cells

Special Issue Reprint

Advances in the Cellular and Molecular Mechanisms of Cardiovascular Diseases

Edited by
Timothy Martin Palmer and Katie S. Wraith

mdpi.com/journal/cells

MDPI

Advances in the Cellular and Molecular Mechanisms of Cardiovascular Diseases

Advances in the Cellular and Molecular Mechanisms of Cardiovascular Diseases

Guest Editors

Timothy Martin Palmer
Katie S. Wraith

MDPI

Basel • Beijing • Wuhan • Barcelona • Belgrade • Novi Sad • Cluj • Manchester

Guest Editors

Timothy Martin Palmer
Hull York Medical School
University of Hull
Hull
UK

Katie S. Wraith
Hull York Medical School
University of Hull
Hull
UK

Editorial Office
MDPI AG
Grosspeteranlage 5
4052 Basel, Switzerland

This is a reprint of the Special Issue, published open access by the journal *Cells* (ISSN 2073-4409), freely accessible at: https://www.mdpi.com/journal/cells/special_issues/VOT8C9M91E.

For citation purposes, cite each article independently as indicated on the article page online and as indicated below:

Lastname, A.A.; Lastname, B.B. Article Title. *Journal Name* **Year**, *Volume Number*, Page Range.

ISBN 978-3-7258-9173-3 (Hbk)
ISBN 978-3-7258-9174-0 (PDF)
https://doi.org/10.3390/books978-3-7258-9174-0

© 2026 by the authors. Articles in this reprint are Open Access and distributed under the Creative Commons Attribution (CC BY) license. The reprint as a whole is distributed by MDPI under the terms and conditions of the Creative Commons Attribution-NonCommercial-NoDerivs (CC BY-NC-ND) license (https://creativecommons.org/licenses/by-nc-nd/4.0/).

Contents

Katie S. Wraith and Timothy M. Palmer
Advances in the Cellular and Molecular Mechanisms of Cardiovascular Diseases
Reprinted from: *Cells* **2026**, *15*, 1587, https://doi.org/10.3390/cells15171587 . . . . . **1**

Hridya Chempon, Sunita Kumari, Srinivasa Reddy Bonam and Srigiridhar Kotamraju
Metformin Inhibits Cardiac Fibroblast Differentiation by Promoting Fatty Acid β-Oxidation: Implications for Age-Associated Cardiac Fibrosis
Reprinted from: *Cells* **2026**, *15*, 1408, https://doi.org/10.3390/cells15151408 . . . . . **4**

Israel O. Bolanle, Florah T. Moshapa, Gillian A. Durham, James P. Hobkirk, Kirsten Riches-Suman, Mahmoud Loubani, et al.
JAK and MEK Pathway Regulation of Mitochondrial Activity as Possible Targets for Saphenous Vein Smooth Muscle Cell Dysfunction in Diabetes
Reprinted from: *Cells* **2026**, *15*, 1402, https://doi.org/10.3390/cells15151402 . . . . . **25**

Su-Kiat Chua, Bao-Wei Wang, Ying-Ju Yu, Wei-Jen Fang, Chiu-Mei Lin, Cheng-Yen Chuang and Kou-Gi Shyu
Exosomal MALAT1 from Rapid Electrical Stimulation-Treated Atrial Fibroblasts Activates Autophagy by Downregulating miR-204-5p and Upregulating LC3B
Reprinted from: *Cells* **2026**, *15*, 1126, https://doi.org/10.3390/cells15121126 . . . . . **52**

Emanuel Heilein, Lucia Sophie Kilian, Samuel Sossalla, Benjamin Meder, Mirko Völkers, Karen S. Frese, et al.
Strip1 Is a Novel Negative Regulator of Cardiomyocyte Hypertrophy
Reprinted from: *Cells* **2026**, *15*, 540, https://doi.org/10.3390/cells15060540 . . . . . **68**

Nadja Itani, Rolf Schreckenberg, Rainer Schulz, Peter Bencsik, Peter Ferdinandy and Klaus-Dieter Schlüter
Roquin Modulates Cardiac Post-Infarct Remodeling via microRNA Stability Control
Reprinted from: *Cells* **2025**, *14*, 1748, https://doi.org/10.3390/cells14221748 . . . . . **92**

Lucia Spartano, Maria Lombardi, Vincenzo Ardita, Roberto Chiesa, Andrea Aramini, Marcello Allegretti, et al.
Ladarixin Potential over the Effects of IL-8 and of Serum from Patients with Abdominal Aortic Aneurysm on Human Aortic Cells
Reprinted from: *Cells* **2025**, *14*, 1713, https://doi.org/10.3390/cells14211713 . . . . . **105**

Ankita Garg, Malte Juchem, Sinje Biss, Carla Nunes Borisch, Julia Leonardy, Christian Bär, et al.
Prostaglandin D_2 Synthase: A Novel Player in the Pathological Signaling Mechanism of the Aldosterone–Mineralocorticoid Receptor Pathway in the Heart
Reprinted from: *Cells* **2025**, *14*, 1485, https://doi.org/148510.3390/cells14191485 . . . . . **119**

Md Sayed Ali Sheikh, A. Alduraywish, Basil Mohammed Alomair, Muhannad Almubarak and Umme Salma
MicroRNA-21 Protects Hypoxic-Induced Cardiomyocytes Injury by Targeting Smad-7
Reprinted from: *Cells* **2025**, *14*, 1483, https://doi.org/10.3390/cells14191483 . . . . . **137**

Alexander Blagov, Daria Borodko, Ulyana Rozhkova, Stanislav Antonov, Aleksandra Utkina and Tatiana Kovyanova
Targeting the Notch Signaling Pathway to Treat Atherosclerosis
Reprinted from: *Cells* **2026**, *15*, 1463, https://doi.org/10.3390/cells15161463 . . . . . **152**

Daniel Miron Brie, Cristian Mornoș, Ovidiu Adam, Alexandru Tîrziu, Roxana Popescu and Alina Diduța Brie
Inflammatory Mechanisms in Acute Coronary Syndromes: From Pathophysiology to Therapeutic Targets
Reprinted from: *Cells* **2026**, *15*, 72, https://doi.org/10.3390/cells15010072 . . . . . **174**

Muhammad Sanusi, Roopeessh Vempati, Dinakaran Umashankar, Suha Tarannum, Yash Varma, Fawaz Mohammed, et al.
Molecular Mechanisms of Atrial Fibrillation Recurrence After Successful Catheter Ablation
Reprinted from: *Cells* **2026**, *15*, 36, https://doi.org/10.3390/cells15010036 . . . . . **222**

cells

MDPI

Editorial

Advances in the Cellular and Molecular Mechanisms of Cardiovascular Diseases

Katie S. Wraith and Timothy M. Palmer *

Centre for Biomedicine, Hull York Medical School, University of Hull, Hull HU6 7RX, UK; katie.wraith@hyms.ac.uk

* Correspondence: tim.palmer@hyms.ac.uk

Introduction

Cardiovascular diseases (CVDs) remain the leading cause of death worldwide despite major advances in prevention, diagnosis and treatment. While improvements in risk factor management and acute clinical care have reduced mortality in some patient groups, the global burden of atherosclerosis, heart failure, vascular disease and age-associated cardiovascular dysfunction continues to rise. Addressing this challenge requires a deeper understanding of the cellular and molecular mechanisms that drive disease initiation, progression and tissue remodelling. This Special Issue of *Cells*, "Advances in the Cellular and Molecular Mechanisms of Cardiovascular Diseases", brings together a collection of research studies and narrative reviews spanning cardiovascular metabolism, inflammation, cellular signalling, vascular remodelling and gene regulation, highlighting emerging therapeutic opportunities spanning multiple cardiovascular pathologies.

A recurring theme throughout this Special Issue is the central role of metabolic regulation in determining cardiovascular cell phenotype and function. Growing evidence indicates that alterations in mitochondrial activity and substrate utilisation are not simply consequences of disease but active drivers of pathological remodelling [1,2]. Chempon and colleagues (Contribution 1) [3] demonstrate that metformin suppresses cardiac fibroblast differentiation and cellular senescence through preservation of fatty acid β-oxidation and mitochondrial bioenergetics, providing new mechanistic insight into the anti-fibrotic actions of this widely used therapeutic agent. Similarly, Bolanle et al. (Contribution 2) [4] identify JAK- and MEK-dependent regulation of mitochondrial activity in diabetic saphenous vein smooth muscle cells, highlighting signalling pathways that may contribute to vein graft failure and vascular dysfunction in diabetes. Together, these studies reinforce the concept that metabolic pathways represent attractive targets for therapeutic intervention in cardiovascular disease.

The collection also highlights the importance of inflammatory signalling networks in cardiovascular pathology. Chronic vascular inflammation is a major driver of remodelling, aneurysm formation and tissue injury, yet the mechanisms linking inflammatory stimuli to cellular dysfunction remain incompletely understood [5]. Spartano et al. (Contribution 6) [6] demonstrate that pharmacological inhibition of CXCR2/CXCL1 signalling with ladarixin attenuates several pathological responses in endothelial and vascular smooth muscle cells exposed to inflammatory stimuli relevant to abdominal aortic aneurysm. These findings support a growing body of evidence implicating chemokine signalling pathways as potential therapeutic targets for vascular disease. In parallel, Garg et al. (Contribution 7) [7] identify prostaglandin D2 synthase as a previously unrecognised mediator of aldosterone–mineralocorticoid receptor signalling in the heart, establishing a novel link between hormonal signalling, cardiac hypertrophy and fibrotic remodelling.

Another important theme emerging from this Special Issue is the increasing recognition of the fundamental roles post-transcriptional mechanisms play in cardiovascular adaptation to stress and injury. Itani and co-workers (Contribution 5) [8] demonstrate that the RNA-binding proteins Roquin-1 and Roquin-2 regulate cardiac post-infarction remodelling through control of microRNA stability and downstream transcriptional networks. These findings add to a rapidly expanding literature demonstrating that RNA-dependent regulatory pathways are major determinants of cardiovascular cell fate and function and may provide opportunities for highly specific therapeutic targeting [9]. Narrative reviews evaluating the roles of the Notch pathway in atherosclerosis (Contribution 9) [10], new findings on how inflammation drives acute coronary syndromes (Contribution 10) [11] and the molecular impact of catheter ablation on atrial fibrillation (Contribution 11) [12] elegantly summarise current research in these areas.

Taken together, the studies published in this Special Issue show that cardiovascular diseases arise through the complex interaction of metabolic dysfunction, inflammatory signalling, altered cellular plasticity and dysregulated gene expression. Importantly, these processes are interconnected and frequently converge on common pathological endpoints, including fibrosis, vascular remodelling, cellular senescence and impaired tissue repair. The work presented here therefore advances our understanding of cardiovascular disease across multiple biological scales, from intracellular signalling pathways to whole-organ remodelling.

Collectively, these articles also provide compelling evidence that mechanistic cardiovascular research will continue to generate clinically relevant insights with significant translational potential. By identifying new molecular targets, clarifying disease pathways and revealing previously unrecognised regulatory mechanisms, the contributions in this Special Issue expand the foundation upon which future diagnostic and therapeutic strategies will be built. As the burden of cardiovascular disease continues to grow globally, such interdisciplinary and mechanistically driven research will be essential for translating mechanistic insights in the development of more effective approaches to prevention, diagnosis and treatment.

Author Contributions: T.M.P.: writing—original draft preparation; K.S.W.: writing—review and editing. All authors have read and agreed to the published version of the manuscript.

Conflicts of Interest: The authors declare no conflicts of interest.

List of Contributions:

1. Chempon, H.; Kumari, S.; Bonam, S.R.; Kotamraju, S. Metformin Inhibits Cardiac Fibroblast Differentiation by Promoting Fatty Acid β-Oxidation: Implications for Age-Associated Cardiac Fibrosis. *Cells* **2026**, *15*, 1408. https://doi.org/10.3390/cells15151408.
2. Bolanle, I.O.; Moshapa, F.T.; Durham, G.A.; Hobkirk, J.P.; Riches-Suman, K.; Loubani, M.; Sturmey, R.G.; Palmer, T.M. JAK and MEK Pathway Regulation of Mitochondrial Activity as Possible Targets for Saphenous Vein Smooth Muscle Cell Dysfunction in Diabetes. *Cells* **2026**, *15*, 1402. https://doi.org/10.3390/cells15151402.
3. Chua, S.K.; Wang, B.W.; Yu, Y.J.; Fang, W.J.; Lin, C.M.; Chuang, C.Y.; Shyu, K.G. Exosomal MALAT1 from Rapid Electrical Stimulation-Treated Atrial Fibroblasts Activates Autophagy by Downregulating miR-204-5p and Upregulating LC3B. *Cells* **2026**, *15*, 1126. https://doi.org/10.3390/cells15121126.
4. Heilein, E.; Kilian, L.S.; Sossalla, S.; Meder, B.; Völkers, M.; Frese, K.S.; Herch, S.; Frey, N.; Eden, M. Strip1 Is a Novel Negative Regulator of Cardiomyocyte Hypertrophy. *Cells* **2026**, *15*, 540. https://doi.org/10.3390/cells15060540.
5. Itani, N.; Schreckenberg, R.; Schulz, R.; Bencsik, P.; Ferdinandy, P.; Schlüter, K.D. Roquin Modulates Cardiac Post-Infarct Remodeling via microRNA Stability Control. *Cells* **2025**, *14*, 1748. https://doi.org/10.3390/cells14221748.

6. Spartano, L.; Lombardi, M.; Ardita, V.; Chiesa, R.; Aramini, A.; Allegretti, M.; Baccellieri, D.; De Filippis, L.; Foglieni, C. Ladarixin Potential over the Effects of IL-8 and of Serum from Patients with Abdominal Aortic Aneurysm on Human Aortic Cells. *Cells* **2025**, *14*, 1743. https://doi.org/10.3390/cells14211713.
7. Garg, A.; Juchem, M.; Biss, S.; Borisch, C.N.; Leonardy, J.; Bär, C.; Gupta, S.K.; Thum, T. Prostaglandin D2 Synthase: A Novel Player in the Pathological Signaling Mechanism of the Aldosterone–Mineralocorticoid Receptor Pathway in the Heart. *Cells* **2025**, *14*, 1485. https://doi.org/10.3390/cells14191485.
8. Ali Sheikh, M.S.; Alduraywish, A.; Mohammed Alomair, B.; Almubarak, M.; Salma, U. MicroRNA-21 Protects Hypoxic-Induced Cardiomyocytes Injury by Targeting Smad-7. *Cells* **2025**, *14*, 1483. https://doi.org/10.3390/cells14191483.
9. Blagov, A.; Borodko, D.; Rozhkova, U.; Antonov, S.; Utkina, A.; Kovyanova, T. Targeting the Notch Signaling Pathway to Treat Atherosclerosis. *Cells* **2026**, *15*, 1463. https://doi.org/10.3390/cells15161463.
10. Brie, D.M.; Mornoș, C.; Adam, O.; Tîrziu, A.; Popescu, R.; Brie, A.D. Inflammatory Mechanisms in Acute Coronary Syndromes: From Pathophysiology to Therapeutic Targets. *Cells* **2025**, *15*, 72. https://doi.org/10.3390/cells15010072.
11. Sanusi, M.; Vempati, R.; Umashankar, D.; Tarannum, S.; Varma, Y.; Mohammed, F.; Mylavarapu, M.; Zakaria, F.; Nair, R.; Reddy, Y.M.; Toquica Gahona, C. Molecular Mechanisms of Atrial Fibrillation Recurrence After Successful Catheter Ablation. *Cells* **2025**, *15*, 36. https://doi.org/10.3390/cells15010036.

References

1. Chen, L.; Chen, M.; Yang, X.; Hu, Y.; Qiu, C.; Fu, Y.; Lan, X.; Luo, G.; Liu, Q.; Liu, M. Energy metabolism in cardiovascular diseases: Unlocking the hidden powerhouse of cardiac pathophysiology. *Front. Endocrinol.* **2025**, *16*, 1617305. [CrossRef]
2. Ouyang, J.; Wu, D.; Gan, Y.; Tang, Y.; Wang, H.; Huang, J. Unraveling the metabolic–epigenetic nexus: A new frontier in cardiovascular disease treatment. *Cell Death Dis.* **2025**, *16*, 183. [CrossRef]
3. Chempon, H.; Kumari, S.; Bonam, S.R.; Kotamraju, S. Metformin Inhibits Cardiac Fibroblast Differentiation by Promoting Fatty Acid β-Oxidation: Implications for Age-Associated Cardiac Fibrosis. *Cells* **2026**, *15*, 1408. [CrossRef]
4. Bolanle, I.O.; Moshapa, F.T.; Durham, G.A.; Hobkirk, J.P.; Riches-Suman, K.; Loubani, M.; Sturmey, R.G.; Palmer, T.M. JAK and MEK Pathway Regulation of Mitochondrial Activity as Possible Targets for Saphenous Vein Smooth Muscle Cell Dysfunction in Diabetes. *Cells* **2026**, *15*, 1402. [CrossRef]
5. Zhu, J.; Meganathan, I.; MacAruthur, R.; Kassiri, Z. Inflammation in Abdominal Aortic Aneurysm: Cause or Comorbidity? *Can. J. Cardiol.* **2024**, *40*, 2378–2391. [CrossRef]
6. Spartano, L.; Lombardi, M.; Ardita, V.; Chiesa, R.; Aramini, A.; Allegretti, M.; Baccellieri, D.; De Filippis, L.; Foglieni, C. Ladarixin Potential over the Effects of IL-8 and of Serum from Patients with Abdominal Aortic Aneurysm on Human Aortic Cells. *Cells* **2025**, *14*, 1713. [CrossRef]
7. Garg, A.; Juchem, M.; Biss, S.; Borisch, C.N.; Leonardy, J.; Bär, C.; Gupta, S.K.; Thum, T. Prostaglandin D2 Synthase: A Novel Player in the Pathological Signaling Mechanism of the Aldosterone–Mineralocorticoid Receptor Pathway in the Heart. *Cells* **2025**, *14*, 1485. [CrossRef]
8. Itani, N.; Schreckenberg, R.; Schulz, R.; Bencsik, P.; Ferdinandy, P.; Schlüter, K.D. Roquin Modulates Cardiac Post-Infarct Remodeling via microRNA Stability Control. *Cells* **2025**, *14*, 1748. [CrossRef]
9. Dzau, V.J.; Hodgkinson, C.P. RNA Therapeutics for the Cardiovascular System. *Circulation* **2024**, *149*, 707–716. [CrossRef]
10. Blagov, A.; Borodko, D.; Rozhkova, U.; Antonov, S.; Utkina, A.; Kovyanova, T. Targeting the Notch Signaling Pathway to Treat Atherosclerosis. *Cells* **2026**, *15*, 1463. [CrossRef]
11. Brie, D.M.; Mornoș, C.; Adam, O.; Tîrziu, A.; Popescu, R.; Brie, A.D. Inflammatory Mechanisms in Acute Coronary Syndromes: From Pathophysiology to Therapeutic Targets. *Cells* **2026**, *15*, 72. [CrossRef]
12. Sanusi, M.; Vempati, R.; Umashankar, D.; Tarannum, S.; Varma, Y.; Mohammed, F.; Mylavarapu, M.; Zakaria, F.; Nair, R.; Reddy, Y.M.; et al. Molecular Mechanisms of Atrial Fibrillation Recurrence After Successful Catheter Ablation. *Cells* **2026**, *15*, 36. [CrossRef]

Disclaimer/Publisher's Note: The statements, opinions and data contained in all publications are solely those of the individual author(s) and contributor(s) and not of MDPI and/or the editor(s). MDPI and/or the editor(s) disclaim responsibility for any injury to people or property resulting from any ideas, methods, instructions or products referred to in the content.

cells

MDPI

Article

Metformin Inhibits Cardiac Fibroblast Differentiation by Promoting Fatty Acid β-Oxidation: Implications for Age-Associated Cardiac Fibrosis

Hridya Chempon [1,2], Sunita Kumari [1,2], Srinivasa Reddy Bonam [1,2] and Srigiridhar Kotamraju [1,2,*]

[1] Department of Applied Biology, CSIR-Indian Institute of Chemical Technology, Hyderabad 500007, India; hridyacdas@gmail.com (H.C.); sunitaraisr28@gmail.com (S.K.); bsrpharmacy90@gmail.com (S.R.B.)
[2] Academy of Scientific and Innovative Research, Ghaziabad 201002, India
* Correspondence: giridhar.iict@csir.res.in; Tel.: +91-9908213979

Highlights

What are the main findings?

- Metformin enhances FAO to suppress cardiac fibroblast activation.
- Metformin preserves mitochondrial bioenergetics in cardiac fibrosis.

What are the implications of the main findings?

- Metformin reduces cardiac fibrosis by enhancing CPT1-dependent FAO.

Abstract

Cardiac fibrosis is a hallmark of pathological cardiac remodeling, characterized by fibroblast activation, excessive extracellular matrix deposition, and myocardial hypertrophy, ultimately leading to cardiac dysfunction. Aging exacerbates these processes through metabolic stress and impaired mitochondrial bioenergetics. Here, we investigated the anti-fibrotic effects of metformin and the role of fatty acid β-oxidation (FAO) in regulating cardiac fibroblast differentiation. Metformin significantly attenuated transforming growth factor-β (TGF-β)-induced cardiac fibroblast activation and the associated senescence-like phenotype. These effects were accompanied by enhanced FAO and increased mitochondrial oxygen consumption rate (OCR), indicating improved mitochondrial function. Importantly, inhibition of carnitine palmitoyltransferase-1 (CPT1) with etomoxir largely abolished the beneficial effects of metformin on mitochondrial respiration, fibroblast activation, and cellular senescence, demonstrating a critical role for FAO. Mechanistically, metformin increased CPT1 activity and acetyl-CoA levels while reducing malonyl-CoA accumulation, thereby promoting mitochondrial fatty acid utilization. These findings were corroborated in aged Apoe$^{-/-}$ mice, where metformin reduced the expression of cardiac fibroblast differentiation markers and enhanced FAO-associated markers. Collectively, our findings demonstrate that metformin suppresses cardiac fibroblast differentiation and senescence by preserving mitochondrial bioenergetics through FAO-dependent mechanisms, revealing a metabolic basis for its anti-fibrotic actions and supporting its therapeutic potential in age-related cardiovascular disease.

Keywords: metformin; CPT1; FAO; cardiac fibrosis; senescence

1. Introduction

Cardiovascular diseases (CVDs) remain the leading cause of mortality worldwide, and aging is a major risk factor for their development and progression. Age-associated cardiac remodeling is characterized by myocardial hypertrophy, increased ventricular stiffness, impaired cardiac function, and excessive extracellular matrix (ECM) deposition [1]. Among these changes, myocardial fibrosis is a key pathological feature that contributes to cardiac dysfunction, arrhythmias, and heart failure. Cardiac fibrosis is primarily driven by the activation and differentiation of resident cardiac fibroblasts into myofibroblasts, a process largely mediated by transforming growth factor-β (TGF-β) [2,3].

Accumulating evidence suggests that aging promotes fibrotic remodeling through mitochondrial dysfunction, oxidative stress, chronic inflammation, and cellular senescence [4]. Given the high energy demand of the heart, maintenance of mitochondrial function is essential for cardiac homeostasis. The adult myocardium derives the majority of its ATP from mitochondrial fatty acid β-oxidation (FAO), and impairment of this pathway is increasingly recognized as a hallmark of cardiac aging [5,6]. Reduced FAO contributes to metabolic stress, diminished ATP production, and mitochondrial dysfunction, all of which may influence fibroblast activation and pathological remodeling. However, the role of FAO in regulating cardiac fibroblast differentiation during aging still remains elusive.

Mitochondrial FAO is tightly regulated by carnitine palmitoyltransferase-1 (CPT1), the rate-limiting enzyme responsible for transporting long-chain fatty acids into mitochondria for β-oxidation [7]. Aging has been associated with reduced expression and activity of CPT1 and other FAO-related enzymes, resulting in impaired mitochondrial bioenergetics [8]. Emerging studies suggest that metabolic reprogramming is a critical determinant of fibroblast fate and function [9], raising the possibility that restoration of FAO may represent a novel strategy to limit cardiac fibrosis.

AMP-activated protein kinase (AMPK) serves as a central regulator of cellular energy homeostasis and promotes FAO through inhibition of acetyl-CoA carboxylase (ACC), thereby relieving malonyl-CoA-mediated suppression of CPT1. Notably, AMPK activity declines with aging, contributing to metabolic dysfunction and reduced mitochondrial efficiency [10]. Metformin, a widely prescribed antidiabetic drug, activates AMPK and has gained attention for its cardioprotective and geroprotective properties. In our previous studies, metformin was shown to modulate AMPK-mediated H3K79 methylation, which in turn improves mitochondrial function and attenuation of endothelial cell senescence [11,12]. Additionally, in a recent study, we showed that metformin administration delays endothelial cell senescence by potentiating FAO [13]. In addition to improving metabolic homeostasis, metformin was shown to attenuate fibrosis, oxidative stress, and cellular senescence in several pathological settings [14]. However, whether the anti-fibrotic effects of metformin are mediated through restoration of FAO-dependent mitochondrial bioenergetics remains unclear. Addressing this knowledge gap is important because current understanding of metformin-mediated cardioprotection has largely focused on modulation of canonical signaling pathways, whereas the contribution of metabolic substrate utilization, particularly FAO, to fibroblast regulation remains poorly characterized. Determining whether FAO restoration represents a functional mediator of metformin's anti-fibrotic effects may provide new insights into metabolic approaches for preventing age-related cardiac remodeling.

In the present study, we investigated the role of FAO in metformin-mediated regulation of cardiac fibroblast activation and senescence. Using TGF-β-stimulated cardiac fibroblasts and aged $Apoe^{-/-}$ mice, a model with features of hypercholesteremia and age-associated cardiovascular dysfunction, we examined the involvement of the AMPK–ACC–CPT1 signaling axis in fibroblast differentiation. Our findings demonstrate that metformin suppresses fibroblast activation and senescence by enhancing CPT1-dependent FAO and

preserving mitochondrial bioenergetics. These results identify FAO as a critical regulator of cardiac fibroblast fate, and reveal a previously underappreciated metabolic mechanism underlying the anti-fibrotic actions of metformin in age-related cardiac fibrosis.

2. Materials and Methods

2.1. Isolation of Mouse Cardiac Fibroblast Cells

Male 6–8-week-old C57BL/6 mice were sacrificed by cervical dislocation, and hearts were collected after perfusion with PBS. The hearts were transferred to a 60 mm dish, atria were removed, and ventricles were cut in to small pieces and collected. A volume of 2 mL collagenase II solution (Cat. #C6885, Sigma, St. Louis, MO, USA) was added per heart, and the tissue was triturated with a 1 mL pipette tip with a wide opening. The supernatant was collected into a 50 mL centrifuge tube and kept for incubation at 37 °C with continuous shaking for 20 min. Collagenase was inactivated by adding FBS (Cat. #12800017, GIBCO, Paisley, UK) (2 mL per heart), and the cell suspension was transferred to a 15 mL centrifuge tube and centrifuged for 1 min. The pellet was resuspended in DMEM (Cat. #D7777, Sigma, St. Louis, MO, USA) with 10% FBS. Collagenase II solution was added to the remaining tissue and incubated again at 37 °C for 20 min. The above steps were repeated until the tissue was completely dissolved. All of the collected supernatants were clubbed and centrifuged, and the pellet was homogenously suspended in DMEM containing 10% FBS and seeded in Petri dishes. Media was changed after 2 h. After expansion, primary cardiac fibroblasts were passaged, and all experiments were performed using second-passage (P2) cells. Experiments were conducted according to the guidelines formulated for the care and use of animals in scientific research (ICMR, New Delhi, India) at a CPCSEA (Committee for the Purpose of Control and Supervision of Experiments on Animals) registered animal facility. The IAEC approved the experimental protocol at CSIR-IICT (IICT/IAEC/040/2023).

2.2. Real Time-qPCR

Total RNA was extracted using TRIzol reagent (Cat. #T9424, Sigma, St. Louis, MO, USA). The purified RNA was subsequently reverse-transcribed into cDNA using a commercially available cDNA synthesis kit (Cat. #K1622, Thermo Fisher Scientific, Waltham, MA, USA). Quantitative real-time PCR (qPCR) was performed using SYBR Green PCR Master Mix (Cat. #4309155, Thermo Fisher Scientific, Waltham, MA, USA) along with gene-specific primers. Relative gene expression levels were determined using the ΔΔCt method, with 18S rRNA serving as internal reference genes for normalization. Details of the gene-specific primer sequences are listed in Table 1.

2.3. Western Blot Analysis

Cells were lysed using RIPA buffer (Cat. #R0278, Sigma, St. Louis, MO, USA) supplemented with protease inhibitor cocktail (Cat. #P8340, Sigma, St. Louis, MO, USA), phosphatase inhibitor cocktail-2 (Cat. #P5726, Sigma, St. Louis, MO, USA), and phosphatase inhibitor cocktail-3 (Cat. #P0044, Sigma, St. Louis, MO, USA). Equal amounts of protein were separated on 8–15% SDS-PAGE gels and subsequently transferred onto nitrocellulose membranes. The membranes were incubated overnight at 4 °C with specific primary antibodies, followed by incubation with the corresponding secondary antibodies for 1 h at room temperature. Protein bands were visualized using Luminal/Enhancer solution (Millipore, Hercules, CA, USA) and detected with the ChemiDoc XRS+ imaging system (Bio-Rad, Hercules, CA, USA). The primary antibodies used for Western blot analysis were as follows: CPT1 (Cat. #97361S, Cell Signaling Technology, Danvers, MA, USA), AMPK (Cat. #2795S, Cell Signaling Technology, Danvers, MA, USA), p-AMPK (Cat. #2535S, Cell

Signaling Technology, Danvers, MA, USA), ACC (Cat. #3676S, Cell Signaling Technology, Danvers, MA, USA), p-ACC (Cat. #3661S, Cell Signaling Technology, Danvers, MA, USA), α-SMA (Cat. #ab5694, Abcam, Cambridge CB2 0AX, UK), p21 (Cat. #2947S, Cell Signaling Technology, Danvers, MA, USA), p27 (Cat. #SAB4500068, Sigma, St. Louis, MO, USA), and TGF-β (Cat. #3711S, Cell Signaling Technology, Danvers, MA, USA).

Table 1. List of Mouse Primer Sets Used.

Gene	Forward Primer	Reverse Primer
CPT1	AAGTTCTGCCTGACTACGAGG	ATGTTTTGGTGCTTTTCGGAGG
FABP3	CATCATCGAGAAGAACGGGGAT	TTCTGCACATGGATGAGTTTGC
ACSL1	CATCGTCAGAAACAACAGCCTG	GGTCTGTCCGTAGCCTTCATAG
ACADM	CGGAACACTTACTATGGGTCGA	CTGATAGATCTTGGCGTCCCTC
ACADS	CTCCTCCACAGCTAACCTCATC	GGCATACTTCACAGCACAATCC
α-SMA	CTATTCCTTCGTGACCACAGCT	CCGCAGACTCCATACCGATAAA
COL1A1	CTCAAGATGTGCCACTCTGACT	ACCTGTCTCCATGTTGCAGTAG
COL3A1	ACGTAAGCACTGGTGGACAG	GGAGGGCCATAGCTGAACTG
18S	AGTTATGGTTCCTTTGGTCGCT	TTATCTAGAGTCACCAAGCCGC

2.4. Carnitine Palmitoyltranferase-1 (CPT1) Activity

Carnitine palmitoyltransferase-1 (CPT1) enzymatic activity was determined as previously described [15,16]. Briefly, active mitochondrial fractions were isolated using a commercially available mitochondrial isolation kit (Cat. #MITOISO2, Sigma, St. Louis, MO, USA) according to the manufacturer's instructions. Equal amounts of mitochondrial protein were incubated in a reaction mixture containing 116 mM Tris-HCl (pH 8.0), 0.09% Triton X-100, 1.1 mM EDTA (Cat. #E5134, Sigma, St. Louis, MO, USA), 0.12 mM DTNB (Cat. #D8130, Sigma, St. Louis, MO, USA), 0.035 mM palmitoyl-CoA (Cat. #P9716, Sigma, St. Louis, MO, USA), and either 1 mM L-carnitine (Cat. #8.40092, Sigma, St. Louis, MO, USA) or 11 mM D-carnitine (Cat. No. #HY-W012550, MedChemExpress, Monmouth Junction, NJ, USA). The reaction was initiated by adding mitochondrial fraction, and the formation of CoA-SH was continuously monitored for 4 min at 412 nm in a multimode reader.

2.5. Measurement of Acetyl-CoA and Malonyl-CoA Levels

Acetyl-CoA and malonyl-CoA levels were measured using commercially available kits from Sigma (Cat. #MAK039, Sigma, St. Louis, MO, USA) and Krishgen biosystems (Cat. # KBH5628, Krishgen biosystems, Mumbai, India), respectively, as per the manufacturers' instructions.

2.6. Analysis of Mitochondrial Respiration

Mitochondrial function was assessed using an extracellular flux analyzer (XF24; Seahorse Biosciences/Agilent, Santa Clara, CA, USA). Adult mouse cardiac fibroblast cells were seeded at a density of 40,000 cells per well in DMEM. After 16 h, the culture medium was replaced with Seahorse assay medium (Cat. #103575-100, Agilent, CA, USA) supplemented with 10 mM glucose (Cat. #G8270, Sigma, St. Louis, MO, USA), 1 mM pyruvate (Cat. #S8636, Sigma, St. Louis, MO, USA), and 200 mM glutamine (Cat. #G7513, Sigma, St. Louis, MO, USA), followed by incubation for 1 h at 37 °C in a CO_2-free incubator for equilibration. Etomoxir (40 μM), oligomycin (1 μM), FCCP (carbonyl cyanide-p-trifluoromethoxyphenylhydrazone; 1 μM), and Antimycin A+ Rotenone (1 μM each) (Cat. #103270-100, Agilent, Santa Clara, CA, USA) were loaded into Ports A, B, C, and D, respec-

tively. In a separate experiment, adult mouse cardiac fibroblast cells were plated at the same density in DMEM medium and allowed to attach for 8 h. The medium was subsequently replaced with substrate-limited growth medium containing 0.5 mM glucose (Cat. #G8270, Sigma, St. Louis, MO, USA), 1 mM glutamine (Cat. #G7513, Sigma, St. Louis, MO, USA), 1% FBS (Cat. #12800017, GIBCO, Paisley, UK), and 0.5 mM carnitine (Cat. #103693-100, Agilent, Santa Clara, CA, USA), and the cells were incubated in a CO_2 incubator for 16 h. Prior to the assay, the medium was exchanged with substrate-limited assay medium supplemented with 2 mM glucose (Cat. #G8270, Sigma, St. Louis, MO, USA) and 0.5 mM L-carnitine (Cat. #103693-100, Agilent, Santa Clara, CA, USA), followed by incubation for 1 h in a non-CO_2 incubator. Immediately before initiating the assay, 85 µL of 1 × palmitate-BSA (170 µM) (Cat. #103693-100, Agilent, Santa Clara, CA, USA) was added to each well. The oxygen consumption rate (OCR) was determined from the slope of concentration change versus time. Maximal respiration was calculated by subtracting the rotenone and antimycin A-inhibited OCR from the FCCP-stimulated OCR, while ATP production was estimated from the reduction in basal OCR following oligomycin treatment. Coupling efficiency (%) was calculated by dividing ATP production/basal respiration × 100.

2.7. Animal Experiments

Animal studies were performed using 12-month-old male $Apoe^{-/-}$ mice according to the guidelines formulated for the care and use of animals in scientific research (ICMR, India) at a CPCSEA (Committee for the Purpose of Control and Supervision of Experiments on Animals) registered animal facility. The IAEC approved the experimental protocols at CSIR-IICT (IICT/IAEC/024/2022). All animals were housed in a specific pathogen-free (SPF) animal facility under controlled environmental conditions (23 ± 1 °C, 50–60% relative humidity) with a 12 h light/12 h dark cycle and had ad libitum access to standard chow diet and water. A group of 6-month-old male $Apoe^{-/-}$ mice was included as the young control. The 12-month-old $Apoe^{-/-}$ mice were randomly assigned to two groups (n = 10 per group). To evaluate the adequacy of the sample size used, we performed a post hoc sensitivity analysis using G*Power 3.1. One group was administered with metformin (50 mg/kg body weight/day) prepared in 0.5% methylcellulose containing Tween-20, while the other served as the age-matched vehicle control. Both young control group (6-month-old $Apoe^{-/-}$ mice) and age-matched control group (12-month-old $Apoe^{-/-}$ mice) received only 0.5% methylcellulose and Tween-20. Treatments were given once daily by oral gavage for 12 weeks. Throughout the study, all mice were maintained on a standard chow diet containing 11.4% fat. Daily food intake was monitored, and body weight was measured weekly.

2.8. Lipid Staining by Nile Red Assay

Cardiac fibroblast cells or heart tissue sections were stained with Nile Red (1 µg/mL; Cat. #72485, Sigma, St. Louis, MO, USA) for 15 min to visualize lipid content. Following staining, sections were washed three times with PBS to remove excess dye. Fluorescence images were captured using a fluorescence microscope equipped with a rhodamine filter.

2.8.1. Measurement of Cardiac TGF-β Levels by ELISA

TGF-β levels in the cardiac tissue homogenates were quantified using a commercially available ELISA kit (Cat. #KLM0285, Krishgen biosystems, Mumbai, India) according to the manufacturer's instructions.

https://doi.org/10.3390/cells15151408

2.8.2. Masson's Trichrome Staining

Masson's trichrome staining was performed using a commercial staining kit (Cat. #AB150686, Abcam, Cambridge CB2 0AX, UK) according to the manufacturer's instructions. Images were captured using a bright-field microscope.

2.8.3. Sirius Red/Fast Green Collagen Staining

Collagen staining was performed using a Sirius Red/Fast Green collagen Staining Kit (Cat. #9046, Chondrex Inc., Redmond, WA, USA) following the manufacturer's instructions. Images were captured using a bright-field microscope.

2.8.4. Hydroxyproline Assay

Collagen content was determined using a Hydroxyproline Assay Kit (Cat. #E-BC-K062-S, Elabscience, Houston, TX, USA) according to the manufacturer's instructions. Briefly, heart tissue was hydrolyzed with 6 mol/L HCl to release free hydroxyproline. The hydrolysates were reacted with the assay reagents to produce a colored complex, and the absorbance was measured at 558 nm to assess the collagen content.

2.9. PKH 26 Staining

Cardiac fibroblasts were washed with PBS and stained with 2 μM PKH26 (Cat. #HY-D1451, MedChemExpress, Monmouth Junction, NJ, USA) according to the manufacturer's instructions. After staining, cells were washed thoroughly with PBS to remove excess dye and maintained in complete culture medium. Images were acquired using a laser scanning confocal microscope.

2.10. Senescence-Associated β-Galactosidase (SA-β-Gal) Staining

Cellular senescence was assessed using a Senescence β-Galactosidase Staining Kit (Cat. #9860, Cell Signaling Technology, Danvers, MA, USA) according to the manufacturer's instructions. Briefly, cells were washed with PBS, fixed with a fixative solution for 10–15 min at room temperature, and washed twice with PBS. Cells were then incubated with freshly prepared β-galactosidase staining solution at 37 °C in a dry incubator (without CO_2) overnight. Senescent cells exhibiting blue coloration were visualized under a bright-field microscope and images were captured.

2.11. Statistical Analysis

All of the experiments were performed in biological triplicates, and the results are represented as mean ± SD. Data normality and the equality of variances were examined by Shapiro–Wilk test and Brown–Forsythe test, respectively. Data were analyzed by Welch's ANOVA followed by Dunnett's T3 post hoc test for unequal variances, and one-way or two-way ANOVA followed by Tukey's multiple-comparison test for equal variances using GraphPad Prism 10.

3. Results

3.1. Metformin Enhances CPT1 Activity and Fatty Acid β-Oxidation in Adult Mouse Cardiac Fibroblast Cells

Fatty acid β-oxidation (FAO) is the primary pathway for fatty acid catabolism, generating acetyl-CoA for cellular energy production. Activated cardiac fibroblasts have been reported to exhibit impaired oxidative metabolism and reduced FAO [17]. Given our previous finding that chronic metformin treatment enhances FAO in endothelial cells [13], in the current study, we investigated whether metformin could counteract TGF-β-induced alterations in FAO in primary adult mouse cardiac fibroblasts. For this, cells were treated

with TGF-β (10 ng/mL) in the presence or absence of metformin (2 mM) for 48 h. Cells were treated with metformin 12 h prior to the addition of TGF-β. It is to be noted that, intriguingly, while TGF-β alone caused a marked reduction in CPT1 levels, addition of metformin to these cells significantly enhanced the transcript and protein levels of CPT1 (Figure 1A,B). These results were further corroborated by measuring the CPT1 activity, a rate limiting enzyme of FAO (Figure 1C). On a similar note, metformin treatment also led to an increase in the transcript levels of other FAO pathway-related genes (Figure 1D). On the contrary, metformin treatment significantly attenuated TGF-β-induced upregulation of the glycolysis-associated genes (Figure 1E). Collectively, these findings suggest that metformin reverses TGF-β-induced metabolic alterations by restoring FAO while suppressing glycolysis-associated genes expression. Based on the above observations, we next performed Nile Red staining and observed a significant reduction in the intracellular lipid content with metformin + TGF-β treatment conditions compared to TGF-β alone treatment conditions. In contrast, etomoxir (an irreversible inhibitor of CPT1) reversed metformin-mediated reduction in the lipid levels (Figure 1F). This observation suggests that the reduction in the intracellular lipid content in metformin-treated cells is perhaps due to the increased consumption of fatty acids by FAO. Moreover, this result coincides with the increased levels of acetyl-CoA, a key metabolic intermediate and end product of fatty acid β-oxidation, along with a reduction in the levels of malonyl-CoA, a well-established endogenous inhibitor of CPT1-dependent mitochondrial fatty acid uptake, in metformin-treated cells (Figure 1G,H).

Furthermore, to investigate the upstream signaling cascade by which metformin regulates fatty acid β-oxidation, we assessed the activation of AMPK and ACC by immunoblotting. Acetyl-CoA carboxylase (ACC) catalyzes the conversion of acetyl-CoA to malonyl-CoA, a key metabolite that inhibits CPT1-mediated mitochondrial fatty acid uptake. However, phosphorylation of ACC by activated AMPK inhibits its enzymatic activity, thereby reducing malonyl-CoA levels and relieving CPT1 inhibition. Metformin significantly enhanced the levels of phospho-AMPK (Thr-172) with a concomitant increase in phospho-ACC (Ser-79; an inhibitory phosphorylation) compared to TGF-β alone treated cardiac fibroblast cells (Figure 1I–K). Taken together, these findings indicate that metformin promotes FAO in adult mouse cardiac fibroblasts. To determine whether AMPK activation is required for the above observed effects of metformin, cardiac fibroblasts were treated with Compound C, a pharmacological inhibitor of AMPK. Inhibition of AMPK noticeably attenuated the metformin-induced increase in CPT1 transcript levels and its enzyme activity (Figure 2A,B). Consistent with this observation, the transcript levels of other FAO-associated genes were also significantly reduced in Compound C-treated cells (Figure 2C–F). In addition, inhibition of AMPK activation decreased intracellular acetyl-CoA levels while increasing malonyl-CoA levels (Figure 2G,H), indicating suppression of fatty acid β-oxidation. These results demonstrate that activation of the AMPK–ACC axis is essential for metformin-mediated restoration of FAO in TGF-β-stimulated cardiac fibroblasts. Moreover, under these conditions, metformin treatment significantly reduced TGF-β expression, whereas pharmacological inhibition of AMPK with Compound C abolished this effect, as demonstrated by both RT-qPCR and Western blot analyses (Figure 2I–L). Notably, treatment with Compound C alone significantly increased TGF-β levels relative to the untreated control, suggesting that basal AMPK activity negatively regulates TGF-β expression. Together, these results support the conclusion that AMPK activation contributes to the suppressive effect of metformin on TGF-β levels in cardiac fibroblast cells.

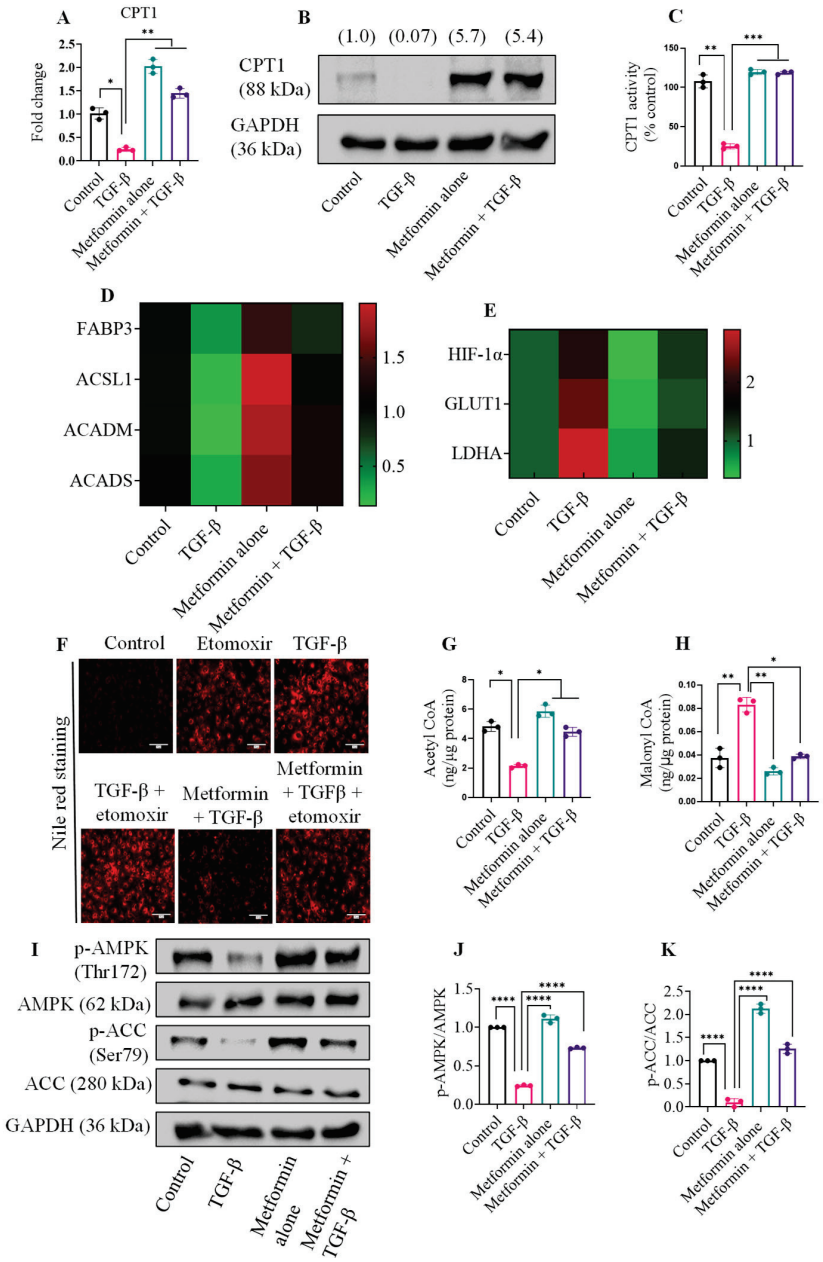


Figure 1. Metformin promotes fatty acid β-oxidation in adult mouse cardiac fibroblasts. (**A**–**C**) Adult mouse cardiac fibroblast cells were pretreated with or without metformin (2 mM) for 12 h followed by TGF-β (10 ng/mL) for 48 h, and CPT1 transcript levels (**A**), protein levels (**B**), and enzyme activity (**C**) were measured. (**D**) Same as *A*, except that transcript levels of *FABP3*, *ACSL1*, *ACADM*, and *ACADS* were measured by RT-qPCR analysis. (**E**) Same as *A*, except that transcript levels of *HIF-1α*, *GLUT1*, and *LDHA* were measured by RT-qPCR analysis. (**F**) Adult mouse cardiac fibroblast cells were pretreated with metformin (2 mM) followed by treatment with TGF-β (10 ng/mL) in the presence or absence of etomoxir (40 µM) for 48 h; lipid accumulation was measured by Nile Red staining, and images were taken in a fluorescence microscope equipped with a rhodamine filter, scale bar = 175 µm. (**G**,**H**) Same as *A*, except that acetyl-CoA levels (**G**) and malonyl-CoA levels (**H**) were measured in cell lysates. (**I**) Same as *A*, except that the indicated protein levels were measured by immunoblot analysis. (**J**,**K**) Quantification of (**I**). GraphPad Prism 10 was used for statistical analysis. Data are presented as mean ± SD from at least three independent experiments. *, $p \leq 0.05$; **, $p \leq 0.005$; ***, $p \leq 0.0005$; ****, $p \leq 0.0001$. Welch's ANOVA followed by Dunnett's T3 post hoc test for unequal variances and one-way ANOVA followed by Tukey's multiple-comparison test for equal variances, depending on variance homogeneity.

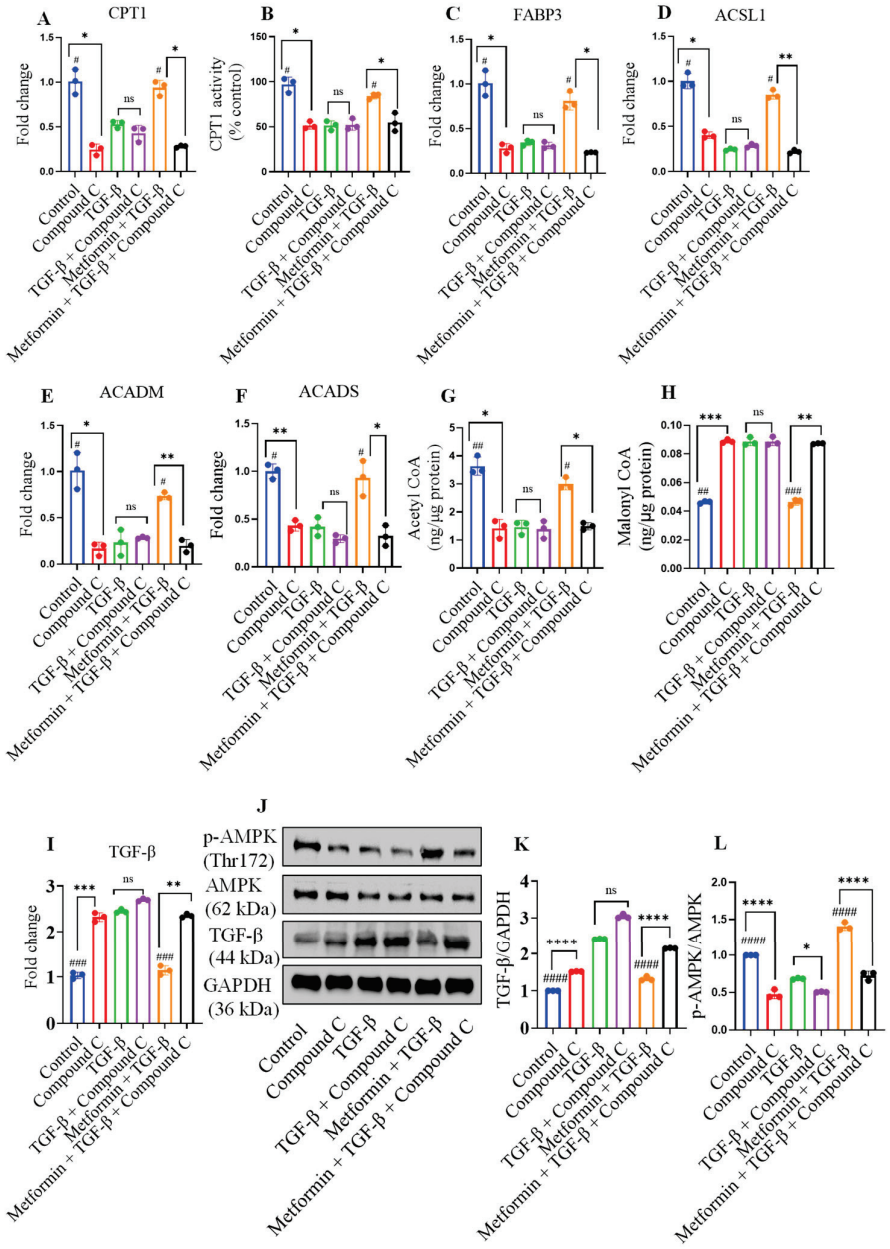


Figure 2. Inhibition of AMPK activation abolishes metformin-mediated enhancement of fatty acid β-oxidation in cardiac fibroblasts. (**A**,**B**) Adult mouse cardiac fibroblasts were treated with Compound C (10 μM) in the presence or absence of metformin (2 mM) for 12 h, followed by TGF-β (10 ng/mL) stimulation for 48 h, and CPT1 transcript levels (**A**) and enzyme activity (**B**) were measured. (**C**–**F**) Same as *A*, except that transcript levels of *FABP3*, *ACSL1*, *ACADM*, and *ACADS* were measured by RT-qPCR analysis. (**G**,**H**) Same as *A*, except that acetyl-CoA levels (**G**) and malonyl-CoA levels (**H**) were measured in cell lysates. (**I**) Same as *A*, except that transcript levels of *TGF-β* (**I**) and the indicated protein levels (**J**) were assessed by RT-qPCR and Western blot analysis, respectively. (**K**,**L**) Quantification of (**J**). GraphPad Prism 10 was used for statistical analysis. Data are presented as mean ± SD from at least three independent experiments. ns is non-significant, *, $p \leq 0.05$; **, $p \leq 0.005$; ***, $p \leq 0.0005$; ****, $p \leq 0.0001$. #, $p \leq 0.05$; ##, $p \leq 0.005$; ###, $p \leq 0.0005$; ####, $p \leq 0.0001$ significantly different from TGF-β. Welch's ANOVA followed by Dunnett's T3 post hoc test for unequal variances and one-way ANOVA followed by Tukey's multiple-comparison test for equal variances, depending on variance homogeneity.

https://doi.org/10.3390/cells15151408

3.2. Metformin Potentiates Mitochondrial Respiration by Enhancing FAO in Adult Mouse Cardiac Fibroblast Cells: Effect of CPT1 Inhibition

Since metformin enhanced CPT1 activity and FAO-related transcript levels like *FABP3*, *ACSL1*, *ACADM*, and *ACADS*, we next assessed its functional relevance by measuring mitochondrial oxygen consumption rate (OCR) using the Seahorse extracellular flux analyzer. Cardiac fibroblast cells were treated with TGF-β alone or in combination with metformin, in the presence or absence of Etomoxir (CPT1 inhibitor). Cells treated with TGF-β exhibited a significant reduction in the basal respiration, maximal respiration, ATP production, and coupling efficiency compared to untreated control cells. Notably, pretreatment with metformin significantly improved the aforementioned parameters (Figure 3A–E). Additionally, in accordance with the results presented in Figure 1, metformin-mediated increases in OCR, ATP production, maximal respiration, and coupling efficiency were markedly attenuated in the presence of etomoxir (Figure 3A–E).

To further validate these observations, we measured the aforementioned parameters under the same treatment conditions using the palmitate-advanced assay following the exogenous addition of palmitic acid (PA), a free fatty acid known to stimulate FAO. Etomoxir significantly attenuated the basal respiration, maximal respiration, ATP production, and coupling efficiency in PA-treated control cells, indicating the dependence of mitochondrial OCR on CPT1-mediated FAO (Figure 4A–E). In contrast, PA failed to restore basal respiration, maximal respiration, ATP production, and coupling efficiency in TGF-β-treated cells compared to PA-treated control cells, thus suggesting impaired utilization of exogenous fatty acids under these conditions (Figure 4A–E). Similar trends were observed in the presence of PA and etomoxir in TGF-β-treated cells (Figure 4A–E). This is consistent with the diminished CPT1 activity by TGF-β, as presented in Figure 1A–C. Notably, metformin markedly preserved basal respiration, maximal respiration, ATP production, and coupling efficiency in TGF-β-treated cells supplemented with PA, while etomoxir significantly attenuated these parameters (Figure 4A–E). Collectively, these findings further support that metformin improves mitochondrial energetics by enhancing CPT1-dependent FAO in mouse cardiac fibroblasts.

3.3. Etomoxir Blunts Metformin-Mediated Attenuation of Cardiac Fibroblast Activation and Cellular Senescence

We next investigated the impact of metformin's ability to potentiate FAO in the regulation of TGF-β-induced cardiac fibroblast differentiation. For this, mouse cardiac fibroblasts were treated with metformin, etomoxir, or TGF-β, either individually or in combination. Morphological changes were initially assessed using PKH26 staining. TGF-β treatment caused cell enlargement, consistent with myofibroblast differentiation compared to a small, spindle-shaped morphology seen in control cells (Figure 5A). Notably, metformin markedly attenuated TGF-β-induced trans-differentiation, with cells retaining a morphology similar to untreated cells (Figure 5A). Interestingly, inhibition of FAO under these conditions by etomoxir diminished the protective effect of metformin against TGF-β-induced fibroblast activation (Figure 5A), indicating that metformin's anti-fibrotic action is likely dependent on enhanced FAO. Accordingly, metformin treatment significantly reduced the transcript levels of fibrosis-associated markers like *α-SMA*, *COL1A1*, and *COL3A1* in TGF-β-treated cells, as well as α-SMA protein levels (Figure 5B–E). Furthermore, TGF-β-induced cardiac fibroblast differentiation coincided with the induction of cellular senescence as measured by senescence-associated β-Gal (SA-β-Gal) staining (Figure 5F,G). Metformin treatment significantly reduced TGF-β-induced senescence, as evidenced by a decreased number of SA-β-Gal-positive cells (Figure 5F,G). Intriguingly, etomoxir significantly abrogated metformin-mediated inhibition of premature senescence in cardiac fibroblast cells (Figure 5F,G). Similar trends were observed with senescence

marker proteins like p21 and p27 by immunoblotting (Figure 5H–J). Thus, it appears that metformin, by potentiating the FAO pathway, alleviates cardiac fibroblast activation and the associated fibroblast senescence.

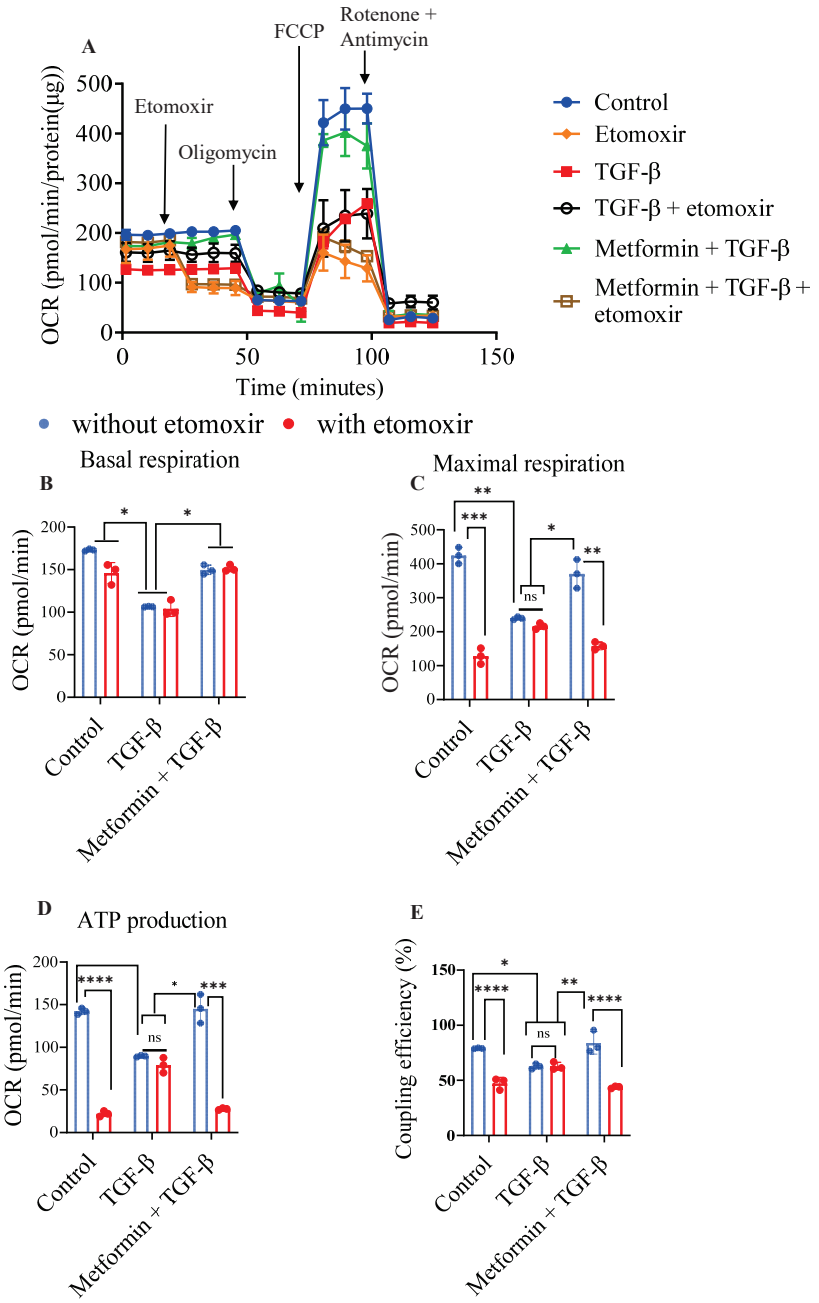


Figure 3. Etomoxir reverses metformin-mediated increase in mitochondrial oxygen consumption rate (OCR) in adult mouse cardiac fibroblast cells. (**A**) Adult mouse cardiac fibroblast cells were pretreated with or without metformin (2 mM) for 12 h followed by TGF-β (10 ng/mL) for 48 h, and the oxygen consumption rates (OCR) were measured by sequentially adding (indicated by arrows) Etomoxir (40 µM), Oligomycin (1 µM), FCCP (1 µM), Rotenone (1 µM), and Antimycin (1 µM) using a Seahorse XF 24 Extracellular Flux Analyzer. (**B**–**E**) Same as A, except that basal respiration (**B**), maximal respiration (**C**), ATP production (**D**), and coupling efficiency (**E**) were measured from the data obtained in A. GraphPad prism 10 was used to perform the statistics. The data shown in the graphs represent the mean ± SD of at least three different experiments. ns is non-significant, *, $p \leq 0.05$; **, $p \leq 0.005$; ***, $p \leq 0.0005$; ****, $p \leq 0.0001$ by two-way ANOVA followed by Tukey's multiple-comparison test.

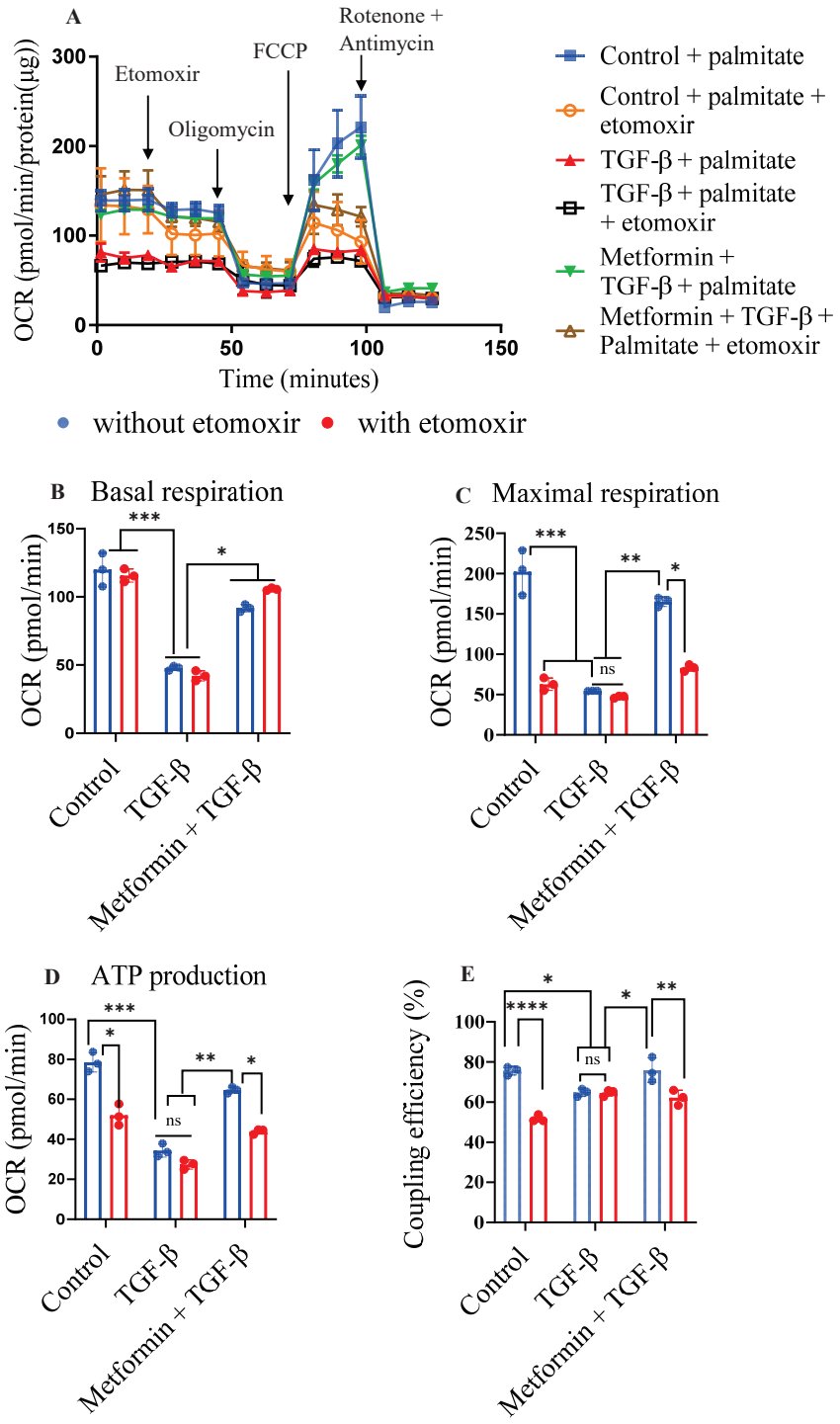


Figure 4. Metformin-mediated increase in mitochondrial oxygen consumption rate (OCR) is due to enhanced FAO in cardiac fibroblasts. (**A**) Adult mouse cardiac fibroblast cells were pretreated with or without metformin (2 mM) for 12 h followed by TGF-β (10 ng/mL) for 48 h and palmitate-BSA fatty acid oxidation substrate assay was performed to measure the mitochondrial OCR as described in methods. (**B**–**D**) Same as *A*, except that basal respiration (**B**), maximal respiration (**C**), ATP production (**D**) and coupling efficiency (**E**) were measured from the data obtained in *A*. GraphPad prism 10 was used to perform the statistics. The data shown in the graphs represent the mean ± SD of at least three different experiments. ns is non-significant, *, $p \leq 0.05$; **, $p \leq 0.005$; ***, $p \leq 0.0005$; ****, $p \leq 0.0001$ by two-way ANOVA followed by Tukey's multiple-comparison test.

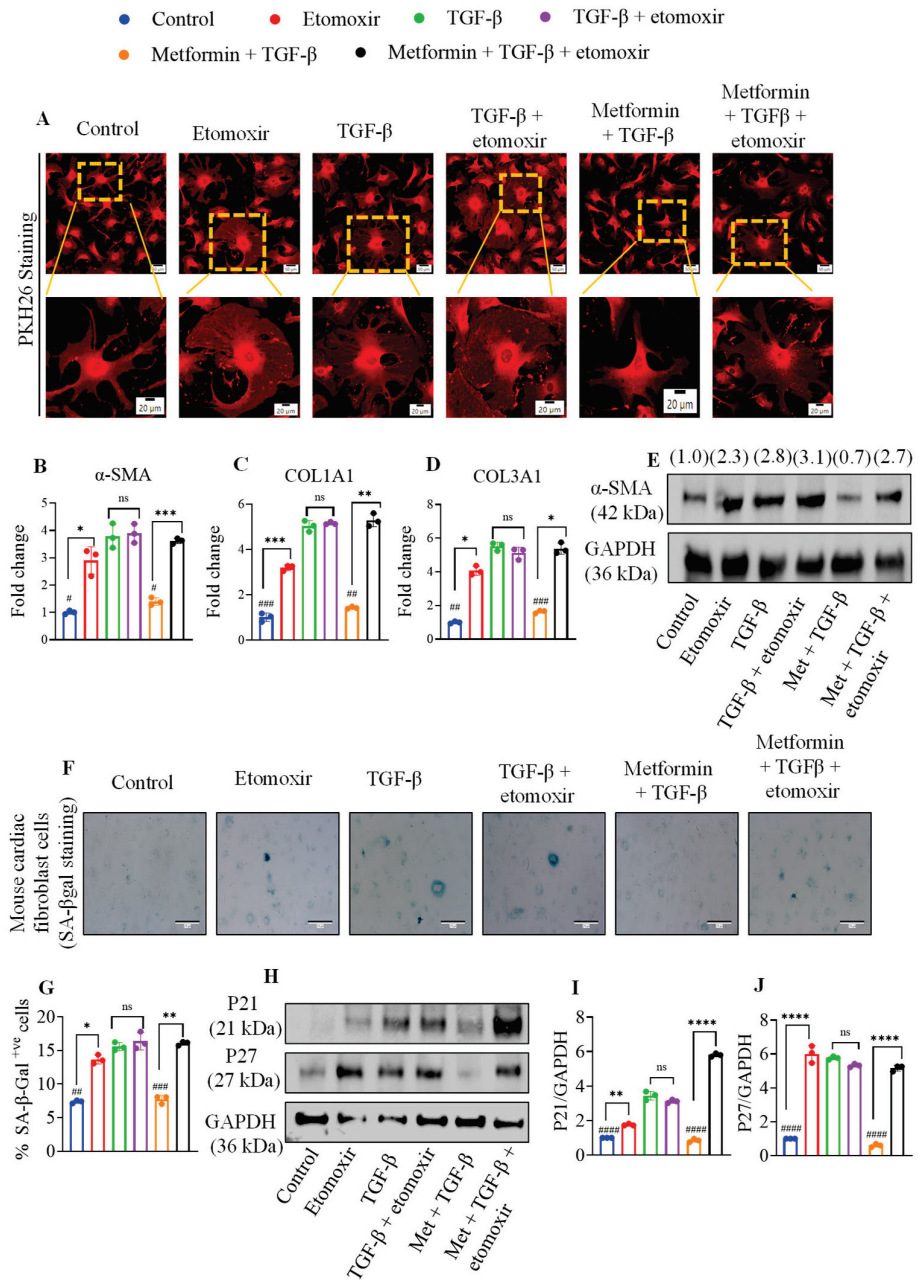


Figure 5. Metformin mitigates cardiac fibrosis markers and cellular senescence by promoting fatty acid β-oxidation. Adult mouse cardiac fibroblast cells were pretreated with metformin (2 mM) followed by treatment with TGF-β (10 ng/mL) in the presence or absence of etomoxir (40 μM) for 48 h. (**A**) Cells were labelled with PKH26 lipophilic dye and images were acquired using a laser scanning confocal microscope (scale bar = 50 μm). (**B**–**D**) Same as *A*, except that transcript levels of the indicated fibrosis markers were measured by RT-qPCR analysis. (**E**) Same as *A*, except that α-SMA protein levels were measured by immunoblotting. (**F**,**G**) Same as *A*, except that cellular senescence (**F**) was measured by SA-β-Gal staining (scale bar = 175 μm) and its quantification (**G**). (**H**) Same as *A*, except that senescence marker proteins like p21 and p27 were measured by immunoblot analysis. (**I**,**J**) Quantification of *H*. GraphPad Prism 10 was used for statistical analysis. Data are presented as mean ± SD from at least three independent experiments. ns is non-significant, *, $p \leq 0.05$; **, $p \leq 0.005$; ***, $p \leq 0.0005$; ****, $p \leq 0.0001$. #, $p \leq 0.05$; ##, $p \leq 0.005$; ###, $p \leq 0.0005$; ####, $p \leq 0.0001$ significantly different from TGF-β. Welch's ANOVA followed by Dunnett's T3 post hoc test for unequal variances and one-way ANOVA followed by Tukey's multiple-comparison test for equal variances, depending on variance homogeneity.

3.4. Metformin Administration Preserves Fatty Acid β-Oxidation Pathway in Aged Apoe$^{-/-}$ Mice Heart: Effect on Age-Associated Cardiac Fibrosis Markers

Cardiac fibrosis, in general, is associated with the progression of age. Aging and hypercholesterolemia are prominent and frequently overlapping contributors to cardiovascular dysfunction [18]. Studies in Apoe$^{-/-}$ mice have demonstrated that chronic hypercholesterolemia coupled with aging promotes adverse metabolic remodeling, leading to heightened inflammation, cardiac hypertrophy, fibrosis, diminished cardiomyogenesis, and increased cardiomyocyte apoptosis [19,20]. To this end, to see if metformin administration improves age-induced alterations in FAO, and in turn, cardiac fibrosis markers, we performed an in vivo experiment in 12-month-old Apoe$^{-/-}$ mice. Metformin (50 mg/kg body weight; a physiologically relevant dose) was administered daily via oral gavage for 12 weeks. In parallel, 6-month-old Apoe$^{-/-}$ mice were included as a young control group alongside age-matched untreated control group. It was observed that CPT1 transcript and protein levels were significantly decreased in 12-month-old mice cardiac tissue compared to 6-month-old mice (Figure 6A–C). CPT1 enzyme activity followed a similar trend (Figure 6D), supporting an age-dependent decline in FAO capacity. Moreover, consistent with our cell culture results, metformin-treated mice cardiac tissue exhibited significantly elevated CPT1 levels compared to aged-matched Apoe$^{-/-}$ control group (Figure 6A–D). In addition, metformin administration also enhanced the transcript levels of other FAO-related genes like *ACSL1*, *FABP3*, *ACADM*, and *ACADS* compared to aged-matched Apoe$^{-/-}$ control group (Figure 6E–H), and are, in part, comparable to 6-month-old mice group. These results were further supported by elevated acetyl-CoA and diminished malonyl-CoA levels in metformin-administered mice group compared to age-matched control mice group (Figure 6I,J). Nile Red staining also revealed a noticeable reduction in lipid content in metformin-treated mice cardiac tissue sections compared to age-matched control mice cardiac tissue (Figure 6K). Similar to the results observed in cardiac fibroblast cells, metformin administration significantly increased AMPK activation and ACC phosphorylation (inhibitory phosphorylation) in cardiac tissue homogenates (Figure 6L–N), thus suggesting that metformin, by enhancing the AMPK–ACC axis, potentiates FAO in aged Apoe$^{-/-}$ mice. To further determine if metformin influences the aging-associated cardiac profibrotic signaling, we measured TGF-β levels in heart tissue homogenates by ELISA. Metformin administration caused a significant reduction in aging-associated TGF-β levels (Figure 7A). These results were paralleled with a significant reduction in the profibrotic markers like α-SMA, COL1A1, and COL3A1 in metformin-administered mice heart tissues compared to age-matched control mice group (Figure 7B–F). The aforementioned profibrotic marker levels in metformin treated group are comparable to 6-month-old mice group (Figure 7B–F). Consistent with these findings, Masson's trichrome and Sirius Red/Fast Green staining demonstrated greater collagen deposition in the hearts of aged-Apoe$^{-/-}$ control mice compared with 6-month-old mice. Notably, metformin administration markedly attenuated collagen deposition (Figure 7G–J). These observations were further validated by hydroxyproline levels in the heart tissues (Figure 7K). Overall, these results indicate that metformin alleviates cardiac fibroblast activation in the heart tissue and improves age-associated cardiac fibrosis, in part, by preserving FAO.

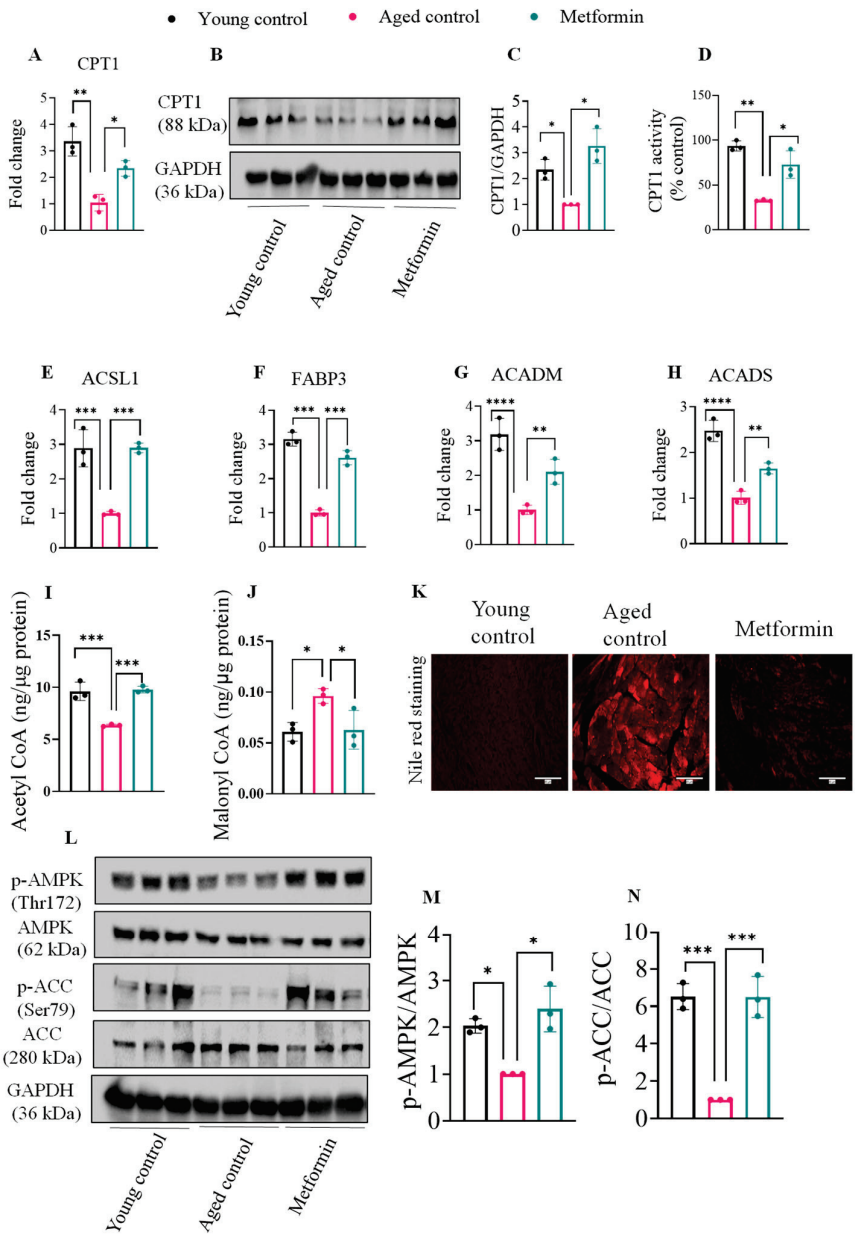


Figure 6. Metformin administration enhances CPT1 levels and fatty acid β-oxidation (FAO) pathway in the hearts of aged Apoe$^{-/-}$ mice. (**A**–**D**) *CPT1* Transcript (**A**), protein (**B**,**C**), and enzyme activity (**D**) were measured in Apoe$^{-/-}$ mice heart (n = 3 per group). (**E**–**H**) Transcript levels of *FABP3*, *ACSL1*, *ACADM*, and *ACADS* were measured in Apoe$^{-/-}$ mice heart tissue by RT-qPCR analysis (n = 3 per group). (**I**,**J**) Acetyl-CoA (**I**) and Malonyl-CoA (**J**) levels were measured in Apoe$^{-/-}$ mice heart tissue (n = 3 per group). (**K**) Lipid content was measured by Nile Red staining in Apoe$^{-/-}$ mice heart sections and images were taken in a fluorescence microscope equipped with a rhodamine filter (n = 3 per group; scale bar = 85 µm). (**L**) Indicated protein levels were measured in Apoe$^{-/-}$ mice heart tissue homogenates (n = 3 per group) by immunoblot analysis. (**M**,**N**) Quantification of *L*. GraphPad Prism 10 was used for statistical analysis. Data are presented as mean ± SD from at least three independent experiments. *, $p \leq 0.05$; **, $p \leq 0.005$; ***, $p \leq 0.0005$; ****, $p \leq 0.0001$. Welch's ANOVA followed by Dunnett's T3 post hoc test for unequal variances and one-way ANOVA followed by Tukey's multiple-comparison test for equal variances, depending on variance homogeneity.

https://doi.org/10.3390/cells15151408

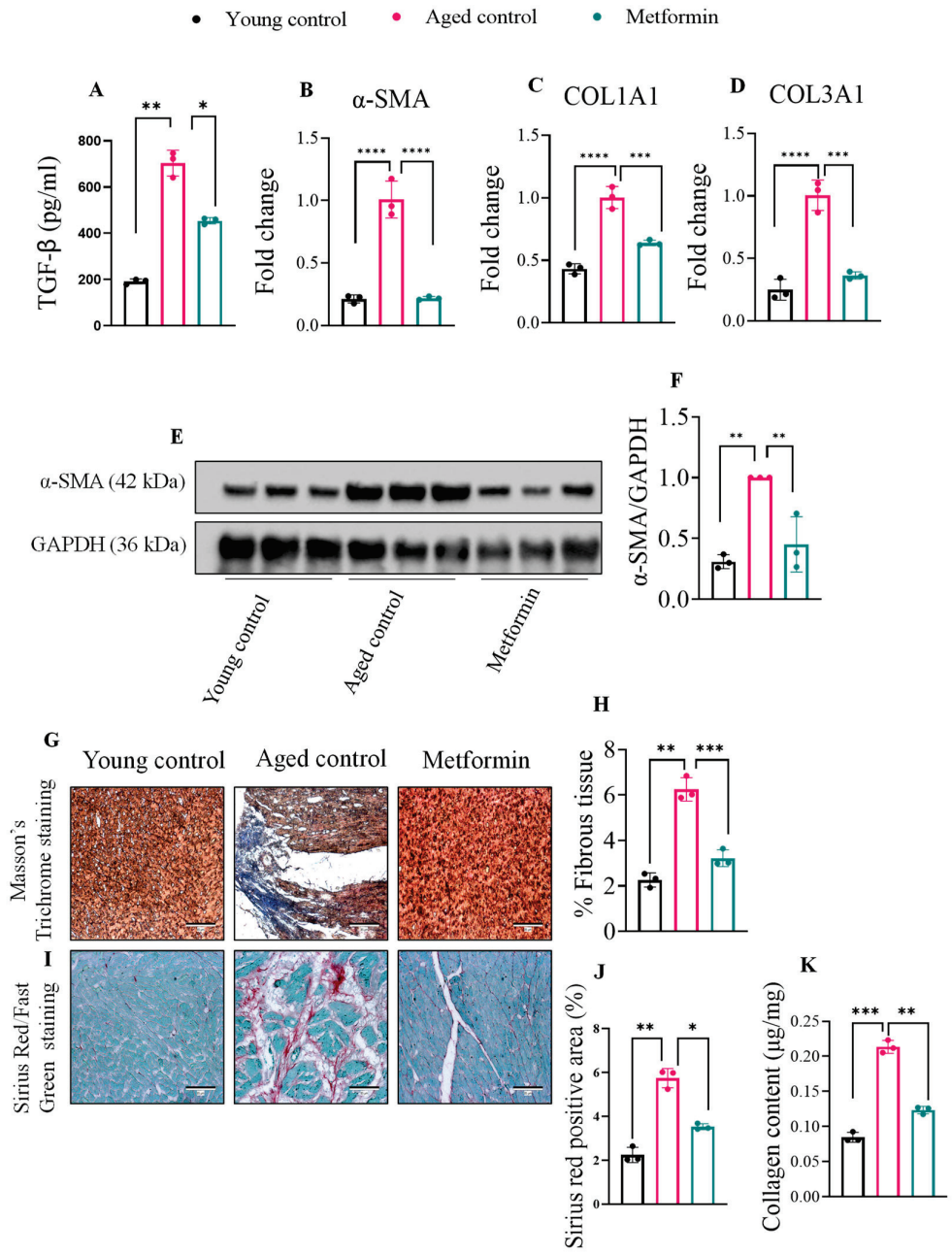


Figure 7. Metformin administration attenuates cardiac fibrosis markers in Apoe$^{-/-}$ mice. (**A**) TGF-β levels were measured in Apoe$^{-/-}$ mice heart tissue homogenates by ELISA (n = 3 per group). (**B**–**D**) Transcript levels of the indicated fibrosis markers were measured in Apoe$^{-/-}$ mice heart tissue by RT-qPCR analysis (n = 3 per group). (**E**) α-SMA protein levels were measured in Apoe$^{-/-}$ mice heart tissue homogenates by immunoblotting (n = 3 per group). (**F**) Quantification of *E*. (**G**) Masson's trichome staining for collagen accumulation in the heart sections (n = 3 per group; scale bar = 85 µm). (**H**) Quantification of *G*. (**I**) Sirius Red/Fast Green staining for collagen accumulation in the heart sections (n = 3 per group; scale bar = 85 µm). (**J**) Quantification of *I*. (**K**) Total collagen content in heart tissues by hydroxyproline assay (n = 3 per group). GraphPad Prism 10 was used for statistical analysis. Data are presented as mean ± SD from at least three independent experiments. *, $p \leq 0.05$; **, $p \leq 0.005$; ***, $p \leq 0.0005$; ****, $p \leq 0.0001$. Welch's ANOVA followed by Dunnett's T3 post hoc test for unequal variances and one-way ANOVA followed by Tukey's multiple-comparison test for equal variances, depending on variance homogeneity.

https://doi.org/10.3390/cells15151408

4. Discussion

Cardiac fibrosis is a hallmark of cardiovascular aging and represents a major determinant of myocardial stiffness, ventricular dysfunction, and heart failure. Although accumulating evidence implicates metabolic dysfunction as a key driver of age-associated cardiac remodeling, the metabolic mechanisms governing cardiac fibroblast activation remain incompletely understood. In the present study, we demonstrate that metformin suppresses TGF-β-induced cardiac fibroblast activation and senescence by restoring CPT1-dependent fatty acid β-oxidation (FAO) through activation of the AMPK–ACC signaling axis. Furthermore, metformin preserved FAO and attenuated fibrosis-associated markers in aged Apoe$^{-/-}$ mice, identifying FAO as a critical regulator of fibroblast fate and cardiac fibrotic remodeling during aging.

Fibroblast activation is increasingly recognized as a metabolically demanding process requiring extensive cellular reprogramming. Recent advances have highlighted that fibroblast activation is accompanied by dynamic metabolic adaptations, including changes in mitochondrial function, substrate utilization, and lipid metabolism, suggesting that metabolic state is not merely a consequence of fibrosis, but an active regulator of fibroblast phenotype [21,22]. Consistent with these reports, TGF-β-treated cardiac fibroblasts in our study exhibited reduced CPT1 expression and activity, diminished expression of FAO-related genes, and impaired mitochondrial respiration. Metformin effectively reversed these changes, restoring CPT1 activity, enhancing expression of *ACSL1*, *FABP3*, *ACADM*, and *ACADS*, and improving mitochondrial bioenergetics. Furthermore, in addition to enhancing FAO, metformin suppressed the TGF-β-induced expression of glycolytic markers, including *HIF-1α*, *GLUT1*, and *LDHA*, suggesting that metformin favors a metabolic profile associated with increased FAO and reduced glycolysis during cardiac fibroblast differentiation. These findings suggest that maintenance of FAO is essential for preserving fibroblast metabolic homeostasis and preventing pathological activation.

Several studies have demonstrated that metformin exerts anti-fibrotic effects in the heart, kidney, liver, and lung, primarily through activation of AMPK and inhibition of profibrotic pathways such as TGF-β/Smad signaling, NF-κB activation, and oxidative stress responses [23–26]. In experimental models of cardiac fibrosis, metformin attenuates myofibroblast differentiation and extracellular matrix deposition through AMPK-dependent suppression of TGF-β signaling [25]. In tune with this, in the current study, we observed that metformin suppresses TGF-β levels predominantly through activation of the AMPK signaling pathway in cardiac fibroblast cells. Additionally, in an independent lab finding, we observed that metformin attenuated TGF-β-induced cardiac fibroblast proliferation, suggesting that its anti-fibrotic actions extend beyond inhibition of myofibroblast differentiation. Studies in renal and pulmonary fibrosis have demonstrated that activation of AMPK by metformin limits fibroblast activation and tissue remodeling [23,26]. These findings are consistent with previous reports describing the cardiovascular beneficial effects of metformin through AMPK-dependent mechanisms, including attenuation of pathological remodeling and improvement of cardiovascular outcomes [27]. However, the downstream metabolic mechanisms responsible for these beneficial effects have remained largely unresolved. Our findings extend these observations by identifying FAO as a key metabolic effector downstream of AMPK. Specifically, metformin increased AMPK phosphorylation and inhibitory phosphorylation of ACC, resulting in reduced malonyl-CoA levels, enhanced CPT1 activity, and increased fatty acid utilization. Thus, beyond its established effects on profibrotic signaling pathways, metformin appears to reprogram fibroblast metabolism toward a more oxidative phenotype that is resistant to activation and senescence.

CPT1 is the rate-limiting enzyme responsible for mitochondrial transport of long-chain fatty acids, and plays a central role in maintaining cardiac metabolic flexibility.

https://doi.org/10.3390/cells15151408

Aging-associated declines in CPT1 activity and FAO have been linked to mitochondrial dysfunction, lipid accumulation, and impaired cardiac energetics [28,29]. In agreement with these observations, aged Apoe$^{-/-}$ mice exhibited reduced CPT1 expression and activity together with increased fibrotic remodeling. Notably, metformin restored CPT1 activity, reduced intracellular lipid accumulation, and increased acetyl-CoA levels both in vitro and in vivo. Importantly, pharmacological inhibition of CPT1 with etomoxir largely abolished the beneficial effects of metformin on mitochondrial respiration, ATP production, fibroblast activation, and senescence. These findings provide direct functional evidence that enhanced FAO is required for metformin-mediated cardioprotection.

Another important finding of the present study is the close relationship between FAO and cellular senescence. Senescent cardiac fibroblasts contribute to age-related fibrosis through the senescence-associated secretory phenotype, which promotes chronic inflammation and extracellular matrix deposition [30,31]. Accumulating evidence suggests that therapeutic targeting or elimination of senescent fibroblast populations can attenuate age-associated tissue fibrosis, supporting cellular senescence as an attractive therapeutic target in chronic fibrotic disorders [32,33]. In the present study, metformin significantly attenuated TGF-β-induced SA-β-Gal^{+ve} fibroblast cells and reduced p21 and p27 levels, whereas inhibition of CPT1 reversed these effects. These observations suggest that impaired FAO may act as a metabolic trigger linking mitochondrial dysfunction to fibroblast senescence and fibrotic remodeling. Interestingly, these findings are consistent with our previous studies demonstrating that metformin delays endothelial senescence through AMPK-dependent mechanisms involving mitochondrial biogenesis, H3K79 trimethylation, and enhanced FAO [11,13]. Together, these studies support the concept that restoration of mitochondrial metabolism is a common mechanism underlying the geroprotective actions of metformin across multiple cardiovascular cell types.

The physiological relevance of these observations was further validated in aged Apoe$^{-/-}$ mice, a model characterized by hypercholesterolemia, metabolic dysfunction, and accelerated cardiovascular aging [20,34]. Metformin restored FAO-related gene expression, enhanced CPT1 activity, activated AMPK signaling, and significantly reduced cardiac fibrosis markers. These findings indicate that preservation of FAO contributes substantially to the anti-fibrotic effects of metformin during aging-associated cardiac remodeling. While these results are interesting, one of the limitations of the present study is the use of aged Apoe$^{-/-}$ mice, which exhibit dyslipidemia and enhanced atherosclerotic susceptibility and therefore do not completely model physiological aging. Moreover, few studies have employed additional pro-fibrotic stimuli, such as high-fat diet feeding or angiotensin II infusion, to induce more pronounced cardiac fibrosis in Apoe$^{-/-}$ mice [35,36]. Although this model is relevant to aging-associated cardiovascular disease [20], the contribution of ApoE deficiency and associated metabolic and vascular abnormalities to cardiac fibrosis cannot be fully excluded. Accordingly, the present findings should be interpreted in the context of aging-associated cardiac fibrosis under atherosclerosis-prone conditions. Future studies using naturally aged wild-type mice will be important to determine whether metformin exerts comparable anti-fibrotic effects during normal aging. Another limitation of this study is the relatively small number of biological samples used for individual in vivo analyses. Nevertheless, the consistency of findings across complementary histological, molecular, and biochemical approaches supports the overall conclusions. Additionally, in this study, we have not assessed the in vivo cardiac functional parameters. Although metformin reduced myocardial collagen accumulation and the expression of pro-fibrotic markers, these findings do not directly establish an improvement in cardiac performance. Future studies incorporating comprehensive cardiac functional assessment will be neces-

sary to determine whether the structural anti-fibrotic effects of metformin translate into improved systolic and/or diastolic function in aged Apoe$^{-/-}$ mice.

5. Conclusions

The present study identifies CPT1-dependent FAO as a previously underappreciated metabolic regulator of cardiac fibroblast activation and senescence. Our findings establish the AMPK–ACC–CPT1 pathway as a critical mechanistic link between metformin treatment and suppression of cardiac fibrosis. By restoring mitochondrial fatty acid metabolism and cellular bioenergetics, metformin limits fibroblast activation and age-associated fibrotic remodeling. These results not only provide new mechanistic insight into the cardioprotective actions of metformin, but also highlight targeting FAO as a promising therapeutic strategy for combating age-related cardiac fibrosis.

Author Contributions: Conceptualization, H.C. and S.K. (Srigiridhar Kotamraju); methodology, H.C., S.K. (Sunita Kumari), S.R.B., and S.K. (Srigiridhar Kotamraju); software, H.C., S.K. (Sunita Kumari), S.R.B., and S.K. (Srigiridhar Kotamraju); validation, H.C., S.K. (Sunita Kumari), S.R.B., and S.K. (Srigiridhar Kotamraju); formal analysis, H.C. and S.K. (Srigiridhar Kotamraju); investigation, H.C. and S.K. (Sunita Kumari); resources, S.K. (Srigiridhar Kotamraju); data curation, H.C. and S.K. (Sunita Kumari); writing—original draft preparation, H.C. and S.K. (Sunita Kumari); writing—review and editing, S.R.B. and S.K. (Srigiridhar Kotamraju); visualization, H.C.; supervision, S.K. (Srigiridhar Kotamraju); project administration, S.K. (Srigiridhar Kotamraju); funding acquisition, S.K. (Srigiridhar Kotamraju). All authors have read and agreed to the published version of the manuscript.

Funding: This work was supported by a grant from the Council of Scientific and Industrial Research (OLP-015), India.

Institutional Review Board Statement: The mice study performed in this work was reviewed and approved by the institutional animal ethical committee (IAEC/IICT/024/2022 and IAEC/IICT/040/2023) according to the guidelines formulated for care and use of animals in scientific research (ICMR, India) at a CPCSEA (Committee for the Purpose of Control and Supervision of Experiments on Animals) registered animal facility.

Informed Consent Statement: Not Applicable.

Data Availability Statement: The data that support the findings of this study are available from the corresponding author upon reasonable request.

Acknowledgments: Chempon H, Kumri S acknowledge CSIR, New Delhi, India, for the award of research fellowships. Sriravali Pulipaka and Muralidharan K for providing animals and animal experimentation. We thank the Department of Knowledge and Information Management, CSIR-IICT, Hyderabad, India, for performing the plagiarism check of this manuscript (IICT/Pubs./2026/201). The graphical abstract was created using Biorender.com under the paid version.

Conflicts of Interest: The authors declare no conflicts of interest.

Abbreviations

The following abbreviations are used in this manuscript:

FAO	Fatty acid β-oxidation
TGF-β	Transforming growth factor-β
CPT1	Carnitine palmitoyltransferase-1
OCR	Mitochondrial oxygen consumption rate
AMPK	AMP-activated protein kinase
ACC	Acetyl-CoA carboxylase
FABP3	Fatty Acid-Binding Protein 3
ACSL1	Acyl-CoA Synthetase Long Chain Family Member 1
ACADM	Medium-Chain Acyl-CoA Dehydrogenase

ACADS	Short-chain acyl-CoA dehydrogenase
α-SMA	Alpha-Smooth Muscle Actin
COL1A1	Collagen Type I Alpha 1 Chain
COL3A1	Collagen Type III Alpha 1 Chain

References

1. Zheng, P.; Yan, W.; Ding, Y.; Zhang, Y.; Chen, Z.; Qian, J.; Ge, J. Cardiovascular ageing: Hallmarks, signaling pathways, diseases and therapeutic targets. *Signal Transduct. Target. Ther.* **2026**, *11*, 142. [CrossRef] [PubMed]
2. Biernacka, A.; Dobaczewski, M.; Frangogiannis, N.G. TGF-β signaling in fibrosis. *Growth Factors* **2011**, *29*, 196–202. [CrossRef] [PubMed]
3. Gibb, A.A.; Lazaropoulos, M.P.; Elrod, J.W. Myofibroblasts and Fibrosis: Mitochondrial and Metabolic Control of Cellular Differentiation. *Circ. Res.* **2020**, *127*, 427–447. [CrossRef] [PubMed]
4. Baechle, J.J.; Chen, N.; Makhijani, P.; Winer, S.; Furman, D.; Winer, D.A. Chronic inflammation and the hallmarks of aging. *Mol. Metab.* **2023**, *74*, 101755. [CrossRef] [PubMed]
5. Sithara, T.; Drosatos, K. Metabolic Complications in Cardiac Aging. *Front. Physiol.* **2021**, *12*, 669497. [CrossRef] [PubMed]
6. Xie, S.; Xu, S.C.; Deng, W.; Tang, Q. Metabolic landscape in cardiac aging: Insights into molecular biology and therapeutic implications. *Signal Transduct. Target. Ther.* **2023**, *8*, 114. [CrossRef] [PubMed]
7. McCann, M.R.; George De la Rosa, M.V.; Rosania, G.R.; Stringer, K.A. L-Carnitine and Acylcarnitines: Mitochondrial Biomarkers for Precision Medicine. *Metabolites* **2021**, *11*, 51. [CrossRef] [PubMed]
8. Bang, S.; Choi, S.H.; Jeong, S.M. Beyond Bioenergetics: Emerging Roles of Mitochondrial Fatty Acid Oxidation in Stress Response and Aging. *Cells* **2025**, *14*, 1956. [CrossRef] [PubMed]
9. Bois, A.; Grandela, C.; Gallant, J.; Mummery, C.; Menasché, P. Revitalizing the heart: Strategies and tools for cardiomyocyte regeneration post-myocardial infarction. *npj Regen. Med.* **2025**, *10*, 6. [CrossRef] [PubMed]
10. Burkewitz, K.; Zhang, Y.; Mair, W.B. AMPK at the nexus of energetics and aging. *Cell Metab.* **2014**, *20*, 10–25. [CrossRef] [PubMed]
11. Karnewar, S.; Neeli, P.K.; Panuganti, D.; Kotagiri, S.; Mallappa, S.; Jain, N.; Jerald, M.K.; Kotamraju, S. Metformin regulates mitochondrial biogenesis and senescence through AMPK mediated H3K79 methylation: Relevance in age-associated vascular dysfunction. *Biochim. Biophys. Acta Mol. Basis Dis.* **2018**, *1864*, 1115–1128. [CrossRef] [PubMed]
12. Pulipaka, S.; Singuru, G.; Sahoo, S.; Shaikh, A.; Thennati, R.; Kotamraju, S. Therapeutic efficacies of mitochondria-targeted esculetin and metformin in the improvement of age-associated atherosclerosis via regulating AMPK activation. *Geroscience* **2024**, *46*, 2391–2408. [PubMed]
13. Pulipaka, S.; Chempon, H.; Singuru, G.; Sahoo, S.; Shaikh, A.; Kumari, S.; Thennati, R.; Kotamraju, S. Mitochondria-targeted esculetin and metformin delay endothelial senescence by promoting fatty acid β-oxidation: Relevance in age-associated atherosclerosis. *Mech. Ageing Dev.* **2024**, *219*, 111931. [CrossRef] [PubMed]
14. Malaekeh-Nikouei, A.; Shokri-Naei, S.; Karbasforoushan, S.; Bahari, H.; Baradaran Rahimi, V.; Heidari, R.; Askari, V.R. Metformin beyond an anti-diabetic agent: A comprehensive and mechanistic review on its effects against natural and chemical toxins. *Biomed. Pharmacother.* **2023**, *165*, 115263. [CrossRef] [PubMed]
15. Kumari, S.; Sahoo, S.; Pulipaka, S.; Thomas, A.; Kuncha, M.; Kotamraju, S. Palmitic acid fuels triple-negative breast cancer through metadherin-dependent fatty acid β-oxidation: Relevance to high fat diet-induced breast cancer progression. *Cell. Signal.* **2026**, *139*, 112320. [CrossRef] [PubMed]
16. Talari, N.K.; Mattam, U.; Meher, N.K.; Paripati, A.K.; Mahadev, K.; Krishnamoorthy, T.; Sepuri, N.B.V. Lipid-droplet associated mitochondria promote fatty-acid oxidation through a distinct bioenergetic pattern in male Wistar rats. *Nat. Commun.* **2023**, *14*, 766. [CrossRef] [PubMed]
17. Tian, G.; Zhou, J.; Quan, Y.; Kong, Q.; Li, J.; Xin, Y.; Wu, W.; Tang, X.; Liu, X. Voltage-dependent anion channel 1 (VDAC1) overexpression alleviates cardiac fibroblast activation in cardiac fibrosis via regulating fatty acid metabolism. *Redox Biol.* **2023**, *67*, 102907. [CrossRef] [PubMed]
18. Liu, H.H.; Li, J.J. Aging and dyslipidemia: A review of potential mechanisms. *Ageing Res. Rev.* **2015**, *19*, 43–52. [CrossRef] [PubMed]
19. Hastings, M.H.; Zhou, Q.; Wu, C.; Shabani, P.; Huang, S.; Yu, X.; Singh, A.P.; Guseh, J.S.; Li, H.; Lerchenmüller, C.; et al. Cardiac ageing: From hallmarks to therapeutic opportunities. *Cardiovasc. Res.* **2025**, *121*, 1474–1488. [CrossRef] [PubMed]
20. Vasquez, E.C.; Peotta, V.A.; Gava, A.L.; Pereira, T.M.; Meyrelles, S.S. Cardiac and vascular phenotypes in the apolipoprotein E-deficient mouse. *J. Biomed. Sci.* **2012**, *19*, 22. [CrossRef] [PubMed]
21. Zhao, X.; Psarianos, P.; Ghoraie, L.S.; Yip, K.; Goldstein, D.; Gilbert, R.; Witterick, I.; Pang, H.; Hussain, A.; Lee, J.H.; et al. Metabolic regulation of dermal fibroblasts contributes to skin extracellular matrix homeostasis and fibrosis. *Nat. Metab.* **2019**, *1*, 147–157. [CrossRef] [PubMed]

22. Frangogiannis, N.G. Cardiac fibrosis: Cell biological mechanisms, molecular pathways and therapeutic opportunities. *Mol. Asp. Med.* **2019**, *65*, 70–99. [CrossRef] [PubMed]
23. Sato, N.; Takasaka, N.; Yoshida, M.; Tsubouchi, K.; Minagawa, S.; Araya, J.; Saito, N.; Fujita, Y.; Kurita, Y.; Kobayashi, K.; et al. Metformin attenuates lung fibrosis development via NOX4 suppression. *Respir. Res.* **2016**, *17*, 107. [CrossRef] [PubMed]
24. Wu, M.; Xu, H.; Liu, J.; Tan, X.; Wan, S.; Guo, M.; Long, Y.; Xu, Y. Metformin and Fibrosis: A Review of Existing Evidence and Mechanisms. *J. Diabetes Res.* **2021**, *2021*, 6673525. [CrossRef] [PubMed]
25. Xiao, H.; Ma, X.; Feng, W.; Fu, Y.; Lu, Z.; Xu, M.; Shen, Q.; Zhu, Y.; Zhang, Y. Metformin attenuates cardiac fibrosis by inhibiting the TGFbeta1-Smad3 signalling pathway. *Cardiovasc. Res.* **2010**, *87*, 504–513. [CrossRef] [PubMed]
26. Yi, H.; Huang, C.; Shi, Y.; Cao, Q.; Chen, J.; Chen, X.M.; Pollock, C.A. Metformin Attenuates Renal Fibrosis in a Mouse Model of Adenine-Induced Renal Injury Through Inhibiting TGF-β1 Signaling Pathways. *Front. Cell Dev. Biol.* **2021**, *9*, 603802. [CrossRef] [PubMed]
27. Bu, Y.; Peng, M.; Tang, X.; Xu, X.; Wu, Y.; Chen, A.F.; Yang, X. Protective effects of metformin in various cardiovascular diseases: Clinical evidence and AMPK-dependent mechanisms. *J. Cell. Mol. Med.* **2022**, *26*, 4886–4903. [CrossRef] [PubMed]
28. Lesnefsky, E.J.; Chen, Q.; Hoppel, C.L. Mitochondrial Metabolism in Aging Heart. *Circ. Res.* **2016**, *118*, 1593–1611. [CrossRef] [PubMed]
29. Tocchi, A.; Quarles, E.K.; Basisty, N.; Gitari, L.; Rabinovitch, P.S. Mitochondrial dysfunction in cardiac aging. *Biochim. Biophys. Acta* **2015**, *1847*, 1424–1433. [CrossRef] [PubMed]
30. Osorio, J.M.; Espinoza-Pérez, C.; Rimassa-Taré, C.; Machuca, V.; Bustos, J.O.; Vallejos, M.; Vargas, H.; Díaz-Araya, G. Senescent cardiac fibroblasts: A key role in cardiac fibrosis. *Biochim. Biophys. Acta Mol. Basis Dis.* **2023**, *1869*, 166642. [CrossRef] [PubMed]
31. Vijayakumar, A.; Wang, M.; Kailasam, S. The Senescent Heart—"Age Doth Wither Its Infinite Variety". *Int. J. Mol. Sci.* **2024**, *25*, 3581. [CrossRef] [PubMed]
32. Childs, B.G.; Durik, M.; Baker, D.J.; van Deursen, J.M. Cellular senescence in aging and age-related disease: From mechanisms to therapy. *Nat. Med.* **2015**, *21*, 1424–1435. [CrossRef] [PubMed]
33. González-Gualda, E.; Baker, A.G.; Fruk, L.; Muñoz-Espín, D. A guide to assessing cellular senescence in vitro and in vivo. *FEBS J.* **2021**, *288*, 56–80. [CrossRef] [PubMed]
34. Wang, Y.X. Cardiovascular functional phenotypes and pharmacological responses in apolipoprotein E deficient mice. *Neurobiol. Aging* **2005**, *26*, 309–316. [CrossRef] [PubMed]
35. Ma, K.L.; Liu, J.; Ni, J.; Zhang, Y.; Lv, L.L.; Tang, R.N.; Ni, H.F.; Ruan, X.Z.; Liu, B.C. Inflammatory stress exacerbates the progression of cardiac fibrosis in high-fat-fed apolipoprotein E knockout mice via endothelial-mesenchymal transition. *Int. J. Med. Sci.* **2013**, *10*, 420–426. [CrossRef] [PubMed]
36. Zack, M.; Boyanovsky, B.B.; Shridas, P.; Bailey, W.; Forrest, K.; Howatt, D.A.; Gelb, M.H.; de Beer, F.C.; Daugherty, A.; Webb, N.R. Group X secretory phospholipase A(2) augments angiotensin II-induced inflammatory responses and abdominal aortic aneurysm formation in apoE-deficient mice. *Atherosclerosis* **2011**, *214*, 58–64. [CrossRef] [PubMed]

Disclaimer/Publisher's Note: The statements, opinions and data contained in all publications are solely those of the individual author(s) and contributor(s) and not of MDPI and/or the editor(s). MDPI and/or the editor(s) disclaim responsibility for any injury to people or property resulting from any ideas, methods, instructions or products referred to in the content.

cells

MDPI

Article

JAK and MEK Pathway Regulation of Mitochondrial Activity as Possible Targets for Saphenous Vein Smooth Muscle Cell Dysfunction in Diabetes

Israel O. Bolanle [1,2,*], Florah T. Moshapa [3,4], Gillian A. Durham [1,5], James P. Hobkirk [6,7], Kirsten Riches-Suman [8], Mahmoud Loubani [9], Roger G. Sturmey [1] and Timothy M. Palmer [1,*]

1 Biomedical Institute for Multimorbidity, Centre for Biomedicine, Hull York Medical School, University of Hull, Hull HU6 7RX, UK; g.durham@imperial.ac.uk (G.A.D.)
2 Department of Bioengineering, Imperial College London, London SW7 2AZ, UK
3 School of Pharmacy and Medical Sciences, Faculty of Life Sciences, University of Bradford, Bradford BD7 1DP, UK; moshapaf@ub.ac.bw
4 School of Pharmacy, Faculty of Health Sciences, University of Botswana, Gaborone P/Bag-0022, Botswana
5 Pears Cumbria School of Medicine, University of Cumbria, Carlisle CA1 2HH, UK
6 School of Sport Exercise and Rehabilitation Sciences, University of Hull, Hull HU6 7RX, UK; james.hobkirk3@nhs.net
7 School of Cardiovascular & Metabolic Health, British Heart Foundation Glasgow Cardiovascular Research Centre, University of Glasgow, Glasgow G12 8TA, UK
8 School of Chemistry and Biosciences, Faculty of Life Sciences, University of Bradford, Bradford BD7 1DP, UK; k.riches@bradford.ac.uk
9 Department of Cardiothoracic Surgery, Castle Hill Hospital, Cottingham HU16 5JQ, UK; mahmoud.loubani@nhs.net
* Correspondence: olapeju.bolanle@hyms.ac.uk (I.O.B.); tim.palmer@hyms.ac.uk (T.M.P.)

Highlights

What are the main findings?

- We have identified JAK and MEK pathways as targets to regulate specific aspects of mitochondrial function in human saphenous vein smooth muscle cells (HSVSMCs).
- We have also shown how these pathways are impaired in HSVSMCs from type 2 diabetic patients (T2DM), a condition linked to poorer outcomes following coronary artery bypass graft surgery.

What is the implication of the main finding?

- These pathways represent potential targets for regulation of HSVSMC function that can be explored for drug development to limit saphenous vein graft failure in T2DM.

Abstract

While glucose-driven mitochondrial dysfunction has been proposed to promote vascular dysfunction responsible for saphenous vein graft failure (VGF) following bypass surgery, the impact of type 2 diabetes mellitus (T2DM) on mitochondrial function in human saphenous vein smooth muscle cells (HSVSMCs) responsible for maladaptive remodelling is unknown. Our aim was to identify signalling pathways that mediate any mitochondrial dysfunction in HSVSMCs in vitro and assess the impact of T2DM. HSVSMCs explanted from surplus HSV tissues from consenting T2DM and non-diabetic patients undergoing coronary artery bypass graft surgery were treated with known activators and inhibitors of the JAK/STAT and MAPK/ERK pathways. Following this, real-time oxygen consumption rate (OCR) and extracellular acidification rate (ECAR) measures of mitochondrial function were then determined. Our findings revealed that both IL-6/sIL-6Rα trans-signalling complexes and platelet-derived growth factor-BB (PDGF-BB) significantly increased OCR

in HSVSMCs from T2DM patients but not non-diabetic controls. Meanwhile, only PDGF-BB increased ECAR in HSVSMCs from T2DM patients but not in non-diabetic controls. The observed increases in OCR and ECAR were abolished by JAK1/2-selective inhibitor ruxolitinib. Furthermore, thrombin caused a significant increase in OCR, specifically in HSVSMCs from T2DM patients, and this effect was abolished by the MEK1/2-selective inhibitor trametinib. Both ruxolitinib and trametinib significantly reduced basal OCR and ECAR in HSVSMCs from both T2DM and non-diabetic patients. Together, these findings demonstrate a JAK/STAT- and MAPK/ERK-mediated regulation of mitochondrial function in HSVSMCs. As such, they represent potential targets for regulation of HSVSMC function that can be explored for drug development to limit saphenous VGF in T2DM.

Keywords: type 2 diabetes mellitus; oxygen consumption rate; extracellular acidification rate; JAK/STAT; MAPK/ERK1,2

1. Introduction

Glucose-dependent alterations in cellular function have been suggested to promote proliferation and migration of vascular smooth muscle cells (VSMCs), which are linked to vein graft failure (VGF) [1–3]. VSMCs from type 2 diabetes mellitus (T2DM) patients have distinct functional properties [4,5], including significantly greater migratory activity than those from non-diabetic controls [5,6]. Additionally, T2DM is known to trigger changes in mitochondrial function [7], and together, these findings hint at a link between T2DM, mitochondrial dysfunction, and VGF. Metabolic reprogramming, adaptive oxygen consumption, and glucose utilisation are now appreciated as key mechanisms by which cells such as arterial endothelial and malignant cancer cells sustain high proliferative rates even in hostile environments in which the supplies of oxygen and essential nutrients are limited [8–10]. However, the impact of T2DM and possible downstream signalling pathways that regulate these processes in human saphenous vein smooth muscle cells (HSVSMCs), a crucial cell type implicated in the vascular dysfunction responsible for saphenous VGF, remains unclear [2,3].

Mitochondrial oxygen consumption rate (OCR) and extracellular acidification rate (ECAR) have been described as gold standard measures for the determination of mitochondrial function in vascular endothelial cells (ECs), VSMCs, and platelets [11–13]. Since oxidative phosphorylation measured by OCR accounts for most of the increase in cellular ATP demand, the activity of this pathway is a major indicator of metabolic function [14,15]. Measurement of OCR in the presence of certain inhibitors can offer valuable information on mitochondrial bioenergetic profiles. The components of oxygen consumption that are linked to ATP production can be determined by inhibitors that target the various complexes in the electron transport chain [15]. These components include the so-called coupled OCR, as well as the contribution made to OCR by passive or active proton leakage across the inner mitochondrial membrane, the difference between maximal oxygen consumption and basal (spare capacity), and non-mitochondrial oxygen consumption. Together, these tests offer a detailed picture of mitochondrial function [16].

In contrast, ECAR provides a measure of the lactic acid produced by cells whilst in culture. This is typically excreted by cells when lactate dehydrogenase converts pyruvate to lactate to replenish NAD+, which is necessary to sustain glycolysis [17,18]. The flow through catabolic pathways necessary to produce ATP is, therefore, connected to a cell's ECAR. The ECAR is also linked to ATP turnover, as the rates of ATP synthesis and consumption are equivalent in steady state [19]. Even though it is technically difficult to quantify

https://doi.org/10.3390/cells15151402

ATP turnover, however, it may be demonstrated that fluctuations in extracellular fluxes are correlated with changes in ATP turnover rates [19]. For these reasons, mitochondrial OCR and ECAR are now appreciated as key parameters in assessing altered metabolic homeostasis in pathological conditions [11].

JAK/STAT and ERK 1/2 signalling pathways are important in numerous human physiological processes [20,21]. Importantly, activating these pathways with interleukin-6 (IL-6), platelet-derived growth factor-BB (PDGF-BB), Angiotensin II (Ang II) or thrombin can promote either vascular cell migration or proliferation events which are responsible for vascular remodelling [22–25]. However, their involvement in the modulation of mitochondrial function of vascular cells is poorly understood. Of importance is the fact that in patients with coronary artery disease (CAD) with or without T2DM, coronary artery bypass graft (CABG) using the autologous saphenous vein remains a major procedure for restoration of blood supply to the heart [26,27]. Patients with T2DM who have CAD, however, are more susceptible to neointimal hyperplasia (NIH), vascular remodelling, and stenosis that result in VGF [28]. While the underlying mechanisms responsible for this are unclear, activities of the activators of the JAK/STAT and MAPK/ERK signalling pathways are upregulated in T2DM patients [21]. To prevent VGF, it may therefore be possible to identify novel therapeutic targets by identifying characteristic metabolic modifications mediated by these downstream signalling pathways. Therefore, in this study, we assessed the roles of JAK/STAT and MAPK/ERK in regulating mitochondrial functions (OCR and ECAR), as well as the potential impact of T2DM on these processes in HSVSMCs in vitro.

2. Materials and Methods

2.1. Materials

HSV samples were collected between January 2020 and May 2022 from patients undergoing elective coronary artery bypass graft procedure. Table 1 summarises the information on the tissue donors. Other materials used in this study and further details on the tissue donors are listed in the Supplementary Materials Tables S1 and S2.

Table 1. Patient information for HSV samples.

	Description	T2DM	Non-T2DM
1	Number of samples	17	38
2	Age	Range: 56–80 Mean ± SD: 69.2 ± 6.2	Range: 47–84 Mean ± SD: 66.4 ± 8.9
3	Sex	Male—15 Female—2	Male—36 Female—2
4	Ethnicity	White British—17	White British—37 Asian—1
5	Reason for surgery	CAD	CAD

CAD: coronary artery disease; T2DM: type 2 diabetes mellitus; SD: standard deviation.

2.2. Methods

2.2.1. HSVSMC Isolation

As shown in Table 1, surplus HSV tissues were obtained from consenting (written) T2DM and non-diabetic patients undergoing coronary artery bypass graft (CABG) surgery at the Hull University Teaching Hospitals NHS Trust Department of Cardiothoracic Surgery, Castle Hill Hospital, Cottingham, UK, under UK Health Research Authority ethical approval (NHS REC:15/NE/0138). The procedures we used to obtain and process surplus HSV tissues adhered to the guidelines outlined in the 2024 revision of the Declaration of

Helsinki [29]. HSV tissues (length 0.5–4 cm) were stored at 4 °C for a maximum of 48 h in Dulbecco's modified Eagle medium (DMEM) supplemented with 100 IU/mL penicillin, 100 μg/mL streptomycin, and 0.25 μg/mL fungizone. VSMCs were explanted from HSV as previously described [30]. Briefly, HSV tissue was placed in a 10 cm dish with enough medium to cover it, and a sterile blade was used to remove the perivascular fat, vein branches, connective tissue, and adventitia. The vein was then dissected longitudinally, and the endothelial and tunica intima layers gently removed with sterile surgical scissors and forceps. Then, HSV tissue was dissected into small fragments (~1 mm^3) which were transferred into a 25 cm^2 tissue culture flask with 2 mL of SmGM2 and cultured at 37 °C in 5% (*v*/*v*) CO_2 in humidified atmosphere. Once HSVSMCs had migrated from the explant tissue, after approximately two weeks, the growth medium was topped up with 0.5 mL fresh SmGM2 twice weekly. Addition of 0.5 mL fresh SmGM2 continued until a total of 5 mL of growth medium had been added; then, 2.5 mL of growth medium was removed and replenished with fresh 2.5 mL SmGM2 until 90% confluence. Thereafter, HSVSMCs were transferred to a 75 cm^2 tissue culture flask and fed with 10 mL of SmGM2, which was replaced twice weekly until cells reached 90% confluency and expanded for either cryopreservation in liquid nitrogen or downstream experimental applications. The integrity of HSVSMC preparations was confirmed by the presence of SMC markers and absence of fibroblast and endothelial cell markers by immunofluorescence staining and confocal microscopy as we have previously described [31].

2.2.2. Cell Culture, SDS-PAGE and Immunoblotting

HSVSMCs were maintained with SmGM2 at normal glucose concentration (5 mM) in a T75 flask and kept in a cell culture incubator maintained at 37 °C and 5% (*v*/*v*) CO_2 in a humidified atmosphere. For all experiments, cells were allowed to be 80–90% confluent before subculturing. All experiments were done with Passage 4 of HSVSMCs, and all cells were free of mycoplasma contamination. SDS-PAGE and Immunoblotting were performed as we have previously described [31].

2.2.3. HSVSMC Mitochondrial Stress Analysis of OCR and ECAR

HSVSMCs were seeded in Seahorse XFp 8-well plates at a density of 10,000 cells/well and allowed to grow over 24 h. Cells were then treated with the respective inhibitors of the downstream signalling pathways. To evaluate the contribution of JAK/STAT signalling pathways, cells were treated with 0.1 μM JAK1/2-selective inhibitor ruxolitinib [32] for 90 min, after which IL-6 (5 ng/mL) and sIL-6Rα (25 ng/mL) (IL-6/sIL-6Rα) or 10 ng/mL PDGF-BB was added for a further 24 h. To examine a role for ERK1,2 signalling pathways, cells were treated with 10 nM MEK1,2-selective inhibitor trametinib [33] for 90 min after which 100 nM Ang II or 1 U/mL thrombin were used to treat cells over 24 h. Also, the probes of the XFp 8-well plate were hydrated overnight by adding 200 μL/well of Seahorse calibrant and 400 μL into the ridges of the plate to prevent evaporation [34]. A humidified incubator was used to incubate this hydrated sensor containing XFp 8-well plates overnight at 37 °C.

On the day of assay, modulators of mitochondrial respiration, 20 μL oligomycin (1.5 μM), 22 μL carbonyl cyanide p-(trifluoromethoxy) phenylhydrazone (FCCP) (5 μM), and 25 μL rotenone (5 μM) and antimycin A (5 μM) complex were added to the injection ports of the pre-hydrated Seahorse XFp 8-well plate [34]. The Seahorse XFp 8-well plate was kept in the non-CO_2 incubator for 30 min to allow the drugs to equilibrate. Each treatment was done in duplicate. Following this, plates were mounted in the Agilent (Santa Clara, CA, USA) Seahorse XFp Analyzer (model number 102745-100) and allowed to calibrate. While calibrating, the growth media on the pre-treated cells were withdrawn and 180 μL of the

XF DMEM medium was added to each well. Following calibration, the cells were mounted in the Agilent Seahorse XFp Analyzer (model number 102745-100), and real-time OCR and ECAR of the pre-treated cells were determined [34]. After the assay, the treated cells were lysed, and protein concentrations were determined using a BCA assay. Peak OCR and ECAR values, with or without treatments, following the injection of each modulator of mitochondrial respiration were normalised with the determined protein concentrations. Four biological replicates were performed using samples from different patients. Samples from these same donors were used across treatments.

2.2.4. Real-Time Quantitative PCR

qPCR was used to determine the mtDNA expression of the mitochondrially encoded gene for cytochrome c oxidase subunit I (COI), a key protein in the mitochondrial respiratory chain [35,36]. A total volume of 20 µL PCR mixture, comprising 1 ng of cDNA, 10 µL of SYBR Green Master Mix (Bio-Rad, Hercules, CA, USA), 1 µL of the appropriate primer (Table 2), and 7.4 µL of RNase-free H_2O, was added to each well of a 96-well PCR plate. The 96-well plate was then installed in the StepOne machine after being sealed with optical adhesive film. StepOne software v2.3 was used to perform the real-time quantitative PCR (qPCR) following the manufacturer's recommendations. The cycle conditions for real-time qPCR were optimised and set at 95 °C for 10 min, followed by 35 cycles of 95 °C for 30 s, 57 °C for 30 s, and 72 °C for 30 s. Every assay was carried out twice, and the average was determined. RNase-free water served as the negative control. Each sample's average C_T values were computed and normalised to 18S RNA controls.

Table 2. Two PCR primer sequences.

Gene	Primer Sequence (5′-3′)
MT-COI	Forward—CCT ACT CCT GCT CGC ATC TG Reverse—AGA GGG GCG TTT GGT ATT GG
18S	Forward—GTA ACC CGT TGA ACC CCA TT Reverse—CCA TCC AAT CGG TAG TAG CG

2.2.5. Statistical Analysis

Statistical analysis was carried out using GraphPad Prism® 6, San Diego, CA, USA. Data are presented as mean ± standard error of mean (SEM) and were analysed using an independent *t*-test and both one-way and two-way analysis of variance, followed by both Dunnett's and Holm–Šidák's post hoc tests to determine significant differences between means, where $p < 0.05$ was considered statistically significant.

3. Results

3.1. Effect of IL-6/sIL-6Rα on OCR in HSVSMCs from T2DM and Non-Diabetic Patients

Studies have shown that T2DM is associated with elevated levels of pleiotropic cytokines such as IL-6, which can cause a number of adverse cellular effects, including mitochondrial dysfunction [20]. However, the mechanism(s) and impact on mitochondrial function of VSMCs are unknown. First, we determined the concentration of ruxolitinib sufficient to significantly inhibit IL-6/sIL-6Rα-mediated phosphorylation of STAT3 on Tyr705 (Figure 1). Then, as shown in Figure 2A, an IL-6/sIL-6Rα trans-signalling complex was found to significantly increase OCR in HSVSMCs from T2DM patients at maximal respiration ($p < 0.05$ versus unstimulated cells, $n = 4$), but not in those from non-diabetic HSVSMCs (Figure 2B). The IL-6/sIL-6Rα-stimulated increase in OCR found in HSVSMCs from T2DM patients was abolished by pre-treatment with JAK1/2-selective inhibitor ruxolitinib (Figure 2A), at the predetermined concentration (0.1 µM) (Figure 1). Furthermore,

https://doi.org/10.3390/cells15151402

ruxolitinib significantly decreased OCR in HSVSMCs from non-diabetic patients at basal and maximal respiration with or without IL-6/sIL-6Rα stimulation ($p < 0.05$ versus unstimulated cells, $n = 4$; Figure 2B). No significant differences in OCR between HSVSMCs from T2DM and non-diabetic patients were observed (Figure 2C).

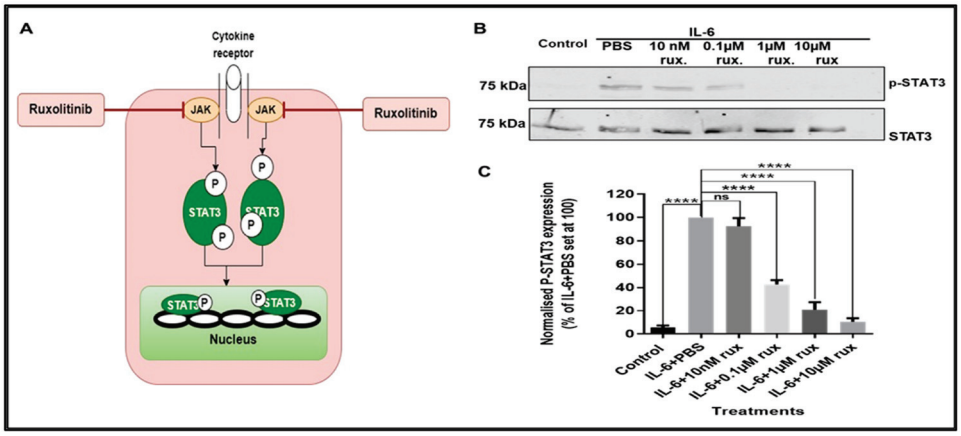


Figure 1. Downstream activation and inhibition of the JAK/STAT signalling pathway. (**A**) Schematic of downstream activation and inhibition of the JAK/STAT signalling pathway. The JAK/STAT pathway transmits information from chemical signals outside of a cell to the cell nucleus, where it activates genes through transcription. This is mediated by activation of receptors such as IL-6R and proteins, Janus kinases (JAKs), and signal transducer and activator of transcription (STAT). Ruxolitinib (JAK 1/2-selective inhibitor) blocks this signalling pathway. (**B**) Representative Western blot of downstream inhibition of IL-6/sIL-6Rα-stimulated JAK1/2-mediated phosphorylation of STAT3 (98 kDa) on Tyr705 by ruxolitinib. Lower panel: expression of total STAT3. (**C**) Densitometric analysis of p-STAT3 normalised to total STAT3. Data are expressed as mean ± SEM and from $n = 4$ biological replicates using HSVSMC samples from different non-diabetic patients. Statistical significance was assessed using one-way ANOVA followed by Dunnett's post hoc test to determine significant differences between means. IL-6: IL-6/sIL-6Rα; PBS: phosphate-buffered saline; rux: ruxolitinib. **** $p < 0.0001$; ns: not significant.

3.2. Effect of IL-6/sIL-6Rα on the ECAR in HSVSMCs from T2DM and Non-Diabetic Patients

The effect of pro-inflammatory cytokines such as IL-6 on ECAR in vascular cells is currently unclear. ECAR serves as a proxy measure of glycolysis [17]. We therefore determined the ECAR of HSVSMCs from T2DM and non-diabetic patients after treatment with IL-6/sIL-6Rα, following pre-treatment with or without ruxolitinib. ECAR was measured simultaneously during mitochondrial stress tests. Consequently, ECAR values are interpreted here as an index of non-mitochondrial acidification and the compensatory glycolytic response to mitochondrial inhibition. Our findings suggest that IL-6/sIL-6Rα did not cause any significant change in the ECAR of HSVSMCs from either T2DM or non-diabetic patients (Figure 3A,B). However, with or without IL-6/sIL-6Rα stimulation, ruxolitinib significantly ($p < 0.05$ versus unstimulated cells, $n = 4$) decreased resting ECAR and maximal ECAR compensation, and ($p < 0.01$ versus unstimulated cells, $n = 4$) decreased non-mitochondrial ECAR in HSVSMCs from non-diabetic patients (Figure 3B). No significant differences in the ECAR of HSVSMCs from T2DM and non-diabetic patients after stimulation with IL-6/sIL-6R were observed (Figure 3C).

https://doi.org/10.3390/cells15151402

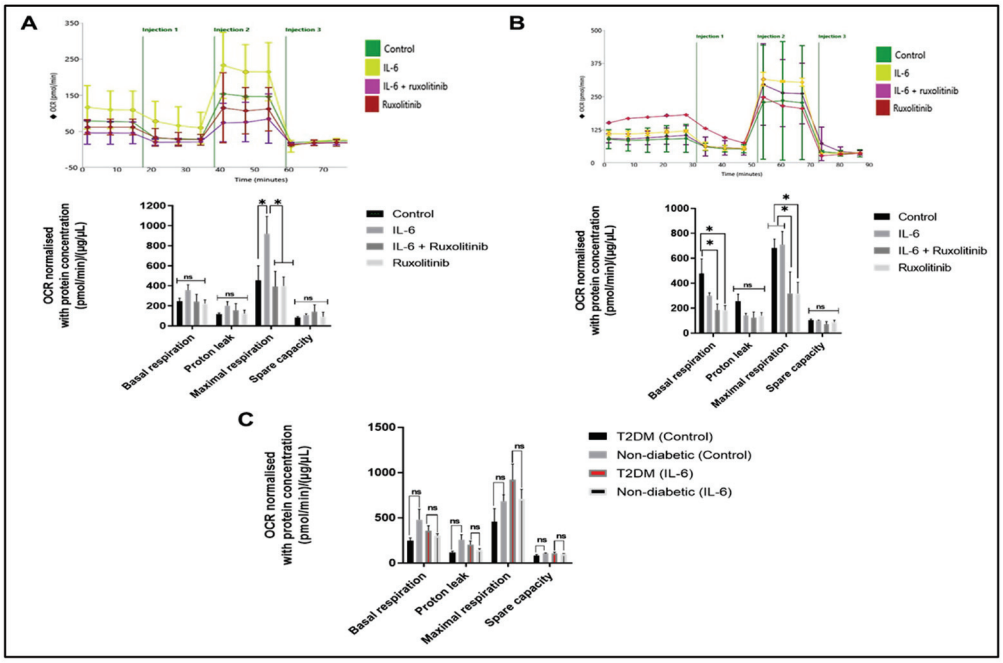


Figure 2. Mitochondrial stress analysis to determine the OCR of HSVSMCs from T2DM and non-T2DM patients after stimulation with IL-6/sIL-6Rα +/− ruxolitinib. (**A**) **Upper panel:** representative time course curve of OCR of HSVSMCs from T2DM patients treated with IL-6/sIL-6Rα (IL-6 (5 ng/mL) and sIL-6Rα (25 ng/mL)) +/− ruxolitinib (0.1 µM) and untreated control from T2DM patients. **Lower panel:** comparative analysis of normalised peak OCR between treatment groups and untreated control at basal glycolysis, and after addition of inhibitors of mitochondrial respiration and the uncoupler. Normalised data are presented as mean ± SEM from $n = 4$ biological replicates using HSVSMC samples from different T2DM patients. (**B**) **Upper panel:** representative time course curve of OCR of HSVSMCs from non-diabetic patients treated with IL-6/sIL-6Rα (IL-6 (5 ng/mL) and sIL-6Rα (25 ng/mL)) +/− ruxolitinib (0.1 µM) and untreated control from non-diabetic patients. **Lower panel:** comparative analysis of normalised peak OCR between treatment groups and untreated control at basal glycolysis, and after addition of inhibitors of mitochondrial respiration and the uncoupler. Normalised data are presented as mean ± SEM from $n = 4$ biological replicates using HSVSMC samples from different non-diabetic patients. (**C**) Comparison of normalised peak OCR of unstimulated and IL-6/sIL-6Rα-stimulated HSVSMCs from T2DM patients versus non-diabetic control. Normalised data are presented as mean ± SEM and statistical significance was assessed using an independent *t*-test, $n = 4$ biological replicates using HSVSMC samples from different T2DM and non-diabetic patients. In the lower panels of Figures (**A**,**B**), normalised data from different treatment conditions were compared with data from the normalised untreated control. Statistical significance was assessed using an independent *t*-test and both one-way and two-way ANOVA, followed by Dunnett's and Holm–Šidák's post hoc tests to determine significant differences between means. * $p < 0.05$. IL-6: IL-6/sIL-6Rα; OCR: oxygen consumption rate.

3.3. Effect of PDGF-BB on the OCR in HSVSMCs from T2DM and Non-Diabetic Patients

Given that the OCR is proportional to mitochondrial respiration [17], it is unclear how growth factors like PDGF alter this cellular metabolic index (OCR) in HSVSMCs. To investigate this, the OCRs of HSVSMCs from T2DM patients and non-diabetic controls were assessed after treatment with PDGF-BB in the presence or absence of ruxolitinib. As shown in Figure 4A, PDGF-BB significantly increased OCR in HSVSMCs from T2DM patients ($p < 0.05$ versus unstimulated cells, $n = 4$) and maximum respiration ($p < 0.01$ versus unstimulated cells, $n = 4$). However, PDGF-BB had no significant effect on the OCR of HSVSMCs from non-diabetic patients (Figure 4B). This increase in OCR in T2DM patient HSVSMCs was abolished by pre-treatment with ruxolitinib (Figure 4A). Ruxolitinib also significantly reduced OCR at maximum respiration ($p < 0.05$ versus unstimulated cells

and $p < 0.01$ versus PDGF-BB-stimulated cells, $n = 4$) in HSVSMCs from T2DM patients (Figure 4A)—a pattern also seen in HSVSMCs from non-diabetic controls (Figure 4B) ($p < 0.05$ versus unstimulated and PDGF-BB-stimulated, $n = 4$). In contrast, there were no significant differences between OCRs in HSVSMCs from T2DM and non-diabetic patients (Figure 4C).

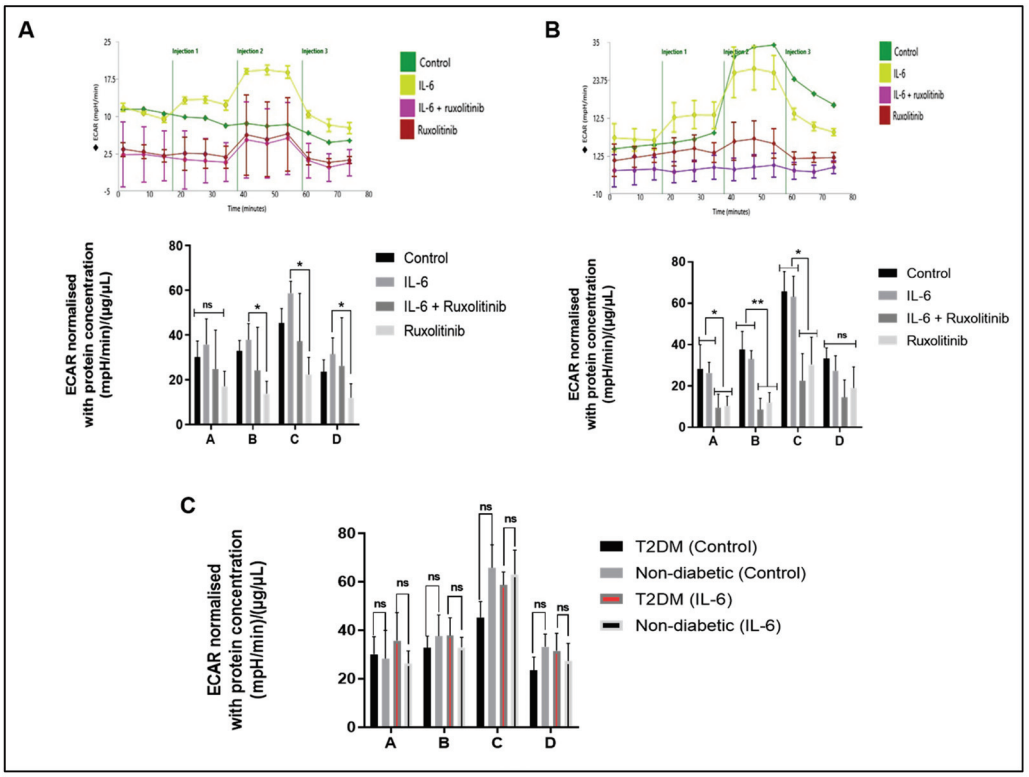


Figure 3. Mitochondrial stress analysis to determine the ECAR of HSVSMCs from T2DM and non-T2DM patients after stimulation with IL-6/sIL-6Rα +/− ruxolitinib. (**A**) **Upper panel:** representative time course curve of ECAR of HSVSMCs from T2DM patients treated with IL-6/sIL-6Rα (IL-6 (5 ng/mL) and sIL-6Rα (25 ng/mL)) +/− ruxolitinib (0.1 µM) and untreated control from diabetic patients. **Lower panel:** comparative analysis of normalised peak ECAR between treatment groups and untreated control at basal glycolysis, and after addition of inhibitors of mitochondrial respiration and the uncoupler. Normalised data are presented as mean ± SEM from $n = 4$ biological replicates using HSVSMC samples from different T2DM patients. (**B**) **Upper panel:** representative time course curve of ECAR of HSVSMCs from non-diabetic patients treated with IL-6/sIL-6Rα (IL-6 (5 ng/mL) and sIL-6Rα (25 ng/mL)) +/− ruxolitinib (0.1 µM) and untreated control from non-diabetic patients. **Lower panel:** comparative analysis of normalised peak ECAR between treatment groups and untreated control at basal glycolysis, and after addition of inhibitors of mitochondrial respiration and the uncoupler. Normalised data are presented as mean ± SEM from $n = 4$ biological replicates using HSVSMC samples from different non-diabetic patients. (**C**) Comparison of normalised peak ECAR of unstimulated and IL-6/sIL-6Rα-stimulated HSVSMCs from T2DM patients versus non-diabetic control. Normalised data are presented as mean ± SEM and statistical significance was assessed using an independent *t*-test, $n = 4$ biological replicates using HSVSMC samples from different T2DM and non-diabetic patients. In the lower panels of Figure 3 (**A**,**B**), normalised data from different treatment conditions were compared with data from the normalised untreated control. Statistical significance was assessed using an independent *t*-test and both one-way and two-way ANOVA, followed by Dunnett's and Holm–Šidák's post hoc tests to determine significant differences between means. * $p < 0.05$; ** $p < 0.01$. ns: not significant; IL-6: IL-6/sIL-6Rα; A: resting ECAR; B: oligomycin-induced ECAR; C: ECAR response to uncoupling; D: non-mitochondrial ECAR; ECAR: extracellular acidification rate.

https://doi.org/10.3390/cells15151402

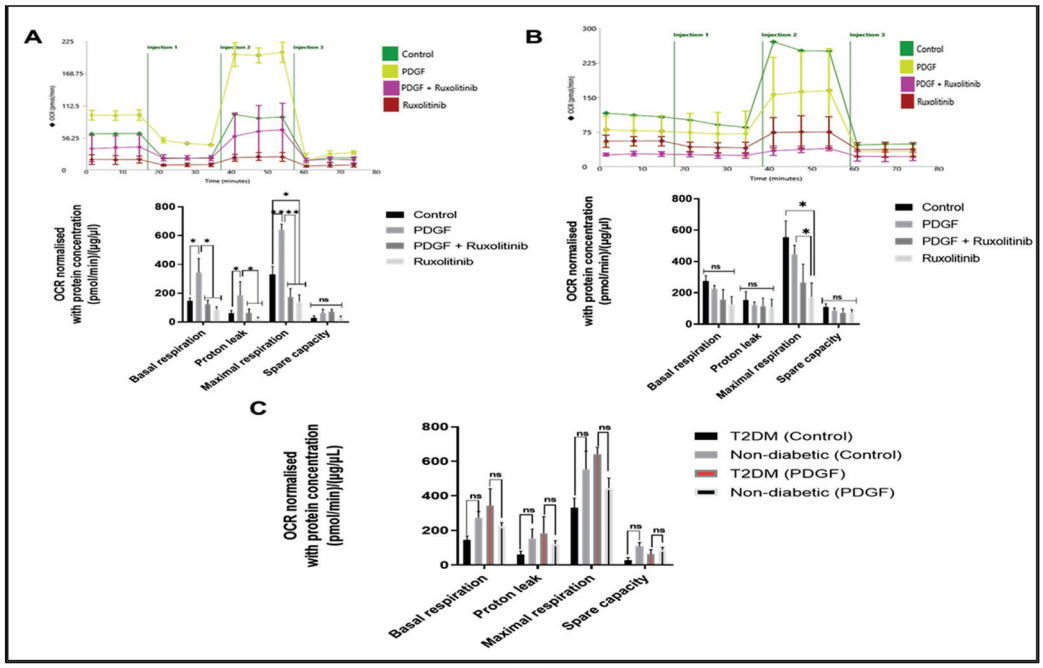


Figure 4. Mitochondrial stress analysis to determine the OCR of HSVSMCs from T2DM and non-T2DM patients after stimulation with PDGF-BB +/− ruxolitinib. (**A**) **Upper panel:** representative time course curve of OCR of HSVSMCs from T2DM patients treated with PDGF-BB (10 ng/mL) +/− ruxolitinib (0.1 µM) and untreated control from diabetic patients. **Lower panel:** comparative analysis of normalised peak OCR between treatment groups and untreated control at basal glycolysis, and after addition of inhibitors of mitochondrial respiration and the uncoupler. Normalised data are presented as mean ± SEM from $n = 4$ biological replicates using HSVSMC samples from different T2DM patients. (**B**) **Upper panel:** representative time course curve of OCR of HSVSMCs from non-diabetic patients treated with PDGF-BB (10 ng/mL) +/− ruxolitinib (0.1 µM) and untreated control from non-diabetic patients. **Lower panel:** comparative analysis of normalised peak OCR between treatment groups and untreated control at basal glycolysis, and after addition of inhibitors of mitochondrial respiration and the uncoupler. Normalised data are presented as mean ± SEM from $n = 4$ biological replicates using HSVSMC samples from different non-diabetic patients. (**C**) Comparison of normalised peak OCR of unstimulated and PDGF-BB-stimulated HSVSMCs from T2DM patients versus non-diabetic control. Normalised data are presented as mean ± SEM and statistical significance was assessed using an independent *t*-test, $n = 4$ biological replicates using HSVSMC samples from different T2DM and non-diabetic patients. In the lower panels of Figure 4 (**A**,**B**), normalised data from different treatment conditions were compared with data from the normalised untreated control. Statistical significance was assessed using an independent *t*-test and both one-way and two-way ANOVA, followed by Dunnett's and Holm–Šidák's post hoc tests to determine significant differences between means. * $p < 0.05$; ** $p < 0.01$. ns: not significant; PDGF: PDGF-BB; OCR: oxygen consumption rate.

3.4. Effect of PDGF-BB on the ECAR in HSVSMCs from T2DM and Non-Diabetic Patients

We next determined the ECAR response of HSVSMCs from T2DM and non-diabetic control patients treated with or without PDGF-BB following pre-treatment with or without ruxolitinib and in response to mitochondrial disruption. As shown in Figure 5A, PDGF-BB significantly increased resting ECAR, as well as ECAR compensation, ECAR in response to uncoupling, and non-mitochondrial ECAR in HSVSMCs from T2DM patients ($p < 0.05$ versus unstimulated cells, $n = 4$) but not in non-diabetic controls (Figure 5B). Furthermore, ruxolitinib significantly decreased resting ECAR, ECAR compensation, ECAR in response to uncoupling, and non-mitochondrial ECAR in HSVSMCs from non-diabetic patients ($p < 0.05$ versus unstimulated and PDGF-BB-stimulated cells but not in those from T2DM patients (Figure 5B). Direct comparison of the ECAR of HSVSMCs from T2DM versus non-diabetic patients also revealed a significantly higher ECAR in response to uncoupling

https://doi.org/10.3390/cells15151402

in HSVSMCs from T2DM patients compared with non-diabetic controls ($p < 0.05$, $n = 4$; Figure 5C).

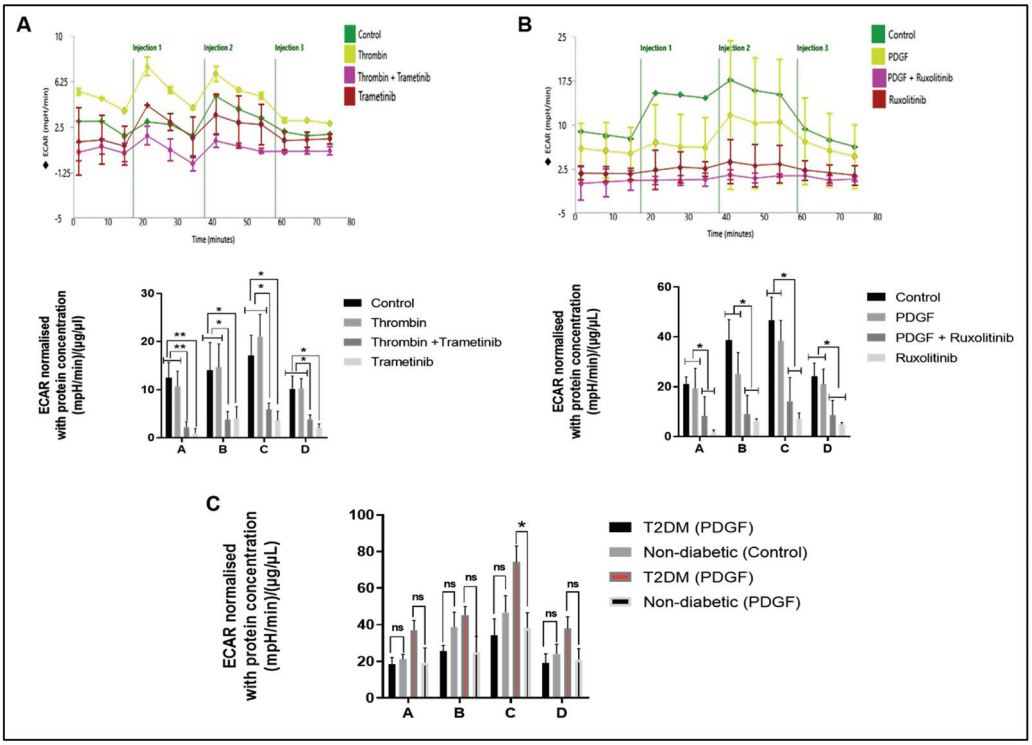


Figure 5. Mitochondrial stress analysis to determine the ECAR of HSVSMCs from T2DM and non-T2DM patients after stimulation with PDGF-BB +/− ruxolitinib. (**A**) **Upper panel:** representative time course curve of ECAR of HSVSMCs from T2DM patients treated with PDGF-BB (10 ng/mL) +/− ruxolitinib (0.1 µM) and untreated control from diabetic patients. **Lower panel:** comparative analysis of normalised peak ECAR between treatment groups and untreated control at basal glycolysis, and after addition of inhibitors of mitochondrial respiration and the uncoupler. Normalised data are presented as mean ± SEM from $n = 4$ biological replicates using HSVSMC samples from different T2DM patients. (**B**) **Upper panel:** representative time course curve of ECAR of HSVSMCs from non-diabetic patients treated with PDGF-BB (10 ng/mL) +/− ruxolitinib (0.1 µM) and untreated control from non-diabetic patients. **Lower panel:** comparative analysis of normalised peak ECAR between treatment groups and untreated control at basal glycolysis, and after addition of inhibitors of mitochondrial respiration and the uncoupler. Normalised data are presented as mean ± SEM from $n = 4$ biological replicates using HSVSMC samples from different non-diabetic patients. (**C**) Comparison of normalised peak ECAR of unstimulated and PDGF-BB-stimulated HSVSMCs from T2DM patients versus non-diabetic control. Normalised data are presented as mean ± SEM and statistical significance was assessed using an independent *t*-test, $n = 4$ biological replicates using HSVSMC samples from different T2DM and non-diabetic patients. In the lower panels of Figure 5 (**A**,**B**), normalised data from different treatment conditions were compared with data from the normalised untreated control. Statistical significance was assessed using an independent *t*-test and both one-way and two-way ANOVA, followed by Dunnett's and Holm–Šidák's post hoc tests to determine significant differences between means. * $p < 0.05$; ** $p < 0.01$. ns: not significant; PDGF: PDGF-BB; A: Resting ECAR; B: Oligomycin-induced ECAR; C: ECAR response to uncoupling; D: Non-mitochondrial ECAR; ECAR: extracellular acidification rate.

3.5. mtDNA Expression in HSVSMCs from T2DM and Non-Diabetic Patients After Treatment with IL-6/sIL-6Rα and PDGF-BB +/−Ruxolitinib

As JAK/STAT activators IL-6/sIL-6Rα and PDGF-BB caused a significant increase in the OCR of HSVSMCs from T2DM (Figures 2A and 4A) but not non-diabetic patients (Figures 2B and 4B), it was therefore necessary to ascertain whether this increase was

associated with a parallel increase in mitochondria. Therefore, qPCR of the mitochondrially encoded gene for COI was used to determine mtDNA expression [35,36].

As shown in Figure 6A, there was no significant difference in mtDNA expression in HSVSMCs from T2DM patients after treatment with IL-6/sIL-6Rα+/−ruxolitinib compared with the untreated control. Similarly, in the HSVSMCs from non-diabetic patients, there was no significant difference in mtDNA expression after treatment with IL-6/sIL-6Rα+/−ruxolitinib compared with the untreated control (Figure 6B). Comparison between HSVSMCs from T2DM patients versus the non-diabetic control treated with IL-6/sIL-6Rα+/−ruxolitinib showed no significant difference (Figure 6C). Furthermore, as shown in Figure 6D, there was no significant difference in mtDNA expression in HSVSMCs from T2DM patients after treatment with PDGF-BB+/−ruxolitinib compared with the untreated control. Similarly, in the HSVSMCs from non-diabetic patients, there was no significant difference in mtDNA expression after treatment with PDGF-BB+/−ruxolitinib compared with the untreated control (Figure 6E). Also, comparison between HSVSMCs from T2DM patients versus the non-diabetic control treated with PDGF-BB+/−ruxolitinib showed no significant difference (Figure 6F).

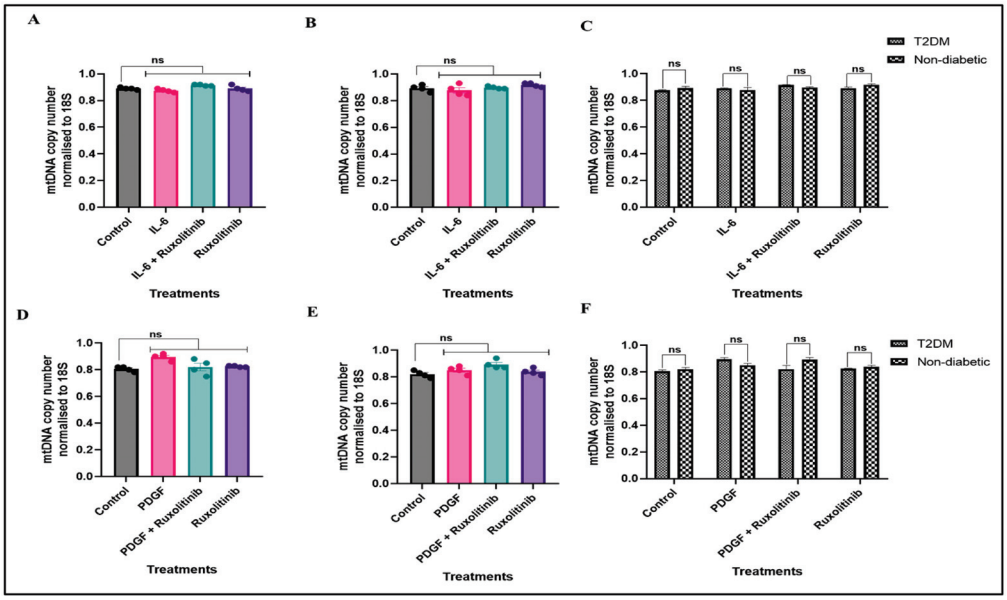


Figure 6. mtDNA expression of HSVSMCs from T2DM and non-diabetic patients after treatment with IL-6/sIL-6Rα or PDGF-BB +/− ruxolitinib, along with qPCR analysis of mtDNA expression of the mitochondrially encoded gene for COI as a marker of mtDNA expression normalised to 18S. **Top panel:** (**A**) T2DM patients, (**B**) non-diabetic patients, and (**C**) comparison between T2DM patients versus the non-diabetic control treated with IL-6/sIL-6Rα (IL-6 (5 ng/mL) and sIL-6Rα (25 ng/mL)) +/− ruxolitinib (0.1 μM). **Bottom panel:** (**D**) T2DM patients, (**E**) non-diabetic patients, and (**F**) comparison between T2DM patients versus the non-diabetic control treated with PDGF-BB (10 ng/mL) +/− ruxolitinib (0.1 μM). All data were normalised to 18S, and normalised data from different treatment conditions were compared with data from the normalised untreated control for statistical difference. Data are presented as mean ± SEM from n = 4 experiments using HSVSMC from different patients. Statistical significance was assessed using an independent t-test and both one-way and two-way ANOVA, followed by Dunnett's and Holm–Šidák's post hoc tests to determine significant differences between means. ns: not significant; IL-6: IL-6/sIL-6Rα; PDGF: PDGF-BB.

3.6. Effect of Ang II on OCR of HSVSMCs from T2DM and Non-Diabetic Patients

While Ang II has been shown to promote VSMC migration and proliferation by activating the MAP/ERK1,2 pathway [37], it is not totally clear how Ang II modulates these processes. However, we hypothesise that the increased cell proliferation and migration

induced by Ang II [37] may necessitate higher ATP synthesis, which would increase oxygen consumption. Therefore, we assessed the effect of Ang II +/− MEK1/2-selective inhibitor trametinib on the OCR of HSVSMCs from patients with and without T2DM. The optimised concentration of trametinib that significantly ($p < 0.05$ versus untreated cells, $n = 4$) inhibited activation of ERK1,2 in HSVSMCs from non-diabetic patients was 10 nM trametinib (Figure 7). Hence, this concentration was used in subsequent experiments. As shown in Figure 8A,B, Ang II (100 nM) did not significantly alter the OCR of HSVSMCs from T2DM and non-diabetic patients, respectively, even though the same concentration of Ang II stimulated a transient increase in ERK1,2 phosphorylation in HSVSMCs (Figure 9). However, trametinib with or without Ang II stimulation significantly reduced OCRs at basal respiration ($p < 0.01$ versus unstimulated and Ang II-stimulated cells, $n = 4$) and maximal respiration ($p < 0.05$ versus unstimulated and Ang II-stimulated cells, $n = 4$) in HSVSMCs from T2DM patients (Figure 8A). Similarly, in HSVSMCs from non-diabetic patients, Ang II treatment did not significantly alter the OCR (Figure 8B). Furthermore, trametinib caused a significant reduction in the OCRs at basal respiration ($p < 0.01$ with Ang II stimulation; $p < 0.001$ without Ang II stimulation, both versus unstimulated and Ang II-stimulated cells, $n = 4$) in HSVSMCs from non-diabetic patients (Figure 8B). Interestingly, trametinib caused a significant reduction in the OCRs at maximal respiration ($p < 0.05$ with or without Ang II stimulation versus unstimulated and Ang II-stimulated cells, $n = 4$) in HSVSMCs from non-diabetic patients (Figure 8B). Also, direct comparison of OCRs after treatment with Ang II revealed a significant increase in the OCR of HSVSMCs from T2DM patients at maximal respiration ($p < 0.05$ versus HSVSMCs from non-diabetic patients, $n = 4$; Figure 8C).

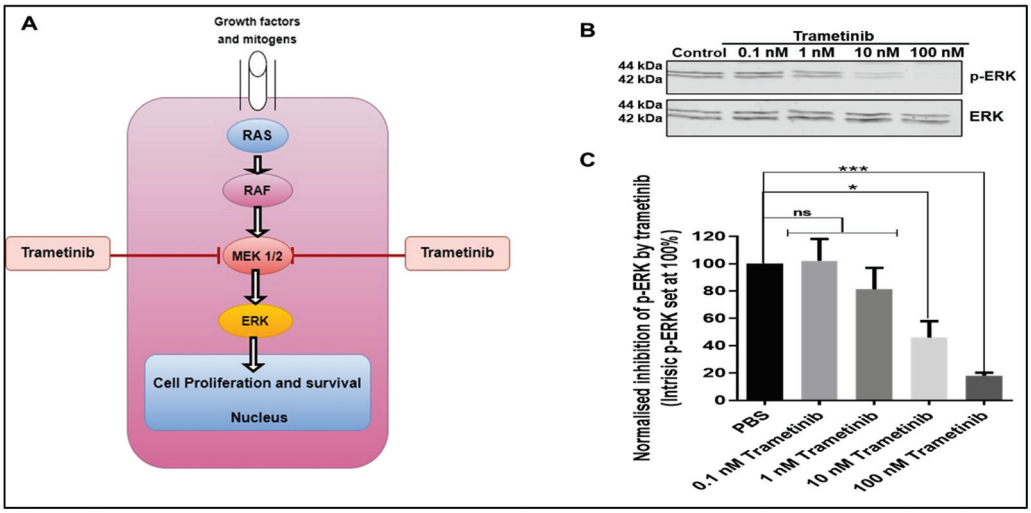


Figure 7. Downstream activation and inhibition of the MAPK/ERK signalling pathway. (**A**) Schematic of downstream activation and inhibition of the MEK/ERK signalling pathway. Mitogens trigger activation of the small GTPase Ras protein, which in turn activates the Ser/Thr-directed protein kinase Raf, which phosphorylates and activates MEK 1/2. MEK1/2 then phosphorylates and stimulates ERK1,2 (Thr202/185 and Tyr204/187 in human ERK1/2 respectively). ERK further activates a panel of substrates that promote cell proliferation. (**B**) Upper panel: representative Western blot of downstream inhibition of the MEK 1/2 by trametinib. Lower panel: expression of total ERK (44/42 kDa). (**C**) Densitometric analysis of p-ERK at both 44/42 kDa normalised to total ERK at both 44/42 kDa. Data are expressed as mean ± SEM and from $n = 4$ biological replicates using HSVSMC samples from different non-diabetic patients. Statistical significance was assessed using one-way ANOVA followed by Dunnett's post hoc test to determine significant differences between means. PBS: phosphate-buffered saline. * $p < 0.05$; *** $p < 0.001$. ns: not significant.

https://doi.org/10.3390/cells15151402

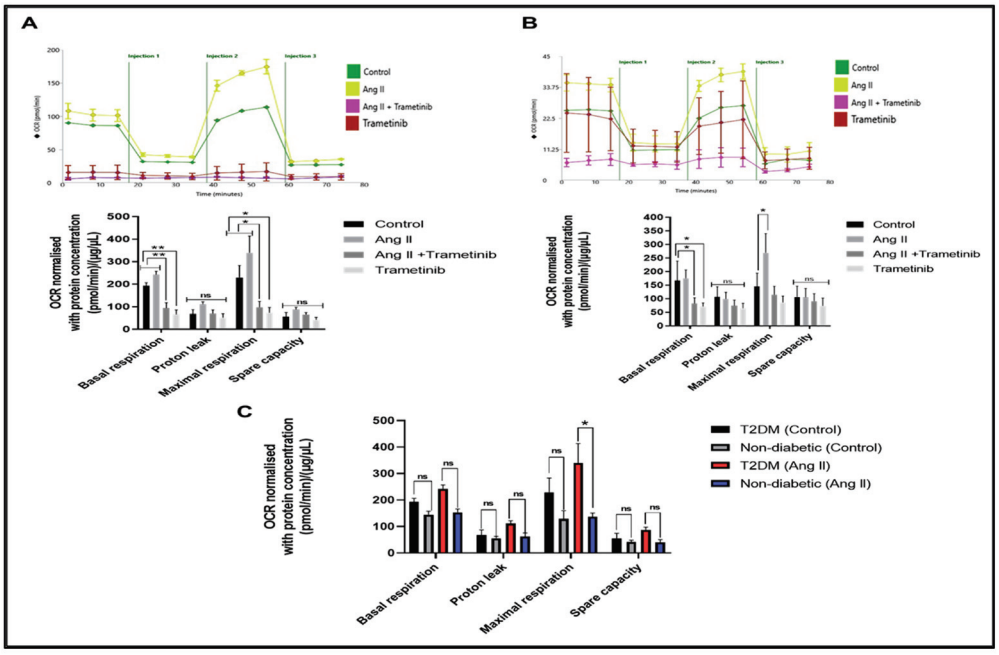


Figure 8. Mitochondrial stress analysis to determine the OCR of HSVSMCs from T2DM and non-T2DM patients after stimulation with Ang II +/− trametinib. (**A**) **Upper panel:** representative time course curve of the OCR of HSVSMCs from T2DM patients treated with Ang II (100 nM) +/− trametinib (10 nM) and untreated control from diabetic patients. **Lower panel:** comparative analysis of normalised peak OCR between treatment groups and untreated control at basal glycolysis, and after addition of inhibitors of mitochondrial respiration and the uncoupler. Normalised data are presented as mean ± SEM from $n = 4$ biological replicates using HSVSMC samples from different T2DM patients. (**B**) **Upper panel:** representative time course curve of the OCR of HSVSMCs from non-diabetic patients treated with Ang II (100 nM) +/− trametinib (10 nM) and untreated control from non-diabetic patients. **Lower panel:** biological replicates using HSVSMC samples from different non-diabetic patients. (**C**) Comparison of normalised peak OCR of unstimulated and Ang II-stimulated HSVSMCs from T2DM patients versus non-diabetic control. Normalised data are presented as mean ± SEM and statistical significance was assessed using an independent *t*-test, $n = 4$ biological replicates using HSVSMC samples from different T2DM and non-diabetic patients. In the lower panels of Figure 8 (**A**,**B**), normalised data from different treatment conditions were compared with data from the normalised untreated control. Statistical significance was assessed using an independent *t*-test and both one-way and two-way ANOVA, followed by Dunnett's and Holm–Šidák's post hoc tests to determine significant differences between means. * $p < 0.05$; ** $p < 0.01$. ns: not significant; Ang II: Angiotensin II; OCR: oxygen consumption rate.

3.7. Effect of Ang II on ECAR of HSVSMCs from T2DM and Non-Diabetic Patients

There is evidence that Ang II may cause mitochondrial oxidative damage in vascular endothelial cells, which could reduce NO bioavailability and increase vascular oxidative stress [21]. While this finding emphasises the role of Ang II in controlling metabolic homeostasis in endothelial cells, its effect on ECAR of HSVSMCs is unknown. Therefore, we evaluated the effects of Ang II +/− trametinib on the ECAR of HSVSMCs from T2DM patients and non-diabetic controls in response to mitochondrial inhibition. As shown in Figure 10A, Ang II treatment did not significantly alter the ECAR in HSVSMCs from T2DM patients. However, in HSVSMCs from T2DM patients, trametinib significantly reduced resting ECARs ($p < 0.05$ with Ang II stimulation, $p < 0.01$ without Ang II stimulation, $n = 4$), and oligomycin-induced ECAR ($p < 0.05$ with Ang II stimulation, $p < 0.01$ without Ang II stimulation, $n = 4$). Furthermore, trametinib significantly reduced ECARs in response to uncoupling ($p < 0.05$ with Ang II stimulation, $p < 0.01$ without Ang II stimulation, $n = 4$), and non-mitochondrial ECAR ($p < 0.05$ with Ang II stimulation, $p < 0.01$ without

Ang II stimulation, $n = 4$) in HSVSMCs from T2DM patients. Similarly, in HSVSMCs from non-diabetic patients, there was no significant change to ECAR in response to Ang II (Figure 10B). Conversely, trametinib caused a significant reduction in resting ECARs ($p < 0.01$ with or without Ang II stimulation, $n = 4$), oligomycin-induced ECAR ($p < 0.01$ with or without Ang II stimulation, $n = 4$), ECAR in response to uncoupling ($p < 0.05$ with or without Ang II stimulation, $n = 4$), and non-mitochondrial ECAR ($p < 0.05$ with or without Ang II stimulation, $n = 4$) in HSVSMCs from non-diabetic patients (Figure 10B). However, no significant differences were observed in the ECARs between Ang II-stimulated HSVSMCs from T2DM and non-diabetic patients (Figure 10C).

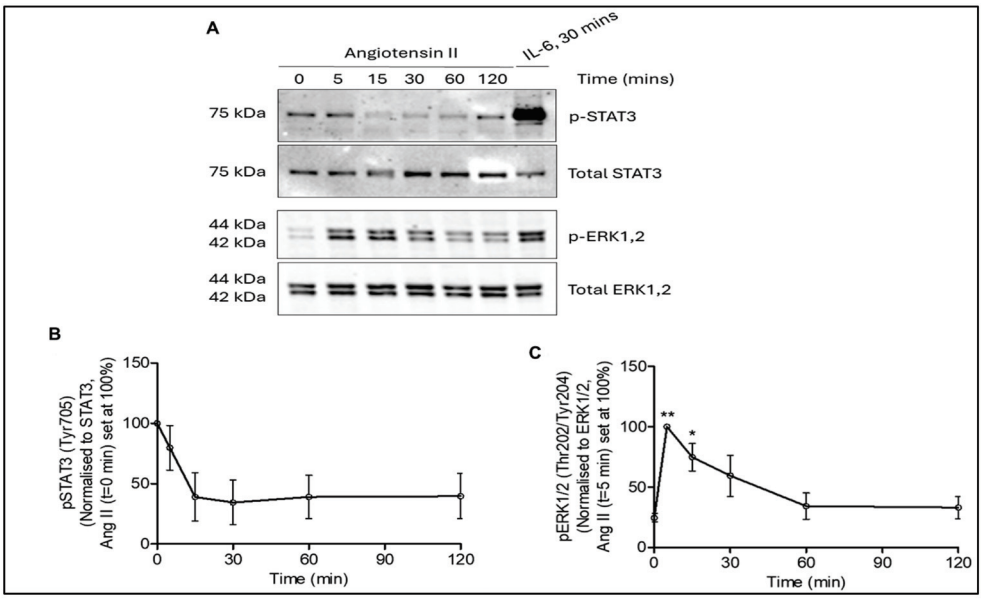


Figure 9. Time course of the effects of Angiotensin II treatment on STAT3 and ERK1/2 phosphorylation in HSVSMCs. HSVSMCs were either treated with vehicle or Angiotensin II (Ang II) (0.1 μM) for the indicated times or sIL-6Rα/IL-6 for 30 min before cell harvest. (**A**) Protein-equalised cell lysates were fractionated by SDS-PAGE for immunoblotting. P-STAT3 (Tyr705) (**B**) and P-ERK1/2 (Thr202/Tyr204) (**C**) levels were normalised to total STAT3 and ERK1/2, respectively, and measured relative to the maximum response (set at 100%). Data are presented as mean ± SEM. Data are expressed as mean ± SEM and from $n = 4$ biological replicates using HSVSMC samples from different non-diabetic patients. Statistical significance was assessed using one-way ANOVA followed by Dunnett's post hoc test to determine significant differences between means. * $p < 0.05$; ** $p < 0.01$ versus t = 0 min (min).

3.8. Effect of Thrombin on OCR of HSVSMCs from T2DM and Non-Diabetic Patients

Thrombin has been associated with vascular remodelling via a number of potential mechanisms, including activation of the MAPK/ERK signalling pathway [25]. However, it is still unknown how thrombin affects mitochondrial respiration, a crucial mediator of VSMC metabolic function. Given that understanding the metabolic homeostasis of VSMCs is crucial for targeting vascular remodelling, we therefore assessed the impact of thrombin +/− trametinib on the OCR of HSVSMCs from T2DM and non-diabetic controls. Thrombin caused a significant increase ($p < 0.05$ versus unstimulated cells) in OCR of HSVSMCs from T2DM patients at maximal respiration which was abolished by trametinib (Figure 11A). On the other hand, trametinib significantly reduced OCR at basal respiration ($p < 0.05$ with or without thrombin stimulation versus unstimulated cells, $n = 4$). Furthermore, in HSVSMCs from non-diabetic patients, thrombin did not significantly change OCR, although trametinib significantly reduced (at both basal and maximal respiration) OCRs ($p < 0.05$ with or without thrombin stimulation versus unstimulated cells, $n = 4$; Figure 11B). Meanwhile,

https://doi.org/10.3390/cells15151402

direct comparison of OCRs in thrombin-treated HSVSMCs from T2DM and non-diabetic patients revealed there was a significant increase in OCR at maximal respiration ($p < 0.01$, $n = 4$) and spare capacity ($p < 0.05$, $n = 4$) (Figure 11C). Moreover, spare capacity was significantly higher in control T2DM HSVSMCs versus non-diabetic control cells.

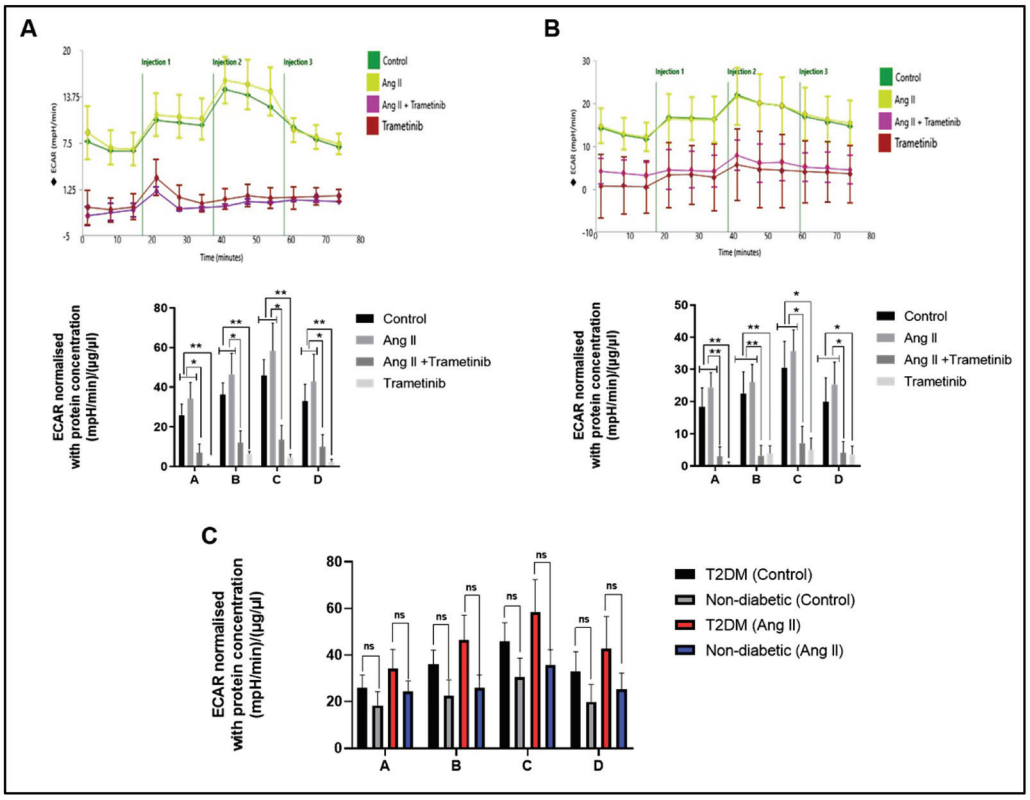


Figure 10. Mitochondrial stress analysis to determine the ECAR of HSVSMCs from T2DM and non-T2DM patients after stimulation with Ang II +/− trametinib. (**A**) **Upper panel:** representative time course curve of ECAR of HSVSMCs from T2DM patients treated with Ang II (100 nM) +/− trametinib (10 nM) and untreated control from diabetic patients. **Lower panel:** comparative analysis of normalised peak ECAR between treatment groups and untreated control at basal glycolysis, and after addition of inhibitors of mitochondrial respiration and the uncoupler. Normalised data are presented as mean ± SEM from $n = 4$ biological replicates using HSVSMC samples from different T2DM patients. (**B**) **Upper panel:** representative time course curve of ECAR of HSVSMCs from non-diabetic patients treated with Ang II (100 nM) +/− trametinib (10 nM) and untreated control from non-diabetic patients. **Lower panel:** comparative analysis of normalised peak ECAR between treatment groups and untreated control at basal glycolysis, and after addition of inhibitors of mitochondrial respiration and the uncoupler. Normalised data are presented as mean ± SEM from $n = 4$ biological replicates using HSVSMC samples from different non-diabetic patients. (**C**) Comparison of normalised peak ECAR of unstimulated and PDGF-BB-stimulated HSVSMCs from T2DM patients versus non-diabetic control. Normalised data are presented as mean ± SEM and statistical significance was assessed using an independent *t*-test, $n = 4$ biological replicates using HSVSMC samples from different T2DM and non-diabetic patients. In the lower panels of Figure 10 (**A**,**B**), normalised data from different treatment conditions were compared with data from the normalised untreated control. Statistical significance was assessed using an independent *t*-test and both one-way and two-way ANOVA, followed by Dunnett's and Holm–Šidák's post hoc tests to determine significant differences between means. * $p < 0.05$; ** $p < 0.01$. ns: not significant; Ang II: Angiotensin II; A: resting ECAR; B: oligomycin-induced ECAR; C: ECAR response to uncoupling; D: non-mitochondrial ECAR; ECAR: extracellular acidification rate.

https://doi.org/10.3390/cells15151402

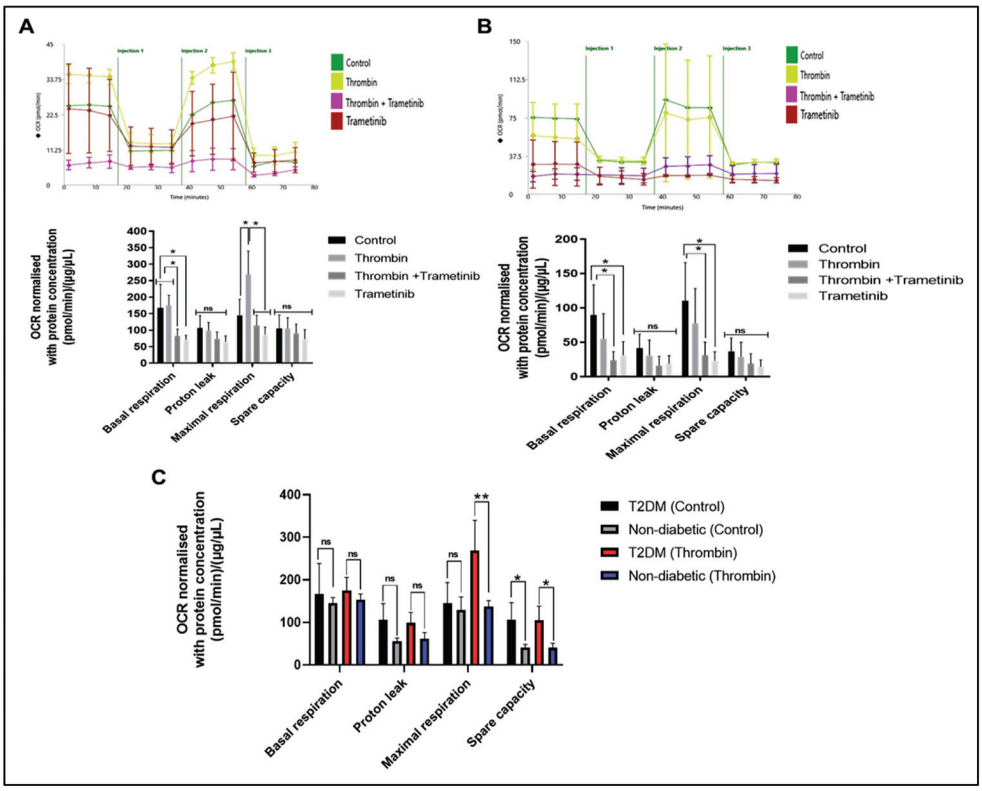


Figure 11. Mitochondrial stress analysis to determine the OCR of HSVSMCs from T2DM and non-T2DM patients after stimulation with thrombin +/− trametinib. (**A**) **Upper panel:** representative time course curve of OCR of HSVSMCs from T2DM patients treated with thrombin (1 U/mL) +/− trametinib (10 nM) and untreated control from diabetic patients. **Lower panel:** comparative analysis of normalised peak OCR between treatment groups and untreated control at basal glycolysis, and after addition of inhibitors of mitochondrial respiration and the uncoupler. Normalised data are presented as mean ± SEM from $n = 4$ biological replicates using HSVSMC samples from different T2DM patients. (**B**) **Upper panel:** representative time course curve of OCR of HSVSMCs from non-T2DM patients treated with thrombin (1 U/mL) +/− trametinib (10 nM) and untreated control from non-diabetic patients. **Lower panel:** comparative analysis of normalised peak OCR between treatment groups and untreated control at basal glycolysis, and after addition of inhibitors of mitochondrial respiration and the uncoupler. Normalised data are presented as mean ± SEM from $n = 4$ biological replicates using HSVSMC samples from different non-diabetic patients. (**C**) Comparison of normalised peak OCR of unstimulated and thrombin-stimulated HSVSMCs from T2DM patients versus non-diabetic control. Normalised data are presented as mean ± SEM and statistical significance was assessed using an independent *t*-test, $n = 4$ biological replicates using HSVSMC samples from different T2DM and non-diabetic patients. In the lower panels of Figure 11 (**A**,**B**), normalised data from different treatment conditions were compared with data from the normalised untreated control. Statistical significance was assessed using an independent *t*-test and both one-way and two-way ANOVA, followed by Dunnett's and Holm–Šidák's post hoc tests to determine significant differences between means. * $p < 0.05$. ns: not significant; ECAR: extracellular acidification rate.

3.9. Effect of Thrombin on ECAR of HSVSMCs from T2DM and Non-Diabetic Patients

Currently, there are no documented research findings highlighting the effects of the MAPK/ERK pathway on ECAR of VSMCs despite the significance of ECAR as a tool for measuring glycolytic flux in cells [38]. Therefore, we assessed the effect of thrombin +/− trametinib on the ECAR of HSVSMCs from T2DM and non-diabetic controls. As shown in Figure 12A, thrombin did not cause any significant alteration in the ECAR of HSVSMCs from T2DM patients. However, trametinib significantly reduced resting ECARs, oligomycin-induced ECAR, ECAR in response to uncoupling, and non-mitochondrial ECAR ($p < 0.01$ with or without thrombin, $n = 4$) in HSVSMCs from T2DM patients (Figure 12A). Similarly,

in HSVSMCs from non-diabetic patients, while there was no significant alteration in ECAR after thrombin stimulation, trametinib significantly reduced the OCRs at resting ECAR ($p < 0.01$ with or without thrombin, $n = 4$), ECAR in response to uncoupling ($p < 0.05$ with or without thrombin, $n = 4$), and non-mitochondrial ECAR ($p < 0.05$ with thrombin, $n = 4$) in HSVSMCs from non-diabetic patients (Figure 12B). Also, the ECAR in response to uncoupling in thrombin-stimulated HSVSMCs from T2DM patients was significantly higher when compared with those from non-diabetic patients ($p < 0.05$, $n = 4$; Figure 12C).

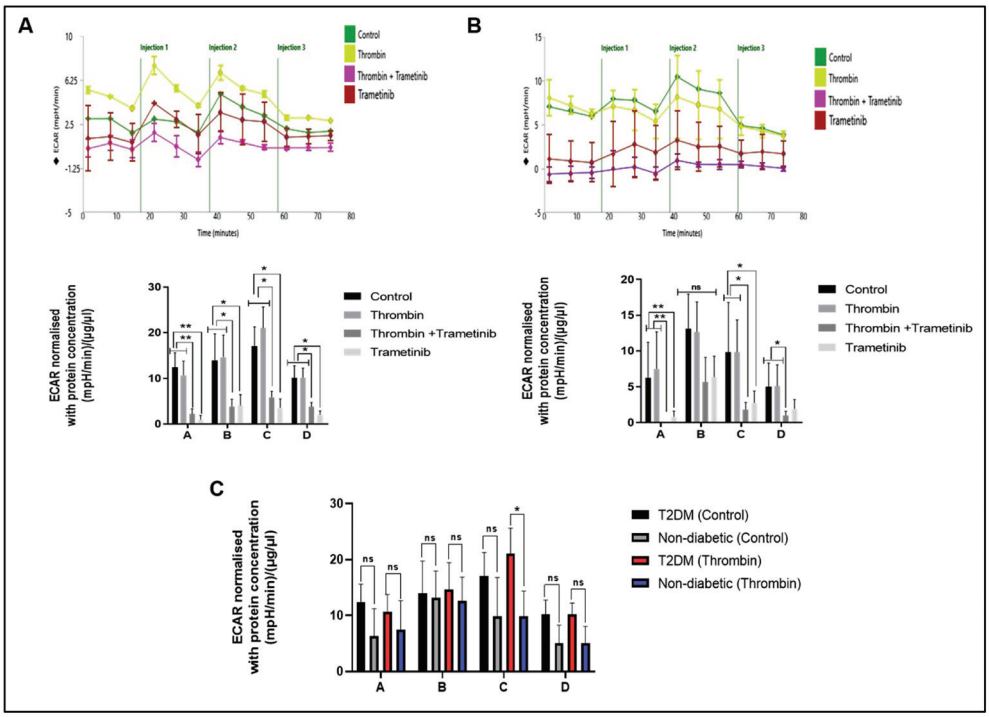


Figure 12. Mitochondrial stress analysis to determine the ECAR of HSVSMCs from T2DM and non-T2DM patients after stimulation with thrombin +/− trametinib. (**A**) **Upper panel:** representative time course curve of ECAR of HSVSMCs from T2DM patients treated with thrombin (1 U/mL) +/− trametinib (10 nM) and untreated control from diabetic patients. **Lower panel:** comparative analysis of normalised peak ECAR between treatment groups and untreated control at basal glycolysis, and after addition of inhibitors of mitochondrial respiration and the uncoupler. Normalised data are presented as mean ± SEM from $n = 4$ biological replicates using HSVSMC samples from different T2DM patients. (**B**) **Upper panel:** representative time course curve of ECAR of HSVSMCs from non-diabetic patients treated with thrombin (1 U/mL) +/− trametinib (10 nM) and untreated control from non-diabetic patients. **Lower panel:** comparative analysis of normalised peak ECAR between treatment groups and untreated control at basal glycolysis, and after addition of inhibitors of mitochondrial respiration and the uncoupler. Normalised data are presented as mean ± SEM from $n = 4$ biological replicates using HSVSMC samples from different non-diabetic patients. (**C**) Comparison of normalised peak ECAR of unstimulated and thrombin-stimulated HSVSMCs from T2DM patients versus non-diabetic control. Normalised data are presented as mean ± SEM and statistical significance was assessed using an independent *t*-test, $n = 4$ biological replicates using HSVSMC samples from different T2DM and non-diabetic patients. In the lower panels of Figure 12 (**A**,**B**), normalised data from different treatment conditions were compared with data from the normalised untreated control. Statistical significance was assessed using an independent *t*-test and both one-way and two-way ANOVA, followed by Dunnett's and Holm–Šidák's post hoc tests to determine significant differences between means. * $p < 0.05$; ** $p < 0.01$. ns: not significant; A: resting ECAR; B: oligomycin-induced ECAR; C: ECAR response to uncoupling; D: non-mitochondrial ECAR; ECAR: extracellular acidification rate.

https://doi.org/10.3390/cells15151402

3.10. mtDNA Expression in HSVSMCs from T2DM and Non-Diabetic Patients After Treatment with Ang II and Thrombin +/− Trametinib

Ang II caused a significant increase in the OCR of HSVSMCs from T2DM at maximal respiration ($p < 0.05$ versus HSVSMCs from non-diabetic patients, $n = 4$; Figure 8C). Also, the OCR of HSVSMCs from T2DM patients, but not from non-diabetic patients, was significantly increased by thrombin (Figure 11). It was therefore important to determine whether this could be explained by an increase in mitochondria number in response to stimulation by Ang II and thrombin. Therefore, the expression of the mitochondrially encoded gene for COI after treatment with Ang II and thrombin +/− trametinib was determined using qPCR [35,36].

As shown in Figure 13A, there was no significant difference in mtDNA expression in HSVSMCs from T2DM patients after treatment with Ang II +/− trametinib compared with the untreated control. Also, in the HSVSMCs from non-diabetic patients, there was no significant difference in mtDNA expression after treatment with Ang II+/− trametinib compared with the untreated control (Figure 13B). Comparison between HSVSMCs from T2DM patients versus the non-diabetic control treated with Ang II +/− trametinib showed no significant difference (Figure 13C). As shown in Figure 13D, there was no significant difference in mtDNA expression in HSVSMCs from T2DM patients after treatment with thrombin +/− trametinib compared with the untreated control. There was also no significant difference in mtDNA expression in HSVSMCs from non-diabetic patients after treatment with thrombin +/− trametinib compared with the untreated control (Figure 13E). Also, comparison between HSVSMCs from T2DM patients versus the non-diabetic control treated with thrombin +/− trametinib showed no significant difference (Figure 13F).

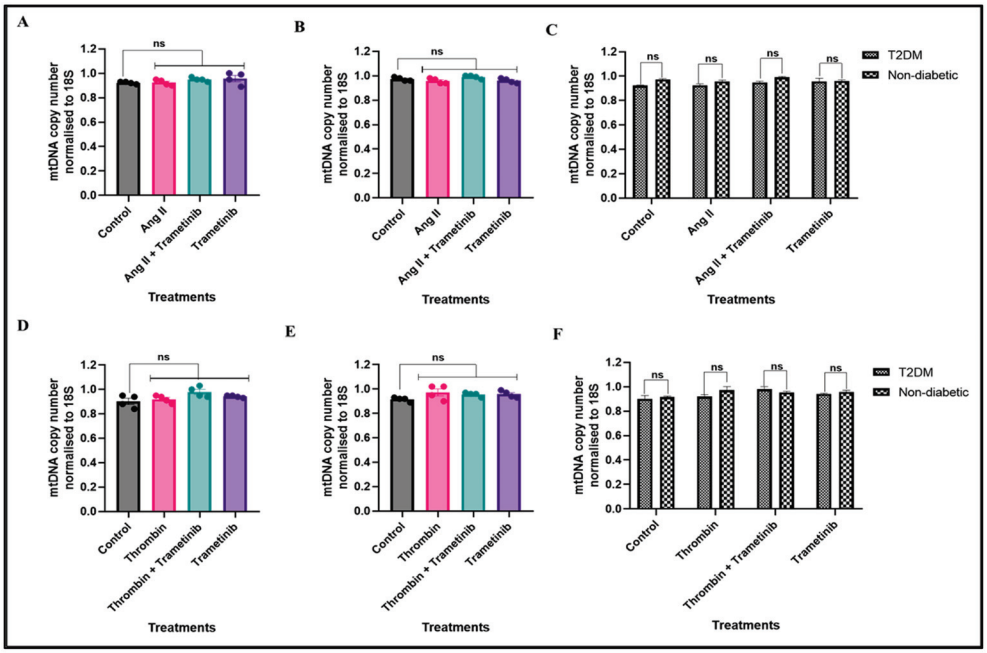


Figure 13. mtDNA expression in HSVSMCs from T2DM and non-diabetic patients after treatment with Ang II and thrombin +/− trametinib. mtDNA expression of the mitochondrially encoded gene for COI as a marker of mtDNA expression in response to stimulation by Ang II and thrombin. **Top panel:** (**A**) T2DM patients, (**B**) non-diabetic patients, and (**C**) comparison between T2DM patients versus non-diabetic control treated with Ang II (100 nM) +/− trametinib (10 nM). **Bottom Panel:** (**D**) T2DM patients, (**E**) non-diabetic patients, and (**F**) comparison between T2DM patients versus non-diabetic control treated with thrombin (1 U/mL) +/− trametinib (10 nM). All data were normalised

to 18S, and normalised data from different treatment conditions were compared with data from the normalised untreated control for statistical difference. Data are presented as mean ± SEM from n = 4 experiments using HSVSMC from different patients. Statistical significance was assessed using an independent t-test and both one-way and two-way ANOVA, followed by Dunnett's and Holm–Šidák's post hoc tests to determine significant differences between means. ns: not significant; Ang II: Angiotensin II.

4. Discussion

VSMCs have garnered attention as a possible target to treat vascular pathologies due to their role in neointima hyperplasia (NIH) and venous graft stenosis [39–42]. More so, HSV wall thickening is caused by the HSVSMCs shifting from a differentiated to a dedifferentiated phenotype, resulting in uncontrolled cell migration and proliferation responsible for long-term VGF [43]. The rate of VGF after 10 years is about 50% and is suggested to be worse (70%) in T2DM patients [44,45]. Furthermore, it has been established that VSMCs from T2DM patients exhibit unique functional characteristics and are more migratory than those of non-diabetic controls [5,6]. Additionally, there is evidence that T2DM triggers changes in the mitochondrial function of VSMCs of mice [46]. However, for HSVSMCs—important cells linked to the vascular dysfunction causing saphenous VGF—the effects of T2DM on the mitochondrial function and potential downstream signalling mechanisms that regulate these processes are unknown. Hence, our findings have highlighted some of the downstream signalling pathways that are involved in regulating these mitochondrial functions alongside possible effects of T2DM on these functions.

While it is well established that the levels and activities of proinflammatory cytokines such as IL-6 are increased in T2DM [47], the exact impact on mitochondrial OCR and ECAR in VSMCs—and, specifically, HSVSMCs—is unclear. Our study has now shown that IL-6/sIL-6Rα increases mitochondrial respiration through the JAK/STAT pathway, as the IL-6/sIL-6Rα-induced increase in the OCR of HSVSMCs from T2DM but not non-diabetic patients was abolished by JAK1/2-selective inhibitor ruxolitinib (Figure 2). Ruxolitinib also caused a reduction in the basal OCR of HSVSMCs from both T2DM and non-diabetic patients (Figure 2). The JAK/STAT pathway is an emerging target in inflammation, a major feature of cardiovascular diseases. Hence, anti-inflammatory drugs are increasingly being considered in the management of cardiovascular events, including those resulting from vascular dysfunction [48]. For instance, current available treatments for pulmonary hypertension (PH), which is caused by remodelling of the pulmonary arteries marked by endothelial dysfunction and proliferation of smooth muscle cells, are vasodilatory drugs, which do not stop disease progression [48]. It has been well demonstrated that the JAK/STAT molecular pathway plays an essential role in the vascular remodelling linked to pulmonary hypertension [49]. Interestingly, our results showed that stimulation of HSVSMCs with IL-6/sIL-6Rα did not significantly modify the ECAR of HSVSMCs from either T2DM or non-diabetic patients, suggesting that glycolysis is unaffected by the JAK/STAT pathway. The reason for this is still unclear; however, it has been shown that IL-6/sIL-6Rα shifted the control for ATP synthesis towards processes that generate the mitochondrial membrane potential [50]. This suggests that IL-6/sIL-6Rα induces a metabolic state where cellular functions are limited by the mitochondrial energy supply, limiting the conversion of glucose to lactate, which determines ECAR [50]. However, it is important to acknowledge that ECAR in this assay is not a pure or calibrated readout of glycolytic flux. Nonetheless, it remains a valid indicator of the compensatory metabolic response to mitochondrial perturbation. The differences in ECAR dynamics observed therefore likely reflect underlying alterations in metabolic plasticity; specifically, the capacity to shift between oxidative and glycolytic ATP production in cells from patients with diabetes.

https://doi.org/10.3390/cells15151402

Similarly, PDGF-BB increased the OCR of HSVSMCs from T2DM patients at basal and maximal respiration and these were again both abolished by ruxolitinib (Figure 4), which suggests that the modulation of mitochondrial respiration by PDGF-BB is also JAK 1/2-dependent. Conversely, there was no significant increase in the OCR of HSVSMCs from non-diabetic subjects in response to PDGF-BB (Figure 4). Also, in both HSVSMCs from T2DM and non-diabetic patients, ruxolitinib caused a significant reduction in the basal and PDGF-stimulated OCR under all conditions (Figure 4). The importance of mitochondrial metabolism as a key regulator of cell growth and proliferation is becoming increasingly appreciated [51]. Increased glycolysis and glutamine usage are seen in rapidly dividing cells, which contribute to the production of energy, reducing equivalents, and the carbon and nitrogen building blocks necessary for daughter cell synthesis [51]. Growth factors like PDGF have been found to boost glycolysis and mitochondrial activity in rat aortic VSMCs [52]. Additionally, studies on pre-clinical models and human pulmonary arterial SMCs have demonstrated that VSMCs have greater rates of glycolysis [53,54]. These studies also indicated a role for mitochondrial fission in pulmonary arterial SMC proliferation, with pulmonary arterial SMC mitochondria in cellular and pre-clinical pulmonary arterial hypertension (PAH) models found to be dysmorphic and hyperpolarised [53,54]. While little is known about how mitochondrial structure controls the phenotypic and metabolic properties of HSVSMCs, it has been demonstrated that such changes in mitochondrial morphology have a direct impact on cell differentiation and proliferation of rat aortic SMCs [55,56]. Furthermore, despite numerous studies that have linked PDGF to vascular dysfunction [56–60], a role for PDGF in mitochondrial respiration and its metabolic components has not yet been investigated in HSVSMCs. The significance of our findings is highlighted by the discovery that PDGF-BB can control mitochondrial respiration in HSVSMCs via the JAK/STAT pathway, which is less well-known for PDGF's downstream activity than other pathways such as ERK1,2 and Akt [61].

Conversely, ruxolitinib reduced ECAR in HSVSMCs from both T2DM and non-diabetic patients (Figures 3 and 4) and also abolished the PDGF-BB-induced increase in ECAR in HSVSMCs from T2DM patients (Figure 4). These findings suggest a JAK-mediated modulation of mitochondrial glycolysis of HSVSMCs. The JAK/STAT pathway is an established therapeutic target for immune and inflammatory conditions that promote several CVDs [48]. Furthermore, emerging findings have suggested that patients with PAH of different types have pulmonary arteries with overactive JAK/STAT pathways [49,62]. Additionally, several cytokines, including IL-6, IL-13, and IL-11, as well as growth factors, including PDGF, VEGF, and TGFβ1, activate the JAK/STAT pathway and trigger pulmonary remodelling, which contributes to the onset of PAH [49]. Therefore, targeting the cellular signalling pathways implicated in vascular dysfunction to prevent vascular remodelling may also be a viable option for preventing VGF.

Furthermore, our results showed that Ang II did not cause any noticeable alteration in OCR of HSVSMCs from both T2DM and non-diabetic patients. However, trametinib reduced OCR at basal and maximal respiration of HSVSMCs from both T2DM and non-diabetic patients (Figure 8). This suggests that mitochondrial respiration can be modulated through the ERK1,2 signalling pathway. Furthermore, the OCR of HSVSMCs from T2DM and non-diabetic patients did not significantly differ from each other in either the absence or presence of Ang II (Figure 8). While we have described this in HSVSMCs for the first time, it was previously demonstrated that Ang II caused a reduction in the OCR of HUVECs [63]. In this study [63], it was shown that Ang II reduced OCR at basal and maximal respiration compared with the control group. The explanation for this is unclear at this time.

In addition, the ERK1,2 pathway can indirectly modulate cellular metabolic homeostasis through tumour-suppressor liver kinase B1-induced activation of AMPK, a crucial regu-

lator of energy homeostasis, under low-energy situations in most cellular contexts [64,65]. When activated, AMPK blocks most of the biosynthetic pathways required for cell growth, reducing ATP utilisation, and activates catabolic pathways that produce ATP, enabling cells to restore energy equilibrium [65]. Furthermore, it has been shown that Ang II decreased the OCR of mitochondria isolated from the kidney cortex of both non-diabetic controls and type 1 diabetic rats via AT2 receptor-mediated nitric oxide release [66]. It was further demonstrated in this study that whereas Ang II increases the OCR at mitochondria leak respiration in diabetic animals via AT1 receptors, AT1 receptors do not influence mitochondria function in control mice [66]. Together, these findings suggest that while Ang II can elicit its effects on mitochondrial function activity through multiple signalling pathways, in the current study we have looked specifically at the effect of Ang II as a known activator of ERK1,2 signalling in HSVSMCs, where it did not cause any significant alteration in the OCR in cells from T2DM or non-diabetic patients. Also, while there were no significant alterations in the ECAR of HSVSMCs from both T2DM and non-diabetic patients after stimulation with Ang II, trametinib caused a significant reduction in ECAR in HSVSMCs from both T2DM and non-diabetic patients (Figure 10).

We also found that thrombin significantly increased the OCR in HSVSMCs from T2DM but not non-diabetic patients, and that this was attenuated by trametinib (Figure 13). Direct comparison of the OCR of HSVSMCs from T2DM and non-diabetic patients revealed that thrombin significantly increased the OCR of HSVSMCs from T2DM patients compared to non-diabetic control subjects at maximal glycolysis and spare capacity (Figure 11). In addition, trametinib reduced basal OCR in HSVSMCs from both T2DM and non-diabetic patients (Figure 11). Previous findings have revealed that thrombin triggered a significant rise in OCR in platelets [67,68]. While these two studies used platelets from healthy donors [67,68], similar studies using unstimulated platelets from T2DM patients indicated reduced OCR when compared with those from healthy donors [69]. We have now demonstrated an increase in the OCR of HSVSMCs from T2DM patients, but not non-diabetic patients, following thrombin stimulation. The fact that trametinib attenuated this increase in OCR suggests that thrombin elicited its effect through the ERK1,2 pathway, although the underlying mechanism is not entirely clear.

Trametinib, the MEK1/2 inhibitor employed in this study not only abolished the thrombin-induced increase in the OCR of HSVSMCs from T2DM patients but also reduced the OCR of HSVSMCs from both T2DM and non-diabetic patients. Trametinib binds to unphosphorylated MEK1/2 preferentially, blocking Raf-dependent phosphorylation and activation of MEK [70]. While it might be premature to assume that the ability of trametinib to abolish the MEK-mediated increase in OCR in HSVSMCs from T2DM patients would be of any clinical benefit, trametinib used alone or in combination with B-Raf inhibitor dabrafenib is, however, a clinical tool used to manage malignant melanoma driven by constitutively active Val600Glu- and Val600Lys-mutated B-Raf [71]. Dabrafenib binds the ATP binding site of the mutated B-Raf protein, specifically the Val600Glu mutation. This inhibits the kinase activity of B-Raf and ultimately ERK1,2, resulting in programmed cell death [72].

It has long been recognised that mitochondrial dysfunction contributes significantly to the underlying pathogenesis of a number of age-related diseases, including cancers, CVDs and neurodegenerative diseases [73–75]. Hence, mtDNA expression is increasingly used to evaluate the role of mitochondria in diseases as its measurement is a straightforward proxy for mitochondrial function [73,74]. Furthermore, mtDNA expression levels offer direct insights into a cell's metabolic activity, energy generation capacity, and general mitochondrial health because it encodes crucial protein subunits for the respiratory chain [73,74]. Additionally, mtDNA expression provides an opportunity to determine changes not only

in disease conditions but also as a genetic marker [73]. In this study, we used mtDNA expression to investigate whether the observed alterations in OCR and ECAR detected in HSVSMCs from T2DM patients after the activation of the JAK/STAT and the MAPK/ERK signalling pathways were caused by an increase in mtDNA expression or by other factors that are unknown but may be related to T2DM. From our findings, there were no significant changes in mtDNA expression after treatment with the different treatment conditions, and when compared between T2DM patients and non-T2DM controls (Figures 6 and 13). These data therefore suggest that the observed changes in OCR relate to increased metabolic activity by the mitochondria. Therefore, while it is not entirely clear, the observed increase in OCR and ECAR in HSVSMCs from T2DM patients and not from non-diabetic controls could be due to the T2DM status. However, while mtDNA expression, the proxy we used in this study, is very useful as an indicator of mitochondrial function, we acknowledge that determining the mtDNA copy number would have been more appropriate [76]. This is because mitochondria are capable of producing an excess of transcripts that are controlled and maintained post-transcriptionally, and often RNA levels and final protein output do not always correlate [77].

In summary, understanding any link between T2DM and compromised vascular function, specifically in autologous saphenous veins used as conduits in bypass surgery in T2DM patients, is critical to improving vein graft patency and patient outcomes. Our study has identified downstream signalling pathways that regulate mitochondrial function in HSVSMCs and described how T2DM may modify these functions. The significance of these findings lies in the fact that proliferation and migration of vascular cells, including SMCs, have been linked to vascular remodelling and restenosis responsible for VGF. Furthermore, SMCs from T2DM patients have been shown to be more migratory than those from non-diabetic patients [5,6]. Taken together, because increased oxygen and enhanced glycolysis are required to generate more ATP to drive these cellular processes, identifying the pathways through which this can be effectively modulated is significant for the development of novel therapeutic opportunities to limit vein graft failure. Given the clinical relevance of our findings and the potential for the identified pathways to be targets to improve vein graft potency, we acknowledge that further investigations will be required to strengthen these initial findings. For example, determining whether these variations result from modified receptor expression, increased STAT3 or ERK1/2 activation, modifications to mitochondrial priming, or other metabolic adaptations linked to diabetes would be useful. Furthermore, investigating potential downstream mediators of mitochondrial regulation, such as mitochondrial STAT3, as well as changes in ATP synthesis, electron transport chain activity, and mitochondrial membrane potential, would be useful to establish the MAPK/ERK1,2 and JAK/STAT signalling pathways as key targets to enhance vein graft patency.

5. Conclusions

Through this study, we have demonstrated a JAK- and MEK-mediated regulation of mitochondrial function (OCR and ECAR) alongside a possible effect of T2DM on these processes in HSVSMCs—key cells implicated in the vascular dysfunction that is responsible for VGF. Our findings have therefore contributed to the body of knowledge identifying possible novel glucose-dependent alterations that cause vascular dysfunction in T2DM patients. These findings therefore offer a background and rationale for future investigations to develop novel therapies to improve vein graft patency.

Supplementary Materials: The following supporting information can be downloaded at: https://www.mdpi.com/article/10.3390/cells15151402/s1, Table S1: Materials; Table S2: Patients' characteristics with medication history and sample ID number.

Author Contributions: Conceptualization, I.O.B., F.T.M., K.R.-S., R.G.S. and T.M.P.; methodology, I.O.B., F.T.M., G.A.D., J.P.H., M.L., K.R.-S., R.G.S. and T.M.P.; software, I.O.B., F.T.M., K.R.-S. and T.M.P.; validation, I.O.B., F.T.M., K.R.-S., R.G.S. and T.M.P.; formal analysis, I.O.B., F.T.M., K.R.-S. and T.M.P.; investigation, I.O.B., F.T.M., G.A.D., J.P.H., M.L., K.R.-S., R.G.S. and T.M.P.; resources, I.O.B., F.T.M., J.P.H., M.L. and T.M.P.; data curation, I.O.B., F.T.M., G.A.D., J.P.H. and T.M.P.; writing—original draft preparation, I.O.B., F.T.M. and T.M.P.; writing—review and editing, I.O.B., F.T.M., K.R.-S., R.G.S. and T.M.P.; visualization, I.O.B. and F.T.M.; supervision, M.L., K.R.-S., R.G.S. and T.M.P.; project administration, I.O.B. and T.M.P.; funding acquisition, I.O.B., F.T.M. and T.M.P. All authors have read and agreed to the published version of the manuscript.

Funding: Research in TMP's laboratory was supported by the Hull and East Riding Cardiac Trust Fund. IOB received scholarships from the Tertiary Education Trust Fund (TETFund) and University of Benin, Nigeria, and the Hull York Medical School, University of Hull, UK. FTM was supported by a University of Botswana PhD scholarship.

Institutional Review Board Statement: The study was conducted in accordance with the Declaration of Helsinki and approved by UK Health Research Authority ethical approval (protocol code NHS REC:15/NE/0138 and approval date 31 March 2019).

Informed Consent Statement: Written informed consent was obtained from all subjects involved in the study.

Data Availability Statement: Data will be made available upon request.

Conflicts of Interest: The authors declare no conflicts of interest.

Abbreviations

The following abbreviations are used in this manuscript:

AMPK	Adenosine monophosphate-activated protein kinase
Ang II	Angiotensin II
AT1	Angiotensin 1 receptor
AT2	Angiotensin 2 receptor
ATP	Adenosine triphosphate
BCA	Bicinchoninic acid
BSA	Bovine serum albumin
CABG	Coronary artery bypass graft
CAD	Coronary artery disease
CVD	Cardiovascular disease
DMEM	Dulbecco's modified Eagle medium
DMSO	Dimethyl sulfoxide
DNA	Deoxyribonucleic acid
DPBS	Dulbecco's phosphate-buffered saline
ECAR	Extracellular acidification rate
EDTA	Ethylenediaminetetraacetic acid
ERK	Extracellular signal-regulated kinase
FCCP	Carbonyl cyanide p-(trifluoromethoxy)phenylhydrazone
GAPDH	Glyceraldehyde-3-phosphate dehydrogenase
HSVSMC	Human saphenous vein smooth muscle cell
HUVEC	Human umbilical vein endothelial cell; IL-6, interleukin-6
JAK	Janus kinase
MAPK	Mitogen-activated protein kinase
NAD	Nicotinamide adenine dinucleotide
NIH	Neointimal hyperplasia
NOS	Nitric oxide synthase
OCR	Oxygen consumption rate
PAH	Pulmonary arterial hypertension

PBS	Phosphate-buffered saline
PBST	Phosphate-buffered saline with Tween® detergent
PDGF	Platelet-derived growth factor
PH	Pulmonary hypertension
sIL-6Ra	Soluble interleukin-6 receptor
STAT	Signal transducer and activator of transcription
T2DM	Type 2 diabetes mellitus
TGF	Transforming growth factor
VEC	Vascular endothelial cell
VGF	Vein graft failure
VSMC	Vascular smooth muscle cell

References

1. Yang, X.; Qian, K. Protein O-GlcNAcylation: Emerging mechanisms and functions. *Nat. Rev. Mol. Cell Biol.* **2017**, *18*, 452–465. [CrossRef] [PubMed]
2. Bolanle, I.O.; Riches-Suman, K.; Loubani, M.; Williamson, R.; Palmer, T.M. Revascularisation of type 2 diabetics with coronary artery disease: Insights and therapeutic targeting of O-GlcNAcylation. *Nutr. Metab. Cardiovasc. Dis.* **2021**, *31*, 1349–1356. [PubMed]
3. Bolanle, I.O.; Riches-Suman, K.; Williamson, R.; Palmer, T.M. Emerging roles of protein O-GlcNAcylation in cardiovascular diseases: Insights and novel therapeutic targets. *Pharmacol. Res.* **2021**, *165*, 105467. [PubMed]
4. Bolanle, I.O.; Palmer, T.M. *O*-GlcNAcylation and Phosphorylation Crosstalk in Vascular Smooth Muscle Cells: Cellular and Therapeutic Significance in Cardiac and Vascular Pathologies. *Int. J. Mol. Sci.* **2025**, *26*, 3303. [CrossRef] [PubMed]
5. Madi, H.A.; Riches, K.; Warburton, P.; O'Regan, D.J.; Turner, N.A.; Porter, K.E. Inherent differences in morphology, proliferation, and migration in saphenous vein smooth muscle cells cultured from nondiabetic and Type 2 diabetic patients. *Am. J. Physiol. Cell Physiol.* **2009**, *297*, C1307–C1317. [CrossRef] [PubMed]
6. Riches-Suman, K.; Hussain, A. Identifying and targeting the molecular signature of smooth muscle cells undergoing early vascular ageing. *Biochim. Biophys. Acta Mol. Basis Dis.* **2022**, *1868*, 166403. [CrossRef] [PubMed]
7. Pinti, M.V.; Fink, G.K.; Hathaway, Q.A.; Durr, A.J.; Kunovac, A.; Hollander, J.M. Mitochondrial dysfunction in type 2 diabetes mellitus: An organ-based analysis. *Am. J. Physiol. Endocrinol. Metab.* **2019**, *316*, E268–E285. [CrossRef] [PubMed]
8. Boroughs, L.K.; DeBerardinis, R.J. Metabolic pathways promoting cancer cell survival and growth. *Nat. Cell Biol.* **2015**, *17*, 351–359. [CrossRef] [PubMed]
9. Fang, Y.H.; Piao, L.; Hong, Z.; Toth, P.T.; Marsboom, G.; Bache-Wiig, P.; Rehman, J.; Archer, S.L. Therapeutic inhibition of fatty acid oxidation in right ventricular hypertrophy: Exploiting Randle's cycle. *J. Mol. Med.* **2012**, *90*, 31–43. [PubMed]
10. Caruso, P.; Dunmore, B.J.; Schlosser, K.; Schoors, S.; Dos Santos, C.; Perez-Iratxeta, C.; Lavoie, J.R.; Zhang, H.; Long, L.; Flockton, A.R.; et al. Identification of MicroRNA-124 as a Major Regulator of Enhanced Endothelial Cell Glycolysis in Pulmonary Arterial Hypertension via PTBP1 (Polypyrimidine Tract Binding Protein) and Pyruvate Kinase M2. *Circulation* **2017**, *136*, 2451–2467. [CrossRef] [PubMed]
11. Aibibula, M.; Naseem, K.M.; Sturmey, R.G. Glucose metabolism and metabolic flexibility in blood platelets. *J. Thromb. Haemost.* **2018**, *16*, 2300–2314. [CrossRef] [PubMed]
12. Al-Mehdi, A.B.; Pastukh, V.M.; Swiger, B.M.; Reed, D.J.; Patel, M.R.; Bardwell, G.C.; Pastukh, V.V.; Alexeyev, M.F.; Gillespie, M.N. Perinuclear mitochondrial clustering creates an oxidant-rich nuclear domain required for hypoxia-induced transcription. *Sci. Signal.* **2012**, *5*, ra47. [CrossRef] [PubMed]
13. Coutelle, O.; Hornig-Do, H.T.; Witt, A.; Andree, M.; Schiffmann, L.M.; Piekarek, M.; Brinkmann, K.; Seeger, J.M.; Liwschitz, M.; Miwa, S.; et al. Embelin inhibits endothelial mitochondrial respiration and impairs neoangiogenesis during tumor growth and wound healing. *EMBO Mol. Med.* **2014**, *6*, 624–639. [CrossRef] [PubMed]
14. Brinster, R.L. Nutrition and metabolism of the ovum, zygote and blastocyst. In *Handbook of Physiology*; American Physiological Society (APS): Washington DC, USA, 1973; Volume 11, pp. 165–185.
15. Sturmey, R.G.; Leese, H.J. Energy metabolism in pig oocytes and early embryos. *Reproduction* **2003**, *126*, 197–204. [CrossRef] [PubMed]
16. Leese, H.J.; Guerif, F.; Allgar, V.; Brison, D.R.; Lundin, K.; Sturmey, R.G. Biological optimization, the Goldilocks principle, and how much is lagom in the preimplantation embryo. *Mol. Reprod. Dev.* **2016**, *83*, 748–754. [CrossRef] [PubMed]
17. Plitzko, B.; Loesgen, S. Measurement of Oxygen Consumption Rate (OCR) and Extracellular Acidification Rate (ECAR) in Culture Cells for Assessment of the Energy Metabolism. *Bio Protoc.* **2018**, *8*, e2850. [CrossRef] [PubMed]

18. Yetkin-Arik, B.; Vogels, I.M.C.; Nowak-Sliwinska, P.; Weiss, A.; Houtkooper, R.H.; Van Noorden, C.J.F.; Klaassen, I.; Schlingemann, R.O. The role of glycolysis and mitochondrial respiration in the formation and functioning of endothelial tip cells during angiogenesis. *Sci. Rep.* **2019**, *9*, 12608. [CrossRef] [PubMed]
19. Ferrick, D.A.; Neilson, A.; Beeson, C. Advances in measuring cellular bioenergetics using extracellular flux. *Drug Discov. Today* **2008**, *13*, 268–274. [CrossRef] [PubMed]
20. Abid, H.; Ryan, Z.C.; Delmotte, P.; Sieck, G.C.; Lanza, I.R. Extramyocellular interleukin-6 influences skeletal muscle mitochondrial physiology through canonical JAK/STAT signaling pathways. *FASEB J.* **2020**, *34*, 14458–14472. [CrossRef] [PubMed]
21. Cao, R.; Tian, H.; Zhang, Y.; Liu, G.; Xu, H.; Rao, G.; Tian, Y.; Fu, X. Signaling pathways and intervention for therapy of type 2 diabetes mellitus. *MedComm* **2023**, *4*, e283. [CrossRef] [PubMed]
22. Zhao, C.; Wang, Z.; Chen, L.; Xu, Y.; Sun, X.; Tu, K.; Lv, L.; Xue, G. Arctigenin ameliorates neointima formation induced by vascular injury by inhibiting inflammatory response and proliferation through the IL-6/JAK2/STAT3 pathway. *Mol. Cell. Biochem.* **2026**, *481*, 1355–1367. [CrossRef] [PubMed]
23. Song, H.T.; Cui, Y.; Zhang, L.L.; Cao, G.; Li, L.; Li, G.; Jia, X.J. Ruxolitinib attenuates intimal hyperplasia via inhibiting JAK2/STAT3 signaling pathway activation induced by PDGF-BB in vascular smooth muscle cells. *Microvasc. Res.* **2020**, *132*, 104060. [CrossRef] [PubMed]
24. Pinzar, E.; Wang, T.; Garrido, M.R.; Xu, W.; Levy, P.; Bottari, S.P. Angiotensin II induces tyrosine nitration and activation of ERK1/2 in vascular smooth muscle cells. *FEBS Lett.* **2005**, *579*, 5100–5104. [CrossRef] [PubMed]
25. Hsieh, H.L.; Tung, W.H.; Wu, C.Y.; Wang, H.H.; Lin, C.C.; Wang, T.S.; Yang, C.M. Thrombin induces EGF receptor expression and cell proliferation via a PKC(δ)/c-Src-dependent pathway in vascular smooth muscle cells. *Arterioscler. Thromb. Vasc. Biol.* **2009**, *29*, 1594–1601. [CrossRef] [PubMed]
26. Yusuf, S.; Zucker, D.; Passamani, E.; Peduzzi, P.; Takaro, T.; Fisher, L.; Kennedy, J.; Davis, K.; Killip, T.; Norris, R.; et al. Effect of coronary artery bypass graft surgery on survival: Overview of 10-year results from randomised trials by the Coronary Artery Bypass Graft Surgery Trialists Collaboration. *Lancet* **1994**, *344*, 563–570. [CrossRef] [PubMed]
27. National Health Service (NHS) Inform. Coronary Heart Bypass Graft. 2020. Available online: https://www.nhsinform.scot/tests-and-treatments/surgical-procedures/coronary-artery-bypass-graft (accessed on 25 June 2023).
28. Motwani, J.G.; Topol, E.J. Aortocoronary saphenous vein graft disease: Pathogenesis, predisposition, and prevention. *Circulation* **1998**, *97*, 916–931. [CrossRef] [PubMed]
29. Resneck, J.S., Jr. Revisions to the Declaration of Helsinki on Its 60th Anniversary: A Modernized Set of Ethical Principles to Promote and Ensure Respect for Participants in a Rapidly Innovating Medical Research Ecosystem. *JAMA* **2025**, *333*, 15–17. [CrossRef] [PubMed]
30. Riches, K.; Alshanwani, A.R.; Warburton, P.; O'Regan, D.J.; Ball, S.G.; Wood, I.C.; Turner, N.A.; Porter, K.E. Elevated expression levels of miR-143/5 in saphenous vein smooth muscle cells from patients with Type 2 diabetes drive persistent changes in phenotype and function. *J. Mol. Cell. Cardiol.* **2014**, *74*, 240–250. [CrossRef] [PubMed]
31. Bolanle, I.O.; Durham, G.A.; Hobkirk, J.P.; Loubani, M.; Sturmey, R.G.; Palmer, T.M. Do T2DM and Hyperglycaemia Affect the Expression Levels of the Regulating Enzymes of Cellular O-GlcNAcylation in Human Saphenous Vein Smooth Muscle Cells? *Diabetology* **2024**, *5*, 162–177. [CrossRef]
32. Fetter, T.; Smith, P.; Guel, T.; Braegelmann, C.; Bieber, T.; Wenzel, J. Selective Janus Kinase 1 Inhibition Is a Promising Therapeutic Approach for Lupus Erythematosus Skin Lesions. *Front. Immunol.* **2020**, *11*, 344. [CrossRef] [PubMed]
33. Cheng, Y.; Tian, H. Current Development Status of MEK Inhibitors. *Molecules* **2017**, *22*, 1551. [CrossRef] [PubMed]
34. Muller, B.; Lewis, N.; Adeniyi, T.; Leese, H.J.; Brison, D.R.; Sturmey, R.G. Application of extracellular flux analysis for determining mitochondrial function in mammalian oocytes and early embryos. *Sci. Rep.* **2019**, *9*, 16778. [CrossRef] [PubMed]
35. Hebert, P.D.; Cywinska, A.; Ball, S.L.; deWaard, J.R. Biological identifications through DNA barcodes. *Proc. R. Soc. Lond. Ser. B* **2003**, *270*, 313–321. [CrossRef] [PubMed]
36. Rodrigues, M.S.; Morelli, K.A.; Jansen, A.M. Cytochrome c oxidase subunit 1 gene as a DNA barcode for discriminating Trypanosoma cruzi DTUs and closely related species. *Parasites Vectors* **2017**, *10*, 488. [CrossRef] [PubMed]
37. Yaghini, F.A.; Song, C.Y.; Lavrentyev, E.N.; Ghafoor, H.U.; Fang, X.R.; Estes, A.M.; Campbell, W.B.; Malik, K.U. Angiotensin II-induced vascular smooth muscle cell migration and growth are mediated by cytochrome P450 1B1-dependent superoxide generation. *Hypertension* **2010**, *55*, 1461–1467. [CrossRef] [PubMed]
38. Mookerjee, S.A.; Brand, M.D. Measurement and Analysis of Extracellular Acid Production to Determine Glycolytic Rate. *J. Vis. Exp.* **2015**, *106*, e53464.
39. Ortiz-Muñoz, G.; Martin-Ventura, J.L.; Hernandez-Vargas, P.; Mallavia, B.; Lopez-Parra, V.; Lopez-Franco, O.; Muñoz-Garcia, B.; Fernandez-Vizarra, P.; Ortega, L.; Egido, J.; et al. Suppressors of cytokine signaling modulate JAK/STAT-mediated cell responses during atherosclerosis. *Arterioscler. Thromb. Vasc. Biol.* **2009**, *29*, 525–531. [CrossRef] [PubMed]

40. Xiang, S.; Dong, N.G.; Liu, J.P.; Wang, Y.; Shi, J.W.; Wei, Z.J.; Hu, X.J.; Gong, L. Inhibitory effects of suppressor of cytokine signaling 3 on inflammatory cytokine expression and migration and proliferation of IL-6/IFN-γ-induced vascular smooth muscle cells. *J. Huazhong Univ. Sci. Technol. Med. Sci.* **2013**, *33*, 615–622. [CrossRef] [PubMed]
41. Xiang, S.; Liu, J.; Dong, N.; Shi, J.; Xiao, Y.; Wang, Y.; Hu, X.; Gong, L.; Wang, W. Suppressor of cytokine signaling 3 is a negative regulator for neointimal hyperplasia of vein graft stenosis. *J. Vasc. Res.* **2014**, *51*, 132–143. [CrossRef] [PubMed]
42. Wang, D.; Uhrin, P.; Mocan, A.; Waltenberger, B.; Breuss, J.M.; Tewari, D.; Mihaly-Bison, J.; Huminiecki, Ł.; Starzyński, R.R.; Tzvetkov, N.T.; et al. Vascular smooth muscle cell proliferation as a therapeutic target. Part 1: Molecular targets and pathways. *Biotechnol. Adv.* **2018**, *36*, 1586–1607. [CrossRef] [PubMed]
43. Miano, J.M.; Cserjesi, P.; Ligon, K.L.; Periasamy, M.; Olson, E.N. Smooth muscle myosin heavy chain exclusively marks the smooth muscle lineage during mouse embryogenesis. *Circ. Res.* **1994**, *75*, 803–812. [CrossRef] [PubMed]
44. Veith, F.J.; Gupta, S.K.; Ascer, E.; White-Flores, S.; Samson, R.H.; Scher, L.A.; Towne, J.B.; Bernhard, V.M.; Bonier, P.; Flinn, W.R.; et al. Six-year prospective multicenter randomized comparison of autologous saphenous vein and expanded polytetrafluoroethylene grafts in infrainguinal arterial reconstructions. *J. Vasc. Surg.* **1986**, *3*, 104–114. [CrossRef]
45. Fitzgibbon, G.M.; Kafka, H.P.; Leach, A.J.; Keon, W.J.; Hooper, G.D.; Burton, J.R. Coronary bypass graft fate and patient outcome: Angiographic follow-up of 5,065 grafts related to survival and reoperation in 1,388 patients during 25 years. *J. Am. Coll. Cardiol.* **1996**, *28*, 616–626. [CrossRef] [PubMed]
46. Koval, O.M.; Nguyen, E.K.; Mittauer, D.J.; Ait-Aissa, K.; Chinchankar, W.C.; Grumbach, I.M. Regulation of Smooth Muscle Cell Proliferation by Mitochondrial Ca2+ in Type 2 Diabetes. *Int. J. Mol. Sci.* **2023**, *24*, 12897. [CrossRef] [PubMed]
47. Akbari, M.; Hassan-Zadeh, V. IL-6 signalling pathways and the development of type 2 diabetes. *Inflammopharmacology* **2018**, *26*, 685–698. [CrossRef] [PubMed]
48. Baldini, C.; Moriconi, F.R.; Galimberti, S.; Libby, P.; De Caterina, R. The JAK-STAT pathway: An emerging target for cardiovascular disease in rheumatoid arthritis and myeloproliferative neoplasms. *Eur. Heart J.* **2021**, *42*, 4389–4400. [CrossRef] [PubMed]
49. Roger, I.; Milara, J.; Montero, P.; Cortijo, J. The Role of JAK/STAT Molecular Pathway in Vascular Remodeling Associated with Pulmonary Hypertension. *Int. J. Mol. Sci.* **2021**, *22*, 4980. [CrossRef] [PubMed]
50. Berthiaume, F.; MacDonald, A.D.; Kang, Y.H.; Yarmush, M.L. Control analysis of mitochondrial metabolism in intact hepatocytes: Effect of interleukin-1β and interleukin-6. *Metab. Eng.* **2003**, *5*, 108–123. [CrossRef] [PubMed]
51. Moncada, S.; Higgs, E.A.; Colombo, S.L. Fulfilling the metabolic requirements for cell proliferation. *Biochem. J.* **2012**, *446*, 1–7. [CrossRef] [PubMed]
52. Perez, J.; Hill, B.G.; Benavides, G.A.; Dranka, B.P.; Darley-Usmar, V.M. Role of cellular bioenergetics in smooth muscle cell proliferation induced by platelet-derived growth factor. *Biochem. J.* **2010**, *428*, 255–267. [CrossRef] [PubMed]
53. Marsboom, G.; Toth, P.T.; Ryan, J.J.; Hong, Z.; Wu, X.; Fang, Y.H.; Thenappan, T.; Piao, L.; Zhang, H.J.; Pogoriler, J.; et al. Dynamin-related protein 1-mediated mitochondrial mitotic fission permits hyperproliferation of vascular smooth muscle cells and offers a novel therapeutic target in pulmonary hypertension. *Circ. Res.* **2012**, *110*, 1484–1497. [CrossRef] [PubMed]
54. Bonnet, S.; Michelakis, E.D.; Porter, C.J.; Andrade-Navarro, M.A.; Thébaud, B.; Bonnet, S.; Haromy, A.; Harry, G.; Moudgil, R.; McMurtry, M.S.; et al. An abnormal mitochondrial-hypoxia inducible factor-1alpha-Kv channel pathway disrupts oxygen sensing and triggers pulmonary arterial hypertension in fawn hooded rats: Similarities to human pulmonary arterial hypertension. *Circulation* **2006**, *113*, 2630–2641. [CrossRef] [PubMed]
55. Mitra, K. Mitochondrial fission-fusion as an emerging key regulator of cell proliferation and differentiation. *Bioessays* **2013**, *35*, 955–964. [CrossRef] [PubMed]
56. Salabei, J.K.; Hill, B.G. Mitochondrial fission induced by platelet-derived growth factor regulates vascular smooth muscle cell bioenergetics and cell proliferation. *Redox Biol.* **2013**, *1*, 542–551. [CrossRef] [PubMed]
57. Hayashi, K.; Saga, H.; Chimori, Y.; Kimura, K.; Yamanaka, Y.; Sobue, K. Differentiated phenotype of smooth muscle cells depends on signaling pathways through insulin-like growth factors and phosphatidylinositol 3-kinase. *J. Biol. Chem.* **1998**, *273*, 28860–28867. [CrossRef] [PubMed]
58. Hayashi, K.; Shibata, K.; Morita, T.; Iwasaki, K.; Watanabe, M.; Sobue, K. Insulin receptor substrate-1/SHP-2 interaction, a phenotype-dependent switching machinery of insulin-like growth factor-I signaling in vascular smooth muscle cells. *J. Biol. Chem.* **2004**, *279*, 40807–40818. [CrossRef] [PubMed]
59. Wang, C.C.; Gurevich, I.; Draznin, B. Insulin affects vascular smooth muscle cell phenotype and migration via distinct signaling pathways. *Diabetes* **2003**, *52*, 2562–2569. [CrossRef] [PubMed]
60. Radhakrishnan, Y.; Busby, W.H., Jr.; Shen, X.; Maile, L.A.; Clemmons, D.R. Insulin-like growth factor-I-stimulated insulin receptor substrate-1 negatively regulates Src homology 2 domain-containing protein-tyrosine phosphatase substrate-1 function in vascular smooth muscle cells. *J. Biol. Chem.* **2010**, *285*, 15682–15695. [CrossRef] [PubMed]
61. Zhao, Y.; Biswas, S.K.; McNulty, P.H.; Kozak, M.; Jun, J.Y.; Segar, L. PDGF-induced vascular smooth muscle cell proliferation is associated with dysregulation of insulin receptor substrates. *Am. J. Physiol. Cell Physiol.* **2011**, *300*, C1375–C1385. [CrossRef] [PubMed]

62. Milara, J.; Ballester, B.; Morell, A.; Ortiz, J.L.; Escrivá, J.; Fernández, E.; Perez-Vizcaino, F.; Cogolludo, A.; Pastor, E.; Artigues, E.; et al. JAK2 mediates lung fibrosis, pulmonary vascular remodelling and hypertension in idiopathic pulmonary fibrosis: An experimental study. *Thorax* **2018**, *73*, 519–529. [CrossRef] [PubMed]
63. Chang, Y.; Li, Y.; Ye, N.; Guo, X.; Li, Z.; Sun, G.; Sun, Y. Atorvastatin protects the proliferative ability of human umbilical vein endothelial cells inhibited by angiotensin II by changing mitochondrial energy metabolism. *Int. J. Mol. Med.* **2018**, *41*, 33–42. [CrossRef] [PubMed]
64. Papa, S.; Choy, P.M.; Bubici, C. The ERK and JNK pathways in the regulation of metabolic reprogramming. *Oncogene* **2019**, *38*, 2223–2240. [CrossRef] [PubMed]
65. Hardie, D.G.; Schaffer, B.E.; Brunet, A. AMPK: An Energy-Sensing Pathway with Multiple Inputs and Outputs. *Trends Cell Biol.* **2016**, *26*, 190–201. [CrossRef] [PubMed]
66. Friederich-Persson, M.; Persson, P. Mitochondrial angiotensin II receptors regulate oxygen consumption in kidney mitochondria from healthy and type 1 diabetic rats. *Am. J. Physiol. Ren. Physiol.* **2020**, *318*, F683–F688. [CrossRef] [PubMed]
67. Ravi, S.; Chacko, B.; Sawada, H.; Kramer, P.A.; Johnson, M.S.; Benavides, G.A.; O'Donnell, V.; Marques, M.B.; Darley-Usmar, V.M. Metabolic plasticity in resting and thrombin activated platelets. *PLoS ONE* **2015**, *10*, e0123597. [CrossRef] [PubMed]
68. Sowton, A.P.; Millington-Burgess, S.L.; Murray, A.J.; Harper, M.T. Rapid kinetics of changes in oxygen consumption rate in thrombin-stimulated platelets measured by high-resolution respirometry. *Biochem. Biophys. Res. Commun.* **2018**, *503*, 2721–2727. [CrossRef] [PubMed]
69. Avila, C.; Huang, R.J.; Stevens, M.V.; Aponte, A.M.; Tripodi, D.; Kim, K.Y.; Sack, M.N. Platelet mitochondrial dysfunction is evident in type 2 diabetes in association with modifications of mitochondrial anti-oxidant stress proteins. *Exp. Clin. Endocrinol. Diabetes* **2012**, *120*, 248–251. [CrossRef] [PubMed]
70. Gentry, L.; Samatar, A.A.; Der, C.J. Inhibitors of the ERK mitogen-activated protein kinase cascade for targeting RAS mutant cancers. *Enzymes* **2013**, *34*, 67–106. [CrossRef] [PubMed]
71. Kim, K.B.; Kefford, R.; Pavlick, A.C.; Infante, J.R.; Ribas, A.; Sosman, J.A.; Fecher, L.A.; Millward, M.; McArthur, G.A.; Hwu, P.; et al. Phase II study of the MEK1/MEK2 inhibitor Trametinib in patients with metastatic BRAF-mutant cutaneous melanoma previously treated with or without a BRAF inhibitor. *J. Clin. Oncol.* **2013**, *31*, 482–489. [CrossRef] [PubMed]
72. Hashem, O.; Shahin, A.I.; Al Hindawi, M.A.; Fageeri, M.F.; Al-Sbbagh, S.A.; Tarazi, H.; El-Gamal, M.I. An overview of RAF kinases and their inhibitors (2019–2023). *Eur. J. Med. Chem.* **2024**, *275*, 116631. [CrossRef] [PubMed]
73. Kotrys, A.V.; Szczesny, R.J. Mitochondrial Gene Expression and Beyond-Novel Aspects of Cellular Physiology. *Cells* **2019**, *9*, 17. [CrossRef] [PubMed]
74. D'Erchia, A.M.; Atlante, A.; Gadaleta, G.; Pavesi, G.; Chiara, M.; De Virgilio, C.; Manzari, C.; Mastropasqua, F.; Prazzoli, G.M.; Picardi, E.; et al. Tissue-specific mtDNA abundance from exome data and its correlation with mitochondrial transcription, mass and respiratory activity. *Mitochondrion* **2015**, *20*, 13–21. [CrossRef] [PubMed]
75. Gómez-Serrano, M.; Camafeita, E.; Loureiro, M.; Peral, B. Mitoproteomics: Tackling Mitochondrial Dysfunction in Human Disease. *Oxidative Med. Cell. Longev.* **2018**, *2018*, 1435934. [CrossRef] [PubMed]
76. Longchamps, R.J.; Castellani, C.A.; Yang, S.Y.; Newcomb, C.E.; Sumpter, J.A.; Lane, J.; Grove, M.L.; Guallar, E.; Pankratz, N.; Taylor, K.D.; et al. Evaluation of mitochondrial DNA copy number estimation techniques. *PLoS ONE* **2020**, *15*, e0228166. [CrossRef] [PubMed]
77. Rubalcava-Gracia, D.; Larsson, N.G. Mammalian mtDNA gene expression: Concepts learned from in vivo models. *Biochim Biophys. Acta Mol. Cell Res.* **2026**, *1873*, 120158. [CrossRef] [PubMed]

Disclaimer/Publisher's Note: The statements, opinions and data contained in all publications are solely those of the individual author(s) and contributor(s) and not of MDPI and/or the editor(s). MDPI and/or the editor(s) disclaim responsibility for any injury to people or property resulting from any ideas, methods, instructions or products referred to in the content.

cells

MDPI

Article

Exosomal MALAT1 from Rapid Electrical Stimulation-Treated Atrial Fibroblasts Activates Autophagy by Downregulating miR-204-5p and Upregulating LC3B

Su-Kiat Chua [1,2,*], Bao-Wei Wang [2], Ying-Ju Yu [2], Wei-Jen Fang [2], Chiu-Mei Lin [1,3], Cheng-Yen Chuang [2] and Kou-Gi Shyu [2]

[1] School of Medicine, College of Medicine, Fu Jen Catholic University, New Taipei 24205, Taiwan; mei882153@gmail.com
[2] Division of Cardiology, Department of Internal Medicine, Shin Kong Wu Ho-Su Memorial Hospital, Taipei 11101, Taiwan; baowei@ms22.hinet.net (B.-W.W.); kinki1983yu@gmail.com (Y.-J.Y.); wjfang0719@gmail.com (W.-J.F.); medicine.chuang@gmail.com (C.-Y.C.); shyukg@ms12.hinet.net (K.-G.S.)
[3] Department of Emergency Medicine, Shin Kong Wu Ho-Su Memorial Hospital, Taipei 11101, Taiwan
* Correspondence: benchua1131@hotmail.com; Tel.: +886-2-2833-2211 (ext. 2084)

Highlights

What are the main findings?

- RES selectively induces exosomal MALAT1 secretion in human atrial fibroblasts (HCF-aa), which acts as a competing endogenous RNA (ceRNA) to putatively sequester miR-204-5p, thereby de-repressing LC3B expression and activating autophagy.
- Luciferase reporter assays, gain- and loss-of-function experiments, and immunofluorescence confocal microscopy confirm a MALAT1/miR-204-5p/LC3B signaling axis as a mechanistic driver of autophagic activation in atrial fibroblasts under rapid electrical stress.

What are the implications of the main findings?

- Exosomal MALAT1 extends its role as a master orchestrator of non-coding RNA networks in atrial fibroblasts, adding regulation of autophagy to its previously established functions in apoptosis (miR-499a-5p/SOX6) and electrical remodeling (miR-1/Tbx18/Cx43).
- The MALAT1/miR-204-5p/LC3B axis represents a potential therapeutic target for modulating autophagy-mediated atrial structural remodeling in atrial fibrillation.

Abstract

Background: Atrial fibrillation (AF) is the most common sustained cardiac arrhythmia and is strongly associated with atrial structural remodeling driven by activated cardiac fibroblasts. Autophagy has been implicated in AF-related atrial remodeling; however, the non-coding RNA mechanisms that govern autophagic activation in atrial fibroblasts under rapid electrical stress remain poorly understood. **Methods:** Human cardiac fibroblasts from adult atria (HCF-aa) were subjected to rapid electrical stimulation (RES) at 0.5 V/cm and 10 Hz. Expression levels of exosomal metastasis-associated lung adenocarcinoma transcript 1 (MALAT1), cytoplasmic miR-204-5p, and microtubule-associated protein light chain 3B (LC3B) were measured using quantitative real-time PCR and Western blot analyses. Luciferase reporter assays were performed to confirm direct molecular interactions. The functional roles of MALAT1 siRNA, miR-204-5p mimics/antagomirs, rapamycin, and 3-methyladenine (3-MA) on LC3B expression and autophagic activation were assessed by Western blot and immunofluorescence confocal microscopy for LC3B puncta formation.

Results: RES significantly induced exosomal MALAT1 expression in a voltage- and time-dependent manner, peaking at 2 h post-stimulation, while cytoplasmic MALAT1 levels remained unchanged. Cytoplasmic miR-204-5p exhibited an initial transient rise followed by a significant decline at 2 h, inversely correlating with peak MALAT1 levels. LC3B mRNA and protein expression subsequently increased, peaking at 6 and 16 h, respectively. Luciferase reporter assays confirmed that miR-204-5p directly binds both the MALAT1 transcript and the 3′-UTR of LC3B mRNA. MALAT1 knockdown augmented miR-204-5p levels and suppressed LC3B expression, while miR-204-5p overexpression attenuated RES-induced LC3B upregulation and LC3B puncta accumulation. Conversely, miR-204-5p inhibition further enhanced autophagic activation, as evidenced by increased LC3B puncta density. **Conclusions:** In HCF-aa subjected to RES, MALAT1 functions intracellularly as a competing endogenous RNA to putatively sequester miR-204-5p, thereby de-repressing LC3B expression and promoting autophagic activation. Concurrent exosomal secretion of MALAT1 may additionally serve as a paracrine signal to neighboring cells, though this requires future conditioned-media transfer experiments to confirm.

Keywords: atrial fibrillation; MALAT1; miR-204-5p; LC3B; autophagy; rapid electrical stimulation; exosome; competing endogenous RNA

1. Introduction

Atrial fibrillation (AF) is the most common sustained cardiac arrhythmia in clinical practice, affecting over 33 million individuals worldwide and carrying a substantially elevated risk of stroke, heart failure, and overall mortality [1]. Tachycardia-induced atrial structural and electrical remodeling are two cardinal features of AF pathogenesis [2]. Cardiac fibroblasts, long regarded as passive structural sentinels, are now recognized as active participants in atrial remodeling through fibroblast–myocyte coupling, whereby electrically silent fibroblasts modulate cardiomyocyte action potentials, thereby perpetuating the arrhythmogenic substrate [3]. Rapid electrical stimulation (RES) of human cardiac fibroblasts from adult atria (HCF-aa) has been established as a validated in vitro model that faithfully recapitulates key features of AF-associated fibroblast activation [4,5].

Recent studies have highlighted the pivotal role of long non-coding RNAs (lncRNAs) and microRNAs (miRNAs) in the molecular regulation of AF [6]. Metastasis-associated lung adenocarcinoma transcript 1 (MALAT1) is a highly conserved lncRNA that modulates gene expression as a competing endogenous RNA (ceRNA), sequestering specific miRNAs and thereby derepressing their target messenger RNAs [7]. Exosomes—nanoscale extracellular vesicles that carry diverse non-coding RNA cargo and mediate intercellular communication—play a critical role in transmitting MALAT1-mediated signals in cardiovascular biology [8]. We have previously demonstrated that RES of HCF-aa significantly induces exosomal MALAT1 secretion, and that this exosomal MALAT1 sponges miR-499a-5p to upregulate SOX6 expression and modulate fibroblast apoptosis [4]. In a related study, we further showed that exosomal miR-1 released by RES-exposed HCF-aa represses Tbx18 and consequently upregulates connexin 43 (Cx43) expression [5]. These findings suggest that exosomal MALAT1 orchestrates a broader non-coding RNA network in electrically stressed atrial fibroblasts; however, additional downstream targets of this axis remain to be identified.

MicroRNA-204-5p (miR-204-5p) has emerged as a clinically relevant miRNA in AF and is significantly downregulated in the coronary sinus plasma of AF patients [9]. Mechanistically, miR-204-5p functions as a potent suppressor of autophagy by directly targeting

microtubule-associated protein light chain 3B (LC3B): seminal work demonstrated that miR-204 binds the 3′-UTR of LC3B to inhibit autophagic activation, a finding subsequently validated in cardiac ischemia–reperfusion models [10,11]. The conversion of cytosolic LC3B-I to its lipidated autophagosome form, LC3B-II, is a defining hallmark of autophagy activation and has been observed to be dysregulated in both human atrial tissues from AF patients and in animal models of rapid atrial pacing, implicating autophagy as a potential contributor to atrial electrical remodeling [12,13]. Despite these observations, whether MALAT1 regulates miR-204-5p and thereby modulates LC3B-mediated autophagy in atrial fibroblasts under conditions of rapid electrical stress has not been investigated.

The present study aims to elucidate a novel regulatory axis involving exosomal MALAT1, miR-204-5p, and LC3B in HCF-aa subjected to RES. We hypothesize that RES-induced exosomal MALAT1 putatively sequesters miR-204-5p, thereby derepressing LC3B expression and activating autophagy in atrial fibroblasts. Elucidating this signaling cascade may advance our understanding of AF pathogenesis and identify potential therapeutic targets for atrial fibroblast-mediated remodeling.

2. Materials and Methods

2.1. Cell Culture of HCF-aa

Human cardiac fibroblasts-adult atrial (HCF-aa) were obtained from ScienCell Research Laboratories (San Diego, CA, USA). These cells were cultured in fibroblast medium supplemented with essential and nonessential amino acids, vitamins, hormones, growth factors, and 2% fetal bovine serum. The medium was buffered with HEPES and bicarbonate to maintain a stable pH of 7.4. The cells were incubated in a humidified 5% CO_2 atmosphere at 37 °C to ensure optimal growth. For all experimental protocols, HCF-aa were used at passages 3 to 6 to maintain phenotypic consistency.

2.2. In Vitro Rapid Electrical Stimulation (RES)

The HCF-aa were subjected to RES using an established protocol. Upon reaching confluence, the culture medium was replaced with serum-free Fibroblast Medium (ScienCell, Cat No: 2301, Carlsbad, CA, USA) for 6 h prior to stimulation. Cells were then transferred to an EPS-01 culture pacer dish (BioEast, Taipei, Taiwan) equipped with parallel platinum electrodes to prevent electrolysis. The RES was delivered as a unipolar square waveform at 10 Hz (duration, 50 ms; interval, 50 ms). A voltage gradient of 0.5 V/cm was applied. Control cells were maintained under identical conditions without electrical stimulation.

2.3. Extraction of Exosomes from Cell Media

Exosomes were isolated from cell culture media using the Total Exosome Isolation Reagent (Invitrogen, Thermo Fisher Scientific, Waltham, MA, USA) according to the manufacturer's guidelines. Briefly, the cell-free media were centrifuged at 2000× *g* for 30 min to remove cellular debris. The resulting supernatant was mixed with the isolation reagent at a 2:1 ratio and incubated overnight at 4 °C. The mixture was then centrifuged at 10,000× *g* for 1 h at 4 °C. The exosome pellet was resuspended in phosphate-buffered saline (PBS) and quantified using an ExoQuant™ quantification assay kit (BioVision, Milpitas, CA, USA).

Using this protocol, isolated vesicles have previously been confirmed to fall within the expected exosomal size range of 50–150 nm, and exosomal identity has been validated by CD9 and CD81 Western blots in our prior publications employing the same isolation platform. Comprehensive characterization per MISEV2023 guidelines, including nanoparticle tracking analysis, transmission electron microscopy, and full tetraspanin marker profiling, was not performed in the present study and is acknowledged as a limitation [14].

https://doi.org/10.3390/cells15121126

2.4. Reverse Transcription and Real-Time Quantitative PCR

Total cytoplasmic RNA was extracted using TRIzol reagent (Invitrogen, Thermo Fisher Scientific, Waltham, MA, USA) according to the manufacturer's protocol. For exosomal RNA extraction, the Total Exosome RNA and Protein Isolation Kit (Invitrogen, Thermo Fisher Scientific) was used as previously described. Prior to RNA extraction, exosome quantity was standardized across all experimental conditions using the ExoQuant™ quantification assay kit (BioVision, Milpitas, CA, USA) to ensure equal exosome input. RNA quality of each exosome preparation was confirmed using a BiOptic Qsep100 analyzer (BiOptic Inc., Taipei, Taiwan) with an RNA cartridge kit; all samples were analyzed in duplicate, and electropherogram profiles were generated to verify RNA integrity before proceeding to reverse transcription.

Reverse transcription of total RNA was performed using random hexamers and a High-Capacity cDNA Reverse Transcription Kit (Applied Biosystems, Thermo Fisher Scientific, Waltham, MA, USA). Quantitative PCR was conducted using Fast SYBR® Green Master Mix (Applied Biosystems, Thermo Fisher Scientific, Waltham, MA, USA) on an ABI StepOnePlus cycler with the following cycling conditions: 95 °C for 15 min, followed by 40 cycles of 94 °C for 15 s, 55 °C for 30 s, and 70 °C for 30 s.

Relative gene expression levels were calculated using the $2^{-\Delta CT}$ method, where $\Delta CT = CT(\text{target gene}) - CT(\text{control condition})$, as previously described. All expression values are presented as fold-change relative to the unstimulated control group, which was assigned a reference value of 1.0. This method normalizes expression to the matched experimental control condition and does not require a housekeeping gene, consistent with the approach used in our prior peer-reviewed work employing the same experimental platform.

2.5. Construction of Expression Vectors and Transfection

To confirm the direct interaction between miR-204-5p and MALAT1, a 500 bp human MALAT1 DNA fragment encompassing the predicted miR-204-5p binding site (nucleotides 1650–1671; binding site sequence: 5′-AAGAGUAGCAUGAGGAAGGAAA-3′) was artificially synthesized and cloned into a pUC57 intermediate vector. The insert was subsequently digested with restriction enzymes and ligated into the pmirNanoGLO luciferase reporter vector (Promega, Madison, WI, USA) to generate the wild-type MALAT1 reporter construct. Similarly, a 500 bp human LC3B 3′-UTR fragment encompassing the predicted miR-204-5p binding site (nucleotides 41–62; binding site sequence: 5′-UUACCAAGGAAAAAAAAGGGAU-3′) was cloned using the same strategy. Mutant constructs were generated by site-directed mutagenesis of the conserved miR-204-5p binding sites within each 500 bp fragment. All cloned plasmids were confirmed by DNA sequencing. This approach was performed as previously described.

Cells were transfected at 60–75% confluence using ViaFect™ Transfection Reagent (Promega) or Lipofectamine RNAiMax (Thermo Fisher Scientific, Waltham, MA, USA) according to the manufacturer's protocols. The miR-204-5p mimics (5′-UUCCCUUUGUCAUCCUAUGCCU-3′), antagomirs (5′-AGGCAUAGGAUGACAAAGGGAA-3′), and MALAT1 siRNA (Cat. no. 4392420, Thermo Fisher Scientific) were delivered by transfection as specified for each experimental condition.

2.6. Luciferase Activity Assay

2.6.1. 3′-UTR Luciferase Binding Assay

To confirm direct miR-204-5p binding to MALAT1 and the LC3B 3′-UTR, the 500 bp wild-type and mutant reporter constructs described in Section 2.5 were cloned into the pmirNanoGLO dual luciferase reporter vector (Promega, Madison, WI, USA), as previously described. HCF-aa were co-transfected with reporter plasmids and miR-204-5p wild-type

https://doi.org/10.3390/cells15121126

or mutant mimics using ViaFect™ Transfection Reagent (Promega). After 24 h, luciferase activity was measured using the Nano-Glo Dual-Luciferase Reporter Assay System (Promega) on a Glomax Multi Detection System luminometer (Promega). Firefly luciferase activity was normalized to Renilla luciferase activity to control for transfection efficiency. This assay evaluates miRNA-mediated post-transcriptional repression via direct 3′-UTR binding, rather than transcriptional activity.

2.6.2. Promoter Activity Assay

To evaluate transcriptional regulation, human promoter constructs were generated and ligated into the pGL3-basic luciferase plasmid vector (Mission Biotech, Taipei, Taiwan). Plasmids were transfected into HCF-aa using ViaFect™ Transfection Reagent (Promega). Luciferase activity was measured as previously described to determine promoter-driven transcriptional activity in response to RES and molecular interventions. This assay is entirely independent of the 3′-UTR binding system described in Section 2.6.1.

2.7. Western Blot Analysis

Cells were harvested by scraping and centrifuged at 300× *g* for 10 min at 4 °C. The resulting pellet was resuspended, homogenized in RIPA Lysis and Extraction Buffer (Thermo Fisher Scientific, Rockford, IL, USA), and centrifuged at 14,000× *g* for 15 min at 4 °C. Protein content was determined using a Bio-Rad Protein Assay (Bio-Rad Laboratories, Hercules, CA, USA). Equal amounts of protein (30 µg per lane) were loaded onto 15% sodium dodecyl sulfate-polyacrylamide gels for optimal resolution of LC3B-I (~16 kDa) and LC3B-II (~14 kDa), and subjected to electrophoresis. Proteins were transferred to polyvinylidene difluoride (PVDF) membranes (0.2 µm pore size; Merck Millipore, Darmstadt, Germany) by wet transfer at 100 V for 90 min at 4 °C. Membranes were blocked with 5% non-fat dry milk in Tris-buffered saline with 0.1% Tween-20 (TBST) for 1 h at room temperature, followed by overnight incubation at 4 °C with primary antibodies against LC3B (Santa Cruz Biotechnology, Cat. no. sc-271837, Dallas, TX, USA) and β-actin (mouse monoclonal anti-β-actin, Sigma-Aldrich, Saint Louis, MO, USA). After washing with TBST, membranes were incubated with horseradish peroxidase-conjugated secondary antibodies for 1 h at room temperature, and signals were detected using enhanced chemiluminescence (ECL) reagent (Thermo Fisher Scientific). To ensure linearity of detection for LC3B-I/II quantification, all samples were confirmed to fall within the linear range of exposure prior to densitometric analysis. Band densitometry was performed using ImageJ software (version 1.54; National Institutes of Health, Bethesda, MD, USA). Equal protein loading was further verified by quantifying β-actin band intensity. The LC3B-II/LC3B-I ratio, normalized to β-actin, was used as the primary metric for quantifying autophagy. The detailed procedure has been described previously [4,15].

2.8. Immunofluorescence Staining

HCF-aa were fixed in 4% paraformaldehyde for 1 h and washed with PBS. The cells were incubated with a primary antibody against LC3B at 4 °C for 12 h, followed by a fluorescently conjugated secondary antibody for 1–2 h in the dark. Nuclei were stained with DAPI, and the cytoskeleton was visualized with phalloidin. Samples were examined using confocal microscopy, and at least three random fields were captured per sample to quantify LC3B puncta density.

2.9. Statistical Analysis

Data are presented as mean ± standard deviation (SD) from at least three independent experiments. Statistical significance was assessed using one-way analysis of variance (ANOVA), followed by Tukey–Kramer post hoc tests for multiple comparisons. A *p*-value

of less than 0.05 was considered statistically significant. One-way ANOVA was applied under the assumption of approximate normality, which is biologically justified for fold-change expression data derived from independent controlled experiments, and is consistent with our previously published methodology [4,15]. We acknowledge that formal normality testing is not feasible with $n = 3$; non-parametric validation using the Kruskal–Wallis test with larger sample sizes is recommended for future studies.

3. Results

3.1. RES Up-Regulates Exosomal MALAT1 Expression in a Dose- and Time-Dependent Manner

To investigate whether RES modulates MALAT1 secretion via exosomes, we performed dose–response and time-course experiments in HCF-aa. As illustrated in Figure 1A, exposure to RES at 0.5 V/cm and 10 Hz for 2 h resulted in a significant induction of exosomal MALAT1 expression (2.7 ± 2.4-fold relative to control, $p < 0.001$). In contrast, lower (0.25 V/cm; 1.04 ± 0.09-fold) and higher (0.75 V/cm; 1.26 ± 0.18-fold) voltage gradients did not significantly increase MALAT1 levels compared with the control group (1.01 ± 0.06-fold). Based on these findings, a voltage intensity of 0.5 V/cm was selected for all subsequent investigations.

The temporal dynamics of this induction followed a distinct bell-shaped pattern (Figure 1B). While no significant change was observed at 0.5 h (0.92 ± 0.27-fold), exosomal MALAT1 levels rose significantly at 1 h (1.97 ± 0.31-fold, $p < 0.001$) and reached a peak at 2 h post-stimulation (2.95 ± 0.42-fold, $p < 0.001$). Following the peak, MALAT1 levels gradually declined but remained significantly elevated through 8 h (1.51 ± 0.17-fold) compared to the unstimulated control group (1.01 ± 0.05-fold).

3.2. Reciprocal Expression of miR-204-5p and LC3B in Response to RES

As shown in Figure 2A, cytoplasmic miR-204-5p expression exhibited a transient increase at 1-h post-RES (1.83 ± 0.21-fold, $p < 0.05$), followed by a significant decline at 2 h (0.84 ± 0.11-fold, $p < 0.05$ vs. 1 h), falling below the control group's baseline (1.03 ± 0.13). This reduction in miR-204-5p expression coincided precisely with the peak levels of exosomal MALAT1 observed in Figure 1, supporting the hypothesis that MALAT1 acts as a ceRNA to putatively sequester miR-204-5p.

In parallel, we observed a delayed but robust induction of LC3B mRNA expression (Figure 2B). Following the nadir of miR-204-5p at 2 h, LC3B mRNA levels began to rise significantly at 4 h (2.09 ± 0.18-fold, $p < 0.05$ vs. control) and reached a peak at 6 h (2.68 ± 0.34-fold, $p < 0.05$ vs. control). LC3B expression remained significantly elevated (approximately 2.0-fold) through 24 h of continuous RES.

To confirm whether the RES-induced increase in LC3B mRNA translates to functional protein expression, we performed Western blot analysis to detect LC3B-I and LC3B-II levels in HCF-aa (original gel images are provided in Supplementary Figure S1; Figure 2C). Consistent with our mRNA findings, RES elicited a robust, time-dependent accumulation of LC3B protein (Figure 2D). While early stages of RES (1–2 h) showed only modest increases (1.31 ± 0.06 and 1.41 ± 0.15-fold, respectively), a significant induction was observed starting at 4 h (1.75 ± 0.32-fold, $p < 0.05$ vs. control). Protein expression continued to rise, reaching a peak at 16 h (2.71 ± 0.24-fold) and maintaining a high plateau through 24 h (2.60 ± 0.27-fold).

https://doi.org/10.3390/cells15121126

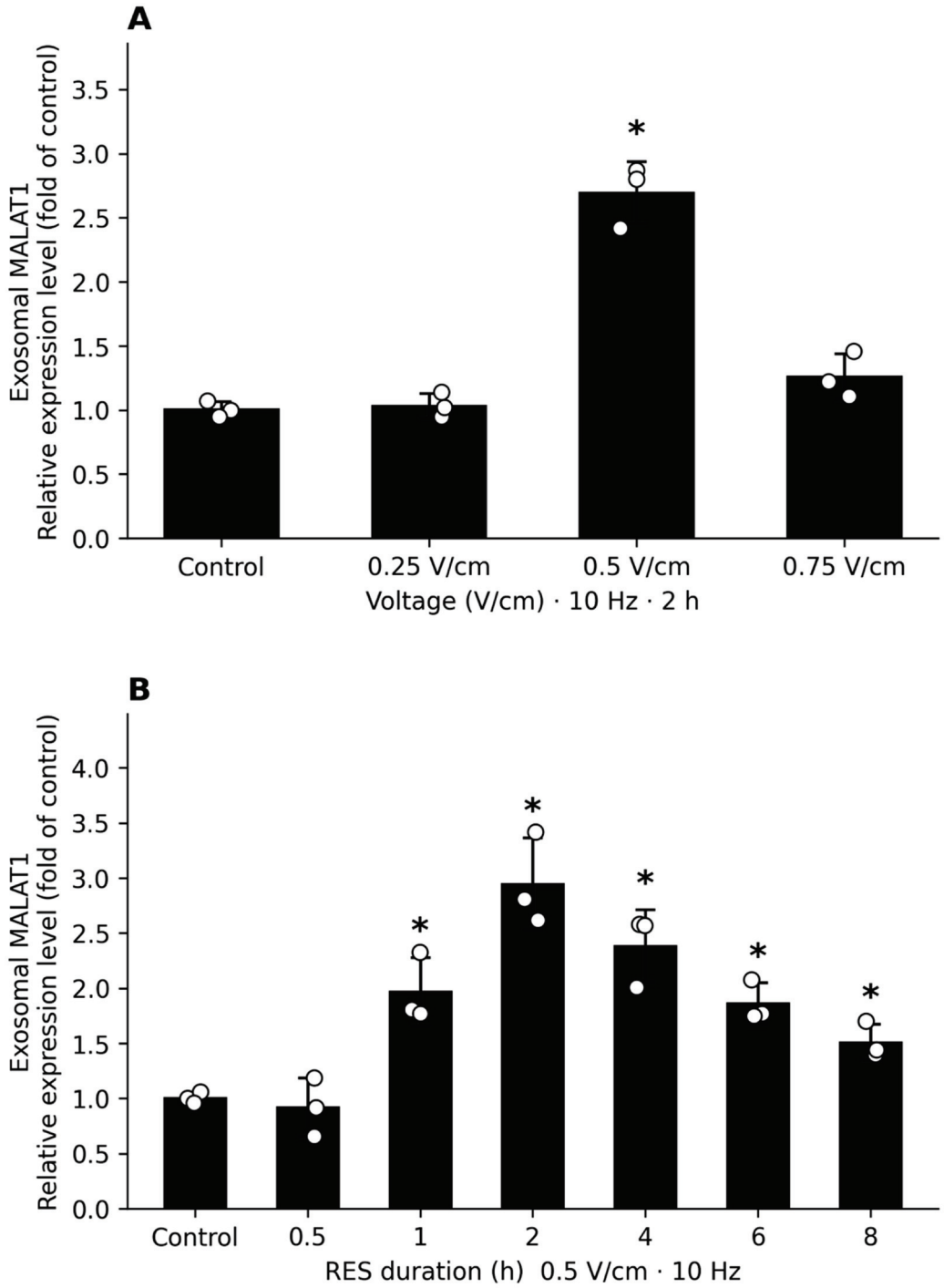


Figure 1. Rapid electrical stimulation (RES) induces the expression of exosomal MALAT1 in HCF-aa. (**A**) Exosomal MALAT1 mRNA expression levels in HCF-aa subjected to RES at varying voltage gradients (0.25, 0.5, and 0.75 V/cm) at 10 Hz for 2 h. (**B**) Time-dependent changes in exosomal MALAT1 mRNA levels in HCF-aa exposed to RES (0.5 V/cm and 10 Hz) for 0.5 to 8 h. The control group was cultured for 8 h without RES. Relative MALAT1 expression was determined by qPCR and normalized to the control group. The open circles are the individual data points. Data represent mean ± SD (n = 3 per group). * $p < 0.001$ versus the control group.

https://doi.org/10.3390/cells15121126

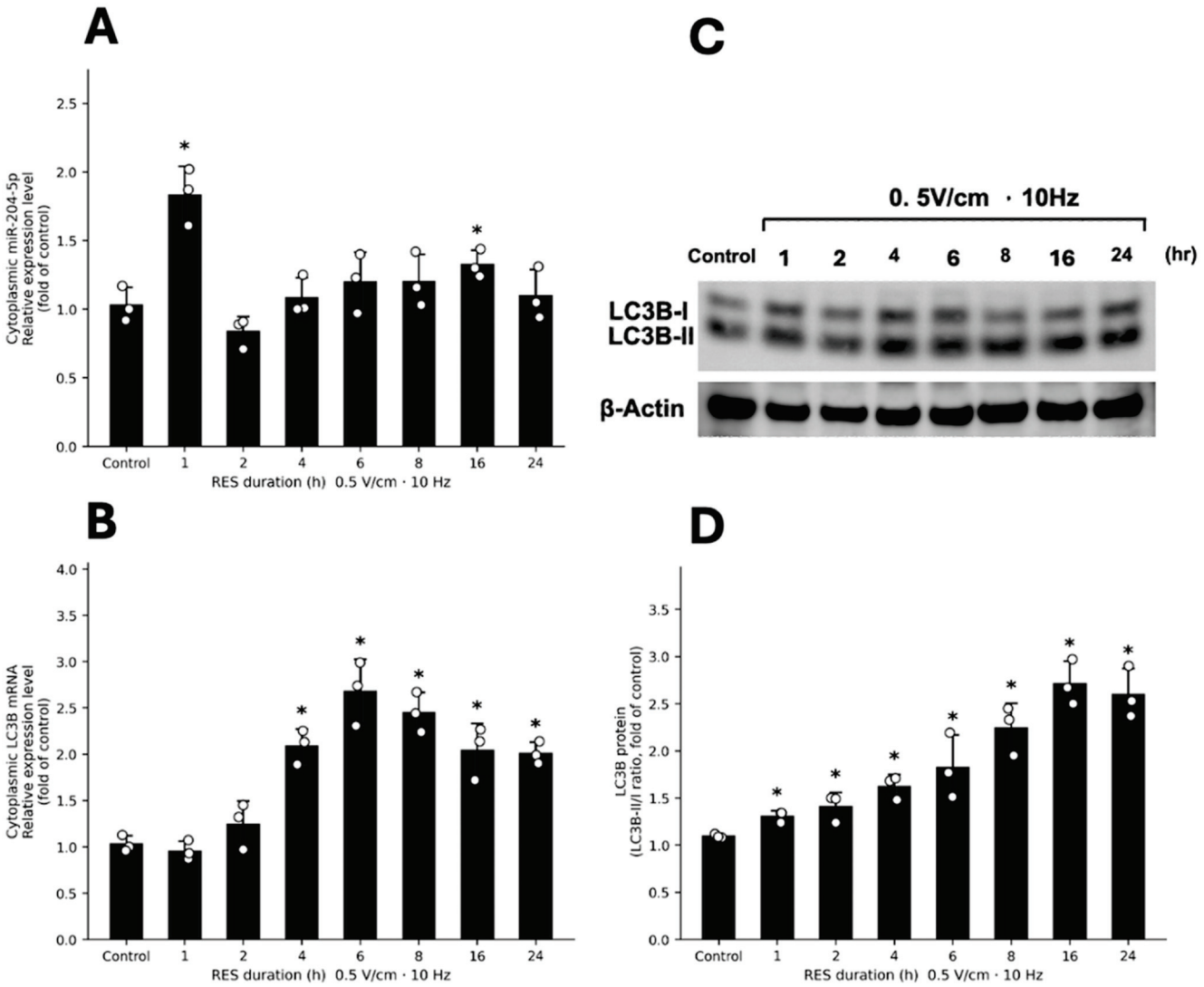


Figure 2. Rapid electrical stimulation (RES) modulates miR-204-5p, LC3B mRNA, and LC3B protein expression in HCF-aa. (**A**) Time-course analysis of cytoplasmic miR-204-5p expression levels in HCF-aa subjected to RES (0.5 V/cm, 10 Hz) for 1 to 24 h. (**B**) Quantitative expression of cytoplasmic LC3B mRNA in HCF-aa under the same RES conditions. (**C**) Representative Western blot images showing LC3B-I, LC3B-II, and β-actin in HCF-aa subjected to RES for 1 to 24 h; original gel images are provided in Supplementary Figure S1. (**D**) Quantitative analysis of LC3B protein expression (LC3B-II/I ratio) normalized to β-actin. The open circles are the individual data points. The control group was cultured for 24 h without RES. Data represent mean ± SD (n = 3 per group). * $p < 0.05$ versus the control group.

3.3. MALAT1 Regulates LC3B Expression by Sponging miR-204-5p

As shown in Figure 3A, while RES (0.5 V/cm, 10 Hz for 6 h) resulted in a moderate increase in cytoplasmic miR-204-5p levels (1.36 ± 0.07-fold vs. 0.91 ± 0.17-fold in control), the knockdown of MALAT1 using siRNA further augmented this expression significantly (2.14 ± 0.28-fold, $p < 0.05$). This observation indicates that endogenous MALAT1 putatively sequesters miR-204-5p during periods of electrical stress.

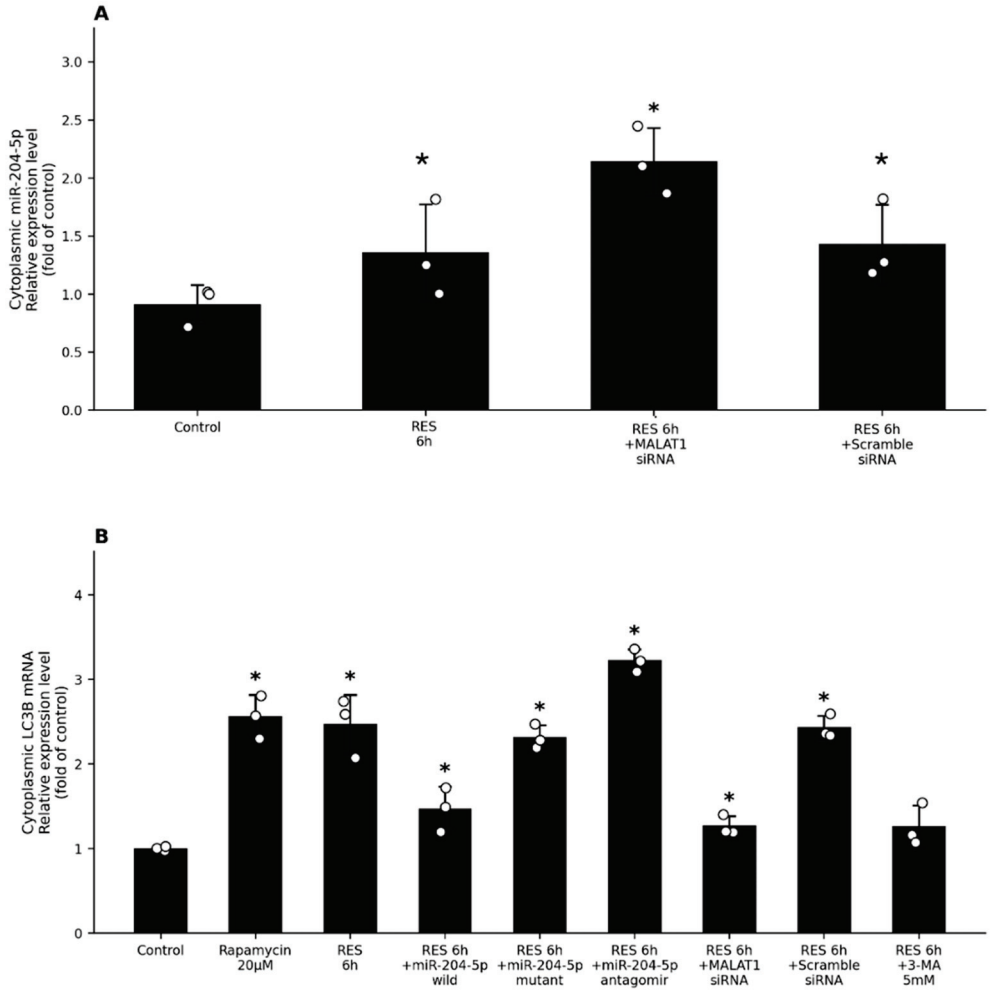


Figure 3. MALAT1 acts as a ceRNA for miR-204-5p to regulate LC3B expression in HCF-aa under RES. (**A**) Cytoplasmic miR-204-5p expression levels in HCF-aa subjected to RES (0.5 V/cm, 10 Hz for 6 h) with or without MALAT1 siRNA or scramble siRNA transfection. (**B**) Relative LC3B mRNA expression levels in HCF-aa under various experimental conditions, including treatment with rapamycin (20 μM), miR-204-5p wild-type/mutant mimics, miR-204-5p antagomir, MALAT1 siRNA, and 3-methyladenine (3-MA, 5 mM). The open circles are the individual data points. Data represent mean ± SD (n = 3). * $p < 0.05$ versus the control group.

RES induced a robust upregulation of LC3B mRNA (2.47 ± 0.35-fold), comparable to rapamycin (2.56 ± 0.25-fold) (Figure 3B). Transfection with miR-204-5p wild-type mimics significantly attenuated the RES-induced increase in LC3B (1.47 ± 0.26-fold), whereas the mutant mimic had no significant effect (2.31 ± 0.14-fold). Conversely, inhibition of miR-204-5p with an antagomir further enhanced LC3B expression (2.89 ± 0.46-fold). Crucially, MALAT1 siRNA treatment effectively reversed the RES-induced upregulation of LC3B (1.27 ± 0.12-fold), mimicking the effect of 3-MA (1.26 ± 0.25-fold).

3.4. miR-204-5p Directly Binds to MALAT1 and the LC3B 3′-UTR

Sequence analysis revealed a predicted binding site for miR-204-5p on the MALAT1 transcript at nucleotides 1650–1671 (Figure 4A). Co-transfection with miR-204-5p wild-type mimics significantly reduced the luciferase activity of the WT-MALAT1 construct to 0.506 ± 0.071-fold compared to the RES control group (1.011 ± 0.051-fold, $p < 0.05$). Importantly, the inhibitory effect of miR-204-5p was completely abolished when the predicted binding site on MALAT1 was mutated (0.993 ± 0.072-fold), confirming that MALAT1 acts as a direct molecular sponge for miR-204-5p.

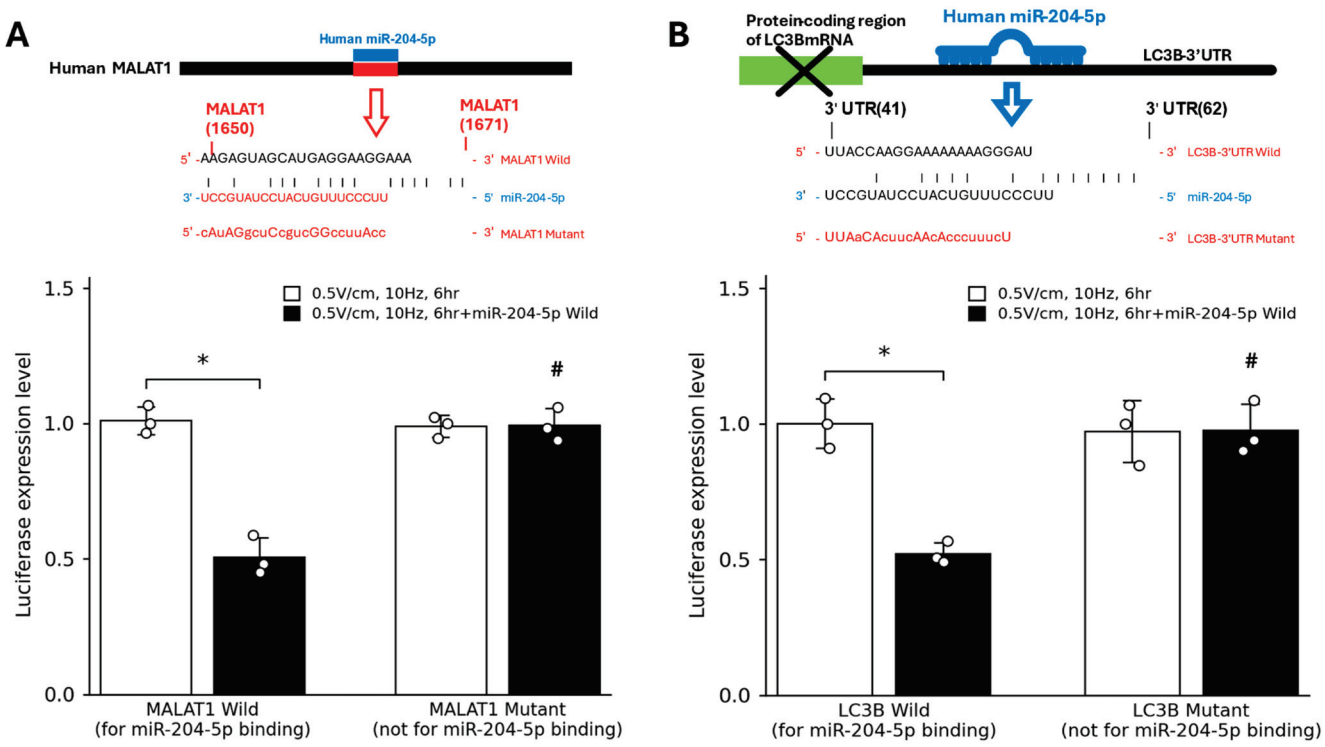


Figure 4. miR-204-5p directly targets MALAT1 and the 3′-UTR of LC3B mRNA. (**A**) Luciferase activity of wild-type (WT) and mutant MALAT1 constructs in HCF-aa. The schematic illustrates the predicted binding site of miR-204-5p on human MALAT1 (nucleotides 1650–1671). (**B**) Luciferase activity of WT and mutant LC3B 3′-UTR constructs. The predicted miR-204-5p binding site within the 3′-UTR of LC3B is at nucleotides 41–62. Luciferase activity was measured 24 h post-transfection and normalized to control levels. The open circles are the individual data points. Data represent mean ± SD (n = 3). * $p < 0.05$ vs. RES group; # $p < 0.05$ vs. RES + miR-204-5p wild-type group.

Furthermore, the predicted miR-204-5p binding site within the 3′-UTR of LC3B was located at nucleotides 41–62 (Figure 4B). MiR-204-5p mimics significantly suppressed luciferase activity in the WT-LC3B 3′-UTR, resulting in a 48% decrease (0.521 ± 0.040-fold vs. 1.001 ± 0.091-fold in the control, $p < 0.05$). This suppression was reversed upon mutation of the binding site (0.976 ± 0.098-fold).

3.5. The MALAT1/miR-204-5p Axis Is Essential for RES-Induced LC3B Protein Expression

As shown in Figure 5A, 16 h of RES significantly induced LC3B protein expression (2.36 ± 0.48-fold vs. 1.05 ± 0.06-fold in the control, $p < 0.05$), a response similar to that of rapamycin (2.55 ± 0.30-fold). The induction of LC3B was abolished by 3-MA (1.04 ± 0.15-fold), confirming activation of the autophagic pathway.

The RES-induced upregulation of LC3B protein was significantly reversed by transfection of miR-204-5p wild-type mimics (0.99 ± 0.14-fold) or MALAT1 siRNA (0.86 ± 0.01-fold), whereas miR-204-5p mutant mimics had no significant effect (2.53 ± 0.18-fold) (Figure 5B). Conversely, miR-204-5p antagomir further enhanced LC3B protein levels (3.12 ± 0.33-fold, $p < 0.05$). These protein-level findings are highly consistent with our mRNA and luciferase data, suggesting that the cytoplasmic MALAT1 pool, replenished in part through exosomal trafficking, is functionally important for LC3B-mediated autophagic activation in RES-stimulated HCF-aa; whether exosomal MALAT1 additionally acts as a paracrine mediator to recipient cells requires future conditioned media transfer experiments to confirm.

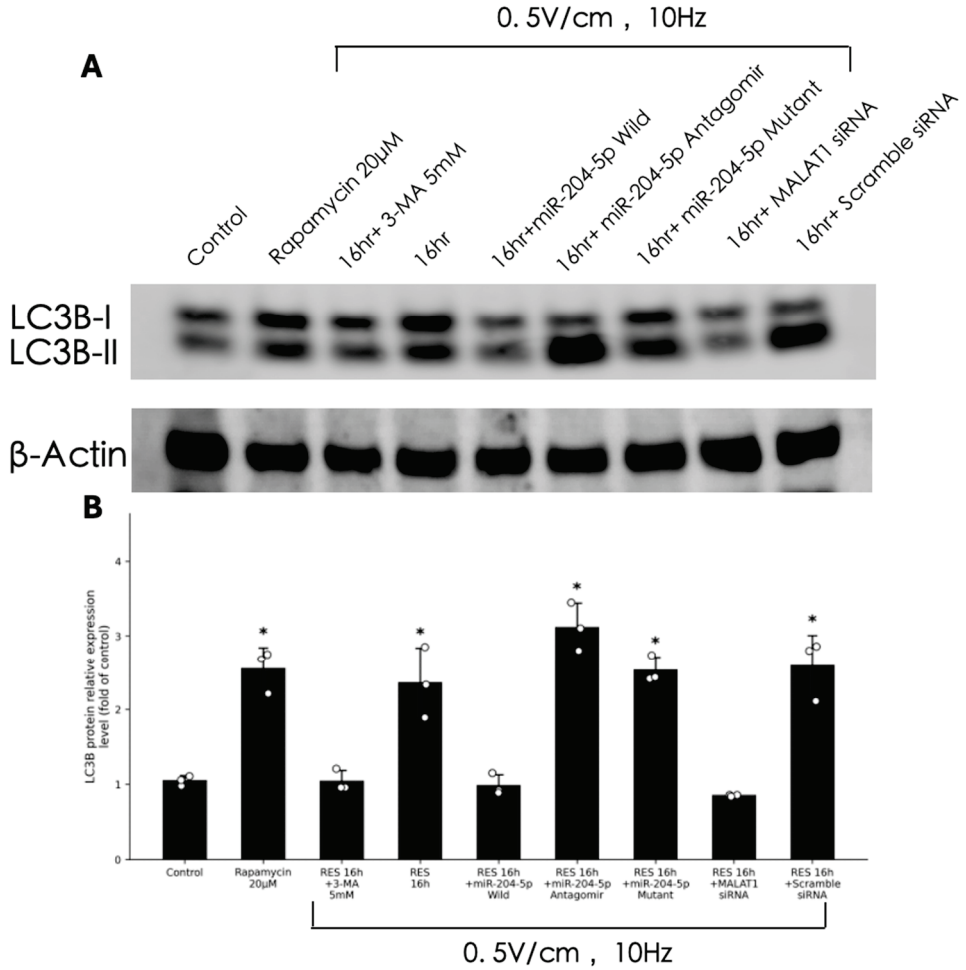


Figure 5. MALAT1 and miR-204-5p mediate RES-induced LC3B protein expression in HCF-aa. (**A**) Representative Western blot analysis of LC3B-I, LC3B-II, and β-actin in HCF-aa under various conditions after 16 h of RES (0.5 V/cm, 10 Hz). Conditions include control, RES alone, rapamycin (20 μM), 3-MA (5 mM), miR-204-5p wild-type/mutant mimics, miR-204-5p antagomir, and MALAT1 siRNA. Original gel images are provided in Supplementary Figure S2. (**B**) Quantitative analysis of LC3B protein levels (LC3B-II/I ratio) normalized to β-actin. The open circles are the individual data points. Data represent mean ± SD (n = 3). * $p < 0.05$ versus the control group.

3.6. RES Activates Autophagy as Evidenced by LC3B Puncta Accumulation

Immunofluorescence confocal microscopy was performed to quantify LC3B-positive puncta—a well-established surrogate marker of autophagic flux [15]—in HCF-aa under various experimental conditions (Figure 6). Under baseline conditions, HCF-aa exhibited sparse LC3B signals (23.33 ± 8.82%/HPF). Rapamycin (20 μM) served as a positive control and significantly increased LC3B-positive cells (76.08 ± 5.28%/HPF, $p < 0.05$ vs. control). Consistent with Western blot data, 16 h of RES markedly increased the proportion of LC3B-positive cells (69.84 ± 2.75%/HPF, $p < 0.05$ vs. control), which was abolished by 3-MA (21.19 ± 9.85%/HPF).

Transfection with miR-204-5p wild-type mimic significantly attenuated RES-induced LC3B puncta (13.93 ± 3.75%/HPF, $p < 0.05$ vs. RES alone). Conversely, miR-204-5p antagomir further augmented LC3B accumulation (82.34 ± 11.35%/HPF). Knockdown of MALAT1 by siRNA markedly reduced RES-induced LC3B positivity (15.81 ± 0.74%/HPF), whereas scramble siRNA had no significant effect (73.15 ± 5.78%/HPF). These morphological data provide direct visual evidence that the MALAT1/miR-204-5p signaling axis is essential for RES-induced autophagic activation in atrial fibroblasts.

https://doi.org/10.3390/cells15121126

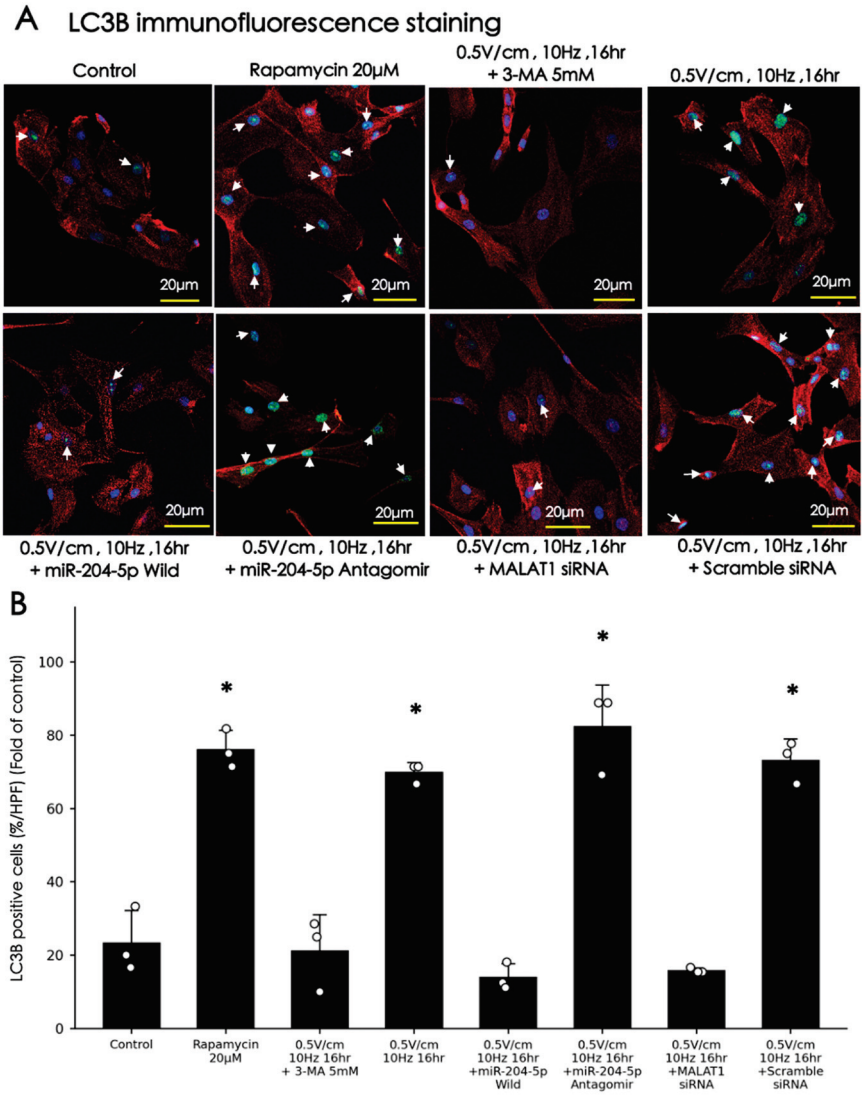


Figure 6. The MALAT1/miR-204-5p axis regulates autophagic activation in HCF-aa under RES, as assessed by LC3B immunofluorescence staining. Quantification reflects the percentage of LC3B-positive cells per high-power field; a validated semi-quantitative metric applied consistently across all experimental conditions. (**A**) Representative confocal microscopy images showing LC3B immunoreactive signals (green puncta, white arrows) in HCF-aa under the indicated conditions. Nuclei were counterstained with DAPI (blue), and the cytoskeleton was visualized with phalloidin (red). Scale bar = 20 μm. (**B**) Quantitative analysis of LC3B-positive cells (% per high-power field, expressed as fold of control). The open circles are the individual data points. Data represent mean ± SD (n = 3 per group). * $p < 0.05$ vs. control group.

4. Discussion

This study provides novel mechanistic insights into the molecular regulation of autophagy in HCF-aa subjected to RES, focusing on the interplay among MALAT1, miR-204-5p, and the autophagy marker LC3B. While MALAT1-mediated ceRNA regulation of autophagy has been reported in other cellular contexts, including gastric cancer [16] and macrophages under hyperglycemic conditions, the present study extends this regulatory paradigm specifically to human atrial fibroblasts subjected to rapid electrical stimulation, identifying the MALAT1/miR-204-5p/LC3B axis as a potential contributor to autophagy-mediated atrial fibroblast remodeling in the context of AF.

The intracellular ceRNA mechanism is directly supported by MALAT1 siRNA rescue experiments, demonstrating that reduction of the cytoplasmic MALAT1 pool elevates

miR-204-5p and suppresses LC3B; exosomal MALAT1 secretion may additionally facilitate paracrine signal propagation to neighboring cells, a mechanism validated in the same regulatory axis in our prior publication, and warrants further investigation through conditioned media transfer experiments in future studies.

RES significantly increased exosomal MALAT1 expression in a voltage- and time-dependent manner, peaking at two hours post-stimulation. Importantly, cytoplasmic MALAT1 levels did not change significantly, indicating a selective mechanism for exosomal packaging and secretion of MALAT1 in response to electrical stress [17]. MALAT1 has previously been shown to respond to diverse cellular stresses, including hypoxia and oxidative stress [8], and its rapid exosomal induction by RES suggests it may serve as an early mediator of the fibroblast stress response.

The dynamic changes in miR-204-5p expression following RES are particularly noteworthy. An initial transient upregulation at one hour was followed by a significant decline at two hours, coinciding precisely with the peak of exosomal MALAT1—an inverse temporal relationship that strongly supports the ceRNA hypothesis. The luciferase reporter assays provide direct molecular evidence, confirming that miR-204-5p binds to a specific site on the MALAT1 transcript (nucleotides 1650–1671) and that mutation of this site abolishes the inhibitory effect. MALAT1 knockdown with siRNA further corroborated the functional relevance of this sponging relationship. The growing evidence that lncRNAs modulate miRNA function through ceRNA competition [18] further supports the regulatory mechanism identified here. While luciferase reporter assays confirm direct miR-204-5p binding to MALAT1 and the LC3B 3′-UTR, they do not establish the physiological stoichiometric feasibility of ceRNA competition; the relative intracellular abundance of MALAT1 versus miR-204-5p was not quantified in this study, and future work measuring copy numbers per cell would be required to formally validate the ceRNA model under physiological conditions.

Our findings regarding LC3B expression and autophagic activation further substantiate the proposed regulatory axis. The upregulation of LC3B mRNA beginning at four hours and peaking at six hours was temporally consistent with the prior decline in miR-204-5p. The direct targeting of the LC3B 3′-UTR by miR-204-5p was confirmed by luciferase assay, establishing LC3B as a bona fide miR-204-5p target—consistent with seminal reports demonstrating miR-204-mediated suppression of LC3B in renal carcinoma [10] and in cardiomyocyte ischemia–reperfusion models [11]. Autophagic activation was further corroborated by immunofluorescence confocal microscopy, demonstrating a marked increase in cytoplasmic LC3B puncta density following RES [15]. Pharmacological modulation with rapamycin and 3-MA provided directional support for autophagic involvement; however, 3-MA exerts off-target inhibitory effects on both class I and class III PI3K and should therefore be interpreted as a pharmacological comparator rather than an autophagy-specific inhibitor. Future validation with more selective agents, such as chloroquine or ATG-targeted siRNA, would be required to confirm pathway specificity.

The clinical implications of these findings are potentially significant. The MALAT1/miR-204-5p/LC3B axis may represent a novel layer of fibroblast-specific regulation that contributes to the autophagic remodeling of the atrial substrate during AF. Fibroblast autophagy has been increasingly recognized as a determinant of fibroblast activation and myofibroblast transdifferentiation [8] processes central to atrial fibrosis and perpetuation of the arrhythmogenic substrate. Furthermore, exosomal MALAT1 may serve as a paracrine signal transmitting autophagic cues from stressed fibroblasts to neighboring cardiomyocytes [19].

Several limitations of the present study should be acknowledged. First, our experiments were conducted exclusively in vitro using HCF-aa subjected to RES, which may not fully recapitulate the complex in vivo fibrillating-atrium environment. Validation in animal

models of AF and in human atrial tissue specimens will be necessary. Second, autophagic activation was assessed by LC3B expression and accumulation of puncta by immunofluorescence; direct ultrastructural confirmation by transmission electron microscopy was not performed and represents an important direction for future work. Third, the downstream consequences of LC3B-mediated autophagic activation for fibroblast function remain to be determined in future co-culture and in vivo studies. Furthermore, autophagic flux was not directly assessed using lysosomal inhibitors such as bafilomycin A1, nor was p62/SQSTM1 protein turnover measured; future studies incorporating these approaches will be necessary to definitively distinguish autophagy induction from impaired autophagic clearance. Additionally, the causal role of exosomal MALAT1 as an intercellular paracrine signal was not directly tested; experiments involving the transfer of conditioned media and the inhibition of exosome uptake would be required to formally establish its functional delivery to recipient cells. In addition, exosome isolation was performed using a validated, commercially available precipitation-based kit consistent with our previously published methodology [4]; however, comprehensive biophysical characterization, including nanoparticle tracking analysis, transmission electron microscopy, and tetraspanin marker profiling (CD63, CD81, TSG101), was not performed in accordance with MISEV2023 guidelines, and co-isolation of non-vesicular particles cannot be formally excluded. Finally, although equal protein loading was confirmed by Bio-Rad Protein Assay and LC3B values were normalized to β-actin by ImageJ densitometry, minor inter-blot variability across independent replicates is acknowledged; original unprocessed gel images are available upon request.

In conclusion, our study reveals a novel regulatory axis in which RES-induced exosomal MALAT1, as a ceRNA, putatively sequesters miR-204-5p, thereby derepressing LC3B expression and activating autophagy in atrial fibroblasts (Figure 7). These findings advance our understanding of the regulation of non-coding RNA-mediated autophagy in atrial fibroblasts under electrical stress and suggest that the MALAT1/miR-204-5p/LC3B axis may serve as a potential therapeutic target for modulating autophagy-mediated atrial structural remodeling.

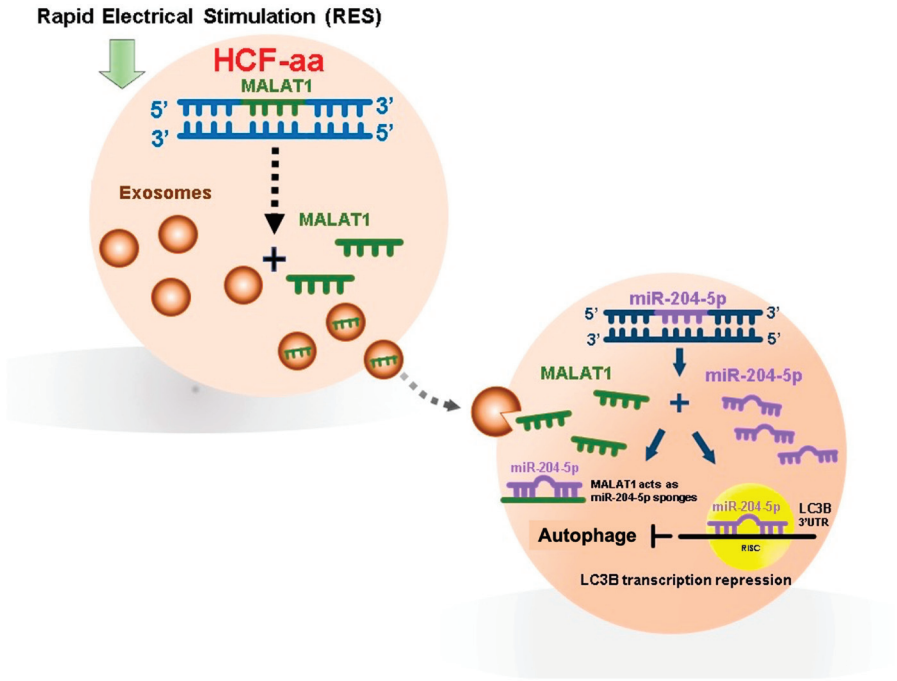


Figure 7. Schematic representation of the proposed molecular mechanism. Rapid electrical stimulation (RES) of HCF-aa triggers significant upregulation of exosomal MALAT1. Within the RES-stimulated HCF-aa, MALAT1 functions intracellularly as a ceRNA, potentially sequestering miR-204-5p.

Concurrent exosomal secretion of MALAT1 may additionally serve as a paracrine mediator to neighboring cells, pending confirmation by conditioned media transfer experiments. This sequestration prevents miR-204-5p from binding to the 3′-UTR of LC3B mRNA, thereby relieving miR-204-5p-mediated repression of LC3B expression. The resulting upregulation of LC3B activates autophagic signaling in atrial fibroblasts subjected to rapid electrical stress.

Supplementary Materials: The following supporting information can be downloaded at: https://www.mdpi.com/article/10.3390/cells15121126/s1, Figure S1: Original gel images used in Figure 2C (time-course Western blot of LC3B-I and LC3B-II in HCF-aa subjected to RES for 1–24 h; $n = 3$ per group); Figure S2: Original gel images used in Figure 5A (Western blot of LC3B-I and LC3B-II in HCF-aa under various functional interventions after 16 h of RES; $n = 3$ per group).

Author Contributions: Conceptualization, S.-K.C. and B.-W.W.; methodology, B.-W.W. and K.-G.S.; validation, S.-K.C., B.-W.W. and C.-M.L.; formal analysis, Y.-J.Y., W.-J.F. and K.-G.S.; investigation, Y.-J.Y. and K.-G.S.; resources, K.-G.S.; data curation, Y.-J.Y. and C.-Y.C.; writing—original draft preparation, S.-K.C.; writing—review and editing, S.-K.C.; visualization, C.-M.L. and C.-Y.C.; supervision, S.-K.C.; funding acquisition, S.-K.C. All authors have read and agreed to the published version of the manuscript.

Funding: This research was funded by Shin Kong Wu Ho Su Memorial Hospital.

Institutional Review Board Statement: Not applicable.

Informed Consent Statement: Not applicable.

Data Availability Statement: The original contributions presented in this study are included in the article/Supplementary Materials. Further inquiries can be directed to the corresponding author.

Acknowledgments: The authors would like to thank the staff of the Division of Cardiology, Shin Kong Wu Ho-Su Memorial Hospital, for their technical assistance and support throughout this study.

Conflicts of Interest: The authors declare no conflicts of interest. The funders had no role in the design of the study; in the collection, analyses, or interpretation of data; in the writing of the manuscript; or in the decision to publish the results.

References

1. Chugh, S.S.; Havmoeller, R.; Narayanan, K.; Singh, D.; Rienstra, M.; Benjamin, E.J.; Gillum, R.F.; Kim, Y.H.; McAnulty, J.H., Jr.; Zheng, Z.-J.; et al. Worldwide epidemiology of atrial fibrillation: A Global Burden of Disease 2010 Study. *Circulation* **2014**, *129*, 837–847. [CrossRef] [PubMed]
2. Hindricks, G.; Potpara, T.; Dagres, N.; Arbelo, E.; Bax, J.J.; Blomström-Lundqvist, C.; Boriani, G.; Castella, M.; Dan, G.-A.; Dilaveris, P.E.; et al. 2020 ESC Guidelines for the diagnosis and management of atrial fibrillation developed in collaboration with the European Association for Cardio-Thoracic Surgery (EACTS): The Task Force for the diagnosis and management of atrial fibrillation of the European Society of Cardiology (ESC) Developed with the special contribution of the European Heart Rhythm Association (EHRA) of the ESC. *Eur. Heart J.* **2021**, *42*, 373–498. [CrossRef]
3. Zhang, J.; Tao, R.; Campbell, K.F.; Carvalho, J.L.; Ruiz, E.C.; Kim, G.C.; Schmuck, E.G.; Raval, A.N.; da Rocha, A.M.; Herron, T.J.; et al. Functional cardiac fibroblasts derived from human pluripotent stem cells via second heart field progenitors. *Nat. Commun.* **2019**, *10*, 2238. [CrossRef] [PubMed]
4. Chuang, C.-Y.; Wang, B.-W.; Yu, Y.-J.; Fang, W.-J.; Lin, C.-M.; Shyu, K.-G.; Chua, S.-K. Exosomal MALAT1 from rapid electrical stimulation-treated atrial fibroblasts enhances Sox-6 expression by downregulating miR-499a-5p. *Cells* **2024**, *13*, 1942. [CrossRef] [PubMed]
5. Chuang, C.-Y.; Wang, B.-W.; Yu, Y.-J.; Fang, W.-J.; Lin, C.-M.; Shyu, K.-G.; Chua, S.-K. Exosomal microRNA-1 regulates Cx43 expression via Tbx18 in culture atrial fibroblasts under rapid electrical stimulation. *Acta Cardiol. Sin.* **2026**, *42*, 47–61. [CrossRef] [PubMed]
6. Nappi, F.; Avtaar Singh, S.S.; Jitendra, V.; Alzamil, A.; Schoell, T. The roles of microRNAs in the cardiovascular system. *Int. J. Mol. Sci.* **2023**, *24*, 14277. [CrossRef] [PubMed]
7. Tay, Y.; Rinn, J.; Pandolfi, P.P. The multilayered complexity of ceRNA crosstalk and competition. *Nature* **2014**, *505*, 344–352. [CrossRef] [PubMed]

8. Michalik, K.M.; You, X.; Manavski, Y.; Doddaballapur, A.; Zörnig, M.; Braun, T.; John, D.; Ponomareva, Y.; Chen, W.; Uchida, S.; et al. Long noncoding RNA MALAT1 regulates endothelial cell function and vessel growth. *Circ. Res.* **2014**, *114*, 1389–1397. [CrossRef] [PubMed]
9. Harada, M.; Okuzaki, D.; Yamauchi, A.; Ishikawa, S.; Nomura, Y.; Nishimura, A.; Motoike, Y.; Koshikawa, M.; Hitachi, K.; Tsuchida, K.; et al. Circulating miR-20b-5p and miR-330-3p are novel biomarkers for progression of atrial fibrillation. *PLoS ONE* **2023**, *18*, e0283942. [CrossRef] [PubMed]
10. Mikhaylova, O.; Stratton, Y.; Hall, D.; Kellner, E.; Ehmer, B.; Drew, A.F.; Gallo, C.A.; Plas, D.R.; Biesiada, J.; Meller, J.; et al. VHL-regulated miR-204 suppresses tumor growth through inhibition of LC3B-mediated autophagy in renal clear cell carcinoma. *Cancer Cell* **2012**, *21*, 532–546. [CrossRef] [PubMed]
11. Xiao, J.; Zhu, X.; He, B.; Zhang, Y.; Kang, B.; Wang, Z.; Ni, X. MiR-204 regulates cardiomyocyte autophagy induced by ischemia-reperfusion through LC3-II. *J. Biomed. Sci.* **2011**, *18*, 35. [CrossRef] [PubMed]
12. Yuan, Y.; Zhao, J.; Gong, Y.; Wang, D.; Wang, X.; Yun, F.; Liu, Z.; Zhang, S.; Li, W.; Zhao, X.; et al. Autophagy exacerbates electrical remodeling in atrial fibrillation by ubiquitin-dependent degradation of L-type calcium channel. *Cell Death Dis.* **2018**, *9*, 873. [CrossRef] [PubMed]
13. Goette, A.; Lendeckel, U.; Kuchenbecker, A.; Bukowska, A.; Peters, B.; Klein, H.U.; Huth, C.; Röcken, C. Impaired cardiac autophagy in patients developing postoperative atrial fibrillation. *J. Thorac. Cardiovasc. Surg.* **2011**, *142*, 1452–1460. [CrossRef]
14. Théry, C.; Witwer, K.W.; Aikawa, E.; Alcaraz, M.J.; Anderson, J.D.; Andriantsitohaina, R.; Antoniou, A.; Arab, T.; Archer, F.; Atkin-Smith, G.K.; et al. Minimal information for studies of extracellular vesicles 2018 (MISEV2018): A position statement of the International Society for Extracellular Vesicles and update of the MISEV2014 guidelines. *J. Extracell. Vesicles* **2018**, *7*, 1535750. [CrossRef] [PubMed]
15. Shyu, K.-G.; Wang, B.-W.; Pan, C.-M.; Lin, C.-M.; Fang, W.-J. Exosomal MALAT1 from macrophages treated with high levels of glucose upregulates LC3B expression via miR-204-5p downregulation. *J. Chin. Med. Assoc.* **2024**, *87*, 581–589. [CrossRef] [PubMed]
16. Klionsky, D.J.; Abdel-Aziz, A.K.; Abdelfatah, S.; Abdellatif, M.; Abdoli, A.; Abel, S.; Abeliovich, H.; Abildgaard, M.H.; Abudu, Y.P.; Acevedo-Arozena, A.; et al. Guidelines for the use and interpretation of assays for monitoring autophagy (4th edition). *Autophagy* **2021**, *17*, 1–382. [CrossRef] [PubMed]
17. Shao, G.; Zhao, Z.; Zhao, W.; Hu, G.; Zhang, L.; Li, W.; Xing, C.; Zhang, X. Long non-coding RNA MALAT1 activates autophagy and promotes cell proliferation by downregulating microRNA-204 expression in gastric cancer. *Oncol. Lett.* **2020**, *19*, 805–812. [CrossRef] [PubMed]
18. Yuan, Y.; Han, X.; Zhao, X.; Zhang, H.; Vinograd, A.; Bi, X.; Duan, X.; Cao, Y.; Gao, Q.; Song, J.; et al. Circulating exosome long non-coding RNAs are associated with atrial structural remodeling by increasing systemic inflammation in atrial fibrillation patients. *J. Transl. Int. Med.* **2024**, *12*, 106–118. [CrossRef] [PubMed]
19. Zhou, Q.; Liu, L.; Zhou, J.; Chen, Y.; Xie, D.; Yao, Y.; Cui, D. Novel insights into MALAT1 function as a microRNA sponge in NSCLC. *Front. Oncol.* **2021**, *11*, 758653. [CrossRef] [PubMed]

Disclaimer/Publisher's Note: The statements, opinions and data contained in all publications are solely those of the individual author(s) and contributor(s) and not of MDPI and/or the editor(s). MDPI and/or the editor(s) disclaim responsibility for any injury to people or property resulting from any ideas, methods, instructions or products referred to in the content.

cells

MDPI

Article

Strip1 Is a Novel Negative Regulator of Cardiomyocyte Hypertrophy

Emanuel Heilein [1,2], Lucia Sophie Kilian [3], Samuel Sossalla [4], Benjamin Meder [1,2], Mirko Völkers [1,2], Karen S. Frese [1,2], Sabine Herch [1], Norbert Frey [1,2] and Matthias Eden [1,2,*]

[1] Department of Internal Medicine III, University of Heidelberg, 69120 Heidelberg, Germany; emanuel@heilein.de (E.H.); mirko.voelkers@med.uni-heidelberg.de (M.V.); karen.frese@med.uniheidelberg.de (K.S.F.); sabine.herch@med.uni-heidelberg.de (S.H.); norbert.frey@med.uni-heidelberg.de (N.F.)
[2] German Centre for Cardiovascular Research, 69120 Heidelberg, Germany
[3] Department of Internal Medicine III (Cardiology and Angiology), University Hospital Schleswig-Holstein, 24105 Kiel, Germany
[4] Department of Cardiology, Giessen and Kerckhoff Heart and Lung Centre, University of Giessen, 61231 Bad Nauheim, Germany
* Correspondence: matthias.eden@med.uni-heidelberg.de

Abstract

Pathological cardiac hypertrophy is a critical factor leading to cardiomyopathy and ultimately heart failure. While several signaling pathways controlling cardiac hypertrophy have been identified, the molecular mechanisms underlying their precise regulation remain incompletely understood. Strip1, a structural component of STRIPAK complexes, has been implicated in various cellular functions; however, its role in cardiomyocytes is uncharacterized. Here we identify Strip1 as a potent anti-hypertrophic factor, controlling cell size and the hypertrophic gene program in neonatal rat ventricular cardiomyocytes (NRVCMs). STRIP1 expression was found to be significantly reduced in human dilated and ischemic cardiomyopathies (DCM/ICM), as well as in murine stress model induced by transverse aortic constriction (TAC). In a knockdown model with morpholino-driven STRIP1 reduction in zebrafish in vivo, impaired cardiac function and heart failure–like features were observed. Interestingly, Strip1 localized to the nucleolus in NRVCMs, suggesting a putative nuclear/epigenetic role in cardiomyocytes. Furthermore, our data support association of Strip1 with cardiac STRIPAK complex, modulating kinase activities, including MST1/MST2 and MST4. Mechanistically, Strip1 appears to influence prohypertrophic signaling, including Hippo- and Calcineurin/NFAT-related pathways, which may contribute to pathological cardiac remodeling. Collectively, these findings establish Strip1 as an important modulator of cardiomyocyte hypertrophy and a potential therapeutic target for cardiomyopathy and heart failure.

Keywords: strip1; heart failure; cardiac hypertrophy; cardiomyopathy; STRIPAK; NRVCM; nucleolus; in vitro; cardiac signaling

1. Introduction

Cardiac hypertrophy represents a fundamental adaptive response of the heart to increased workload, aimed at maintaining function and reducing ventricular wall stress [1]. Physiological hypertrophy, as observed, e.g., in athletes, is beneficial and reversible [2]. In contrast, pathological hypertrophy, triggered by chronic pressure overload, is a process distinct in both morphology and molecular profile that often leads to heart failure and

thus poses a major risk for cardiovascular morbidity and mortality [1,2]. It is driven by a complex network of intracellular signaling pathways that remain incompletely understood, highlighting the need to identify novel regulatory pathways that govern this pathological progression [2,3].

Striatin-interacting phosphatase and kinase (STRIPAK) complexes represent evolutionarily highly conserved multiprotein assemblies that have gained attention as critical regulators of numerous physiological and pathological processes, including tumorgenesis, embryonic neural development, and vascular formation [4–6]. Recent evidence has increasingly highlighted their importance in cardiac function, particularly in relation to hypertrophy and heart failure [6]. Initial insights into the role of STRIPAK in cardiac function emerged from studies on its components, PP2A, striatins, and SLMAP [7–9]. Protein phosphatase 2A (PP2A), which acts within the STRIPAK complex by restraining kinase activity [6], has been identified as a key negative regulator of pathological cardiac remodeling, as transgenic mice overexpressing PP2A are protected from isoproterenol-induced cardiac hypertrophy [9]. Furthermore, heterozygous gene deletion of Striatins in mice identified them as inhibitors of angiotensin II-induced cardiac hypertrophy, while SLMAP was shown to alter the structure of the sarcomeric reticulum and calcium uptake, thereby regulating cardiac contractility [7,8].

We recently identified a STRIPAK member, MST4, as a novel cardiac kinase with potential relevance in heart disease. While its role in cardiomyocytes had not been previously explored, we found MST4 to be highly enriched in rodent hearts and markedly upregulated in human samples from patients with DCM. In NRVCMs, MST4 interacts with STRIPAK components and localizes to the intercalated disc. Its overexpression induces cardiomyocyte hypertrophy, enhances contractility, and reduces apoptosis. Phosphoproteomic analyses revealed potential targets at the intercalated disc, supporting a role of MST4 in regulating cardiomyocyte growth and survival in the context of cardiac remodeling [10]. In addition to its role within STRIPAK complexes, MST4 has been shown to phosphorylate the cytoskeletal protein Ezrin at Thr567, associated with changes in actin organization, which is used as a readout of MST4 kinase activity [11].

Previously we also discovered striatin-interacting protein 2 (Strip2), which we termed "myocardium-enriched, calcium channel–associated protein" (Myoscape), to play a key role in cardiac structure and function, including regulation of cardiac hypertrophy and contractility [12]. Myoscape deficiency in mice resulted in progressive heart failure characterized by myocardial hypertrophy, accompanied by a significant reduction in fractional shortening, the latter also occurring upon knockdown in zebrafish. Furthermore, a reactivation of fetal gene expression (Nppa, Nppb) was observed [12], as well as increased Calcineurin/NFAT signaling, both being associated with cardiac hypertrophy [13–15]. Moreover, Myoscape protein levels were found to be reduced by approximately 80% in myocardial tissue from patients with DCM compared to nonfailing human control hearts [12].

Striatin-interacting protein 1 (Strip1), a paralog of Myoscape, plays important roles in mammalian cells, regulating cellular signaling and actin cytoskeletal organization, affecting cell morphology and migration, but its function in the heart remains unexplored [16,17]. As a central adaptor of the STRIPAK complex, Strip1 connects STRIPAK components and ensures the positioning of PP2A near its targets, including Hippo kinases (MST1/2) and GCK III kinases (MST3/MST4), thereby playing a crucial role in their regulation [17–21]. MST1 and MST2 are the key kinases of the Hippo pathway, which serves as a critical regulator of organ size, cell proliferation, and tissue homeostasis [22]. Phosphorylation of MOB1 serves as a critical activation step for downstream Hippo signaling, as activation of the LATS–MOB1 complex ultimately leads to inactivation of the transcriptional co-activators YAP and TAZ, which serve as the downstream effectors [23]. Moreover, for

https://doi.org/10.3390/cells15060540

several members of the Hippo pathway, including MST1 [24], involvement in pathological cardiac processes has already been described in detail. [23]. Since Strip1 regulates the aforementioned kinase activity in various non-cardiac cell types [6,17,18,20–22], we investigated whether Strip1 influences these cardiac-relevant STRIPAK components and Hippo pathway members in cardiomyocytes. We further assessed whether Strip1 serves a functional role in regulating pathological cardiomyocyte hypertrophy. This study addresses a key knowledge gap by exploring Strip1's subcellular localization, its integration into cardiac STRIPAK, as well as Hippo and Calcineurin/NFAT regulation and its potential role as an anti-hypertrophic regulator.

2. Materials and Methods

2.1. Isolation and Culture of NRVCMs

NRVCMs were isolated from 1- to 2-day-old pooled male and female Wistar rats (Charles River Laboratories, Sulzfeld, Germany). Left ventricles were minced in ADS buffer (116 mM NaCl, 19.7 mM HEPES, 9.4 mM $NaH_2PO_4 \cdot H_2O$, 5.55 mM glucose, 5.36 mM KCl, 0.83 mM $MgSO_4$; all from Sigma-Aldrich, Merck KGaA, Darmstadt, Germany) and digested with 1 mL/heart of ADS containing 0.5 mg/mL collagenase type II (Thermo Fisher Scientific GmbH, Karlsruhe, Germany) and 0.6 mg/mL pancreatin (Sigma-Aldrich) for 20 min at 37 °C.

Cell suspensions were filtered (70 µm), and digestion was terminated with newborn calf serum (Thermo Fisher Scientific; 1:5 dilution). The process was repeated 2–3 times. Cells were centrifuged (950 rpm, 15 min), and cardiomyocytes were enriched by Percoll density gradient (1500 g, 30 min; Cytiva, Freiburg, Germany).

Cells were seeded in DMEM (Thermo Fisher Scientific) containing 10% fetal bovine serum (Cat #10270), 100 U/mL penicillin, 100 µg/mL streptomycin, and 2 mM L-glutamine (Cat #10378-016; all from Thermo Fisher Scientific GmbH, Dreieich, Germany), and cultured at 37 °C with 5% CO_2, which served as the standard condition for both NRVCMs and adult rat ventricular cardiomyocytes (ARVCMs). For additional hypertrophic response NRVCMs were treated with 100µM Phenylephrine or 10 µM Isoproterenol (Sigma-Aldrich Chemie GmbH, Steinheim, Germany, Deutschland Cat #P6126/Cat #I5627).

2.2. Isolation and Culture of ARVCMs

Adult cardiomyocytes were isolated from female six-week-old Wistar rats by retrograde perfusion using a Langendorff system, as previously described [10]. After heparin injection and excision, hearts were perfused via the aorta with isolation buffer (120.4 mM NaCl, 14.7 mM KCl, 0.6 mM KH_2PO_4, 0.6 mM $NaH_2PO_4 \cdot H_2O$, 1.2 mM $MgSO_4 \cdot 7H_2O$, 10 mM HEPES, 4.6 mM $NaHCO_3$, 30 mM taurine, 10 mM 2,3-butanedione monoxime, 5.5 mM glucose; all from Sigma-Aldrich, Merck KGaA, Darmstadt, Germany), followed by enzymatic digestion with collagenase II (Worthington Biochemical Corp, Lakewood, US.) and 40 µM $CaCl_2$.

Cells were dissociated in stop buffer (isolation buffer containing 1% BSA and 12.5 µM $CaCl_2$; Sigma-Aldrich, Merck KGaA) and filtered through a 200 µm mesh. Calcium was reintroduced stepwise (100, 400, and 900 µM; 10 min each), and 100,000 ARVCMs were seeded per well on laminin-coated Nunc™ Lab-Tek™ chamber slides (Cat #154461, Thermo Fisher Scientific GmbH, Dreieich, Germany).

Cells were maintained in M199-based medium (supplemented with 10 mM creatine, 20 mM taurine, 1% BSA, 100 U/mL penicillin, 100 µg/mL streptomycin, and 2 mM L-glutamine; all from Thermo Fisher Scientific GmbH, Dreieich, Germany) and processed for immunofluorescence staining the following day.

https://doi.org/10.3390/cells15060540

2.3. Human Myocardial Samples

Human left ventricular myocardial samples were obtained from explanted hearts of patients suffering from end-stage heart failure (NYHA class IV) who underwent heart transplantation due to either DCM (n = 10) or ICM (n = 9). Control myocardial tissues (n = 6) originated from nonfailing donor hearts collected during standard post-transplant assessments, as previously described [10]. Detailed clinical parameters such as age, sex, comorbidities, or medication at the time of transplantation were not available for all samples and were therefore not included in the analysis. All procedures followed approval by the ethics committee of the University Medical Center Göttingen. Samples were immediately excised in the operating theater, rapidly frozen in liquid nitrogen, and stored at −80 °C until analysis.

2.4. Cloning and Generation of Adenovirus

The coding sequence of rat Strip1 was amplified from cardiac DNA using the GATEWAY Cloning platform, with attB-flanked primers (fwd: 5′-GGGGACAAGTTTGTACAAAAAAGCTGGCACCatgccatgagtaagggattcctttc-3′ and rev: 5′-GGGGACCACTTTGTACAAGAAAGCTGGGTCGCCagacaaggcgacagggaca-3′) and inserted into the pDONR221 entry vector (Thermo Fisher Scientific GmbH, Karlsruhe, Germany) via BP recombination using Gateway® BP Clonase™ II Enzyme Mix (Cat #11789-020, Invitrogen™, Thermo Fisher Scientific). After verification by sequencing (Eurofins GSC Luxembourg S.A., Rollingergrund, Luxembourg), the insert was transferred to the pAd/CMV/V5-DEST™ vector (Cat #V493-20, Invitrogen™, Thermo Fisher Scientific) using Gateway® LR Clonase™ II Enzyme Mix (Cat #11791-020, Invitrogen™, Thermo Fisher Scientific).

Recombinant adenoviruses (AdStrip1) were produced in HEK293A cells and harvested by three freeze–thaw cycles. Viral supernatants were cleared by centrifugation, aliquoted, and stored at −80 °C until use.

2.5. Overexpression of STRIP1 in NRVCMs

NRVCMs were infected 24 h post-isolation with AdStrip1 or control adenovirus (AdLacZ, Thermo Fisher Scientific) at a concentration of 50 infectious units (ifu) per cell. Infection was performed in DMEM containing penicillin/streptomycin and L-glutamine, but lacking fetal bovine serum. Virus-containing medium remained on the cells for 48 h before medium replacement. Cells were collected 72 h post-infection for downstream analysis.

2.6. siRNA-Mediated Knockdown of STRIP1 in NRVCMs

NRVCMs were transfected with either Silencer™ Select Strip1 siRNA (Thermo Fisher Scientific GmbH, Karlsruhe, Germany; Cat #4390771; sense: 5′-GCA UCA AGG UGA UCC GGA Att-3′, antisense: 5′-UUC CGG AUC ACC UUG AUG Ctg-3′) or Silencer™ Select Negative Control No. 1 siRNA (Cat #4390843, Thermo Fisher Scientific) using the TransMessenger® Transfection Reagent (Cat #301525, Qiagen GmbH, Hilden, Germany).

Transfection complexes were prepared according to the manufacturer's instructions. Briefly, 128 pmol siRNA were combined with Enhancer R and Buffer EC-R, followed by addition of TransMessenger reagent. The complexes were diluted in serum- and antibiotic-free DMEM/F-12 medium (Thermo Fisher Scientific) and applied to the cells. 3 h after transfection, the medium was replaced with serum-reduced culture medium (and again after 48 h) and harvested after 72 h.

Transfections were performed in triplicate wells per condition (Strip1 or negative control siRNA) across multiple plates for parallel downstream analyses.

2.7. Zebrafish Morpholino-Mediated STRIP1-Knockdown

Zebrafish (*Danio rerio*) were maintained and bred under standardized laboratory conditions as previously described [12]. All experimental procedures were approved by institutional authorities and performed in accordance with the Guide for the Care and Use of Laboratory Animals (NIH Publication No. 85-23).

250 μM morpholino-modified antisense oligonucleotides targeting the splice donor site of intron 2 of zebrafish *strip1* (5′-TAGCACATAAACCGACACCGTCCAT-3′) or a standard control morpholino (Gene Tools, Philomath, USA) were microinjected into fertilized eggs. To inhibit pigmentation, 0.003% 1-phenyl-2-thiourea (PTU; Cat #P7629, Sigma-Aldrich, Merck KGaA, Darmstadt, Germany) was added to the embryo medium.

Still images and videos were recorded at 48 and 72 h post-fertilization using a Zeiss MCU II stereomicroscope (Zeiss Microscopy, Oberkochen, Germany).

Cardiac function was quantified from bright-field video recordings using Fiji/ImageJ. Ventricular contractility was assessed by fractional shortening (FS) as previously described by Eden et al. [12]. Briefly, end-diastolic and end-systolic frames were identified based on maximal and minimal ventricular dimensions, respectively, and the ventricular short-axis diameter was measured at a consistent anatomical position. Fractional shortening was calculated as the relative change between end-diastolic and end-systolic ventricular diameter.

Pericardial effusion was quantified from a representative frame with clearly visible cardiac anatomy. The inner contour of the pericardial sac and outlining of the heart area were manually delineated, and a pericardial effusion index was calculated as the relative fraction of the pericardial cavity not occupied by the heart. All measurements were performed using identical anatomical landmarks and imaging conditions.

2.8. Transverse Aortic Constriction (TAC) in Mice

The TAC procedure was conducted on male C57BL/6 mice aged between 8 and 10 weeks (Charles-River Laboratories, Sulzfeld, Germany), as described in our previous publication [10]. In short, following lateral thoracotomy, a 6-0 Prolene suture was placed around the transverse aorta, tightening it against a 27-gauge needle to induce controlled stenosis. The thorax was then closed and the pneumothorax was resolved. Control (sham) animals underwent identical surgical steps without the actual ligation. This experiment was conducted following approval by the local ethics committee and in accordance with the regulations set forth by the Ministry for Energy Transition, Agriculture, Environment, and Rural Areas of Schleswig-Holstein.

2.9. Cyclic Biaxial Stretch in NRVCMs

Mechanical stretch was applied to NRVCMs using an established in vitro model, which has been shown to induce a hypertrophic response with upregulation of classical hypertrophy-associated gene expression markers [10].

Cells were seeded at a density of 1×10^7 cells per well onto collagen type I–coated silicone elastomer-bottomed 6-well plates (Bioflex® Collagen Type I Culture Plate, Cat #BF-3001C, Dunn Labortechnik GmbH, Asbach, Germany) in DMEM supplemented with 10% fetal bovine serum (Cat #10270) and 1× penicillin-streptomycin-glutamine (Cat #10378-016; all from Thermo Fisher Scientific, Dreieich, Germany). After 24 h of incubation, cells were washed with PBS and maintained in serum-free DMEM.

Biaxial cyclic stretch (118% total elongation, 1 Hz) was applied for 48 h using the Flexcell® FX-6000™ Tension System with FlexSoft® FX-6000™ V1.0 software (Flexcell International Corporation, Burlington, NC, USA). Unstretched cells cultured under identical conditions on collagen-coated Bioflex® plates served as controls.

2.10. Protein Extraction and Immunoblotting

NRVCMs were lysed by three freeze–thaw cycles in RIPA buffer (1% NP-40, 1% sodium deoxycholate, 0.1% SDS, 150 mM NaCl, 10 mM sodium phosphate, 1 mM DTT, pH 7.2; all from Sigma-Aldrich, Merck KGaA, Darmstadt, Germany) supplemented with phosphatase inhibitors (Cat #P5726, #P0044) and protease inhibitors (Cat #04693132001, Roche Diagnostics GmbH, Mannheim, Germany). Lysates were cleared (14,000× *g*, 10 min, 4 °C), and protein concentration was determined using the DC Protein Assay (Cat #5000111, Bio-Rad Laboratories GmbH, München, Germany).

Mouse and human heart tissues were homogenized in RIPA buffer with ceramic beads (Cat #KT03961-1-003.2, Peqlab, VWR International GmbH, Darmstadt, Germany) and processed similarly. Proteins were separated on 10–12% Criterion™ XT Bis-Tris gels (Bio-Rad), transferred to PVDF membranes (Cat #IPVH00010, Merck Millipore, Burlington, MA, USA) by wet transfer, and blocked with 5% milk in TBS-T (Cat #70166, Sigma-Aldrich).

Membranes were incubated with primary antibodies (Table 1) overnight (4 °C), followed by HRP-conjugated secondary antibodies (Cat #111-035-144, Dianova GmbH, Hamburg, Germany; 1:10,000). Signal detection was performed using ECL Prime (Cat #RPN2232, Cytiva via VWR) and imaged via FluorChem Q (Biozym, Hessisch Oldendorf, Germany) or X-ray films (Cat #34089, Thermo Fisher Scientific). Densitometry was conducted with Fiji (ImageJ2, Version 2.3.0/1.53t) software [25,26], values were normalized to housekeeping or total protein as appropriate.

Table 1. Primary antibodies used for Immunoblotting and Immunofluorescence.

Target	Supplier	Catalog No.	Host Species	Dilution
STRIP1 (OTI7B8)	Novus Biologicals, Centennial, CO, USA	NBP2-45715	Mouse	1:5000 (WB), 1:250 (Co-IP), 1:100 (IF)
MST4 (EP1864Y)	Abcam PLC, Cambridge, UK	ab52491	Rabbit	1:150,000–1:100,000 (WB), 1:500 (IF)
FAM40B	Proteintech, Planegg, Germany	25163-1-AP	Rabbit	1:10,000–1:1000 (WB), 1:100 (IF)
Phospho-MST3/4/STK25 (T174/178/190)	Abcam PLC, Cambridge, UK	ab76579	Rabbit	1:1300 (WB)
Phospho-Ezrin (Thr567)	BioVision, Milpitas, CA, USA	A-1970	Rabbit	1:500–1:1000 (WB)
Ezrin	Novus Biologicals, Centennial, CO, US	NBP2-16396	Rabbit	1:10,000 (WB)
Phospho-YAP (Ser397) LATS1 Phospho-MOB1 (Thr35) MOB1 MST1 MST2 SAV1 Phospho-YAP (Ser127) YAP/TAZ	Cell Signaling Technology Europe B.V., Leiden, The Netherlands	13619 3477 8699 13730 3682 3952 13301 13008 8418	Rabbit	1:1000 (WB)
β-Actin	Santa Cruz Biotechnology, Heidelberg, Germany	sc-47778	Mouse	1:50,000 (WB)
Desmin	Abcam PLC, Cambridge, UK	ab15200	Rabbit	1:700 (IF)
SLMAP	Novus Biologicals, Centennial, CO, USA	NBP1-81398	Rabbit	1:1000 (IF)

Table 1. *Cont.*

Target	Supplier	Catalog No.	Host Species	Dilution
Nucleolin	Novus Biologicals, Centennial, CO, USA	NB600-241	Rabbit	1:50 (IF)
Normal mouse IgG control	Sigma Aldrich, Taufkirchen, Germany	12-371	Mouse	1:250 (Co-IP)
Adenovirus Type 5 Hexon (FITC)	Thermo Scientific, Merelbeke, Belgium	PA1-73053	Goat	1:50 (IF)

2.11. Co-Immunoprecipitation (Co-IP)

Co-IP from NRVCMs was performed using erythrocyte lysing buffer (50 mM HEPES, 250 mM NaCl, 5 mM EDTA, 1% NP-40; all from Sigma-Aldrich, Merck KGaA, Darmstadt, Germany) as previously described [10]. Briefly, 500 µg protein from clarified lysates were incubated overnight at 4 °C with STRIP1 antibody or control IgG (Table 1) at 1:250. Immune complexes were captured using Dynabeads Protein G (Cat #10004D, Thermo Fisher Scientific, Dreieich, Germany) for 4 h at 4 °C, washed five times, and eluted in Laemmli buffer at 95 °C for 5 min. After bead removal, supernatants were used for immunoblotting.

2.12. RNA Isolation, cDNA Synthesis and qPCR

Total RNA from NRVCMs was isolated using the Quick-RNA™ MiniPrep Kit (Cat #R1055, Zymo Research Europe GmbH, Freiburg, Germany) including on-column DNase I digestion. RNA concentration and purity (A260/A280) were assessed using a NanoDrop™ Lite Spectrophotometer (Thermo Fisher Scientific GmbH, Karlsruhe, Germany; Cat #ND-LITE-PR).

Reverse transcription of 500 ng RNA was performed with the iScript™ cDNA Synthesis Kit (Cat #1708891BUN, Bio-Rad Laboratories GmbH, Feldkirchen, Germany), and cDNA was diluted to 1 ng/µL. Quantitative PCR was conducted using the iTaq™ Universal SYBR® Green Supermix (Cat #1725124, Bio-Rad) on a QuantStudio™ 5 Real-Time PCR System (Life Technologies Holdings Pte Ltd., Singapore). Primer sequences used are listed in Table 2. Expression levels were normalized to RPL32 and calculated by the $2^{-\Delta\Delta Ct}$ method. Control samples were set to a reference value of 1. All reactions were run in technical triplicates, including no-template controls; statistical analysis was based on biological triplicates.

Table 2. Primers used for qRT-PCR.

Target	Forward Sequence	Reverse Sequence
STRIP1 rat	ACG AGC TTC CAG AGC TAA CC	ACA CCA CCA GCA TCA TAG TCC
STRIP1 mouse	CTT CCG GAT CCA TGT GTC AGA	AGC TGC ACT CTC CAA AGG TA
STRIP2 rat	CTT CCG AAC TGA ACT GAG TTT CT	CAA ATC CAC CAA GGG TAA ACA
STRIP2 mouse	CCA GGA CCA TGA TGT TAG TGG TG	GCT TAT CAT ATC GGC GGC TG
RPL32 rat/mouse	GGT GGC TGC CAT CTG TTT TAC G	CCG CAC CCT GTT GTC AAT GC
NPPA rat/mouse	GGA GCA AAT CCT GTG TAC AGT G	ACC TCA TCT TCT ACC GGC AT
NPPB rat/mouse	GCA GCA TGG ATC TCC AGA AGG	CTG CAG CCA GGA GGT CTT CC
RCAN1.4 rat/mouse	TAG CTC CCT GAT TGC TTG TG	GGA TTC AAA TTT GGC CCT GG

https://doi.org/10.3390/cells15060540

2.13. Immunofluorescence Staining

For localization studies, 100,000 NRVCMs or ARVCMs per well were seeded on laminin-coated Nunc™ Lab-Tek™ chamber slides (Sigma-Aldrich Chemie GmbH, Steinheim, Germany; L2020-1MG; 154461, Thermo Fisher Scientific GmbH, Dreieich, Germany) and fixed after 16 h. For high-throughput quantification of NRVCM cell area, 20,000 cells per well were plated in 96-well plates (Thermo Fisher Scientific) and fixed after treatment.

Cells were washed three times with PBS and fixed using 4% paraformaldehyde in PBS (P6148, Sigma-Aldrich, Merck KGaA, Darmstadt, Germany). After washing, cells were permeabilized using 0.3% Triton™ X-100 in PBS (T8787, Sigma-Aldrich), followed by additional washes. Blocking was performed in 10% normal horse serum in PBS (Gibco™, Thermo Fisher Scientific GmbH) for 1 h at room temperature.

Primary antibodies (Table 1) were diluted in blocking buffer and incubated overnight at 4 °C in a humidified chamber. After washing, fluorophore-conjugated secondary antibodies (Thermo Fisher Scientific) were applied for 1 h at room temperature in the dark.

Cells were mounted on coverslips (0107032, Marienfeld Superior, Lauda-Königshofen, Germany) using Fluoromount™ containing DAPI (F4680, Sigma-Aldrich, Merck KGaA).

Images for cell area analysis were acquired using an In Cell Analyzer 2200 (GE Healthcare Life Sciences, Buckinghamshire, UK; 29-0278-86). For each experimental condition, multiple cells were analyzed per biological replicate. Confocal microscopy for colocalization studies was performed using a TCS SP8 X system (Leica Microsystems CMS GmbH, Wetzlar, Germany; 8110002344), and image channels were merged with Fiji (ImageJ2, Version 2.3.0/1.53t) software [25,26].

2.14. Protein Sequence Alignment

The amino acid sequences of human STRIP1 (UniProt ID: Q5VSL9) and STRIP2 (UniProt ID: Q9ULQ0) were retrieved from the UniProt database [27]. Pairwise alignment was performed using the EMBOSS Matcher tool V6.6.0 provided by the EMBL-EBI web server [28]. Default settings were used, and results were visualized to identify conserved regions.

2.15. Structure Prediction

Predicted quaternary structures of human STRIP1 (AlphaFold ID: AF-Q5VSL9-F1, version 4) and STRIP2 (AlphaFold ID: AF-Q9ULQ0-F1, version 4) were obtained from the AlphaFold Protein Structure Database (https://alphafold.ebi.ac.uk/, accessed on 24 May 2024). Structural features and domain organization were assessed for comparison.

2.16. Use of Generative Artificial Intelligence Tools

Generative artificial intelligence (GenAI) tools, including ChatGPT versions 4.0, 4o, o4-mini, 4.5 and 5, as well as Perplexity—which is based on models such as GPT-4o, Claude 3.7 Sonnet—were employed to assist in text generation and to support literature and source retrieval during manuscript preparation.

2.17. Statistical Analysis

All statistical analyses were performed using GraphPad Prism 9 (version 9.5.1; GraphPad Software, San Diego, CA, USA). Normality and homogeneity of variance were assessed where appropriate. Outliers were identified using the ROUT method with a Q value of 1%. *n* represents the number of biological replicates; for qPCR and immunoblot analyses, technical replicates were averaged prior to statistical analysis. For cardiomyocyte cell area measurements, the mean cell area of each biological replicate was calculated

and used as the statistical unit for all comparisons. Individual cell measurements were used solely for visualization and were not treated as independent replicates. Comparisons between two groups were conducted using unpaired Student's *t*-tests assuming equal standard deviations and normal distribution. DCM and ICM groups were compared to nonfailing controls by ordinary one-way ANOVA without matching or pairing. Dunnett's multiple comparisons test was applied as the post hoc procedure. Unless otherwise stated, data are presented as mean ± SEM, and error bars in bar graphs represent the standard error of the mean (SEM).

3. Results

3.1. Strip1 Interacts with Key STRIPAK Components in Cardiomyocytes

To investigate the role of Strip1 in cardiomyocyte signaling, we first examined its integration within the multi-enzyme STRIPAK complex in cardiomyocytes. Based on established models from other cell types (Jeong et al. 2021 [17]; Shi et al. 2016 [5]; Tang et al. 2019 [18]), Strip1 is proposed to function as a scaffold within the cardiac STRIPAK complex interacting directly with the phosphatase PP2A, MST4, and striatins, as illustrated in Figure 1a. The two-arm STRIPAK architecture is also presumed for the cardiac STRIPAK, with one arm involving Strip1 and the other SLMAP/SIKE1 anchoring GCKIII/GCKII kinases potentially regulated by PP2A [5,17,18]. Co-immunoprecipitation assays from NRVCM lysates showed that Strip1 was detected in association with key STRIPAK components Strip2 and the GCKIII kinase MST4 (Figure 1b), supporting its integral role within cardiac STRIPAK formation. Immunofluorescence microscopy of ARVCMs revealed Strip1's cytosolic colocalization with MST4 (Figure 1c,d) as well as an overlapping localization with SLMAP in cytosolic and perinuclear regions (Figure 1e,f). Furthermore, a notable nuclear presence of Strip1 was observed (Figure 1e,f). These findings suggest a multifaceted subcellular distribution of Strip1, likely reflecting distinct functional roles.

https://doi.org/10.3390/cells15060540

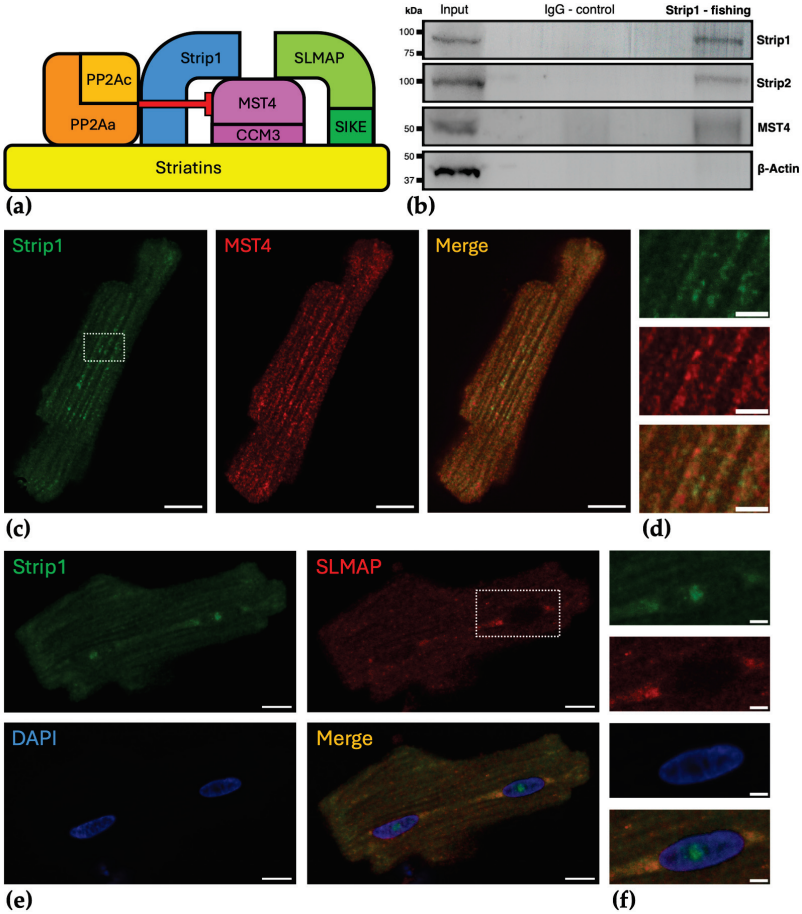


Figure 1. Strip1's association with key cardiomyocyte STRIPAK components and its subcellular localization. (**a**) Proposed STRIPAK complex schematic in cardiomyocytes, based on diverse models from various contexts and cell types by Jeong et al. [17], Tang et al. 2019 [18] and Shi et al. 2016 [5], illustrating Strip1 centrally positioned with interactions to PP2A, striatins, and GCKII/GCKIII kinases, here represented by MST4 as a GCKIII kinase. Red T-shaped bar indicates inhibition of GCKII/GCKIII by PP2A [5,17,18]; (**b**) Co-IP from NRVCM lysates using Strip1 antibody for pulldown. Immunoblotting for Strip2 and MST4 detects bands in Strip1 pulldown samples, while β-actin serves as a negative control. Uncropped full-length blots are shown in Supplementary Figure S1; (**c**) Immunofluorescence staining of ARVCMs for Strip1 (green) and MST4 (red) demonstrates cytosolic colocalization in merged image; boxed area is enlarged in (**d**); (**e**) Immunofluorescence staining of ARVCMs for Strip1 (green) and SLMAP (red) with DAPI nuclear counterstain shows colocalization in the cytosol and perinuclear region; additional nuclear localization of Strip1 is observed; (**f**) boxed region from (**e**) enlarged; Scale bars: (**c**,**e**) 10 µm; (**d**,**f**) 3 µm;.

3.2. Structurally Similar Strip1 and Strip2 Show Independent Regulation and Distinct Subcellular Localization in Cardiomyocytes

Amino acid sequence alignment of human Strip1 and Strip2 (UniProt accessions Q5VSL9 and Q9ULQ0) performed with EMBOSS Matcher highlighted conserved regions, underscoring their structural similarity (Figure 2a). Further, predicted structures generated with AlphaFold confirmed analogous domain organization and confidence levels between the two proteins (Figure 2b,c). These similarities in primary and tertiary structures suggest that the paralogs may also share related functional roles. Functional modulation in NRVCMs using adenoviral overexpression and siRNA knockdown showed that STRIP1 levels can be specifically manipulated without altering STRIP2 expression at the mRNA level, indicating independent regulation (Figure 2d). Immunofluorescence in native ARVCMs showed that while both proteins colocalize in cytosolic and perinuclear regions, Strip1 uniquely localizes to a discrete intranuclear structure corresponding to the nucleolus,

confirmed by co-staining with the nucleolar marker Nucleolin (Figure 2e–g). This distinct localization might indicate specialized nuclear functions for Strip1 not shared by Strip2.

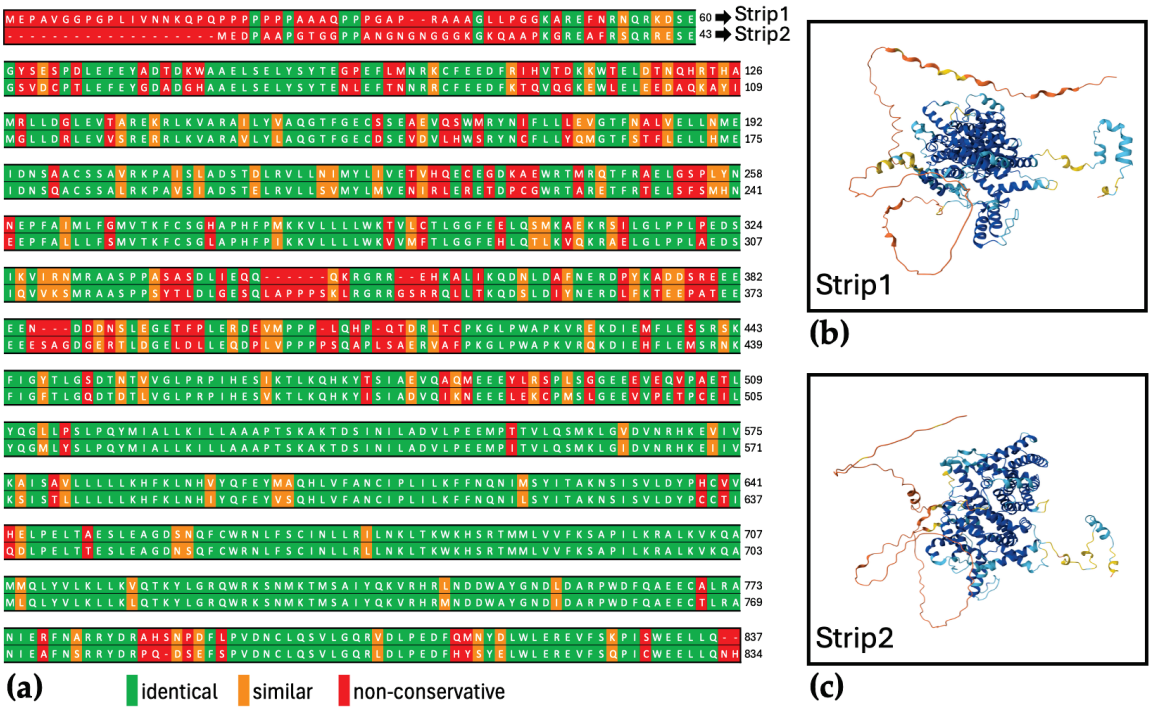


Figure 2. *Cont.*

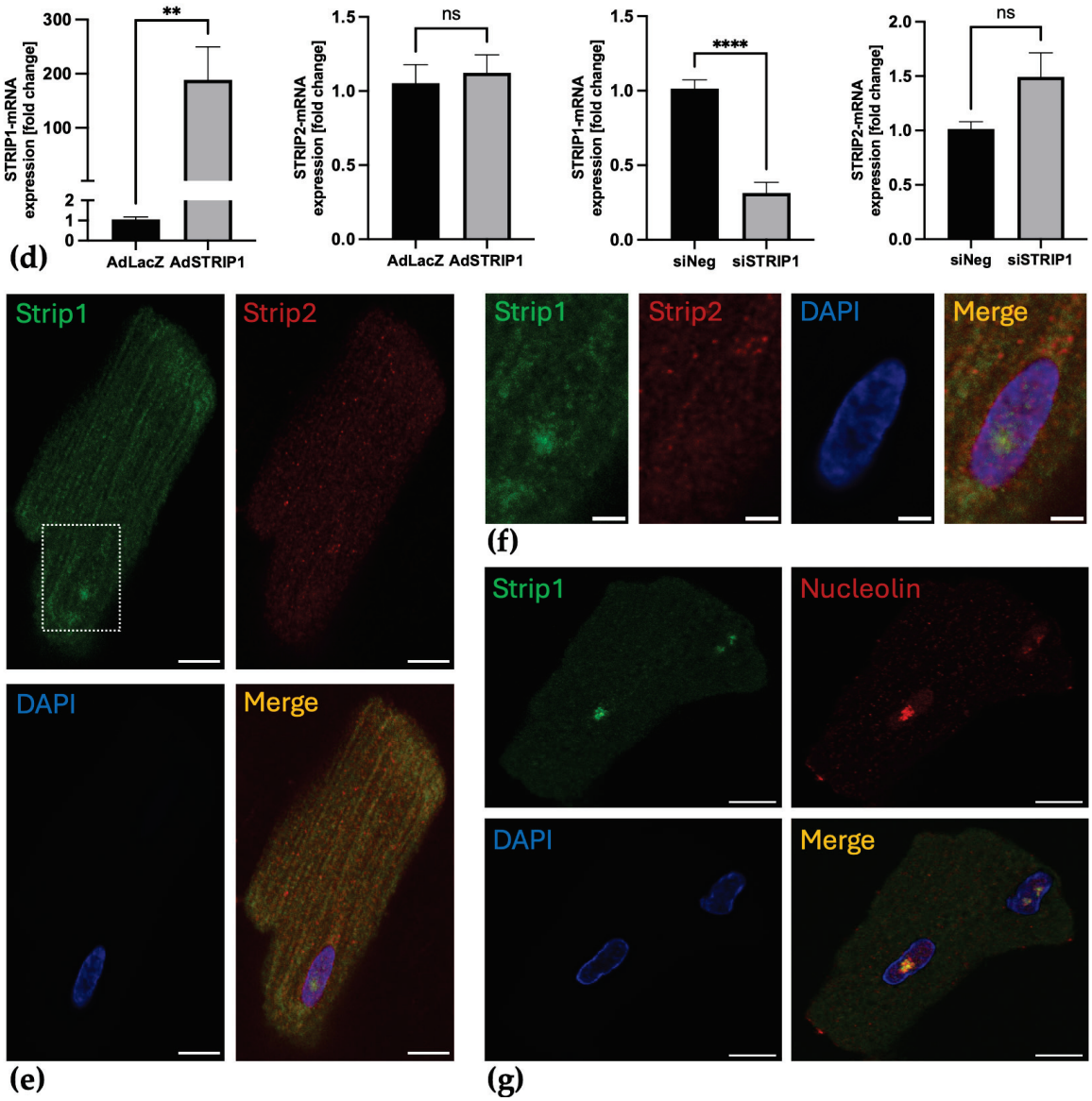


Figure 2. Structural similarity and distinct expression patterns of Strip1 and Strip2 in cardiomyocytes. (**a**) Alignment of Strip1 and Strip2 amino acid sequences using EMBOSS Matcher highlights conserved regions [28]; (**b**) Predicted structures of Strip1 and (**c**) Strip2 generated using AlphaFold [29,30] reveal similar domain organization. Color indicates per-residue model confidence (pLDDT): very high (pLDDT > 90, dark blue), high (70–90, light blue), low (50–70, yellow), and very low (<50, orange) [29,30]; (**d**) qPCR analysis of STRIP1 and STRIP2 mRNA following adenoviral-mediated overexpression of STRIP1 (AdSTRIP1, 50 ifu, 72 h—control: AdLacZ) or siRNA-mediated knockdown (siSTRIP1, 128 pmol, 96 h; control: siControl) in NRVCMs. While STRIP1 levels are significantly increased after AdSTRIP1 and decreased after siSTRIP1 compared to control, STRIP2 expression remains unchanged (n = 3); (**e**) Immunofluorescence staining of ARVCMs for Strip1 (green) and Strip2 (red) shows cytosolic and perinuclear colocalization; Strip1 additionally accumulates in an intranuclear round focus; (**f**) Enlarged view of boxed region from (**e**); (**g**) Immunofluorescence staining of ARVCMs for Strip1 and nucleolar marker Nucleolin demonstrates nucleolar colocalization; nuclei are counterstained with DAPI (blue); Scale bars: (**e**,**g**) 10 µm; (**f**) 3 µm; Student's t-test; ns = not significant; ** $p < 0.01$; **** $p < 0.0001$; Data are shown as mean ± SEM.

3.3. Strip1 Expression Is Reduced in Human Cardiomyopathy and Under Mechanical Stress

We next assessed Strip1 expression in human heart samples from patients with end-stage DCM or ICM, relative to nonfailing controls. Western blot analysis demonstrated a significant reduction of Strip1 protein in both DCM and ICM groups compared to nonfailing

controls (Figure 3a,b). These clinical observations were mirrored in a murine model of pressure overload induced by transverse aortic constriction (TAC), where Strip1 protein levels significantly declined compared to sham-operated controls (Figure 3c,d), suggesting a mechanosensitive expression of STRIP1. Indeed, an in vitro mechanical stretch of NRVCMs showed downregulation of STRIP1 mRNA after 48 h, supporting the notion that mechanical stress directly influences STRIP1 expression (Figure 3e). Collectively, these data indicate that STRIP1 downregulation is a hallmark of pathological remodeling associated with heart failure and mechanical stress.

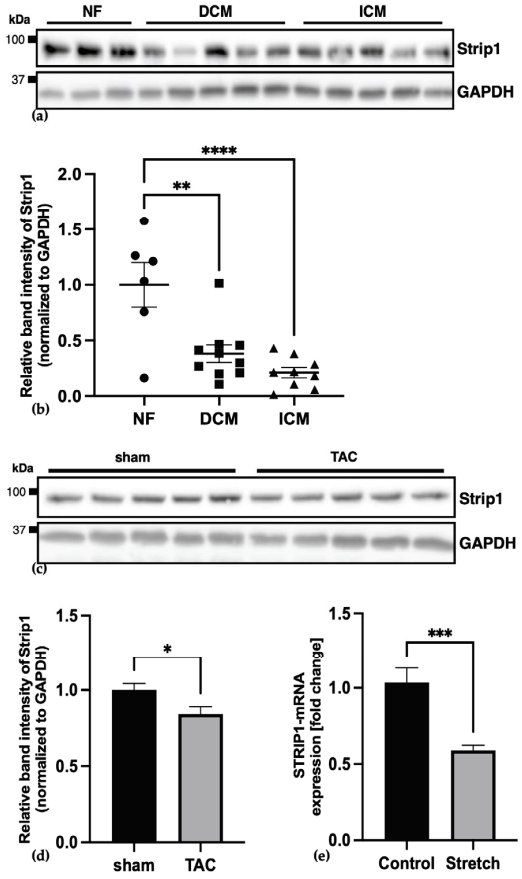


Figure 3. STRIP1 expression is reduced in human cardiomyopathy and models of mechanical stress. (**a**) Western blot analysis of Strip1 in human heart tissue from nonfailing (NF), DCM and ICM patients, with GAPDH as the loading control; (**b**) Densitometric quantification normalized to GAPDH shows significantly reduced STRIP1 expression in both DCM (n = 10 individuals) and ICM (n = 9) compared to nonfailing controls (n = 6); the representative blot does not show all biological replicates; (statistics: one-way ANOVA; * $p < 0.05$); (**c**) Western blot analysis of Strip1 in mouse heart samples reveals significantly decreased Strip1 protein levels following transverse aortic constriction (TAC) (n = 5) compared to sham-operated controls (n = 5), as quantified by (**d**) densitometry of the bands; (**e**) qPCR in NRVCMs after 48 h of mechanical stretch reveals significant downregulation of STRIP1 expression compared to unstretched control cells (n = 3); (**a**,**c**) Uncropped full-length blots are shown in Supplementary Figure S2; Student's t-test; ns = not significant; * $p < 0.05$; ** $p < 0.01$; *** $p < 0.001$; **** $p < 0.0001$; Data are shown as mean ± SEM.

3.4. Strip1 Acts as a Negative Regulator of Cardiomyocyte Hypertrophy

Functional analyses in NRVCMs demonstrated that adenoviral-mediated overexpression of STRIP1 significantly reduced cardiomyocyte surface area relative to LacZ controls, indicating an antihypertrophic effect (Figure 4a). In contrast, STRIP1 knockdown via siRNA did not significantly alter cell size compared to control siRNA (Figure 4a,b). Compared with native NRVCMs, adenovirus-treated cells, including AdLacZ controls, displayed an

increased cell size. No further obvious morphological alterations were observed apart from changes in cell size. At the molecular level, hypertrophic marker genes NPPA, NPPB, and RCAN1.4 were significantly downregulated following STRIP1 overexpression, suggesting that STRIP1 inhibits pathological hypertrophy (Figure 4c). This reduction was further pronounced when AdSTRIP1-infected NRVCMs were subjected to additional hypertrophic stimulation during the final 24 h using phenylephrine (PE) or isoproterenol (ISO) (Figure 4d), indicating that STRIP1 overexpression attenuates hypertrophic marker gene expression in response to adrenergic stress. Notably, the reduction in RCAN1.4, a known marker of calcineurin–NFAT pathway activity, suggests that Strip1 also suppresses this pro-hypertrophic signaling pathway (Figure 4c). In contrast, siRNA-mediated STRIP1 knockdown showed a trend toward increased expression of hypertrophic marker genes compared to control siRNA, both under basal conditions and following PE or ISO stimulation, although these changes did not reach statistical significance (Supplementary Figure S3). While fractional shortening was reduced in MO STRIP1 embryos compared to control morpholino-treated embryos, this difference did not reach statistical significance (Figure 4e,f). In contrast, pericardial effusion was significantly increased in MO STRIP1 embryos and was particularly pronounced at 72 h post fertilization, indicating compromised cardiac performance despite modest effects on systolic contractility (Figure 4e,f). No gross morphological abnormalities were observed in STRIP1 morphant zebrafish embryos compared to controls. Overall body morphology appeared comparable between groups. A tendency toward increased curvature of paravertebral skeletal muscle was noted in some morphants, but this was not further analyzed. Given the known limitations of morpholino-based approaches, including potential off-target effects, these in vivo findings are interpreted with caution. Accordingly, they provide supportive functional evidence for impaired cardiac performance following STRIP1 loss during development but are not intended as a standalone model of pathological hypertrophy. These results collectively underscore Strip1's essential role in preventing pathological hypertrophy and maintaining cardiac function.

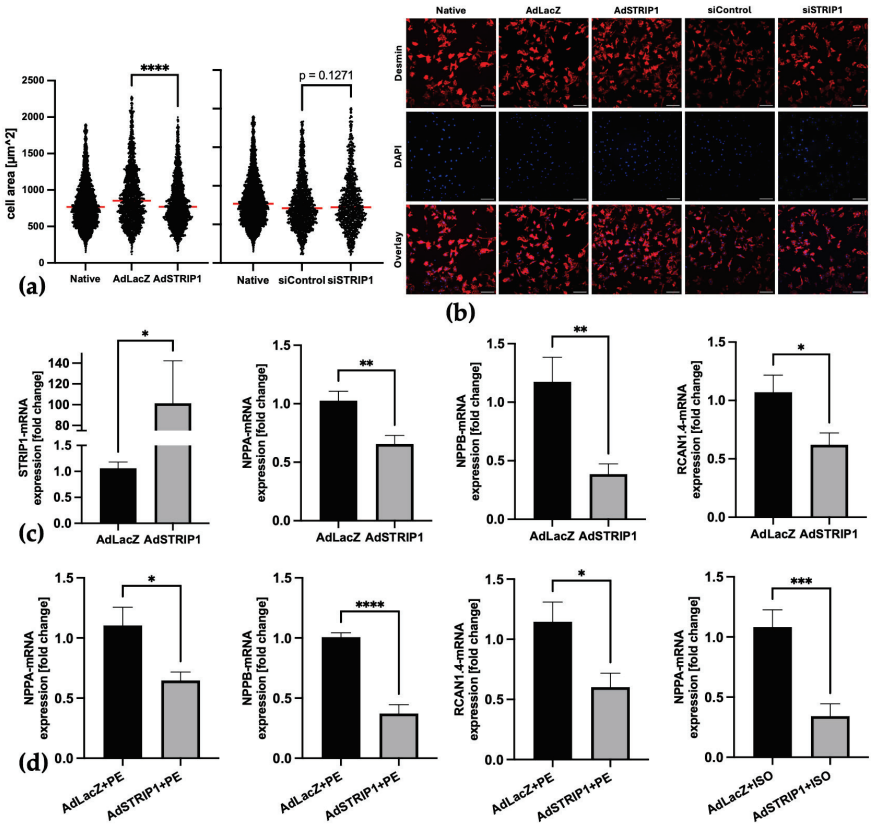


Figure 4. *Cont.*

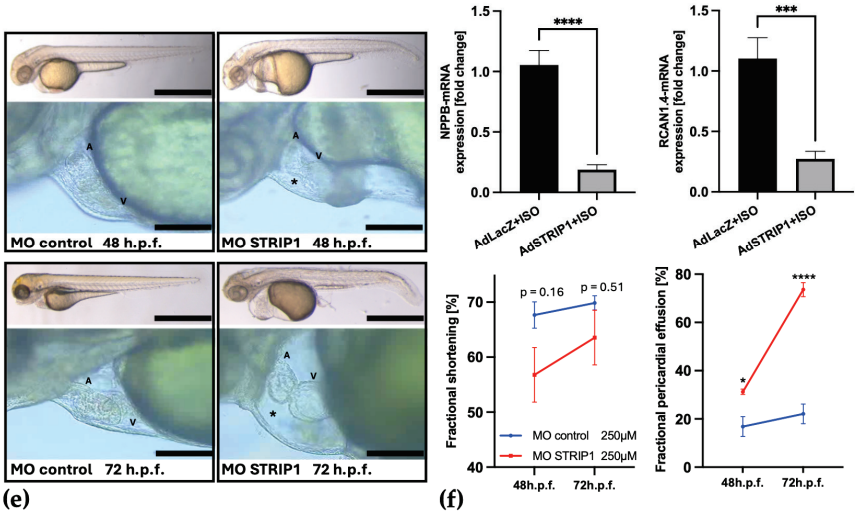


Figure 4. Strip1 modulates cardiomyocyte hypertrophy in vitro and in vivo. (**a**) Quantification of NRVCM area (µm^2) under conditions: Native, siControl, siSTRIP1, AdLacZ and AdSTRIP1. Cell area in AdSTRIP1 is significantly reduced compared to AdLacZ, while NRVCMs after siSTRIP1 show no significant difference from siControl. Apart from changes in cell size, no obvious morphological alterations were observed. For visualization, the scatter plot displays individual cell measurements. Statistical analyses were performed using the mean cell area of each biological replicate as the statistical unit (n = 3 biological replicates); (**b**) Representative immunofluorescence images for each condition, showing Desmin (cell bodies), DAPI (nuclei), and merged overlays; High-resolution images of Figure 4b are shown in Supplementary Figure S4; (**c**) qPCR analysis shows that NPPA, NPPB, and RCAN1.4 mRNA expression is significantly reduced 72 h after AdSTRIP1 infection (50 ifu) compared to AdLacZ control in NRVCMs (n = 3); (**d**) with additional stimulation during the final 24 h with phenylephrine (PE, 100 µM or isoproterenol (ISO, 10 µM), this significant reduction in NPPA, NPPB and RCAN1.4 becomes more pronounced; (**e**,**f**) Zebrafish embryos with morpholino-induced STRIP1 knockdown (MO STRIP1; n = 5) at 48 hpf and 72 hpf (hours post fertilization) show reduced but non-significant fractional shortening compared to control morpholino-treated embryos (MO control; n = 4). In contrast, MO STRIP1 embryos exhibited significant pericardial effusion (=*), pronounced at 72 hpf (A = atrium, V = ventricle); Scale bars: (**b**) 100 µm; (**e**,**f**) 60 µm in whole-embryo image & 20 µm in cardiac close-up; Student's t-test; ns = not significant; * $p < 0.05$; ** $p < 0.01$; *** $p < 0.001$; **** $p < 0.0001$; Data are shown as mean ± SEM.

3.5. Strip1 Modulates Hippo Signaling and MST4 Kinase Activity

To explore downstream signaling pathways influenced by Strip1, we analyzed Hippo pathway–related signaling, previously implicated in STRIPAK signaling in non-myocytes [22,31]. In NRVCMs, adenoviral-mediated STRIP1 overexpression led to increased phosphorylation of MOB1, while total protein levels of YAP, MST1, MST2, and TAZ were significantly decreased relative to controls (Figure 5a–f). As these analyses were limited to total protein abundance for several components, these changes should not be interpreted as direct measures of pathway activity but rather suggest an association of cardiac Strip1 with Hippo-related signaling. Furthermore, STRIP1 knockdown elevated phosphorylated MST4 levels without altering total MST4 protein, providing direct evidence for altered MST4 kinase activation (Figure 5g–i), a GCKIII kinase and established STRIPAK component. Taken together, these results suggest that Strip1 is associated with the regulation of selected STRIPAK-related kinases, including Hippo pathway–associated components and the GCKIII kinase MST4, rather than establishing comprehensive regulation of GCKII kinases or Hippo pathway activity in cardiomyocytes.

https://doi.org/10.3390/cells15060540

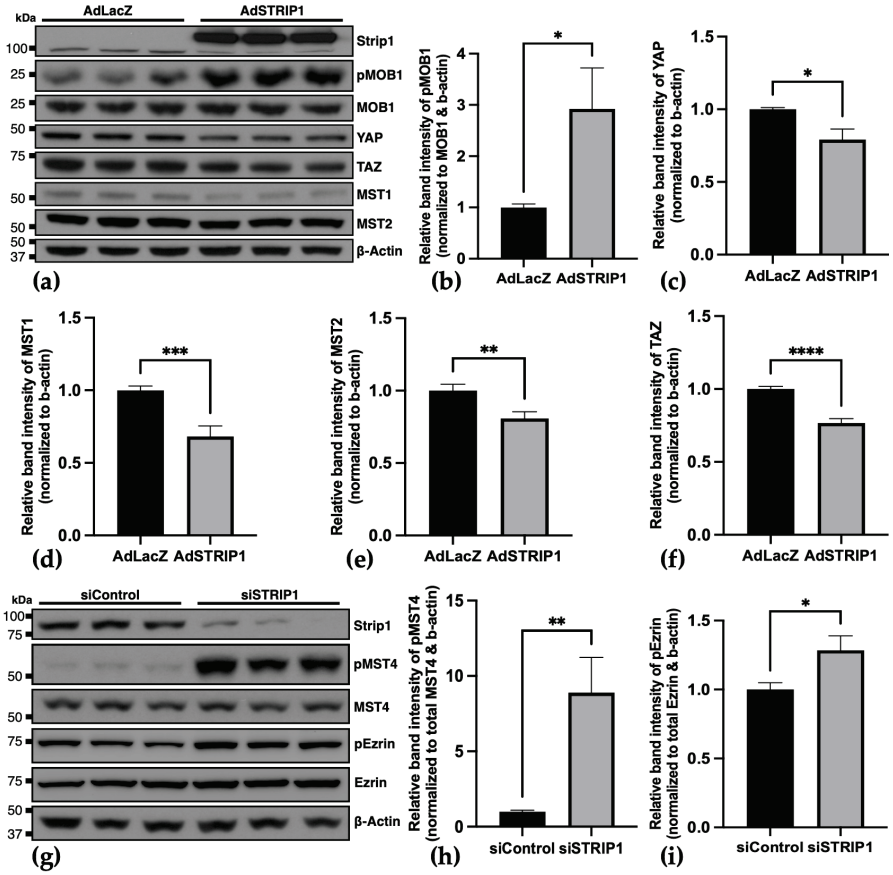


Figure 5. Strip1 modulates Hippo-pathway-related components and MST4 activity in NRVCMs. (**a**) Western blot analysis of Hippo pathway components in NRVCMs 72 h after infection with AdSTRIP1 (50 ifu) compared to AdLacZ control. (**b**–**f**) Densitometry of bands, normalized to β-actin and, for phosphorylated proteins, additionally to the respective total protein levels. Infection with 50 ifu AdSTRIP1 results in significantly increased (**b**) MOB1 phosphorylation, while total protein levels of (**c**–**f**) YAP, MST1, MST2 and TAZ are reduced significantly compared to control after 72 h. (**g**) Western blot analysis following STRIP1 knockdown (siSTRIP1) in NRVCMs shows a significant increase in phosphorylated MST4 (p-MST4), whereas total MST4 protein levels remain unchanged relative to control. Densitometric quantification of (**h**) p-MST4 relative to total MST4 and (**i**) relative to Ezrin, both normalized to β-actin. (**a**,**g**) Uncropped full-length blots are shown in Supplementary Figures S5 and S6; (**a**–**i**), $n = 3$; Student's t-test; ns = not significant; * $p < 0.05$; ** $p < 0.01$; *** $p < 0.001$; **** $p < 0.0001$; Data are shown as mean ± SEM.

4. Discussion

Our study identifies Strip1 as an essential negative regulator of pathological cardiomyocyte hypertrophy in vitro and in vivo and implicates Strip1 in cardiac STRIPAK-related signaling pathways. Notably, Strip1 overexpression attenuates hypertrophic marker gene induction not only under basal conditions but also in response to adrenergic stress, providing evidence for its function under pathophysiologically relevant stimulation. Importantly, Strip1 expression is markedly reduced in human dilated (DCM) and ischemic (ICM) cardiomyopathy, representing an association with advanced human heart failure and linking our experimental findings to clinically relevant disease states. This is the first evidence directly implicating Strip1 in cardiac biology and remodeling, thereby expanding our understanding of hypertrophic signaling and its translational significance for heart failure.

We recently confirmed the existence of a cardiac STRIPAK complex while investigating the role of MST4 [10]. Co-IP and immunofluorescence analyses showing Strip1 interaction and colocalization with Strip2/Myoscape, MST4, and SLMAP in cardiomyocytes now also

support the involvement of Strip1 in cardiac STRIPAK-associated complexes. Strip1 may serve a core scaffolding role, as established in other cell types [6]. The perinuclear and cytoplasmic colocalization of Strip1 and Strip2 further suggests functional cooperation in cardiomyocytes, consistent with STRIPAK organization in other systems [5].

Strip1 and Strip2 share structural similarity [32] and morpholino-mediated Strip1 knockdown in zebrafish displays impaired cardiac function characterized by significant pericardial effusion and a trend toward reduced contractile performance, similar to Myoscape-deficient zebrafish, which showed severely impaired ventricular contractility and the development of pericardial effusion [12]. Nevertheless, their functions are non-redundant: Strip1 knockout causes embryonic lethality due to impaired mesodermal migration [16], while Strip2-deficient mice survive but develop severe heart failure [12]. The absence of Strip2 compensation following Strip1 knockdown underlines this specificity.

The perinuclear localization of Strip1 in cardiomyocytes resembles STRIPAK component patterns in other cell types, likely reflecting the Golgi or, in the case of SLMAP, the nuclear envelope association [6,33]. However, the apparent accumulation of Strip1 in the nucleolus of ARVCMs is unexpected. In murine podocytes, Strip1 is nuclear but homogeneously distributed throughout the nucleoplasm [34], whereas nucleolar localization has only been described for Strip2 in murine embryonic CGR8 stem cells, alongside its cytosolic and perinuclear distribution [35].

While the nucleolus is primarily known for ribosome production [36], cell cycle regulation and apoptosis [37], a connection between its function and cardiac disease has also been established [38]. For instance, nucleolar enlargement associated with increased ribosomal activity has been observed in human ICM and DCM [39]. Additionally, nucleolar organizer region (NOR) activity correlates positively with cardiac mass and left ventricular hypertrophy in patients with hypertension but is reduced in ICM and heart failure [40], as reviewed by Hariharan et al. [38].

Recently, specific nucleolar proteins, including Nucleolin, Nucleophosmin, and Nucleostemin, have been uncovered to influence cardiomyocyte growth, survival and stress adaptation [38,41,42]. Our immunofluorescence-based observation suggesting a nucleolar association of Strip1 raises the question whether Strip1 joins this growing list of nucleolar proteins, integrating stress signals and growth responses in the heart.

Cardiac hypertrophy, a key contributing factor in the development of cardiomyopathies and heart failure [43], appears to be negatively regulated by Strip1, as indicated by multiple experimental approaches. Strip1 overexpression reduces cardiomyocyte size and expression of hypertrophic markers NPPA and NPPB under basal conditions and further attenuates adrenergic stress–induced expression of NPPA, NPPB, and RCAN1.4 following phenylephrine or isoproterenol stimulation, while knockdown increases expression of Nppa. In contrast, loss-of-function approaches yielded only modest and variable molecular responses, suggesting that reduced Strip1 levels alone are not sufficient to robustly drive hypertrophic gene activation in this setting (Supplementary Figure S1). These in vitro findings are complemented by the zebrafish data, which provide supportive in vivo evidence for compromised cardiac performance following STRIP1 loss rather than a standalone model of pathological hypertrophy.

Therefore, Strip1's downregulation in ICM may reflect a modest and potentially compensatory response, as myocardial hypertrophy is a known initially adaptive response to the functional insufficiency of damaged myocardial tissue under ischemic conditions [44]. Comparable mechanisms of compensatory remodeling may also account for Strip1's downregulation in DCM, an observation consistent with prior reports of decreased Strip2 expression in end-stage DCM patients [12]. Given the relatively small but statistically significant changes observed, this interpretation should be viewed cautiously. Strip1 expression also

declines under mechanical stress—after TAC and in vitro stretch —further supporting its role in modulating hypertrophic adaptation under pathological load.

We observed Strip1's influence on multiple hypertrophy-regulating signaling pathways, likely underlying its anti-hypertrophic effects. One key pathway is Calcineurin/NFAT, a well-characterized mediator of pathological cardiac hypertrophy [45]. Calcineurin activates NFAT, promoting hypertrophic gene expression [46], with sustained activation leading to DCM and heart failure in mouse models [46]. Moreover, in patients with DCM and NYHA class IV heart failure, calcineurin activity is elevated by approximately 80% compared to nonfailing hearts, along with increased activation of NFAT transcription factors [47]. Notably, the calcineurin–NFAT pathway is activated in pressure overload models of pathological hypertrophy but not in endurance training models of physiological hypertrophy [48]. Strip1 overexpression significantly reduces RCAN1.4 expression, which is widely regarded as a robust and sensitive readout of Calcineurin/NFAT pathway activity due to the high density of NFAT binding sites within its promoter region [49]. As RCAN1.4 is induced almost exclusively upon Calcineurin activation in cardiomyocytes, its downregulation both under basal conditions and in response to adrenergic stimulation suggests that Strip1 limits Calcineurin/NFAT-driven pro-hypertrophic signaling [49]. This is consistent with findings in STRIP2 knockout mice, where excessive activation of the calcineurin/NFAT pathway was observed following TAC. [12] Since enhanced Calcineurin activity occurs in both Strip1- and Strip2-deficient conditions, both paralogs likely contribute to suppressing pathological hypertrophy, at least in part via this pathway [12].

Another mechanism may involve Strip1's association with Hippo signaling pathway, which governs heart size via regulation of proliferation during development and hypertrophy in adult cardiomyocytes [23,50]. For one, Strip1 overexpression reduced YAP expression, as assessed at the total protein level. In patients with hypertrophic cardiomyopathy (HCM), YAP activity and gene expression are elevated [51], consistent with findings in NRVCMs where YAP1 overexpression promotes and knockdown attenuates hypertrophy [52].

In transgenic mice, MST1 overexpression induces apoptosis and DCM, while it fails to elicit compensatory hypertrophy in the surviving cardiomyocytes [24]. Yet its expression is reduced upon Strip1 overexpression, which appears counterintuitive. However, only total MST1 expression was assessed, while phosphorylation status, indicating its activation, was not analyzed. Changes in total protein abundance may reflect altered transcription, protein stability, or cellular stress responses rather than pathway activity per se. The increased MOB1 phosphorylation observed upon Strip1 overexpression in NRVCM is further compatible with altered Hippo signaling, in line with findings in HEK293A cells [17]. Notably, STRIP1 knockout in HEK293A cells results in increased MST1 phosphorylation. [22]. Although the effects of Strip1 on Hippo pathway components are not unidirectional, these data collectively suggest a potential association between Strip1 and Hippo-related signaling in cardiomyocytes but should be interpreted cautiously and do not constitute definitive evidence for direct regulation of Hippo pathway activity.

Enhanced phosphorylation of MST4 following STRIP1 knockdown is also consistent with prior reports in other cell types, where Strip1 contributes to MST4 inhibition within the STRIPAK complex [21]. As illustrated in Figure 1a, adapted from established STRIPAK models [5,18], Strip1 likely forms a scaffold with striatins in cardiomyocytes to facilitate recruitment of the phosphatase PP2A to GCKIII kinases such as MST4 [6]. The observed increase in Ezrin phosphorylation at Thr567 upon STRIP1 knockdown in NRVCMs is most likely attributable to the elevated activation of MST4. Previous studies in W4 cells demonstrated MST4-dependent Ezrin phosphorylation at this site [11], whereas direct interaction between Strip1 and Ezrin was not seen in large-scale interactome studies using JEG-3 epithelial cells [53].

Together, these findings suggest that Strip1 not only modulates MST4 activity in NRVCMs but subsequently modulates its effects on downstream substrates. Since MST4 overexpression promotes hypertrophy in NRVCMs [10], while Strip1 has the opposite effect, their inverse expression patterns under mechanical stress and in DCM samples [10] may suggest that Strip1 exerts anti-hypertrophic effects, at least in part by limiting MST4-associated signaling within the STRIPAK complex. In contrast, MST4 is markedly upregulated in samples of DCM and ICM [10]. Similarly, following in vitro biaxial stretch, MST4 expression is upregulated along with stress biomarkers NPPA and NPPB [10], while Strip1 expression is decreased. These reciprocal expression patterns may suggest opposing roles for Strip1 and MST4 in cardiomyocytes and their contribution to cardiac pathology.

A recently identified chromatin-associated complex in cardiomyocytes—comprising Calcineurin, its inhibitor Carabin, MST3, and the histone monomethyltransferase MLL3—has been shown to epigenetically regulate cardiac hypertrophy [54]. Under basal conditions, Carabin inhibits Calcineurin, while MST3 suppresses MLL3 activity via phosphorylation. Upon mechanical stress, induced by TAC, displacement of Carabin and MST3 allows subsequent MLL3 and Calcineurin activation, both promoting hypertrophic gene expression [54]. Our observations that Strip1 affects not only Calcineurin activity but also MST4 phosphorylation, a GCKIII kinase closely related to MST3, suggest that both pathways may converge downstream on MLL3, which regulates cardiac hypertrophy and, like Strip1, is localized to the nucleus.

However, a potential discrepancy arises in that MST3 appears to act as a brake on MLL3-mediated hypertrophy within the complex [54], while our previous data on MST4 [10] suggest a prohypertrophic influence of GCKIII kinases. Together with the observed increase in MST4 activity following STRIP1 knockdown, this raises important questions about the precise role of MST3/4 activity in different cellular contexts and underscores the need for further investigation into how Strip1 interacts with these kinases and the chromatin regulatory machinery [54].

Future investigations should explore the role of Strip1 in cardiomyocyte apoptosis, a promising avenue given the known involvement of nucleolar proteins in apoptotic signaling, as well as the pro-apoptotic roles of the kinases MST1, MST2, and MST4, which we showed to be influenced by Strip1 in NRVCMs. We previously observed reduced cleavage of Caspase-3 and -7 in NRVCMs upon MST4 overexpression, indicating suppression of apoptosis. Conversely, MST4 knockdown significantly increased Caspase-7 activity [10]. Cardiac-specific overexpression of MST1 in transgenic mice has been associated with increased caspase activity and cardiomyocyte apoptosis [24], whereas MST2-deficient mice exhibit reduced apoptosis [55]. Depending on cellular context, however, MST1 and MST2 may also exert anti-apoptotic effects [56,57]. The apparent contradiction, putative pro-apoptotic influence of Strip1 via MST4 regulation versus potentially anti-apoptotic effects via MST1/MST2 downregulation, suggests complex and potentially compensatory mechanisms that warrant further elucidation.

Limitations: Although our data suggest a role for Strip1 in regulating cardiac hypertrophy, a murine knockout model will be required for further validation. As global deletion of STRIP1 is lethal [16], a heart-specific knockout using αMHC-Cre recombination is planned for future studies. The use of morpholino-mediated STRIP1 knockdown in zebrafish represents a limitation, as morpholinos can be associated with off-target or non-specific effects. Therefore, the zebrafish data were used not as a primary basis for mechanistic interpretation, but rather to provide supportive in vivo evidence in line with the in vitro findings. Although no overt morphological defects were observed in STRIP1 morphants, additional uncharacterized structural or functional abnormalities cannot be excluded. Furthermore, mechanistic analyses were largely limited to total protein expression, as phosphorylation status, subcellular localization,

https://doi.org/10.3390/cells15060540

and downstream transcriptional activity—particularly TEAD-dependent output of the Hippo pathway—were not directly assessed. Accordingly, changes in YAP/TAZ abundance are interpreted as suggestive rather than definitive evidence of Hippo pathway modulation. The functional significance of Strip1's putative nucleolar localization remains to be determined, particularly its involvement in ribosome biogenesis, stress responses, or apoptosis, and will require biochemical validation in future studies.

5. Conclusions

In summary, our findings establish Strip1 as a novel and central regulator of pathological cardiac hypertrophy, whose expression is significantly reduced in human DCM and ICM and under mechanical stress—highlighting its potential as a key protective factor during cardiac disease. The observed nucleolar association of Strip1 suggests a previously unrecognized nuclear aspect of its function in cardiomyocytes. Mechanistically, Strip1 limits hypertrophic remodeling in response to adrenergic stress by influencing pro-hypertrophic signaling pathways, including the STRIPAK-associated kinase MST4, as well as Calcineurin/NFAT- and Hippo-related signaling. These findings extend our understanding of cardiac STRIPAK-related functions and suggest Strip1 as a potential regulator and target of pathological cardiac remodeling.

Supplementary Materials: The following supporting information can be downloaded at: http://bit.ly/40GKzBF (accessed on 2 March 2026), Figure S1: Strip1 CoIP Western blots; Figure S2: TAC/mice and human DCM and ICM Western blots; Figure S3: Strip1 knockdown catecholamine stimulation; Figure S4: High-resolution images of cell area measurement; Figure S5: Strip1 overexpression Hippo members Western blots; Figure S6: Strip1 knockdown p-MST4/Ezrin Western blots.

Author Contributions: Conceptualization, M.E. and E.H.; methodology, M.E. and E.H.; software, E.H.; validation, M.E., N.F. and E.H.; formal analysis, M.E. and E.H.; investigation, E.H., M.E., K.S.F., S.H., S.S., M.V., B.M. and L.S.K.; resources, N.F., M.E., S.S., M.V. and B.M.; data curation, E.H., M.E., K.S.F., S.H. and L.S.K.; writing—original draft preparation, E.H. and M.E.; writing—review and editing, M.E., N.F., S.S., M.V., B.M. and E.H.; visualization, E.H. and M.E.; supervision, N.F. and M.E.; project administration, N.F. and M.E. All authors have read and agreed to the published version of the manuscript.

Funding: This research received no external funding.

Institutional Review Board Statement: The study was conducted in accordance with the Declaration of Helsinki and approved by the Ethics Committee of the Medical Faculty, Georg-August-University Göttingen (protocol code 31/9/00, date of approval: 28 May 2009).

Informed Consent Statement: Informed consent was waived because the study used fully anonymized human myocardial tissue obtained either during clinically indicated heart transplantation or during routine post-transplant assessments, under the approval of the Ethics Committee of the University Medical Center Göttingen (protocol code 31/9/00, approval date: 28 May 2009).

Data Availability Statement: Data underlying this study are available within the article and its Supplementary Materials. The raw image datasets from cell size area measurements (approximately 120 GB) and further information are available from the corresponding author upon reasonable request.

Acknowledgments: We gratefully acknowledge the invaluable administrative and technical support provided by Nicole Herzog, Qiang Sun, and Nicola Vallon. Their dedicated assistance in the laboratory was essential for the successful completion of this study. During the preparation of this manuscript, the authors used ChatGPT versions, o4-mini, 4o, 4.0, 4.1-mini, 4.5 and 5, along with Perplexity, powered by models Sonnet, GPT-4o, and Claude 3.7, for the purposes of text generation and literature/source retrieval. The authors have reviewed and edited the output and take full responsibility for the content of this publication.

Conflicts of Interest: The authors declare no conflicts of interest.

Abbreviations

The following abbreviations are used in this manuscript:

AdLacZ	Adenoviral LacZ construct
AdSTRIP1	Adenoviral STRIP1 construct
αMHC-Cre	Alpha-myosin heavy chain–driven Cre recombinase
ARVCMs	Adult ventricular cardiomyocytes
BSA	Bovine serum albumin
Co-IP	Co-immunoprecipitation
DCM	Dilated cardiomyopathy
DMEM	Dulbecco's Modified Eagle Medium
DTT	Dithiothreitol
GAPDH	Glyceraldehyde-3-phosphate dehydrogenase
GCKII/GCKIII	Germinal Center Kinase class II/class III
HCM	Hypertrophic cardiomyopathy
HEPES	4-(2-hydroxyethyl)-1-piperazineethanesulfonic acid
hpf	Hours post fertilization
ICM	Ischemic cardiomyopathy
ifu	Infectious units
ISO	isoproterenol
MLL3	Histone H3K4 mono-methyltransferase MLL3 (KMT2C)
MO STRIP1	morpholino-induced STRIP1 knockdown
MOB1	Mps one binder 1
MST	Mammalian sterile 20-like kinase
Myoscape	Myocardium-enriched, calcium channel–associated protein
NFAT	Nuclear Factor of Activated T-Cells
NOR	Nucleolar organizer region
NPM	Nucleophosmin
NPPA	Natriuretic peptide A gene
NPPB	Natriuretic peptide B gene
NRVCMs	Neonatal rat ventricular cardiomyocytes
NYHA	New York Heart Association functional class
PBS	Phosphate-buffered saline
PE	phenylephrine
PP2A	Protein phosphatase 2A
PTU	1-Phenyl-2-thiourea
RCAN1.4	Regulator of Calcineurin 1 isoform 4
RIPA buffer	Radioimmunoprecipitation assay buffer
RPL32	Ribosomal protein L32 (Housekeeping gene)
SDS	Sodium dodecyl sulfate
SIKE1	Suppressor of IKKε 1
siRNA	Small interfering RNA
siSTRIP1/siNeg	siRNA targeting STRIP1 mRNA/Negative Control
SLMAP	Sarcolemmal membrane-associated protein
TAC	Transverse aortic constriction
TAZ	Transcriptional co-activator with PDZ-binding motif (WWTR1)
UniProt	Universal Protein Resource
YAP	Yes-associated protein

References

1. Nakamura, M.; Sadoshima, J. Mechanisms of physiological and pathological cardiac hypertrophy. *Nat. Rev. Cardiol.* **2018**, *15*, 387–407. [CrossRef]
2. Frey, N.; Olson, E.N. Cardiac hypertrophy: The good, the bad, and the ugly. *Annu. Rev. Physiol.* **2003**, *65*, 45–79. [CrossRef] [PubMed]
3. Molkentin, J.D.; Dorn, G.W., 2nd. Cytoplasmic signaling pathways that regulate cardiac hypertrophy. *Annu. Rev. Physiol.* **2001**, *63*, 391–426. [CrossRef]
4. Kuck, U.; Radchenko, D.; Teichert, I. STRIPAK, a highly conserved signaling complex, controls multiple eukaryotic cellular and developmental processes and is linked with human diseases. *Biol. Chem.* **2019**, *400*, 1005–1022. [CrossRef]
5. Shi, Z.; Jiao, S.; Zhou, Z. STRIPAK complexes in cell signaling and cancer. *Oncogene* **2016**, *35*, 4549–4557. [CrossRef] [PubMed]
6. Hwang, J.; Pallas, D.C. STRIPAK complexes: Structure, biological function, and involvement in human diseases. *Int. J. Biochem. Cell Biol.* **2014**, *47*, 118–148. [CrossRef]
7. Nader, M.; Westendorp, B.; Hawari, O.; Salih, M.; Stewart, A.F.R.; Leenen, F.H.H.; Tuana, B.S. Tail-anchored membrane protein SLMAP is a novel regulator of cardiac function at the sarcoplasmic reticulum. *Am. J. Physiol. Heart Circ. Physiol.* **2012**, *302*, H1138–H1145. [CrossRef] [PubMed]
8. Cull, J.J.; Cooper, S.T.E.; Alharbi, H.O.; Chothani, S.P.; Rackham, O.J.L.; Meijles, D.N.; Dash, P.R.; Kerkela, R.; Ruparelia, N.; Sugden, P.H.; et al. Striatin plays a major role in angiotensin II-induced cardiomyocyte and cardiac hypertrophy in mice in vivo. *Clin. Sci.* **2024**, *138*, 573–597. [CrossRef]
9. Yoon, S.; Kook, T.; Min, H.K.; Kwon, D.H.; Cho, Y.K.; Kim, M.; Shin, S.; Joung, H.; Jeong, S.H.; Lee, S.; et al. PP2A negatively regulates the hypertrophic response by dephosphorylating HDAC2 S394 in the heart. *Exp. Mol. Med.* **2018**, *50*, 1–14. [CrossRef]
10. Eden, M.; Leye, M.; Hahn, J.; Heilein, E.; Luzarowski, M.; Volschow, B.; Tannert, C.; Sossalla, S.; Lucena-Porcel, C.; Frank, D.; et al. Mst4, a novel cardiac STRIPAK complex-associated kinase, regulates cardiomyocyte growth and survival and is upregulated in human cardiomyopathy. *J. Biol. Chem.* **2024**, *300*, 107255. [CrossRef]
11. ten Klooster, J.P.; Jansen, M.; Yuan, J.; Oorschot, V.; Begthel, H.; Di Giacomo, V.; Colland, F.; de Koning, J.; Maurice, M.M.; Hornbeck, P.; et al. Mst4 and Ezrin induce brush borders downstream of the Lkb1/Strad/Mo25 polarization complex. *Dev. Cell* **2009**, *16*, 551–562. [CrossRef]
12. Eden, M.; Meder, B.; Volkers, M.; Poomvanicha, M.; Domes, K.; Branchereau, M.; Marck, P.; Will, R.; Bernt, A.; Rangrez, A.; et al. Myoscape controls cardiac calcium cycling and contractility via regulation of L-type calcium channel surface expression. *Nat. Commun.* **2016**, *7*, 11317. [CrossRef] [PubMed]
13. Drexler, H.; Hanze, J.; Finckh, M.; Lu, W.; Just, H.; Lang, R.E. Atrial natriuretic peptide in a rat model of cardiac failure. Atrial and ventricular mRNA, atrial content, plasma levels, and effect of volume loading. *Circulation* **1989**, *79*, 620–633. [CrossRef]
14. Mukoyama, M.; Nakao, K.; Hosoda, K.; Suga, S.; Saito, Y.; Ogawa, Y.; Shirakami, G.; Jougasaki, M.; Obata, K.; Yasue, H.; et al. Brain natriuretic peptide as a novel cardiac hormone in humans. Evidence for an exquisite dual natriuretic peptide system, atrial natriuretic peptide and brain natriuretic peptide. *J. Clin. Investig.* **1991**, *87*, 1402–1412. [CrossRef]
15. Frey, N.; Olson, E.N. Making matters worse for a broken heart. *J. Clin. Investig.* **2000**, *106*, 1437–1439. [CrossRef]
16. Bazzi, H.; Soroka, E.; Alcorn, H.L.; Anderson, K.V. STRIP1, a core component of STRIPAK complexes, is essential for normal mesoderm migration in the mouse embryo. *Proc. Natl. Acad. Sci. USA* **2017**, *114*, E10928–E10936. [CrossRef]
17. Jeong, B.C.; Bae, S.J.; Ni, L.; Zhang, X.; Bai, X.C.; Luo, X. Cryo-EM structure of the Hippo signaling integrator human STRIPAK. *Nat. Struct. Mol. Biol.* **2021**, *28*, 290–299. [CrossRef]
18. Tang, Y.; Chen, M.; Zhou, L.; Ma, J.; Li, Y.; Zhang, H.; Shi, Z.; Xu, Q.; Zhang, X.; Gao, Z.; et al. Architecture, substructures, and dynamic assembly of STRIPAK complexes in Hippo signaling. *Cell Discov.* **2019**, *5*, 3. [CrossRef] [PubMed]
19. Li, A.X.; Martin, T.A.; Lane, J.; Jiang, W.G. Cellular Impacts of Striatins and the STRIPAK Complex and Their Roles in the Development and Metastasis in Clinical Cancers. *Cancers* **2023**, *16*, 76. [CrossRef] [PubMed]
20. Rodriguez-Cupello, C.; Dam, M.; Serini, L.; Wang, S.; Lindgren, D.; Englund, E.; Kjellman, P.; Axelson, H.; Garcia-Mariscal, A.; Madsen, C.D. The STRIPAK Complex Regulates Response to Chemotherapy Through p21 and p27. *Front. Cell Dev. Biol.* **2020**, *8*, 146. [CrossRef]
21. Madsen, C.D.; Hooper, S.; Tozluoglu, M.; Bruckbauer, A.; Fletcher, G.; Erler, J.T.; Bates, P.A.; Thompson, B.; Sahai, E. STRIPAK components determine mode of cancer cell migration and metastasis. *Nat. Cell Biol.* **2015**, *17*, 68–80. [CrossRef] [PubMed]
22. Chen, R.; Xie, R.; Meng, Z.; Ma, S.; Guan, K.L. STRIPAK integrates upstream signals to initiate the Hippo kinase cascade. *Nat. Cell Biol.* **2019**, *21*, 1565–1577. [CrossRef]
23. Wang, J.; Liu, S.; Heallen, T.; Martin, J.F. The Hippo pathway in the heart: Pivotal roles in development, disease, and regeneration. *Nat. Rev. Cardiol.* **2018**, *15*, 672–684. [CrossRef]
24. Yamamoto, S.; Yang, G.; Zablocki, D.; Liu, J.; Hong, C.; Kim, S.J.; Soler, S.; Odashima, M.; Thaisz, J.; Yehia, G.; et al. Activation of Mst1 causes dilated cardiomyopathy by stimulating apoptosis without compensatory ventricular myocyte hypertrophy. *J. Clin. Investig.* **2003**, *111*, 1463–1474. [CrossRef]

25. Schneider, C.A.; Rasband, W.S.; Eliceiri, K.W. NIH Image to ImageJ: 25 years of image analysis. *Nat. Methods* **2012**, *9*, 671–675. [CrossRef]
26. Schindelin, J.; Arganda-Carreras, I.; Frise, E.; Kaynig, V.; Longair, M.; Pietzsch, T.; Preibisch, S.; Rueden, C.; Saalfeld, S.; Schmid, B.; et al. Fiji: An open-source platform for biological-image analysis. *Nat. Methods* **2012**, *9*, 676–682. [CrossRef]
27. The UniProt Consortium. UniProt: The Universal Protein Knowledgebase in 2025. *Nucleic Acids Res.* **2025**, *53*, D609–D617. [CrossRef]
28. Madeira, F.; Madhusoodanan, N.; Lee, J.; Eusebi, A.; Niewielska, A.; Tivey, A.R.N.; Lopez, R.; Butcher, S. The EMBL-EBI Job Dispatcher sequence analysis tools framework in 2024. *Nucleic Acids Res.* **2024**, *52*, W521–W525. [CrossRef] [PubMed]
29. Jumper, J.; Evans, R.; Pritzel, A.; Green, T.; Figurnov, M.; Ronneberger, O.; Tunyasuvunakool, K.; Bates, R.; Zidek, A.; Potapenko, A.; et al. Highly accurate protein structure prediction with AlphaFold. *Nature* **2021**, *596*, 583–589. [CrossRef] [PubMed]
30. Varadi, M.; Bertoni, D.; Magana, P.; Paramval, U.; Pidruchna, I.; Radhakrishnan, M.; Tsenkov, M.; Nair, S.; Mirdita, M.; Yeo, J.; et al. AlphaFold Protein Structure Database in 2024: Providing structure coverage for over 214 million protein sequences. *Nucleic Acids Res.* **2024**, *52*, D368–D375. [CrossRef]
31. Ribeiro, P.S.; Josue, F.; Wepf, A.; Wehr, M.C.; Rinner, O.; Kelly, G.; Tapon, N.; Gstaiger, M. Combined functional genomic and proteomic approaches identify a PP2A complex as a negative regulator of Hippo signaling. *Mol. Cell* **2010**, *39*, 521–534. [CrossRef]
32. Goudreault, M.; D'Ambrosio, L.M.; Kean, M.J.; Mullin, M.J.; Larsen, B.G.; Sanchez, A.; Chaudhry, S.; Chen, G.I.; Sicheri, F.; Nesvizhskii, A.I.; et al. A PP2A phosphatase high density interaction network identifies a novel striatin-interacting phosphatase and kinase complex linked to the cerebral cavernous malformation 3 (CCM3) protein. *Mol. Cell. Proteom.* **2009**, *8*, 157–171. [CrossRef]
33. Frost, A.; Elgort, M.G.; Brandman, O.; Ives, C.; Collins, S.R.; Miller-Vedam, L.; Weibezahn, J.; Hein, M.Y.; Poser, I.; Mann, M.; et al. Functional repurposing revealed by comparing *S. pombe* and *S. cerevisiae* genetic interactions. *Cell* **2012**, *149*, 1339–1352. [CrossRef]
34. Chen, Z.; Zhang, Y.; Zhao, X. FAM40A alters the cytoskeleton of podocytes in familial focal and segmental glomerulosclerosis by regulating F-actin and nephrin. *Arch. Med. Sci.* **2019**, *15*, 165–173. [CrossRef] [PubMed]
35. Wagh, V.; Doss, M.X.; Sabour, D.; Niemann, R.; Meganathan, K.; Jagtap, S.; Gaspar, J.A.; Ardestani, M.A.; Papadopoulos, S.; Gajewski, M.; et al. Fam40b is required for lineage commitment of murine embryonic stem cells. *Cell Death Dis.* **2014**, *5*, e1320. [CrossRef] [PubMed]
36. Scheer, U.; Hock, R. Structure and function of the nucleolus. *Curr. Opin. Cell Biol.* **1999**, *11*, 385–390. [CrossRef] [PubMed]
37. Sakthivel, D.; Brown-Suedel, A.; Bouchier-Hayes, L. The role of the nucleolus in regulating the cell cycle and the DNA damage response. *Adv. Protein Chem. Struct. Biol.* **2023**, *135*, 203–241. [CrossRef]
38. Hariharan, N.; Sussman, M.A. Stressing on the nucleolus in cardiovascular disease. *Biochim. Biophys. Acta* **2014**, *1842*, 798–801. [CrossRef]
39. Rosello-Lleti, E.; Rivera, M.; Cortes, R.; Azorin, I.; Sirera, R.; Martinez-Dolz, L.; Hove, L.; Cinca, J.; Lago, F.; Gonzalez-Juanatey, J.R.; et al. Influence of heart failure on nucleolar organization and protein expression in human hearts. *Biochem. Biophys. Res. Commun.* **2012**, *418*, 222–228. [CrossRef]
40. Mamaev, N.N.; Gudkova, A.Y.; Amineva, K.K. AgNORs in the myocardium in ischaemic heart disease complicated by heart failure: A postmortem study. *Mol. Pathol.* **1998**, *51*, 102–104. [CrossRef]
41. Ma, H.; Pederson, T. Nucleophosmin is a binding partner of nucleostemin in human osteosarcoma cells. *Mol. Biol. Cell* **2008**, *19*, 2870–2875. [CrossRef] [PubMed]
42. Avitabile, D.; Bailey, B.; Cottage, C.T.; Sundararaman, B.; Joyo, A.; McGregor, M.; Gude, N.; Truffa, S.; Zarrabi, A.; Konstandin, M.; et al. Nucleolar stress is an early response to myocardial damage involving nucleolar proteins nucleostemin and nucleophosmin. *Proc. Natl. Acad. Sci. USA* **2011**, *108*, 6145–6150. [CrossRef]
43. Lyon, R.C.; Zanella, F.; Omens, J.H.; Sheikh, F. Mechanotransduction in cardiac hypertrophy and failure. *Circ. Res.* **2015**, *116*, 1462–1476. [CrossRef]
44. Meerson, F.Z. Insufficiency of hypertrophied heart. *Basic Res. Cardiol.* **1976**, *71*, 343–354. [CrossRef]
45. Leinwand, L.A. Calcineurin inhibition and cardiac hypertrophy: A matter of balance. *Proc. Natl. Acad. Sci. USA* **2001**, *98*, 2947–2949. [CrossRef]
46. Molkentin, J.D.; Lu, J.R.; Antos, C.L.; Markham, B.; Richardson, J.; Robbins, J.; Grant, S.R.; Olson, E.N. A calcineurin-dependent transcriptional pathway for cardiac hypertrophy. *Cell* **1998**, *93*, 215–228. [CrossRef]
47. Diedrichs, H.; Chi, M.; Boelck, B.; Mehlhorn, U.; Schwinger, R.H. Increased regulatory activity of the calcineurin/NFAT pathway in human heart failure. *Eur. J. Heart Fail.* **2004**, *6*, 3–9. [CrossRef]
48. Wilkins, B.J.; Dai, Y.S.; Bueno, O.F.; Parsons, S.A.; Xu, J.; Plank, D.M.; Jones, F.; Kimball, T.R.; Molkentin, J.D. Calcineurin/NFAT coupling participates in pathological, but not physiological, cardiac hypertrophy. *Circ. Res.* **2004**, *94*, 110–118. [CrossRef]
49. Yang, J.; Rothermel, B.; Vega, R.B.; Frey, N.; McKinsey, T.A.; Olson, E.N.; Bassel-Duby, R.; Williams, R.S. Independent signals control expression of the calcineurin inhibitory proteins MCIP1 and MCIP2 in striated muscles. *Circ. Res.* **2000**, *87*, e61–e68. [CrossRef] [PubMed]

50. Windmueller, R.; Morrisey, E.E. Hippo and Cardiac Hypertrophy: A Complex Interaction. *Circ. Res.* **2015**, *117*, 832–834. [CrossRef] [PubMed]
51. Wang, P.; Mao, B.; Luo, W.; Wei, B.; Jiang, W.; Liu, D.; Song, L.; Ji, G.; Yang, Z.; Lai, Y.Q.; et al. The alteration of Hippo/YAP signaling in the development of hypertrophic cardiomyopathy. *Basic Res. Cardiol.* **2014**, *109*, 435. [CrossRef]
52. Del Re, D.P.; Yang, Y.; Nakano, N.; Cho, J.; Zhai, P.; Yamamoto, T.; Zhang, N.; Yabuta, N.; Nojima, H.; Pan, D.; et al. Yes-associated protein isoform 1 (Yap1) promotes cardiomyocyte survival and growth to protect against myocardial ischemic injury. *J. Biol. Chem.* **2013**, *288*, 3977–3988. [CrossRef]
53. Viswanatha, R.; Wayt, J.; Ohouo, P.Y.; Smolka, M.B.; Bretscher, A. Interactome analysis reveals ezrin can adopt multiple conformational states. *J. Biol. Chem.* **2013**, *288*, 35437–35451. [CrossRef]
54. Pane, R.; Laib, L.; Formoso, K.; Detrait, M.; Sainte-Marie, Y.; Bourgailh, F.; Ruffenach, N.; Faugeras, H.; Simon, I.; Lhuillier, E.; et al. Macromolecular Complex Including MLL3, Carabin and Calcineurin Regulates Cardiac Remodeling. *Circ. Res.* **2024**, *134*, 100–113. [CrossRef] [PubMed]
55. Zi, M.; Maqsood, A.; Prehar, S.; Mohamed, T.M.; Abou-Leisa, R.; Robertson, A.; Cartwright, E.J.; Ray, S.G.; Oh, S.; Lim, D.S.; et al. The mammalian Ste20-like kinase 2 (Mst2) modulates stress-induced cardiac hypertrophy. *J. Biol. Chem.* **2014**, *289*, 24275–24288. [CrossRef] [PubMed]
56. Abdollahpour, H.; Appaswamy, G.; Kotlarz, D.; Diestelhorst, J.; Beier, R.; Schaffer, A.A.; Gertz, E.M.; Schambach, A.; Kreipe, H.H.; Pfeifer, D.; et al. The phenotype of human STK4 deficiency. *Blood* **2012**, *119*, 3450–3457. [CrossRef]
57. Park, J.; Kim, G.H.; Lee, J.; Phuong, B.T.C.; Kong, B.; Won, J.E.; Won, G.W.; Lee, Y.H.; Han, H.D.; Lee, Y. MST2 silencing induces apoptosis and inhibits tumor growth for estrogen receptor alpha-positive MCF-7 breast cancer. *Toxicol. Appl. Pharmacol.* **2020**, *408*, 115257. [CrossRef] [PubMed]

Disclaimer/Publisher's Note: The statements, opinions and data contained in all publications are solely those of the individual author(s) and contributor(s) and not of MDPI and/or the editor(s). MDPI and/or the editor(s) disclaim responsibility for any injury to people or property resulting from any ideas, methods, instructions or products referred to in the content.

cells

MDPI

Article

Roquin Modulates Cardiac Post-Infarct Remodeling via microRNA Stability Control

Nadja Itani [1], Rolf Schreckenberg [1], Rainer Schulz [1], Peter Bencsik [2,3], Peter Ferdinandy [2,4,5] and Klaus-Dieter Schlüter [1,*]

1 Physiologisches Institut, Justus-Liebig-Universität Gießen, 35392 Gießen, Germany; nadja.itani@physiologie.med.uni-giessen.de (N.I.); rolf.schreckenberg@physiologie.med.uni-giessen.de (R.S.); rainer.schulz@physiologie.med.uni-giessen.de (R.S.)
2 Pharmahungary Group, 6722 Szeged, Hungary; peter.bencsik@pharmahungary.com (P.B.); peter.ferdinandy@pharmahungary.com (P.F.)
3 Department of Pharmacology and Pharmacotherapy, University of Szeged, 6722 Szeged, Hungary
4 Department of Pharmacology and Pharmacotherapy, Semmelweis University, 1094 Budapest, Hungary
5 Center for Pharmacology and Drug Research & Development, Semmelweis University, 1085 Budapest, Hungary
* Correspondence: klaus-dieter.schlueter@physiologie.med.uni-giessen.de; Tel.: +49-641-99-47-212

Abstract: Through binding to complementary mRNAs, microRNAs (miRNAs) mediate gene silencing. The stability and half-life of microRNAs are controlled by two isoforms of the RNA-binding protein Roquin. This study aimed at identifying the role of Roquin to miRNA-dependent regulation of the transcriptome in the post-ischemic heart. Both Roquin isoforms are highly conserved between rats and humans and constitutively expressed in cardiomyocytes. In both cell species, hypoxia induces a down-regulation of Roquin-1 and Roquin-2. An integrative miRNA-and-mRNA analysis (MMIA) identified miR-23b-5p as a potential interaction partner of Roquins. The open data bank TargetScan8.0 suggests that the transcription factor ZBTB20 is a potential target of miR-23b-5p. The level of expression of *ZBTB20* correlated with the functional recovery of rat hearts after myocardial infarction. Moreover, the down-regulation of Roquin-2 in AC16 cells by siRNA under normoxic conditions was associated with an up-regulation of miR-23b-5p and a down-regulation of *ZBTB20*. Furthermore, in the case of hypoxia-dependent down-regulation of Roquin, the subsequent down-regulation of *ZBTB20* was reversed with the help of an antagomir against miR-23b-5p. In conclusion, hypoxia-induced down-regulation of the two Roquin isoforms was associated with an increased stability of miR-23b-5p, a Roquin-2-dependent miRNA, which subsequently led to silencing of the transcription factor ZBTB20.

Keywords: ZBTB20; miR-23b-5p; post-infarct remodeling

1. Introduction

Revascularization of occluded coronary vessels leads to reperfusion injury. The extent and nature of this tissue damage affect the subsequent remodeling of the post-infarcted heart. However, such structural remodeling processes require protein synthesis and degradation. Both processes depend at least in part on transcriptional regulation. A number of specific mechanisms are involved in the transcriptional regulation of genes, such as the regulation of transcription factor expression and activity, epigenetic modifications of genes, control of mRNA half-life, and control of mRNA regulators such as microRNAs (miRNAs). RNA-binding proteins such as Roquin can control the stability and half-life of

RNA molecules, including mRNA and miRNAs. However, Roquin expression and function have not yet been addressed in post-infarct remodeling.

Roquins, a family of RNA-binding proteins, contain two family members named Roquin-1 and Roquin-2. Both proteins show a high degree of evolutionary conservation. Their involvement in immune defense in Drosophila has already been demonstrated, but they also play a role in immune regulation in mammals [1,2]. It has been proposed that Roquins originate from the cellular defense of eukaryotic cells against RNA pathogens [3]. As they were first recognized by their effects on immune cells, it is in line with this finding that Roquin deficiency is associated with inflammation in nearly all tissues [4]. In the heart, Roquin deficiency causes T-cell-dependent inflammation [5]. The mechanisms by which Roquins affect transcription, translation, and cell function are complex and contain mRNA deadenylation [6], RNA degradation in connection with Regnase [7], targeting of miRNAs [8], and interference with the Akt signaling pathway [9]. In addition, Roquins also have E3 ubiquitin ligase activity and can degrade proteins [10]. Roquin expression can be inhibited by mucosa-associated lymphoma translocation protein 1 (MALT1) [11,12] and miR-223 [13]. Furthermore, it has already been demonstrated that ischemia in the liver influences the expression of Roquin-1 [14].

Inflammatory processes and altered transcription contribute to post-infarction remodeling, and both processes are influenced by Roquin. However, there are yet no data available about the effect of ischemia and reperfusion on the expression and function of Roquins in the heart. The present study therefore aimed to identify potential cardiac signaling pathways that are influenced by Roquin. To shed light on this topic, the regulation of Roquin expression in post-infarcted cardiac tissue also needs to be examined. We previously analyzed the expression of miRNAs in the reperfused myocardium of rat hearts [15]. We now extended our previous work and used these data and a quantitative mRNA expression approach to perform an integrative miRNA-and-mRNA analysis (MMIA). This approach formed the basis by which potential cardiac targets of Roquin were discovered and led to the identification of miR-23b-5p. Subsequent screening of the TargetScan8.0 database identified the zinc finger and BTB domain containing protein 20 (ZBTB20) as a potential down-stream target of miR-23b-5p. We then used siRNA and antagomir approaches to validate a newly discovered Roquin-2–miR-23-b5p–ZBTB20 cascade that appears to be important for post-ischemic remodeling.

2. Materials and Methods

2.1. Ethics Statement of Animal Studies

This investigation conforms with the Guide for the Care and Use of Laboratory Animals published by the US National Institute of Health (NIH publication No. 85-23, revised 1996). The animal study protocol (isolation of rat cardiomyocytes) was approved by the Institutional Review Board (or Ethics Committee) of the Justus Liebig University, Giessen, Germany (752_M; 17 August 2023). All other data used in this study from rat tissues were taken from the data set already used before in a different context [15].

2.2. Animal Studies

All tissue samples used in this study were obtained from female Wistar-Hannover rats weighing 215–265 g. The sample material was collected as part of an earlier study and further examined in the current work under the new objective. All details regarding surgical procedures, analysis of left ventricular function, and the extraction and processing of miRNA and mRNA are explained in detail in the study that has already been published [15].

2.3. Isolation of Rat Ventricular Myocytes and Non-Myocytes

Ventricular heart muscle and non-muscle cells were isolated from male Wistar rats as described before [16]. Briefly, after hearts were excised under deep anesthesia, they were quickly mounted on a Langendorff system and perfused with collagenase-containing buffer. Myocytes and non-myocytes were separated by sedimentation and subsequent resuspension. After isolation and separation, myocytes and non-myocyte cells were quickly frozen in liquid nitrogen and stored until used at −80 °C.

2.4. Cell Culture

Human AC16 cardiomyocytes were cultured on 100 mm dishes (Falcon, type 3003, Corning Inc., Corning, NY, USA) in Dulbecco's Modified Eagle's Medium (D6429, EMD Millipore Corp., Billerica, MA, USA), added with 12.5% heat-inactivated FBS (35-079-CV, Corning Inc., USA) and under 1% antibiotic–antifungal coverage (30-004-CI, Corning Inc., USA) according to the protocol (#SCC109, EMD Millipore Corp., USA). In this study, all AC16-based experiments were performed with cells that were initially transferred into 60 mm culture dishes (Falcon, type 3002, Corning Inc., USA).

SiRNA transfection was performed according to the Lipofectamine RNAiMAX transfection protocol (life technologies, Carlsbad, CA, USA). For each transfection of a 35 mm culture dish, 4.5 µL of a Lipofectamine transfection reagent was mixed with cold 150 µL Opti-MEM (Thermo fisher, Waltham, MA, USA) and 1.5 µL siRNA for Roquin-1 (HS_KIAA2025, Qiagen, Venlo, The Netherlands), Roquin-2 (HS_MNAB, Qiagen), or for the control (SI03650318, Qiagen) and incubated for 5 min at room temperature. The cell density on the culture dish was 70% confluent for transfection. The cells were then transfected and incubated at 37 °C for up to 48 h.

For the plasmid transfection of the AC16 cell line, the plasmid RC3H1 Human Untagged Clone was used with the vector pCMV6 entry (SC306712, ORIGENE, Rockville, MD, USA). First, the freeze-dried plasmid was dissolved in sterile water according to the manufacturer's instructions. Then, 1 µg of plasmid DNA was diluted in 250 µL of cold Opti-MEM and carefully mixed with 4 µL of TurboFectin 8.0 Transfection Reagent (TF81001, ORIGENE, USA). The whole mixture was incubated for 15 min at room temperature, and the cells were transfected at a confluence of 70%. The incubation was carried out for 48 h at 37 °C.

Experiments using an in vitro hypoxia–reoxygenation model were performed in the following way: AC16 cells were exposed to a hypoxic chamber (94.9% N_2, 5.0% CO_2, 0.1% O_2) for 48 h, followed by reoxygenation for one hour under normoxic conditions (5% CO_2, 95% room air). Control cultures were incubated for the same time period under normoxic conditions. The incubation temperature was 37 °C.

2.5. Real-Time RT-PCR

Total RNA was isolated from cardiac tissue, isolated cells, and AC16 cardiomyocytes using peqGold TriFast (peqlab, Biotechnologie GmbH, Burgwedel, Germany) according to the manufacturer's protocol. cDNA synthesis was performed using SuperScript™ III reverse transcriptase (#18080093, Invitrogen™, Carlsbad, CA, USA) after incubation with 1 U DNase/µg RNA for 15 min at 37 °C. miRNA cDNA synthesis was performed using a microscript microRNA cDNA synthesis kit from Norgen Biotek (ordered via BioCat GmbH, Heidelberg, Germany). Real-time quantitative PCR was performed with the CFX Connect Real-Time PCR Detection System (Bio-Rad Laboratories, Inc., Dreieich, Germany) using iQ™ SYBR® Green Supermix (Bio-Rad Laboratories, Inc., Germany). For information on the primers used, see Supplementary Table S1.

2.6. SDS-PAGE and Western Blot

Total protein was extracted from cardiac tissue, isolated cells, and AC16 cardiomyocytes using Cell Lysis Buffer (10×) (Cell Signaling, Danvers, MA, USA) according to the manufacturer's protocol. The homogenate was centrifuged at 14,000× *g* for 10 min at 4 °C, and the supernatant was treated with Laemmli buffer. Protein samples were loaded onto NuPAGE Bis-Tris Precast gels (10%; Life Technology, Darmstadt, Germany) followed by transfer to nitrocellulose membranes. The blots were incubated with an antibody against Roquin-1/2 (MABF288; Life Technology, Darmstadt, Germany) and subsequently with the secondary antibody Goat-Anti-Rat (Jackon ImmunoResearch Europe Ltd., Cambridgeshire, UK).

2.7. Statistical Analysis

Data from all groups underwent initial testing for variance (Levene test) and normal distribution (Shapiro–Wilk test). Subsequently, two-sided *T*-tests (2 groups) or a two-sided ANOVA (comparison of multiple groups) was used to compare groups. *p*-Values below 0.05 are indicated as such in the figure legends. Correlation analysis was performed by Pearson correlation using SPSS23. Data are expressed as correlation coefficient β and exact *p*-values.

3. Results

3.1. Expression of Roquin Isoforms in Rat Heart Tissue

A quantitative comparison of the expression of RC3H1 and RC3H2, the two genes encoding Roquin-1 and Roquin-2, respectively, was performed in isolated adult rat cardiomyocytes and non-myocytes. As indicated in Figure 1A, the primers used in this study to quantify the mRNA expression of Roquin-1 and Roquin-2 have the same primer efficiency. This made it possible to quantitatively compare the expression of both isoforms using PCR thresholds (Figure 1B). Beta-2-Microglobulin (B2M) expression was used as a loading control and showed comparable expression in myocytes and non-myocytes (Figure 1B). Non-myocytes showed a lower threshold and therefore higher expression of RC3H1, whereas in cardiomyocytes RC3H2 showed lower thresholds. The data indicate a cell-specific difference in the expression profile of Roquin isoforms. When the expression in cardiomyocytes is normalized to RC3H2, it becomes clear that the expression of RC3H2 in non-myocytes is marginal (Figure 1C).

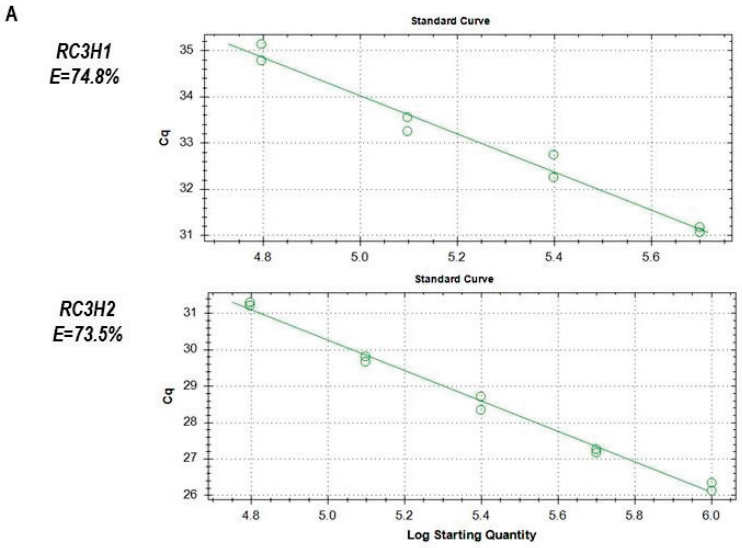


Figure 1. *Cont.*

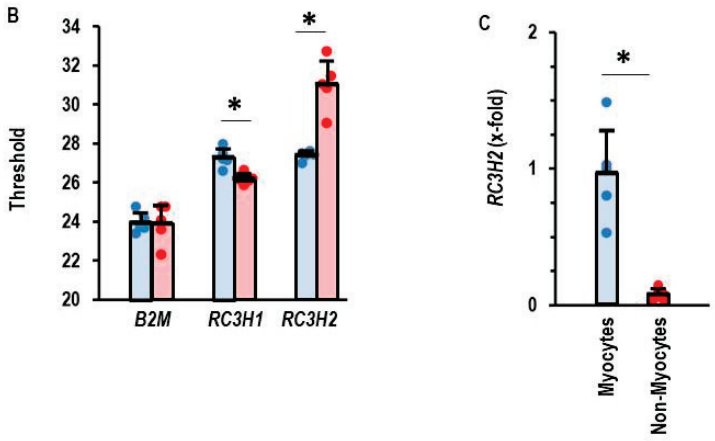


Figure 1. Expression of Roquin mRNA in rat heart tissue. (**A**) Primer efficiency for *RC3H1* and *RC3H2*. (**B**) Thresholds for PCR analysis for the house-keeping gene beta-2-microglubulin (*B2M*), *RC3H1*, and *RC3H2*. Myocytes in blue and non-myocytes in red. (**C**) Normalized expression of *RC3H2* in myocytes and non-myocytes with mean expression of *RC3H2* in cardiomyocytes set as 1. Data are given as means + S.D. (in black) and individual data points. *: $p < 0.05$ between myocytes and non-myocytes. *T*-test with Levene test for variance testing and Shapiro–Wilk test for normal distribution.

3.2. Screening for miRNAs That Are Potentially Affected by Roquins

Roquins act as RNA-binding molecules and can directly interact with mature miRNAs and Argonaute 2, which leads to inhibition of miRNA function and blocks Dicer-mediated processing of their precursor forms [17]. To identify potential miRNAs targeted by Roquins, we performed an integrative miRNA-and-mRNA analysis (MMIA). MiRNA expression was initially determined by RNA sequencing and secondarily by RT-PCR in rat ventricular samples taken seven days after the start of reperfusion or from non-ischemic controls [15]. mRNA expression was analyzed by RT-PCR. MiR-34c-3p showed the strongest inverse correlation to RC3H2 and RC3H1 (Figure 2A), but the data could not be confirmed by an alternative approach in which the expression of miR-34c-3p was quantified by RT-PCR instead of RNA sequencing (*RNA-Sequencing: β = −0.616 vs. RT-PCR: β = +0.992*). However, RC3H2 and miR-23b-5p were inversely expressed, regardless of whether the data were generated by RNA sequencing or RT-PCR analysis (Figure 2B,C). Based on this type of analysis, we considered miR-23b-5p as a potential target of Roquin. RC3H2 was down-regulated in all post-ischemic tissues, irrespective of infarct sparing procedures such as pre- and post-conditioning (Figure 2D). In contrast, miR-23b-5p was up-regulated in the same tissues (Figure 2E).

A

RC3H2	-log2 p	β	RC3H1	-log2 p	β
miR-34c-3p	9.145	-0.616	miR-34c-3p	5.966	-0.496
miR-672-5p	8.960	-0.610	miR-23b-5p	4.921	-0.445
miR-23b-5p	8.904	-0.608	miR-155-5p	4.837	-0.441
miR-32-3p	8.893	-0.608	miR-32-3p	4.574	-0.427
miR-1247-5p	8.240	-0.586	miR-672-5p	4.238	-0.408
miR-298-5p	7.465	-0.558	miR-1247-5p	3.837	-0.385
miR-155-5p	6.809	-0.532	miR-298-5p	3.095	-0.336

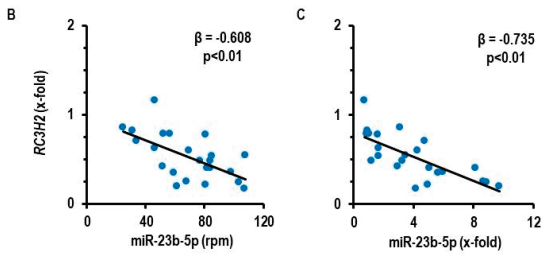


Figure 2. *Cont.*

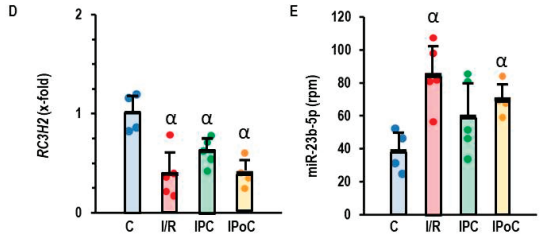


Figure 2. Correlation between *RC3H2* and *RC3H1* expression and the expression of miR-23b-5p in rat heart tissue. (**A**) Pearson correlation with *p*-values and β coefficient. (**B**,**C**) Correlation between the expression of *RC3H2* and miR-23b-5p quantified by RNA sequencing, expressed as rpm (**B**) or by RT-PCR, expressed as fold change of non-ischemic controls. (**D**) Expression of *RC3H2* in the left ventricle of samples from control rats (C), 45 min ischemia and 7-day reperfusion (I/R), 45 min ischemia with pre-conditioning and 7-day reperfusion (IPC), and 45 min ischemia with subsequent pre-conditioning and 7-day reperfusion (IPoC). (**E**) Expression of miR-23b-5p (expressed as reads per million, rpm) in the left ventricle of samples from control rats (C), 45 min ischemia and 7-day reperfusion (I/R), 45 min ischemia with pre-conditioning and 7-day reperfusion (IPC), and 45 min ischemia with subsequent pre-conditioning and 7-day reperfusion (IPoC). Data are given as means + S.D. and individual data points. α: $p < 0.05$ different from control rats (C). Two-sided ANOVA with Student–Newman–Keuls post hoc analysis. Exact *p*-values are given for correlation analysis.

3.3. Identification of ZBTB20 as a Potential Target of miR-23b-5p

Once we identified miR-23b-5p as a potential target of Roquin-2, we were interested in identifying potential targets of this miRNA. The data bank TargetScan8.0 suggested ZBTB20 as a potential target of miR-23b-5p. The ZBTB20 gene has three consequential pairing sites for rno-miR-23b-5p and six consequential pairing sites for hsa-miR-23b-5p. If the assumption is correct that miR-23b-5p targets ZBTB20, it must be predicted that this gene is down-regulated in rat heart tissues that showed an increased expression of miR-23b-5p. This assumption was confirmed, as *ZBTB20* is indeed down-regulated in post-ischemic hearts (Figure 3A). As predicted by the relationship between ZBTB20 and cardiac function (Ren et al. 2020; Ren et al. 2024 [18,19]), a strong correlation between *ZBTB20* expression and left ventricular function was found (Figure 3B).

3.4. Silencing of Roquin in AC16 Cells

The results on rat heart tissue suggest that ischemic events down-regulate the expression of Roquins, which can then no longer repress the expression of miR-23b-5p. miR-23b-5p subsequently targets the expression of ZBTB20, and down-regulation of this protein translates the signal cascade to a reduced cardiac function. However, these experiments on rat tissues did not validate whether RC3H2 expression correlates with Roquin-2 protein expression. Post-transcriptional modifications may alter such a direct relationship. Moreover, no causal relationship between Roquin expression and miR-23b-5p was shown, only an association of their expression under post-ischemic conditions. To validate the proposed relationship between Roquin, miR-23b-5p, and ZBTB20, expression at the protein level must be confirmed and gene expression must be examined independently of ischemic or hypoxic events. As there is currently no convincing antibody available to detect Roquin in rat tissue, we used AC16 cardiomyocytes, derived from human ventricular tissue, to prove this relationship.

Like rat cardiomyocytes, AC16 cells also constitutively express both Roquin isoforms at the mRNA level (Figure 4A). The application of siRNA against RC3H1 specifically down-regulated the mRNA of Roquin-1, just as the siRNA against RC3H2 exclusively affected the mRNA of Roquin-2 (Figure 4B,C). Moreover, successful down-regulation was also confirmed on the protein levels (Figure 4D–F). Therefore, we used siRNA directed against Roquin isoforms to validate the relationship between Roquin and miR-23b-5p expression.

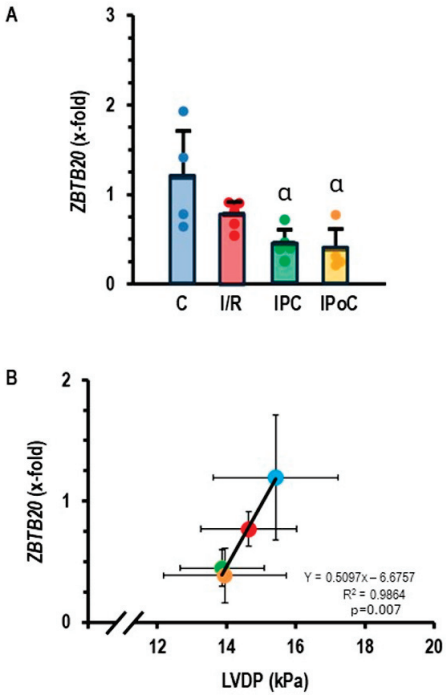


Figure 3. (**A**) Expression of *ZBTB20* in the left ventricle of samples from control rats (C), 45 min ischemia and 7-day reperfusion (I/R), 45 min ischemia with pre-conditioning and 7-day reperfusion (IPC), and 45 min ischemia with subsequent pre-conditioning and 7-day reperfusion (IPoC). Data are normalized to the expression of non-ischemic controls. Data are given as means + S.D. (in black) and data points. α: $p < 0.05$ versus control. Two-sided ANOVA with Student–Newman–Keuls post hoc analysis. (**B**) Correlation between *ZBTB20* expression and left ventricular developed pressure (LVDP). Exact *p*-value is given for the Pearson correlation analysis.

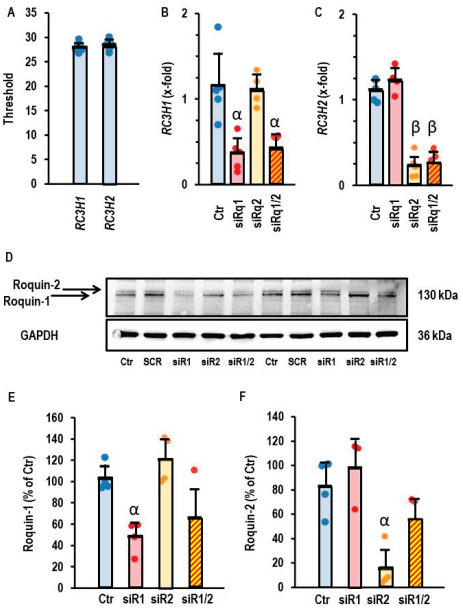


Figure 4. Effect of siRNA directed against RC3H1 and RC3H2 in AC16 cells. (**A**) Thresholds of PCR analysis for both genes. (**B**) Expression of RC3H1 in AC16 cells after incubation with siRNA directed against both Roquin isoforms. (**C**) Expression of RC3H2 in AC16 cells after incubation with siRNA directed both against Roquin isoforms. Data are given as means + S.D. (in black) and individual data points. β: $p < 0.05$ between siR2 vs. Ctr. and siR1. α: $p < 0.05$ for siR1 vs. Ctr and siR2. Two-way ANOVA with Student–Newman–Keuls post hoc analysis. (**D**) Western blot showing the expression of both Roquin isoforms in cells that were or were not (Ctr) transfected with siRNA against Roquin. (**E**,**F**) Quantification of the Western blot shown in (**D**) with α, $p < 0.05$ vs. Ctr.

3.5. Relationship Between Roquin-2 Expression and miR-23b-5p in AC16 Cells

Down-regulation of Roquin-2 led to a compensatory up-regulation of miR-23b-5p in normoxic AC16 cells (Figure 5A). Moreover, down-regulation of Roquin-2 also led to a down-regulation of *ZBTB20*, a potential target of miR-23b-5p (Figure 5B). These data suggest that Roquin deficiency and not hypoxia drives the up-regulation of miR-23b-5p and the subsequent down-regulation of *ZBTB20*.

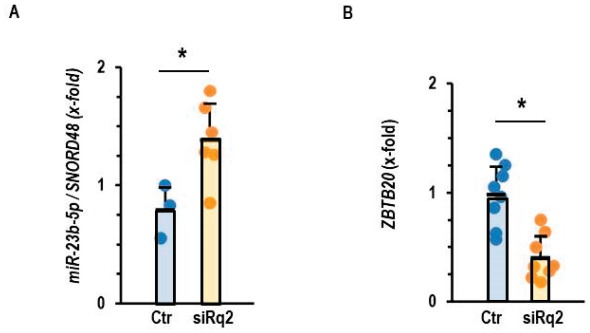


Figure 5. Effect of Roquin silencing on the expression of miR-23b-5p and *ZBTB20*. (**A**) Expression of miR-23b-5p in AC16 cells after incubation with siRNA directed against Roquin 2. (**B**) Expression of *ZBTB20* in AC16 cells after incubation with siRNA directed against Roquin-2. Data are given as means + S.D. (in black) and individual data points. *: $p < 0.05$ vs. Ctr. with unpaired *T*-tests.

3.6. Hypoxia-Dependent Regulation of Roquin in AC16 Cells

In rat tissue, we found a down-regulation of Roquin in post-ischemic tissue, regardless of infarct-sparing procedures. This suggested that ischemia or hypoxia triggers the down-regulation of Roquins and not any events related to reperfusion. This assumption was confirmed in the AC16 cell line, as Roquin-2 was down-regulated at the mRNA and protein level in post-hypoxic cells (Figure 6A–C). As shown above for the silencing of Roquin expression under normoxic conditions, the hypoxia-dependent down-regulation of Roquin was also associated with increased expression of miR-23b-5p and reduced expression of *ZBTB20* (Figure 6D,E).

3.7. Effect of Antagomir Treatment Against miR-23b-5p on ZBTB20 Expression

Lastly, we validated the requirement for miR-23b-5p induction as a crucial step for the down-regulation of *ZBTB20*. Again, we down-regulated Roquin expression in AC16 cells using siRNA directed against Roquin-2 and blocked miR-23b-5p activity by antagomir treatment. Antagomir did not affect the down-regulation of Roquin-2 (Figure 7A), but the loss of *ZBTB20* expression was alleviated (Figure 7B).

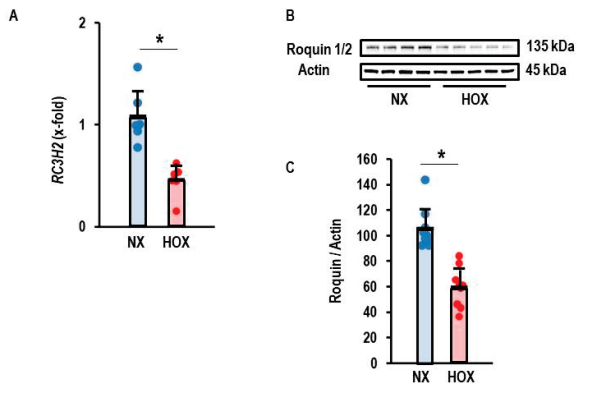


Figure 6. *Cont.*

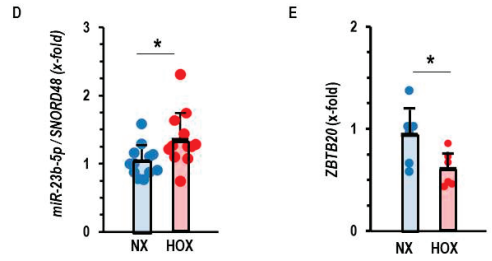


Figure 6. Effect of hypoxia (Hox) on the expression of Roquin. (**A**) Expression of RC3H2. Data are normalized to normoxic controls (Nx). (**B**) Western blot indicating the effect of hypoxia (Hox) on the expression of Roquin and quantification of the Western blot in (**C**) with $p < 0.05$ (unpaired *T*-test with Levene test for variance testing and Shapiro–Wilk test for normal distribution). (**D**) Expression of miR-23b-5p normalized to *SNORD48* as loading control. (**E**) Expression of *ZBTB20*. Data are given as means + S.D. (in black) and individual data points. *: $p < 0.05$ vs. Ctr. unpaired *T*-test with Levene test for variance testing and Shapiro–Wilk test for normal distribution.

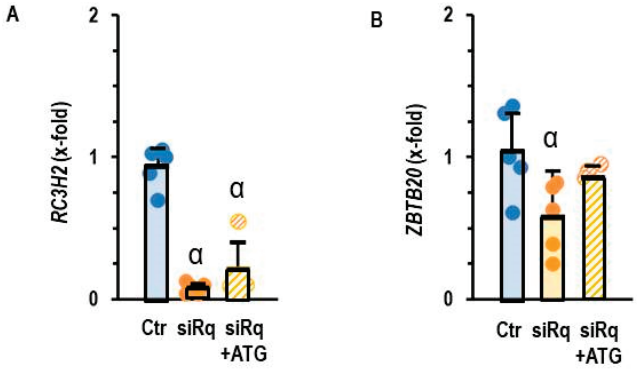


Figure 7. Expression of (**A**) *RC3H2* and (**B**) *ZBTB20* in AC16 cells with silencing of Roquin and antagomir treatment against miR23b-5p (ATG). Data are given as means + S.D. (in black) and individual data points. α: $p < 0.05$ versus control. Two-sided ANOVA with Student–Newman–Keuls post hoc analysis.

4. Discussion

Our study has revealed a previously undiscovered mechanism by which hypoxia influences ventricular remodeling: hypoxia down-regulates the expression of Roquin in cardiomyocytes, leading to the subsequent up-regulation of miR-23b-5p and ultimately to down-regulation of its target gene *ZBTB20*. This mechanism is important for the subsequent function of the post-ischemic myocardium.

The precise regulation of protein expressions in cells is essential for maintaining cell integrity. Transcription, translation, and protein degradation are primarily involved in maintaining intracellular protein homeostasis. As outlined in the introduction, Roquins belong to an interesting family of proteins that were originally identified as RNA-binding proteins in immune cells and are involved in the regulation of protein expression. They can bind to single-stranded RNA molecules (mRNA and miRNA), thereby reducing transcript concentration and subsequently the translation of RNA into protein [11,17]. They can also affect protein stability via ubiquitination. Roquins can act independently, but in some cases, they can also work together with proteins such as Regnase to regulate target mRNAs. However, studies on other cell types have shown that Regnase can function independently of Roquin [5,20]. Moreover, the expression of Roquin is regulated by MALT1.

Roquins have been characterized as modifiers of immune cell responses, but they are expressed in a broad way in other tissues as well. Our study demonstrates the constitutive expression of Roquin-1 and Roquin-2 in terminally differentiated rat cardiomyocytes and human AC16 cells, a cell line derived from human ventricular cardiomyocytes fused with

SV40-transformed fibroblasts. The use of rat terminally differentiated cardiomyocytes and a human cell line has both advantages and disadvantages. The advantages we used in this study are the comparison of cells from two species, the possibility to use antibodies directed against Roquin, and the capability of manipulating cells using siRNA. We also confirmed the expression of Regnase and MALT1 in these cells, but the expression of these proteins was not affected by hypoxia–reoxygenation or ischemia–reperfusion. They were therefore not further investigated in this study.

The role of Roquin in cardiac tissue has not yet been investigated, with the exception of a contribution to T-cell-dependent dysregulation associated with cardiac inflammation [5]. In contrast to this study, our data clearly show that Roquin is expressed in non-immune heart cells, such as cardiomyocytes. Furthermore, we observed a down-regulation of Roquin in post-ischemic rat hearts and post-hypoxic human cardiomyocytes. Interestingly, miR-223 was previously identified as an miRNA that triggers the degradation of Roquin and can also be used as a biomarker after myocardial infarction [21]. Thus, hypoxia may induce the expression of miR-223, which then triggers the hypoxia-dependent degradation of Roquin, but this requires future studies to identify the molecular mechanism more precisely. Our data show a comparative down-regulation of Roquin mRNA and protein expression, suggesting that regulation occurs on the transcriptional level.

We investigated via RNA sequencing the expression of multiple miRNAs in the rat heart under non-ischemic conditions and seven days after ischemia–reperfusion with and without infarct-sparing procedures such as pre- and post-conditioning [15]. We then correlated the expression of these miRNAs with that of Roquin mRNA to identify potential targets of Roquin. Overall, we have indeed identified several miRNAs that show a strong inverse correlation with Roquin expression, suggesting that these miRNAs are also potential targets of Roquin. It is important to validate the expression of these miRNAs with two independent methods—RNA sequencing and RT-PCR. After validation of miRNA expression with these two independent methods, we identified miR-23b-5p as a potential target of Roquins in cardiac cells. These correlations were subsequently confirmed in AC16 cells with Roquin silencing under normoxic conditions. Our data show that it is indeed Roquin deficiency, and not hypoxia itself, that triggers the inverse regulation of miR-23b-5p.

Next, we used the TargetScan8.0 data bank to identify potential targets of miR-23b-5p. Based on conserved sequences in both rat and human gene sequences, *ZBTB20* was identified as a potential down-stream target of miR-23b-5p. A deficiency of ZBTB20 is associated with cardiac dysfunction and a lack of cardiac reserve and exercise capacity in mice [18,19]. Mechanistically, ZBTB20 is required for phospholamban expression, and its deficiency leads to SERCA2a overactivation and increased Ca^{2+} loading of the sarcoplasmic reticulum (SR). Here, we show that hypoxia-dependent down-regulation of Roquin increased the expression of miR-23b-5p. This is subsequently linked to a reduction in *ZBTB20* expression, and this is associated with reduced left ventricular function. Furthermore, siRNA-induced down-regulation of Roquin and subsequent induction of miR-23b-5p did not lead to a reduction in *ZBTB20* expression when antagomir against miR-23b-5p was administered simultaneously.

As in all studies, our study has some limitations that cannot properly be addressed in this manuscript but require future attention. The lack of a proper antibody to detect Roquin-2 in rat tissue means that we could confirm the co-regulation of roquin mRNA and protein only in AC16 cells. However, we have no reason to assume that this will be different in rats. The different expression profile between Roquin-1 and Roquin-2 in rat tissue and AC16 cells requires attention, i.e., the role of Roquin-1 remains unclear, as we could not find any major difference between either isoform in this study. Furthermore, we believe that no differences occur between the Roquin expression in males and females,

but this was not really checked in this study. From the data so far, there is no evidence to assume such a difference. Finally, the in vitro part has the limitation that the cells were not exposed to physiological pO_2 levels, as they were cultured in a standard incubator using room air and 5% pCO_2. Thus, the challenge to hypoxia and reoxygenation does not exactly mimic the in vivo situation of ischemia–reperfusion. Nevertheless, this limitation is overbalanced by the finding of a similar type of regulation between in vivo and in vitro conditions and the ability to use siRNA and antagomirs to manipulate Roquin expression.

In summary, this is the first study to demonstrate the constitutive expression of Roquin isoforms in cardiomyocytes, their down-regulation in post-hypoxic tissues, an effect on miR-23b-5p and thus on *ZBTB20*, and finally an association with reduced cardiac function (Figure 8). Overall, the mechanisms identified may contribute to our understanding of why cardioprotective measures such as pre-conditioning and post-conditioning alone cannot completely prevent post-ischemic cardiac dysfunction, as they do not address hypoxia-induced alterations. Furthermore, our study suggests that the development of new techniques aimed to increase the expression of Roquins could lead to improved recovery after myocardial infarction.

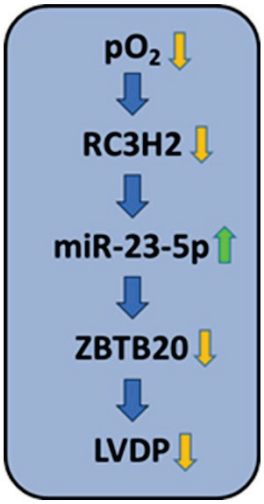


Figure 8. Summary of the findings: Hypoxia down-regulates the expression of *RC3H2* (Roquin-2), as demonstrated by exposing AC16 cells to hypoxia and rat hearts to ischemia (Figures 2D and 6A–C). Down-regulation of Roquin-2, as shown at the mRNA and protein level, increases the stability of miR-23b-5p (Figure 2A–C, Figures 5A, 6D and 7A). Increased expression of miR-23b-5p subsequently led to reduced expression of ZBTB20 (Figures 5B, 6E and 7B), and this is associated with decreased function (left ventricular developed pressure, LVDP; Figure 3B).

Supplementary Materials: The following supporting information can be downloaded at https://www.mdpi.com/article/10.3390/cells14221748/s1, Table S1: Information on PCR Primers.

Author Contributions: Conceptualization, R.S. (Rainer Schulz), P.F., and K.-D.S.; methodology, R.S. (Rolf Schreckenberg) and P.B.; software, P.B. and K.-D.S.; validation, N.I., R.S. (Rolf Schreckenberg), and K.-D.S.; formal analysis, N.I. and R.S. (Rolf Schreckenberg); investigation, N.I. and R.S. (Rolf Schreckenberg); resources, R.S. (Rainer Schulz), P.F., and K.-D.S.; data curation, K.-D.S.; writing—original draft preparation, K.-D.S.; writing—review and editing, N.I., R.S. (Rolf Schreckenberg), and K.-D.S.; visualization, K.-D.S.; supervision, R.S. (Rolf Schreckenberg) and K.-D.S.; project administration, R.S. (Rainer Schulz) and P.F.; funding acquisition, R.S. (Rainer Schulz) and P.F. All authors have read and agreed to the published version of the manuscript.

Funding: This research was funded by the International Excellence Research Cooperation Program 2024-1.2.3-HU-RIZONT and supported by the Hungarian National Scientific Research Fund (OTKA-138223). This study was also supported by project no. 2.3.1-21-2022-00003 'National Heart Laboratory, Hungary', implemented with the support of the European Union.

Institutional Review Board Statement: The animal study protocol was approved by the Institutional Review Board (or Ethics Committee) of Justus Liebig University, Giessen, Germany (752_M; 17 August 2023).

Informed Consent Statement: Not applicable.

Data Availability Statement: Original data can be requested from the corresponding author.

Acknowledgments: The authors thank Nadine Woitasky for excellent technical support.

Conflicts of Interest: Authors Peter Bencsik and Peter Ferdinandy were employed by the Pharmahungary Group. The remaining authors declare that the research was conducted in the absence of any commercial or financial relationships that could be construed as a potential conflict of interest.

Abbreviations

The following abbreviations are used in this manuscript:

miRNA	Micro-RNA
MMIA	miRNA-and-mRNA integrative analysis
siRNA	Small-inhibitory RNA
ZBTB20	Zinc finger and BTB domain containing protein 20

References

1. Du, B.; Liu, L. RNA-binding protein roquin negatively regulates STING-dependent innate immune response in Drosophila. *Yi Chuan* **2020**, *42*, 1201–1210. [CrossRef] [PubMed]
2. Diaz-Munoz, M.D.; Osma-Garcia, I.C. The RNA regulatory programs that govern lymphocyte development and function. *Wiley Interdiscip. Rev. RNA* **2022**, *13*, e1683. [CrossRef] [PubMed]
3. Hamid, F.M.; Makeyev, E.V. Exaptive origins of regulated mRNA decay in eukaryotes. *Bioessays* **2016**, *38*, 830–838. [CrossRef] [PubMed]
4. Montufar-Solis, D.; Vigneswaran, N.; Nakra, N.; Schaefer, J.S.; Klein, J.R. Hematopoietic not systemic impairment of roquin expression accounts for intestinal inflammation in roquin-deficient mice. *Sci. Rep.* **2014**, *4*, 4920. [CrossRef]
5. Cui, X.; Mino, T.; Yoshinaga, M.; Nakatsuka, Y.; Hia, F.; Yamasoba, D.; Tsujimura, T.; Tomonaga, K.; Suzuki, Y.; Uehata, T.; et al. Regnase-1 and roquin nonredundantly regulate Th1 differentiation causing cardiac inflammation and fibrosis. *J. Immunol.* **2017**, *199*, 4066–4077. [CrossRef]
6. Essig, K.; Kronbeck, N.; Guimaraes, J.C.; Lohs, C.; Schlundt, A.; Hoffmann, A.; Behrens, G.; Brenner, S.; Kowalska, J.; Lopez-Rodriguez, C.; et al. Roquin targets mRNAs in a 3'-UTR-specific manner by different modes of regulation. *Nat. Commun.* **2018**, *9*, 3810. [CrossRef]
7. Jeltsch, K.M.; Hu, D.; Brenner, S.; Zöller, J.; Heinz, G.A.; Nagel, D.; Vogel, K.U.; Rehage, N.; Warth, S.C.; Edelmann, S.L.; et al. Cleavage or roquin and regnase-1 by the paracaspase MALT1 releases theit cooperatively repressed targets to promote TH17 differentiation. *Nat. Immunol.* **2014**, *15*, 1079–1089. [CrossRef]
8. Baumjohann, D.; Heissmeyer, V. Posttranscriptional gene regulation of T follicular helper cells by RNA-binding proteins and microRNAs. *Front. Immunol.* **2018**, *9*, 1794. [CrossRef]
9. Essig, K.; Hu, D.; Guimaraes, J.C.; Alerauge, D.; Edelmann, S.; Raj, T.; Kranich, J.; Behrens, G.; Heiseke, A.; Floess, S.; et al. Roquin suppresses the PI3K-mTOR signaling pathway to inhibit T helper cell differentiation and conversion of Treg to Tfr cells. *Immunity* **2017**, *47*, 1067–1082. [CrossRef]
10. Athanasopoulos, V.; Ramiscal, R.R.; Vinuesa, C.G. ROQUIN signalling pathways in innate and adaptive immunity. *Eur. J. Immunol.* **2016**, *46*, 1082–1090. [CrossRef]
11. Schlundt, A.; Niessing, D.; Heissmeyer, V.; Sattler, M. RNA recognition by roquin in posttranscriptional gene regulation. *Wiley Interdiscip. Rev. RNA* **2016**, *7*, 455–469. [CrossRef] [PubMed]
12. Schmidt, H.; Raj, T.; O'Neill, T.J.; Muschaweckh, A.; Giesert, F.; Negraschus, A.; Hoefig, K.P.; Behrens, G.; Esser, L.; Baumann, C.; et al. Unrestrained cleavage of Roquin-1 by MALT1 induces spontaneous T cell activation and the development of autoimmunity. *Proc. Natl. Acad. Sci. USA* **2023**, *120*, e2309205120. [CrossRef] [PubMed]

13. Schaefer, J.S.; Montufar-Solis, D.; Vigneswaran, N.; Klein, J.R. Selective upregulation of microRNA expression in peripheral blood leukocytes in IL-10$^{-/-}$ mice precedes expression in the colon. *J. Immunol.* **2011**, *187*, 5834–5841. [CrossRef] [PubMed]
14. Zheng, L.; Ling, W.; Zhu, D.; Li, Z.; Kong, L. Roquin-1 regulates macrophage immune response and participates in hepatic ischemia-reperfusion injury. *J. Immunol.* **2020**, *204*, 1322–1333. [CrossRef]
15. Schreckenberg, R.; Klein, J.; Kutsche, H.S.; Schulz, R.; Gömöri, K.; Bencsik, P.; Benczik, B.; Agg, B.; Saghy, E.; Ferdinandy, P.; et al. Ischaemic post-conditioning in rats: Responder and non-responder differ in transcriptome of mitochondrial proteins. *J. Cell. Mol. Med.* **2020**, *24*, 5528–5541. [CrossRef]
16. Nippert, F.; Schreckenberg, R.; Schlüter, K.-D. Isolation and cultivation of adult rat cardiomyocytes. *J. Vis.* **2017**, *128*, 56634. [CrossRef]
17. Srivastava, M.; Duan, G.; Kershaw, N.J.; Athanasopoulos, V.; Yeo, J.H.C.; Ose, T.; Hu, D.; Brown, S.H.J.; Jergic, S.; Patel, H.R.; et al. Roquin binds microRNA-146a and Argonaute2 to regulate microRNA homeostasis. *Nat. Commun.* **2015**, *6*, 6253. [CrossRef]
18. Ren, A.-J.; Chen, C.; Zhang, S.; Liu, M.; Wie, C.; Wang, K.; Ma, X.; Song, Y.; Wang, R.; Zhang, H.; et al. Zbtb20 deficiency causes cardiac contractile dysfunction in mice. *FASEB J.* **2020**, *34*, 13862–13876. [CrossRef]
19. Ren, A.-J.; Wei, C.; Liu, Y.-J.; Liu, M.; Wang, P.; Fan, J.; Wang, K.; Zhang, S.; Qin, Z.; Ren, Q.-X.; et al. ZBTB20 regulates SERCA2a activity and myocardial contractility through phospholamban. *Circ. Res.* **2024**, *134*, 252–265. [CrossRef]
20. Mino, T.; Murakawa, Y.; Fukao, A.; Vandenbon, A.; Wessels, H.H.; Ori, D.; Uehata, T.; Tartey, S.; Akira, S.; Suzuki, Y.; et al. Regnase-1 and roquin regulate a common element in inflammatory mRNAs by spatiotemporally distinct mechanisms. *Cell* **2015**, *161*, 1058–1073. [CrossRef]
21. Elbaz, M.; Faccini, J.; Laperche, C.; Grazide, M.-H.; Ruidavets, J.-B.; Vindis, C. MiR-223 and MiR-186 are associated with long-term mortality after myocardial infarction. *Biomolecules* **2022**, *12*, 1243. [CrossRef]

Disclaimer/Publisher's Note: The statements, opinions and data contained in all publications are solely those of the individual author(s) and contributor(s) and not of MDPI and/or the editor(s). MDPI and/or the editor(s) disclaim responsibility for any injury to people or property resulting from any ideas, methods, instructions or products referred to in the content.

cells

MDPI

Article

Ladarixin Potential over the Effects of IL-8 and of Serum from Patients with Abdominal Aortic Aneurysm on Human Aortic Cells

Lucia Spartano [1,†], Maria Lombardi [1,†], Vincenzo Ardita [2], Roberto Chiesa [2], Andrea Aramini [3], Marcello Allegretti [3], Domenico Baccellieri [2], Lidia De Filippis [3] and Chiara Foglieni [1,*]

[1] Cardiovascular Research Center, IRCCS Ospedale San Raffaele, 20132 Milan, Italy
[2] Division of Vascular Surgery, IRCCS Ospedale San Raffaele, Vita-Salute San Raffaele University, 20132 Milan, Italy
[3] Dompé Farmaceutici S.p.A., 20122 Milan, Italy
* Correspondence: foglieni.chiara@hsr.it
† These authors contributed equally to this work.

Abstract: Early cellular alterations in abdominal aortic aneurysm (AAA) are scarcely investigated. Aortic remodeling inflammation-related suggested the CXCR2/CXCL1/IL-8 axis as a therapeutic target. This study investigates CXCR1/CXCR2 antagonism in primary human aortic endothelial (HAOEC) and smooth muscle cells (HAOSMC) conditioned with IL-8 or serum from patients with AAA (sPT). Ladarixin (10 μM Lad or 25 μM) served as an inhibitor. Readouts included RT-qPCR for *CXCL1*, *CXCL8*, *CXCR2*, *MMP9*, *NFKB1*, and *VEGF-A*; zymography for MMP9 activity confocal microscopy for F-actin and mitochondria; NADPH/NADH diaphorase histochemistry for redox activity; and ATP assay. In HAOEC, IL-8 downregulated *CXCR2*, increased MMP9 activity, and induced cytoskeletal and mitochondria disorganization without altering NADH/NADPH diaphorases but increasing ATP release. At concentration of 10 μM Lad rescued cell organization and gene expression. sPT upregulated *CXCL8*, *CXCR2*, and *MMP9*, decreased NADH/NADPH diaphorases, and altered cytoskeleton and mitochondria organization in HAOEC. At concentration of 10 μM Lad (partially) and 25 μM Lad reverted gene upregulation and mitochondria distribution; both doses increased diaphorase and released ATP. HAOSMC were scantily susceptible to IL-8 and weakly responsive to sPT, slightly upregulating *CXCR2* and *VEGF-A* but increasing proMMP9 gelatinolysis. Ladarixin recovered proMMP9 activity and modulated *CXCL1*. AAA-like vascular cell alterations involve multiple inflammatory factors and are modulable by inhibition of IL-8 receptors. The results underline careful dose calibration.

Keywords: primary human aortic endothelial (HAOEC); primary smooth muscle cells (HAOSMC); Interleukin 8 (IL-8); CXCR2/CXCL1/IL-8 axis; Metalloprotease 9 (MMP9); Ladarixin (Lad)

1. Introduction

Vascular wall damage in abdominal aortic aneurism (AAA) involves complex cellular and molecular immune–inflammatory pathogenic factors [1]. Besides the amplificatory effect associated with intraluminal NETosis or thrombosis [2], the circulating inflammatory microenvironment and oxidative stress-associated deregulation of NAD(P)H enzymes and metalloproteases (MMPs) [3] may affect constitutive vascular wall cells from the early phases of AAA development. Endothelial changes precede the injury of underneath smooth muscle cells (SMC) and the loosening of the extracellular matrix [3]. The role of endothelial

interaction with other cells belonging to the vascular wall during AAA formation has been postulated, but functional data about pro-aneurysmatic activation of the aortic cells are still scanty [3]. In LDR-/- mice, the deficiency of Angiotensin II receptor in aortic endothelium, but not in smooth muscle cells, attenuated the AAA development, and in the rat xenograft model of AAA involving dysendothelialization, rescue of the luminal lining by endothelial cell transplantation supported aortic wall stabilization through partially preserving the integrity of the internal elastic media [4,5]. The altered functionality of nitric oxide synthase and NAD(P)H oxidases in the endothelium activated by inflammation lead to increased production of oxygen radicals, inducing MMPs activation and abnormal matrix degradation, and affecting SMC functions, and ultimately contributing to aortic wall swelling and AAA development [3].

The administration of medications protecting the aortic luminal endothelium could be supportive in the reduction of the risk of AAA formation and rupture. This is relevant in the setting of AAA, as current pharmacological approaches (e.g., antihypertensive and antiplatelet drugs, statins, ACE inhibitors, and renin–angiotensin inhibitors) do not target AAA development but co-morbidities and risk factors. The identification of an optimal drug treatment is compulsory for going beyond monitoring of small AAA and surgery big AAA [1].

In the inflammatory background of AAA and specifically in the cyto-chemokines-related pathways, the CXCR2/CXCL1/IL-8 axis represents a putative therapeutic target in AAA, playing a causal role and pharmacologically modulable on *in vivo* murine elastase-induced AAA [6] and in *ex-vivo* cultured AAA tissues, as recently proposed by our group [7]. Here, we have mimicked the early phases of AAA in terms of activation of *in vitro* human aortic endothelial cells (EC) and SMC, exploring the dysfunctional effects of chronic stimulation with IL-8 or multiple circulating mediators on the homeostasis of the vascular wall cells.

We have also extended to activated EC and SMC the mechanistic investigation of the inhibition CXCR2/CXCL1/IL-8 axis, using the same dual CXCR1/CXCR2 antagonist Ladarixin (Lad) applied in the previous study [7]. Lad was mostly known for its application in cancer and type 1 diabetes, where this molecule is undergoing clinical trials [8]. Moreover, Lad contributed to protection against diabetic retinopathy in streptozotocin-treated rats [9] and impaired neutrophil migration without altering adhesive properties of the inflamed endothelium [10], hinting to a potential application in the vascular context. Accordingly with previous reports, including our recent findings on *ex vivo* cultured AAA tissues, we mainly focused on few readouts, i.e., *CXCR2/CXCL1/IL-8* and *MMP9* expressed genes, the activities of MMP9 and NAD(P)H oxidases, ATP release, mitochondrial and cytoskeletal organization [11–14].

2. Materials and Methods

2.1. Blood for Cell Conditioning

Serum samples (10 mL) from characterized male patients (Supplementary Table S2) with diagnosis of unruptured large AAA, according to the current European guidelines [15], hospitalized and undergoing infrarenal abdominal aortic aneurysmectomy at Vascular Surgery Unit of IRCCS San Raffaele Hospital, were used for cell conditioning. The donors were involved in a previously published study where further characteristics were described [14]. The research protocol (ID. AAA1, approved on 28 October 2021 and emended on 15 February 2023 by the Institutional Ethic Committee) conformed to the World Medical Association Declaration of Helsinki, and all enrolled individuals donating blood signed an informed consent.

Upon collection in vacutainer serum tubes, the blood was centrifuged at 2500× *g* 10 min at 4 °C, to obtain serum, which was aliquoted and stored at −80 °C until use.

The serum levels of several pro/anti-inflammatory mediators related to the CXCR2/CXCL1/IL-8 axis, namely CXCL1 CXCL2, IL-1α, IL-1β, IL-10, IL-6, IL-8, and TNF-α, were measured by Luminex multiplexed technology using FLEX MAP 3D LUMINEX instrument equipped with Bio Plex 6.2 software (all from R&D System, Minneapolis, MN, USA). Samples were stored at −80 °C and thawed only once, run in duplicate, and determined vs. standard curve, following the manufacturer' instructions.

2.2. Cell Culture

Primary human aortic endothelial and smooth muscle cells (HAOEC and HAOSMC, from single donors 43 and 53 years old, Caucasian males, Cat. # 304-05a and # 354-05a, respectively) were cultured using specific cell culture medium (095211F-500 Human EC Growth Medium and 095311-500 Human SMC Growth Medium, respectively) following the manufacturer' instructions and kept in standard 5% CO_2 incubator at 37 °C. The materials were provided by Cell Applications, Inc., San Diego, CA, USA.

Two chronic conditioning stimuli were studied: human recombinant IL-8 (human recombinant IL-8, SRP3098, Sigma-Aldrich, Milano, Italy) and human serum from patients with AAA (sPT). Briefly, the cells were settled in 24-well plates and in parallel on μ-Slides 8 well ^{high} Glass Bottom (N.80807, Ibidi GmbH, Gräfelfing, Germany) coated with Bovine Collagen Type I (N.47257, SERVA Electrophoresis GmbH, Heidelberg, Germany). After reaching about 50% confluence, the cells were treated with medium supplemented either with progressively increased amounts of IL-8 (IL-8 10 ng/mL, IL-8 30 ng/mL, IL-8 50 ng/mL), or sPT (2% sPT twice, then 5% sPT), following the protocol schematized in Supplementary Figure S1. Lad (10 μM or 25 μM) was added to culture 4 h before the end of the stimulation. Thereafter, the cell supernatants were harvested from cells in multiwells, which were rinsed in Dulbecco's phosphate buffer (PBS) and either fixed in 1% paraformaldehyde in PBS (PFA) for histochemistry assays or frozen for RNA and protein extraction. At the end of stimulation, cells in μ-slides were incubated with MitoTracker CMX-ROS (300 nM, 30 min, 37 °C, N. M7512 Invitrogen, ThermoFisher, Waltham, MA, USA) diluted in warm cell culture medium to label active mitochondria, then fixed with 1% PFA.

2.3. Immunofluorescence

Fixed cells were permeabilized with 0.1%Triton X-100 in PBS for 10 min, non-specific binding was blocked by 1% bovine serum albumin in PBS (blocking) for 30 min RT. F-actin was stained by Phalloidin (1:100, 30 min RT, P5282, Sigma-Aldrich, Milano, Italy) diluted in blocking. The cell phenotype was verified by Rabbit anti-Human VE-Cadherin (1:200, o/n 4 °C, AB-J3158, Immunological Sciences, Roma, Italy) or Mouse anti-human α smooth muscle actin (1:500, o/n 4 °C, MAB1420, R&D, Bio-Techne, Minneapolis, MN, USA), revealed by secondary antibody (Donkey-anti-Mouse IgG or Donkey-anti-Rabbit IgG AlexaFluor488-conjugated, diluted 1:500, incubated for 45 min RT, Thermo Fisher Life technologies Inc., Carlsbad, CA, USA). Upon rinse in PBS, the nuclei were stained with 4′,6-diamidino-2-phenylindole (DAPI, 0.2 nmol/L, 10 min, RT, D9542, Sigma-Aldrich, Milano, Italy). Slides mounted within 15%glycerol in PBS were analyzed under Olympus FluoVIEW 3000 RS confocal microscope using a UPLSAPO 60XS (NA 1.3) *Sil* objective. Multiframe images were obtained, then combined in 2D projections by the Fiji open-source software, ImageJ-based. The 2D images were collected in panels by using AdobePhotoshop CS [16].

2.4. Gel Zymography

Gelatin zymography was performed to evaluate the MMP gelatinolytic activities into cell supernatants. Briefly, samples diluted in Laemmli buffer were resolved on 8% SDS-PAGE containing 0.1% gelatin. Gels were washed in 2.5% Triton X-100 at RT on orbital shaker, then incubated overnight at 37 °C in 0.05 M Tris-HCl pH 8.8 containing 0.02% NaN_3 and 5 mM$CaCl_2$. Staining with 0.1% Coomassie blue and de-staining with 5% methanol and 7% acetic acid solution followed. Areas of digestion were visualized as non-stained regions. Optical densitometry was performed with Fiji software [16].

2.5. NADH/βNADPH Diaphorase Histochemistry

Fixed HAOEC were rinsed in PBS for 5 min at room temperature, then incubated (o/n, 37 °C) in 1 mM NADH/βNADPH and 0.2 mM Nitroblue Tetrazolium (cod. N. 10128023001, 10128024001, and N6876, respectively, Sigma-Aldrich, Milano, Italy) diluted in 100 mM Tris-HCl buffer pH 8.0 containing 0.1% Triton X-100. The oxidation of NAD(P)H generated hydrogen ions which bind to Nitroblue Tetrazolium, allowing the formation of a stable blue formazan. The redox reaction was stopped rinsing cells in PBS, and absorption was quantified by Victor 3V reader (450–630 nm). The cells were also visualized and photographed using an Eclipse 55i microscope equipped with a DS-L1 camera (Nikon, Tokyo, Japan) [17].

2.6. ATP Assays

ATP content was determined in cell supernatants by a bioluminescence assay based on luciferase's absolute requirement for ATP in producing light (ATP Determination Kit, A22066, Invitrogen, ThermoFisher, Waltham, MA, USA) according to the manufacturers' instruction, as previously described [18]. Samples were run in triplicate and luminescence was measured on Infinite F200 microplate reader (TECAN Group Ltd., Männedorf, Switzerland).

2.7. RNA Isolation and Quantitative Real-Time PCR

Total mRNA was extracted using miRNeasy Tissue/Cells Advanced Mini Kit (Qiagen, Hilden, Germany). Synthesis of cDNA from 200 ng of mRNA was carried out by reverse transcription using High-Capacity RNA-to-cDNA Kit (Invitrogen, Carlsbad, CA, USA). Quantitative real-time PCR (RT-qPCR) was performed using TaqMan® Universal Master Mix II and Taqman primer/Fam-labeled probes (Table S1, Applied Biosystems, Foster City, CA, USA) determining the relative levels of the expressed genes. All the procedures were carried out according to the manufacturers' instruction. Samples were run in triplicate, target gene levels were normalized to that of βactin mRNA, and relative expression was determined using the $2^{-\Delta Ct}$ method. The gene expression is presented as ratio applying the formula:

$$R = 2^{-\Delta Ct} \text{ (stimulated cells)} / 2^{-\Delta Ct} \text{ (untreated cells)}.$$

2.8. Statistics

The normality of the distribution of experimental data was assessed by Shapiro–Wilk test. Parametric or non-parametric tests were used depending on the normality of the data distribution. Differences among variables were calculated by using Wilcoxon or *t*-test, and with mixed-effects analysis or Friedman test for multiple comparisons. Simple linear regression or non-linear fits were evaluated to relate experimental parameters. Probability values <0.05 were considered significant. Prism 9.5.0 software (Graphpad Software Inc., La Jolla, San Diego, CA, USA) was used.

3. Results

3.1. Primary HAOEC Conditioned with IL-8 and Treated with Lad: Gene Expression and MMP9 Activities

To evaluate pro-aneurysmatic effects of chronic, progressively increasing concentrations IL-8 over aortic endothelial cells and the modulatory effects of Lad, we conditioned HAOEC with IL-8 before treating cells with the drug (Figure S1). IL-8 induced downregulation of CXCR2 gene expression with respect to untreated cells, restored by 10 μM Lad but not by 25 μM Lad (Figure 1A).

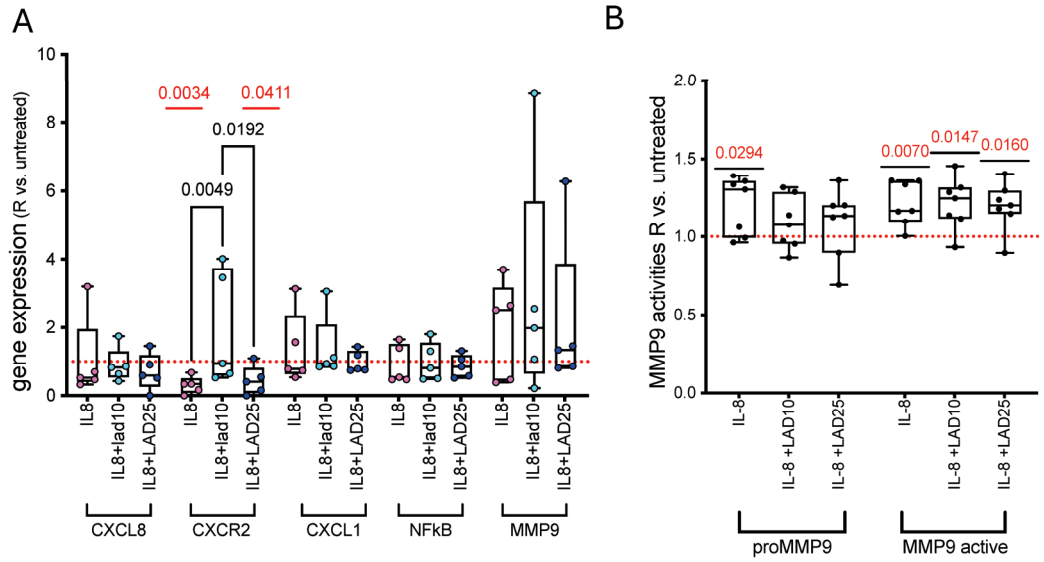


Figure 1

Figure 1. Gene expression levels and released MMP9 activities in IL-8 conditioned HAOEC. The expression level of *CXCL8, CXCR2, CXCL1, NFκB*, and *MMP9* genes measured by RT-qPCR in HAOEC (n = 5) is shown (**A**). Changes in MMP9 gelatinolytic activities in cell supernatants (n = 7) are plotted (**B**). Data are presented as ratio vs. untreated cells in boxes (min to max). Dots indicate single-sample values and $p < 0.05$ significant differences among treatments by Friedman test between single treatment and vs. untreated cells by Wilcoxon or *t*-test, depending on the normality of distribution. Pairwise comparisons are shown in each plot in red (comparison vs. untreated cells) and black (comparison between conditioned cells).

No significant changes in *CXCL8, CXCL1, NFKB*, and *MMP9* gene expressions were found in the presence/absence of Lad (Figure 1A), thus supporting a close functional relation between IL-8 and its receptor.

Lad antagonism on CXCR2 in AAA-cultured tissue modulated the activities of MMP9 isoforms [7]. To understand whether the modulation of released MMP9 was a downstream effect of IL-8 stimulus and Lad treatment, gel zymography was performed on HAOEC supernatants. Gelatinolytic activities of both proMMP9 and MMP9 active isoforms increased in the supernatants of HAOEC conditioned with IL-8 (Figure 1B and Figure S2A), whilst the activities of proMMP9 by HAOEC treated with 10 μM Lad and 25 μM Lad were assimilable to untreated cells, indicating recovery action. At difference, active MMP9 was significantly higher in the presence of both 10 μM Lad and 25 μM Lad than in untreated HAOEC (Figure 1B). These data supported the role of IL-8 in negative remodeling of the extracellular matrix and the potential, even partial, regulatory efficacy of Lad.

3.2. Primary HAOEC Conditioned with IL-8 and Treated with Lad: Energetics and Cytoskeleton

In HAOEC conditioned with IL-8, the NADH and NADPH diaphorases (oxidative activity of mitochondrial complex I and V, respectively) failed to show significant alterations (Figure S2B,C). In agreement, no change in the amounts of the released ATP was found, excepted for a moderate increase in cells conditioned with IL-8 and treated with 10 μM Lad vs. those only stimulated with IL-8 (Figure S2B). Interestingly, MitoTracker showed that the intracytoplasmic mitochondria organization changed in HAOEC treated with IL-8, with condensation of active mitochondria in the perinuclear area, and partially recovered upon treatment with Lad (Figure S2D). A slight alteration in VE-Cadherin pattern and the formation of stress fibers confirming the responsiveness of HAOEC to IL-8 and a structural recovery with Lad treatment were observed (Figure S2E,F).

3.3. Primary HAOEC Conditioned with Human Serum and Treated with Ladarixin: Gene Expression and MMP9 Activities

To assess whether and how the pro-aneurysmatic response of HAOEC changes in the presence of complex inflammation-related stimulation including IL-8, the cells were conditioned with serum from patients with AAA (sPT) (Figures S1 and S3A).

Upregulation of CXCL8, CXCR2, and MMP9 genes without changes in NFkB, VEGF-A, and CXCL1 (Figure 2A) were found in HAOEC conditioned with sPT. Treatment with 25 μM Lad reverted the upregulated gene expression to untreated cell level.

Despite the increase of *MMP9* expressed gene, no changes in the gelatinolytic activities of released MMP9 protein were detected in HAOEC conditioned with sPT with respect to untreated cells, either in the presence/absence of Lad (Figure 2B and Figure S3B), suggesting a regulation of metalloproteinases not restrained to IL-8 action or requiring high cytokine levels. In HAOEC conditioned with sPT in the presence of 25 μM Lad, the gelatinolysis by MMP9 active was associated to that of proMMP9 and to that in the absence of Lad (Figure S3C). The gelatinolysis by proMMP9 was linearly related to the amount of CXCL1 and IL-1β proteins in sPT (Figure S3D); this association reverted with 10 μM Lad but not with 25 μM Lad. Moreover, in the presence of 10 μM Lad, both MMP9 activities resulted negatively related also to IL-8 and IL-1βcontent in sPT.

3.4. Primary HAOEC Conditioned with Human Serum and Treated with Lad: Energetics and Cytoskeleton

In HAOEC conditioned with sPT, the NADH diaphorase was negatively related to the amount of IL-8 in sPT and positively to that of IL-1β (Figure S4A). The sPT-conditioning led to a decrease in NADH diaphorase, consistent with oxidative stress. Recovery was observed in the presence of Lad, significant with 25 μM Lad, which was also higher than untreated cells (Figure 2C,D). This was supportive of oxidoreductase regulation by Lad. Conversely, the NAPDH diaphorase did not change in HAOEC conditioned with sPT vs. untreated but was significantly lower than in cells treated with 10 μM Lad and 25 μM Lad (Figure 2C,D). The NADH and NADPH diaphorase activities were both higher in 25 μM Lad-treated HAOEC vs. untreated. Analogously, the release of ATP did not change following sPT conditioning, but increased with respect to untreated cells in HAOEC treated with both 10 μM Lad and 25 μM Lad (Figure 2E). Taken together, these data are compatible with an effect of increasing mitochondrial activity by Lad in sPT-conditioned cells.

At difference from what observed with IL-8, the mitochondria appeared diffusely distributed following sPT. A perinuclear localization comparable to that of untreated cells was observed with 25 μM Lad (Figure 2F). The actin cytoskeleton was altered with formation of peripheral stress fibers by conditioning with sPT, and a minor rescue of thin fibers was observed only with 25 μM Lad (Figure S4B).

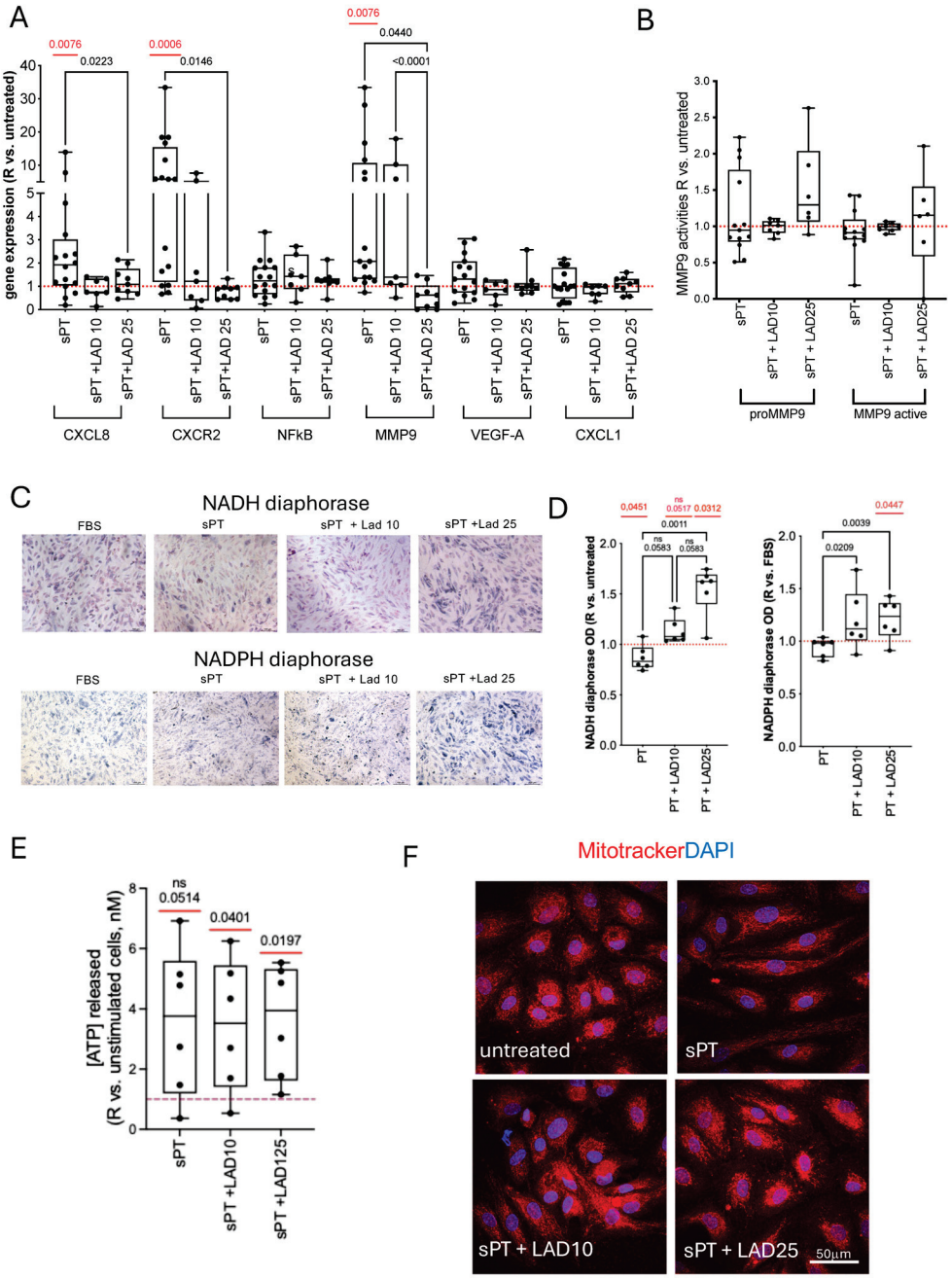


Figure 2

Figure 2. Gene expression levels, MMP9 gelatinolysis, NAD(P)H diaphorases, and ATP release in sPT-conditioned HAOEC. Gene expression by RT-qPCR of CXCL8, CXCR2, NFκB, MMP9, VEGF-A, and CXCL1 after cells conditioning +/- treatment with Lad is presented (n = 16, n = 7, and n = 9, respectively, (**A**)). Changes in gelatinolysis by released MMP9 after cells conditioning +/- treatment with Lad (n = 7) are presented (**B**). Representative light microscopy images of NADH and NADPH diaphorase histochemistry (objective 10x) are shown (**C**). Quantification of NADH/NADPH diaphorase activities (n = 6) (**D**) and ATP release in cell supernatants (n = 6, (**E**)) are plotted. Representative confocal microscopy images of MitoTracker-labeled mitochondria (red, (**F**)) are shown on HAOEC. Nuclei are stained with DAPI (blue). Data in (**A**,**B**,**D**,**E**) are presented as ratio vs. untreated cells in boxes (min to max). Dots indicate single-sample values and $p < 0.05$ significant differences by mixed-effects analysis in (**A**,**B**). Pairwise comparisons are shown in each plot in red (comparison vs. untreated cells) and black (comparison between conditioned cells).

3.5. Primary HAOSMC: Conditioned with IL-8 and Treated with Lad

In HAOSMC conditioned with IL-8, no significant change in the expression of CXCL8, CXCR2, CXCL1, NFKB, and MMP9 genes was determined. Treatment with 10 μM Lad, but not with 25 μM Lad, downregulated the MMP9 gene in IL-8-conditioned HAOSMC compared to untreated cells (Figure 3A).

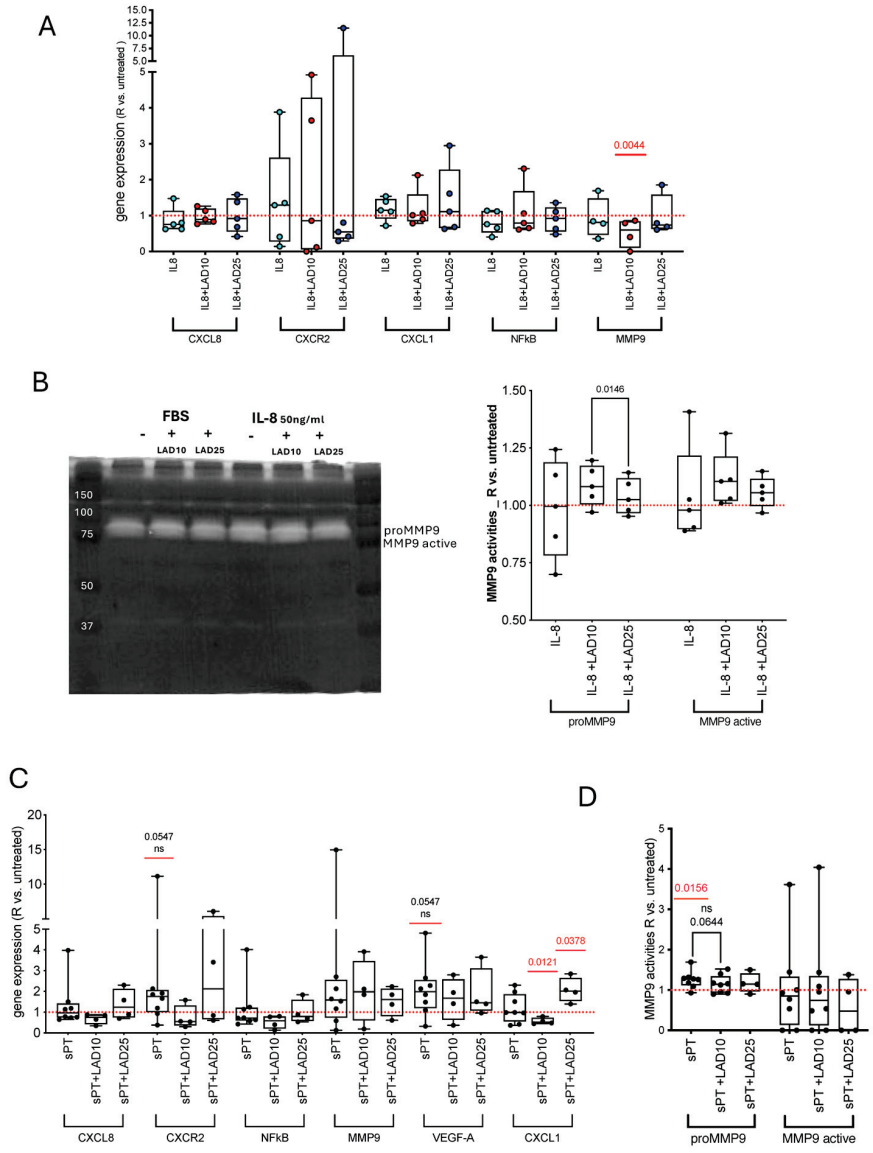


Figure 3

Figure 3. Gene expression levels and MMP9 activities in IL-8 and sPT-conditioned HAOSMC. Gene expression by RT-qPCR of *CXCL8*, *CXCR2*, *NFκB*, *MMP9*, *VEGF-A*, and *CXCL1* after HAOSMC conditioning with IL-8 +/− treatment with Lad (n = 5, (**A**)). Representative gel zymography image of HAOSMC conditioned with IL8 and changes in MMP9 gelatinolysis (n = 5, (**B**)) are presented as ratio vs. untreated cells. Gene expression of *CXCL8*, *CXCR2*, *NFκB*, *MMP9*, *VEGF-A*, and *CXCL1*, by RT-qPCR in sPT-conditioned HAOSMC +/- treatment with Lad (n = 8, n = 4 and n = 4, respectively, (**C**)) and changes in MMP9 gelatinolysis (n = 5, (**D**)) are shown as ratio vs. untreated cells. Data are presented as boxes (min to max). Dots indicate single-sample values and $p < 0.05$ significant differences among treatments by mixed-effects analysis, between single treatment and untreated cells by Wilcoxon or *t*-test depending on the normality of distribution. Pairwise comparisons are shown in each plot in red (comparison vs. untreated cells) and black (comparison between conditioned cells).

The zymography on supernatants from HAOSMC conditioned with IL-8 failed to show changes in MMP9 protein activities with respect to untreated cells (Figure 3B). Moreover, although a significant difference was found in proMMP9 gelatinolysis between IL-8-conditioned HAOSMC treated with 10 μM Lad vs. Lad 25 μM, there was no difference vs. untreated cells. Mitotracker and α smooth muscle actin indicated that no dramatic changes were also induced at mitochondrial (Figure S5A) and cytoskeletal levels (Figure S5B). These data supported a non-prominent role for IL-8 pathway in HAOSMC, unaffected by Lad.

3.6. Primary HAOSMC Conditioned with Human Serum and Treated with Ladarixin

No significant modulation of gene expression was measured upon sPT-conditioning of HAOSMC, but trends towards upregulation of CXCR2 and VEGF-A were observed (Figure 3C). Moreover, an opposite modulation of CXCL1 with 10 μM Lad (downregulation) and 25 μM Lad (upregulation) in conditioned vs. untreated HAOSMC was found, suggestive of a rebound effect with Lad 25 μM.

The proMMP9 gelatinolytic activity significantly increased in HAOSMC conditioned with sPT vs. untreated cells, and a trend towards reduction was observed following treatment with 10 μM Lad (Figure 3D and Figure S5C). The data were not related to the amounts of inflammatory mediators in sPT. Taken together, these findings support a scarce responsiveness of HAOSMC to sPT and a limited reactivity to Lad in non-activated conditions.

4. Discussion

Since the early 90s, AAA development has been causally related to increase of IL-8 cytokine amount and activity at aortic wall level [6,19–21]. A functional link between CXCR2/CXCL1/IL-8 axis and MMP9 activity in cultured lesioned aortic tissues from AAA and the MMP9 modulation via IL-8 receptor antagonism was demonstrated [7]. We show differences in the responsiveness of primary aortic cells to IL-8 and to serum from patients with AAA, and the modulatory effects over cell responses by the IL-8 receptor antagonist Lad, in the optics of viable therapeutic approaches against aortic damage.

IL-8 promoted in dose-dependent manner, either survival (via MMP9 enhancement and capillary tube formation) or dysfunction (via alteration of cytoskeleton and tight junctions) of *in vitro* endothelial cells [22,23], and was a functional modulator of SMC [24,25]. The decrease of *CXCR2* upon exposure of HAOEC to mature IL-8 (under conditions of progressively increasing, chronic inflammatory stimulation [26]) may represent a defensive reaction against alteration of the endothelial chemoattractant and of cell-to-cell interaction properties, compatible with first-line localization and protective role of HAOEC *in vivo* [27]. The absence of changes in other genes may indicate no activation of autocrine pathway or angiogenesis [28]. Instead, the IL-8-associated increase of the MMP9 protein activity is compatible with the chemokine role as extracellular matrix degradation enhancer. None of these effects is elicited in HAOSMC, thus indicating different intracellular mechanisms associated with IL-8 processing by vascular cells. Biological activities of IL-8 change upon site-specific proteolytic modification, mediated by MMP9 and other metalloproteinases, whose deregulation in pathological conditions like AAA supports the relevance of IL-8 cleavage in inflammatory settings [29].

Differences in responsiveness to IL-8 may be related to cell diversity in the vascular beds. Human saphenous vein cells provide an example: isolated SMC were able to produce and secrete IL-8 but lacked binding sites, whilst endothelial cells produced and bound IL-8 [30]. The aortic artery cells differ from those of the saphenous vein, as HAOSMC

endogenously express higher levels of *CXCL8* and *CXCR2* than HAOEC but scarcely react to the prolonged conditioning with IL-8.

The behavior of HAOEC is distinct from that of HAOSMC also with sPT-conditioning. This complex inflammatory stimulus triggers early signs of endothelial dysfunction in HAOEC (i.e., upregulation of *CXCL8*, *CXCR2*, and *MMP9* genes in the presence of variable MMP9 protein activity) but extracellular matrix/angiogenesis-related changes in HAOSMC. (i.e., increased proMMP9 gelatinolysis and borderline significant upregulation of *CXCR2* and *VEGF-A* genes). Despite the intrinsic constitutive differences, both HAOEC and HAOSMC respond to pharmacological antagonism of IL-8 receptors by Lad, which demonstrates rescuing efficacy.

In HAOEC, the sPT effect over MMP9 protein is linearly related to the serum content of CXCL1 (member of the ELR CXC family, as IL-8 [31,32]) and to IL-1β. Conversely, the efficacy of 10 μM Lad in rescuing gelatinolysis is negatively associated to the amounts of IL-8, IL-1β, and CXCL1 in sPT [7], and the rebound effect on proMMP9 by 25 μM Lad to the content of CXCL1. These findings highlight a non-exclusive role of IL-8 in the pro-aneurysmatic activation of aortic endothelium and suggest a connection at endothelial level between the drug action and the multifactorial composition of the stimulus.

Interplay between Lad and CXCL1 is also found in HAOSMC conditioned with sPT, where 10 μM Lad and 25 μM Lad exert opposite actions over gene expression, assimilable to stabilization and rebound effects, respectively. The association of CXCL1 increase to the inflammatory activation of rat vascular SMC induced by hypertension [33], to the causes of hypertension and MMP9 release in human diseases [32,34], and to AAA growth [35] support the potential relevance of Lad effects over CXCL1 in the perspective of AAA therapy. Together with the higher efficiency of 10 μM Lad vs. 25 μM Lad in modulating proMMP9 gelatinolysis in aortic cells, and in agreement with previous data on AAA tissue cultures [7], these findings suggest 10 μM Lad as a candidate dose for further studies.

Consequences of inflammation of the vascular wall and of intracellular pathways activated by IL-8 [36] may be multifaceted, and causal relationships with SMC remodeling and oxidative stress/respiration were demonstrated, pointing to a role for NADPH oxidases [3,37]. Although IL-8-driven alteration of NAD(P)H-dependent redox balance and ATP production at endothelial level [38] was reported in sepsis [39], if and how inflammation triggers endothelial dysfunction via cell remodeling and redox activity alteration under AAA-like conditions is almost unexplored. Our findings show that IL-8 leads to reinforcement of F-actin peripheral fibers [23] and mitochondria aggregation in HAOEC but not in HAOSMC. These changes are not paralleled by variation in NAD(P)H diaphorases (related to respiratory chain activity and nitric oxide synthesis, respectively [11,13,40]), and in ATP release. In sPT-conditioned HAOEC, the NADH diaphorase is associated to the sPT content of IL-8 and of IL-1β in opposite ways, and conditioning induces a decrease in both diaphorase activities, a trend towards increasing ATP secretion, and mitochondria spatial reorganization. Overall, these findings support early-stage remodeling in HAOEC, insufficiency of IL-8 but need of multiple mediators to trigger bioenergetic changes.

As in whole vessels ATP fuels vasodilation and maintenance of vascular tone [41], the variation in ATP released by HAOEC in the absence of shear stress/blood flow but presence of inflammatory stimuli may provide preliminary indication of how inflammation contributes to alter the artery diameter in AAA. Further studies investigating this mechanism under either static or dynamic conditions are required.

In the sPT-conditioning setting, treatment with Lad has augmentative, dose-dependent effects over energetics in HAOEC, and 25 μM Lad restores the mitochondrial pattern, significantly increasing diaphorases and ATP release. The reaction of HAOEC to Lad extends the drug effects beyond extracellular matrix regulation, possibly to the reversion

of the energetic unbalance due to sPT, results in mitochondria overwork buffered by ATP release, and underlines that drug calibration is pivotal.

The pattern of aortic cell responsiveness to Lad is also supportive of the need for combination therapy in AAA, in agreement with the failure in patients of therapies based on IL-8 inhibition, and effective on animal models [36].

5. Conclusions

In conclusion, IL-8 chronic stimulus plays a role in the post-translational regulation of MMP9 and in the modulation of *CXCR2* gene in HAOEC, and AAA patient' serum acts more widely over expressed genes of the CXCR2/CXCL1/IL-8 axis, underlining the synergistic/antagonistic interplay among serum inflammatory mediators in affecting the vascular wall. Moreover, the action of sPT, but not of IL-8, on HAOEC involves unbalance of redox-associated NAD(P)H enzymes, ultimately affecting the release of ATP.

HAOSMC are almost unresponsive to IL-8 but respond to AAA patient' serum at MMP9 post-translational level, compatibly with the prominent increase of extracellular matrix degradation in AAA.

IL-8 antagonism by Lad is partially efficient in recovering the IL-8 effects and fully efficient against those due to sPT. Characterizing whether Lad action in aortic cells involves specific engagements other than with IL-8 receptors goes beyond the purposes of this study. Finally, rebound effects following 25 μM Lad suggest being careful with dose calibration and indicate 10 μM Lad as a possible therapeutic candidate for vascular damage in AAA, warranting further studies.

Supplementary Materials: The following supporting information can be downloaded at: https://www.mdpi.com/article/10.3390/cells14211713/s1, Figure S1 Schematic representation of the cell treatments. Table S1. 1 FAM-probes for RT-qPCR. Table S2. Basic characteristics of blood donors. Figure S2 HAOEC conditioned with IL-8. Figure S3. HAOEC conditioned with sPT. Figure S4. HAOEC conditioned with sPT. Figure S5. MMP9 activities, staining Mitotracker and αSMA of conditioned HAOSMC.

Author Contributions: C.F., L.D.F., M.A. and A.A., conceptualization and design; V.A., R.C. and D.B., patients' recruitment, characterization; L.S., M.L. and C.F., investigation; L.S., M.L., C.F., V.A., R.C. and D.B., methodology and formal analysis; L.S., M.L. and C.F., writing—original draft preparation. C.F., L.D.F., A.A. and M.A., writing—review and editing. All authors have read and agreed to the published version of the manuscript.

Funding: Dompé Farmaceutici S.p.A supported this work as a part of the project "Fondo crescita sostenibile-Proposal n. 1410 bando MISE DM 02/08/2019".

Institutional Review Board Statement: The study was conducted in accordance with the Declaration of Helsinki, and approved by the Institutional Review Board (or Ethics Committee) of Ospedale San Raffaele IRCCS (protocol ID. AAA1, approved on 28 October 2021 and emended on 15 February 2023 by the Institutional Ethic Committee).

Informed Consent Statement: Informed consent was obtained from all subjects involved in the study.

Data Availability Statement: The main data presented in this study are available either in the article tables or in Supplementary Materials. Data from serum donors are subjected to privacy law and available on request from the corresponding author.

Acknowledgments: We thank Roberto Bertini, Dompé Farmaceutici S.p.A, for the useful information on the chemistry of Ladarixin and its *in vitro* use, and the team of Vascular Surgery Unit at IRCCS Ospedale San Raffaele for the support in patients' sample collection. We would also like to thank

the ALEMBIC Facility, an advanced microscopy laboratory established by the San Raffaele Scientific Institute, and the Vita-Salute San Raffaele University, for providing the confocal microscope.

Conflicts of Interest: A.A., M.A., and L.D.F are employees of Dompé Farmaceutici S.p.A. The remaining authors declare no conflicts of interest.

References

1. Golledge, J.; Thanigaimani, S.; Powell, J.T.; Tsao, P.S. Pathogenesis and management of abdominal aortic aneurysm. *Eur. Heart J.* **2023**, *44*, 2682–2697. [CrossRef]
2. Michalska, M.; Grochowiecki, T.; Jakimowicz, T.; Nazarewski, S. A Review of the Impact of Neutrophils and Neutrophil Extracellular Traps (NETs) on the Development of Aortic Aneurysms in Animal and Human Studies. *Med. Sci. Monit. Int. Med. J. Exp. Clin. Res.* **2021**, *27*, e935134. [CrossRef] [PubMed]
3. Sun, J.; Deng, H.; Zhou, Z.; Xiong, X.; Gao, L. Endothelium as a Potential Target for Treatment of Abdominal Aortic Aneurysm. *Oxidative Med. Cell. Longev.* **2018**, *2018*, 6306542. [CrossRef]
4. Franck, G.; Dai, J.; Fifre, A.; Ngo, S.; Justine, C.; Michineau, S.; Allaire, E.; Gervais, M. Reestablishment of the endothelial lining by endothelial cell therapy stabilizes experimental abdominal aortic aneurysms. *Circulation* **2013**, *127*, 1877–1887. [CrossRef]
5. Rateri, D.L.; Moorleghen, J.J.; Balakrishnan, A.; Owens, A.P., 3rd; Howatt, D.A.; Subramanian, V.; Poduri, A.; Charnigo, R.; Cassis, L.A.; Daugherty, A. Endothelial cell-specific deficiency of Ang II type 1a receptors attenuates Ang II-induced ascending aortic aneurysms in LDL receptor$^{-/-}$ mice. *Circ. Res.* **2011**, *108*, 574–581. [CrossRef]
6. Kokje, V.B.C.; Gäbel, G.; Dalman, R.L.; Koole, D.; Northoff, B.H.; Holdt, L.M.; Hamming, J.F.; Lindeman, J.H.N. CXCL8 hyper-signaling in the aortic abdominal aneurysm. *Cytokine* **2018**, *108*, 96–104. [CrossRef]
7. Lombardi, M.; Spartano, L.; Nicolo, S.; Ardita, V.; Chiesa, R.; Aramini, A.; Allegretti, M.; Baccellieri, D.; De Filippis, L.; Foglieni, C. Modulation of MMP9 and CXCR2/CXCL1/IL-8 axis in human abdominal aortic aneurysm tissues by ladarixin. *Cardiovasc. Res.* **2024**, *120*, 1832–1834. [CrossRef] [PubMed]
8. Korbecki, J.; Bosiacki, M.; Pilarczyk, M.; Kot, M.; Defort, P.; Walaszek, I.; Chlubek, D.; Baranowska-Bosiacka, I. The CXCL1-CXCR2 Axis as a Component of Therapy Resistance, a Source of Side Effects in Cancer Treatment, and a Therapeutic Target. *Cancers* **2025**, *17*, 1674. [CrossRef]
9. Boccella, S.; Morace, A.M.; Giorgio, C.; Guida, F.; Perrone, M.; Manzo, I.; Belardo, C.; Jones, M.; Maione, S.; Aramini, A.; et al. Effects of CXCR1/2 Blockade with Ladarixin on Streptozotocin-Induced Type 1 Diabetes Mellitus and Peripheral Neuropathy and Retinopathy in Rat. *Diabetes Metab. J.* **2025**, *49*, 990–1005. [CrossRef]
10. Napoli, M.; Sitaru, S.; Budke, A.; Kammerl, A.; Querner, G.; Immler, R.; Rohwedder, I.; Seifert, S.; Ferraro, B.; Weckbach, L.; et al. The dual non-competitive CXCR1/2 inhibitor ladarixin impairs neutrophil extravasation without altering intravascular adhesion. *Haematologica* **2025**. [CrossRef] [PubMed]
11. Aliev, G.; Smith, M.A.; Turmaine, M.; Neal, M.L.; Zimina, T.V.; Friedland, R.P.; Perry, G.; LaManna, J.C.; Burnstock, G. Atherosclerotic lesions are associated with increased immunoreactivity for inducible nitric oxide synthase and endothelin-1 in thoracic aortic intimal cells of hyperlipidemic Watanabe rabbits. *Exp. Mol. Pathol.* **2001**, *71*, 40–54. [CrossRef]
12. Ejiri, J.; Inoue, N.; Tsukube, T.; Munezane, T.; Hino, Y.; Kobayashi, S.; Hirata, K.; Kawashima, S.; Imajoh-Ohmi, S.; Hayashi, Y.; et al. Oxidative stress in the pathogenesis of thoracic aortic aneurysm: Protective role of statin and angiotensin II type 1 receptor blocker. *Cardiovasc. Res.* **2003**, *59*, 988–996. [CrossRef]
13. Morin, A.M.; Stanboli, A. Nitric oxide synthase in cultured endothelial cells of cerebrovascular origin: Cytochemistry. *J. Neurosci. Res.* **1993**, *36*, 272–279. [CrossRef]
14. Zhang, J.; Tang, Y.; Zhang, S.; Xie, Z.; Ma, W.; Liu, S.; Fang, Y.; Zheng, S.; Huang, C.; Yan, G.; et al. Mitochondrial NAD(+) deficiency in vascular smooth muscle impairs collagen III turnover to trigger thoracic and abdominal aortic aneurysm. *Nat. Cardiovasc. Res.* **2025**, *4*, 275–292. [CrossRef] [PubMed]
15. Wanhainen, A.; Verzini, F.; Van Herzeele, I.; Allaire, E.; Bown, M.; Cohnert, T.; Dick, F.; van Herwaarden, J.; Karkos, C.; Koelemay, M.; et al. Editor's Choice—European Society for Vascular Surgery (ESVS) 2019 Clinical Practice Guidelines on the Management of Abdominal Aorto-iliac Artery Aneurysms. *Eur. J. Vasc. Endovasc. Surg. Off. J. Eur. Soc. Vasc. Surg.* **2019**, *57*, 8–93. [CrossRef] [PubMed]
16. Mantione, M.E.; Lombardi, M.; Baccellieri, D.; Ferrara, D.; Castellano, R.; Chiesa, R.; Alfieri, O.; Foglieni, C. IL-1β/MMP9 activation in primary human vascular smooth muscle-like cells: Exploring the role of TNFα and P2X7. *Int. J. Cardiol.* **2019**, *278*, 202–209. [CrossRef] [PubMed]
17. Foglieni, C.; Cavarelli, M.; Piscopiello, M.; Fulgenzi, A.; Ferrero, M.E. Mn bioavailability by polarized Caco-2 cells: Comparison between Mn gluconate and Mn oxyprolinate. *Nutr. J.* **2011**, *10*, 77. [CrossRef]
18. Lombardi, M.; Mantione, M.E.; Baccellieri, D.; Ferrara, D.; Castellano, R.; Chiesa, R.; Alfieri, O.; Foglieni, C. P2X7 receptor antagonism modulates IL-1β and MMP9 in human atherosclerotic vessels. *Sci. Rep.* **2017**, *7*, 4872. [CrossRef]

19. Koch, A.E.; Kunkel, S.L.; Pearce, W.H.; Shah, M.R.; Parikh, D.; Evanoff, H.L.; Haines, G.K.; Burdick, M.D.; Strieter, R.M. Enhanced production of the chemotactic cytokines interleukin-8 and monocyte chemoattractant protein-1 in human abdominal aortic aneurysms. *Am. J. Pathol.* **1993**, *142*, 1423–1431.
20. Levesque, M.; Bath, L.; Ducas, A.; Boyd, A. Increased Interleukin-8 Expression in Regions of High Intraluminal Thrombus Deposition in Human Abdominal Aortic Aneurysms. *JVS-Vasc. Sci.* **2020**, *1*, 256–257. [CrossRef]
21. Middleton, R.K.; Bown, M.J.; Lloyd, G.M.; Jones, J.L.; London, N.J.; Sayers, R.D. Characterisation of Interleukin-8 and monocyte chemoattractant protein-1 expression within the abdominal aortic aneurysm and their association with mural inflammation. *Eur. J. Vasc. Endovasc. Surg. Off. J. Eur. Soc. Vasc. Surg.* **2009**, *37*, 46–55. [CrossRef]
22. Li, A.; Dubey, S.; Varney, M.L.; Dave, B.J.; Singh, R.K. IL-8 directly enhanced endothelial cell survival, proliferation, and matrix metalloproteinases production and regulated angiogenesis. *J. Immunol.* **2003**, *170*, 3369–3376. [CrossRef]
23. Yu, H.; Huang, X.; Ma, Y.; Gao, M.; Wang, O.; Gao, T.; Shen, Y.; Liu, X. Interleukin-8 regulates endothelial permeability by down-regulation of tight junction but not dependent on integrins induced focal adhesions. *Int. J. Biol. Sci.* **2013**, *9*, 966–979. [CrossRef] [PubMed]
24. Hastings, N.E.; Feaver, R.E.; Lee, M.Y.; Wamhoff, B.R.; Blackman, B.R. Human IL-8 regulates smooth muscle cell VCAM-1 expression in response to endothelial cells exposed to atheroprone flow. *Arterioscler. Thromb. Vasc. Biol.* **2009**, *29*, 725–731. [CrossRef]
25. Yue, T.L.; Wang, X.; Sung, C.P.; Olson, B.; McKenna, P.J.; Gu, J.L.; Feuerstein, G.Z. Interleukin-8. A mitogen and chemoattractant for vascular smooth muscle cells. *Circ. Res.* **1994**, *75*, 1–7. [CrossRef] [PubMed]
26. Shimizu, K.; Mitchell, R.N.; Libby, P. Inflammation and cellular immune responses in abdominal aortic aneurysms. *Arterioscler. Thromb. Vasc. Biol.* **2006**, *26*, 987–994. [CrossRef]
27. Reutershan, J.; Morris, M.A.; Burcin, T.L.; Smith, D.F.; Chang, D.; Saprito, M.S.; Ley, K. Critical role of endothelial CXCR2 in LPS-induced neutrophil migration into the lung. *J. Clin. Investig.* **2006**, *116*, 695–702. [CrossRef] [PubMed]
28. Martin, D.; Galisteo, R.; Gutkind, J.S. CXCL8/IL8 stimulates vascular endothelial growth factor (VEGF) expression and the autocrine activation of VEGFR2 in endothelial cells by activating NFkappaB through the CBM (Carma3/Bcl10/Malt1) complex. *J. Biol. Chem.* **2009**, *284*, 6038–6042. [CrossRef]
29. Metzemaekers, M.; Abouelasrar Salama, S.; Vandooren, J.; Mortier, A.; Janssens, R.; Vandendriessche, S.; Ganseman, E.; Martens, E.; Gouwy, M.; Neerinckx, B.; et al. From ELISA to Immunosorbent Tandem Mass Spectrometry Proteoform Analysis: The Example of CXCL8/Interleukin-8. *Front. Immunol.* **2021**, *12*, 644725. [CrossRef]
30. Schönbeck, U.; Brandt, E.; Petersen, F.; Flad, H.D.; Loppnow, H. IL-8 specifically binds to endothelial but not to smooth muscle cells. *J. Immunol.* **1995**, *154*, 2375–2383. [CrossRef]
31. Geiser, T.; Dewald, B.; Ehrengruber, M.U.; Clark-Lewis, I.; Baggiolini, M. The interleukin-8-related chemotactic cytokines GRO alpha, GRO beta, and GRO gamma activate human neutrophil and basophil leukocytes. *J. Biol. Chem.* **1993**, *268*, 15419–15424. [CrossRef]
32. Zhang, L.; Li, Q.; Zhou, C.; Zhang, Z.; Zhang, J.; Qin, X. Immune-dysregulated neutrophils characterized by upregulation of CXCL1 may be a potential factor in the pathogenesis of abdominal aortic aneurysm and systemic lupus erythematosus. *Heliyon* **2023**, *9*, e18037. [CrossRef]
33. Zhao, J.; Nishimura, Y.; Kimura, A.; Ozawa, K.; Kondo, T.; Tanaka, T.; Yoshizumi, M. Chemokines protect vascular smooth muscle cells from cell death induced by cyclic mechanical stretch. *Sci. Rep.* **2017**, *7*, 16128. [CrossRef]
34. Korbecki, J.; Maruszewska, A.; Bosiacki, M.; Chlubek, D.; Baranowska-Bosiacka, I. The Potential Importance of CXCL1 in the Physiological State and in Noncancer Diseases of the Cardiovascular System, Respiratory System and Skin. *Int. J. Mol. Sci.* **2022**, *24*, 205. [CrossRef] [PubMed]
35. Márquez-Sánchez, A.C.; Koltsova, E.K. Immune and inflammatory mechanisms of abdominal aortic aneurysm. *Front. Immunol.* **2022**, *13*, 989933. [CrossRef] [PubMed]
36. Matsushima, K.; Yang, D.; Oppenheim, J.J. Interleukin-8: An evolving chemokine. *Cytokine* **2022**, *153*, 155828. [CrossRef]
37. Zhang, Z.; Xu, H.N.; Li, S.; Davila, A., Jr.; Chellappa, K.; Davis, J.G.; Guan, Y.; Frederick, D.W.; Chu, W.; Zhao, H.; et al. Rapamycin maintains NAD(+)/NADH redox homeostasis in muscle cells. *Aging* **2020**, *12*, 17786–17799. [CrossRef] [PubMed]
38. Dumitrescu, S.I.; Jinga, M.; Cochior, D.; Bontas, E.; Parepa, I.; Nita, D.; Gabriel, C.; Ţintoiu, I.C. Endothelial Dysfunction in Aortic Aneurysm. In *New Approaches to Aortic Diseases from Valve to Abdominal Bifurcation*; Academic Press: London, UK, 2018; pp. 25–39.
39. Miyoshi, T.; Yamashita, K.; Arai, T.; Yamamoto, K.; Mizugishi, K.; Uchiyama, T. The role of endothelial interleukin-8/NADPH oxidase 1 axis in sepsis. *Immunology* **2010**, *131*, 331–339. [CrossRef]

40. Seckler, J.M.; Shen, J.; Lewis, T.H.J.; Abdulameer, M.A.; Zaman, K.; Palmer, L.A.; Bates, J.N.; Jenkins, M.W.; Lewis, S.J. NADPH diaphorase detects S-nitrosylated proteins in aldehyde-treated biological tissues. *Sci. Rep.* **2020**, *10*, 21088. [CrossRef]
41. Wilson, C.; Lee, M.D.; Buckley, C.; Zhang, X.; McCarron, J.G. Mitochondrial ATP Production is Required for Endothelial Cell Control of Vascular Tone. *Function* **2023**, *4*, zqac063. [CrossRef]

Disclaimer/Publisher's Note: The statements, opinions and data contained in all publications are solely those of the individual author(s) and contributor(s) and not of MDPI and/or the editor(s). MDPI and/or the editor(s) disclaim responsibility for any injury to people or property resulting from any ideas, methods, instructions or products referred to in the content.

cells

MDPI

Article

Prostaglandin D_2 Synthase: A Novel Player in the Pathological Signaling Mechanism of the Aldosterone–Mineralocorticoid Receptor Pathway in the Heart

Ankita Garg [1,†], Malte Juchem [1,2,†], Sinje Biss [1], Carla Nunes Borisch [1], Julia Leonardy [1], Christian Bär [1,2,3,‡], Shashi Kumar Gupta [1,‡,§] and Thomas Thum [1,*,‡]

[1] Institute of Molecular and Translational Therapeutic Strategies (IMTTS), Hannover Medical School, 30625 Hannover, Germany
[2] Fraunhofer Institute for Toxicology and Experimental Medicine (ITEM), 30625 Hannover, Germany
[3] Fraunhofer Cluster of Excellence Immune-Mediated Diseases (CIMD), 30625 Hannover, Germany
* Correspondence: thum.thomas@mh-hannover.de
† These authors contributed equally to this work.
‡ These authors jointly directed the work.
§ Current address: Council of Scientific and Industrial Research—Central Drug Research Institute, Lucknow 226031, India.

Abstract: Background: A deregulated aldosterone (Aldo)–mineralocorticoid receptor (MR) pathway is linked to cardiovascular disease (CVD), including hypertension and heart failure. Despite the association of elevated plasma Aldo levels with cardiac stress, inflammation, myocardial fibrosis, and cardiac remodeling, the underlying mechanisms remain elusive. **Methods:** To study the impact of Aldo–MR pathway overactivation on cardiac health, a novel mouse model with AAV9-mediated MR overexpression and Aldo administration via subcutaneous osmotic pumps was generated. Echocardiographic analyses, transcriptome sequencing, and loss-of-function experiments of an identified lead candidate gene were performed. Additionally, cardiac tissue samples from human patients with end-stage heart failure were analyzed in the study. **Results:** Mice with an overactivated Aldo–MR pathway exhibited increased neutrophil gelatinase-associated lipocalin (NGAL) expression, cardiac dysfunction, hypertrophy, and fibrosis. Transcriptomics identified prostaglandin D_2 synthase (*Ptgds*) as a novel downstream effector of the cardiac Aldo–MR pathway. SiRNA-mediated inhibition of *Ptgds* in primary cardiomyocytes reduced NGAL levels and the hypertrophic impact of Aldo, suggesting a role in mediating Aldo-induced cardiac pathologies. Elevated expression of *PTGDS* was observed in hiPSC-CMs treated with the pro-hypertrophic cytokine leukemia inhibitory factor (LIF) and in end-stage heart failure patients, ascertaining its importance in cardiac disease settings. **Conclusions:** PTGDS is a newly identified mediator of Aldo–MR-induced cardiac remodeling and may represent a potential therapeutic target for CVD.

Keywords: Aldo–MR pathway; cardiovascular disease; remodeling; cardiac hypertrophy; adeno-associated virus

1. Introduction

Heart failure is a chronic clinical syndrome characterized by the inability of the heart muscle to pump sufficient blood throughout the body. This incapacity can originate from various reasons such as atherosclerosis, high blood pressure, cardiomyopathy, arrhythmias, or congenital heart disease. Cardiovascular diseases (CVDs) refer to conditions that affect

the blood vessels or the heart and represent the leading cause of deaths and morbidity across the world, emanating an aggressive socio-economic burden on humanity and a substantial challenge for the scientific community [1].

Several studies advocate the role of a deregulated aldosterone–mineralocorticoid receptor (Aldo–MR) pathway in driving these cardiovascular pathologies, indicating the high importance of this pathway [2]. Under normal physiological conditions, the Aldo–MR pathway regulates the Na^+-H_2O balance in the body via kidneys' ductal tubes, thereby maintaining the blood pressure [3,4]. However, an over-activated Aldo–MR pathway has been involved in myocardial infarction (MI), hypertension, and cardiac remodeling, including cardiac fibrosis, apoptosis, hypertrophy, inflammation, and oxidative cardiac stress, eventually leading to heart failure [5–9]. The therapeutic value of the Aldo–MR pathway has been explored using various MR antagonists that improved cardiac functions as observed in the clinical trials RALES, EPHESUS, and EMPHASIS-HF [10–13]. In addition to the studies showing an inverse correlation of activation and blockage of MR with cardiac health, inhibition of NGAL (downstream effector of Aldo–MR pathway) in mice was also found to limit cardiac damage induced by MI and ischemia-reperfusion injury [14–17]. Although a crucial role of the Aldo–MR pathway in mediating cardiac pathologies is evident, the detailed underlying mechanisms are still poorly understood.

To have an in-depth understanding of these cardiac pathologies, researchers have devised several small murine models such as coronary artery ligation (myocardial damage), transient occlusion of coronary artery (ischemia reperfusion damage), cryo-infarction, aortic constriction (pressure overload), and various transgenic models (e.g., mutation of α-actin protein for dilated cardiomyopathy) [18]. These physiological models hold great importance as they closely mimic cardiac pathological conditions and provide valuable mechanistic insight. Several knockout and transgenic models such as LDLR$-/-$ mice (for familial hypercholesterolemia) and ApoE$-/-$ mice (for atherosclerosis) are also available for exploring cellular pathways and evaluation of novel therapies [18]. Interestingly, a transgenic model for aldosterone-mediated cardiac hypertrophy was also developed by specific overexpression of 11β-hydroxysteroid dehydrogenase type 2 in cardiomyocytes that showed aggravated hypertrophy which improved upon treatment with Aldo antagonist eplerenone [19]. However, these models mainly focus on the genetic predisposition of cardiac pathologies, while the involvement of the Aldo–MR pathway in cardiac conditions is mostly acquired with age in adulthood rather than being genetic. Therefore, we developed a mouse model (adult mice, age 8–10 weeks) for Aldo–MR pathway activation where MR was overexpressed via AAV9 followed by subcutaneous implantation of osmotic pump implants for constant Aldo administration (Figure 1A). This model closely mimics the acquired Aldo–MR pathway over-activation in adulthood in mice without any predisposed cardiac conditions since birth. Here, using this mouse model, we identified key players involved in the Aldo–MR pathway-mediated cardiac remodeling and their functionalities.

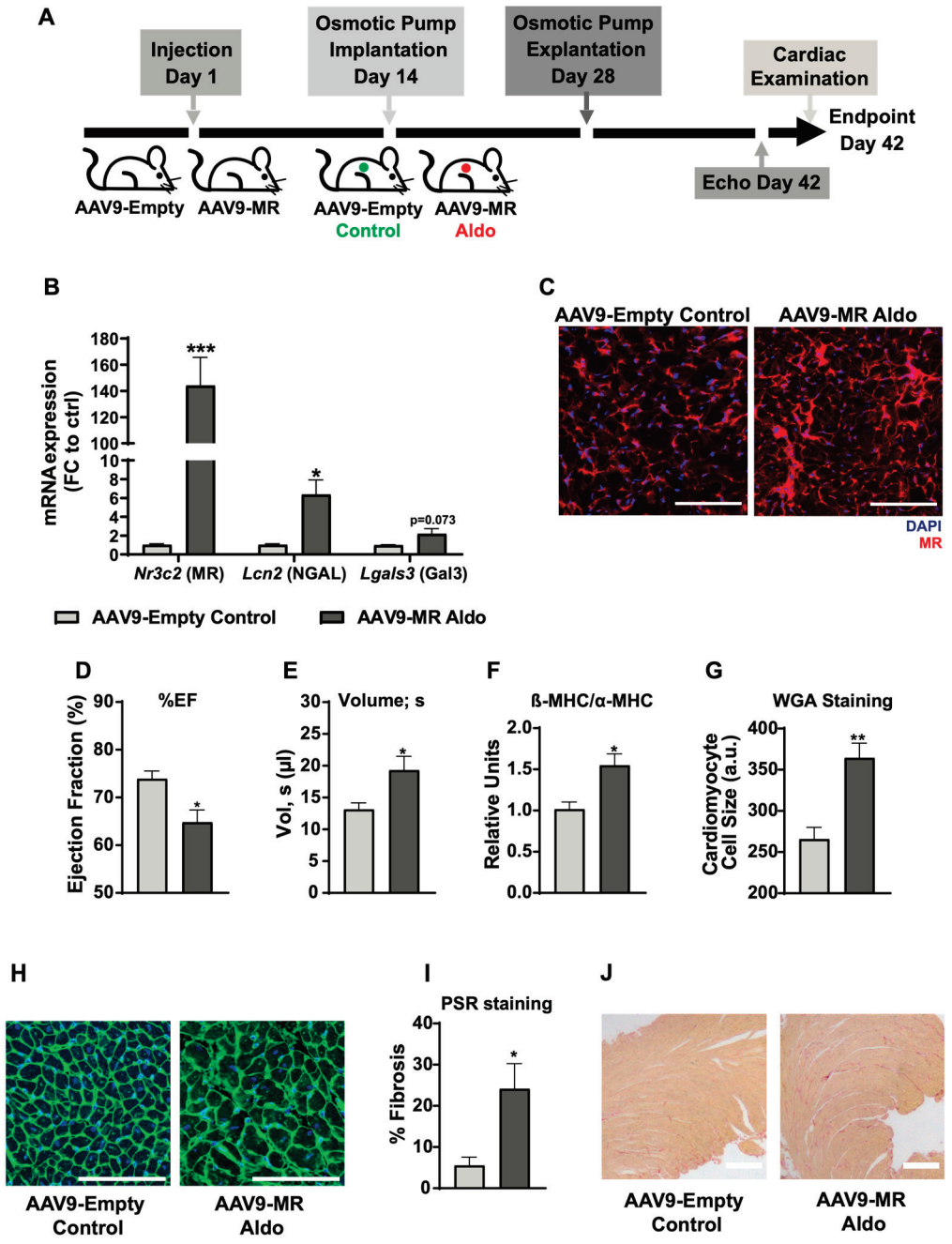


Figure 1. Aldo–MR over-activation mouse model. (**A**) A schematic overview of the experimental design for AAV9-mediated MR-overexpression in a murine model with pharmacological aldosterone treatment. (**B**) mRNA expression of various genes in mouse hearts treated with AAV9-Empty-Control and AAV9-MR-Aldo as measured by RT-PCR. (**C**) Fluorescent images obtained after Anti-MR staining of mouse heart cryo-sections from AAV9-Empty-Control and AAV9-MR-Aldo animal groups (n = 5–6 animals per group). (**D**,**E**) Echocardiographic analysis in the AAV9-mediated MR-overexpression system showing a change in ejection fraction percentage (**D**) and end-systolic volume (**E**) as a measure of cardiac function in mice with AAV9-Empty-Control and AAV9-MR-Aldosterone treatment (n = 5–6 animals per group). (**F**) Ratio of mRNA expression of β-MHC and α-MHC as analyzed by RT-PCR in mice with AAV9-Empty-Control and AAV9-MR-Aldosterone treatment (n = 5–6 animals per group). (**G**–**J**) Cell size measurement from heart tissue slices (**G**) after WGA staining (**H**), and percent of fibrosis (**I**) analyzed after Picro-Sirius red staining (**J**) in mice with AAV9-Empty-Control and AAV9-MR-Aldosterone treatment (n = 5–6 animals per group). All data are represented as mean ± SEM. * $p \leq 0.05$, ** $p \leq 0.01$, *** $p \leq 0.001$. Scale bars indicate 100 (**C**,**H**) or 200 (**J**) µm.

2. Materials and Methods

2.1. Animal Model

For this study, 8–10-week-old male C57BL/6N mice were used. The sample size was determined by the original exploratory design of the study ($n = 5$ for control and $n = 6$ for overexpression group). On day 1 of the experimental timeline, AAV9-Empty/AAV9-MR was injected (i.v.) in the animals at a concentration of 2×10^{12} viral particles per animal (injection volume: 100 µL). After 14 days of AAV injection, osmotic pumps (Alzet® model; ALZET LLC, Campbell, CA, USA) with either saline (0.9% NaCl) or aldosterone (concentration: 300 µg/kg/day) were implanted in mice with AAV9-Empty and AAV9-MR, respectively. Aldosterone was also dissolved in saline solution (0.9% NaCl) to ensure proper control. The pumps were explanted after another 14 days, i.e., 4 weeks from the start of the trial. As post-operative care during pump implantation and explantation, animals were given Novalgin via the drinking water (200 mg/kg) for the next three days. After another 14 days, i.e., 6 weeks from the start of the trial or endpoint of the experiment, echocardiographic data were recorded using the Vevo 2100 system (FUJIFILM VisualSonics Inc., Toronto, ON, Canada) before sacrificing the mice. Pressure volume measurements were obtained using a 1F microtip PV catheter (PVR 1045; Millar Instruments, Houston, TX, USA) coupled with a Powerlab/4Sacquisition system (AD instruments, Oxford, UK), maintaining the temperature at 37 °C. For performing various functional assays, hearts were harvested, frozen, and stored at −80 °C. Cardiac functions were analyzed from the echocardiographic data in M-mode and B-mode using VevoLab software (version 5.10.0, FUJIFILM VisualSonics Inc., Toronto, ON, Canada). To randomize and blind the animal study, an internal numbering system was incorporated by a blinded independent researcher. All research conditions and key design features were defined in advance and documented in the approved animal experimental application.

2.2. Human Tissue Samples

Heart-failure or healthy control cardiac tissue was collected as previously described [20]. This research was conducted with the endorsement of the institutional ethics committees at the Medical College of Wisconsin in Milwaukee, WI, USA, and the Hannover Medical School in Germany.

2.3. Cell Culture

For neonatal rat cardiomyocytes, 1- to 3-day-old rats were sacrificed, and cardiomyocytes were isolated from the explanted hearts following a previously described protocol [21]. For AAV virus production, HEK293T cells were cultured in DMEM (Dulbecco's Modified Eagle Medium; Gibco, Thermo Fisher Scientific, Waltham, MA, USA) with 4.5 g/L D-Glucose, L-Glutamine, 10% FCS, and 1% penicillin/streptomycin. Aldosterone (Sigma-Aldrich, St. Louis, MO, USA) treatment was conducted for 24 h at a concentration of 1 µM unless stated otherwise. The inhibition of *Ptgds* was obtained using siRNA #mm.si.Ptgds.13.1 (Integrated DNA Technologies, Inc., Coralville, IA, USA) transfection at a concentration of 100 nM using Lipofectamine 2000 (Life Technologies, Thermo Fisher Scientific, Waltham, MA, USA) in OptiMEM medium (Gibco, Thermo Fisher Scientific, Waltham, MA, USA).

2.4. RNA and Real-Time PCR

RNA isolation for cell culture samples and tissue samples (from mice) was performed using TriFast (peqGOLD; VWR chemicals, Avantor Inc., Radnor, PA, USA) following the manufacturer's protocol. The RNA concentration and quality were checked using Multi-Mode Reader Synergy HT (Biotek, Agilent Technologies, Santa Clara, CA, USA), Take

3 session, and Gen5 software (version: 1 November 2005, Biotek). Thereafter, reverse transcription of the isolated RNA (200 ng–1000 ng) was performed using a Biozym cDNA Synthesis Kit (Biozym Scientific GmbH, Hessisch Oldendorf, Germany, Cat. No. 331470) with Oligo dT primers following the manufacturer's instructions. For quantitative measurement, real-time PCR was performed using SYBR-Green mix (iQ™ SYBR® Green Supermix; Bio-Rad Laboratories, Inc., Hercules, CA, USA; Cat. No. 170-8882) with gene-specific primers (Supplemental Table S2) in an Applied Biosystems ViiA7 instrument (Thermo Fisher Scientific, Waltham, MA, USA).

2.5. Western Blotting

Cell lysis buffer (1×) (Cell Signaling Technology, Danvers, MA, USA) along with Pefabloc (Sigma-Aldrich) was used to lyse the cell pellet. Protein quantification was performed using Bradford reagent (Bio-Rad Laboratories). For resolving the proteins, 25 µg of protein per sample was loaded onto SDS polyacrylamide gel along with Precision Plus Protein WesternC standard (Bio-Rad Laboratories). Furthermore, blots were prepared by transferring the proteins from SDS polyacrylamide gel to polyvinylidene fluoride membrane in a Mini PROTEAN Tetra cell (Bio-Rad Laboratories). The following primary antibodies were used to detect the proteins of interest: MR (Abcam; ab2774) and GAPDH (Abcam, Cambridge, UK; ab8245). Secondary antibody conjugated with HRP (anti-mouse IgG, HRP-linked antibody #7076; Cell Signaling Technology) was used for detection of bands.

2.6. Adeno-Associated Virus Preparation

MR sequence was obtained from Ensembl Genome browser and was cloned into the pAAV vector using SalI and HindIII (Thermo Fischer Scientific, Waltham, MA, USA). For AAV9 and AAV6 virus production, a previously described protocol was used [22]. To produce AAV9 and AAV6, the pDP9rs or pDP6rs serotype helper plasmids were used, respectively.

2.7. RNA-Sequencing and Raw Data Processing

RNA was isolated as described above from n = 3 heart tissue samples for AAV9-Empty-Control and AAV9-MR-Aldo mice. The RNA quality was analyzed by using the Bioanalyzer System (Agilent Technologies, Santa Clara, CA, USA) in terms of RNA integrity number (RIN). An Illumina NextSeq 550 sequencer was used to perform the sequencing run at Research Core Unit Genomics (RCUG) of Hannover Medical School.

At first, 500 ng of total RNA per sample was utilized as an input for an rRNA depletion procedure with a 'NEBNext® rRNA Depletion Kit (Human/Mouse/Rat), 96 rxns' (E6310X; New England Biolabs, Ipswich, MA, USA), followed by stranded cDNA library generation using a 'NEBNext® Ultra II Directional RNA Library Prep Kit for Illumina' (E7760L; New England Biolabs, Ipswich, MA, USA). All steps were performed as recommended in user manual E7760 (Version 1.0_02-2017; NEB), except that all reactions were downscaled to 2/3 of the initial volumes. Furthermore, one additional purification step was introduced at the end of the standard procedure, using 1× 'Agencourt® AMPure® XP Beads' (#A63881; Beckman Coulter, Inc., Brea, CA, USA). cDNA libraries were barcoded by a single indexing approach, using 'NEBNext Multiplex Oligos for Illumina—Set 1' (Index Primer 2, 4, 5, 6, 7, 12). All generated cDNA libraries were amplified with 9 cycles of final PCR. Fragment length distribution of individual libraries was monitored using a 'Bioanalyzer High-Sensitivity DNA Assay' (5067-4626; Agilent Technologies). Quantification of libraries was performed by use of the 'Qubit® dsDNA HS Assay Kit' (Q32854; Thermo Fisher Scientific).

Equal molar amounts of six libraries in total were pooled for a common sequencing run. Accordingly, each analyzed library constitutes 16.6% of the overall flowcell capacity. The combined library pool was denatured with NaOH and was finally diluted to 1.5 pM

according to the Denature and Dilute Libraries Guide (Document #15048776 v02; Illumina). An amount of 1.3 mL of denatured pool was loaded on an Illumina NextSeq 550 sequencer using a High-Output Flowcell for 75bp paired-end reads (#20024907; Illumina Inc., San Diego, CA, USA). The obtained BCL files were converted to FASTQ files using bcl2fastq Conversion Software version v2.20.0.422 (Illumina).

The FASTQ files were adapter- and quality-trimmed using Trim Galore! (version 0.4.1) with default settings as described in the User Guide except for the setting of the quality cutoff (-q/–quality) which was set to a Phred score of 15. Trim Galore! used Cutadapt (version 1.9.1) as subroutine. Quality control of FASTQ files was performed by FastQC (version 0.11.4) before and after trimming.

After trimming, FASTQ files were mapped against a reference genome with the splice-aware aligner STAR (version 2.5.4a) to generate BAM files. The BAM files were built in a 2-pass mapping (two-pass Mode Basic) and were finally sorted (out SAM type BAM SortedByCoordinate). All other settings were left as default as described in the manual. The genome index files were created by STAR with default settings using *Mus musculus* sequence and annotation data taken from GENCODE.org (GRCm38.p6 release M17).

Quantification was performed with feature counts from the subread package (version 1.6.1) for paired-end reads (-p) with default settings except for the setting of strandedness (-s 2) and the minimum mapping quality score (-Q 10). Annotation data were again taken from GENCODE.org (GRCm38.p6 release M17). Normalization and differential expression analysis was performed with DESeq2 (Galaxy Tool Version 2.11.40.2) with default settings except for "Output normalized counts table", which was set to "Yes".

Differentially expressed genes (DEGs) with base mean values > 5 and an adjusted p-value < 0.05 were selected for further analysis (Supplemental Table S1). The heat map was generated using the ClustVis online tool [23].

2.8. Immunostaining

In order to stain the neonatal rat cardiomyocytes for cell size measurement, 4% paraformaldehyde was used to fix the cells for 10 min followed by permeabilization with 0.1% Triton-X-100 for another 10 min. Blocking was performed in 5% donkey serum for 30 min prior to overnight incubation with primary antibody, namely monoclonal Anti-α-Actinin (Sarcomeric) (A7811; Sigma-Aldrich) at a dilution of 1:500 in 5% donkey serum. Then, cells were incubated with the secondary antibody Anti-Mouse-Alexa 594 (Invitrogen, Waltham, MA, USA) and DAPI for 1 h. In between each step, the cells were washed with DPBS (Gibco) 3 times. Finally, fluorescence microscopy (Nikon Eclipse Ti microscope, Minato (Tokio), Japan) was used to acquire images which were further analyzed with NIS Elements (Nikon) BR imaging software (version 3.22.00).

2.9. Immunohistochemistry

For heart tissue from in vivo mice experiments, 5 µm paraffin-embedded heart sections were prepared with a Leica microtome. An additional step of dewaxing and antigen retrieval was performed in freshly prepared citrate buffer (pH 6.0) at a temperature of 96–98 °C for 20 min in case of wheat germ agglutinin (WGA, Invitrogen, Thermo Fisher Scientific, Waltham, MA, USA) staining for cardiomyocyte cell size measurement. Sections were then brought to room temperature and then washed with PBS. After fixation and permeabilization, the sections were stained with Alexa Fluor 488-labeled WGA and DAPI. A Nikon Eclipse Ti microscope was used to obtain images at 20× magnification, which were further analyzed using NIS Elements (version 3.22.00, Nikon, Minato (Tokio), Japan) BR imaging software.

To analyze the fibrosis in heart tissues, Picro-Sirius red staining was performed on paraffin-embedded heart sections. The images were acquired using a Nikon Eclipse Ci microscope with a 2× magnification. Sirius red dye stained the collagen content on the heart section which was then quantified as a percentage of total area of each heart section by using Adobe Photoshop CC2018.

2.10. Cell Size Measurement

After immunostaining of NRCMs, images were acquired spanning different areas of respective wells (10–11 images per well). An area of approximately 200 cardiomyocytes was measured using NIS Elements software, and the average value was calculated. The area was normalized to control the samples.

Similarly, for paraffin-embedded heart sections, the images were obtained from 5–6 different regions of the heart. An area of more than 250 cardiomyocytes was measured and averaged per animal. The area was normalized to control the samples.

2.11. Statistics

In this study, the experiments were performed 3 or more times as independent biological replicates with three technical replicates in each experiment. We analyzed the data using Prism 7 (Graph Pad) software (version 7.05) and represented it as mean ± SEM throughout the study. An unpaired two-tailed Student's *t*-test was used for calculating the significance amongst two groups while a one-way ANOVA with Tukey's post hoc test was performed for more than two groups. We considered a p-value < 0.05 as statistically significant in the present study.

3. Results

3.1. Aldo–MR Pathway Activation Showed Pathological Phenotype in Mice

To understand the impact of an activated Aldo–MR pathway on cardiac physiology, an Adeno-associated virus-9 (AAV9)-based MR overexpression mouse model was generated along with Aldo treatment using osmotic pumps (Figure 1A). The AAV9 serotype of the AAVs possesses a natural tropism for cardiomyocytes in vivo which makes it a suitable serotype under the given experimental conditions. We observed a significant overexpression of MR in mice treated with AAV9-MR as compared to the AAV9-Empty group as analyzed by RT-PCR (Figure 1B). The overexpression was further confirmed at the protein level by immunohistochemistry staining of the cryo-sections from mouse hearts with AAV9-MR-Aldo or AAV9-Empty-Control treatment using Anti-MR antibodies (Figure 1C). Activation of the Aldo–MR pathway was analyzed by the mRNA expression levels of *Lcn2* (NGAL) and *Lgals3* (Gal3) which are well-established downstream effector molecules of an activated Aldo–MR pathway. Confirming the pathway activation, an increase in both the effector molecules was observed (Figure 1B). Echocardiographic analysis of the two experimental groups showed that the Aldo–MR pathway activation caused a decline in cardiac function as observed by a decrease in left ventricular ejection fraction and an increased end-systolic volume (Figure 1D,E; no significant difference in body weight development was observed between the two groups as depicted in Figure S3). Consistently, we detected thickening of the left ventricular anterior wall, along with a significant increase in left ventricular mass upon AAV9-MR-Aldo treatment (Figure S4; Representative echocardiographic M-mode images are shown in Figure S5). However, no signs of diastolic dysfunction were observed at this stage as the IVRT and E/e′ ratio did not differ between the groups (Figure S6).

Furthermore, the mRNA expression levels of myosin heavy chain (MHC) proteins alpha (α) and beta (β) were analyzed by RT-PCR, as a shift in the ratio of these MHC

proteins in favor of β-MHC indicates cardiac remodeling. Interestingly, a higher ratio of β-MHC/α-MHC in Aldo-MR overactivation animals as compared to the control animals was observed, indicating the onset of cardiac remodeling (Figure 1F). Since cardiac hypertrophy and fibrosis are major factors contributing towards maladaptive cardiac functioning, WGA and Picro-Sirius red stainings were performed in paraffin sections of the mouse hearts to measure cell size and fibrosis, respectively, in the two animal groups. In line with our previous results, a significant increase in both cell size and fibrosis was observed in animals with Aldo-MR overactivation compared to those in the control group (Figure 1G–J). Thus, our findings suggest that Aldo–MR pathway activation can trigger a diseased cardiac phenotype.

3.2. Novel Players Involved in the Aldo–MR-Pathway-Mediated Cardiac Pathology

Since a diseased cardiac phenotype was observed in mice with Aldo–MR pathway activation, we aimed to identify novel players driving the pathological signaling mechanism of the Aldo–MR pathway. Therefore, we performed a global RNA sequencing in heart tissue samples from mice transduced either with AAV9-MR or AAV9-Empty, which were further treated with aldosterone or saline (control), respectively (three mice per group). Differentially expressed genes (DEGs) were filtered out by setting a base mean threshold of five, and genes which were significantly (adjusted *p*-value of <0.05) up- or down-regulated in the Aldo–MR-activated group compared to those in the control group were selected (Figure 2A). In total, 125 genes were up-regulated while 67 genes were down-regulated in the MR-overexpression mouse model with Aldo treatment as compared to those of the control animals (Supplementary Table S1). The heat map generated using ClustVis [23] shows the DEGs among the two groups indicating that Aldo–MR pathway activation significantly changes the transcriptome of cardiac tissue from mice (Figure 2B). A volcano plot is shown in Figure 2C, with significantly DEGs indicated above the horizontal line ($-\log_{10}$ of an adjusted *p*-value of 0.05). Additionally, gene set enrichment analysis (GSEA) was performed with Enrichr [24–26] using the 192 significantly DEGs as the input. Ranked by *p*-value, the top ten enriched biological processes are mostly related to tumor necrosis factor production, inflammatory processes, as well as lipid storage and oxidation (Figure 2D). To shortlist top candidate genes from all DEGs, we performed a literature review to identify possible mediators of the biological processes indicated by GSEA but also of the cardiac pathology observed in our animal model. This approach yielded a list of 17 candidate genes (*Angpl4*, *Amy1*, *Ptgds*, *Itgb2*, *Ucp3*, *Cd37*, *ItgaI*, *Ikzf3*, *RasaI3*, *Cd52*, *Thbs1*, *Mthfd2*, *Itgb7*, *Grap2*, *Pdh4*, *Hpse*, *Chrna2*) that are highlighted in red in the volcano plot (Figure 2C).

To confirm the global sequencing results, these 17 top candidates were validated in independent heart tissue samples by RT-PCR from AAV9-MR-Aldo and AAV9-Empty-Control mice. The expression levels of seven genes were validated to be significantly up- or down-regulated in the complete sample set of the MR-overexpression animal study. We observed a significant increase in the mRNA expression of *Ptgds*, *ItgaI*, *Mthfd2*, *Itgb2*, *RasaI3*, and *Itgb7*, whereas *Angpl4* expression displayed a significant decrease in mice with Aldo–MR-overexpression as compared to control mice (Figure 2E). These genes were selected for further investigations in our in vitro system.

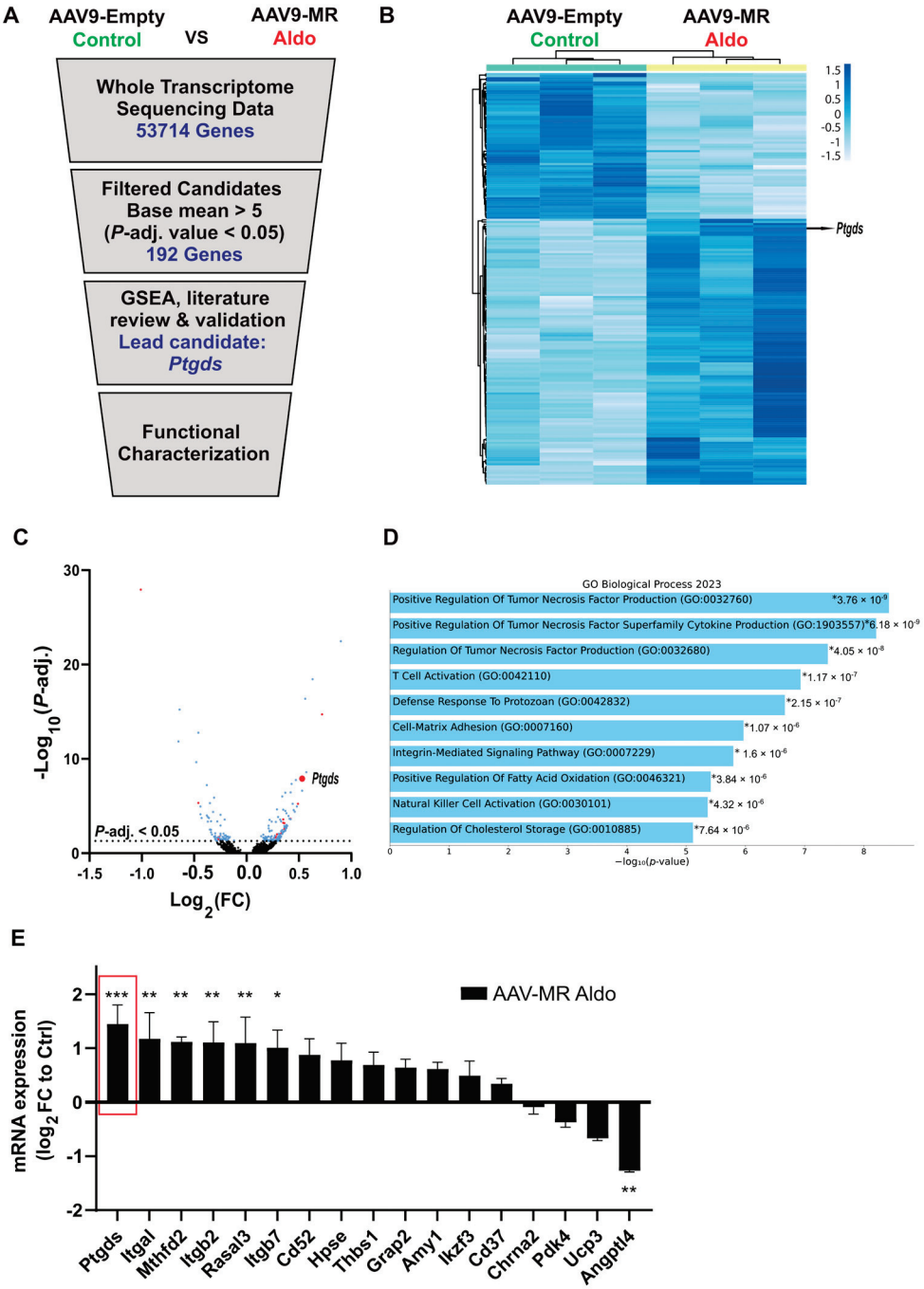


Figure 2. Identification of novel players involved in the Aldo–MR pathway. (**A**) Pipeline used to filter candidates involved in the Aldo–MR pathway using global RNA sequencing of the AAV9-mediated MR-overexpression mice with aldosterone treatment compared to control mice. (**B**) Heat map of 192 significantly differentially regulated genes obtained from the global RNA sequencing with *Ptgds* highlighted in the heat map. Rows are centered and unit variance scaling is applied. Correlation distance and average linkage are used for clustering of both rows and columns. (**C**) Volcano plot showing the significantly up- and down-regulated genes in blue (adjusted p-value < 0.05) with the shortlisted candidates highlighted in red. Lead candidate *Ptgds* is labelled and indicated by a larger red point. (**D**) Enriched GO biological processes analyzed using Enrichr. Ranked according to p-value. (**E**) mRNA expression of various shortlisted genes in heart tissues from the complete sample set of mice treated with AAV9-Empty-Control and AAV9-MR-Aldosterone as measured by RT-PCR. Gene expression was calculated relative to the housekeeper gene *Gapdh* and normalized to the AAV9-Empty-Control group (n = 5–6 animals per group). All data are represented as mean ± SEM. * $p \leq 0.05$, ** $p \leq 0.01$, *** $p \leq 0.001$.

3.3. Ptgds Participates in Aldo–MR-Mediated Cardiac Hypertrophy

To better understand the mechanism of action in the Aldo–MR pathway, we incorporated an in vitro system that mimics our Aldo–MR over-activation mouse model. In contrast to cell lines, normal cell morphology and function observed in vivo are preserved in primary cells. Therefore, we used neonatal rat cardiomyocytes (NRCMs) which provide an excellent in vitro system for the characterization of functional and molecular mechanisms in the heart. An AAV6-mediated MR-overexpression was performed in NRCMs to investigate mechanistic involvement of the identified top candidates. The schematic plasmid map of pAAV-MR used to achieve the overexpression of MR both in vitro and in vivo is shown in Supplementary Figure S1. NRCMs were transduced with AAV6-MR or AAV6-Empty with MOIs = 5×10^4 for 48 h and were further treated with 1 μM Aldo or ethanol as control for 24 h, and the mRNA expression of various candidate genes was measured via RT-PCR. Robust MR overexpression in NRCMs was validated by RT-PCR, immunofluorescence, and Western blotting (Figure 3A−C).

Similar to our previous results in vivo, the expression of *Ptgds* was highly increased in NRCMs with AAV6-mediated MR-overexpression which increased further by Aldo treatment (Figure 3D). Interestingly, 1 μM Aldo treatment alone did not increase the expression of *Ptgds* in the AAV6-Empty control group. Among the other genes that could be detected in the in vitro model, only *Angptl4* showed a similar trend as observed in the animal study where the transduction of AAV6-MR led to a significant reduction in expression, while the treatment with Aldo further reduced the *Angptl4* expression compared to that of the control (Figure 3D).

In line with our findings, *Ptgds* was previously identified as a direct downstream target of MR in adipocytes [27]; however, the specific role of *Ptgds* in the context of the Aldo–MR pathway in cardiomyocytes is still unknown. *Angptl4* also showed promising potential as it has an inverse correlation with MR overexpression which makes it an ideal candidate for *Angptl4*-overexpression-based therapies. However, a literature survey of *Angptl4* was contradictory, showing a positive association with cardiac diseases rather than having cardio-protective effects. For example, increased levels of *Angptl4* were observed in cardiometabolic disorders including atherosclerosis and type 2 diabetes while a loss of function genetic variant of *AngptI4* reduced the risk for coronary artery disease. Therefore, we selected *Ptgds* for further investigation in the in vitro system.

3.4. Ptgds Is Involved in Cardiac Pathologies

Since *Ptgds* expression levels were up-regulated upon Aldo–MR pathway activation, we hypothesized that its inhibition might reverse the cardiac disease phenotype. Hence, we performed an siRNA-mediated *Ptgds* inhibition in NRCMs. Three different siRNAs against *Ptgds* (siPtgds13.1, 13.2, 13.3) were tested for their inhibition efficacy of *Ptgds* as compared to a siRNA-negative control (siCtrl) by RT-PCR (Supplementary Figure S2). SiRNA13.1 was selected for future experiments owing to its high inhibition efficiency for *Ptgds*.

The expression of *Lcn2* (NGAL) was measured as a marker for MR pathway activation. After si-Ptgds transfection, the expression of NGAL was significantly decreased in comparison to the si-Control treated cells. Importantly, si-*Ptgds* treatment rescued the levels of NGAL expression also after Aldo treatment (Figure 4A), showing the effect of *Ptgds* inhibition on the Aldo–MR pathway.

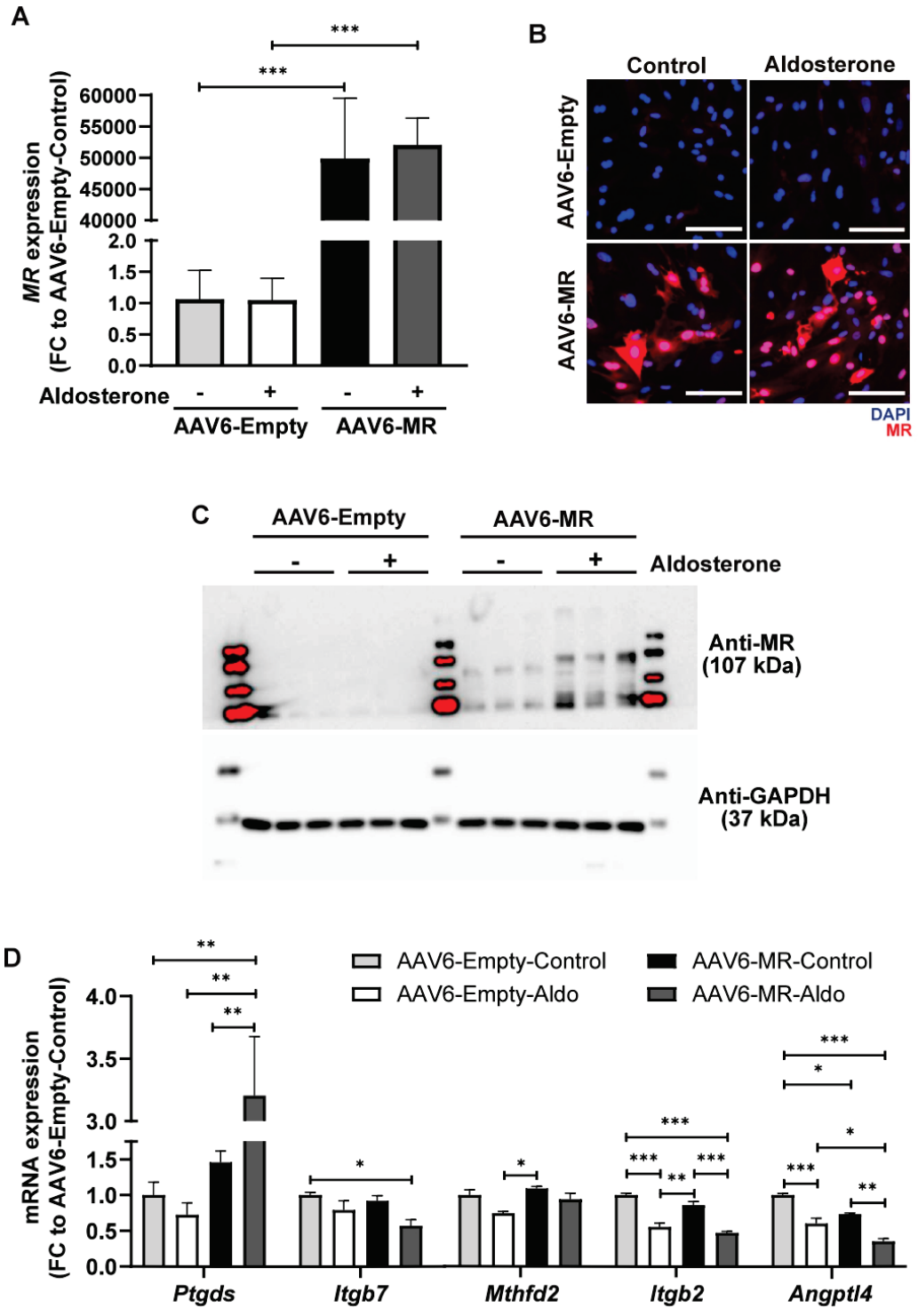


Figure 3. Target validation in NRCMs with AAV6-mediated MR-overexpression and Aldo treatment. (**A**) mRNA expression analysis of MR in NRCMs transduced with AAV6-MR or AAV6-Empty in the presence of Aldo (1 µM) or ethanol control. Gene expression was calculated relative to housekeeper gene *Gapdh* and normalized to the AAV9-Empty control without Aldo treatment. (**B**,**C**) Fluorescent images (**B**) of AAV6-mediated MR-overexpression in NRCMs (MR (red) and DAPI (blue)) and Western blots incubated with Anti-MR and Anti-GAPDH antibodies (**C**) of lysates from NRCMs after transduction with AAV6-Empty or AAV6-MR in the presence of Aldo (1 µM) or ethanol control. (**D**) mRNA expression of the detectable top candidate genes as measured in NRCMs transduced with AAV6-MR or AAV6-Empty in the presence of Aldo (1 µM) or ethanol via RT-PCR. Gene expression was calculated relative to housekeeper *Gapdh* and normalized to AAV6-Empty-Control. Scale bar indicates 100 µm. All data are represented as mean ± SEM. $n = 3$, * $p \leq 0.05$, ** $p \leq 0.01$, *** $p \leq 0.001$.

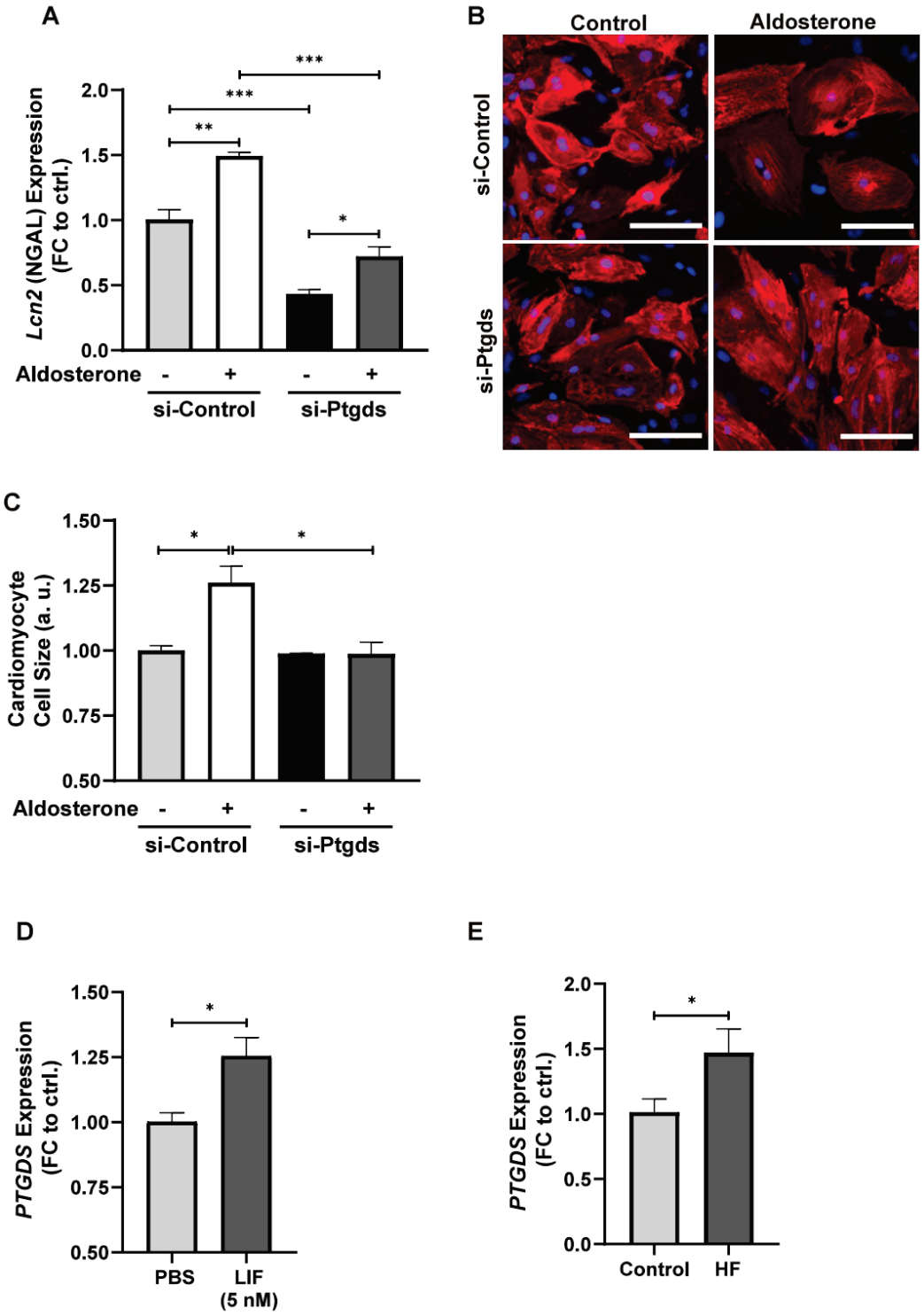


Figure 4. *Ptgds* involved in cardiac pathologies. (**A**) *Lcn2* (NGAL) mRNA expression after transfection of NRCMs with siPtgds or siCtrl at a concentration of 100 nM and ethanol/Aldo treatment (0.1 μM) as measured by RT-PCR. (**B**,**C**) Fluorescent images (**B**) obtained after α-actinin (red) and DAPI (blue) immunostaining of NRCMs and cardiomyocyte cell size measurement (**C**) after siPtgds or siCtrl transfection (100 nM) and ethanol/Aldo treatment (0.1 μM) (n = 2). (**D**,**E**) mRNA expression of *PTGDS* after the treatment with 5 nM LIF or control (PBS) in hiPSC-CMs (n = 3) (**D**) and in heart tissue samples from patients with end-stage heart failure and controls (n = 22/12) (**E**) as measured by RT-PCR. All data are represented as mean ± SEM. * $p \leq 0.05$, ** $p \leq 0.01$, *** $p \leq 0.001$. Scale bar indicates 100 μm. a.u., arbitrary units.

Since Aldo–MR activation leads to a hypertrophic phenotype, as observed in our animal study, we analyzed if *Ptgds* inhibition could reverse this effect. Interestingly, there was no significant change in cell size under control conditions without Aldo stimulation and *Ptgds* inhibition. However, under Aldo treatment, the hypertrophic effect was significantly reversed by the inhibition of *Ptgds* indicating that *Ptgds* specifically alters Aldo induced hypertrophy and did not have apparent effects under physiological conditions (Figure 4B,C). These results suggest the involvement of *Ptgds* in the hypertrophic effects of the Aldo–MR pathway.

For further validation, the expression of *PTGDS* was measured in human-induced pluripotent stem cell (iPSC)-derived cardiomyocytes (hiPSC-CM) after treatment with 5 nM LIF or PBS as control via RT-PCR. LIF (leukemia inhibitory factor) is a pleiotropic cytokine that is known to induce cardiomyocyte hypertrophy [28]. *PTGDS* expression was significantly increased in hiPSCs-CMs after LIF treatment as compared to that of the control (Figure 4D), corroborating the notion that *PTGDS* is involved in the development of cardiac hypertrophy even in human-based models, suggesting translational importance of *PTGDS* as a therapeutic target in Aldo–MR-derived cardiac remodeling.

Furthermore, the expression of *PTGDS* was measured in heart tissue samples from patients with end-stage heart failure compared to control patients. Consolidating our previous results, we observed a significant increase in the expression of *PTGDS* in patients with end stage heart failure as compared to controls. Thus, *PTGDS* shows high potential to be developed as a therapeutic target against Aldo–MR-mediated cardiac pathologies.

4. Discussion

An over-activated Aldo–MR pathway has been associated with cardiovascular conditions such as hypertension, myocardial infarction, and subsequent heart failure [2]. Therefore, we aimed to identify novel molecular targets and to characterize their potential for interference with pathological Aldo–MR signaling.

Using an AAV9-mediated MR overexpression system activated with Aldo-infused pumps, a diseased cardiac phenotype consisting of cellular hypertrophy, fibrosis, and deteriorated cardiac functions was observed showing that an abnormally activated Aldo–MR pathway has severe detrimental impacts on cardiac health. In line with our observations, a study using cardiac-specific hMR overexpression identified a critical coronary endothelial dysfunction [29] while another study associated it with ventricular arrhythmias which was prevented by an MR antagonist [30]. Although the AAV9 serotype is considered the gold standard for in vivo cardiac transgene delivery in mice [31], a high expression of transgenes is observed in the liver, lungs, and kidneys [32]. Therefore, caution is warranted, as a contribution of extra-cardiac MR to the disease phenotype cannot be ruled out. Thus, cardiac-specific promoters such as α-MHC or cTnT in place of the CMV promoter would reduce the extra-cardiac MR overexpression aiding the investigation of cardiac-specific effects. Moreover, despite not being the primary focus of the present study, follow-up investigations might also want to evaluate the effects of MR overexpression with Aldo stimulation on the blood pressure of mice.

Global RNA sequencing of heart tissue samples from our animal model identified *Ptgds* as a key player in the Aldo–MR pathway, which was found to be up-regulated with over-activation of the Aldo–MR pathway in cardiomyocytes. Urbanet et al. previously identified PTGDS as a downstream target of MR in adipocytes [27], which is consistent with our findings in cardiac settings. We further confirmed its role in Aldo-mediated hypertrophy where *Ptgds* inhibition reduced the hypertrophic effect of Aldo on NRCMs. The inhibition of *Ptgds* also decreased the levels of *Lcn2* (NGAL), suggesting its involvement in NGAL-mediated cardiac pathologies. Even though the association between *Ptgds*- and

Aldo–MR-related cardiac diseases has not been explored much, its expression is elevated in myocardial infarction [33] and it is advocated as a biomarker for cardiovascular risk prediction due to its association with heart failure and acute coronary syndrome [34]. Interestingly, we also observed an increase in *PTGDS* in hiPSC-CMs treated with LIF, a pro-hypertrophic compound [28], as well as in patients with end-stage heart failure. These results consolidate the importance of *Ptgds* as a pivotal factor in cardiovascular pathologies. Additionally, GSEA revealed that the overactivation of the Aldo–MR pathway in the present mouse experiments led to the enrichment of genes associated with biological processes related to the activation of the immune system and the production of tumor necrosis factor (TNF) and TNF superfamily cytokines. Interestingly, a potential link between these biological processes and the observed general cardiac pathologies, such as cardiomyocyte hypertrophy and cardiac fibrosis, might be found in our lead candidate gene, *Ptgds*. Specifically, the gene *Ptgds* encodes for prostaglandin D synthase, responsible for synthesizing one of many bioactive prostanoid lipids termed prostaglandin D2 (PGD2) [35]. The connection between prostanoids and inflammation [36,37], including TNF synthesis and signaling [38–40] is well established in the literature. Depending on the cell type and receptor PGD2 in particular acts upon, it exhibits both pro- and anti-inflammatory effects. In the heart specifically, both beneficial and detrimental effects are associated with PGD2 [41]. Adding to the complexity, Fitzpatrick et al. demonstrated the rapid conversion of PGD2 into active metabolites [42]. One such metabolite is Prostaglandin F 2 alpha (PGF2α) that can be produced by prostaglandin F synthase from PGD2 [43]. Notably, PGF2α is known to induce cardiomyocyte hypertrophy in vitro [44], and stimulation of the PGF2α receptor (FP) in vivo leads to hypertrophic hearts. Moreover, in cardiac fibroblasts, PGF2α is a contributor to myocardial fibrosis by stimulating collagen deposition [45]. Future studies should focus on evaluating whether direct targeting of *Ptgds* or, perhaps, a more specific pharmacological intervention, such as FP receptor inhibition, could prove to be a valid therapeutic strategy in the context of Aldo–MR-pathway-related cardiac pathologies. Encouragingly, a study of FP receptor gene silencing suggested that it can ameliorate diabetic cardiomyopathy and myocardial fibrosis [46], making it a promising avenue for further studies.

This study has some limitations. First, the experimental design did not include additional control groups such as AAV9-Empty-Aldo and AAV9-MR-Control, which restricts certain comparisons. Second, blood pressure was not directly assessed, limiting our ability to link structural and functional changes to hemodynamic alterations. Instead, we invasively determined the maximum left ventricular pressure (P_{max}; Figure S6). However, this is a contractility-related parameter and not a proxy for systolic pressure. Although not the primary focus of the present study, future investigations should also evaluate the impact of MR overexpression combined with Aldo stimulation on blood pressure to better understand its contribution to cardiac remodeling. Finally, mechanistic insights into the regulation of PTGDS expression were beyond the scope of present study, which should be addressed in future studies.

Given the demonstrated involvement of *Ptgds* in regulating glucose transport, insulin resistance, and glucose intolerance under diabetic conditions [47], it is pertinent to further explore these metabolic effects of *Ptgds* with regards to the Aldo–MR pathway and cardiac remodeling. Moreover, an AAV-mediated *Ptgds* overexpression study in combination with a detailed investigation of its effects on prostanoid levels would be useful in broadening our understanding of its effects on cardiac health and identifying novel effector molecules of this pathway.

5. Conclusions

Our findings demonstrate that sustained activation of the MR–Aldo pathway drives adverse cardiac remodeling, characterized by fibrosis, hypertrophy, and impaired function, validating AAV9-MR-Aldo as a relevant mouse model. Transcriptomic profiling identified *Ptgds* as a candidate mediator of this process, and functional experiments showed that silencing *Ptgds* reversed hypertrophy in vitro. Importantly, elevated *PTGDS* expression was also observed in human iPSC-derived cardiomyocytes and in patients with end-stage heart failure, underscoring its translational relevance. Future studies should clarify the mechanisms regulating PTGDS expression and its metabolic consequences, which may open new therapeutic avenues in heart failure.

Supplementary Materials: The following supporting information can be downloaded at: https://www.mdpi.com/article/148510.3390/cells14191485/s1, Figure S1: Vector map of pAAV-CMV-MR; Figure S2: Analyzing *Ptgds* expression after its siRNA-mediated inhibition. Figure S3: Change in body weight over the course of the experiment; Figure S4: Left ventricular parameters point towards cardiac remodeling; Figure S5: Representative echocardiographic M-mode images; Figure S6: Parameters of hemodynamic and diastolic function; Table S1: List of differentially expressed genes; Table S2: Gene-specific primers for qPCR.

Author Contributions: Conceptualization, A.G., S.K.G. and T.T.; formal analysis, A.G., M.J., C.N.B. and S.B.; funding acquisition, C.B. and T.T.; investigation, A.G. and J.L.; methodology, A.G.; resources, C.B. and T.T.; supervision, C.B., S.K.G. and T.T.; validation, S.B. and J.L.; visualization, A.G. and M.J.; writing—original draft, A.G. and M.J.; writing—review and editing, M.J., C.N.B. and C.B. All authors have read and agreed to the published version of the manuscript.

Funding: This study received financial aid from Deutsche Forschungsgemeinschaft (DFG, SFB Transregio TRR-267, to TT and CB).

Institutional Review Board Statement: The experiments involving human tissue were conducted in accordance with the Declaration of Helsinki and approved by the Institutional Review Board of the Medical College of Wisconsin, Milwaukee, WI, USA, and the Hannover Medical School Ethikkommission, Hannover, Germany (No. 2997-2016, on 25 June 2016). The animal study was performed with the consent of Hannover Medical School and Niedersachsen Landesamt für Verbraucherschutz (No. 15/1915; approved: 23 September 2015) in accordance with the issued directives.

Informed Consent Statement: Informed consent was obtained from all subjects involved in the study.

Data Availability Statement: RNA-sequencing data will be made publicly available via the GEO database under the accession number GSE308485, or following this link: https://www.ncbi.nlm.nih.gov/geo/query/acc.cgi?acc=GSE308485 (accessed on 14 September 2025).

Acknowledgments: We extend our gratitude to Karina Zimmer and Janet Remke for their help in the animal study. Sequencing data used in this publication were generated by the Research Core Unit Genomics (RCUG) at Hannover Medical School. We heartily thank Ke Xiao for her valuable advice and guidance on bioinformatic data analysis. We also acknowledge the technical support of Kristian Scherf and Annette Just during the study. We thank the Department of Medicine, the Cardiovascular Center, and the Department of Physiology at the Medical College of Wisconsin (Milwaukee, Milwaukee, WI, USA) for providing human heart tissue control samples used in this study under institutional IRB approval and a material transfer agreement.

Conflicts of Interest: TT is founder and CSO/CMO of Cardior Pharmaceuticals, a fully owned subsidiary of Novo Nordisk A/S Europe (outside of this manuscript). TT and CB are named inventors on patents related to RNA-based therapies, which have been licensed; however, these are not connected to the current work. The other authors declare no conflicts of interest.

Abbreviations

The following abbreviations are used in this manuscript:

AAV	Adeno-associated virus
CVD	Cardiovascular disease
DEGs	Differentially expressed genes
FP	Prostaglandin F2 alpha receptor
GSEA	Gene set enrichment analysis
hiPSC-CMs	Human-induced pluripotent stem cell-derived cardiomyocytes
LIF	Leukemia inhibitory factor
MI	Myocardial infarction
MR	Mineralocorticoid receptor
PGD2	Prostaglandin D2
PGF2α	Prostaglandin F2 alpha
Ptgds	Prostaglandin D2 synthase
siRNA	Small interfering ribonucleic acid
TNF	Tumor necrosis factor

References

1. Virani, S.S.; Alonso, A.; Benjamin, E.J.; Bittencourt, M.S.; Callaway, C.W.; Carson, A.P.; Chamberlain, A.M.; Chang, A.R.; Cheng, S.; Delling, F.N.; et al. Heart Disease and Stroke Statistics—2020 Update a Report from the American Heart Association. *Circulation* **2020**, *141*, 139–596. [CrossRef]
2. Buonafine, M.; Bonnard, B.; Jaisser, F. Mineralocorticoid Receptor and Cardiovascular Disease. *Am. J. Hypertens.* **2018**, *31*, 1165–1174. [CrossRef]
3. Rossier, B.C.; Staub, O.; Hummler, E. Genetic Dissection of Sodium and Potassium Transport along the Aldosterone-Sensitive Distal Nephron: Importance in the Control of Blood Pressure and Hypertension. *FEBS Lett.* **2013**, *587*, 1929–1941. [CrossRef]
4. Patel, S.; Rauf, A.; Khan, H.; Abu-Izneid, T. Renin-Angiotensin-Aldosterone (RAAS): The Ubiquitous System for Homeostasis and Pathologies. *Biomed. Pharmacother.* **2017**, *94*, 317–325. [CrossRef] [PubMed]
5. Brilla, C.G.; Weber, K.T. Mineralocorticoid Excess, Dietary Sodium, and Myocardial Fibrosis. *J. Lab. Clin. Med.* **1992**, *120*, 893–901. [PubMed]
6. Fraccarollo, D.; Thomas, S.; Scholz, C.J.; Hilfiker-Kleiner, D.; Galuppo, P.; Bauersachs, J. Macrophage Mineralocorticoid Receptor Is a Pleiotropic Modulator of Myocardial Infarct Healing. *Hypertension* **2019**, *73*, 102–111. [CrossRef]
7. Fraccarollo, D.; Berger, S.; Galuppo, P.; Kneitz, S.; Hein, L.; Schütz, G.; Frantz, S.; Ertl, G.; Bauersachs, J. Deletion of Cardiomyocyte Mineralocorticoid Receptor Ameliorates Adverse Remodeling after Myocardial Infarction. *Circulation* **2011**, *123*, 400–408. [CrossRef]
8. Hayashi, M.; Tsutamoto, T.; Wada, A.; Maeda, K.; Mabuchi, N.; Tsutsui, T.; Matsui, T.; Fujii, M.; Matsumoto, T.; Yamamoto, T.; et al. Relationship between Transcardiac Extraction of Aldosterone and Left Ventricular Remodeling in Patients with First Acute Myocardial Infarction: Extracting Aldosterone through the Heart Promotes Ventricular Remodeling after Acute Myocardial Infarction. *J. Am. Coll. Cardiol.* **2001**, *38*, 1375–1382. [CrossRef] [PubMed]
9. De Angelis, N.; Fiordaliso, F.; Latini, R.; Calvillo, L.; Funicello, M.; Gobbi, M.; Mennini, T.; Masson, S. Appraisal of the Role of Angiotensin II and Aldosterone in Ventricular Myocyte Apoptosis in Adult Normotensive Rat. *J. Mol. Cell Cardiol.* **2002**, *34*, 1655–1665. [CrossRef]
10. Zannad, F.; McMurray, J.J.V.; Krum, H.; van Veldhuisen, D.J.; Swedberg, K.; Shi, H.; Vincent, J.; Pocock, S.J.; Pitt, B. Eplerenone in Patients with Systolic Heart Failure and Mild Symptoms. *N. Engl. J. Med.* **2011**, *364*, 11–21. [CrossRef]
11. Pitt, B.; Remme, W.; Zannad, F.; Neaton, J.; Martinez, F.; Roniker, B.; Bittman, R.; Hurley, S.; Kleiman, J.; Gatlin, M. Eplerenone, a Selective Aldosterone Blocker, in Patients with Left Ventricular Dysfunction after Myocardial Infarction. *N. Engl. J. Med.* **2003**, *348*, 1309–1321. [CrossRef]
12. Pitt, B.; Williams, G.; Remme, W.; Martinez, F.; Lopez-Sendon, J.; Zannad, F.; Neaton, J.; Roniker, B.; Hurley, S.; Burns, D.; et al. The EPHESUS Trial: Eplerenone in Patients with Heart Failure Due to Systolic Dysfunction Complicating Acute Myocardial Infarction. Eplerenone Post-AMI Heart Failure Efficacy and Survival Study. *Cardiovasc. Drugs Ther.* **2001**, *15*, 79–87. [CrossRef]
13. Pitt, B.; Zannad, F.; Remme, W.J.; Cody, R.; Castaigne, A.; Perez, A.; Palensky, J.; Wittes, J. The Effect of Spironolactone on Morbidity and Mortality in Patients with Severe Heart Failure. *N. Engl. J. Med.* **1999**, *341*, 709–717. [CrossRef]

14. Tarjus, A.; Martínez-Martínez, E.; Amador, C.; Latouche, C.; El Moghrabi, S.; Berger, T.; Mak, T.W.; Fay, R.; Farman, N.; Rossignol, P.; et al. Neutrophil Gelatinase-Associated Lipocalin, a Novel Mineralocorticoid Biotarget, Mediates Vascular Profibrotic Effects of Mineralocorticoids. *Hypertension* **2015**, *66*, 158–166. [CrossRef] [PubMed]
15. Martínez-Martínez, E.; Buonafine, M.; Boukhalfa, I.; Ibarrola, J.; Fernández-Celis, A.; Kolkhof, P.; Rossignol, P.; Girerd, N.; Mulder, P.; López-Andrés, N.; et al. Aldosterone Target NGAL (Neutrophil Gelatinase-Associated Lipocalin) Is Involved in Cardiac Remodeling After Myocardial Infarction Through NFκB Pathway. *Hypertension* **2017**, *70*, 1148–1156. [CrossRef]
16. Bauersachs, J.; Fraccarollo, D. Mineralocorticoid Receptor-Dependent Adverse Remodeling After Myocardial Infarction Mediated by UNGALant Activation of NFκB. *Hypertension* **2017**, *70*, 1080–1081. [CrossRef] [PubMed]
17. Yang, B.; Fan, P.; Xu, A.; Lam, K.S.; Berger, T.; Mak, T.W.; Tse, H.-F.; Yue, J.W.; Song, E.; Vanhoutte, P.M.; et al. Improved Functional Recovery to I/R Injury in Hearts from Lipocalin-2 Deficiency Mice: Restoration of Mitochondrial Function and Phospholipids Remodeling. *Am. J. Transl. Res.* **2012**, *4*, 60.
18. Egido, J.; Zaragoza, C.; Gomez-Guerrero, C.; Martin-Ventura, J.L.; Blanco-Colio, L.; Lavin, B.; Mallavia, B.; Tarin, C.; Mas, S.; Ortiz, A. Animal Models of Cardiovascular Diseases. *J. Biomed. Biotechnol.* **2011**, *2011*, 1–13.
19. Qin, W.; Rudolph, A.E.; Bond, B.R.; Rocha, R.; Blomme, E.A.G.; Goellner, J.J.; Funder, J.W.; McMahon, E.G. Transgenic Model of Aldosterone-Driven Cardiac Hypertrophy and Heart Failure. *Circ. Res.* **2003**, *93*, 69–76. [CrossRef]
20. Viereck, J.; Bührke, A.; Foinquinos, A.; Chatterjee, S.; Kleeberger, J.A.; Xiao, K.; Janssen-Peters, H.; Batkai, S.; Ramanujam, D.; Kraft, T.; et al. Targeting Muscle-Enriched Long Non-Coding RNA H19 Reverses Pathological Cardiac Hypertrophy. *Eur. Heart J.* **2020**, *41*, 3462–3474. [CrossRef] [PubMed]
21. Gupta, S.K.; Foinquinos, A.; Thum, S.; Remke, J.; Zimmer, K.; Bauters, C.; de Groote, P.; Boon, R.A.; de Windt, L.J.; Preissl, S.; et al. Preclinical Development of a MicroRNA-Based Therapy for Elderly Patients With Myocardial Infarction. *J. Am. Coll. Cardiol.* **2016**, *68*, 1557–1571. [CrossRef]
22. Gupta, S.K.; Garg, A.; Bär, C.; Chatterjee, S.; Foinquinos, A.; Milting, H.; Streckfus-Bomeke, K.; Fiedler, J.; Thum, T. Quaking Inhibits Doxorubicin-Mediated Cardiotoxicity Through Regulation of Cardiac Circular RNA Expression. *Circ. Res.* **2018**, *122*, 246–254. [CrossRef] [PubMed]
23. Metsalu, T.; Vilo, J. ClustVis: A Web Tool for Visualizing Clustering of Multivariate Data Using Principal Component Analysis and Heatmap. *Nucleic Acids Res.* **2015**, *43*, W566–W570. [CrossRef] [PubMed]
24. Xie, Z.; Bailey, A.; Kuleshov, M.V.; Clarke, D.J.B.; Evangelista, J.E.; Jenkins, S.L.; Lachmann, A.; Wojciechowicz, M.L.; Kropiwnicki, E.; Jagodnik, K.M.; et al. Gene Set Knowledge Discovery with Enrichr. *Curr. Protoc.* **2021**, *1*, 90. [CrossRef] [PubMed]
25. Kuleshov, M.V.; Jones, M.R.; Rouillard, A.D.; Fernandez, N.F.; Duan, Q.; Wang, Z.; Koplev, S.; Jenkins, S.L.; Jagodnik, K.M.; Lachmann, A.; et al. Enrichr: A Comprehensive Gene Set Enrichment Analysis Web Server 2016 Update. *Nucleic Acids Res.* **2016**, *44*, 90–97. [CrossRef]
26. Chen, E.Y.; Tan, C.M.; Kou, Y.; Duan, Q.; Wang, Z.; Meirelles, G.V.; Clark, N.R.; Ma'ayan, A. Enrichr: Interactive and Collaborative HTML5 Gene List Enrichment Analysis Tool. *BMC Bioinform.* **2013**, *14*, 128. [CrossRef]
27. Urbanet, R.; Cat, A.N.D.; Feraco, A.; Venteclef, N.; El Mogrhabi, S.; Sierra-Ramos, C.; De La Rosa, D.A.; Adler, G.K.; Quilliot, D.; Rossignol, P.; et al. Adipocyte Mineralocorticoid Receptor Activation Leads to Metabolic Syndrome and Induction of Prostaglandin D2 Synthase. *Hypertension* **2015**, *66*, 149–157. [CrossRef]
28. Kodama, H.; Fukuda, K.; Pan, J.; Makino, S.; Baba, A.; Hori, S.; Ogawa, S. Leukemia Inhibitory Factor, a Potent Cardiac Hypertrophic Cytokine, Activates the JAK/STAT Pathway in Rat Cardiomyocytes. *Circ. Res.* **1997**, *81*, 656–663. [CrossRef]
29. Favre, J.; Gao, J.; di Zhang, A.; Remy-Jouet, I.; Ouvrard-Pascaud, A.; Dautreaux, B.; Escoubet, B.; Thuillez, C.; Jaisser, F.; Richard, V. Coronary Endothelial Dysfunction after Cardiomyocyte-Specific Mineralocorticoid Receptor Overexpression. *Am. J. Physiol. Heart Circ. Physiol.* **2011**, *300*, 2035–2043. [CrossRef]
30. Ouvrard-Pascaud, A.; Sainte-Marie, Y.; Bénitah, J.P.; Perrier, R.; Soukaseum, C.; Cat, A.N.D.; Royer, A.; Quang, K.L.; Charpentier, F.; Demolombe, S.; et al. Conditional Mineralocorticoid Receptor Expression in the Heart Leads to Life-Threatening Arrhythmias. *Circulation* **2005**, *111*, 3025–3033. [CrossRef]
31. Pacak, C.A.; Mah, C.S.; Thattaliyath, B.D.; Conlon, T.J.; Lewis, M.A.; Cloutier, D.E.; Zolotukhin, I.; Tarantal, A.F.; Byrne, B.J. Recombinant Adeno-Associated Virus Serotype 9 Leads to Preferential Cardiac Transduction in Vivo. *Circ. Res.* **2006**, *99*, 3–9. [CrossRef]
32. Zincarelli, C.; Soltys, S.; Rengo, G.; Rabinowitz, J.E. Analysis of AAV Serotypes 1-9 Mediated Gene Expression and Tropism in Mice after Systemic Injection. *Mol. Ther.* **2008**, *16*, 1073–1080. [CrossRef]
33. Zhao, Q.; Wu, K.; Li, N.; Li, Z.; Jin, F. Identification of Potentially Relevant Genes for Myocardial Infarction Using RNA Sequencing Data Analysis. *Exp. Ther. Med.* **2018**, *15*, 1456–1464. [CrossRef]
34. Orenes-Piñero, E.; Manzano-Fernández, S.; López-Cuenca, Á.; Marín, F.; Valdés, M.; Januzzi, J.L. β-Trace Protein: From GFR Marker to Cardiovascular Risk Predictor. *Clin. J. Am. Soc. Nephrol.* **2013**, *8*, 873–881. [CrossRef] [PubMed]
35. Biringer, R.G. The Enzymology of the Human Prostanoid Pathway. *Mol. Biol. Rep.* **2020**, *47*, 4569–4586. [CrossRef]

36. Ricciotti, E.; Fitzgerald, G.A. Prostaglandins and Inflammation. *Arterioscler. Thromb. Vasc. Biol.* **2011**, *31*, 986–1000. [CrossRef] [PubMed]
37. Hirata, T.; Narumiya, S. Prostanoids as Regulators of Innate and Adaptive Immunity. *Adv. Immunol.* **2012**, *116*, 143–174.
38. Fujino, H.; Regan, J.W. Prostaglandin F2α Amplifies Tumor Necrosis Factor-α Promoter Activity by the FPB Prostanoid Receptor. *Biochem. Biophys. Res. Commun.* **2004**, *317*, 1114–1120. [CrossRef]
39. Koyani, C.N.; Windischhofer, W.; Rossmann, C.; Jin, G.; Kickmaier, S.; Heinzel, F.R.; Groschner, K.; Alavian-Ghavanini, A.; Sattler, W.; Malle, E. 15-Deoxy-Δ12,14-PGJ2 Promotes Inflammation and Apoptosis in Cardiomyocytes via the DP2/MAPK/TNFα Axis. *Int. J. Cardiol.* **2014**, *173*, 472. [CrossRef] [PubMed]
40. Kunisch, E.; Jansen, A.; Kojima, F.; Löffler, I.; Kapoor, M.; Kawai, S.; Rubio, I.; Crofford, L.J.; Kinne, R.W. Prostaglandin E2 Differentially Modulates Proinflammatory/Prodestructive Effects of TNF-Alpha on Synovial Fibroblasts via Specific E Prostanoid Receptors/CAMP. *J. Immunol.* **2009**, *183*, 1328–1336. [CrossRef]
41. Beccacece, L.; Abondio, P.; Bini, C.; Pelotti, S.; Luiselli, D. The Link between Prostanoids and Cardiovascular Diseases. *Int. J. Mol. Sci.* **2023**, *24*, 4193. [CrossRef]
42. Fitzpatrick, F.A.; Wynalda, M.A. Albumin-Catalyzed Metabolism of Prostaglandin D2. Identification of Products Formed in Vitro. *J. Biol. Chem.* **1983**, *258*, 11713–11718. [CrossRef]
43. Watanabe, K. Prostaglandin F Synthase. *Prostaglandins Other Lipid Mediat.* **2002**, *68–69*, 401–407. [CrossRef] [PubMed]
44. Adams, J.W.; Migita, D.S.; Yu, M.K.; Young, R.; Hellickson, M.S.; Castro-Vargas, F.E.; Domingo, J.D.; Lee, P.H.; Bui, J.S.; Henderson, S.A. Prostaglandin F2 Alpha Stimulates Hypertrophic Growth of Cultured Neonatal Rat Ventricular Myocytes. *J. Biol. Chem.* **1996**, *271*, 1179–1186. [CrossRef] [PubMed]
45. Ding, W.Y.; Ti, Y.; Wang, J.; Wang, Z.H.; Xie, G.L.; Shang, Y.Y.; Tang, M.X.; Zhang, Y.; Zhang, W.; Zhong, M. Prostaglandin F2α Facilitates Collagen Synthesis in Cardiac Fibroblasts via an F-Prostanoid Receptor/Protein Kinase C/Rho Kinase Pathway Independent of Transforming Growth Factor B1. *Int. J. Biochem. Cell Biol.* **2012**, *44*, 1031–1039. [CrossRef] [PubMed]
46. Ding, W.Y.; Liu, L.; Wang, Z.H.; Tang, M.X.; Ti, Y.; Han, L.; Zhang, L.; Zhang, Y.; Zhong, M.; Zhang, W. FP-Receptor Gene Silencing Ameliorates Myocardial Fibrosis and Protects from Diabetic Cardiomyopathy. *J. Mol. Med.* **2014**, *92*, 629–640. [CrossRef]
47. Ragolia, L.; Hall, C.E.; Palaia, T. Lipocalin-Type Prostaglandin D(2) Synthase Stimulates Glucose Transport via Enhanced GLUT4 Translocation. *Prostaglandins Other Lipid Mediat.* **2008**, *87*, 34–41. [CrossRef]

Disclaimer/Publisher's Note: The statements, opinions and data contained in all publications are solely those of the individual author(s) and contributor(s) and not of MDPI and/or the editor(s). MDPI and/or the editor(s) disclaim responsibility for any injury to people or property resulting from any ideas, methods, instructions or products referred to in the content.

cells

MDPI

Article

MicroRNA-21 Protects Hypoxic-Induced Cardiomyocytes Injury by Targeting Smad-7

Md Sayed Ali Sheikh [1,*], A. Alduraywish [1], Basil Mohammed Alomair [1], Muhannad Almubarak [1] and Umme Salma [2]

[1] Internal Medicine Department, College of Medicine, Jouf University, Sakaka 72345, Saudi Arabia; dr-aaad@ju.edu.sa (A.A.); bmalomair@ju.edu.sa (B.M.A.); maalmubarak@ju.edu.sa (M.A.)
[2] Gynecology and Obstetrics Department, College of Medicine, Jouf University, Sakaka 72345, Saudi Arabia; dusalma@ju.edu.sa
* Correspondence: drsheikh07@hotmail.com or dshekh@ju.edu.sa

Abstract: Globally acute myocardial infarction is the leading independent cause of unexpected death. This study aimed to explore the diagnostic and molecular impact of miR-21, miR-488, and miR-126 in acute myocardial infarction patients (AMI). We enrolled 95 non-ST-elevation myocardial infarction (NSTEMI) patients, 152 ST-elevation myocardial infarction (STEMI) patients, and 95 healthy individuals, additionally using three-month-old mice and their ventricular-derived H9c2 cells. The circulatory plasma miR-21 and miR-488 levels were significantly upregulated, while plasma miR-126 levels were remarkably downregulated in NSTEMI and STEMI subjects. The receiver operating characteristic curve showed that plasma miR-21, miR-488, and miR-126 were able to clearly differentiate NSTEMI and STEMI from healthy subjects. Moreover, H9c2 hypoxic cells treated with inhibitor miR-21 markedly reduced intracellular ROS levels, capase-3 activities levels, and cellular apoptosis rates and significantly enhanced cellular viability through up regulation of Smad-7 mRNA and protein expressions. In geriatric STEMI and NSTEMI subjects, plasma miR-21 levels were evidently higher than in comparatively younger subjects. Upregulated plasma miR-21 and miR-488 levels and downregulated miR-126 levels might be considered potential clinical biomarkers for myocardial infarction patients, while inhibition of miR-21, which significantly reduced hypoxia-exposed H9c2 cellular injury via targeting Smad-7, could be a new therapeutic target for AMI patients. Low levels plasma miR-21 may have a significant impact on delaying the aging process.

Keywords: microRNAs; acute myocardial infarction; biomarkers; H9c2 cells; Smad-7; aging

1. Introduction

Acute myocardial infarction (AMI) is the number one cause of death and disability in both developed and developing countries of all races [1]. Early and correct diagnosis of AMI has a significant impact on the treatment and prognosis of the patient. The diagnosis of AMI is mainly based on clinical presentation, ECG changes, and biochemical markers. However, clinical presentation and ECG changes in elderly and diabetic patients are often nonspecific. Currently, cardiac troponins (cTnT or cTnI) are widely used biomarkers for the early evaluation of AMI in clinical practice. Moreover, several recent studies have found that cardiac troponins are not only elevated in AMI but also elevated in end-stage renal disease, severe heart failure, atrial fibrillation, septic shock, and chronic stable coronary artery disease, even in apparently healthy subjects. Therefore, a novel biomarker for early and reliable

diagnosis of AMI is still lacking [1,2]. MicroRNAs (miRNAs) are small, evolutionarily conserved, non-coding RNA molecules that play an essential role in post-transcriptional gene expression through translational repression or mRNA destabilization. Moreover, miRNAs have been directly and indirectly associated with the pathogenesis of numerous cardiovascular diseases [3]. Various molecular mechanisms of AMI, such as platelet activation and aggregation in the arterial wall, coronary atherosclerotic plaque rupture, and even cardiac cell death after occlusion of coronary arteries, are critically regulated by miRNAs [4].

Myocardial ischemic injury is one of the leading causes of myocardial cell death in AMI, and certain cardiac-specific miRNAs critically regulate the ischemic pathway through modification by their targets [5]. Those miRNAs, measurable in various body fluids, including blood, are considered circulating microRNAs. Circulating miRNAs are highly constant in extreme hot and freezing temperatures and exhibit remarkable defensive power against plasma RNAse due to binding with microvesicles and proteins. Therefore, plasma or serum miRNAs fulfill all the criteria as a standard biomarker [6]. Several recent clinical researchers have acknowledged that circulatory miRNA levels are significantly deregulated in patients with atherosclerosis, hypertension, arrhythmia, stable coronary heart disease, unstable coronary heart disease, coronary plaque rupture, acute coronary syndrome, and acute myocardial infarction [2,5–10]. Moreover, cardiac-specific circulatory miR-208b and miR-499 were reported as potential clinical biomarkers for acute myocardial infarction patients [2,6,11]. It has been demonstrated that disturbed blood flow and hyperlipidemia surprisingly altered the relative miR-21 expression patterns in cultured human endothelial cells and subsequently enhanced the dysfunction of the endothelial wall and initiation of atherosclerotic plaque formation through several pro-inflammatory targets, including NF-κB (nuclear factor κB)-mediated VCAM-1 (vascular cell adhesion molecule-1) [4,12]. A clinical study reported that miR-21 is prominently involved in coronary atherosclerosis formation in coronary heart disease patients through forkhead box P3 (foxp3) and TGF-β1/Smad-7 signaling pathways [13]. Moreover, altered Smad-7 expressions have a protective role in post-myocardial wound repair through fibroblast activation [14].

Biological aging is considered a major non-modifiable risk factor for myocardial infarction. Dysregulated miR-101-3p, miR-142, miR-146, miR-409-3p, miR-142, and miR-146 expressions have been directly associated with aging [2]. However, the effect of miR-21 in hypoxia-induced H9c2 cellular damage and its relationship with Smad-7 and the aging process are largely unknown. Several researchers documented that miR-21, miR-488, and miR-126 have been linked with cardiovascular diseases, but the diagnostic significance of these miRNAs for the early evaluation of non-ST-segment and ST-segment-elevated acute myocardial infarction patients is not fully explored. Therefore, we assessed the clinical significance of these miRNAs for the early prediction of AMI patients. In addition, we also investigated the molecular impact of cardio-enriched miR-21 in hypoxia-injured H9c2 cells and its association with Smad-7 and aging.

2. Section of Material and Methods

2.1. Study of Human Research Participants

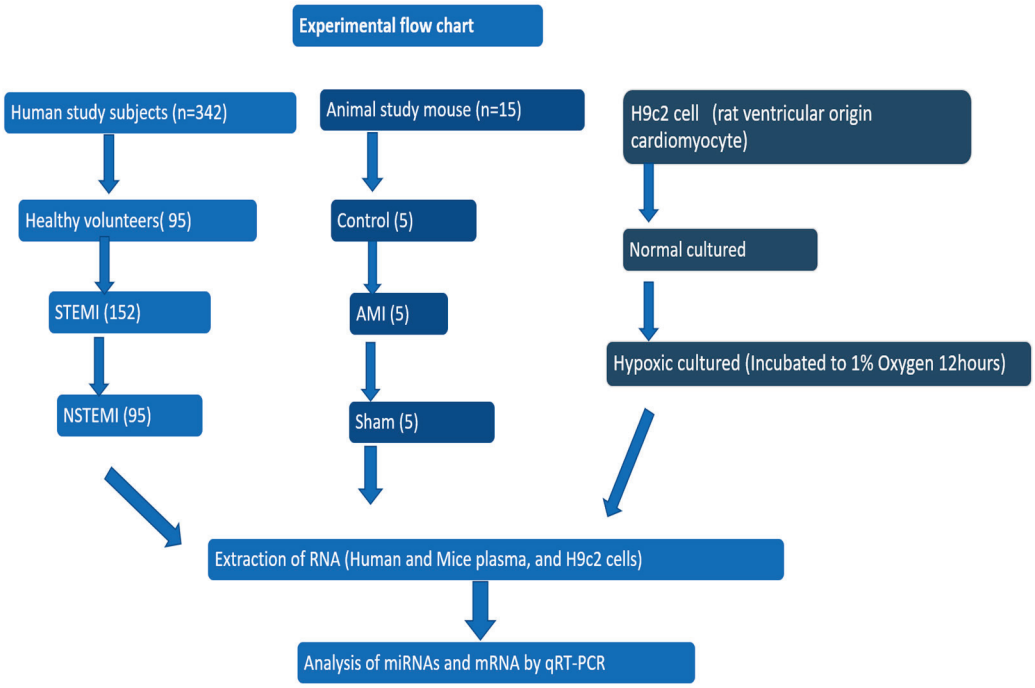
Our research is a case–control-based, cross-sectional study of 95 non-ST-elevated acute myocardial infarction patients (NSTEMI), 152 ST-elevated acute myocardial infarction patients (STEMI), and 95 healthy subjects, aged between 30–89 years, whom we recruited from February 2022 to July 2023 (n = 342) at the tertiary specialized Xiangya Hospital. NSTEMI and STEMI patients were diagnosed according to ACC/AHA/ESC/WHF Task Force Practice Guidelines [1]. Blood samples were collected within 12 h of acute chest pain. Moreover, AMI patients were diagnosed based on at least two of the following

criteria: (I) more than 30 min of acute retrosternal ischemic-type chest pain; (II) ST-segment elevation or depression of more than 1 mm; and (III) elevated plasma cTnI (>0.1 ng/mL). Patients were excluded from our study if they had a known history of previous myocardial infarction, prior intravenous thrombolytic or anticoagulant therapy, arrhythmia, heart failure, percutaneous coronary intervention, coronary artery bypass graft surgery, chronic renal failure, liver failure, or malignant disease. We considered healthy subjects in our study if they had no history of cardiovascular or cerebrovascular diseases and were free from chronic inflammatory diseases. This clinical study was carried out following the medical research principles of the Helsinki Declaration by The World Medical Association and approved by Central South University's Xiangya first affiliated hospital, and prior to the study, consent was obtained from all the study subjects.

2.2. Animal Study Groups

From Xiangya's Laboratory Animal Center, 12-week-old C57BL/6 male mice were collected. We performed our experiments according to the Guidelines of the Chinese National Institute of Health Care for Laboratory Animals and in accordance with the ethical standards of the Veterinary Center of Xiangya School of Medicine.

A total of 15 mice were divided into three groups of equal sizes: (1) the healthy group, (2) the AMI group, and (3) the sham group (same surgical procedures without coronary artery ligation). AMI was generated as described previously [14,15]. Briefly, mice were kept under general anesthesia by using 100 mg/kg ketamine and 1 mg/kg acepromazine, maintaining proper mechanical ventilation; then, the left anterior descending coronary artery was permanently occluded by the 6/0 silk suture to confirm myocardial ischemia. Blood samples were collected from AMI mice at 12 h of ligated left anterior descending coronary artery (LAD) into a K2-EDTA-coated tube and subsequently obtained pure plasma. Experimental protocols are given in more detail in the flow chart, Scheme 1.



Scheme 1. Experimental protocols.

2.3. H9c2 Cell Culture, Hypoxic Model, Transfection, and Hoechst Staining

From the Shanghai Institute of Health Science, rat ventricular cardiomyocyte-originated H9c2 cells were obtained and grown at 37 °C in 95% humidity and 5% CO_2 by using

Dulbecco's Modified Eagle Medium and bovine serum, which were replaced every three days by new culture mediums, with approximately 85% of cell growth transferred to the newer flasks. Moreover, the H9c2 hypoxic model was established by exposing the cells to 1% oxygen, 5% CO_2, and 95% nitrogen for 12 h at 37 °C using a modular incubator (Model 3131, Forma Scientific, Marietta, OH, USA). Furthermore, H9c2 cells were categorized into (1) the control group (constant maintenance with 37 °C temperature, 95% oxygen, and 5% CO_2), and (2) the hypoxic group. Moreover, Lipofectamine 2000, miR-21 inhibitor (100 nM), and NC miR-21 (100 nM) reagents were added to H9c2 cells and incubated for 12 h as per the manufacturer's instruction (Invitrogen, Carlsbad, CA, USA) to develop the transfection. Cellular Hoechst Staining was performed according to the company's instructions.

2.4. Luciferase Reporter Gene Expression

Luciferase assaying technique was conducted to the determination of miR-21 target gene.

The potential target site for miR-21 was predicted using the gene analysis software Target Scan (http://www.targetscan.org/) with the complementary sequence of the 3′ untranslated region of Smad-7. Moreover, the 3′-UTRs of Smad-7 inhibitor miR-21 (5′-UC AACAUCAGUCUGAUAAGCUA-3′), and NC miR-21 (5′-UUCUCCGAACGUGUCACGUT-3′) were transfected into H9c2 cells in 24-well plates using Lipofectamine 2000 for 12 h. The luciferase gene expressions were demonstrated using the Dual-Luciferase Reporter assay reagents, following the manufacturers' protocols (Beyotime, Shanghai, China), and Renilla was used as an inner control. Fluorescent sensitivity was considered to detect the relative values.

2.5. Caspase-3 Activities Assessment

Expressions of caspase-3 levels were demonstrated with caspase-3 activity assay reagents as per the company's guidelines (Beyotime, Shanghai, China). Firstly, a standard curve was performed using the standard pNA sample from the assay kit. Afterward, 96-well plates of normal and transfected H9c2 cells were lysed through buffer solution, followed by centrifugation at 4 °C and 16,000× *g* for 15 min. Finally, the optical density of each well was assessed at a 450 nm wavelength with a microplate reader (Sunnyvale, CA, USA), and the expressions of caspase-3 activities were calculated compared with controls.

2.6. Detection of Intracellular ROS Concentration

As per the company's instructions, the non-fluorescent probe 2′,7′-dichlorofluorescein diacetate was used (Beyotime, Shanghai, China) to determine the intracellular concentrations of ROS production. Firstly, properly cultured H9c2 cells were transfected by inhibitors and negative controls of miR-21 and inoculated for 12 h in the hypoxic medium. Subsequently, DCFH-DA was added to 96-well plates, inoculated at 37 °C for 15 min, and, afterward, washed with FBS three times. Finally, ROS concentrations were measured with a microplate fluorometer at a 480 nm wavelength (Molecular Devices, Sunnyvale, CA, USA).

2.7. Cellular Viability Assay

Cellular survivability was assessed with the Cell Counting Kit-8, following the company's (Beyotime, China) instruction. After proper growth of H9c2 cells in 96-multi-well plates, subsequently, CCK-8 solutions (10 μL) were added to each well plate of normal, hypoxia-treated, and hypoxia-under-treated miR-21 and incubated for 2 h. Lastly, cellular proliferation was evaluated through an absorbance reader at a 450 nm wavelength (Sunnyvale, CA, USA), with the process repeated four times for each group to ensure validity.

2.8. RNA Isolation and Detection of miRNA Expressions

TRIZOL chemicals were added with plasma and also in properly cultured cardiomyocytes as per the company's instruction (Invitrogen, USA) for obtaining RNA molecules.

Bulge-loop reverse transcription microRNA primers were used to reverse-transcribe RNA to cDNA following the company's instructions (RiboBio, Guangzhou, China). SYBR Green microRNA RT-PCR kits (Takara, Dalian, China) were used to detect the expression levels of miR-21, miR-488, and miR-126 with a quantitative real-time PCR system. The relative expression each miRNA was measured by the comparative Ct (cycle threshold) $2^{-\Delta Ct}$ method. MicroRNA-156a was applied to an endogenous control of miR-21, miR-488, and miR-126 expression. Moreover, miRNAs expressions were categorized as high (Ct 15–25), good (Ct 25–32), and undetectable (Ct > 38). More details were explained in our previous study [2,14–16]. Target gene primers are shown in Table 1.

Table 1. Primer sequences used in RT-PCR.

Genes	Upstream Primer Sequences (5′–3′)	Downstream Primer Sequences (5′–3′)
miR-21	GCCGCTAGCTTATCAGACTGATGT	GTGCAGGGTCCGAGGT
miR-488	ACACTCCAGCTGGGTTGAAAGGCTGTTTC	TGGTGTCGTGGAGTCG
miR-126	GCATCGTCGTACCGT GAGTAAT	GTGCAGGGTCCGAGGTA TTC
miR-156	AGGCGCCTGACAGAAGAGAGT	GTGCAGGGTCCGAGGT
Smad 7	TTT GTG TAT TTA TTT CTT TCT CTC	CAC TCT CGT CTT CTC CTC

2.9. Statistical Methods

IBM statistic version SPSS 22 was applied for statistical calculations. Comparisons between groups for continuous variables were performed using one-way ANOVA interpretation, the Mann–Whitney test, or the Student's *t*-test, with Tukey's post hoc test for multiple groups. For categorical variables, the Chi-square (χ^2) test or Fischer's exact test was used as appropriate. All the figures were drawn through GraphPad Prism version 6 and values are expressed as mean ± SEM. Clinical biomarker impact analysis for plasma miRNAs of patients with AMI was carried out through a graphical presentation of receiver operating characteristics (ROCs). A p-value < 0.05 was considered statistically significant.

3. Results

3.1. Baseline Information of the Participants

For the current study, a total of 342 patients were recruited: 95 participants with NSTEMI, including 56 men and 39 women (63.7 ± 11.9 years); 152 patients with STEMI, including 85 men and 67 women (62.4 ± 13.2 years); and 95 healthy volunteers, including 48 men and 47 women (average age: 58.9 ± 12.6 years). The clinical parameters of C-reactive protein, a family history of CAD, ventricular ejection fraction rates, and serum creatinine values were statistically significant between healthy individuals and STEMI and NSTEMI patients but were non-significant between STEMI and NSTEMI subjects. However, all other baseline variables were non-significant among healthy individuals with STEMI and NSTEMI subjects. More details are explained in Table 2.

Table 2. Baseline clinical information of the participants.

Clinical Variables	Healthy Participants (n = 95)	STEMI (n = 152)	NSTEMI (n = 95)	P_1	P_2	P_3
Age, years	58 ± 12	62 ± 13	63 ± 11	0.497	0.483	0.806
Sex, male/female	48/47	85/67	56/39	0.295	0.144	0.107
Diabetes	-	50 (33%)	30 (32%)	-	-	0.994
Smokers	52.3 (55%)	102 (67%)	61 (64%)	0.751	0.743	0.928
Obesity	-	20 (13%)	10 (11%)	-	-	0.664
Lipid disorders	-	123 (81%)	80 (84%)	-	-	0.503

Table 2. *Cont.*

Clinical Variables	Healthy Participants (n = 95)	STEMI (n = 152)	NSTEMI (n = 95)	P_1	P_2	P_3
High blood pressure	-	85 (56%)	57 (59%)	-	-	0.719
Family history of CAD	5.7 (6%)	68 (45%)	45 (47%)	0.000	0.000	0.931
Peripheral vascular diseases	-	20 (13%)	16 (17%)	-	-	0.475
Heart rate, bpm	80.2 ± 8.5	84.6 ± 11.8	83.7 ± 10.9	0.648	0.597	0.882
Glucose (mmol/L)	4.6 ± 0.8	5.48 ± 0.9	5.37 ± 0.6	0.098	0.116	0.692
Serum creatinine (mg/dL)	0.91 ± 0.8	1.3 ± 1.2	1.4 ± 1.2	0.000	0.000	0.187
C-reactive protein, mg/L	4.2 ± 3.1	20.6 ± 9.2	22.5 ± 8.4	0.000	0.000	0.155
Platelets (x109/L)	213.1 ± 4.2	217.5 ± 6.2	220.7 ± 6.8	0.279	0.253	0.487
Cardiac Troponin I (μg/L)	-	45.6 ± 59.3	47.8 ± 61.5	-	-	0.108
Left ventricular ejection fraction %	56.7 ± 12.8	45.3 ± 9.6	47.8 ± 9.2	0.000	0.000	0.851
Aspirin	-	126 (83%)	72 (76%)	-	-	0.127
Clopidogrel	-	52 (34%)	28 (29%)	-	-	0.104
Beta-blockers	-	128 (84%)	79 (83%)	-	-	0.972
Angiotensin-converting-enzyme inhibitors	-	59 (39%)	39 (41%)	-	-	0.713
Angiotensin receptor blockers	-	21 (14%)	16 (17%)	-	-	0.681
Nitrates	-	131 (86%)	80 (84%)	-	-	0.895
Lipid-lowering agents	-	122 (80%)	74 (78%)	-	-	0.782
Midazolam	-	41 (27%)	28 (29%)	-	-	0.883

P_1 (healthy and STEMI); P_2 (healthy versus NSTEMI); P_3 (STEMI and NSTEMI).

3.2. Expression of Plasma miRNAs (miR-21, miR-488, miR-126) in Acute Myocardial Infarction Patients and Mice AMI

Circulatory miR-21 and miR-488 concentrations were significantly upregulated, while miR-126 expression levels were considerably decreased, both in NSTEMI and STEMI subjects in comparison with healthy volunteers. Moreover, plasma concentrations of miR-21 and miR-488 were slightly higher, and miR-126 concentrations were comparatively lower in STEMI subjects as compared to NSTEMI subjects, but their differences were not statistically significant (Figure 1A–C). We noticed a greatly increased circulatory miR-21 and miR-488 relative expression in our AMI mice model groups compared to control groups. In addition, plasma miR-126 levels were remarkably downregulated in AMI mice groups compared to those of controls. However, the levels of circulatory miR-21, miR-488, and miR-126 among controls and sham groups were not statistically significant (Figure 1D–F).

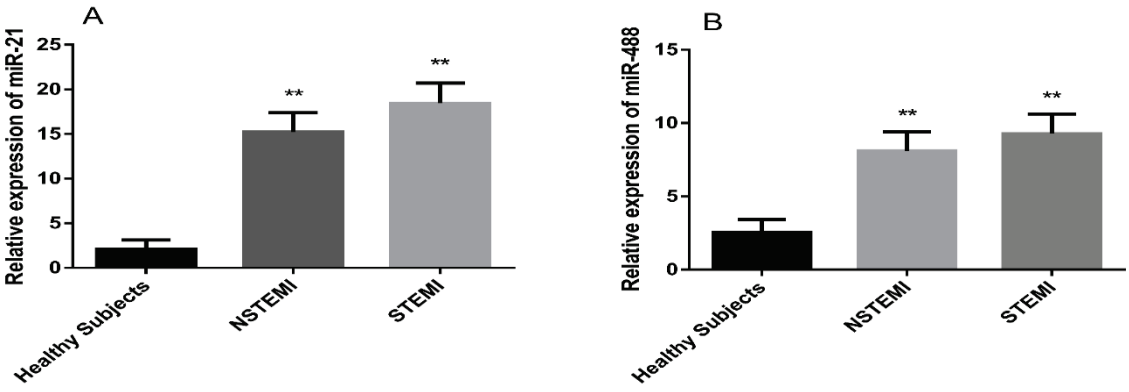


Figure 1. *Cont.*

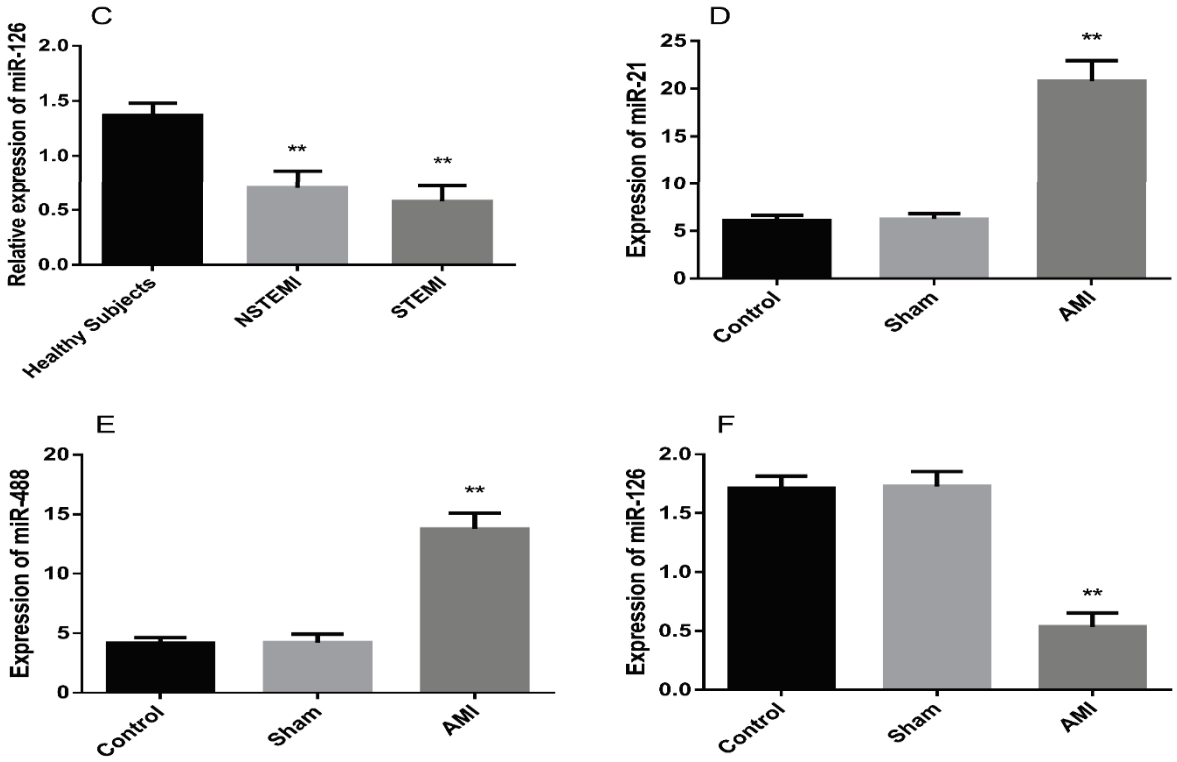


Figure 1. Plasma microRNA concentrations in human subjects and AMI mice models. (**A**) Relative miR-21 expressions in healthy individuals versus NSTEMI and STEMI subjects; (**B**) relative expressions of miR-488 between healthy control subjects and NSTEMI and STEMI patients; (**C**) comparisons of circulating miR-126 expressions between healthy controls and NSTEMI and STEMI patients. (**D**) Relative plasma miR-21 expression in control versus AMI mice models; (**E**) concentrations of plasma miR-488 among AMI mice and controls; (**F**) relative expression of miR-126 within control groups and AMI mice groups. ** $p < 0.001$.

3.3. Diagnostic Impact of Plasma miRNAs for AMI Patients

We performed a ROC curve analysis to explore the diagnostic accuracy of circulatory miR-21, miR-488, and miR-126 for AMI patients. Plasma miR-21 showed a promising potential to discriminate NSTEMI (AUC 0.955) and STEMI (AUC 0.967) patients from control subjects (Figure 2A,B). Moreover, the plasma concentration of miR-488 accurately distinguished NSTEMI (AUC 0.926) and STEMI (AUC 0.934) patients from healthy individuals (Figure 2C,D). Furthermore, circulatory plasma miR-126 clearly separated NSTEMI (AUC 0.825) and STEMI (AUC 0.869) patients from healthy subjects (Figure 2E,F). Therefore, our findings indicate that altered miR-21, miR-488, and miR-126 levels in plasma are novel clinical biomarkers for the early detection of AMI.

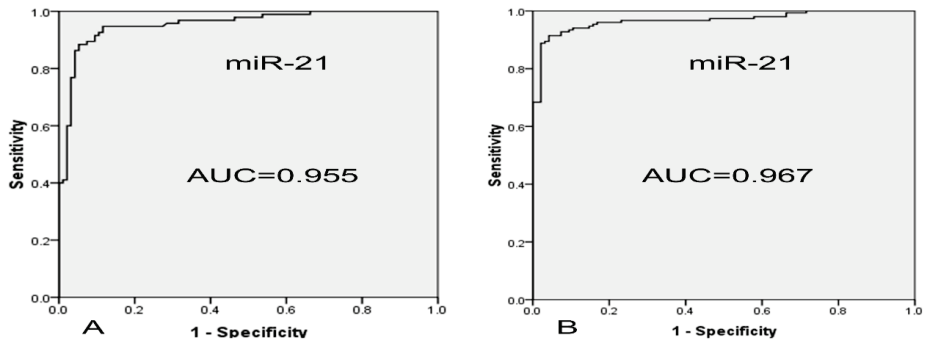


Figure 2. *Cont.*

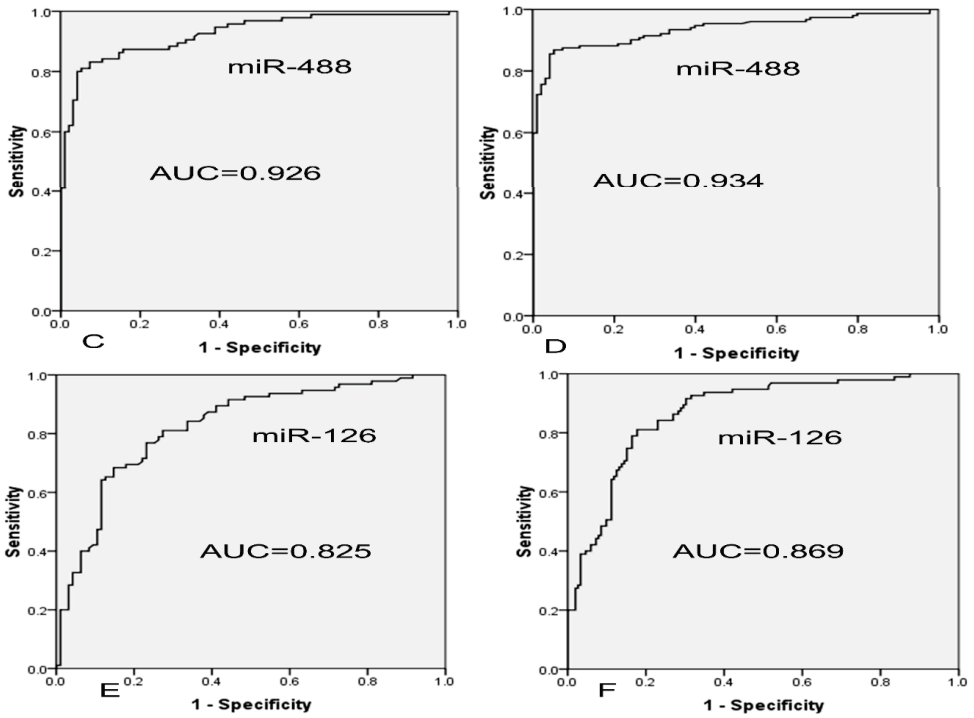


Figure 2. The diagnostic value is illustrated with ROC analysis from plasma miRNAs of AMI patients: (**A**) miR-21, healthy subjects versus NSTEMI patients; (**B**) miR-21, healthy subjects versus STEMI patients; (**C**) miR-488, healthy subjects versus NSTEMI patients; (**D**) miR-488, healthy subjects versus STEMI patients; (**E**) miR-126, healthy subjects versus NSTEMI patients; and (**F**) miR-126, healthy subjects versus STEMI patients.

3.4. Expression and Luciferase Reporter Assay of miR-21, miR-488, and miR-126 in H9c2 Cells

The relative expressions of cardiac-enriched miR-21, miR-488, and miR-126 were upregulated by 2.6-fold and 2.8-fold, respectively, in 12 h hypoxia-exposed H9c2 cells compared to normoxic cells (Figure 3A,B) ($p < 0.001$), while the miR-126 expression level markedly decreased by 5.6-fold in hypoxia-injured H9c2 cells compared to normal cells (Figure 3C). Moreover, a significant decline in miR-21 concentration was noted in hypoxia cells treated with the miR-21 inhibitor compared to untreated cells, and nonsignificant expression was observed within hypoxic and negative controls (Figure 3D). To evaluate the molecular insight of hypoxia-induced cardiomyocyte inflammatory damage linked with alteration of miR-21, we used Target Scan analysis and luciferase gene expression and found that Smad-7 is a target gene of miR-21. Moreover, the luciferase expressions were significantly downregulated in 12 h hypoxia-incubated H9c2 cells compared to normal cells, but the negative control and hypoxic H9c2 cell groups were non-significant. The inhibition of miR-21 markedly regulated luciferase activity in hypoxia-exposed H9c2 cells (Figure 3E).

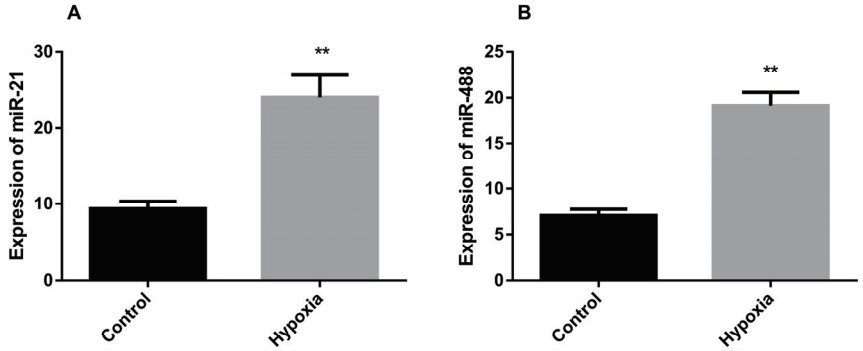


Figure 3. *Cont.*

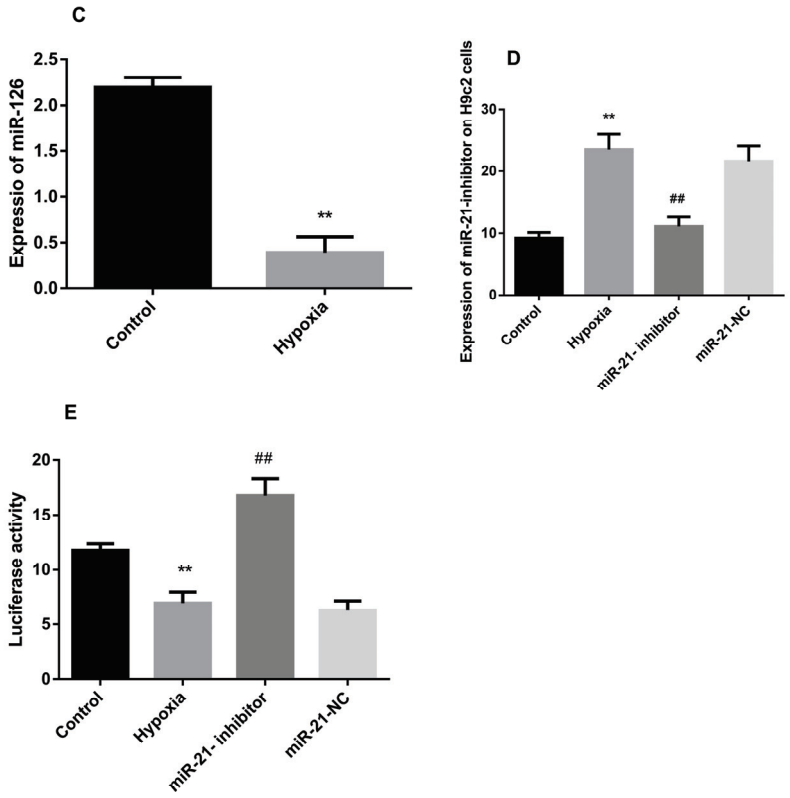


Figure 3. The expression of miRNAs in H9c2 cells. (**A**) Relative expression of miR-21 among control and hypoxia groups; (**B**) expression of miR-488 in hypoxic and normoxic cells; (**C**) relative miR-126 expression between normal culture and hypoxia groups cells; (**D**) effects of miR-21 on hypoxia-induced H9c2cells; (**E**) luciferase reporter gene expressions. ** $p < 0.001$, hypoxia vs. control groups; ## $p < 0.001$, hypoxia vs. hypoxia with miR-21 treatment groups.

3.5. Effects of Inhibitor miR-21 on Smad-7 and Hypoxia-Exposed H9c2 Cells

The Smad-7 mRNA expression levels were remarkably decreased by 4.1-fold in the hypoxia group as compared to normal H9c2 cells. On the contrary, Smad-7 expressions in hypoxic H9c2 cells treated with the miR-21 inhibitor were significantly elevated by 3.3-fold compared to untreated hypoxic cells, but there was no effect noticed within the negative (NC) control and hypoxic group (Figure 4A). Furthermore, ROS expression levels were obviously upregulated by 4-fold in the 12 h hypoxic group as compared to normoxic H9c2 cells, while ROS levels were prominently down-regulated by two-fold in hypoxia-exposed miR-21-inhibited H9c2 cells compared to only-hypoxia-incubated H9c2 cells. However, there were no changes observed among NCs and hypoxia H9c2 cells (Figure 4B). We revealed that caspase-3 activities were significantly elevated by 9-fold in the hypoxic group compared to normal H9c2 cells, whereas inhibition of miR-21 remarkably reduced hypoxia-induced caspase-3 activities by 7-fold, as compared to hypoxia-injured H9c2 cells, but the expression of caspase-3 levels between the hypoxic group and negative control was non-significant (Figure 4C). In addition, cellular viability greatly decreased by 2-fold in the hypoxic H9c2 group compared to normal controls, whereas cellular survivability increased by 1.9-fold in miR-21-inhibited hypoxic H9c2 cells compared to hypoxic cells ($p < 0.001$) (Figure 4D). The cellular apoptosis rate was calculated through Hoechst staining, and we found markedly elevated cellular apoptosis rates in the hypoxia group compared to the control; in hypoxia-exposed H9c2 cells treated with the miR-21 inhibitor, the cellular apoptosis rate was significantly reduced in the hypoxia group compared to the control ($p < 0.001$) (Figure 4E,F). Therefore, our findings suggest that the inhibition of miR-21 enormously suppressed caspase-3 as well as ROS expression and outstandingly improved

cellular viability during hypoxia-induced H9c2 cellular injury by regulating its target Smad-7 mRNA and protein expressions.

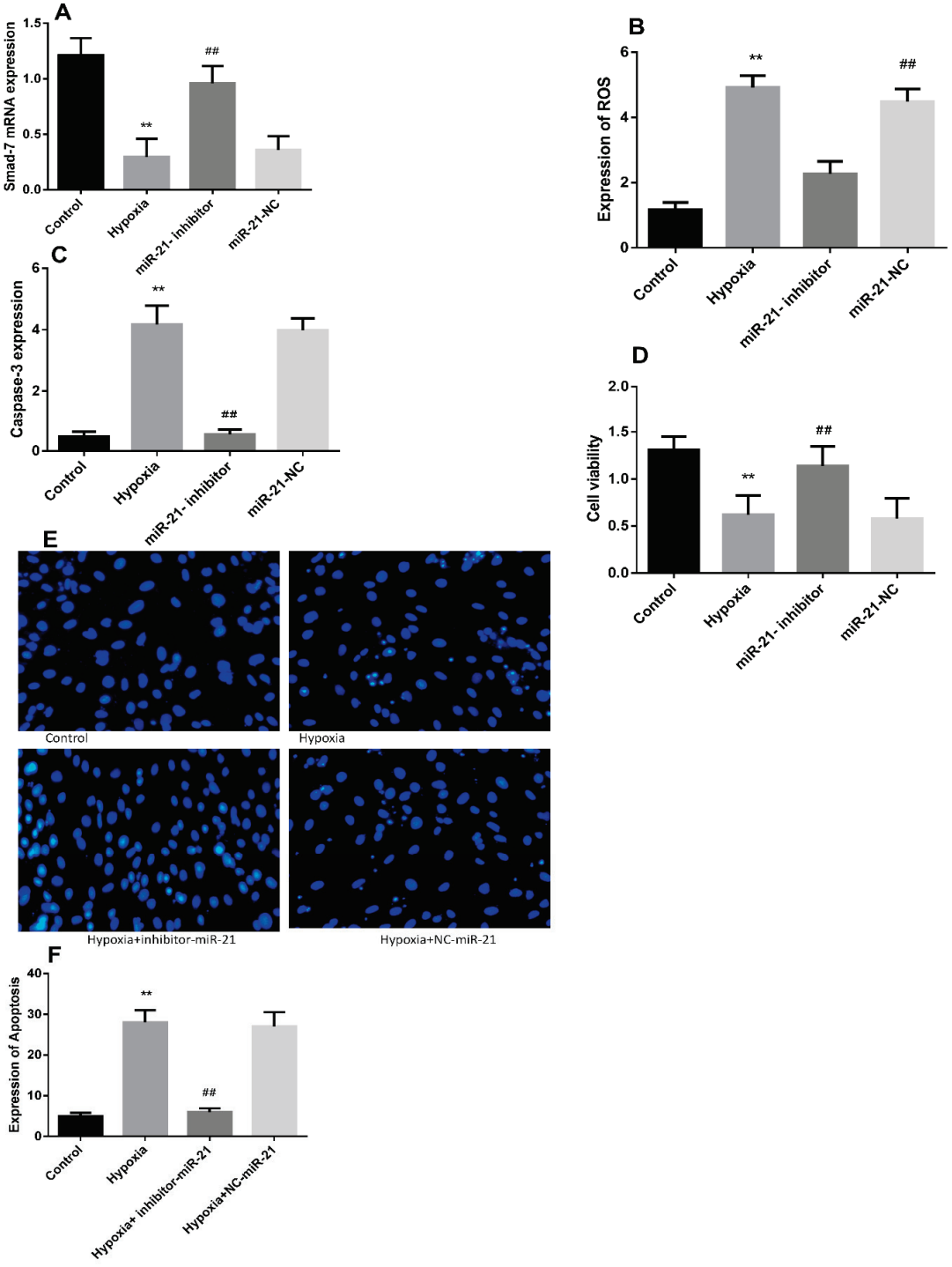


Figure 4. Effect of miR-21 inhibitor on H9c2 cells. (**A**) Smad-7 mRNA levels. (**B**) ROS concentrations. (**C**) Caspase-3 expression. (**D**) Cell viability. (**E**) Measurement of apoptosis through Hoechst. (**F**) Ratio of apoptosis levels. ** $p < 0.001$, hypoxia vs. control groups; $^{\#\#}$ $p < 0.001$, hypoxia vs. hypoxia with miR-21 treatment groups.

3.6. The miR-21 Relationship with Aging and Gender

In the older groups (70–89 years), both STEMI and NSTEMI subjects significantly upregulated plasma miR-21 levels compared to younger (30–49 years) patients. In the

elder patients' group (50–69 years), miR-21 expression was reasonably higher than in the younger groups (30–49 years) but was statistically insignificant (Figure 5A,B). In healthy volunteers, miR-21 expressions slowly rose with increasing age. However, the volume of plasma miR-21 between male and female subjects in either healthy or disease groups was statistically insignificant. (Figure 5C). This finding, attributed to miR-21, has a strong link to aged AMI patients, suggesting that low miR-21 levels may prevent the aging process, as well as treat AMI subjects.

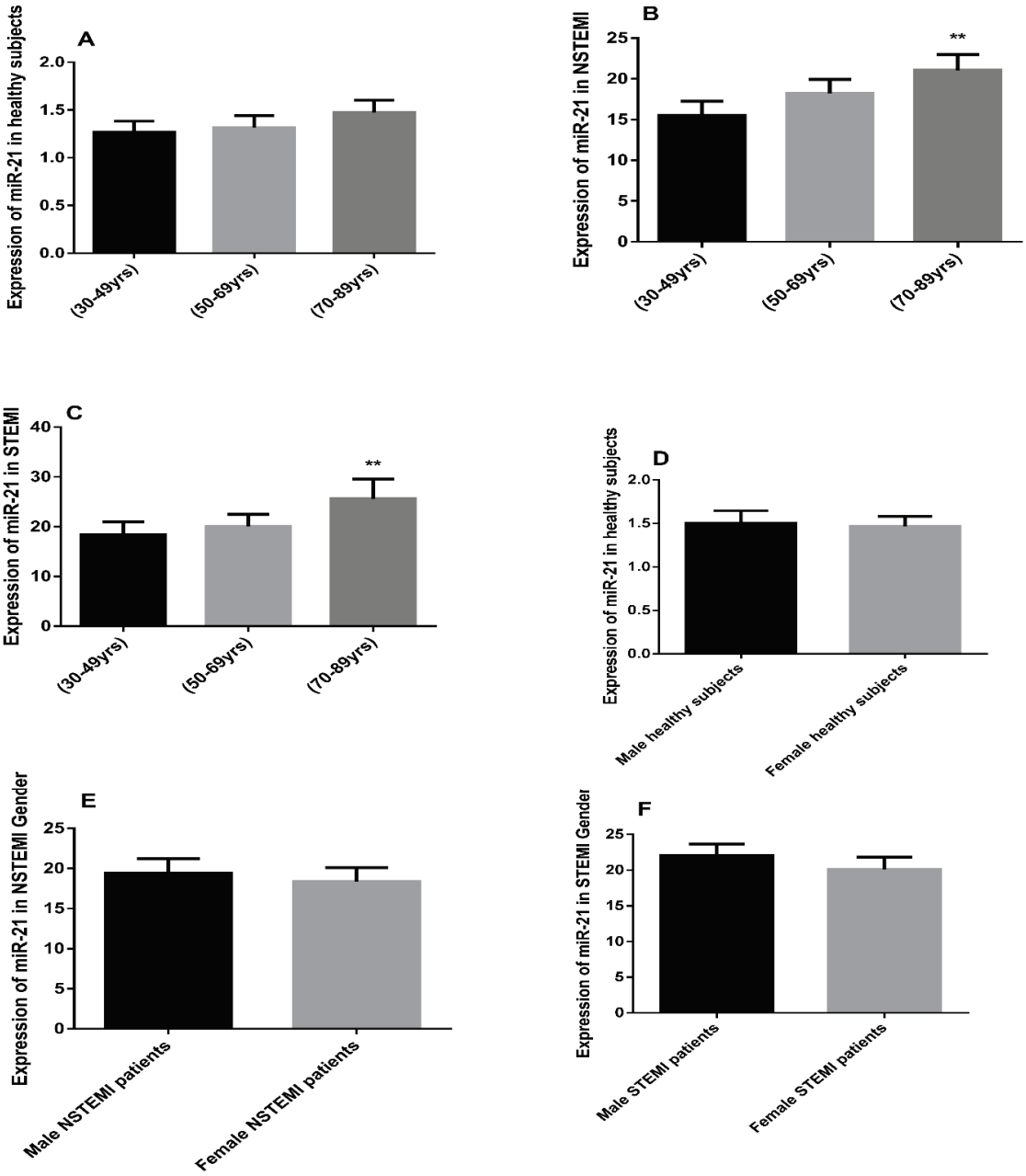


Figure 5. Correlation between aging and miR-21 and association with gender. (**A**) The relative miR-21 expression among healthy subjects. (**B**) The expression of miR-21 within (70–89 years), (50–69 years), and (30–49 years) NSTEMI groups. (**C**) The patterns of miR-21 levels among (30–49 years), (50–69 years), and (70–89 years) STEMI groups. (**D**) Expression level of miR-21 between healthy male and female individuals. (**E**) Male versus female NSTEMI patients' miR-21 expressions. (**F**) miR-21 concentrations among male and female STEMI participants. ** $p < 0.001$.

4. Discussion

Sudden unexpected cardiac death predominantly occurred due to acute myocardial infarction (AMI). Accurate and timely diagnosis of AMI can guarantee urgent initiation of reperfusion treatment that directly reduces the mortality rate. Several clinical and animal studies have suggested that selected cardiac-enriched circulating miRNAs such as miR-1, miR-133, and miR-223 have a significant diagnostic role in the evaluation of AMI patients [2,6,10]. In our study, we observed markedly upregulated circulatory plasma concentrations of miR-488 and miR-21, while finding potentially downregulated miR-126 levels in both the NSTEMI and STEMI group compared to healthy participants. Recently some researchers acknowledged that miR-21 was critically involved in coronary stenosis and highly upregulated in AMI subjects, as well as in hypoxia-injured cardiomyocyte (H9c2) cells; they recommended circulatory miR-21 as having a significant diagnostic impact on acute MI patients, which is consistent with the results of our study [17,18]. Furthermore, circulatory concentrations of plasma miR-21 were noticeably more upregulated in our AMI mice models than in controls. Significantly elevated miR-21 expression patterns were also demonstrated by Yang et al. in mouse models of AMI, and miR-21 prevents excessive inflammation and cardiac dysfunction after myocardial infarction through targeting kelch repeat and BTB (POZ) domain-containing 7 (KBTBD7), considered a new therapeutic molecule for MI; these results are also partially associated with our results [18,19]. It has been recognized that miR-21 is greatly involved in vascular inflammation, foam cell formation, atherosclerosis plaque formation, and also controlling cardiac fibrosis through Smad-7 [20,21]. In our H9c2 cellular study, to find out the underlying molecular mechanism of miR-21 in protecting against hypoxia-induced cardiac cell damage, we performed Target Scan and luciferase reporter gene analysis and confirmed that Smad-7 acts as a potential target gene for miRNA-21. We found that ROS, caspase-3, irreversible cellular damages, and concentrations of miR-21 were markedly elevated, whereas the relative expression of Smad-7 was evidently reduced in 12 h hypoxia-incubated H9c2 cells as compared to normal culture cells. In contrast, Smad-7 expressions were prominently elevated and significantly diminished cellular ROS concentrations and caspase-3 levels, while considerably amplifying the viability of hypoxic H9c2 cells treated with the miR-21 inhibitor. We recommend that the knockdown of miR-21 has significant potential to prevent cardiac cell death through regulating its target, Smad-7. Moreover, recent hypoxia-injured ventricular H9c2 cell studies also demonstrated that markedly elevated expressions of miR-21 increased caspase-3 activity, ROS generation, and cellular death, while hypoxic H9c2 cells treated with the miR-21 inhibition significantly reduced intracellular ROS and caspase-3 levels and remarkably augmented cardiac cellular viability by regulating PDCD4, Akap8, and Bard1 expressions through modification of Wnt/β-catenin, PTEN/PI3K/AKT, and NF-κB pathways [15,22]. These studies, along with our findings, strongly support that miR-21 significantly regulates caspase-3 activity, intracellular ROS generation, and hypoxia-induced H9c2 cellular injury through the modulation of Smad-7 expression.

Our study first recognized the significantly higher expression of plasma miR-488 in acute MI patients and AMI mice models than in controls. Additionally, we detected that miR-488 expressions were remarkably upregulated in hypoxia-exposed H9c2 cells compared to normoxic control groups. Zhen research groups have shown that high expression of circulating miR-488 is a good biomarker for the identification of atherosclerosis patients, and downregulation of miR-488 can inhibit vascular smooth muscle cell (VSMC) proliferation and migration [23]. Verjans et al. reported that macrophages transfected with mimic-miR-488-5p significantly decrease sICAM-1, IL-1ra, IL-16, CXCL1, and TNFα cytokine levels and regulate heart failure conditions in human patients and rat models [24]. However, in our present study, we found that circulatory miR-126 expressions

were significantly decreased in both NSTEMI and STEMI patients, AMI mice models, and hypoxia-induced injured H9c2 cells compared to control groups, which is in strong agreement with other recent studies [10,16]. Luo et al. established that expressions of miR-126 levels were prominently decreased in AMI rat models and 24 h hypoxia-exposed H9c2 cell injury. However, overexpression of miR-126 obviously reduced inflammatory markers (TNF-α, IL-6, and IL-1β), apoptosis rates, and cardiomyocyte fibrosis and significantly improved cardiac cell viability and promoted angiogenesis [25].

Moreover, to explore diagnostic accuracy, we performed a receiver operating characteristic (ROC) curves analysis. ROC analysis revealed AUC values for plasma miR-21 in NSTEMI (0.955) and STEMI (0.967), miR-488 in NSTEMI (0.926) and STEMI (0.934), and miR-126 in NSTEMI (0.825) and STEMI (0.869) compared to those of healthy volunteers. These findings strongly suggest that upregulated plasma miR-21 and miR-488 and downregulated miR-126 levels are able to clearly differentiate NSTEMI and STEMI patients from healthy control subjects and could be novel clinical biomarkers for the identification of AMI patients. Furthermore, aging is an independent major risk factor for atherosclerotic acute coronary syndrome, and our study showed that plasma miR-21 was significantly higher in geriatric AMI patients, and other studies also found miR-21 is correlated with cellular aging [2,26,27]. To avoid technical faults related to the PCR method, we analyzed all the samples four times for human, animal, and H9c2 cells with a single investigator, and miRNAs with Ct values less than 15 and more than 38 were not considered in this study, which guaranteed that our findings were more accurate and more reasonable.

5. Limitations of the Study

However, our study was only conducted in one provisional multidisciplinary hospital among the Han population with relatively few clinical samples. Therefore, different ethnic populations with larger clinical samples investigations will be required to validate these miRNAs as a useful new biomarker before being applied to clinical practice. Required further study to find out CRP and creatinine's molecular relationship with our selected miRNAs. Moreover, we did not examine the inflammatory relationship between TGF-β1 and Smad-7, further elucidation of TGF-β1 and Smad-7 signaling pathways is essential to explore their molecular mechanism during hypoxic-induced H9c2 cellular injury. Moreover, we do not know the regular drugs those were taken by AMI patients that were made any effects on miRNAs expressions, and these medications also had any effects on Animal and cell models, need to further research.

6. Conclusions

We recommend that augmented miR-21, miR-488, and decreased miR-126 plasma concentrations may play critical roles in the early stage of AMI and may be used as novel clinical predictors for diagnosis of NSTEMI and STEMI patients. In addition, miR-21 has a notable correlation with aging. Inhibition of miR-21 prevents H9c2 cardiac cell death during hypoxic challenges through regulating Smad-7, providing a possible therapeutic strategy for AMI patients.

Author Contributions: Conceptualization, M.S.A.S. and U.S.; Methodology and Resources, U.S.; Investigation, M.S.A.S., A.A., U.S., and M.A.; Software, M.A.; Writing—original draft, M.S.A.S.; Writing—Review, M.S.A.S., A.A., and B.M.A.; Formal Analysis, M.S.A.S., A.A., and B.M.A.; Validation, Data Curation, and Writing—Review and Editing, A.A. and M.A.; Funding Acquisition, Project Administration, and Supervision, M.S.A.S. and A.A. All authors have read and agreed to the published version of the manuscript.

Funding: This work was funded by the Deanship of Scientific Research at Jouf University under grand no. 39/589.

Institutional Review Board Statement: The study was conducted in accordance with the Declaration of Helsinki and approved by the Institutional Review Board (or Ethics Committee) of The Xiangya hospital institutional Ethical Committee of Central South University (protocol code 088110011/2 and date of approval 21 July 2019) for studies involving humans.

Informed Consent Statement: Informed consent was obtained from all subjects involved in the study.

Data Availability Statement: Data will be available upon request from the corresponding author.

Acknowledgments: We are sincerely thankful for and appreciative of the great help from the Cardiology Department of Xiangya Hospital, specially from Yang tian Lun, Xia Ke, and Li Fei.

Conflicts of Interest: The authors declare no conflicts of interest.

References

1. Martin, S.S.; Aday, A.W.; Allen, N.B.; Almarzooq, Z.I.; Anderson, C.A.; Arora, P.; Avery, C.I.; Baker-Smith, C.M.; Bansal, N.; Beaton, A.Z.; et al. 2025 Heart Disease and Stroke Statistics: A Report of US and Global Data From the American Heart Association. *Circulation* **2025**, *8*, e41–e660.
2. Sayed, M.S.A.; Salma, U. Impact of microRNAs on cardiovascular diseases and aging. *J. Int. Med. Res.* **2024**, *10*, 3000605241279190.
3. Lozano-Velasco, E.; Inácio, J.M.; Sousa, I.; Guimarães, A.R.; Franco, D.; Moura, G.; Belo, J.A. miRNAs in Heart Development and Disease. *Int. J. Mol. Sci.* **2024**, *3*, 1673. [CrossRef]
4. Stojkovic, S.; Wadowski, P.P.; Haider, P.; Weikert, C.; Pultar, J.; Lee, S.; Eichelberger, B.; Hengstenberg, C.; Wojta, A.; Panzer, S.; et al. Circulating MicroRNAs and Monocyte-Platelet Aggregate Formation in Acute Coronary Syndrome. *Thromb. Haemost.* **2021**, *7*, 913–922. [CrossRef]
5. Liang, G.; Guo, C.; Tang, H.; Zhang, M. miR-30a-5p attenuates hypoxia/reoxygenation-induced cardiomyocyte apoptosis by regulating PTEN protein expression and activating PI3K/Akt signaling pathway. *BMC Cardiovasc. Disord.* **2024**, *1*, 236. [CrossRef] [PubMed]
6. Stojkovic, S.; Wojta, J. Circulatory microRNAs in acute coronary syndrome: An update. *Kardiol. Pol.* **2024**, *12*, 1192–1199.
7. Wang, L.; Zhu, Q.; Cheng, B.; Jiang, N.; Dong, C. Value of Let-7a-5p in Essential Hypertension. *J. Clin. Hypertens.* **2025**, *3*, 70033. [CrossRef]
8. Natsume, Y.; Oaku, K.; Takahashi, K.; Nakamura, W.; Oono, A.; Hamada, S.; Yamazoe, M.; Ihara, K.; Sasaki, T.; Goya, M.; et al. Analysis of Human and Experimental Murine Samples Identified Novel Circulating MicroRNAs as Biomarkers for Atrial Fibrillation. *Circ. J.* **2018**, *4*, 965–973. [CrossRef]
9. Andiappan, R.; Govindan, R.; Ramasamy, T.; Poomarimuthu, M. Circulating miR-133a-3p and miR-451a as potential biomarkers for diagnosis of coronary artery disease. *Acta Cardiol.* **2024**, *7*, 813–823. [CrossRef] [PubMed]
10. Hernández-López, J.R.; Flores-García, M.; García-Flores, E.; Cazarín-Santos, B.G.; Peña-Duque, M.A.; Sánchez-Muñoz, F.; Ballinas-Verdugo, M.A.; Delgadillo-Rodríguez, H.; Martínez-Ríos, M.A.; Angles-Cano, E.; et al. Circulating Microvesicles Enriched in miR-126-5p and miR-223-3p: Potential Biomarkers in Acute Coronary Syndrome. *Biomedicines* **2025**, *2*, 510. [CrossRef]
11. Agiannitopoulos, K.; Pavlopoulou, P.; Tsamis, K.; Bampali, K.; Samara, P.; Nasioulas, G.; Mertzanos, G.; Babalis, D.; Lamnissou, K. Expression of miR-208b and miR-499 in Greek Patients with Acute Myocardial Infarction. *In Vivo* **2018**, *2*, 313–318.
12. Lu, Y.; Thavarajah, T.; Gu, W.; Cai, J.; Xu, Q. Impact of miRNA in Atherosclerosis. *Arter. Thromb. Vasc. Biol.* **2018**, *9*, e159–e170. [CrossRef]
13. Li, S.; Fan, Q.; He, S.; Tang, T.; Liao, Y.; Xie, J. MicroRNA-21 negatively regulates Treg cells through a TGF-β1/Smad-independent pathway in patients with coronary heart disease. *Cell. Physiol. Biochem.* **2015**, *3*, 866–878. [CrossRef] [PubMed]
14. Su, Y.; Shi, D.; Xia, G.; Liu, Y.; Xu, L.; Dao, L.; Lu, X.; Shen, C.; Xu, C. Carbonic Anhydrase 3 is required for cardiac repair post myocardial infarction via Smad7-Smad2/3 signaling pathway. *Int. J. Biol. Sci.* **2024**, *5*, 1796–1814. [CrossRef]
15. Shen, H.; Yao, Z.; Zhao, W.; Zhang, Y.; Yao, C.; Tong, C. miR-21 enhances the protective effect of loperamide on rat cardiomyocytes against hypoxia/reoxygenation, reactive oxygen species production and apoptosis via regulating Akap8 and Bard1 expression. *Exp. Ther. Med.* **2018**, *2*, 1312–1320. [CrossRef]
16. Wang, W.; Zheng, Y.; Wang, M.; Yan, M.; Jiang, J.; Li, Z. Exosomes derived miR-126 attenuates oxidative stress and apoptosis from ischemia and reperfusion injury by targeting ERRFI1. *Gene* **2019**, *690*, 75–80. [CrossRef]
17. Xu, L.; Tian, L.; Yan, Z.; Wang, J.; Xue, T.; Sun, Q. Diagnostic and prognostic value of miR-486-5p, miR-451a, miR-21-5p and monocyte to high-density lipoprotein cholesterol ratio in patients with acute myocardial infarction. *Heart Vessel.* **2023**, *3*, 318–331. [CrossRef]
18. Sahebi, R.; Gandomi, F.; Shojaei, M.; Farrokhi, E. miRNA-21-5p and miRNA-21-3p as key biomarkers of myocardial infarction. *Health Sci. Rep.* **2024**, *7*, e2228. [CrossRef]

19. Yang, L.; Wang, B.; Zhou, Q.; Wang, Y.; Liu, X.; Liu, Z.; Zhan, Z. MicroRNA-21 prevents excessive inflammation and cardiac dysfunction after myocardial infarction through targeting KBTBD7. *Cell Death Dis.* **2018**, *7*, 769. [CrossRef]
20. Canfrán-Duque, A.; Rotllan, N.; Zhang, X.; Fernández-Fuertes, M.; Ramírez-Hidalgo, C.; Araldi, E.; Daimiel, L.; Busto, R.; Fernández-Hernando, C.; Suárez, Y. Macrophage deficiency of miR-21 promotes apoptosis, plaque necrosis, and vascular inflammation during atherogenesis. *EMBO Mol. Med.* **2017**, *9*, 1244–1262. [CrossRef]
21. Yuan, J.; Chen, H.; Ge, D.; Xu, Y.; Xu, H.; Yang, Y.; Gu, M.; Zhou, Y.; Zhu, J.; Ge, T.; et al. Mir-21 Promotes Cardiac Fibrosis After Myocardial Infarction Via Targeting Smad7. *Cell. Physiol. Biochem.* **2017**, *6*, 2207–2219. [CrossRef]
22. Hao, L.; Wang, J.; Liu, N. Long noncoding RNA TALNEC2 regulates myocardial ischemic injury in H9c2 cells by regulating miR-21/PDCD4-medited activation of Wnt/β-catenin pathway. *J. Cell. Biochem.* **2019**, *8*, 12912–12923. [CrossRef]
23. Li, Z.; Xu, C.; Sun, D. MicroRNA-488 serves as a diagnostic marker for atherosclerosis and regulates the biological behavior of vascular smooth muscle cells. *Bioengineered* **2021**, *1*, 4092–4099. [CrossRef]
24. Verjans, R.; Derks, W.J.A.; Korn, K.; Sönnichsen, B.; van Leeuwen, R.E.; Schroen, B.; van Bilsen, M.; Heymans, S. Functional Screening Identifies MicroRNAs as Multi-Cellular Regulators of Heart Failure. *Sci. Rep.* **2019**, *1*, 6055. [CrossRef]
25. Luo, Q.; Guo, D.; Liu, G.; Chen, G.; Hang, M.; Jin, M. Exosomes from MiR-126-Overexpressing Adscs Are Therapeutic in Relieving Acute Myocardial Ischaemic Injury. *Cell. Physiol. Biochem.* **2017**, *6*, 2105–2116. [CrossRef]
26. Mensà, E.; Guescini, M.; Giuliani, A.; Bacalini, M.G.; Ramini, D.; Corleone, G.; Ferracin, M.; Fulgenzi, G.; Graciotti, L.; Prattichizzo, F.; et al. Small extracellular vesicles deliver miR-21 and miR-217 as pro-senescence effectors to endothelial cells. *J. Extracell. Vesicles* **2020**, *9*, 1725285. [CrossRef]
27. Chang, W.T.; Shih, J.Y.; Lin, Y.W.; Huang, T.L.; Chen, Z.C.; Chen, C.L.; Chu, J.S.; Liu, P.Y. miR-21 upregulation exacerbates pressure overload-induced cardiac hypertrophy in aged hearts. *Aging* **2022**, *14*, 5925–5945. [CrossRef]

Disclaimer/Publisher's Note: The statements, opinions and data contained in all publications are solely those of the individual author(s) and contributor(s) and not of MDPI and/or the editor(s). MDPI and/or the editor(s) disclaim responsibility for any injury to people or property resulting from any ideas, methods, instructions or products referred to in the content.

cells

MDPI

Review

Targeting the Notch Signaling Pathway to Treat Atherosclerosis

Alexander Blagov [1,*], Daria Borodko [1], Ulyana Rozhkova [2], Stanislav Antonov [1], Aleksandra Utkina [3] and Tatiana Kovyanova [2]

[1] Laboratory of Molecular Genetic Modeling of Inflammaging, Institute of General Pathology and Pathophysiology, 8, Baltiiskaya Street, 125315 Moscow, Russia
[2] Institute for Atherosclerosis Research, 4-1-207, Osennyaya Street, 121609 Moscow, Russia
[3] Department of Commodity Expertise and Customs Business, Plekhanov Russian University of Economics, 36, Stremyanny Lane, 115054 Moscow, Russia
* Correspondence: al.blagov2014@gmail.com

Abstract

Atherosclerosis remains the principal underlying cause of myocardial infarction, ischemic stroke and peripheral artery disease, and its progression reflects a complex interplay between lipid accumulation, endothelial dysfunction, chronic vascular inflammation and maladaptive remodeling of the arterial wall. The Notch signaling pathway, an evolutionarily conserved juxtacrine communication system, has emerged as a central regulator of every cell type implicated in atherogenesis, including endothelial cells, vascular smooth muscle cells, monocytes/macrophages and T lymphocytes. Depending on the receptor–ligand pairing, the hemodynamic context and the cellular compartment involved, Notch signaling can be either atheroprotective or atherogenic, a duality that has complicated efforts to translate mechanistic insight into therapy. This review summarizes current knowledge of the molecular architecture of the Notch pathway in the vasculature, dissects its cell type-specific and stage-specific contributions to atherosclerotic plaque initiation, progression, calcification and destabilization, and critically appraises pharmacological strategies designed to modulate Notch activity, including γ-secretase inhibitors, ligand- and receptor-directed monoclonal antibodies, soluble decoy receptors, microRNA-based approaches and drug repurposing strategies such as statins. Particular attention is paid to the cardiovascular toxicities that have emerged from oncology trials of Notch pathway inhibitors, which illustrate both the pharmacological tractability and the narrow therapeutic window of this pathway. We conclude that Notch-directed therapy for atherosclerosis is mechanistically well justified but will require cell type-selective and context-selective delivery strategies to be clinically viable.

Keywords: notch signaling; atherosclerosis; endothelial dysfunction; vascular smooth muscle cells; macrophage polarization; Jagged1; delta-like ligand 4; gamma-secretase inhibitor; vascular inflammation; therapeutic target

1. Introduction

Atherosclerosis is a chronic disease of medium- and large-sized arteries characterized by the sub-endothelial retention of apolipoprotein B-containing lipoproteins, recruitment and differentiation of monocytes into lipid-laden macrophages, proliferation and phenotypic switching of vascular smooth muscle cells (VSMCs), and progressive fibrous and, in advanced lesions, calcific remodeling of the vessel wall [1]. Phenotypic switching refers to the capacity of medial VSMCs, which under physiological conditions are quiescent,

non-proliferative and specialized for contraction, to lose this contractile identity and convert to a proliferative, migratory, extracellular matrix-secreting "synthetic" phenotype in response to injury, inflammatory cytokines and altered mechanical or lipid cues in the vessel wall; these dedifferentiated VSMCs migrate from the media into the intima, where they contribute directly to plaque growth and, depending on context, can further transdifferentiate toward macrophage-like, osteochondrogenic or mesenchymal stem cell-like states that shape both plaque expansion and fibrous cap stability [2]. Atherosclerosis is a multifactorial disease driven by the interaction of non-modifiable risk factors, including age, male sex and family history/genetic predisposition, with modifiable risk factors such as hypertension, dyslipidemia, cigarette smoking, diabetes mellitus, obesity and physical inactivity, all of which converge on the endothelium and the vessel wall to initiate and accelerate the pathological process described above; the clinical consequences of the resulting arterial plaque burden include myocardial infarction, ischemic stroke, peripheral artery disease and sudden cardiac death, which together account for the leading share of global cardiovascular mortality [3]. Despite considerable progress in lipid-lowering and anti-inflammatory pharmacotherapy, atherosclerotic cardiovascular disease continues to account for a very large share of global mortality, which has sustained interest in signaling pathways that coordinate the behavior of the several cell types that jointly build the atherosclerotic plaque.

The Notch pathway is one of a small number of signaling systems that is reused throughout metazoan development to control cell fate decisions [4], and canonical Notch signal transduction proceeds through a well-defined sequence of proteolytic and transcriptional events [5]. It has been co-opted by the adult vasculature to regulate arterial identity, angiogenic sprouting, endothelial quiescence and smooth muscle differentiation [6]. Critically, endothelial Notch signaling also plays a pivotal role in angiocrine signaling, whereby ligand- and receptor-dependent Notch activity in the endothelium couples vessel growth and quiescence to organ-specific paracrine outputs that instruct the behavior of neighboring parenchymal, stromal and immune cells; this angiocrine dimension of endothelial Notch biology has been comparatively underemphasized in the atherosclerosis literature relative to its established roles in vascular morphogenesis and is discussed further below [7]. Germline studies in mice have shown that Notch pathway components are essential for cardiac valve and outflow tract morphogenesis [8]. Because Notch signaling depends on direct membrane contact between a receptor-bearing cell and a ligand-bearing neighbor, it is uniquely suited to encode the local, cell-to-cell information exchange that governs the heterocellular architecture of the artery wall—an architecture that is fundamentally disrupted in atherosclerosis.

Human genetics provides some of the strongest evidence that dysregulated Notch signaling produces overt disease phenotypes. Somatic activating mutations in NOTCH1 are found in more than half of human T-cell acute lymphoblastic leukemias [9], establishing the general principle that quantitative dysregulation of Notch signal strength, and not merely its presence or absence, can be pathogenic. In the cardiovascular system specifically, heterozygous loss-of-function NOTCH1 mutations cause a spectrum of developmental aortic valve anomalies together with severe, adult-onset valve calcification in autosomal-dominant human pedigrees [10], dominant cysteine-altering mutations in NOTCH3 cause cerebral autosomal-dominant arteriopathy with subcortical infarcts and leukoencephalopathy (CADASIL), a stroke- and dementia-causing small-vessel disease [11], and mutations in the ligand JAG1 cause Alagille syndrome, a multisystem disorder with prominent cardiovascular involvement [12]. Consistent with these human phenotypes, genetic studies in mice show that Notch3 is required for arterial identity and postnatal maturation of VSMCs [13], and that the ligand DLL4 is dosage-sensitive during artery development,

such that even heterozygous loss causes embryonic vascular defects and lethality [14,15]; a broader survey of Notch pathway mutants confirmed that haploinsufficiency at several nodes of the pathway produces arteriovenous malformations [16]. These monogenic and developmental phenotypes demonstrate unambiguously that Notch dosage is critical for the structural integrity of arteries.

Over the past two decades, an expanding body of experimental work has shown that Notch signaling is also reactivated, in a receptor- and context-dependent manner, in the adult atherosclerotic vessel wall [17,18]. Somewhat counterintuitively, activation of the same core pathway can be atheroprotective when engaged by NOTCH1 in endothelial cells exposed to high, unidirectional shear stress, and atherogenic when engaged by JAG1–NOTCH4 or DLL4 in endothelial cells exposed to low, oscillatory shear stress, or when engaged in monocyte-derived macrophages and VSMCs [19]. This activation of the pathway in atherosclerosis is not merely inferred from review-level synthesis: direct primary evidence includes immunohistochemical demonstration of Notch pathway component upregulation in luminal endothelium overlying human and murine atherosclerotic lesions, and colocalization of activated Notch1 with CD68+ macrophages that is further increased in human vulnerable plaques, findings that have been extended by macrophage-specific genetic loss-of-function studies confirming a causal, pro-atherogenic role for Notch1 activation in this compartment [20]. This apparent paradox—the same pathway acting as both a guardian and a driver of vascular disease—is the central challenge that any Notch-directed therapeutic strategy for atherosclerosis must resolve. In this review, we first summarize the molecular logic of canonical and non-canonical Notch signaling, then examine its roles in the principal cellular participants in atherogenesis, and finally evaluate the pharmacological and biological strategies currently available, or in development, to modulate Notch signaling for the treatment of atherosclerosis, including a critical discussion of the cardiovascular safety signals that have emerged from clinical experience with Notch inhibitors developed for oncology indications.

2. Molecular Architecture of the Notch Signaling Pathway

2.1. Canonical Notch Signaling

Mammals express four Notch receptors (NOTCH1–4) and five canonical ligands of the DSL (Delta/Serrate/Lag-2) family: Delta-like ligand 1, 3 and 4 (DLL1, DLL3, DLL4) and Jagged1 and Jagged2 (JAG1, JAG2) [4,5]. Both receptors and ligands are type I single-pass transmembrane proteins, so that productive signaling requires direct contact between the signal-sending and signal-receiving cell. Following synthesis, the Notch receptor is cleaved once in the trans-Golgi network by a furin-like convertase (S1 cleavage), yielding a heterodimeric receptor displayed at the plasma membrane. Engagement of a ligand on a neighboring cell exerts a mechanical pulling force on the receptor extracellular domain, unmasking a negative regulatory region and permitting a second cleavage (S2) by an ADAM-family metalloprotease. This step generates a membrane-tethered stub that is then subjected to intramembrane proteolysis (S3 cleavage) by the γ-secretase complex, releasing the Notch intracellular domain (NICD) into the cytoplasm [5]. The NICD translocates to the nucleus, where it associates with the DNA-binding protein RBP-J (also known as CSL or CBF1), displacing a co-repressor complex and recruiting the coactivator Mastermind to activate transcription of target genes, most notably the basic helix–loop–helix repressors of the Hes and Hey families [5]. Consistent with the importance of tightly regulated proteolytic release of the NICD, mice doubly deficient for the Notch target genes Hey1 and Hey2 develop severe congenital cardiac defects due to impaired epithelial-to-mesenchymal transition during valve formation [21]. Because ligand-induced receptor cleavage is essentially irreversible and each Notch molecule signals only once, the pathway

https://doi.org/10.3390/cells15161463

lacks the second-messenger amplification typical of many other signaling systems; instead, signal strength and duration are encoded by the number of productive receptor–ligand engagements, the local concentration and glycosylation state of ligands, and the specific receptor–ligand pairing, all of which can differ markedly between vascular cell types and hemodynamic environments.

2.2. Non-Canonical Notch Signaling and Ligand-Dependent Bias

In addition to the canonical RBP-J-dependent pathway, Notch receptors and ligands participate in non-canonical, transcription-independent signaling events. Membrane-tethered NOTCH1 fragments generated by S2 cleavage can associate with adherens junction components, including VE-cadherin and the Rho-GEF Trio, to regulate junctional stability independently of NICD release and nuclear signaling [22]. Ligands, too, can act outside the canonical receptor-activation cascade: Jagged1 has recently been shown to function as a Notch-independent mechanotransducer, engaging VEGFR2/ERK signaling through Src-dependent mechanisms in endothelial cells exposed to fluid shear stress, in a manner that does not require canonical Notch cleavage [23]. Furthermore, ligands presented in cis (on the same cell as the receptor) generally inhibit rather than activate Notch signaling in trans, a phenomenon termed cis-inhibition, which allows a single cell that co-expresses both a Notch receptor and a Notch ligand to modulate its own responsiveness to signals from neighboring cells. In practical terms, this means that a ligand molecule engages Notch receptors productively only when it is presented by a neighboring cell (in trans); when the same ligand is instead expressed on the surface of the receptor-bearing cell itself (in cis), it binds and sequesters the receptor without triggering the proteolytic activation cascade, thereby acting as a competitive brake rather than an activator. Because most vascular cells co-express several Notch receptors and ligands simultaneously, the net signaling output of any given cell is therefore not simply set by which ligands and receptors are present, but by the balance between cis-inhibitory and trans-activating interactions, a property that allows cells to sharpen boundaries between distinct signaling states and that adds a further, receptor-intrinsic layer of context-dependence to Notch outputs in the vessel wall. Mechanistically, this asymmetry arises because trans-activation and cis-inhibition rely on different physical requirements for productive receptor engagement. Trans-activation depends on the mechanical pulling force generated when a ligand anchored to the plasma membrane of a neighboring cell is endocytosed together with the bound Notch ectodomain, a tugging step that is only possible across a cell–cell junction and that mechanically exposes the S2 cleavage site to ADAM-family proteases; a ligand and receptor confined to the same cell membrane cannot generate this trans-cellular pulling force. Instead, single-cell imaging and mathematical modeling of the Notch-Delta system have shown that co-expressed receptor and ligand on one cell rapidly form a stable, mutually inactivating cis-complex that sequesters both molecules away from the pool available for productive trans-engagement, so that cis-pairing acts as a fast, cell-autonomous “off-switch” that effectively titrates a cell’s own Notch responsiveness rather than triggering its proteolytic activation cascade [24]. These non-canonical and cis-regulatory features substantially expand the combinatorial repertoire of the Notch system and help explain why manipulating a single receptor or ligand can produce markedly different, sometimes opposite, phenotypes depending on the cellular and mechanical context.

2.3. Post-Translational Regulation: Glycosylation and Ligand Affinity Tuning

The affinity and outcome of a given Notch receptor–ligand interaction is further tuned by glycosylation of the receptor extracellular domain. Fringe family glycosyltransferases add N-acetylglucosamine residues to O-fucose modifications on specific epidermal growth

factor-like repeats of the Notch ectodomain; mass-spectrometric mapping has shown that modification at distinct repeats potentiates Delta-like ligand binding while simultaneously inhibiting Jagged1-induced activation of the same receptor [25]. Of the three mammalian Fringe paralogues, Lunatic Fringe exerts a dominant effect over Manic and Radical Fringe on NOTCH1 signaling output, such that the relative expression of Lunatic Fringe in a given vascular cell can determine whether that cell preferentially responds to Delta-like or Jagged ligands [26]. This Fringe-dependent switch in ligand preference was first established mechanistically by Benedito and colleagues, who showed in the developing retinal vasculature that Jagged1 is a comparatively weak NOTCH1 agonist that behaves as a potent, Fringe-modulated proangiogenic antagonist of Dll4-Notch signaling, so that the balance between these two ligands, rather than the presence of either alone, dictates tip- versus stalk-cell selection and vascular sprouting; this same Fringe-gated Dll4/Jagged1 antagonism is directly relevant to the differential, sometimes opposing, roles of these two ligands in the endothelium of the atherosclerotic vessel wall discussed in Section 3.1 [27]. Because vascular cells differentially express Fringe enzymes depending on developmental stage, flow environment and disease state, the glycosylation status of the endothelial or smooth muscle Notch receptor pool represents an additional, cell-intrinsic layer of regulation that can bias the outcome of ligand engagement without any change in the absolute abundance of either ligand class. The three Fringe paralogues show distinct, non-redundant expression patterns across the vessel wall. Manic Fringe is constitutively expressed by vascular endothelial cells of arteries, veins and capillaries and is further upregulated in pathologically remodeling, hyperangiogenic endothelium, where its loss impairs endothelial proliferation, migration and sprouting, indicating a specific endothelial requirement for this paralogue [28]. Radical Fringe, in contrast, is comparatively enriched in mural cells, and its expression rises markedly in senescent human pericytes, where it modulates the glycosylation, turnover and signaling output of NOTCH3, including of the CADASIL-associated NOTCH3 mutant proteins that accumulate in degenerating vascular smooth muscle and pericytes, pointing to an age- and mural cell-specific role for this paralogue that is distinct from Manic Fringe's endothelial function [29]. This glycosylation-based bias mechanism is not yet well characterized in the atherosclerotic vessel wall specifically, but by analogy with its role in other tissues, it offers a further, largely unexploited, layer at which pharmacological or gene-based intervention could in principle be used to favor atheroprotective over atherogenic Notch signaling outputs. Notch pathway components relevant to vascular biology and atherosclerosis are summarized in Table 1.

Table 1. Core Notch pathway components relevant to vascular biology and atherosclerosis.

Component	Type	Predominant Vascular Expression	Role in Atherosclerosis-Relevant Vascular Biology
NOTCH1	Receptor	Arterial endothelium; VSMC	Mechanosensor; atheroprotective under laminar shear stress; drives VSMC dedifferentiation when aberrantly activated [30]
NOTCH2	Receptor	Endothelial cells	Downregulated by TNF-α/IL-1β; contributes to endothelial dysfunction [31]
NOTCH3	Receptor	VSMC/pericytes	Required for arterial mural cell differentiation and survival; mutated in CADASIL; mediates osteogenic transdifferentiation [11,13,32,33]

https://doi.org/10.3390/cells15161463

Table 1. *Cont.*

Component	Type	Predominant Vascular Expression	Role in Atherosclerosis-Relevant Vascular Biology
NOTCH4	Receptor	Endothelial cells	Paired with JAG1 at low-oscillatory-shear, atherosusceptible sites; pro-atherogenic; also supports endothelial quiescence when intact [34,35]
JAG1	Ligand	Endothelium; antigen-presenting cells; mural cells	Cis-inhibits NOTCH1; trans-activates NOTCH4; promotes leukocyte recruitment; non-canonical VEGFR2/ERK mechanotransducer; maintains NOTCH3 in mural cells [23,34,36,37]
JAG2	Ligand	Endothelium; VSMC	Developmental vascular roles; less well characterized in adult atherosclerosis
DLL1	Ligand	Endothelium; antigen-presenting cells	Promotes pro-inflammatory (Th1/Th17) T-cell differentiation [38,39]
DLL4	Ligand	Arterial/tip endothelial cells; macrophages	Upregulated by IL-1β, TNF-α, hyperlipidemia; drives macrophage M1-like polarization and suppresses M2-like; target of anti-DLL4 antibodies [40–44]
RBP-J (CSL/CBF1)	Transcription factor	Ubiquitous	Canonical nuclear effector of NICD; induces IRF8-dependent M1-like macrophage program; also supports selected M2-like genes [45–48]
HES1/HES5, HEY1/HEY2	Target genes	Endothelium; VSMC; valve interstitial cells	Downstream effectors of NICD–RBP-J; repress contractile/osteogenic genes; Hey1/Hey2 required for valve EMT [21,49]
γ-Secretase complex	Protease complex	Ubiquitous	Catalyzes S3 cleavage releasing NICD from all Notch receptors; principal target of GSIs (e.g., DAPT) [5,50,51]

3. Notch Signaling in the Principal Cell Types of the Atherosclerotic Vessel Wall

3.1. Endothelial Cells: A Mechanosensitive Switch Between Atheroprotection and Atherogenesis

The endothelium is the first vascular compartment to sense hemodynamic forces, and atherosclerotic lesions form preferentially at arterial branch points and curvatures where blood flow is disturbed and oscillatory, rather than in regions of high, unidirectional laminar shear stress [30]. Endothelial NOTCH1 behaves as a bona fide mechanosensor: canonical NOTCH1 activity scales with the magnitude of fluid shear stress, is required for the maintenance of endothelial junctional integrity, cell elongation and suppression of proliferation under laminar flow, and its endothelial-specific deletion increases hypercholesterolemia-induced atherosclerosis in the murine aorta, establishing NOTCH1 as atheroprotective in this context [30]. Mechanistically, NOTCH1 mechanotransduction appears to combine a ligand-dependent and a ligand-independent component rather than acting as a purely intrinsic force sensor. On one hand, comparison of blood and lymphatic endothelial cells that express comparable levels of NOTCH1, DLL4, JAG1 and VE-cadherin showed that laminar shear stress activates NOTCH1 proteolysis only in the blood vascular subtype, indicating that flow-responsive activation is not explained simply by receptor-ligand co-expression but requires a cell type-specific configuration of the DLL4-NOTCH1 complex at the junction, consistent with force-dependent unmasking of the ADAM10 cleavage site

during ligand engagement under flow. On the other hand, shear stress also engages the mechanosensitive ion channel Piezo1, and the resulting calcium influx increases ADAM10 activity, providing a second, receptor-extrinsic route by which mechanical force can amplify NOTCH1 proteolysis independently of any single ligand; downstream, the liberated NOTCH1 intracellular domain associates with VE-cadherin to stabilize adherens junctions, linking the mechanosensing step directly to the junctional-integrity phenotype described above. NOTCH1 is therefore best understood as a mechanosensor whose activation is jointly gated by flow-dependent ligand engagement and by a parallel, ADAM10-sensitizing Piezo1-calcium axis, rather than by either mechanism alone [52]. Complementary human tissue data support this conclusion: NOTCH1 is constitutively expressed at high levels in adult arterial endothelium relative to smooth muscle, and its expression and downstream signaling are markedly suppressed by a high-fat diet and by circulating inflammatory lipids, an effect that antagonizes endothelial activation, so that mice with only one functional Notch1 allele in the endothelium develop more extensive diet-induced atherosclerosis [53]. The suppression of endothelial NOTCH1 by hyperlipidemia is not merely a correlative diet effect but reflects a direct, ligand-independent transcriptional mechanism: specific oxidized phospholipid species that accumulate under high-fat feeding rapidly repress NOTCH1 and JAG1 expression through activation of the transcription factor STAT3, and this Notch suppression is reversed when circulating cholesterol is lowered, indicating that circulating oxidized lipids actively silence the atheroprotective Notch1 axis rather than NOTCH1 loss being a secondary consequence of established atherosclerosis [53]. More broadly, native atherosusceptible and atheroresistant regions of the arterial tree show reproducible differences in endothelial gene expression and phenotype that mirror the effects of disturbed versus laminar shear stress applied experimentally, and Notch pathway genes feature prominently among the flow-responsive transcripts that distinguish these regions [54,55].

In striking contrast to this atheroprotective role of NOTCH1, the ligand JAG1 together with the receptor NOTCH4 is preferentially expressed at atherosusceptible sites exposed to low, oscillatory shear stress, and endothelial-specific deletion of Jag1 reduces atherosclerotic lesion burden at these sites in murine and porcine arteries, indicating that JAG1–NOTCH4 signaling is pro-atherogenic [34]. Single-cell transcriptomic analysis of Jag1-deficient endothelium suggests that JAG1 suppresses reparative, proliferative and migratory endothelial subsets that would otherwise counteract disturbed-flow-induced dysfunction, providing a plausible mechanism for the pro-atherogenic action of this ligand [34]. Mechanistically, this reflects a shift in endothelial cell-state composition rather than a uniform toxic effect on all endothelial cells: JAG1-NOTCH4 signaling represses a specific transcriptional program associated with proliferation, migration and repair, so that in its absence disturbed-flow endothelium is enriched for these reparative subsets, whereas active JAG1-NOTCH4 signaling depletes them and leaves the endothelium dominated by cell states that are less able to counteract flow-induced injury, adhesion-molecule induction and barrier dysfunction; this loss of reparative capacity, rather than a direct pro-inflammatory transcriptional program analogous to that driven by NOTCH1, is proposed as the principal mechanism by which JAG1-NOTCH4 signaling enhances atherosclerosis susceptibility at sites of disturbed flow [34]. Complementary zebrafish experiments show that the absence of blood flow itself upregulates the ligand Dll4 in the developing vasculature, indicating that flow tonically suppresses certain Notch ligands in vivo and that loss of flow, as occurs at recirculating or stagnant sites in diseased arteries, could remove this brake [56]. Because JAG1 can act as a cis-inhibitor of NOTCH1—that is, it can bind and neutralize NOTCH1 when the two are expressed on the same endothelial cell, rather than activating it as it would from a neighboring cell—elevated JAG1 expression at disturbed-flow regions may simultaneously suppress atheroprotective NOTCH1 signaling while engaging the distinct,

atherogenic NOTCH4 receptor pool, offering one explanation for how the same pathway components can produce opposite regional outcomes within a single vessel [23].

Independent of its role as a mechanosensor, Notch signaling regulates several features of endothelial dysfunction that are central to atherogenesis. Enforced NOTCH1 activation—achieved experimentally by overexpressing the constitutively active Notch1 intracellular domain, the same gain-of-function approach used in the analogous tumor-endothelium studies discussed above—in cultured and in vivo endothelium upregulates pro-inflammatory cytokines (IL-6, IL-8, IL-1α), induces a senescent phenotype, and correlates with coronary artery disease risk in genotyped patient cohorts, while Notch pathway components are selectively upregulated in the luminal endothelium overlying atherosclerotic lesions in both mouse and human aortas [57]. Inflammatory stimuli such as TNF-α and IL-1β further dysregulate endothelial Notch signaling, in particular by downregulating NOTCH2 and NOTCH4, contributing to endothelial barrier dysfunction and adhesion molecule expression [31]. Endothelial Jagged1–RBP-J signaling has also been shown to promote recruitment of inflammatory leukocytes to the vessel wall and to exacerbate atherosclerosis in mouse models [36], and in a rat cardiac allograft model of transplant arteriosclerosis, TNF-mediated downregulation of Notch4 impaired endothelial quiescence and provoked endothelial cell activation and apoptosis, an effect that could be reproduced by direct Notch4 silencing and that was linked mechanistically to loss of RBP-J-dependent survival signaling [35,58]. Conversely, forced activation of a Notch1–Jagged1 autocrine circuit in cultured endothelial cells is sufficient to induce VCAM1 expression on its own and to amplify IL-1β-driven VCAM1 induction, directly linking Notch1 gain-of-function to a classical adhesion-molecule readout of endothelial activation [59]. The pathophysiological consequences of this circuit are illustrated most completely outside the atherosclerosis literature itself, in tumor endothelium, where sustained Notch1 intracellular domain activity induces a senescence-like endothelial phenotype together with VCAM1 upregulation, thereby promoting neutrophil infiltration and leukocyte–endothelial adhesion; because tumor-associated endothelial Notch1 activation, VCAM1 induction and senescence recapitulate the same triad implicated in atherosclerotic endothelial dysfunction, this work provides an important, complementary mechanistic precedent for the role of endothelial Notch1 gain-of-function in driving vascular inflammation and leukocyte recruitment within the plaque [60]. Endothelial microRNA regulation adds a further layer to this network: shear-responsive miR-126-5p maintains endothelial proliferative reserve by suppressing the non-canonical Notch1 inhibitor Dlk1, and mice lacking miR-126-5p show reduced endothelial Notch1 activation and exacerbated atherosclerotic lesion formation, whereas restoring miR-126-5p reduces lesion size, illustrating a distinct, atheroprotective arm of endothelial Notch1 signaling operating through de-repression by a flow-sensitive microRNA [61]. Beyond atherosclerosis proper, endothelial NOTCH1 is required for normal postnatal angiogenesis and ischemia-induced neovascularization [62], and its proteolytic activation in this setting is promoted by the cysteine protease cathepsin K, which increases NICD generation and downstream Hes/Hey target gene expression in ischemic tissue, again illustrating that the same receptor supports reparative vascular functions in some contexts even as its dysregulation promotes disease in others [63]. Beyond its role in shaping lesion-related inflammation and remodeling, Notch signaling also plays an active, ongoing role in maintaining the quiescence of the established, non-diseased vasculature, a function that is directly relevant to the safety of pharmacological Notch inhibition discussed in Section 5. Genetic or antibody-mediated inhibition of endothelial Notch signaling in the adult heart impairs endothelial fatty acid transport and provokes pathological angiogenesis, metabolic remodeling and heart failure, demonstrating that tonic Notch activity is required to actively restrain angiogenesis and preserve normal cardiac vascular and

https://doi.org/10.3390/cells15161463

metabolic homeostasis rather than being dispensable outside disease states [64]. Consistent with this quiescence-maintaining function, forced endothelial expression of constitutively active Notch4 is sufficient to produce arteriovenous malformations in multiple organs, including the liver, uterus and skin, a phenotype that regresses upon withdrawal of the activating stimulus, underscoring that the adult vasculature depends on continuously balanced, rather than simply present or absent, Notch signaling to maintain normal vessel architecture [65].

3.2. Vascular Smooth Muscle Cells: NOTCH3 and the Contractile-to-Synthetic Phenotypic Switch

Among the four Notch receptors, NOTCH3 shows the most restricted and abundant expression in adult vascular smooth muscle, where it is required for normal arterial mural cell differentiation, postnatal maturation and survival [13]. The physiological importance of NOTCH3 in VSMCs is illustrated most dramatically by CADASIL, in which stereotyped cysteine-altering NOTCH3 mutations cause pathological accumulation of the receptor extracellular domain around degenerating smooth muscle cells of small cerebral arteries [32], a process that has been reproduced in transgenic mice expressing mutant NOTCH3 and that recapitulates the granular osmiophilic material and progressive arteriopathy seen in patients [66]. Although CADASIL is a disease of small cerebral arterioles rather than of large-vessel atherosclerosis, it provides unambiguous proof-of-principle that dysregulated NOTCH3 signaling, whether through gain- or loss-of-function mechanisms, is sufficient to produce a severe occlusive arteriopathy in humans. Under physiological conditions, NOTCH3 expression in mural cells is itself maintained by an autoregulatory loop that requires endothelial-expressed JAG1, coupling the endothelial and smooth muscle compartments of the vessel wall [37], and reciprocal signaling through JAG1 promotes NOTCH3-dependent contractile differentiation of human coronary artery smooth muscle cells in three-dimensional coculture systems [67,68], underscoring that VSMC phenotype in the mature vessel wall is actively maintained by ongoing paracrine Notch signaling from the overlying endothelium rather than being fixed during development alone. In keeping with this, global loss of Notch3 is further associated with defective angiogenesis and impaired mural cell investment of new vessels [69], broadening the phenotypic consequences of NOTCH3 loss beyond large-vessel structural integrity to microvascular remodeling more generally.

In the context of atherosclerosis and neointimal remodeling, Notch signaling—engaged through NOTCH1 as well as NOTCH3—drives the transition of VSMCs from a quiescent, contractile phenotype toward a proliferative, synthetic and migratory phenotype. Pharmacological inhibition of γ-secretase with the compound DAPT restores expression of contractile marker genes, suppresses VSMC proliferation, and reduces intimal hyperplasia in a rat vein-graft model of restenosis [50], and, in models of diabetic microangiopathy, dysregulated Jagged1–Notch1 signaling has similarly been linked to abnormal, dysfunctional neovascularization and delayed angiogenic repair [70]. These findings position Notch signaling as a convergence point for multiple drivers of vascular remodeling, spanning mechanical injury, restenosis and metabolic disease.

Notch signaling additionally participates in the osteogenic trans-differentiation of VSMCs that underlies vascular calcification, a hallmark of advanced atherosclerotic plaques and an independent predictor of cardiovascular events. Direct activation of Notch signaling in human aortic smooth muscle cells induces the osteogenic master regulator Msx2 and subsequent alkaline phosphatase activity and matrix mineralization in a manner dependent on Notch–RBP-J signaling [49], and Notch3 activation downstream of hepatocyte growth factor/c-Met signaling similarly promotes VSMC osteogenic differentiation in vitro [33]. microRNA-34a, whose expression rises with vascular aging and in response to

atherogenic and uremic stimuli, promotes VSMC senescence and a senescence-associated secretory phenotype by downregulating SIRT1, and this senescence program favors the osteochondrogenic transdifferentiation of VSMCs and medial calcification [71]; mechanistically, miR-34a has been shown to promote calcification specifically through downregulation of SIRT1 and the receptor tyrosine kinase Axl [72]. A parallel, valve-specific literature shows that Notch1 normally represses osteogenic gene programs in aortic valve interstitial cells [73], that mice haploinsufficient for the Notch effector RBPJK develop diet-induced calcific aortic valve disease with macrophage infiltration and pro-osteogenic signaling [74], that a disease-associated Notch1 mutation promotes valvular calcification through enhanced myofibroblast mechanotransduction [75], and that pharmacological targeting of the mechanosensitive protein cadherin-11 can prevent Notch1-mediated calcific aortic valve disease in animal models [76]—collectively illustrating a coherent, receptor-specific link between disrupted Notch signaling, altered mechanotransduction and ectopic osteogenic differentiation that spans both the valvular and arterial vasculature.

3.3. Macrophages and the Innate Immune Response

Monocyte-derived macrophages are the dominant immune cell population within atherosclerotic plaques, where they take up modified lipoproteins to become foam cells, secrete pro-inflammatory mediators, and, in advanced lesions, undergo apoptosis and defective efferocytosis to form the necrotic lipid core that predisposes to plaque rupture [1]. Notch signaling was first shown to be functionally upregulated following macrophage activation, where it modulates gene expression programs relevant to antigen presentation and cytotoxic activity [45], and canonical Notch–RBP-J signaling has subsequently been shown to amplify Toll-like receptor 4 (TLR4)-induced expression of classically activated, pro-inflammatory M1-like macrophage genes by controlling translation of the transcription factor IRF8 [46]. Consistent with a pro-inflammatory, M1-like-promoting role, forced Notch intracellular domain expression in macrophages upregulates M1-like-associated genes and increases tumor cell cytotoxicity in antitumor immune models [77], whereas myeloid-specific disruption of RBP-J favors an alternatively activated, M2-like phenotype in models of chitin-induced M2-like polarization [47], although RBP-J also supports selected components of the M2-like transcriptional program in the liver, where its myeloid-specific loss ameliorates hepatic fibrosis by attenuating inflammation [48]—indicating that the relationship between Notch signaling and macrophage polarity is more nuanced than a simple M1-like/M2-like binary switch.

In the specific setting of vascular and metabolic disease, endothelial-derived Delta-like ligand 4 was among the first Notch ligands shown to directly induce Notch signaling in macrophages with pro-inflammatory consequences [40], and subsequent work demonstrated that a high-fat, high-cholesterol diet increases Dll4 expression in atheromata and that systemic blockade of Dll4 with a neutralizing antibody attenuates both atherosclerotic lesion formation and the associated metabolic derangements in hyperlipidemic mice, an effect attributed at least in part to reduced macrophage-driven inflammation [41]. Macrophage-derived Dll4 has similarly been shown to promote lesion development in a vein-graft model relevant to bypass graft failure [78], and, at the cellular level, Dll4 signaling through Notch1 selectively impairs the differentiation of blood monocytes into anti-inflammatory M2-like macrophages while promoting their apoptosis, without affecting M1-like differentiation, providing a mechanistic basis for how a single ligand can simultaneously favor pro-inflammatory macrophage programs and actively deplete the reparative, inflammation-resolving macrophage pool within the plaque [42]. At the level of cellular metabolism, Notch signaling has also been shown to reprogram macrophage mitochondrial function toward a pro-inflammatory bioenergetic profile, providing a further, metabolic layer through

https://doi.org/10.3390/cells15161463

which Notch sustains the M1-like phenotype through a specific, dual mechanism rather than a generic metabolic shift: the Notch1 intracellular domain is recruited directly to nuclear and mitochondrial genes encoding respiratory chain components, increasing mitochondrial oxidative phosphorylation, while, in parallel, Notch-dependent induction of pyruvate dehydrogenase phosphatase 1 raises pyruvate dehydrogenase activity and glucose flux into the tricarboxylic acid cycle; the resulting increase in oxidative flux elevates mitochondrial reactive oxygen species (mtROS) production, and this mtROS signal feeds back to reinforce transcriptional induction of the same pro-inflammatory gene program, so that Notch couples a transcriptional and a bioenergetic arm into a single, self-amplifying circuit that sustains macrophage activation [79].

Beyond the innate compartment, Notch ligands presented by antigen-presenting cells within the plaque shape adaptive immunity. In a foundational study, Delta-family ligands were shown to instruct CD4+ T cells toward the Th1 fate, whereas Jagged-family ligands instruct the alternate Th2 fate, establishing that ligand identity, rather than Notch activation as such, dictates the polarity of the adaptive immune response [38]. It should be noted that this foundational Th1/Th2 finding, like most of the T-cell Notch ligand studies discussed in this section, was established in general immunological or autoimmune disease models rather than in atherosclerosis itself; its relevance to the vessel wall is therefore inferred rather than directly demonstrated. Within atherosclerosis specifically, Th1 polarization is comparatively well established as pro-atherogenic, since interferon-γ-producing Th1 cells and their inducing cytokines aggravate lesion development and plaque instability in multiple loss- and gain-of-function mouse studies, whereas the role of Th2 cells is considerably more controversial, with murine loss-of-function studies for Th2 cytokines yielding inconsistent atheroprotective, neutral or even pro-atherogenic effects depending on the specific cytokine, disease stage and genetic background examined, in contrast to the comparatively consistent picture for Th1 and regulatory T cells [80]. Given this uncertainty, a Delta-family ligand bias that favors Th1 responses would be predicted to be net pro-atherogenic on adaptive-immune grounds, whereas the vascular consequence of a Jagged-family, Th2-skewing bias remains genuinely unresolved and represents an important open question for translating this ligand-specific logic to atherosclerosis. Building on this ligand-specific logic, Notch signaling has subsequently been shown to be required for optimal Th17 differentiation in both mouse and human T cells, with pharmacological Notch blockade ameliorating experimental autoimmune encephalomyelitis, a Th17-dependent inflammatory disease model relevant to chronic vascular inflammation [39]; consistent with the earlier Th1/Th2 paradigm, Jagged1 and Delta1 were further shown to differentially regulate the severity and outcome of this same autoimmune model, with blockade of Jagged1 worsening and blockade of Delta1 improving disease [81]. Notch signaling is not confined to effector T-cell subsets: cell-intrinsic Notch activity in regulatory T cells is required for peripheral immune tolerance, and its disruption in Tregs precipitates spontaneous autoimmune and inflammatory pathology in mice [82], suggesting that the balance of Notch ligands available within the atherosclerotic plaque microenvironment may simultaneously shape effector T-cell polarization and the counter-regulatory activity of Tregs that normally restrains plaque inflammation. Notch signaling mechanisms are depicted on Figure 1.

https://doi.org/10.3390/cells15161463

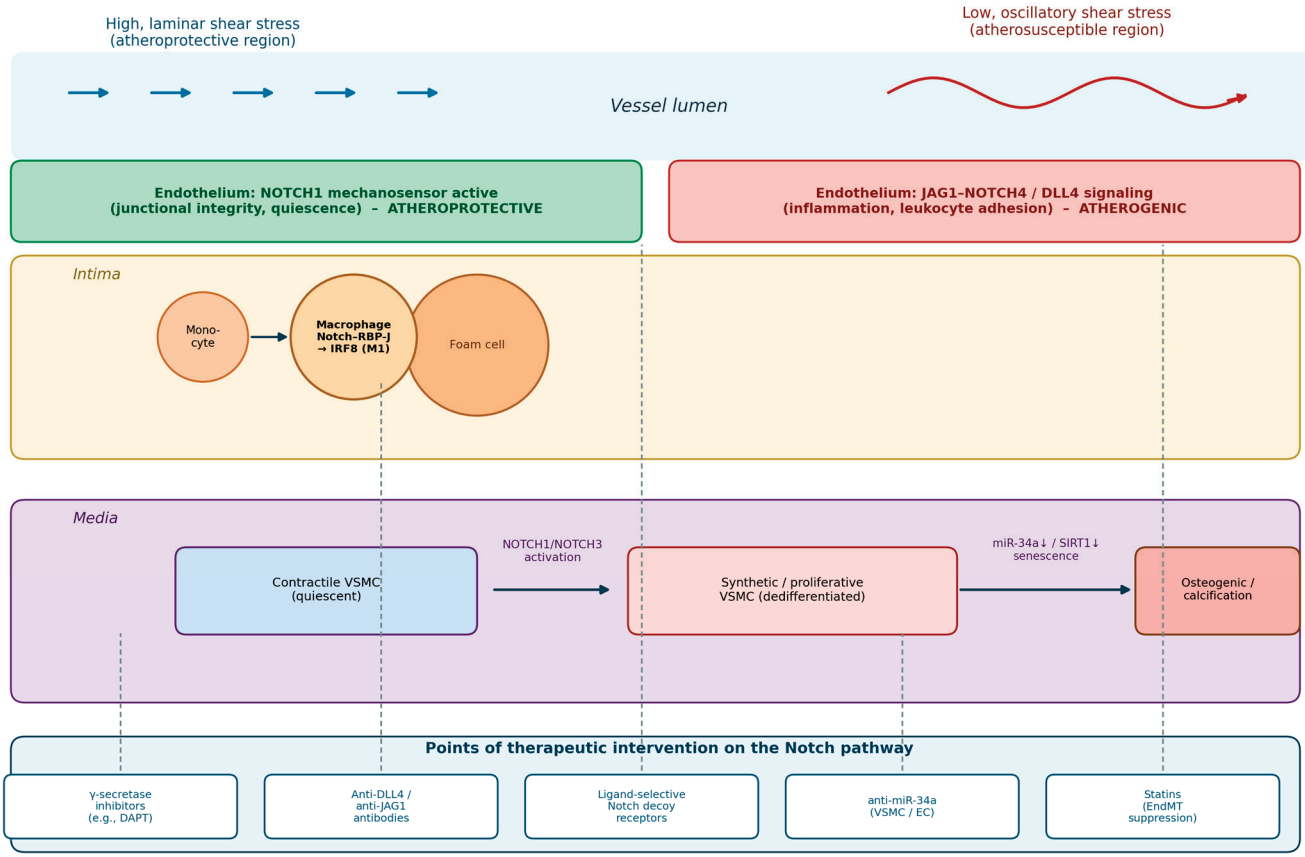


Figure 1. Schematic overview of Notch signaling across the atherosclerotic vessel wall. At sites of high, laminar shear stress, endothelial NOTCH1 preserves junctional integrity and quiescence (atheroprotective, green). At sites of low, oscillatory shear stress, endothelial JAG1–NOTCH4/DLL4 signaling promotes leukocyte adhesion and recruitment (atherogenic, red). Recruited monocytes differentiate into macrophages in which Notch–RBP-J signaling promotes M1-like polarization and foam cell formation. In the media, NOTCH1/NOTCH3 signaling drives the transition of vascular smooth muscle cells (VSMC) from a contractile to a synthetic, proliferative phenotype, and chronic signaling together with miR-34a/SIRT1 dysregulation promotes osteogenic transdifferentiation and calcification. The lower panel indicates the principal points at which pharmacological strategies discussed in Section 5 intersect the pathway: γ-secretase inhibitors, anti-DLL4/anti-JAG1 antibodies, ligand-selective Notch decoy receptors, anti-miR-34a oligonucleotides, and statins acting via suppression of endothelial-to-mesenchymal transition (EndMT).

3.4. In Vivo Evidence: Effects of Experimental Notch Manipulation on Atherosclerosis Development

The cell type-specific findings summarized above are drawn from experiments that differ substantially in genetic strategy, species, vascular bed and outcome measure, which can make the net direction of any given manipulation difficult to extract from prose alone. Table 2 therefore consolidates, in one place, the principal in vivo genetic and pharmacological Notch manipulations that have been directly tested in experimental models of atherosclerosis or closely related vascular remodeling, together with their reported effect on lesion or plaque phenotype. As the table illustrates, the direction of effect tracks receptor and cell-type identity rather than simply reflecting "more" or "less" Notch signaling in the vessel as a whole: loss of endothelial NOTCH1 is consistently pro-atherogenic [30,53], whereas loss of endothelial JAG1 [34], blockade of DLL4 [41], or macrophage-restricted loss of NOTCH1 [20] are each atheroprotective, and non-selective pharmacological suppression of the entire pathway with γ-secretase inhibitors is net atheroprotective in the models tested to date [50,51,83], likely because the pro-atherogenic, disturbed-flow-restricted

JAG1–NOTCH4 and macrophage arms of the pathway dominate the aggregate outcome under the conditions examined. This consolidated view reinforces the central argument of this review, developed in Section 4 below, that "the Notch pathway" cannot be treated as a single therapeutic target in atherosclerosis.

Table 2. In vivo effects of experimental Notch pathway manipulation on atherosclerosis and related vascular remodeling.

Manipulation	Model/System	Effect on Atherosclerosis/Lesion Phenotype	Ref.
Endothelial-specific Notch1 deletion or haploinsufficiency	ApoE−/− or hypercholesterolemic mice	Significantly increased lesion burden in the descending aorta and aortic sinus; loss of junctional integrity and increased endothelial proliferation at disturbed-flow sites	[30,53]
Endothelial-specific Jag1 deletion	Murine and porcine arteries	Significantly reduced lesion burden specifically at low-oscillatory-shear, atherosusceptible sites, with no effect at protected sites	[34]
Systemic Dll4 neutralizing antibody	Hyperlipidemic LDL receptor-deficient mice	Attenuated atherosclerotic lesion formation together with amelioration of associated metabolic derangements (adipose inflammation, insulin resistance)	[41]
Macrophage-derived Dll4 (loss-of-function)	Murine vein-graft model	Reduced vein-graft lesion development, supporting a pro-atherogenic role for macrophage-derived Dll4 distinct from its endothelial source	[78]
Macrophage-specific Notch1 deletion	Murine atherosclerosis model	Shifted plaque macrophages toward an M2-like anti-inflammatory profile via the PI3K-oxidative stress axis, consistent with reduced lesion inflammation	[20]
Pan-Notch γ-secretase inhibition (systemic GSI)	ApoE−/− mice, diet-induced atherosclerosis	Reduced diet-induced atherosclerotic lesion formation, demonstrating net atheroprotection despite non-selective pathway blockade over the exposure durations tested	[51]
γ-Secretase inhibition with DAPT	Rat vein-graft model of restenosis	Restored contractile marker gene expression, suppressed VSMC proliferation and reduced intimal hyperplasia	[50]
Notch1 inhibition (siRNA or DAPT) combined with induced low shear stress	ApoE−/− mice, carotid shear-stress modifier model	DAPT reduced low-shear-stress-induced plaque formation and ICAM-1 expression via suppression of NF-κB activation, directly linking flow-driven Notch1 induction to lesion formation in vivo	[83]

4. Notch Signaling Across the Stages of Atherosclerotic Plaque Development

The multiplicity of cell-type-specific Notch effects described above can be integrated into a stage-based model of atherogenesis. During lesion initiation, disturbed flow at atherosusceptible sites upregulates endothelial JAG1/NOTCH4 signaling, suppresses atheroprotective NOTCH1 signaling, and increases expression of adhesion molecules and inflammatory cytokines that favor monocyte recruitment [30,34,55]. During lesion progression, infiltrating monocytes differentiate into macrophages whose polarization state is shaped by local Delta-like ligand and Jagged1 availability [40,42,46], while resident and

migrating VSMCs undergo NOTCH1/NOTCH3-dependent dedifferentiation, proliferation and migration into the intima, expanding the fibrous cap and, in some contexts, contributing to its structural reinforcement [49,50]. In advanced lesions, chronic Notch pathway activity intersects with cellular senescence programs, in particular via the miR-34a/SIRT1 axis, to promote osteochondrogenic transdifferentiation of VSMCs and medial or intimal calcification, a feature associated with both plaque stability in some contexts and abrupt clinical events in others [71,72]. Finally, at the level of the fibrous cap and lipid core, ongoing macrophage Notch–RBP-J signaling sustains a pro-inflammatory, M1-like-skewed macrophage phenotype and actively suppresses the reparative M2-like macrophage pool, impeding efferocytosis and lesion resolution and favoring necrotic core expansion and potentially plaque instability [42,46]. This staged view underscores that "the Notch pathway" is not a single therapeutic target in atherosclerosis but rather a family of related signaling modules whose net effect on disease depends critically on which receptor, which ligand, which cell type and which stage of lesion development is being considered.

5. Therapeutic Strategies Targeting the Notch Pathway in Atherosclerosis

Given the pleiotropic, context-dependent roles of Notch signaling in the vessel wall, therapeutic strategies have pursued several distinct levels of intervention: global pharmacological inhibition of the terminal proteolytic step common to all Notch receptors (γ-secretase inhibitors), selective antagonism of individual ligands or receptors using monoclonal antibodies or engineered decoy receptors, indirect modulation through microRNA-based agents, and repurposing of existing cardiovascular drugs, particularly statins, that have off-target effects on Notch-dependent endothelial and smooth muscle phenotypes. Table 1 summarizes the principal molecular components of the pathway relevant to vascular biology, and Table 3 summarizes the therapeutic strategies discussed below together with their stage of development and principal limitations.

Table 3. Notch-targeted therapeutic strategies for atherosclerosis.

Strategy	Representative Agent(s)	Mechanism	Stage of Development	Key Limitations/Safety Signals
Pan-Notch γ-secretase inhibition	DAPT and related GSIs	Blocks S3 cleavage of all four Notch receptors	Preclinical (ApoE−/− mice; vein-graft/restenosis models) [50,51]	Non-selective (additional γ-secretase substrates); gastrointestinal and lymphoid toxicity limit chronic use
Anti-DLL4 monoclonal antibodies	Demcizumab (OMP-21M18)	Blocks DLL4–NOTCH1 ligand engagement	Phase I/Ib oncology trials [43,44,84]	Hypertension, pulmonary hypertension, reversible heart failure with prolonged dosing [85]
Notch2/3-selective antibodies	Tarextumab	Selective receptor antagonism sparing NOTCH1	Phase I/II oncology [86]	Narrower target engagement; chronic cardiovascular safety not established
Ligand-selective decoy receptors	Engineered Notch-Fc decoys (Dll4- or Jagged-selective)	Sequester a specific ligand class without activating the receiving cell	Preclinical (tumor angiogenesis models) [87]	Not yet tested in atherosclerosis models; delivery/PK optimization needed
MicroRNA-based modulation	miR-126-5p mimics; anti-miR-34a oligonucleotides	Restores endothelial Notch1/Dlk1 balance; normalizes Notch3-associated VSMC senescence/calcification	Preclinical (murine atherosclerosis and vascular calcification models) [61,71,72]	Vascular cell-type-specific delivery remains challenging
Drug repurposing	Statins (e.g., simvastatin)	Suppresses EndMT via GGTase–RhoA–YAP–SOX9 axis; activates Notch-dependent endothelial differentiation	Established clinical use; mechanistic Notch/EndMT link described [88,89]	Effect on Notch signaling is indirect and pleiotropic; Notch-specific contribution to clinical benefit unclear

5.1. Gamma-Secretase Inhibitors

γ-Secretase inhibitors (GSIs) such as DAPT block the terminal S3 cleavage step required for release of the NICD from all four Notch receptors, and were originally developed against other targets before being repurposed as pan-Notch inhibitors in oncology and vascular research; indeed, the discovery that activating NOTCH1 mutations drive a majority of T-cell leukemias provided much of the initial rationale for developing GSIs as targeted anticancer agents [9]. In atherosclerosis-relevant models, the GSI DAPT restores contractile gene expression and suppresses VSMC proliferation in a rat vein-graft model of intimal hyperplasia [50]. More directly, systemic administration of a γ-secretase inhibitor reduces diet-induced atherosclerotic lesion formation in apolipoprotein E-deficient mice, providing in vivo evidence that pan-Notch inhibition can be net atheroprotective in this model, at least over the exposure durations tested [51]. It is important to note that the anti-atherosclerotic effect of pan-Notch GSIs cannot be attributed to Notch blockade alone, since γ-secretase constitutively cleaves dozens of other type I transmembrane substrates that are independently relevant to vascular and inflammatory biology, including N- and E-cadherin, whose cleavage disrupts endothelial and smooth muscle cell–cell adhesion; CD44, a receptor implicated in leukocyte adhesion and macrophage foam-cell behavior; the receptor tyrosine kinase ErbB4; and the low-density lipoprotein receptor-related protein (LRP), which participates directly in lipoprotein handling by the vessel wall. Consequently, part of the atheroprotective effect attributed to GSIs in ApoE-deficient mice and vein-graft models may reflect concurrent inhibition of these non-Notch substrates rather than Notch blockade per se, a caveat that is difficult to exclude with pan-Notch inhibitors and that further motivates the shift toward ligand- and receptor-selective strategies discussed below [90]. However, because γ-secretase also cleaves numerous other type I transmembrane substrates besides Notch receptors, and because pan-Notch blockade indiscriminately silences both atheroprotective (NOTCH1) and atherogenic (NOTCH4, JAG1-dependent) signaling, GSIs carry an unfavorable therapeutic index for chronic cardiovascular use; class-wide toxicities related to Notch-dependent differentiation programs in the gut and lymphoid system have also limited their systemic use in oncology, reinforcing that pan-pathway inhibition is unlikely to be an acceptable long-term strategy for a chronic disease such as atherosclerosis.

5.2. Ligand- and Receptor-Directed Monoclonal Antibodies

A more selective approach exploits monoclonal antibodies directed against individual Notch ligands or receptors, an approach extensively developed in oncology to block tumor angiogenesis and cancer stem cell maintenance. Antibodies against Delta-like ligand 4, such as demcizumab, have been evaluated in multiple phase I and phase Ib oncology trials in combination with cytotoxic chemotherapy [43,44]. These trials are informative for cardiovascular pharmacology chiefly because of the adverse events they revealed: dose- and duration-dependent cardiopulmonary toxicity, including grade 3 hypertension, pulmonary hypertension and, in a subset of patients receiving prolonged high-dose therapy, congestive heart failure that was reversible upon drug discontinuation in most cases [44]. A systematic analysis of clinical trials of DLL4-inhibiting antibodies confirmed pulmonary hypertension as a class-associated complication occurring independently of left ventricular dysfunction, implicating disordered angiogenesis and vascular remodeling secondary to sustained DLL4/NOTCH1 blockade in the pulmonary circulation [85]. A parallel phase Ib trial combining demcizumab with paclitaxel in platinum-resistant ovarian cancer similarly documented cardiopulmonary adverse events consistent with this class effect [84]. These findings, while derived from an oncology population receiving substantially higher and more sustained receptor blockade than would likely be used for an atherosclerosis

indication, provide a cautionary, real-world demonstration that pharmacological inhibition of the DLL4–NOTCH axis has a genuine and clinically important cardiovascular liability, and they argue for very careful dose-finding, intermittent dosing schedules, or vascular bed-restricted delivery if anti-DLL4 or anti-Jagged1 antibodies are ever to be considered for atherosclerosis. Antibodies selectively targeting NOTCH2/NOTCH3, such as tarextumab, illustrate ongoing efforts within oncology to narrow the toxicity window of Notch pathway antibodies by sparing NOTCH1, efforts whose lessons are directly transferable to any future cardiovascular development program [86].

5.3. Soluble Decoy Receptors

An alternative antibody-independent strategy uses soluble, Fc-fused fragments of the Notch extracellular domain (Notch decoys) engineered to selectively sequester either Delta-like ligands or Jagged ligands without themselves activating signaling in the responding cell. Because Jagged- and Delta-like ligand-mediated Notch signaling can produce distinct, sometimes opposing, vascular phenotypes, ligand-selective decoys in principle allow one arm of the pathway to be neutralized while sparing the other, a level of selectivity that is difficult to achieve with conventional pan-Notch γ-secretase inhibition [87]. Although this technology has so far been developed principally for tumor angiogenesis, the underlying design principle—selective neutralization of a single ligand class rather than global receptor blockade—is directly applicable to the endothelial JAG1–NOTCH4 axis implicated in atherogenesis at sites of disturbed flow, and represents one of the more mechanistically elegant, if still preclinical, strategies for future cardiovascular development.

5.4. MicroRNA-Based and Epigenetic Strategies

Because several microRNAs sit directly upstream or downstream of Notch pathway components in vascular cells, microRNA mimics or antagomirs offer an indirect route to modulate Notch-dependent phenotypes with potentially greater cell-type selectivity than direct pathway inhibition. Restoring the flow-sensitive microRNA miR-126-5p, which normally maintains endothelial Notch1 activity by repressing the inhibitor Dlk1, reduces atherosclerotic lesion formation and promotes endothelial recovery in murine models [61]. In VSMCs, miR-34a intersects with SIRT1 signaling to regulate proliferation, senescence and osteogenic transdifferentiation; genetic ablation or pharmacological inhibition of miR-34a reduces vascular calcification and senescence markers in murine models [71,72], nominating anti-miR-34a oligonucleotides as a candidate strategy to indirectly normalize Notch3/SIRT1 signaling in the aging, atherosclerotic vessel wall. More broadly, because Notch ligand and receptor expression is subject to extensive post-transcriptional control, combining microRNA-based agents with cell-type-restricted delivery vehicles is an attractive, though still largely preclinical, strategy to achieve the cell-selective Notch modulation that pan-pathway inhibitors cannot provide.

5.5. Repurposing Established Cardiovascular Drugs: Statins and Notch-Associated Endothelial Phenotypes

Statins, the cornerstone of lipid-lowering pharmacotherapy in atherosclerotic cardiovascular disease, exert pleiotropic vascular effects beyond LDL-cholesterol reduction, including improvement of endothelial function. Recent work has shown that simvastatin suppresses endothelial-to-mesenchymal transition (EndMT), a process implicated in vascular endothelial dysfunction, in part through epigenetic modulation of a GGTase–RhoA–YAP–SOX9 signaling axis, indicating that at least part of the vasculoprotective, pleiotropic benefit of statin therapy may operate through mechanisms convergent with Notch-associated endothelial phenotypes rather than through cholesterol lowering alone [88]. This crosstalk has a long experimental history: simvastatin was shown more than a decade earlier to promote

the differentiation of bone marrow stromal cells into functional endothelial cells specifically via activation of the Notch signaling pathway, an effect abolished by γ-secretase inhibition or Notch1 knockdown [89]. Because statins are already in widespread, well-tolerated clinical use for atherosclerotic cardiovascular disease, and because endothelial-to-mesenchymal transition and Notch-driven endothelial senescence and inflammation converge mechanistically, this crosstalk supports the rationale for combining conventional lipid-lowering therapy with more selective, emerging Notch-directed agents, and raises the possibility that some of the anti-atherosclerotic benefit already achieved with statins in large outcome trials is partly attributable to favorable modulation of vascular Notch signaling.

6. Safety Considerations and Translational Challenges

The single most important lesson to emerge from clinical experience with Notch pathway inhibitors, gained almost entirely in oncology, is that this pathway has a narrow therapeutic index in the cardiovascular system. Anti-DLL4 antibodies produce dose- and duration-dependent hypertension, pulmonary hypertension and, in a subset of patients receiving prolonged high-dose exposure, congestive heart failure [43,44,84,85], while pan-Notch γ-secretase inhibitors carry class-wide gastrointestinal and immunological toxicity related to loss of Notch signaling in intestinal and lymphoid progenitor compartments. These toxicities are mechanistically continuous, not incidental, with the pathway's normal vasculoprotective functions: NOTCH1 signaling maintains endothelial junctional integrity and vascular quiescence [22,30], and profound pharmacological suppression of this signal—rather than the more subtle rebalancing that might be achievable with ligand-selective or vascular bed-restricted agents—predictably destabilizes the endothelium and pulmonary vasculature. Any future Notch-directed therapy for atherosclerosis will therefore need to achieve at least one, and probably several, of the following: (i) selectivity for a single ligand or receptor, for example, JAG1/NOTCH4 rather than pan-Notch [34,87]; (ii) restriction of drug exposure to a specific vascular bed or cell type, through nanoparticle or antibody–drug conjugate delivery; (iii) intermittent or low-dose regimens designed to titrate pathway activity rather than to abolish it; and (iv) combination with existing, well-tolerated background therapy such as statins, which may already provide partial, indirect normalization of Notch-associated endothelial phenotypes and could allow lower doses of a direct Notch-targeted agent to be used [88,89]. In addition, because most direct clinical experience with Notch inhibitors comes from short-term oncology regimens, the long-term cardiovascular safety of chronic, low-intensity Notch modulation—the exposure profile that would be required for a chronic disease such as atherosclerosis—remains essentially untested and will require dedicated long-term toxicology and, eventually, cardiovascular outcome studies.

7. Future Perspectives

Several converging lines of investigation suggest realistic paths toward a favorable therapeutic index for Notch-directed atherosclerosis therapy. First, single-cell and spatial transcriptomic mapping of Notch receptor and ligand expression across atherosusceptible and atheroresistant arterial regions should make it possible to define more precisely which receptor–ligand pairs are selectively upregulated at disease-prone sites, refining candidate targets beyond the JAG1–NOTCH4 axis already identified [34]. Second, ligand-selective decoy receptors and next-generation antibody engineering that improve the pharmacokinetic and tissue-distribution profile of anti-DLL4 or anti-JAG1 agents may substantially widen the safety margin relative to first-generation oncology antibodies [86,87]. Third, nanoparticle- or antibody–conjugate-based delivery platforms capable of restricting Notch pathway modulation to macrophages or to endothelium at atherosusceptible sites, rather

than achieving systemic pathway blockade, would in principle allow the pro-inflammatory, M1-like-skewing arm of macrophage Notch–RBP-J signaling to be dampened without compromising NOTCH1-dependent endothelial barrier function elsewhere in the vasculature [42,46]. Fourth, microRNA-based agents directed at nodes such as miR-126-5p and miR-34a that intersect with both Notch and senescence or repair pathways may offer a more gradual, combinatorial means of normalizing endothelial and VSMC phenotype than direct pathway blockade [61,71]. Finally, given the mechanistic overlap between statin-mediated modulation of EndMT and Notch pathway biology, prospective biomarker studies nested within existing statin and PCSK9 inhibitor cardiovascular outcome trials could help clarify how much of the clinical benefit of contemporary lipid-lowering therapy is mediated through Notch-dependent endothelial and smooth muscle mechanisms, information that would directly inform the design of combination regimens incorporating future Notch-selective agents.

8. Conclusions

The Notch signaling pathway occupies a central, if paradoxical, position in the biology of atherosclerosis: the same core molecular machinery can protect the endothelium from disturbed-flow-induced dysfunction when engaged through NOTCH1, or actively promote lesion formation when engaged through JAG1–NOTCH4 at atherosusceptible sites, drive VSMC dedifferentiation, proliferation and osteogenic transformation through NOTCH1/NOTCH3, and sustain pro-inflammatory macrophage polarization while suppressing reparative macrophage and T-cell programs through Notch–RBP-J signaling. This context dependence explains why global pathway inhibition with γ-secretase inhibitors, although capable of reducing experimental atherosclerosis and neointimal hyperplasia, carries an unfavorable safety profile, and why clinical experience with anti-DLL4 antibodies in oncology has revealed clinically significant cardiopulmonary toxicity. The path toward a clinically viable Notch-directed therapy for atherosclerosis is therefore unlikely to run through pan-pathway blockade, and more likely to depend on ligand-selective antagonists, decoy receptors, microRNA-based modulators, or vascular bed- and cell type-restricted delivery platforms capable of rebalancing, rather than abolishing, Notch signaling within the diseased artery wall.

Author Contributions: Conceptualization, A.B.; investigation, U.R., S.A. and A.U.; writing—original draft preparation, A.B., D.B. and T.K.; writing—review and editing, U.R., S.A. and A.U.; visualization, D.B.; supervision, A.B.; funding acquisition, A.B. All authors have read and agreed to the published version of the manuscript.

Funding: This research was funded by the Russian Science Foundation, grant number 25-15-00082.

Institutional Review Board Statement: Not applicable.

Informed Consent Statement: Not applicable.

Data Availability Statement: No new data were created or analyzed in this study. Data sharing is not applicable to this article.

Conflicts of Interest: The authors declare no conflicts of interest.

References

1. Libby, P.; Buring, J.E.; Badimon, L.; Hansson, G.K.; Deanfield, J.; Bittencourt, M.S.; Tokgözoğlu, L.; Lewis, E.F. Atherosclerosis. *Nat. Rev. Dis. Primers* **2019**, *5*, 56.
2. Bennett, M.R.; Sinha, S.; Owens, G.K. Vascular smooth muscle cells in atherosclerosis. *Circ. Res.* **2016**, *118*, 692–702. [CrossRef]
3. Herrington, W.; Lacey, B.; Sherliker, P.; Armitage, J.; Lewington, S. Epidemiology of atherosclerosis and the potential to reduce the global burden of atherothrombotic disease. *Circ. Res.* **2016**, *118*, 535–546. [CrossRef] [PubMed]

4. Artavanis-Tsakonas, S.; Rand, M.D.; Lake, R.J. Notch signaling: Cell fate control and signal integration in development. *Science* **1999**, *284*, 770–776. [CrossRef] [PubMed]
5. Kopan, R.; Ilagan, M.X.G. The canonical Notch signaling pathway: Unfolding the activation mechanism. *Cell* **2009**, *137*, 216–233. [CrossRef] [PubMed]
6. Gridley, T. Notch signaling in vascular development and physiology. *Development* **2007**, *134*, 2709–2718. [CrossRef] [PubMed]
7. Hasan, S.S.; Fischer, A. Notch signaling in the vasculature: Angiogenesis and angiocrine functions. *Cold Spring Harb. Perspect. Med.* **2023**, *13*, a041166. [CrossRef] [PubMed]
8. High, F.A.; Epstein, J.A. The multifaceted role of Notch in cardiac development and disease. *Nat. Rev. Genet.* **2008**, *9*, 49–61. [CrossRef] [PubMed]
9. Weng, A.P.; Ferrando, A.A.; Lee, W.; Morris, J.P., 4th; Silverman, L.B.; Sanchez-Irizarry, C.; Blacklow, S.C.; Look, A.T.; Aster, J.C. Activating mutations of NOTCH1 in human T cell acute lymphoblastic leukemia. *Science* **2004**, *306*, 269–271. [CrossRef] [PubMed]
10. Garg, V.; Muth, A.N.; Ransom, J.F.; Schluterman, M.K.; Barnes, R.; King, I.N.; Grossfeld, P.D.; Srivastava, D. Mutations in NOTCH1 cause aortic valve disease. *Nature* **2005**, *437*, 270–274. [CrossRef] [PubMed]
11. Joutel, A.; Corpechot, C.; Ducros, A.; Vahedi, K.; Chabriat, H.; Mouton, P.; Alamowitch, S.; Domenga, V.; Cécillon, M.; Marechal, E.; et al. Notch3 mutations in CADASIL, a hereditary adult-onset condition causing stroke and dementia. *Nature* **1996**, *383*, 707–710. [CrossRef] [PubMed]
12. Li, L.; Krantz, I.D.; Deng, Y.; Genin, A.; Banta, A.B.; Collins, C.C.; Qi, M.; Trask, B.J.; Kuo, W.L.; Cochran, J.; et al. Alagille syndrome is caused by mutations in human Jagged1, which encodes a ligand for Notch1. *Nat. Genet.* **1997**, *16*, 243–251. [CrossRef] [PubMed]
13. Domenga, V.; Fardoux, P.; Lacombe, P.; Monet, M.; Maciazek, J.; Krebs, L.T.; Klonjkowski, B.; Berrou, E.; Mericskay, M.; Li, Z.; et al. Notch3 is required for arterial identity and maturation of vascular smooth muscle cells. *Genes Dev.* **2004**, *18*, 2730–2735. [CrossRef] [PubMed]
14. Duarte, A.; Hirashima, M.; Benedito, R.; Trindade, A.; Diniz, P.; Bekman, E.; Costa, L.; Henrique, D.; Rossant, J. Dosage-sensitive requirement for mouse Dll4 in artery development. *Genes Dev.* **2004**, *18*, 2474–2478. [CrossRef] [PubMed]
15. Gale, N.W.; Dominguez, M.G.; Noguera, I.; Pan, L.; Hughes, V.; Valenzuela, D.M.; Murphy, A.J.; Adams, N.C.; Lin, H.C.; Holash, J.; et al. Haploinsufficiency of delta-like 4 ligand results in embryonic lethality due to major defects in arterial and vascular development. *Proc. Natl. Acad. Sci. USA* **2004**, *101*, 15949–15954. [CrossRef] [PubMed]
16. Krebs, L.T.; Shutter, J.R.; Tanigaki, K.; Honjo, T.; Stark, K.L.; Gridley, T. Haploinsufficient lethality and formation of arteriovenous malformations in Notch pathway mutants. *Genes Dev.* **2004**, *18*, 2469–2473. [CrossRef] [PubMed]
17. Peng, X.; Wang, S.; Chen, H.; Chen, M. Role of the Notch1 signaling pathway in ischemic heart disease (Review). *Int. J. Mol. Med.* **2023**, *51*, 27. [CrossRef] [PubMed]
18. Rizzo, P.; Ferrari, R. The Notch pathway: A new therapeutic target in atherosclerosis? *Eur. Heart J. Suppl.* **2015**, *17*, A74–A76. [CrossRef]
19. Vieceli Dalla Sega, F.; Fortini, F.; Aquila, G.; Campo, G.; Vaccarezza, M.; Rizzo, P. Notch signaling regulates immune responses in atherosclerosis. *Front. Immunol.* **2019**, *10*, 1130. [CrossRef] [PubMed]
20. Zhang, M.; Yue, X.; Zhao, X.; Lu, Y.; Liu, H.; Zhang, Z.; Ma, H.; Wang, X.; Xing, H. Macrophage-specific deletion of Notch-1 induced M2 anti-inflammatory effect in atherosclerosis via activation of the PI3K-oxidative stress axis. *Aging* **2023**, *15*, 15196–15212. [CrossRef] [PubMed]
21. Fischer, A.; Steidl, C.; Wagner, T.U.; Lang, E.; Jakob, P.M.; Friedl, P.; Knobeloch, K.P.; Gessler, M. Combined loss of Hey1 and HeyL causes congenital heart defects because of impaired epithelial to mesenchymal transition. *Circ. Res.* **2007**, *100*, 856–863. [CrossRef] [PubMed]
22. Polacheck, W.J.; Kutys, M.L.; Yang, J.; Eyckmans, J.; Wu, Y.; Vasavada, H.; Hirschi, K.K.; Chen, C.S. A non-canonical Notch complex regulates adherens junctions and vascular barrier function. *Nature* **2017**, *552*, 258–262. [CrossRef] [PubMed]
23. Rodriguez, F.; Virtanen, N.; Kiviluoto, E.; Driessen, R.H.; Zhao, F.; Bouten, C.C.; Stassen, O.M.J.A.; Sahlgren, C.M. Jagged1 is a Notch-independent mechanotransducer in endothelial cells. *bioRxiv* **2025**. [CrossRef]
24. Sprinzak, D.; Lakhanpal, A.; LeBon, L.; Santat, L.A.; Fontes, M.E.; Anderson, G.A.; Garcia-Ojalvo, J.; Elowitz, M.B. Cis-interactions between Notch and Delta generate mutually exclusive signalling states. *Nature* **2010**, *465*, 86–90. [CrossRef] [PubMed]
25. Kakuda, S.; Haltiwanger, R.S. Deciphering the Fringe-mediated Notch code: Identification of activating and inhibiting sites allowing discrimination between ligands. *Dev. Cell* **2017**, *40*, 193–201. [CrossRef] [PubMed]
26. Pennarubia, F.; Nairn, A.V.; Takeuchi, M.; Moremen, K.W.; Haltiwanger, R.S. Modulation of the NOTCH1 Pathway by LUNATIC FRINGE Is Dominant over That of MANIC or RADICAL FRINGE. *Molecules* **2021**, *26*, 5942. [CrossRef] [PubMed]
27. Benedito, R.; Roca, C.; Sörensen, I.; Adams, S.; Gossler, A.; Fruttiger, M.; Adams, R.H. The Notch ligands Dll4 and Jagged1 have opposing effects on angiogenesis. *Cell* **2009**, *137*, 1124–1135. [CrossRef] [PubMed]
28. Cheng, W.K.; Oon, C.E.; Kaur, G.; Sainson, R.C.A.; Li, J.L. Downregulation of Manic fringe impedes angiogenesis and cell migration of renal carcinoma. *Microvasc. Res.* **2022**, *142*, 104341. [CrossRef] [PubMed]

29. Suzuki, S.; Mashiko, T.; Tsukamoto, Y.; Oya, M.; Kotani, Y.; Okawara, S.; Matsumoto, T.; Mizue, Y.; Takeuchi, H.; Okajima, T.; et al. The N-acetylglucosaminyltransferase Radical fringe contributes to defects in JAG1-dependent turnover and signaling of NOTCH3 CADASIL mutants. *J. Biol. Chem.* **2024**, *300*, 107787. [CrossRef] [PubMed]
30. Mack, J.J.; Mosqueiro, T.S.; Archer, B.J.; Jones, W.M.; Sunshine, H.; Faas, G.C.; Briot, A.; Aragón, R.L.; Su, T.; Romay, M.C.; et al. NOTCH1 is a mechanosensor in adult arteries. *Nat. Commun.* **2017**, *8*, 1620. [CrossRef] [PubMed]
31. Quillard, T.; Devalliere, J.; Coupel, S.; Charreau, B. Inflammation dysregulates Notch signaling in endothelial cells: Implication of Notch2 and Notch4 to endothelial dysfunction. *Biochem. Pharmacol.* **2010**, *80*, 2032–2041. [CrossRef] [PubMed]
32. Joutel, A.; Andreux, F.; Gaulis, S.; Domenga, V.; Cecillon, M.; Battail, N.; Piga, N.; Chapon, F.; Godfrain, C.; Tournier-Lasserve, E. The ectodomain of the Notch3 receptor accumulates within the cerebrovasculature of CADASIL patients. *J. Clin. Investig.* **2000**, *105*, 597–605. [CrossRef] [PubMed]
33. Liu, Y.; Wang, T.; Yan, J.; Jiagbogu, N.; Heideman, D.A.M.; Canfield, A.E.; Alexander, M.Y. HGF/c-Met signalling promotes Notch3 activation and human vascular smooth muscle cell osteogenic differentiation in vitro. *Atherosclerosis* **2011**, *219*, 440–447. [CrossRef] [PubMed]
34. Souilhol, C.; Tardajos Ayllon, B.; Li, X.; Diagbouga, M.R.; Zhou, Z.; Canham, L.; Roddie, H.; Pirri, D.; Chambers, E.V.; Dunning, M.J.; et al. JAG1-NOTCH4 mechanosensing drives atherosclerosis. *Sci. Adv.* **2022**, *8*, eabo7958. [CrossRef] [PubMed]
35. Quillard, T.; Coupel, S.; Coulon, F.; Fitau, J.; Chatelais, M.; Cuturi, M.C.; Chiffoleau, E.; Charreau, B. Impaired Notch4 activity elicits endothelial cell activation and apoptosis: Implication for transplant arteriosclerosis. *Arterioscler. Thromb. Vasc. Biol.* **2008**, *28*, 2258–2265. [PubMed]
36. Nus, M.; Martínez-Poveda, B.; MacGrogan, D.; Chevre, R.; D'Amato, G.; Sbroggio, M.; Rodriguez, C.; Martinez-Gonzalez, J.; Andres, V.; Hidalgo, A.; et al. Endothelial Jag1-RBPJ signalling promotes inflammatory leucocyte recruitment and atherosclerosis. *Cardiovasc. Res.* **2016**, *112*, 568–580. [CrossRef] [PubMed]
37. Liu, H.; Kennard, S.; Lilly, B. NOTCH3 expression is induced in mural cells through an autoregulatory loop that requires endothelial-expressed JAGGED1. *Circ. Res.* **2009**, *104*, 466–475. [CrossRef] [PubMed]
38. Amsen, D.; Blander, J.M.; Lee, G.R.; Tanigaki, K.; Honjo, T.; Flavell, R.A. Instruction of distinct CD4 T helper cell fates by different Notch ligands on antigen-presenting cells. *Cell* **2004**, *117*, 515–526. [CrossRef] [PubMed]
39. Keerthivasan, S.; Suleiman, R.; Lawlor, R.; Roderick, J.; Bates, T.; Minter, L.; Anguita, J.; Juncadella, I.; Nickoloff, B.J.; Le Poole, I.C.; et al. Notch signaling regulates mouse and human Th17 differentiation. *J. Immunol.* **2011**, *187*, 692–701. [CrossRef] [PubMed]
40. Fung, E.; Tang, S.M.; Canner, J.P.; Morishige, K.; Arboleda-Velasquez, J.F.; Cardoso, A.A.; Carlesso, N.; Aster, J.C.; Aikawa, M. Delta-like 4 induces Notch signaling in macrophages: Implications for inflammation. *Circulation* **2007**, *115*, 2948–2956. [CrossRef] [PubMed]
41. Fukuda, D.; Aikawa, E.; Swirski, F.K.; Novobrantseva, T.I.; Kotelianski, V.; Gorgun, C.Z.; Chudnovskiy, A.; Yamazaki, H.; Croce, K.; Weissleder, R.; et al. Notch ligand Delta-like 4 blockade attenuates atherosclerosis and metabolic disorders. *Proc. Natl. Acad. Sci. USA* **2012**, *109*, E1868–E1877. [CrossRef] [PubMed]
42. Pagie, S.; Gérard, N.; Charreau, B. Notch signaling triggered via the ligand DLL4 impedes M2 macrophage differentiation and promotes their apoptosis. *Cell Commun. Signal.* **2018**, *16*, 4. [CrossRef] [PubMed]
43. McKeage, M.J.; Kotasek, D.; Markman, B.; Hidalgo, M.; Millward, M.J.; Jameson, M.B.; Harris, D.L.; Stagg, R.J.; Kapoun, A.M.; Xu, L.; et al. Phase IB trial of the anti-cancer stem cell DLL4-binding agent demcizumab with pemetrexed and carboplatin as first-line treatment of metastatic non-squamous NSCLC. *Target. Oncol.* **2018**, *13*, 89–98. [CrossRef] [PubMed]
44. Smith, D.C.; Eisenberg, P.D.; Manikhas, G.; Chugh, R.; Gubens, M.A.; Stagg, R.J.; Kapoun, A.M.; Xu, L.; Dupont, J.; Sikic, B. A phase I dose escalation and expansion study of the anticancer stem cell agent demcizumab (anti-DLL4) in patients with previously treated solid tumors. *Clin. Cancer Res.* **2014**, *20*, 6295–6303. [CrossRef] [PubMed]
45. Monsalve, E.; Pérez, M.A.; Rubio, A.; Ruiz-Hidalgo, M.J.; Baladrón, V.; García-Ramírez, J.J.; Gómez, J.C.; Laborda, J.; Díaz-Guerra, M.J.M. Notch-1 up-regulation and signaling following macrophage activation modulates gene expression patterns known to affect antigen-presenting capacity and cytotoxic activity. *J. Immunol.* **2006**, *176*, 5362–5373. [CrossRef] [PubMed]
46. Xu, H.; Zhu, J.; Smith, S.; Foldi, J.; Zhao, B.; Chung, A.Y.; Outtz, H.; Kitajewski, J.; Shi, C.; Weber, S.; et al. Notch-RBP-J signaling regulates the transcription factor IRF8 to promote inflammatory macrophage polarization. *Nat. Immunol.* **2012**, *13*, 642–650. [CrossRef] [PubMed]
47. Foldi, J.; Shang, Y.; Zhao, B.; Ivashkiv, L.B.; Hu, X. RBP-J is required for M2 macrophage polarization in response to chitin and mediates expression of a subset of M2 genes. *Protein Cell* **2016**, *7*, 908–913. [CrossRef] [PubMed]
48. He, F.; Guo, F.C.; Li, Z.; Yu, H.C.; Ma, P.F.; Zhao, J.L.; Feng, L.; Li, W.N.; Liu, X.W.; Qin, H.Y.; et al. Myeloid-specific disruption of recombination signal binding protein Jκ ameliorates hepatic fibrosis by attenuating inflammation through cylindromatosis in mice. *Hepatology* **2015**, *61*, 303–314. [CrossRef] [PubMed]
49. Shimizu, T.; Tanaka, T.; Iso, T.; Doi, H.; Sato, H.; Kawai-Kowase, K.; Arai, M.; Kurabayashi, M. Notch signaling induces osteogenic differentiation and mineralization of vascular smooth muscle cells: Role of Msx2 gene induction via Notch-RBP-Jk signaling. *Arterioscler. Thromb. Vasc. Biol.* **2009**, *29*, 1104–1111. [PubMed]

50. Zhang, C.; Lu, Y.; Da, X.; Yu, F.; Yu, W.; Xu, W.; Ye, Y.; Zhang, H. γ-Secretase inhibitor DAPT attenuates intimal hyperplasia of vein grafts by inhibition of Notch1 signaling. *Int. J. Mol. Med.* **2014**, *34*, 720–728.
51. Aoyama, T.; Takeshita, K.; Kikuchi, R.; Yamamoto, K.; Cheng, X.W.; Liao, J.K.; Murohara, T. Gamma-secretase inhibitor reduces diet-induced atherosclerosis in apolipoprotein E-deficient mice. *Biochem. Biophys. Res. Commun.* **2009**, *383*, 216–221. [CrossRef] [PubMed]
52. Shepley, B.R.; Bain, A.R. Is Notch1 a neglected vascular mechanosensor? *Physiol. Rev.* **2024**, *104*, 655–658. [CrossRef] [PubMed]
53. Briot, A.; Civelek, M.; Seki, A.; Hoi, K.; Mack, J.J.; Lee, S.D.; Kim, J.; Hong, C.; Yu, J.; Fishbein, G.A.; et al. Endothelial NOTCH1 is suppressed by circulating lipids and antagonizes inflammation during atherosclerosis. *J. Exp. Med.* **2015**, *212*, 2147–2163. [CrossRef] [PubMed]
54. Souilhol, C.; Serbanovic-Canic, J.; Fragiadaki, M.; Chico, T.J.; Ridger, V.; Roddie, H.; Evans, P.C. Endothelial responses to shear stress in atherosclerosis: A novel role for developmental genes. *Nat. Rev. Cardiol.* **2020**, *17*, 52–63. [CrossRef] [PubMed]
55. Davies, P.F.; Civelek, M.; Fang, Y.; Fleming, I. The atherosusceptible endothelium: Endothelial phenotypes in complex haemodynamic shear stress regions in vivo. *Cardiovasc. Res.* **2013**, *99*, 315–327. [CrossRef] [PubMed]
56. Watson, O.; Novodvorsky, P.; Gray, C.; Rothman, A.M.K.; Lawrie, A.; Gerhardt, H.; Crossman, D.C.; Haase, A.; McMahon, K.; Gering, M.; et al. Blood flow suppresses vascular Notch signalling via dll4 and is required for angiogenesis in response to hypoxic signalling. *Cardiovasc. Res.* **2013**, *100*, 252–261. [CrossRef] [PubMed]
57. Liu, Z.J.; Tan, Y.; Beecham, G.W.; Seo, D.M.; Tian, R.; Li, Y.; Vazquez-Padron, R.I.; Pericak-Vance, M.; Vance, J.M.; Goldschmidt-Clermont, P.J.; et al. Notch activation induces endothelial cell senescence and pro-inflammatory response: Implication of Notch signaling in atherosclerosis. *Atherosclerosis* **2012**, *225*, 296–303. [CrossRef] [PubMed]
58. MacKenzie, F.; Duriez, P.; Wong, F.; Noseda, M.; Karsan, A. Notch4 inhibits endothelial apoptosis via RBP-Jkappa-dependent and -independent pathways. *J. Biol. Chem.* **2004**, *279*, 11657–11663. [CrossRef] [PubMed]
59. Verginelli, F.; Adesso, L.; Limon, I.; Alisi, A.; Gueguen, M.; Panera, N.; Giorda, E.; Raimondi, L.; Ciarapica, R.; Campese, A.F.; et al. Activation of an endothelial Notch1-Jagged1 circuit induces VCAM1 expression, an effect amplified by interleukin-1β. *Oncotarget* **2015**, *6*, 43216–43229. [CrossRef] [PubMed]
60. Wieland, E.; Rodriguez-Vita, J.; Liebler, S.S.; Mogler, C.; Moll, I.; Herberich, S.E.; Espinet, E.; Herpel, E.; Menuchin, A.; Chang-Claude, J.; et al. Endothelial Notch1 activity facilitates metastasis. *Cancer Cell* **2017**, *31*, 355–367. [CrossRef] [PubMed]
61. Schober, A.; Nazari-Jahantigh, M.; Wei, Y.; Bidzhekov, K.; Gremse, F.; Grommes, J.; Megens, R.T.A.; Heyll, K.; Noels, H.; Hristov, M.; et al. MicroRNA-126-5p promotes endothelial proliferation and limits atherosclerosis by suppressing Dlk1. *Nat. Med.* **2014**, *20*, 368–376. [CrossRef] [PubMed]
62. Takeshita, K.; Satoh, M.; Ii, M.; Silver, M.; Limbourg, F.P.; Mukai, Y.; Rikitake, Y.; Radtke, F.; Gridley, T.; Losordo, D.W.; et al. Critical role of endothelial Notch1 signaling in postnatal angiogenesis. *Circ. Res.* **2007**, *100*, 70–78. [CrossRef] [PubMed]
63. Jiang, H.; Cheng, X.W.; Shi, G.P.; Hu, L.; Inoue, A.; Yamamura, Y.; Wu, H.; Takeshita, K.; Li, X.; Huang, Z.; et al. Cathepsin K-mediated Notch1 activation contributes to neovascularization in response to hypoxia. *Nat. Commun.* **2014**, *5*, 3838. [CrossRef] [PubMed]
64. Jabs, M.; Rose, A.J.; Lehmann, L.H.; Taylor, J.; Moll, I.; Sijmonsma, T.P.; Herberich, S.E.; Sauer, S.W.; Poschet, G.; Federico, G.; et al. Inhibition of endothelial Notch signaling impairs fatty acid transport and leads to metabolic and vascular remodeling of the adult heart. *Circulation* **2018**, *137*, 2592–2608. [CrossRef] [PubMed]
65. Carlson, T.R.; Yan, Y.; Wu, X.; Lam, M.T.; Tang, G.L.; Beverly, L.J.; Messina, L.M.; Capobianco, A.J.; Werb, Z.; Wang, R. Endothelial expression of constitutively active Notch4 elicits reversible arteriovenous malformations in adult mice. *Proc. Natl. Acad. Sci. USA* **2005**, *102*, 9884–9889. [CrossRef] [PubMed]
66. Ruchoux, M.M.; Domenga, V.; Brulin, P.; Maciazek, J.; Limol, S.; Tournier-Lasserve, E.; Joutel, A. Transgenic mice expressing mutant Notch3 develop vascular alterations characteristic of cerebral autosomal dominant arteriopathy with subcortical infarcts and leukoencephalopathy. *Am. J. Pathol.* **2003**, *162*, 329–342. [CrossRef] [PubMed]
67. Xia, Y.; Bhattacharyya, A.; Roszell, E.E.; Sandig, M.; Mequanint, K. The role of endothelial cell-bound Jagged1 in Notch3-induced human coronary artery smooth muscle cell differentiation. *Biomaterials* **2012**, *33*, 2462–2472. [CrossRef] [PubMed]
68. Bhattacharyya, A.; Lin, S.; Sandig, M.; Mequanint, K. Regulation of vascular smooth muscle cell phenotype in three-dimensional coculture system by Jagged1-selective Notch3 signaling. *Tissue Eng. Part A* **2014**, *20*, 1175–1187. [CrossRef] [PubMed]
69. Liu, H.; Zhang, W.; Kennard, S.; Caldwell, R.B.; Lilly, B. Notch3 is critical for proper angiogenesis and mural cell investment. *Circ. Res.* **2010**, *107*, 860–870. [CrossRef] [PubMed]
70. Guo, Z.; Jia, J.; Tu, Y.; Jin, C.; Guo, C.; Song, F.; Wu, X.; Bao, H.; Fan, W. Altered Jagged1-Notch1 signaling in enhanced dysfunctional neovascularization and delayed angiogenesis after ischemic stroke in HFD/STZ induced type 2 diabetes rats. *Front. Physiol.* **2021**, *12*, 687947. [CrossRef] [PubMed]
71. Zuccolo, E.; Badi, I.; Scavello, F.; Gambuzza, I.; Mancinelli, L.; Macrì, F.; Tedesco, C.C.; Veglia, F.; Bonfigli, A.R.; Olivieri, F.; et al. The microRNA-34a-induced senescence-associated secretory phenotype (SASP) favors vascular smooth muscle cells calcification. *Int. J. Mol. Sci.* **2020**, *21*, 4454. [CrossRef] [PubMed]

72. Badi, I.; Burba, I.; Malpartida, A.B.; Scopece, A.; Sommariva, E.; Vitale, S.; Colombo, G.I.; Pompilio, G.; Raucci, A. miR-34a promotes vascular smooth muscle cell calcification by downregulating SIRT1 (sirtuin 1) and Axl (AXL receptor tyrosine kinase). *Arterioscler. Thromb. Vasc. Biol.* **2018**, *38*, 2079–2090. [CrossRef] [PubMed]
73. Nigam, V.; Srivastava, D. Notch1 represses osteogenic pathways in aortic valve cells. *J. Mol. Cell. Cardiol.* **2009**, *47*, 828–834. [CrossRef] [PubMed]
74. Nus, M.; MacGrogan, D.; Martínez-Poveda, B.; Benito, Y.; Casanova, J.C.; Fernández-Avilés, F.; Bermejo, J.; de la Pompa, J.L. Diet-induced aortic valve disease in mice haploinsufficient for the Notch pathway effector RBPJK/CSL. *Arterioscler. Thromb. Vasc. Biol.* **2011**, *31*, 1580–1588. [CrossRef] [PubMed]
75. Chen, J.; Ryzhova, L.M.; Sewell-Loftin, M.K.; Brown, C.B.; Huppert, S.S.; Baldwin, H.S.; Merryman, W.D. Notch1 mutation leads to valvular calcification through enhanced myofibroblast mechanotransduction. *Arterioscler. Thromb. Vasc. Biol.* **2015**, *35*, 1597–1605. [CrossRef] [PubMed]
76. Clark, C.R.; Bowler, M.A.; Snider, J.C.; Merryman, W.D. Targeting cadherin-11 prevents Notch1-mediated calcific aortic valve disease. *Circulation* **2017**, *135*, 2448–2450. [CrossRef] [PubMed]
77. Wang, Y.C.; He, F.; Feng, F.; Liu, X.W.; Dong, G.Y.; Qin, H.Y.; Hu, X.B.; Zheng, M.H.; Liang, L.; Feng, L.; et al. Notch signaling determines the M1 versus M2 polarization of macrophages in antitumor immune responses. *Cancer Res.* **2010**, *70*, 4840–4849. [CrossRef] [PubMed]
78. Koga, J.; Nakano, T.; Dahlman, J.E.; Figueiredo, J.L.; Zhang, H.; Decano, J.; Khan, O.F.; Niida, T.; Iwata, H.; Aster, J.C.; et al. Macrophage Notch ligand Delta-like 4 promotes vein graft lesion development: Implications for the treatment of vein graft failure. *Arterioscler. Thromb. Vasc. Biol.* **2015**, *35*, 2343–2353. [CrossRef] [PubMed]
79. Xu, J.; Chi, F.; Guo, T.; Punj, V.; Lee, W.N.P.; French, S.W.; Tsukamoto, H. NOTCH reprograms mitochondrial metabolism for proinflammatory macrophage activation. *J. Clin. Investig.* **2015**, *125*, 1579–1590. [CrossRef] [PubMed]
80. Saigusa, R.; Winkels, H.; Ley, K. T cell subsets and functions in atherosclerosis. *Nat. Rev. Cardiol.* **2020**, *17*, 387–401. [CrossRef] [PubMed]
81. Elyaman, W.; Bradshaw, E.M.; Wang, Y.; Oukka, M.; Kivisäkk, P.; Chiba, S.; Yagita, H.; Khoury, S.J. Jagged1 and Delta1 differentially regulate the outcome of experimental autoimmune encephalomyelitis. *J. Immunol.* **2007**, *179*, 5990–5998. [CrossRef] [PubMed]
82. Charbonnier, L.M.; Wang, S.; Georgiev, P.; Sefik, E.; Chatila, T.A. Control of peripheral tolerance by regulatory T cell-intrinsic Notch signaling. *Nat. Immunol.* **2015**, *16*, 1162–1173. [CrossRef] [PubMed]
83. Qin, W.D.; Zhang, F.; Qin, X.J.; Wang, J.; Meng, X.; Wang, H.; Guo, H.P.; Wu, Q.Z.; Wu, D.W.; Zhang, M.X. Notch1 inhibition reduces low shear stress-induced plaque formation. *Int. J. Biochem. Cell Biol.* **2016**, *72*, 63–72. [CrossRef] [PubMed]
84. Coleman, R.L.; Handley, K.F.; Burger, R.; Molin, G.Z.D.; Stagg, R.; Sood, A.K.; Moore, K.N. Demcizumab combined with paclitaxel for platinum-resistant ovarian, primary peritoneal, and fallopian tube cancer: The SIERRA open-label phase Ib trial. *Gynecol. Oncol.* **2020**, *157*, 386–391. [CrossRef] [PubMed]
85. Besse, C.E.; Winicki, N.M.; Puerta, C.; Hernandez, M.; Yuan, J.X.; Thistlethwaite, P.A. Delta-like ligand 4 inhibitor drug treatment induces pulmonary hypertension in cancer clinical trials. *Pulm. Circ.* **2024**, *14*, e12450. [CrossRef] [PubMed]
86. Yen, W.C.; Fischer, M.M.; Axelrod, F.; Bond, C.; Cain, J.; Cancilla, B.; Yeung, V.; Wu, J.; Chartier, C.; Katrina, J.; et al. Targeting Notch signaling with a Notch2/Notch3 antagonist (tarextumab) inhibits tumor growth and decreases tumor-initiating cell frequency. *Clin. Cancer Res.* **2015**, *21*, 2084–2095. [CrossRef] [PubMed]
87. Kangsamaksin, T.; Murtomaki, A.; Kofler, N.M.; Cuervo, H.; Chaudhri, R.A.; Tattersall, I.W.; Rosenstiel, P.E.; Shawber, C.J.; Kitajewski, J. NOTCH decoys that selectively block DLL/NOTCH or JAG/NOTCH disrupt angiogenesis by unique mechanisms to inhibit tumor growth. *Cancer Discov.* **2015**, *5*, 182–197. [CrossRef] [PubMed]
88. Liu, C.; Shen, M.; Tan, W.L.W.; Chen, I.Y.; Liu, Y.; Yu, X.; Yang, H.; Zhang, A.; Liu, Y.; Zhao, M.T.; et al. Statins improve endothelial function via suppression of epigenetic-driven EndMT. *Nat. Cardiovasc. Res.* **2023**, *2*, 467–485. [CrossRef] [PubMed]
89. Xu, J.; Liu, X.; Chen, J.; Zacharek, A.; Cui, X.; Savant-Bhonsale, S.; Liu, Z.; Chopp, M. Simvastatin enhances bone marrow stromal cell differentiation into endothelial cells via Notch signaling pathway. *Am. J. Physiol. Cell Physiol.* **2009**, *296*, C535–C543. [CrossRef] [PubMed]
90. Fortini, M.E. γ-Secretase-mediated proteolysis in cell-surface-receptor signalling. *Nat. Rev. Mol. Cell Biol.* **2002**, *3*, 673–684. [CrossRef] [PubMed]

Disclaimer/Publisher's Note: The statements, opinions and data contained in all publications are solely those of the individual author(s) and contributor(s) and not of MDPI and/or the editor(s). MDPI and/or the editor(s) disclaim responsibility for any injury to people or property resulting from any ideas, methods, instructions or products referred to in the content.

cells

MDPI

Review

Inflammatory Mechanisms in Acute Coronary Syndromes: From Pathophysiology to Therapeutic Targets

Daniel Miron Brie [1,2], Cristian Mornoș [1,2,3], Ovidiu Adam [4], Alexandru Tîrziu [1,5,*], Roxana Popescu [6,7] and Alina Diduța Brie [7,8]

1 Cardiovascular Disease Institute Timisoara, Gheorghe Adam Street, No. 13A, 300310 Timisoara, Romania; mornos.cristian@umft.ro (C.M.)
2 Research Center of the Institute of Cardiovascular Diseases, Gheorghe Adam Street, No. 13A, 300310 Timisoara, Romania
3 Department of Cardiology, "Victor Babes" University of Medicine and Pharmacy, Eftimie Murgu Square, No. 2, 300041 Timisoara, Romania
4 Department of Pediatric Surgery and Orthopedics, "Victor Babes" University of Medicine and Pharmacy, Eftimie Murgu Square, No. 2, 300041 Timisoara, Romania; ovidiu.adam@umft.ro
5 Department of Functional Sciences, "Victor Babes" University of Medicine and Pharmacy, Tudor Vladimirescu Street, No. 14, 300174 Timisoara, Romania
6 ANAPATMOL Research Center, "Victor Babes" University of Medicine and Pharmacy, Tudor Vladimirescu Street, No. 14, 300174 Timisoara, Romania; popescu.roxana@umft.ro
7 Department of Cell and Molecular Biology, Faculty of Medicine, "Victor Babes" University of Medicine and Pharmacy, Eftimie Murgu Square, No. 2, 300041 Timisoara, Romania; alina.brie@umft.ro
8 "Louis Țurcanu" Emergency Children Hospital, Doctor Iosif Nemoianu Street, No. 2, 300011 Timisoara, Romania
* Correspondence: alexandru.tirziu@umft.ro

Abstract

Inflammation plays a pivotal role in the pathogenesis of acute coronary syndromes (ACS), contributing to plaque instability, thrombosis, and myocardial injury. This review aims to comprehensively examine the inflammatory mechanisms underlying ACS and evaluate current and emerging anti-inflammatory therapeutic strategies. We conducted a comprehensive literature review examining the role of inflammatory pathways in ACS pathophysiology, including innate and adaptive immune responses, key inflammatory mediators, and cellular mechanisms. We analyzed current evidence for anti-inflammatory therapies and their clinical outcomes in ACS management. Inflammatory processes in ACS involve complex interactions between innate immune cells (neutrophils, macrophages, monocytes) and adaptive immune cells (T lymphocytes, B cells). Key mechanisms include neutrophil extracellular trap (NET) formation, macrophage polarization, T cell subset imbalances (Th1/Th17 predominance with regulatory T cell dysfunction), and complement activation. Inflammatory biomarkers such as C-reactive protein, interleukin-6, and NET-specific markers demonstrate prognostic value. Anti-inflammatory therapies including colchicine, canakinumab (IL-1β inhibition), and methotrexate have shown cardiovascular benefits in clinical trials. Emerging targets include NET inhibition, T cell modulation, and precision inflammatory profiling approaches. Inflammation represents a critical therapeutic target in ACS beyond traditional risk factor modification. While colchicine and IL-1β inhibition have demonstrated clinical efficacy, future strategies should focus on precision medicine approaches targeting specific inflammatory pathways based on individual patient profiles. Integration of anti-inflammatory therapy with lipid management and antithrombotic strategies offers promise for improving ACS outcomes through comprehensive targeting of the multifactorial pathophysiology underlying coronary artery disease.

Keywords: acute coronary syndrome; inflammation; neutrophil extracellular traps; T lymphocytes; anti-inflammatory therapy; colchicine; interleukin-1; cardiovascular immunology

1. Introduction

Inflammation plays a central role in the pathogenesis of acute coronary syndromes (ACS) by contributing to the initiation, progression, and complications of atherosclerotic plaques [1]. Local inflammatory cells in the coronary arteries release cytokines that activate the endothelium, altering its physiological antiaggregant and anticoagulant properties. This activation promotes plaque instability by reducing extracellular matrix synthesis and increasing its degradation, thereby favoring plaque rupture—a key event in the onset of ACS. Inflammatory cytokines also increase smooth muscle cell reactivity and contribute to thrombus formation following plaque disruption [2]. Both innate and adaptive immune responses regulate the progression of atherosclerosis and plaque stability. Immune cells, such as macrophages and T lymphocytes, secrete inflammatory mediators that enhance the lipid core while reducing the fibrous cap, thereby making plaques more prone to rupture. The 2023 European Society of Cardiology (ESC) guidelines for the management of acute coronary syndrome (ACS) acknowledge the role of inflammation in ACS pathophysiology but do not currently provide specific recommendations for targeting inflammation as a routine therapeutic strategy in ACS management [1].

A recent article discusses the inflammatory response in patients with acute myocardial infarction, drawing inspiration from the title of a famous Western movie, "The Good, the Bad and the Ugly" It is based on the idea that after an acute myocardial infarction, the initial inflammatory response plays a beneficial, defensive role, known as "The Good." This response can be exaggerated in the acute phase, "The Ugly". Additionally, a chronic inflammatory response may persist long after the acute event, thereby realizing the residual inflammatory risk, "The Bad" [3].

The paper demonstrates that inflammation is both beneficial and detrimental after an ACS. A certain amount of inflammation helps the heart heal by removing dead cells and supporting repair processes. On the other hand, too much inflammation can lead to additional damage and complications, such as worsening heart function or triggering additional ACS. Targeted treatments that reduce the harmful inflammation (often referred to as "The Bad" and "The Ugly") while leaving the protective, healing inflammation ("The Good") intact are necessary to aid in recovery after an acute coronary syndrome while preventing the onset of another one. This balance could improve recovery and reduce the risk of complications. The repair process following AMI is likely to involve M2-type macrophages, natural killer (NK) cells, regulatory T lymphocytes (Treg), and cytokines, specifically interleukin-10 (IL-10) and interleukin-2 (IL-2). The acute phase of the inflammatory response is characterized by the activation of polymorphonuclear leukocytes (PMNs), M1 macrophages, the formation of neutrophil extracellular traps (NETs), and the release of cytokines, including interleukin-1α (IL-1α), interleukin-1β (IL-1β), and interleukin-6 (IL-6). After this acute phase, a chronic inflammatory process may develop, resulting in a residual inflammatory risk (RIR). This process involves M1-polarized macrophages, foam cells, and PMNs, as well as the activation of the NLRP3 inflammasome.

So, in the acute phase after a myocardial infarction, anti-inflammatory treatment should protect or stimulate the inflammatory repair processes and limit the acute exaggerated inflammatory response.

https://doi.org/10.3390/cells15010072

This review focuses on the current state of research regarding anti-inflammatory medication in patients with acute myocardial infarction. We want to answer questions such as: What drugs are currently available? What drugs will be available? Will they change treatment guidelines? When is the best time after an acute myocardial infarction to initiate anti-inflammatory treatment? Is anti-inflammatory treatment applicable to all patients with acute coronary syndromes?

2. Inflammatory Mechanisms Involved in Atherosclerotic Plaque Destabilization

Atheromatous plaques that are prone to rapid progression, rupture, or erosion leading to ACS are referred to as vulnerable plaques, as they have specific, well-defined characteristics [4,5]. The term "vulnerable plaque" was first used by Muller et al., who described plaque prone to rupture leading to ACS, histopathologically characterized (based on autopsy studies) by a lipid-rich core, a thin cap fibroatheroma, and an inflammatory infiltrate with macrophages [6]. Although atherosclerotic plaque rupture is the most incriminated mechanism in the pathophysiology of ACS, plaque erosion or the presence of calcified nodules have been described as possible mechanisms [7]. Nowadays, it is recommended to use the term vulnerable plaque to define those atherosclerotic plaques that can cause complications, being used in the designation of all plaques at risk of rupture and thrombosis [8]. An expert consensus proposes several major criteria (active inflammation, a thin cap with a large lipid core, endothelial denudation with superficial platelet aggregation, fissured plaque, and stenosis > 90%) and minor criteria (superficial calcified nodules, glistening yellow aspect on angioscopy, intraplaque hemorrhage, endothelial dysfunction, and outward (positive) remodeling) for diagnosing vulnerable plaque. The vast majority of plaques that cause an ACS are without calcifications, no significant stenosis, or similar to type IV atherosclerotic lesions described in the American Heart Association classification (a well-defined vascular intimal region occupied by extracellular lipids without a significant amount of fibrous tissue and without surface erosion, rupture or thrombus formation) [9].

Inflammation plays a central role in the pathogenesis of ACS, with various inflammatory markers and pathways contributing to disease progression and outcomes.

2.1. NOD-like Receptor Protein Domain-Associated Protein 3 (NLRP3) Inflammasome

The NOD-like receptor protein domain-associated protein 3 (NLRP3) inflammasome plays a critical role in the development and progression of ACS by mediating inflammatory responses that contribute to plaque instability, myocardial injury, and adverse cardiac remodeling [10]. The NLRP3 inflammasome consists of the NLRP3 protein functioning as a sensor for pattern-recognition repeats, danger and pathogen-associated molecular patterns (DAMPs, PAMPs), an adaptor domain (ASC—a caspase-recruiting domain, CARD), and an effector protein (caspase 1). The sensor domain includes an N-terminal pyrin domain, a central NACHT domain vital for ATP-mediated inflammasome assembly and a leucine-rich repeat domain (LRR) [11].

Upon activation by danger signals such as cholesterol crystals, potassium efflux, or ischemic injury, the NLRP3 oligomerizes with the NACHT domains, which further rectruits ASC, which attach to the ASC speck. The activated inflammasome activates caspase 1, which cleaves the pre-IL-1β and pre-IL-18 into their active forms. As a result, IL-1β and IL-18 are released, promoting local vascular inflammation by upregulating the ICAM-1 and VCAM-1 molecules on endothelial cells, promoting immune cell adhesion and infiltration, further contributing to the development and destabilization of atherosclerotic plaques. Additionally, caspase-1 mediates activation of Gasdermin D, which upon oligomerization, forms a plasmallemal pore, triggering pyroptosis. NLRP3 activation can precipitate ACS

https://doi.org/10.3390/cells15010072

events [12] by enhancing the lipid necrotic core and driving IL-1/IL-18-mediated vascular inflammation (pyroptosis) and may constitute a therapeutic target in patients with ACS [13,14].

The inflammasome-driven cytokines exacerbate inflammation within plaques, weakening the fibrous cap through matrix metalloproteinase activation and increasing the likelihood of plaque rupture or erosion, the primary triggers of ACS. Beyond plaque effects, NLRP3 activation in cardiac cells (cardiomyocytes and fibroblasts) during ischemia promotes inflammatory cell death (pyroptosis) and fibrosis. This contributes to adverse ventricular remodeling and impaired cardiac function after myocardial infarction, worsening prognosis [15]. Molecular mechanisms, including microRNAs and protein modifications (such as SUMOylation, phosphorylation and ubiquitylation) tightly regulate NLRP3 activation [16]. Pharmacological inhibition of NLRP3 or its downstream cytokines (e.g., IL-1β) has shown promise in reducing inflammation, limiting cardiac damage, and improving outcomes in preclinical and early clinical studies [13,17].

A recent study highlights the role of the inflammasome signaling pathway in myocardial damage during STEMI. By identifying the genetic expression of inflammasome-related markers like TLR4, NLRP3, and IL-6R in coronary thrombi, the research suggests that these markers are actively involved in the inflammatory response associated with myocardial injury. The findings support targeting the inflammasome signaling pathway as a potential treatment strategy for myocardial infarction. By focusing on this pathway, medical interventions could potentially reduce inflammation and limit heart damage, improving patient outcomes, but the timing of anti-inflammatory treatment is crucial [18].

2.2. Interleukin-1 β (IL-1β)

IL-1β is a pro-inflammatory cytokine that is activated through the NLRP3 inflammasome pathway. IL-1β is highly expressed in atherosclerotic plaques, particularly in complicated and unstable plaques, prone to rupture. IL-1β promotes inflammation by inducing the expression of adhesion molecules (ICAM-1, VCAM-1), chemokines, and matrix metalloproteinases (MMP-9), which degrade the fibrous cap and increase plaque vulnerability [19]. Studies have shown that IL-1β levels are elevated in patients with ACS and correlate with myocardial damage and adverse outcomes. IL-1β stimulates other proatherogenic cytokines such as TNF-α and LIGHT, amplifying vascular inflammation and contributing to plaque progression and rupture [20]. IL-1β exerts direct harmful effects on heart muscle cells by inducing apoptosis (programmed cell death) and hypertrophy, depressing cardiac contractility through nitric oxide-dependent and independent pathways [21]. IL-1β promotes leukocyte trafficking to the site of myocardial injury by enhancing endothelial adhesion molecule expression and chemokine production, which sustains the inflammatory response after myocardial infarction. This inflammatory cascade contributes to infarct healing but can also lead to excessive tissue damage and adverse cardiac remodeling, if uncontrolled [22].

2.3. Interleukin-6 (IL-6)

IL-6 is elevated in patients with ACS, especially in those with unstable angina and acute myocardial infarction, reflecting increased inflammatory activity within atherosclerotic plaques [23]. It is expressed locally in the shoulder regions of plaques, where it enhances recruitment of monocytes and T cells, promoting inflammation and weakening the fibrous cap, thus increasing plaque vulnerability and risk of rupture [24].

IL-6 induces hepatic production of acute-phase reactants such as high-sensitivity C-reactive protein (hs-CRP), amplifying systemic inflammation and generating a prothrombotic state [25–27]. Higher plasma IL-6 levels are correlated with a greater severity of

https://doi.org/10.3390/cells15010072

ACS. They are associated with an increased risk of major adverse cardiovascular events (MACE), including cardiovascular death, myocardial infarction, and hospitalization for heart failure [28]. IL-6 levels provide prognostic information that is independent of traditional risk factors and biomarkers, such as hs-CRP and troponin. Patients in the highest IL-6 quartile have significantly worse outcomes [29]. IL-6 activates the MAPK/ERK1/2 pathway, leading to overexpression of the MMP9, which contributes to extracellular matrix remodeling and fibrosis, processes involved in adverse ventricular remodeling and heart failure following myocardial infarction [27]. IL-6 also activates transcription factors such as NF-κB and PPAR-γ, which contribute to MMP-9 gene transcription in vascular cells and macrophages, promoting inflammatory responses and ECM degradation in atherosclerotic plaques [30].

2.4. Tumor Necrosis Factor α (TNF-α)

TNF-α, abundantly expressed in unstable atherosclerotic plaques, exacerbates local inflammation by activating endothelial cells and recruiting immune cells, thereby promoting plaque vulnerability and increasing the risk of rupture that precipitates acute coronary syndrome (ACS). TNF-α binds platelet TNFR1, activating the arachidonic acid cascade to increase thromboxane A2 production, which promotes platelet activation and aggregation, leading to thrombus formation that can occlude coronary arteries and cause myocardial ischemia [31,32]. Cardiac myocytes produce TNF-α during ischemia that has direct deleterious effects on heart muscle cells, including apoptosis and depressing contractile function [33]. TNF-α binds to TNF receptor 1 (TNFR1) on cardiomyocytes, triggering recruitment of adaptor proteins that activate caspase-8. Activated caspase-8 initiates the apoptotic cascade directly cleaves Bid into truncated Bid (t-Bid), which translocates to mitochondria, promoting the formation of the mitochondrial outer membrane permeabilization pore and release of pro-apoptotic factors such as cytochrome c, Smac/Diablo, and Omi/HtrA2 into the cytosol. Cytochrome c activates caspase-9 which, together with caspase-8, activates caspase-3, the executioner caspase responsible for apoptosis [34,35]. This pathway contributes to left ventricular dysfunction and adverse remodeling after myocardial infarction. Elevated circulating TNF-α levels in ACS patients, including several months after myocardial infarction, are associated with an increased risk of recurrent coronary events, heart failure, and mortality. Persistently high TNF-α levels indicate ongoing inflammatory instability and a worse prognosis [36,37].

2.5. Interleukin-18 (IL-18)

Patients with ACS show significantly elevated circulating IL-18 levels compared to healthy controls. IL-18 concentrations rise rapidly after the acute event and could remain elevated for months, indicating sustained inflammation [38].

IL-18, like IL-1β, is released during the NLRP3-mediated pyroptosis and amplifies vascular inflammation [39]. It promotes the recruitment and activation of immune cells within atherosclerotic plaques, contributing to plaque destabilization and increasing the risk of rupture and thrombosis, which trigger ACS.

IL-18 binds to IL-18Rα, activating NF-κB signaling pathways in vascular cells and macrophages, upregulating the MMP-9 (leading to extracellular matrix remodelling) and the CD36, a multiscavenger receptor that binds and internalizes oxidized LDL-cholesterol lipoprotein particles, favoring foam cell formation [40]. IL-18 also upregulates the production of interferon-γ, further activating macrophages and T/NK cells. Interferon-γ down-regulates collagen production by the vascular smooth muscle cells, leading to plaque fibrous cap thinning, making the plaque more unstable and prone to rupture [41].

https://doi.org/10.3390/cells15010072

Elevated IL-18 levels are associated with a higher risk of adverse clinical events after ACS, including recurrent unstable angina, myocardial infarction, heart failure exacerbation, stroke, and cardiovascular death. IL-18 levels above the median significantly predict worse outcomes, independent of many clinical factors [42]. However, its prognostic value is somewhat attenuated when adjusted for other inflammatory biomarkers, suggesting shared inflammatory pathways. Higher IL-18 levels correlate with male sex, obesity, diabetes, decreased renal function, and other markers of inflammation, reflecting its role in systemic inflammatory burden in ACS patients [39,43].

2.6. Chemokines in Acute Coronary Syndrome

Chemokines are chemotactic molecules that play a role in recruiting immune cells to sites of inflammation. Chemokines influence the migration of leukocytes, including neutrophils, monocytes, and T cells, into atherosclerotic plaques. This influx of inflammatory cells is a hallmark of plaque destabilization and rupture, which are critical events leading to ACS [44,45]. Beyond recruiting immune cells, chemokines directly contribute to the weakening of the fibrous cap of atherosclerotic plaques by inducing the release of matrix-degrading enzymes from macrophages, which degrade the extracellular matrix and promote apoptosis of endothelial cells and smooth muscle cells, further compromising plaque stability [46]. Chemokines can enhance the pro-thrombotic environment within plaques by inducing tissue factor expression in vascular smooth muscle and endothelial cells and promoting platelet activation and aggregation, which are essential steps in the formation of occlusive thrombi following plaque rupture. Elevated levels of various chemokines, including CCL2, CCL3, CCL5, CCL18, CCL19, and CCL21, have been observed in patients with acute coronary syndrome (ACS) and are associated with worse outcomes. These chemokines not only reflect ongoing inflammation but also actively participate in amplifying the inflammatory response within the coronary arteries [47].

CCL2 (prognostic biomarkers and possible therapeutic target) determines monocyte recruitment, plaque destabilization, and predicts major cardiovascular events. CCL2 expression and signaling activate the NF-κB and p42/44 MAPK (ERK1/2) pathways in endothelial cells and monocytes, promoting transcription of proinflammatory genes and adhesion molecules (VCAM-1, ICAM-1) that enhance leukocyte recruitment and retention [48]. In addition to CCR2, CCL2 binds to atypical receptors like ACKR1, which do not induce cell migration but modulate chemokine gradients and inflammatory responses within plaques, influencing local CCL2 activity and plaque microenvironment [49]. Furthermore, CCL2 interacts with other chemokines (CCL4) and receptors (CCR5), activating transcription factors c-Jun and c-Fos, which may regulate CCL2 expression and amplify inflammatory signaling [50].

CCL3, CCL5, and CCL18 determine leukocyte recruitment, and are independently associated with a higher short-term mortality risk [51,52].

Plasma levels of CCL3 are significantly increased in patients with acute myocardial infarction (AMI) and unstable angina, rising rapidly after ischemic events and remaining elevated for months, reflecting ongoing inflammation [53]. CCL3 is produced mainly by leukocytes (macrophages and neutrophils) during inflammation and promotes chemotaxis of neutrophils, T cells, and macrophages to atherosclerotic plaques and ischemic myocardium. This recruitment exacerbates local inflammation and tissue injury. The association between CCL13, vascular inflammation, neutrophil infiltration and plaque progression was proven using CCL13/ApoE-deficient mice expressing lower levels of circulating neutrophils, lower neutrophil infiltration in atherosclerotic plaques and a lower responsivity to CXCL1 when fed with Western-type diet [54].

https://doi.org/10.3390/cells15010072

CXCL1 is highly upregulated in response to ischemic cardiac injury and angiotensin II stimulation. It binds to CXCR2 on monocytes and neutrophils, promoting their chemotaxis into the heart tissue. CXCL1–CXCR2 engagement activates NF-κB and p42/44 MAPK (ERK1/2) pathways in immune and cardiac cells, leading to transcription of proinflammatory cytokines, adhesion molecules (VCAM-1, ICAM-1), and matrix metalloproteinases (MMPs) [48]. CXCL1–CXCR2 signaling contributes to activation of NADPH oxidase (NOX2), which increases ROS production, promoting oxidative stress and further inflammation in cardiac tissues [55].

At the cardiac level, CXCL1 promotes differentiation of cardiac fibroblasts into myofibroblasts, increasing collagen deposition and fibrosis, which impair cardiac function and contribute to heart failure progression. Additionally, by interacting with the Smad2/3 and TGF-β pathways, it leads to pathological atrial remodelling, increasing the susceptibility to atrial fibrillation [55,56]. However, at the vascular level, it exerts a protective role via the same pathway by making the plaque less susceptible to rupture.

Although CXCL5 was more intensively studied in the process of tumor progression, recent efforts have been made to identify its roles in atherosclerotic disease. Similar to CXCL1, CXCL5 binds to CXCR2 on neutrophils and monocytes, promoting their chemotaxis to sites of injury and inflammation [57]. This recruitment amplifies local inflammation and tissue damage. CXCL5 activates intracellular signaling cascades including NF-κB and AKT, which promote transcription of proinflammatory genes, survival signals, and angiogenic factors [58]. In endothelial cells, CXCL5 induces NF-κB-mediated expression of vascular endothelial growth factor A (VEGF-A) via the FOXD1 transcription factor, enhancing angiogenesis and vascular repair processes post-injury. CXCL5 stimulates the MAPK/ERK pathway, which regulates cell proliferation, migration, and survival [59]. This pathway contributes to endothelial cell activation and smooth muscle cell migration. CXCL5 activates epithelial-to-mesenchymal transition (EMT)-related pathways (ERK/Elk-1/Snail and PI3K/AKT/GSK-3β/Snail-Twist), which may have parallels in vascular remodeling and fibrosis after myocardial injury and influencing the development of collateral circulation after an acute coronary syndrome [60]. Supporting evidence for its protective role in coronary artery disease was provided by Ravi et al., who identified a negative correlation between circulating CXCL5 levels and the severity of coronary artery disease, independent of statin use, gender nor age [61].

3. Immune Cells in Acute Coronary Syndrome

3.1. Monocytes and Macrophages

Monocytes are recruited to the arterial wall, where they differentiate into macrophages and phagocytose lipids, becoming foam cells. Foam cells will secrete proinflammatory cytokines, such as IL-1β and TNF-α, which contribute to plaque instability and rupture. Macrophages can polarize into two main phenotypes: M1 (proinflammatory) macrophages, which promote inflammation and plaque vulnerability, and M2 (anti-inflammatory) macrophages, which are more prevalent in advanced plaques and may have protective roles [62–64].

Macrophage infiltration is a crucial and early step in the formation of atherosclerotic plaques. Monocytes migrate into the intima, differentiate into macrophages, and take up oxidized LDL via scavenger receptors (e.g., SR-A, CD36), transforming into foam cells. These foam cells and macrophages produce inflammatory cytokines, such as IL-6 and TNF-α, as well as matrix metalloproteinases, particularly MMP-1 and MMP-9, which degrade extracellular matrix proteins. This degradation weakens the fibrous cap of plaques, making them more prone to rupture and thrombus formation, which can precipitate acute coronary syndrome (ACS) events [65]. Monocytes/macrophages secrete proinflammatory cytokines

https://doi.org/10.3390/cells15010072

that activate neighboring vascular smooth muscle cells, promoting the formation of the extracellular matrix, fibrosis, and further destabilization of the plaques.

The inflammatory milieu created by these cells amplifies local immune responses, attracting more immune cells and sustaining chronic inflammation within the plaque [66]. Monocytes, with their various subpopulations, play a central role in both inflammation and repair mechanisms within the cardiovascular system. Specific subsets of monocytes may promote inflammation, contributing to tissue injury, while others are linked to repair and healing processes after myocardial damage. After MI, monocytes are rapidly recruited to the ischemic heart tissue, where they differentiate into inflammatory macrophages. These macrophages clear dead cells and extracellular debris through phagocytosis, and they secrete proteases and reactive oxygen species, which are essential for tissue remodeling but can also exacerbate injury if produced in excessive amounts [67,68].

The number of monocytes/macrophages increases significantly in the first hours after an MI, and their level remains elevated for about two weeks after an MI. Initially, the infiltrate has a pro-inflammatory role that gradually transitions into a reparative one, contributing to scar formation [64,69].

3.2. Neutrophils

Polymorphonuclear neutrophils (PMNs) play a significant and multifaceted role in ACS, primarily through their involvement in inflammation, plaque destabilization, and thrombosis. These cells are among the first responders to vascular injury, releasing proteolytic enzymes and reactive oxygen species that exacerbate endothelial damage and promote thrombosis. Neutrophils are actively recruited into atherosclerotic plaques, particularly in unstable lesions underlying ACS, such as AMI. Endogenous activation of Toll-like receptor 2 (TLR2) on endothelial cells promotes neutrophil recruitment and accumulation at sites of early plaque erosion, as demonstrated in murine models. They are found in significantly higher numbers in ruptured and eroded plaques compared to stable plaques, suggesting their direct involvement in plaque destabilization [70]. Activated neutrophils release enzymes such as neutrophil elastase, myeloperoxidase (MPO), and matrix metalloproteinases (MMPs). These enzymes degrade extracellular matrix components and basement membranes, contributing to endothelial damage and weakening of the fibrous cap, which can precipitate plaque rupture and thrombus formation. Activated neutrophils can release Neutrophil Extracellular Traps (NETs), web-like structures composed of decondensed chromatin (DNA and histones) decorated with neutrophil granule proteins, such as myeloperoxidase and neutrophil elastase. These NETs provide a matrix that traps platelets, red blood cells, and coagulation factors, facilitating clot formation in coronary arteries and inducing endothelial cell injury and dysfunction, which in turn destabilizes the plaques. NETs stimulate sterile inflammation by activating immune cells and releasing inflammatory mediators, exacerbating vascular injury [71]. NETs form a scaffold within coronary thrombi and correlate positively with infarct size, indicating their role in worsening myocardial injury. DNase, an enzyme that degrades NETs, is associated with reduced infarct size, suggesting a protective mechanism against NET-mediated damage [72].

The ROS production during ischemia activates peptidyl-arginine-deiminase-4 (PAD4), an enzyme that facilitates citrullination of arginine residues in histones (particularly H3 histone), leading to chromatin decondensation. Chromatin unfolding occurs due to the disruption of the ionic interactions between the positively charged arginine residues and the negative charges from the DNA phosphate groups. PAD4 activation also favors translocation of neutrophil elastase and myeloperoxidase into the nucleus that attach to chromatin strands forming NETs. Finally, the nuclear and plasma membranes are lysed, expelling NETs into the extracellular compartment [73].

https://doi.org/10.3390/cells15010072

Increased plasma levels of MPO are associated with an increased risk of coronary artery disease [74], and MPO-DNA complexes are positively correlated with severe adverse cardiovascular events [75].

NET formation is implicated in multiple steps of ACS pathophysiology, from plaque destabilization and arterial thrombosis to reperfusion injury and impaired microvascular flow [76,77]. NETs were identified in human atherothrombotic plaques and retrieved coronary thrombi, being linked to a higher risk of cardiac-related death and stent thrombosis. NETs are also associated with microvascular obstruction and no-reflow after reperfusion, worsening infarct expansion [78,79].

Coronary blood flow restoration during fibrinolysis or PCI increases vascular inflammation significantly, activating the neutrophils which release NETs through the suicidal pathway, augmenting the inflammatory response in a positive feedback fashion [80]. Activated neutrophils express a higher NADPH oxidase activity, which generates reactive oxygen species. ROS are crucial for the formation of NETs by breaking down nuclear and cellular membrane to allow NET release. However, the local oxidative stress also affects myocardial tissues, augmenting cardiac muscle damage and release of pro-inflammatory molecules [81,82]. Excessively accumulated NETs in the ischemic/necrotic myocardium favor the formation of microthrombi by interacting with red blood cells and platelets, contributing to the 'no-reflow' phenomenon [83].

Neutrophils also contribute to the inflammatory milieu by releasing cytokines (IL-1β and IL-18) and interacting with other immune cells, such as macrophages, thereby amplifying local inflammation within the plaque [82].

Elevated circulating neutrophil counts and neutrophil/lymphocyte ratios are associated with unstable coronary artery disease and predict worse cardiovascular outcomes in ACS patients. Neutrophil levels on admission correlate with mortality and major adverse cardiac events, making them useful prognostic markers [84].

3.3. T Lymphocytes

T-cells, especially CD4+ helper T-cells, are more frequently activated in ACS compared to stable angina. Single-cell RNA sequencing has revealed distinct clusters of CD4+ T cells, including effector, naive, cytotoxic, central memory, and regulatory T cells [85]. In ACS, there is a shift toward aggressive effector phenotypes with a high frequency of T helper cell 1 (Th1) and a reduction in regulatory T-cells (Tregs), which normally suppress excessive immune responses [86]. They have a lower activation threshold due to amplified T-cell receptor (TCR) signaling, including increased accumulation of signaling molecules like CD3 complexes, ZAP70, and defective deactivation of LCK kinase [87]. CD4+ T-cells in ACS patients show enhanced activation, lower thresholds for stimulation, and increased cytotoxicity, even capable of killing endothelial and vascular smooth muscle cells [86].

3.3.1. Th1 Cells

Th1 cells, characterized by T-bet expression and IFN-γ production, promote macrophage activation, endothelial dysfunction, and pro-inflammatory plaque phenotypes [88]. Clinical studies demonstrate Th1 enrichment in acute myocardial infarction (AMI) patients, with elevated Th1 frequencies correlating with systemic inflammation markers and plaque vulnerability indices [89]. The IFN-γ produced by Th1 cells mediates pro-atherogenic endothelial and macrophage phenotypes, contributing to plaque destabilization [90].

3.3.2. Th17 Cells

Th17 cells, expressing RORγ and producing IL-17A, facilitate neutrophil recruitment and matrix degradation through metalloproteinase induction [86]. A higher Th17 number is linked to plaque vulnerability and functional decline after ACS [91]. The Th17 pathway can

https://doi.org/10.3390/cells15010072

activate matrix-metalloproteinases with atheroma cap thinning, potentially contributing to plaque rupture events.

3.3.3. Regulatory T Cells (Tregs)

Tregs, characterized by FOXP3 expression and IL-10/TGF-β production, suppress effector T cell responses and promote tissue repair. In ACS patients, reduced or dysfunctional Tregs correlate with worse clinical outcomes and impaired post-infarction remodeling. Tregs support scar formation and healing by inducing macrophage phenotypic change towards the M2 phenotype and limiting excessive inflammatory responses via IL-10 and TGF-β release [92].

3.3.4. CD8+ T Cells

CD8+ T cells exert significant cytotoxic functions in both infarcted myocardium and atherosclerotic plaques. These cells kill target cells via perforin/granzyme and Fas-FasL pathways. Granzyme B-dependent CD8+ activity is linked to adverse remodeling after ischemic injury [93]. Expanded CD4+ CD28-/CD28null and activated CD8+ subsets with effector/senescent features accumulate in the coronary circulation during STEMI and are associated with increased local inflammation [94].

The activation of CD8+ T cells requires TCR recognition of peptide-MHC complexes plus co-stimulation (CD28/B7, CD40/CD40L), and is modulated by immune checkpoints such as CTLA-4 and PD-1 that restrain pathogenic responses [95]. By inhibiting the co-stimulatory axes (CD40 inhibitors, CD28 inhibitors) or augmenting the inhibitory checkpoints (CTLA-4, PD-1 agonists), T cell-mediated vascular inflammation may be mitigated.

The mechanism of atherosclerosis and plaque rupture is summarized in Figure 1.

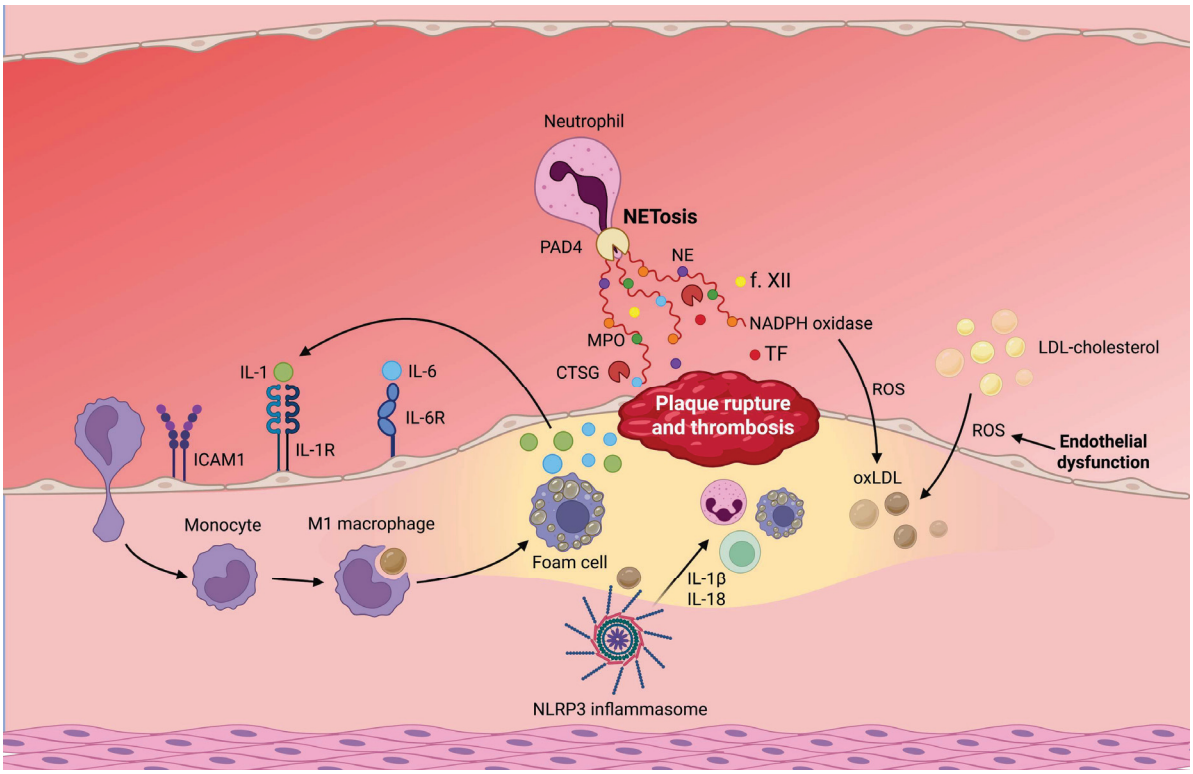


Figure 1. Schematic representation of atherosclerotic plaque rupture and thrombosis. Created in BioRender. Tirziu, A. (2025), https://BioRender.com/mmejda6 [Accessed on 9 November 2025].

4. Inflammatory Markers in Acute Coronary Syndrome

4.1. C-Reactive Protein (CRP)

CRP is an acute-phase protein produced mainly by hepatocytes in response to inflammatory cytokines, including interleukin-1 and interleukin-6 [96]. Its levels rise significantly during ACS, reflecting systemic and vascular inflammation linked to plaque instability and myocardial injury. Elevated CRP levels on admission in ACS patients are strongly associated with worse short- and long-term cardiovascular outcomes, including higher risk of death, myocardial infarction, heart failure, and MACE. In healthy individuals, CRP levels typically range from about 1.2 to 2.0 mg/L [97]. CRP levels start increasing around 6 h after symptom onset in ACS, typically reach peak values between 36 and 50 h (approximately 1.5 to 2 days) after the event [98].

Patients with CRP levels above 3 mg/L have significantly lower survival rates and a higher incidence of complications [99,100]. CRP levels $\geq$ 10 mg/L are commonly used as a cutoff to indicate significant inflammation and a higher risk of adverse outcomes. Elevated CRP above 10 mg/L within 24 to 48 h after ACS onset is associated with worse prognosis and increased long-term mortality [98,100].

CRP levels tend to increase following myocardial injury, with higher levels observed in STEMI and NSTEMI compared to unstable angina. The magnitude of CRP elevation correlates with the extent of myocardial necrosis and inflammatory response [98]. Measuring CRP, especially high-sensitivity CRP (hs-CRP), helps identify patients at higher risk who may benefit from more aggressive treatment and closer monitoring post-ACS. Combining CRP with other markers, such as troponin, enhances risk stratification. Studies have shown that patients who achieve lower CRP levels after treatment, especially with statins, have better outcomes. For example, in the PROVE IT-TIMI 22 trial, ACS patients who reduced their CRP levels below 2 mg/L after intensive statin therapy had significantly lower rates of death or recurrent MI compared to those with CRP levels above 2 mg/L, independent of cholesterol levels [101,102]. Persistently elevated CRP after ACS, even with modern therapies, indicates ongoing inflammation and predicts worse long-term prognosis, including higher mortality and heart failure risk [103]. CRP measurement can thus be used to monitor the inflammatory response and treatment efficacy, guiding more aggressive or tailored therapy in patients with persistently high CRP post-ACS.

4.2. Elevated White Blood Cell and Neutrophil Counts in ACS

Studies consistently show that elevated white blood cell (WBC) counts at admission in ACS patients are linked to higher risks of mortality, recurrent myocardial infarction, and MACE such as cardiac death and target lesion revascularization [104]. Elevated WBC count is an independent predictor of both short-term and long-term mortality in ACS, including STEMI and non-STEMI patients. Patients with higher WBC counts have a significantly increased risk of death during hospitalization and follow-up periods [105]. Higher WBC and neutrophil counts correlate with more severe coronary artery disease, including the presence of active thrombus, multi-vessel disease, and reduced LVEF. Elevated counts are also associated with complications such as congestive heart failure and cardiogenic shock [106].

Higher baseline WBC counts are associated with increased risk of ischemic events (cardiovascular death, MI, stroke) at 30 days and 1 year post-ACS [107].

The neutrophil-to-lymphocyte ratio (NLR) is the commonly used neutrophil ratio in ACS. It is calculated by dividing the absolute neutrophil count by the absolute lymphocyte count from a routine complete blood count. NLR is a simple, widely available, and cost-effective marker of systemic inflammation that has substantial predictive value for myocardial damage, cardiac dysfunction, rehospitalization, and mortality in ACS pa-

https://doi.org/10.3390/cells15010072

tients [108,109]. Elevated NLR reflects heightened inflammation (neutrophilia) combined with relative immunosuppression (lymphopenia), making it a robust biomarker for predicting short- and long-term adverse cardiovascular outcomes in ACS. An NLR cutoff of around 2.5 is commonly used for diagnosing ACS, with a reported sensitivity of about 63.6% and specificity of 80.2%. An NLR exceeding approximately 2.76 is associated with heightened myocardial damage and diminished cardiac function, as evidenced by reduced ejection fraction and fractional shortening. Elevated thresholds, such as NLR > 4 or >4.5, have been linked to adverse outcomes, including increased in-hospital mortality and major adverse cardiac events (MACE). Stratification of NLR into tertiles (e.g., <2.6, 2.6–4.5, >4.5) correlates with escalating risk and disease severity. Furthermore, NLR demonstrates a positive correlation with established clinical risk scores, such as GRACE and SYNTAX, which evaluate prognosis and coronary lesion complexity in acute coronary syndrome (ACS) [110].

Studies demonstrate that higher NLR values are strongly associated with elevated cardiac troponin levels, including high-sensitivity troponin I (hsTnI), which is a sensitive marker of myocardial necrosis. NLR can predict troponin positivity in follow-up, with a cutoff around 2.8 showing good sensitivity (79%) and specificity (73%) for troponin elevation [111]. The combined assessment of NLR with troponin and CRP enhances risk stratification in ACS. Patients with high NLR and CRP levels have significantly higher rates of mortality and major adverse cardiac events (MACCE) compared to those with low levels.

4.3. IL-6

IL-6 levels are elevated in patients with ACS, including acute myocardial infarction and unstable angina, but not in stable angina [27,112]. IL-6 is a powerful predictor of long-term cardiovascular mortality and adverse events after ACS, outperforming traditional markers such as hsCRP. Elevated IL-6 levels are independently associated with increased risk of MACE, cardiovascular death, heart failure, and recurrent myocardial infarction [29]. IL-6 measurement is increasingly used in clinical practice to assess inflammatory status and stratify risk in ACS patients, as it may help identify patients who would benefit from more aggressive or targeted anti-inflammatory therapies [28]. The normal value of IL-6 in healthy adults is generally considered to be less than 5 pg/mL, with some sources citing a range up to about 7 pg/mL depending on the laboratory and assay used. A meta-analysis performed on healthy adults found a pooled average IL-6 level around 5.2 pg/mL (95% CI: 4.6–5.7 pg/mL), with values ranging from 0 to about 43.5 pg/mL in some individuals without apparent disease [113]. Patients with unstable angina have IL-6 levels about three times higher than healthy controls. Higher IL-6 levels are strongly associated with more severe ACS, including STEMI, MACE, cardiovascular death, heart failure, and recurrent myocardial infarction [27]. Reported levels in ACS can vary widely but typically fall between 10 to 50 pg/mL, sometimes much higher depending on severity and timing. A study in patients with STEMI showed IL-6 levels as high as 30–100 pg/mL shortly after symptom onset [114]. Elevated IL-6 levels are associated with a larger infarct size, higher risk of MACE, and worse short- and long-term prognosis. IL-6 levels rise within hours after the onset of myocardial injury and usually peak at 6–24 h, then gradually decline over a few days [115].

4.4. TNF α

The determination of tumor necrosis factor-α (TNF-α) in the context of ACS is primarily associated with its role as both a marker and mediator of inflammation, which is pivotal in the pathogenesis and complications of ACS. Patients with ACS, including those with unstable angina and acute MI, exhibit significantly elevated levels of TNF-α

https://doi.org/10.3390/cells15010072

compared to control groups. This elevation is correlated with the severity of the condition and the incidence of complications such as recurrent angina, hemodynamic instability, and electrical abnormalities [116].

TNF-α plays a critical role in the progression of ischemia by promoting the release of endothelial adhesion molecules, activating leukocytes, and inducing the secretion of thrombocyte-activating factors. These processes collectively exacerbate coronary artery disease and contribute to plaque instability. Elevated levels of TNF-α are recognized as an independent predictor of adverse coronary events and mortality, alongside other inflammatory and injury markers such as IL-6, CRP, and troponin-T.

In patients with ACS who also have rheumatoid arthritis (RA), TNF-α expression on atherosclerotic plaques is even stronger, suggesting a more intense and sustained pro-inflammatory response that may worsen outcomes. Monitoring TNF-α in such patients could guide preventive strategies [32].

Beyond its role as a biomarker, TNF-α signaling influences cardiac physiology and disease processes, mediated partly through NF-κB pathways, highlighting its dual role in inflammation and cardiac tissue response [117].

Additionally, TNF-α levels and genetic polymorphisms have been linked to suicidal ideation in ACS patients, especially in the first two weeks after ACS indicating that TNF-α may also be involved in neuropsychiatric complications post-ACS [118].

The normal value of TNF-α in acute coronary syndrome (ACS) patients is not universally fixed, but studies show that TNF-α levels are significantly elevated in ACS compared to healthy controls. For example, one study found a marked increase in TNF-α levels in ACS patients, with higher levels particularly in those with acute myocardial infarction (MI) compared to unstable angina, and these elevated levels correlated with greater complications [119].

While exact numeric reference ranges vary by assay and population, TNF-α levels in healthy individuals are generally low (often <10 pg/mL), whereas ACS patients often exhibit significantly higher levels, sometimes several-fold above normal baseline values [118].

4.5. Novel Biomarkers in ACS

No blood biomarkers are exclusively specific to coronary vascular inflammation. HsCRP and IL-6 lack specificity for coronary artery disease (CAD), as they reflect systemic inflammation influenced by infections, obesity, or other conditions, limiting their diagnostic accuracy for isolated coronary tree inflammation [120].

However, lipoprotein-associated phospholipase A2 (Lp-PLA2) and myeloperoxidase (MPO) are more relevant to coronary disease, as they target plaque-specific processes, such as the hydrolysis of oxidized phospholipids and neutrophil activation.

Lp-PLA2 localizes to atherosclerotic plaques, particularly in macrophages and necrotic cores, where it amplifies local vascular inflammation rather than reflecting systemic processes like hsCRP. Elevated levels correlate with high-risk plaque features on CT angiography, such as thin fibrous caps and positive remodeling, independent of traditional lipids [121]. Lp-PLA2 predicts coronary events (e.g., ACS) after adjusting for CRP and LDL-C, with thresholds >225–235 ng/mL indicating high vascular risk. However, its association may partly depend on oxidized LDL levels, positioning it as a marker of oxidative stress within coronary inflammation rather than a fully independent causal factor [122].

A 2025 meta-analysis of 22 studies (1110 stable vs. 1298 unstable plaques) reported a pooled sensitivity of 85% (95% CI: 80–89%), specificity of 80% (95% CI: 74–85%), and AUC of 0.89 (95% CI: 0.86–0.92), indicating robust performance across vascular sites including coronaries. The positive likelihood ratio (PLR) was 4.23, and the diagnostic odds ratio (DOR) was 22.55, supporting its utility for plaque vulnerability assessment [123]. In coro-

https://doi.org/10.3390/cells15010072

nary CT angiography contexts, Lp-PLA2 at cutoffs like 183 ng/mL showed 91.7% sensitivity for detecting plaques or stenosis, outperforming some imaging markers alone. However, for event prediction in asymptomatic cohorts, accuracy drops (e.g., 37% sensitivity, 75% specificity in the top quartile). These findings highlight better strength for plaque characterization than primary screening. Heterogeneity in plaque criteria and location affects results, but overall, an AUC > 0.85 confirms good discriminative power. MPO and Lp-PLA2 both detect plaque inflammation but describe different mechanisms, with MPO emphasizing acute oxidative neutrophil activity and Lp-PLA2 targeting chronic macrophage-driven lipid hydrolysis. Neither of these markers has head-to-head superiority for detection alone, but combinations enhance accuracy.

Myeloperoxidase (MPO) acts as a marker of coronary vascular inflammation by reflecting neutrophil activation and oxidative stress within atherosclerotic plaques. Released from neutrophils in inflamed coronary lesions, it promotes LDL oxidation, endothelial dysfunction, and plaque instability. High MPO (>320 pmol/L) predicts major adverse cardiac events in ACS patients, with meta-analyses showing odds ratios up to 3.5 for mortality, complementing troponins for short-term risk stratification. It identifies high-risk patients even with low hsCRP. Consequently, MPO levels highlight plaque-specific oxidative inflammation over general markers [124].

Soluble CD40 ligand (sCD40L) and pentraxin-3 (PTX3) provide improved specificity for endothelial activation and local plaque inflammation compared to hsCRP.

SCD40L serves as a marker of coronary inflammation by mediating interactions between activated platelets, endothelial cells, and immune cells in atherosclerotic plaques, promoting cytokine release, matrix metalloproteinase expression, and plaque instability. Its primary source is from activated platelets during thrombosis (>95%). Levels rise significantly in ACS (e.g., mean 68 ng/mL in STEMI vs. <30 ng/mL in controls), reflecting acute plaque rupture and inflammation intensity.

ROC analysis shows an AUC 0.632 for ACS prediction (cutoff 5.68 ng/mL; sensitivity 82%, specificity 40%), with stronger performance for STEMI over NSTEMI/UA [125]. Elevated sCD40L independently predicts adverse events like recurrent MI and revascularization, though antiplatelet therapy may blunt its levels. sCD40L, MPO, and Lp-PLA2 all mark coronary inflammation but differ in pathways, timing, and performance, with MPO and Lp-PLA2 generally outperforming sCD40L in predictive strength for plaque vulnerability.

MPO and Lp-PLA2 show superior AUC and independence from hsCRP for event prediction, while sCD40L adds value in thrombotic ACS subsets. Combinations (e.g., all three) may optimize detection, though direct trials are lacking.

Pentraxin 3 (PTX3) emerges as a promising future biomarker for detecting vascular inflammation in coronary artery disease (CAD), offering greater specificity than hsCRP or IL-6 by localizing primarily to atherosclerotic lesions rather than reflecting systemic inflammation. PTX3 acts as a soluble pattern recognition receptor rapidly produced at sites of inflammation, such as in coronary plaques, enabling earlier detection of subclinical atherosclerosis. Unlike hsCRP, which is a downstream acute-phase reactant influenced by multiple factors, PTX3 correlates directly with plaque instability and cardiovascular events independent of traditional risk factors. Clinical studies show elevated PTX3 levels predict CAD progression and all-cause mortality in older adults [126].

PTX3 localizes to atherosclerotic plaques as a rapid-response pattern recognition molecule, directly reflecting lesion inflammation and instability rather than broad systemic effects. Studies link elevated PTX3 to CAD progression and mortality, independent of CRP [127].

https://doi.org/10.3390/cells15010072

TRAF3IP2, an IL-17 pathway adaptor, shows upregulated expression in CAD, enabling nomogram-based prediction of stenosis severity via bioinformatics and cohort validation. It bridges inflammation to clinical outcomes more precisely than cytokines [128].

Several biomarkers show promise in distinguishing stable from unstable coronary plaques by reflecting plaque-specific inflammation, matrix degradation, or immune infiltration rather than systemic effects. These include sLOX-1, MMP-9, HSPA2, GEM, and MPO, validated through bioinformatics, OCT imaging, and cohort studies. SLOX-1 and MMP-9 levels are elevated in ruptured plaques, with a combinatorial model (including WBC and CK-MB) achieving moderate sensitivity (62%) and high specificity (98%) for rupture detection in ACS patients via OCT. HSPA2 and GEM, identified as differentially expressed genes, exhibit strong diagnostic AUCs (0.93 and 0.91 in training cohorts) and downregulation in unstable plaques, confirmed by immunohistochemistry [129].

HSPA2 and GEM stand out as protein biomarkers with the highest reported AUC values for distinguishing unstable coronary plaques, based on bioinformatics and machine learning analyses of plaque gene expression. These markers show strong diagnostic performance, with HSPA2 achieving AUC 0.934 in training cohorts and 0.828 in validation, while GEM reaches 0.913 and 0.788, respectively [130].

HSPA2 (a heat shock protein) and GEM (a GTP-binding protein) are downregulated in unstable plaques and correlate with immune cell infiltration patterns like macrophages and neutrophils. Their combined use enhances specificity for plaque instability over systemic markers.

Circulating proteins like soluble LOX-1 (sLOX-1), pregnancy-associated plasma protein A (PAPP-A), and myeloperoxidase (MPO) outperform troponin in predicting plaque instability by detecting early vascular inflammation and rupture before myocardial necrosis occurs [131]. sLOX-1 rises earlier post-ACS than troponin-T, reflecting oxidized LDL uptake in plaques and enabling detection of pre-necrotic instability in prospective cohorts. PAPP-A predicts outcomes in troponin-negative ACS patients with high hazard ratios (up to 7.48), signaling matrix degradation in vulnerable plaques. MPO correlates directly with ongoing rupture in ACS, distinguishing acute instability from stable states better than troponin or CRP.

Plasma proteomics platforms, particularly those using Olink Proximity Extension Assay (PEA) technology, report the highest AUCs for plaque instability markers by analyzing hundreds of circulating proteins simultaneously. Olink PEA panels achieved AUC 0.855 for predicting accelerated plaque progression, surpassing clinical models (ΔAUC 0.137, $p = 0.004$) in CCTA-validated cohorts. Targeted proteomics via mass spectrometry or aptamer-based SomaScan also yield high AUCs (0.80–0.93) for high-risk plaques, identifying signatures like FRIL, CATD, and MMP9 [132].

MicroRNAs (e.g., miR-133a-3p, miR-451a) show promise as upregulated markers in CAD but require validation. These miRNAs are upregulated in CAD plasma, potentially from cardiomyocyte damage or endothelial dysfunction in inflamed coronary plaques. MiR-133a-3p regulates cardiac remodeling and inflammation pathways, while miR-451a links to vascular smooth muscle proliferation and oxidative stress in atherosclerosis. Their stability in circulation positions them as non-invasive indicators of ongoing coronary pathology beyond acute injury. ROC analyses highlight miR-133a-3p and miR-451a as top performers among panels (e.g., with miR-21-5p, miR-221-3p), showing strong discriminatory power for CAD diagnosis versus controls, though specific AUC values and inflammation cutoffs require further validation in larger cohorts. They complement protein markers like MPO by capturing genetic-regulatory aspects of plaque vulnerability. Systematic reviews identify miR-133a-3p as specifically upregulated in ACS versus stable CAD, alongside miR-1, miR-208a/b, and miR-499, due to its cardiac-specific release during acute necrosis and

https://doi.org/10.3390/cells15010072

inflammation. In stable CAD cohorts, levels remain closer to controls or show less elevation, as plaque rupture and thrombosis—hallmarks of ACS—are absent [133]. A key meta-analysis of 9 studies reported a pooled AUC of 0.73 (95% CI: 0.68–0.79) for miR-133a-3p in ACS contexts, rising to 0.89 with healthy controls versus 0.68 with symptomatic ones. Although sensitivity and specificity were not uniformly pooled, they were concordant with the high values found in early studies (e.g., >0.86) [134].

Computed tomography angiography (CCTA) with perivascular fat attenuation index (FAI) directly quantifies coronary inflammation by measuring fat changes around proximal coronary arteries, predicting events independently of hsCRP. Positron emission tomography (PET-CT) using tracers like ^{18}F-FDG targets metabolically active inflamed plaques in coronary vessels with high specificity. These outperform blood markers for localizing inflammation to the coronary circulation [135].

FAI quantifies the shift from lipid-rich (low attenuation) to water-rich (higher attenuation) perivascular adipose tissue (PVAT) caused by paracrine inflammatory signals from the adjacent coronary wall, acting as a "vessel wall thermometer" specific to local vascular inflammation. This spatial gradient around proximal major coronaries (e.g., right coronary artery, left anterior descending) isolates coronary-specific effects, avoiding systemic confounders like infections or obesity that affect hsCRP. FAI predicts plaque instability, hemodynamic impact (e.g., lower CT-FFR), and cardiac events independently of traditional risk scores or hsCRP, enabling risk reclassification in up to 62% of patients. It dynamically responds to anti-inflammatory therapies (e.g., biologics reducing FAI in months), confirming its link to treatable coronary processes. Cutoffs like ≥ -70.1 HU signal high-risk inflammation linked to plaque rupture [136].

An ideal marker for detecting inflammation in ACS would offer high specificity to vascular or plaque inflammation, rise early before necrosis (unlike troponin), predict instability and outcomes independently, and enable point-of-care testing. It must localize to atherosclerotic lesions, distinguishing ACS from non-cardiac inflammation, with rapid kinetics (peaks within hours) and minimal circadian variation, unlike IL-6. High sensitivity/specificity (AUC > 0.90) for risk stratification complements hs-cTn by identifying pre-rupture events in troponin-negative patients. The marker should predict instability in troponin-negative patients, guide anti-inflammatory therapies such as colchicine, and improve net reclassification over hsCRP by integrating with imaging to assess plaque vulnerability.

The future of inflammatory markers in acute coronary syndrome (ACS) holds multiomic panels integrating proteomics, transcriptomics, and AI-driven models, offering superior risk stratification beyond single markers such as hsCRP.

Olink PEA and SomaScan platforms evolve into point-of-care multiplex assays, integrating machine learning (e.g., CatBoost) to achieve AUC > 0.85 for plaque progression, validated against CCTA/OCT. MicroRNA-mRNA networks and deep learning forecast personalized therapies like IL-1β inhibitors [137].

5. Therapeutic Strategies and Implications

5.1. Aspirin

Aspirin plays a significant anti-inflammatory role in ACS, beyond its well-known antiplatelet effects. In ACS, vascular injury involves complex interactions among inflammatory mediators, platelets, and thrombosis. Aspirin at antiplatelet doses (100–300 mg/day) reduces inflammation markers such as CRP or TNF-α [138], macrophage colony-stimulating factor (M-CSF), and monocyte chemoattractant protein-1 (MCP-1). Aspirin exerts immunomodulatory effects by counteracting the increase in pro-inflammatory monocyte subsets (e.g., CD14^{high}CD16^{+} monocytes) seen in ACS. This suggests aspirin can reduce monocytic biomarkers of inflammation, further contributing to plaque stabilization and

https://doi.org/10.3390/cells15010072

improved outcomes [139]. Additionally, aspirin may acetylate COX-2 in vascular cells, shifting its activity to produce 15-epi-lipoxin ("aspirin-triggered lipoxin"), a potent anti-inflammatory mediator. Aspirin also stimulates endothelial nitric oxide synthase (eNOS) and upregulates heme oxygenase-1 (HO-1), enhancing the antioxidative capacity of vascular cells [140]. Mechanistically, aspirin inhibits platelet cyclooxygenase-1 (COX-1), thereby reducing thromboxane A2 formation. This not only prevents platelet aggregation but also decreases thrombin formation and the production of secondary pro-inflammatory mediators, such as sphingosine-1-phosphate. This inhibition helps break the cycle of platelet activation and inflammation that contributes to plaque instability and thrombosis [138]. Aspirin may help decrease the progression of atherosclerosis by protecting LDL from oxidative modification and improving endothelial dysfunction. When LDL is exposed to oxidative stress, aspirin treatment significantly decreases the production of malondialdehyde (a marker of lipid peroxidation) and diminishes the electrophoretic mobility of LDL, both indicators of reduced oxidative modification. These effects are believed to reduce vascular inflammation further and enhance vasodilation. The protective effect is thought to be related to aspirin's ability to inhibit the formation of free radicals and lipid peroxides that drive LDL oxidation [141,142]. The ability of aspirin to protect LDL from oxidative modification is dose-dependent, with higher doses showing protective effects (300 mg/day) and lower doses (75 mg/day) potentially having the opposite effect [143]. Aspirin's anti-inflammatory effects in ACS are achieved primarily through inhibition of COX enzymes, leading to reduced production of inflammatory and prothrombotic mediators, modulation of immune cell activity, and improvement of endothelial function. These mechanisms collectively reduce inflammation, stabilize plaques, and lower the risk of adverse cardiovascular events [144].

While low-dose aspirin (75–100 mg/day) is effective for antiplatelet therapy and cardiovascular prevention, its effect on LDL oxidation may not be beneficial. It could even be pro-oxidative at these doses. The antioxidant, LDL-protective effects of aspirin are observed at higher doses (300 mg/day). Still, these are not typically used for long-term cardiovascular prevention due to the increased risk of side effects and the exceptionally high risk of gastrointestinal bleeding [143,145].

5.2. Statins

Statins have a significant anti-inflammatory effect in ACS, in addition to their well-known lipid-lowering properties.

The JUPITER trial was a large, randomized, double-blind, placebo-controlled trial involving 17,802 participants who were healthy but had low levels of LDL cholesterol (the "bad" cholesterol) and high levels of CRP (>2 mg/L). Participants were assigned to receive either rosuvastatin or a placebo and were followed for an average of 1.9 years. Rosuvastatin reduced LDL cholesterol levels by 50% and CRP levels by 37%, indicating its effectiveness in lowering both cholesterol and inflammation. The findings suggest that statin therapy, particularly with rosuvastatin, could be beneficial for individuals who do not have high cholesterol but do have elevated CRP levels, which is often associated with a higher risk of cardiovascular issues [146]. Statins inhibit nuclear factor kappa B (NF-κB), a key transcription factor that regulates the expression of many inflammatory genes, thereby reducing inflammatory markers such as IL-1β, CRP, IL-6, and TNF-α [147]. Stabilization of atherosclerotic plaques by reducing inflammation within atherosclerotic plaques, making them less likely to rupture and cause acute events, partly due to reduced infiltration of inflammatory cells (like macrophages) and decreased expression of adhesion molecules. Statins reduce the expression of adhesion molecules on endothelial cells (e.g., ICAM-1, lymphocyte function-associated antigen-1) and chemokines such as monocyte chemoattractant

https://doi.org/10.3390/cells15010072

protein-1 (MCP-1). This inhibits the transendothelial migration of leukocytes into the vessel wall, limiting inflammatory cell infiltration into atherosclerotic plaques [148].

Additionally, statins reduce Myeloperoxidase (MPO) activity, decrease oxidative stress and vascular inflammation, and improve endothelial function by enhancing nitric oxide bioavailability, which reduces endothelial activation and inflammation [149].

Statins can reduce inflammatory markers within days of starting therapy, even before significant changes in cholesterol levels occur. This rapid effect is particularly beneficial in the acute phase of ACS [150].

Different types of statins vary in their anti-inflammatory effects in ACS and other cardiovascular conditions, influenced by their chemical properties (lipophilicity vs. hydrophilicity), potency, and dosage. Rosuvastatin and atorvastatin, both potent statins, significantly reduce CRP levels. Lipophilic statins (e.g., simvastatin, atorvastatin) tend to have more pleiotropic effects, including anti-inflammatory actions, compared to hydrophilic statins (e.g., pravastatin, rosuvastatin) [151]. Some evidence suggests rosuvastatin may paradoxically increase certain pro-inflammatory cytokines (e.g., IL-1β) in specific contexts, although it still reduces other markers like IL-6 [152]. However, one study reported that rosuvastatin (20 mg) reduced CRP levels greater than atorvastatin (40 mg; 44 vs. 35%) after 4 weeks of treatment, indicating a more potent anti-inflammatory effect for rosuvastatin [153]. In conclusion, while all statins share anti-inflammatory properties, lipophilic statins like simvastatin and atorvastatin often exhibit stronger anti-inflammatory effects, possibly due to better cellular penetration. Rosuvastatin, a hydrophilic statin, shows potent CRP reduction but may have a mixed impact on other cytokines. The intensity of anti-inflammatory action also depends on the statin dose, with higher doses generally producing greater effects.

In the MIRACLE study, atorvastatin 80 mg in patients with ACS (NSTEMI and UA) reduced the rate of ischemic cardiac events over a 16-week follow-up period, with the effect already visible after 6 weeks [154]. High-dose statin (atorvastatin 80 mg) was also shown to be superior to pravastatin 40 mg in patients with ACS in the PROVE IT-TIMI 22 trial, reducing primary and secondary endpoint (death, myocardial infarction, unstable angina requiring rehospitalization, stroke, or revascularization $\geq$ 30 days) [155].

In registries that included the follow-up of patients with ACS, high-dose statin administration within the first 24 h of first medical contact reduced the incidence of MACE and the risk of in-hospital mortality [156]. A Cochrane review of over 14,000 ACS patients found no significant increase in serious adverse events with early statin initiation (within 14 days of ACS onset) compared to placebo or usual care [157,158].

5.3. PCSK9 Inhibitors

PCSK9 inhibitors have a notable anti-inflammatory role in ACS that extends beyond their potent effects on lowering LDL cholesterol. Emerging evidence from clinical and experimental studies highlights several mechanisms by which PCSK9 inhibition modulates inflammation and vascular health in ACS. PCSK9 levels are significantly elevated during ACS and are associated with increased expression of pro-inflammatory cytokines such as TNF-α, IL-6, IL-1β, IFN-γ, and chemokines like MCP-1. Higher PCSK9 correlates with systemic inflammatory markers, including white blood cell count (WBC), fibrinogen, and high-sensitivity C-reactive protein (hs-CRP). PCSK9 promotes vascular inflammation by enhancing monocyte recruitment, endothelial adhesion molecule expression (e.g., ICAM-1), and the activation of inflammatory cascades, thereby contributing to plaque progression and instability [159]. In the ATHEROREMO-IVUS study, serum PCSK9 levels were correlated with the necrotic core size of atherosclerotic plaques in patients with ACS, independent on the LDL-cholesterol values [160]. Hence, PCSK9 inhibitor administration

https://doi.org/10.3390/cells15010072

in patients with acute coronary syndromes may have specific anti-inflammatory effects that occur in addition to lowering LDLc. Anti-inflammatory mechanisms of PCSK9 inhibitors are to reduce the expression of proinflammatory cytokines such as TNF-α, IL-1β, IL-6 and MCP-1, both in animal models and in human patients [157,160], to modulate immune activation by favoring dendritic cell maturation and activation of T lymphocytes towards a proinflammatory phenotype, to reduce monocyte migration by decreasing the expression of CCR2 and ICAM-1, reduce the activation of inflammatory pathways such as TLR4/NF-κB and LOX-1/NF-κB, leading to reduced expression of proinflammatory genes and increased anti-inflammatory cytokines (e.g., IL-10) [161].

Several meta-analyses and randomized clinical trials have shown that although PCSK9 inhibitors dramatically lower LDL cholesterol, there is no significant decrease in hsCRP compared with placebo or other therapies [157,162,163]. For example, a meta-analysis of 4198 participants showed a minimal and statistically insignificant reduction in hsCRP (−0.04 mg/L) [164]. Similar results have been reported in studies such as EQUATOR [165] and SPIR [166], where the addition of PCSK9 inhibitors to statin therapy did not influence hsCRP levels, despite substantial reductions in LDL-C. We can say that the anti-inflammatory effect of PCSK9 inhibitors is not reflected and cannot be measured by hsPCR. Still, their effect is related to atheroma plaque activity rather than to changes in circulating levels of acute phase reactants. Patients treated with PCSK9 inhibitors had a reduced inflammatory load in carotid atherosclerotic plaques, characterized by lower levels of NLRP3, caspase-1, IL-1β, and TNF-α in carotid plaques, even in subgroups with LDL-C levels below 100 mg/dL [167].

5.4. Ezetimibe

Administration of ezetimibe in combination with statins (rosuvastatin or pitavastatin) in patients with acute coronary syndrome (ACS) resulted in significant decreases in inflammatory markers, such as sPLA2-IIa and interleukin-1β, compared to statin therapy alone. A more minor increase in endothelial adhesion molecules (VCAM-1 and ICAM-1) was also observed in the combination therapy group, suggesting an additional protective effect on the endothelium of the vasculature [168]. Some studies have shown that the anti-inflammatory and cardiovascular protective benefits of ezetimibe cannot be attributed solely to LDL-C reduction. Anti-inflammatory effects, reduction in oxidative stress, and myocardial fibrosis may contribute to a decrease in cardiovascular events and hospitalizations for heart failure after ACS [169]. Data from the IMPROVE-IT trial, which included more than 18,000 patients with ACS, show that the addition of ezetimibe to statin therapy (simvastatin) resulted in a further reduction in hsCRP of about 16% at one month and 14% throughout the study compared with statin monotherapy. More patients treated with ezetimibe/simvastatin achieved the target hsCRP < 2 mg/L compared with those treated with simvastatin alone (50% vs. 29%, $p < 0.001$) [170]. In the ENHANCE trial, the addition of ezetimibe to simvastatin doubled the reduction in hsCRP (49.2% vs. 23.5% with statin alone). However, the decrease in LDL-C was similar between groups. This result suggests an additional mechanism, possibly independent of LDL-C [171].

5.5. Inhibition of NLRP3 Inflammasome in ACS

Inflammasome NLRP3 (NOD-, LRR- and Pyrin domain-containing protein 3) is an essential cytosolic multiprotein complex of the innate immune system involved in the regulation of inflammation and immune response. NLRP3 inflammasome is a key mediator of sterile inflammation in ACS, linking atherosclerotic plaque destabilization to myocardial injury and adverse remodeling. Its inhibition represents a promising strategy for secondary prevention, with strong evidence from preclinical and clinical studies [172–174].

https://doi.org/10.3390/cells15010072

5.6. MCC950

MCC950 is a selective and potent inhibitor of the NLRP3 inflammasome, with promising results in preclinical models of ACS. Administration of MCC950 to mice with myocardial infarction resulted in reduced myocardial fibrosis and improved cardiac function compared with untreated animals [175]. In models of cerebral ischemia/reperfusion (analogous to myocardial reperfusion injury), MCC950 significantly reduced infarct size, edema, and markers of apoptosis, suggesting similar protective potential at the cardiac level as well. This effect is due to the inhibition of caspase-1 and IL-1β release, thereby reducing inflammatory cell death (pyoptosis) [176].

For now, the evidence comes from preclinical animal studies; there are no human clinical data yet on MCC950 in ACS.

5.7. OLT1177

The administration of OLT1177 (dapansutrile) in acute coronary syndromes (ACS) has a promising role as a targeted anti-inflammatory therapy by selectively inhibiting the NLRP3 inflammasome. OLT1177 directly blocks the activation and oligomerization of NLRP3, preventing its interaction with ASC and caspase-1, leading to reduced maturation and release of the proinflammatory cytokines IL-1β and IL-18 [16,96]. It does not affect other inflammasomes (AIM2, NLRC4), which gives it specificity and a superior safety profile [177]. Administration of OLT1177 to animals with myocardial ischemia/reperfusion significantly reduced infarct size (by 36–71%, dose-dependently) and maintained left ventricular systolic function at 24 h and 7 days after injury [178]. OLT1177 reduces the levels of IL-1β, IL-18, IL-6, and other pro-inflammatory cytokines in both tissues and circulation, thereby limiting neutrophil infiltration and oxidative stress. It improves cardiac muscle oxidative metabolism and reduces proinflammatory metabolic markers [179]. OLT1177 is well-tolerated in humans, with no significant adverse effects or biochemical or hematologic changes observed at high doses [177]. Early phase clinical trials have shown benefit in patients with heart failure and gout, and development for cardiovascular indications is ongoing [17].

5.8. Colchicine

Colchicine blocks the assembly of the NLRP3 inflammasome, thereby reducing its activation and the release of proinflammatory cytokines such as interleukin-1β (IL-1β) and IL-18, key molecules in amplifying the inflammatory response after myocardial infarction. Colchicine binds to tubulin and destabilizes microtubules, thereby inhibiting microtubule-dependent functions of inflammatory cells (neutrophils, monocytes/macrophages). This reduces the migration, activation and release of inflammatory mediators by these cells. Colchicine inhibits neutrophil chemotaxis and activation, as well as the formation of neutrophil extracellular traps (NETs), which contribute to tissue injury and thrombosis progression in ACS [180,181].

Results from the Colchicine Cardiovascular Outcomes Trial (COLCOT) show that colchicine (0.5 mg/day) in patients with recent MI (about 14 days after the MI) significantly reduces the risk of major ischemic cardiovascular events compared with placebo in addition to standard treatment. The risk reduction was mainly driven by a decrease in the incidence of stroke and urgent revascularization. No significant differences were observed between groups in cardiovascular mortality or recurrent MI (HR = 0.77 (95% CI: 0.61–0.96), $p = 0.02$ reduction in the risk of major cardiovascular events) [182].

The study did not include detailed measurements of inflammatory biomarkers at baseline and throughout the study, making it difficult to correlate the inflammatory response with the observed clinical benefits directly. The COLCOT did not demonstrate a significant

reduction in total or cardiovascular mortality, but only in composite events, and the number of deaths was almost identical between groups (43 vs. 44) [183].

Results from the COPS (Colchicine in Patients With Acute Coronary Syndrome) trial of colchicine in patients with ACS showed that at 12 months, colchicine did not significantly reduce the risk of major cardiovascular events in patients with ACS (24 events in the colchicine group vs. 38 in the placebo group, $p = 0.09$; HR 0.65), but was associated with an increase in total mortality (8 deaths in the colchicine group vs. 1 in the placebo group, HR 8.20; $p = 0.047$), mainly driven by increased non-cardiovascular mortality (5 vs. 0, $p = 0.024$). In the COPS study, colchicine was administered very early, during hospitalization for ACS, before discharge, immediately after the diagnosis of the acute coronary event. The administration schedule was as follows: 0.5 mg twice daily (1 mg/day) for the first month, followed by 0.5 mg once daily for the next 11 months [181].

The increase in non-cardiovascular mortality observed in the COPS study in patients treated with colchicine has no apparent cause and remains controversial. Detailed analysis showed that four of the five non-cardiovascular deaths were related to sepsis. Still, three of these cases occurred in patients who had discontinued colchicine at least 30 days before death, so were not on active treatment at the time of the event. Another death was caused by cancer, with no known link to colchicine [180]. Colchicine increases the risk of gastrointestinal events and possibly infections, but without a clear association with increased non-cardiovascular mortality on a large scale [184].

Administration of colchicine for 12 months after ACS significantly reduced major cardiovascular events at 24 months, mainly due to a decrease in urgent revascularizations (colchicine 3 cases vs. placebo 16 cases, HR 0.19; 95% CI: 0.05–0.66; $p = 0.009$), without significantly influencing total mortality (colchicine 9 deaths vs. placebo 4 deaths, statistically insignificant difference (HR 2.28; 95% CI: 0.7–7.4; $p = 0.17$) or non-cardiovascular mortality (colchicine 5 deaths vs. placebo 2 deaths, statistically negligible difference (HR 2.54; 95% CI: 0.49–13; $p = 0.27$) [185].

A meta-analysis that included only two trials (COLCOT and COPS) showed that colchicine administration in ACS reduces the risk of MACE (composite events: cardiovascular death, recurrent myocardial infarction, stroke or urgent revascularization) by 25–30%. This effect is primarily driven by a decrease in stroke rates (48–52% reduction) and a reduction in coronary revascularization requirements (23–32% reduction) [184]. With just two randomized controlled trials (RCTs) in the review, the findings might not represent broader clinical experiences. A larger number of studies would provide more confidence in the reliability of the results. Even though both trials investigated the use of colchicine for patients with acute coronary syndrome, there were variations in how the drug was administered. For example, one study used a higher initial dosing regimen than the other. These differences might have affected the outcomes slightly and can limit how broadly the conclusions from the meta-analysis can be applied.

Additionally, the timing of administration of colchicine after an ACS is essential. A sub-analysis of the COLCOT study showed that early treatment, specifically within the first three days after the heart attack, was shown to substantially lower the chance of experiencing a composite event that included heart-related death, another heart attack, stroke, resuscitated cardiac arrest, or the need for urgent hospital procedures like revascularization. The results indicate that initiating treatment in the hospital, rather than waiting until after discharge, can lead to significantly better outcomes for patients [186].

Other large trials, such as CLEAR SYNERGY [187], have not confirmed the benefits observed in COLCOT, suggesting that the effect of colchicine may be more modest or dependent on population selection and timing of initiation of therapy. Results from the CLEAR SYNERGY (OASIS 9) study show that colchicine in patients with acute MI treated

with coronary angioplasty (PCI) did not significantly reduce the risk of major adverse cardiovascular events (MACE) compared with placebo after a median follow-up of almost 3 years. In the CLEAR SYNERGY trial, colchicine was administered to patients with acute myocardial infarction (both STEMI and extended NSTEMI) as soon as possible after percutaneous coronary intervention (PCI), but no later than 72 h after PCI [188]. The CLEAR SYNERGY trial demonstrates that, in patients with acute MI treated by PCI, routine colchicine administration does not reduce MACE compared with placebo (cardiovascular death: 3.3% colchicine vs. 3.2% placebo (HR 1.03); death from any cause: 4.6% colchicine vs. 5.1% placebo (HR 0.90); recurrent MI: 2.9% colchicine vs. 3.1% placebo (HR 0.88); ischemia-driven revascularization: 4.6% colchicine vs. 4.7% placebo (HR 1.01), although it reduces inflammatory markers (hsCRP at 3 months, colchicine: 2.98 mg/dL vs. placebo: 4.27 mg/dL ($p < 0.001$)—significant decrease in inflammation, without substantial clinical impact).

In the colchicine-treated group, there was a higher incidence of gastrointestinal side effects compared with placebo (diarrhea: 10.2% colchicine vs. 6.6% placebo ($p < 0.001$)), without an increase in the number of infections (serious infections: 2.5% colchicine vs. 2.9% placebo ($p = 0.85$)) [187].

Possible explanations between the results of COLCOT and CLEAR SYNERGY would be the very early randomization in patients with STEMI and severe inflammation (CLEAR SYNERGY included more than 7000 patients, mostly with STEMI, randomized very early (on average 1.6 h after PCI, but maximum 72 h post-infarction), insufficient inflammatory control (In CLEAR SYNERGY, levels of C-reactive protein (CRP), a marker of inflammation, remained elevated at 3 months (mean 3.0 mg/L in colchicine vs. 4.3 mg/L in placebo), in contrast to COLCOT, where CRP fell below 2 mg/L), the impact of the COVID-19 pandemic (a significant part of the CLEAR SYNERGY study was conducted during the COVID-19 pandemic, which disrupted health systems and led to underreporting of non-fatal events [heart attacks, revascularizations]), on event reporting and patient care, differences in design and statistical power. CLEAR SYNERGY had more than twice as many events as COLCOT, which may suggest that the positive effect in smaller trials may be overestimated (regression to the mean; in COLCOT, the benefit was driven mainly by reduction in emergency hospitalizations for angina and revascularization, not so much by reduction in deaths or major MIs) [189].

These elements suggest that the benefits of colchicine observed in COLCOT cannot be automatically generalized to all myocardial infarction populations, and its efficacy depends on the clinical context and timing of administration.

5.9. Interleukin-1β Inhibitors

Inhibition of the IL-1β pathway may play a crucial role in the treatment of ACS by modulating the inflammatory response with beneficial effects on both acute and long-term cardiac remodeling.

The pivotal study evaluating canakinumab (an anti-IL-1β monoclonal antibody) in ACS is the Canakinumab Anti-inflammatory Thrombosis Outcomes Study (CANTOS). It included 10,061 patients with a history of myocardial infarction and elevated ultrasensitive C-reactive protein (hsCRP $\geq$ 2 mg/L) who received canakinumab (50 mg, 150 mg or 300 mg) or placebo, administered subcutaneously every 3 months, with a median follow-up of 3.7 years [190].

Canakinumab reduced not only the first major event, but also the total number of serious cardiovascular events (including coronary revascularization), with a relative reduction of about 20% for all doses tested. Canakinumab therapy significantly decreased hsCRP levels compared with placebo, with a greater reduction at higher doses ($p < 0.001$ for all doses). Secondary analyses showed that patients who achieved hsCRP < 2 mg/L after

3 months of treatment had a 25% reduction in major cardiovascular events, a 31% decrease in cardiovascular mortality, and a similar reduction in total mortality. Canakinumab was associated with an increased risk of fatal infections or sepsis (0.31/100 patient-years vs. 0.18/100 patient-years for placebo), but the overall rate of serious adverse events was comparable to placebo.

CANTOS demonstrated for the first time that targeted inhibition of inflammation (by blocking IL-1β) reduces the risk of recurrent cardiovascular events in patients with previous myocardial infarction and residual inflammation, independent of cholesterol lowering.

The effect was more pronounced in responding patients with reduced inflammation (hsCRP < 2 mg/L). Wide clinical use of canakinumab is limited by cost and risk of infection, but the study validates the concept of anti-inflammatory therapy in secondary prevention after ACS [191].

It should be noted that despite the benefits shown in CANTOS, canakinumab has not been imposed in the treatment of patients with ACS due to the increased risk of serious infections (in the CANTOS, the rate of fatal infections was almost double that of placebo), very high costs (over 50,000 USD/year, making it inaccessible for widespread use in ACS) [192], the lack of a formal indication for this pathology (it is only approved for rare auto-inflammatory conditions [e.g., cryopyrin-associated periodic syndromes—CAPS, juvenile systemic arthritis, not for ACS]) and the existence of safer and more affordable alternatives such as colchicine [190].

Anakinra, an IL-1 receptor antagonist, has a promising role in ACS, acting by inhibiting the inflammatory response that contributes to myocardial injury and adverse ventricular remodeling after infarction. The administration of anakinra in patients with STEMI (VCUART3—Virginia Commonwealth University Anakinra Remodeling Trial 3) significantly reduced hsCRP levels compared to placebo (both standard and high dose) during the first 14 days (median 67 IQR 39–120 vs. 214 IQR 131–394 mg-day/L; $p < 0.001$) [193]. There was no significant difference between the standard (once-daily) and high-dose (twice-daily) anakinra treatments in reducing inflammation. This finding suggests that the standard dose is adequate to block the interleukin-1 receptor, thereby modulating the inflammatory response after STEMI. Notably, the trial found a lower incidence of heart failure events, such as hospitalizations and new-onset heart failure, in patients treated with anakinra (9.4%) compared to those treated with placebo (25.7%) ($p = 0.046$). This suggests that targeting the interleukin-1 pathway with anakinra may offer benefits in reducing the risk of complications, such as heart failure, following STEMI.

There were no significant differences in the incidence of severe infections between the anakinra and placebo groups (14% vs. 14%). Injection site reactions were more common with anakinra. No significant differences were noted in the interval changes in left ventricular end-systolic volume or ejection fraction between the anakinra-treated groups and the placebo group. This implies that while anakinra effectively dampens inflammation, it does not significantly alter the structural remodeling of the heart within the measured time frame.

5.10. Low-Dose Interleukin-2 (IL-2)

In the context of acute coronary syndrome (ACS), the administration of low-dose interleukin-2 (IL-2) serves primarily as an immunomodulatory intervention designed to mitigate vascular inflammation through the expansion of regulatory T cells (Tregs). These cells possess significant immune-suppressive and anti-inflammatory properties. At low doses, IL-2 selectively enhances the quantity and functionality of Tregs without markedly increasing effector T cells. Tregs play a crucial role in suppressing the inflammatory processes that contribute to atherosclerosis and acute coronary events. In ACS, vascular inflamma-

https://doi.org/10.3390/cells15010072

tion is a principal factor in disease progression and adverse cardiovascular outcomes. By promoting the expansion of Tregs, low-dose IL-2 effectively reduces this inflammation, potentially stabilizing atherosclerotic plaques and enhancing vascular health [194].

The LILACS trial established that low-dose IL-2 is both safe and biologically effective for patients with acute coronary syndrome (ACS) and stable ischemic heart disease. The study demonstrated an increase in regulatory T cells (Tregs) without any serious adverse events. The target dose required to achieve a significant increase in Tregs was approximately 1.46×10^6 IU [195].

The IVORY trial, a randomized, placebo-controlled study, demonstrated that low-dose IL-2 administration in patients with acute coronary syndrome (ACS) resulted in a significant reduction in arterial inflammation, as assessed by ^{18}F-FDG PET/CT imaging. This outcome was correlated with a notable increase in circulating regulatory T cells (Tregs) and no increase in effector T cells. The treatment was well tolerated. A trend toward fewer major adverse cardiovascular events (MACE) was observed in the IL-2-treated group over a median follow-up period of 2.5 years, indicating potential clinical benefit; however, larger trials are necessary to confirm these findings [194].

Low-dose IL-2 therapy in ACS acts by expanding regulatory T cells, thereby reducing vascular inflammation and potentially lowering the risk of subsequent cardiovascular events. It represents a promising targeted immunomodulatory approach to improve outcomes in high-risk ACS patients with an acceptable safety profile demonstrated in early-phase clinical trials.

5.11. IL-6 Inhibition

Interleukin-6 inhibitors are emerging as potential therapeutic agents in ACS due to IL-6′s central role in propagating inflammation, activating leukocytes and adipose tissue to amplify inflammation, stimulating hepatic production of hs-CRP (a biomarker of cardiovascular risk), promoting endothelial dysfunction, plaque instability, and adverse remodeling post-ACS [196].

Currently, there are no medications specifically approved for targeting IL-6 in acute coronary syndrome (ACS). However, some IL-6 inhibitors approved for other conditions have been studied in ACS with promising but still investigational results [197].

Tocilizumab is a monoclonal antibody against the IL-6 receptor, is approved by the FDA for rheumatoid arthritis, juvenile idiopathic arthritis, and giant cell arteritis [198]. Tocilizumab, an interleukin-6 receptor (IL-6R) antagonist, has been investigated as a potential therapy for acute coronary syndrome (ACS), particularly acute myocardial infarction (AMI), due to its anti-inflammatory properties and its ability to modulate the inflammatory response that contributes to myocardial injury and adverse outcomes. In the randomized, double-blind, placebo-controlled ASSAIL-MI trial [199], patients presenting with STEMI within 6 h of symptom onset received a single intravenous dose of tocilizumab (280 mg) or placebo before PCI. Tocilizumab significantly increased the myocardial salvage index compared to placebo (adjusted between-group difference 5.6 percentage points, $p = 0.04$). There was also less microvascular obstruction in the tocilizumab group, although the difference in final infarct size did not reach statistical significance. Adverse events were similar between groups, and the drug was well tolerated. The results suggest that tocilizumab may reduce reperfusion injury and enhance myocardial salvage in STEMI patients, likely by attenuating the inflammatory response associated with ischemia–reperfusion injury. Despite these encouraging findings, tocilizumab is not yet approved for ACS treatment and remains investigational in this context.

Ziltivekimab, a novel monoclonal antibody targeting IL-6 has shown strong anti-inflammatory effects in patients with chronic kidney disease and high cardiovascular risk by

significantly lowering hsCRP and other inflammatory markers [200]. It is being developed specifically for atherosclerosis but has not yet received approval for ACS or cardiovascular indications. Several major ongoing clinical trials are investigating ziltivekimab, a fully human monoclonal antibody targeting the interleukin-6 (IL-6) ligand, for its ability to reduce inflammation and cardiovascular risk in high-risk patient populations.

The RESCUE trial was a phase 2, randomized, double-blind study evaluating the effects of ziltivekimab, a fully human monoclonal antibody targeting the IL-6 ligand, in patients at high atherosclerotic risk—specifically those with moderate to severe CKD and elevated hsCRP $\geq$ 2 mg/L. Ziltivekimab markedly reduced biomarkers of inflammation and thrombosis relevant to atherosclerosis in a high-risk CKD population [201].

The magnitude of hsCRP reduction (dose-dependent and marked reduction in hsCRP at 12 weeks: 7.5 mg: 77% median reduction, 15 mg: 88% median reduction, 30 mg: 92% median reduction vs. Placebo: 4% median reduction) was about twice that seen with canakinumab (an IL-1β inhibitor) in the CANTOS trial. The safety and efficacy profile supports ongoing investigation in large-scale cardiovascular outcomes trials, such as the ZEUS trial, to determine if these biomarker changes translate into fewer cardiovascular events [202].

Ongoing Trials

The ZEUS Trial (NCT05021835) is a large, phase-3, double-blind, placebo-controlled trial including 6200 adults with acute cardiovascular disease, chronic kidney disease and systemic inflammation (documented by elevated hs-CRP levels), to whom ziltivekimab, 15 mg or placebo is administered subcutaneously once monthly in addition to standard care. The primary aim is to determine whether ziltivekimab reduces major adverse cardiovascular events by serial follow-up for up to 4 years [202,203].

The ARTEMIS trial (NCT06118281) is a phase 3, randomized, placebo-controlled trial that investigates the effect of ziltivekimab, 15 mg or placebo, when initiated during hospital admission for acute myocardial infarction (STEMI), on the recurrence of acute cardiovascular events post-MI.

The HERMES Trial (NCT05636176) is a phase 3, randomized, placebo-controlled trial that explores the effects of ziltivekimab in improving symptoms and outcomes in heart failure [204].

Other anti-inflammatory agents like colchicine reduce IL-6 indirectly and are used off-label in cardiovascular disease. However, colchicine is not a direct IL-6 inhibitor nor approved specifically for IL-6 targeting in ACS.

In summary, while IL-6 is a validated therapeutic target in ACS due to its role in inflammation and plaque instability, no IL-6-targeted medication is currently approved for ACS treatment. Agents like tocilizumab and ziltivekimab are under clinical investigation and may become approved in the future pending results from large-scale cardiovascular outcome trials.

5.12. Lp-PLA2 Inhibition

Darapladib is an oral, selective inhibitor of lipoprotein-associated phospholipase A2 (Lp-PLA2), an enzyme implicated in the inflammatory processes of atherosclerosis and ACS [205]. An observational study from SOLID—TIMI 52 (Stabilization of Plaque Using Darapladib-Thrombolysis in Myocardial Infarction 52) showed that increased IL-6 was associated with increased risk of future cardiovascular events, independent of the risk factors present and baseline hsCRP level [29]. This has also been demonstrated in several meta-analyses, which show that increased levels of IL-6 and hsCRP after an acute coronary

https://doi.org/10.3390/cells15010072

event correlate with prognosis and long-term MACE incidence, making IL-6 blockade an attractive target in the management of ACS [27].

Preclinical studies suggested that darapladib could reduce Lp-PLA2 and Rho kinase activity, lower inflammatory markers (such as CRP), improve nitric oxide production, and reduce cardiomyocyte apoptosis in animal models of atherosclerosis [205]. The most extensive and most definitive study of darapladib in ACS was the SOLID-TIMI 52 trial [206], a multinational, double-blind, placebo-controlled trial enrolling over 13,000 patients within 30 days of hospitalization for ACS. Patients received darapladib or placebo in addition to standard guideline-directed therapy and were followed for a median of 2.5 years. Darapladib did not reduce the risk of major coronary events (a composite of coronary heart disease death, myocardial infarction, or urgent coronary revascularization) compared to placebo (16.3% vs. 15.6% at 3 years; HR 1.00, $p = 0.93$). There were also no significant differences in cardiovascular death, myocardial infarction, stroke, or all-cause mortality between the darapladib and placebo groups. The safety profile was generally acceptable, though darapladib was associated with a higher incidence of odor-related concerns and diarrhea. As a result, darapladib is not approved for use in ACS, and its clinical development for this indication has been discontinued.

5.13. Metothrexate

Methotrexate (MTX) is a well-established anti-inflammatory and immunosuppressive drug, most commonly used in the management of autoimmune diseases such as rheumatoid arthritis (RA). Its potential cardiovascular benefits have been of increasing interest due to the recognized role of inflammation in the development and progression of atherosclerosis and ACS [207]. Multiple studies and meta-analyses have shown that methotrexate use in patients with RA is associated with a reduced risk of cardiovascular events, including ACS, compared to patients not on MTX. This cardioprotective effect is thought to be due to MTX's ability to suppress systemic inflammation, which is a key driver of atherosclerosis and plaque instability, leading to ACS [207,208]. While the benefits of MTX in reducing cardiovascular events are apparent in patients with systemic inflammatory diseases, its role in the general population with established CAD or ACS is less specific. The Cardiovascular Inflammation Reduction Trial (CIRT) [209] investigated low-dose MTX in patients with stable CAD post-MI and did not demonstrate a significant reduction in cardiovascular events or inflammatory biomarkers compared to placebo (incidence rate, 4.13 vs. 4.31 per 100 person-years; hazard ratio, 0.96; 95% confidence interval [CI], 0.79 to 1.16). The lack of efficacy in this population may be due to lower baseline levels of inflammation compared to RA patients. In MethotrexaTE THerapy in ST-Segment Elevation MYocardial InfarctionS (TETHYS). prospective, randomized, phase 2, double-blind, placebo-controlled trial methotrexate in patients with STEMI did not reduce infarct size and further depressed LVEF at 3 months [210]. While MTX's anti-inflammatory mechanisms (adenosine upregulation, cytokine suppression, oxidative stress reduction) are theoretically relevant to STEMI, clinical trials demonstrate no reduction in infarct size or mortality, with potential harm to ventricular function. Current evidence does not support MTX use in STEMI treatment, highlighting the complexity of targeting inflammation in acute myocardial injury [3].

5.14. OxLDL-Targetting

Farina et al. investigated in a phase 2a, double-blind, randomized, placebo-controlled trial the effects of orticumab, an oxLDL epitope-targetting monoclonal antibody, on coronary inflammation and residual inflammatory risk in patients with psoriasis, as oxLDL-induced macrophage activation is inhibited in atherosclerotic plaques. The study aimed to assess orticumab's effects on both skin and coronary disease inflammation in subjects with

https://doi.org/10.3390/cells15010072

psoriasis, as this skin condition associated with increased cardiovascular risk. Orticumab significantly reduced the Fat Attenuation Index (FAI) score in the right coronary artery (RCA) ($p = 0.01$ vs. baseline and $p = 0.02$ vs. placebo) in the subgroup of patients with elevated coronary inflammation at baseline (FAI score $\geq$ 50th centile) [211]. A trend towards reduction was also observed in the left circumflex (LCX) artery ($p = 0.01$ vs. baseline and $p = 0.05$ vs. placebo).

Schwab et al. report a novel use of CAR T cell technology to target atherosclerotic cardiovascular disease, specifically through murine 2D03-CAR Tregs directed against malondialdehyde-modified apolipoprotein B-100 epitope (IEI-E3 and 2D03), underscoring the importance of inducing immune tolerance to OxLDL at plaques using Tregs to stabilize or regress plaques. Targeting OxLDL with CAR Tregs at atherosclerotic lesions presents a localized, effective, and low-risk treatment alternative for refractory patients.

Compared to other therapies, OxLDL-specific CAR Treg treatment may offer long-term benefits with a single administration and lower risk of adverse reactions, enhancing its appeal for clinical use. Although this study provided positive results in murine models, this approach possesses several limitations, including differences in murine and human CAR-T cell behavior, clinical Treg therapy implementation, sorting and expanding natural Tregs and ensuring the stability of antigen-specific Tregs. However, the potential translation of 2D03-CAR Treg therapy from preclinical success to clinical application is promising, given the global functionality and success of CAR T cell manufacturing [212,213].

5.15. PAD4 Inhibition

Since PAD4 is a key enzyme involved in the process of NETosis, drugs targeting this enzyme hold promising potential for reducing cardiovascular risk. Experimental inhibitors, such as GSK484 and chloro-amidine, have shown positive results in murine models of myocardial infarction by reducing infarct size. This effect is attributed to the inhibition of PAD4, which decreases NETosis. By halting the NETosis process, these drugs reduce cardiac ischemia-induced apoptosis of cardiomyocytes and myocardial ischemia–reperfusion injury. Consequently, the overall cardiac function is improved [214,215].

5.16. GLP-1 Receptor Agonists and Inflammation

Medications that act on GLP-1 receptors are known as GLP-1 receptor agonists (GLP-1RAs), and they primarily include injectable and oral agents designed to treat type 2 diabetes and obesity by mimicking the effects of endogenous GLP-1 hormone.

These medications bind and activate GLP-1 receptors, mainly in pancreatic β cells and neurons. The result is enhanced glucose-dependent insulin secretion, inhibition of glucagon release, slowed gastric emptying, regulation of appetite, and cardioprotective effects. These actions make GLP-1RAs effective for glycemic control and weight reduction, as well as for reducing cardiovascular risk in people with diabetes and obesity [216].

GLP-1 receptor agonists have a recognized anti-inflammatory role that extends beyond their glucose-lowering and weight-management effects. These drugs modulate immune responses by acting on GLP-1 receptors expressed on several immune cells, including macrophages, monocytes, and lymphocytes [217]. GLP-1RAs suppress the production of pro-inflammatory cytokines, such as TNF-α, IL-1β, and IL-6, while increasing anti-inflammatory mediators, such as IL-10 and adiponectin. GLP-1RAs activate the AMP-activated protein kinase (AMPK) pathway, which is crucial for suppressing inflammation and promoting metabolic equilibrium [218]. These agents can also shift macrophages from a pro-inflammatory M1 state to an anti-inflammatory M2 phenotype, restoring immune balance in tissues.

https://doi.org/10.3390/cells15010072

GLP-1 receptor agonists, such as liraglutide, semaglutide, and exenatide, have been shown to decrease systemic inflammation by reducing circulating levels of inflammatory biomarkers, including hsCRP, TNF-α, and IL-6, in people with type 2 diabetes, obesity, and cardiovascular disease. Clinical and preclinical evidence indicate that these drugs stabilize atherosclerotic plaques by reducing monocyte adhesion and macrophage accumulation, and they slow atherosclerosis progression by modulating inflammatory pathways [217].

In a controlled trial involving men with type 2 diabetes, weekly semaglutide administration for 6 months resulted in statistically significant decreases in circulating TNF-α and IL-6, demonstrating direct anti-inflammatory benefits [219]. Evidence synthesis across multiple RCTs shows that semaglutide reduces hsCRP by 12–20%, TNF-α by 15–40%, and IL-6 by 10–25%, independent of weight loss or glycemic effects, in patients with type 2 diabetes and obesity.

The SELECT trial, involving over 17,000 high-risk cardiovascular patients without diabetes, found semaglutide reduced high-sensitivity CRP by 12–20% within 4–8 weeks of treatment, even before significant weight loss [220]. Large cardiovascular outcome trials (such as SUSTAIN-6) included patients with prior myocardial infarction or established atherosclerotic disease. They demonstrated significant reductions in major adverse cardiovascular events with semaglutide, but these studies did not specifically focus on inflammation after recent ACS [221]. Post hoc analyses and contemporary registries have shown benefits in reducing recurrent coronary events in patients with prior MI or revascularization. Still, inflammation as a primary outcome was not the focus.

GLP-1 receptor agonists are increasingly considered for secondary prevention after ACS, supported by growing evidence of cardiovascular and anti-inflammatory benefits in high-risk patients. GLP-1 receptor agonists (liraglutide, semaglutide, dulaglutide, exenatide) are recommended for patients with type 2 diabetes and established atherosclerotic cardiovascular disease, including those with prior MI or ACS, to reduce major MACE beyond glucose lowering [222].

RCTs and cohort studies show reductions in hsCRP, IL-6, TNF-α, and improvement in endothelial function, which likely contribute to stabilization of plaque and reduction in recurrent events. Evidence from observational studies and post hoc analyses in MI survivors (mostly liraglutide, some semaglutide) shows reduced risk of recurrent MI, CV mortality, reduced infarct size, and attenuation of LV remodeling when started as early as hospital discharge or soon after ACS. Trials in ACS patients, especially post-PCI STEMI, demonstrate significant myocardial salvage and reduction in inflammatory markers when GLP-1 agents are added as adjunct therapy in the acute phase (within days to weeks) [223]. Guidelines and trials suggest safe initiation during acute hospitalization or soon after discharge, optimizing patient motivation and education. For best results, start GLP-1RAs within the first days to weeks post-ACS unless contraindicated by instability, acute heart failure, GI intolerance, or renal dysfunction. Most evidence in ACS and high CV risk is for liraglutide, semaglutide, and dulaglutide, with largest CV event reduction and anti-inflammatory data for liraglutide and semaglutide [224].

Both ESC [1] and ACC/AHA guidelines [225] recommend GLP-1 receptor agonists as part of the secondary prevention strategy for patients with acute coronary syndrome who have type 2 diabetes or very high cardiovascular risk. These agents, such as semaglutide, liraglutide, and dulaglutide, are supported by evidence showing they reduce major adverse cardiovascular events, with anti-inflammatory benefits contributing to plaque stabilization and vascular protection. Initiation of therapy is appropriate after stabilization, either during hospitalization or in the early post-discharge period. Use in overweight or obese patients without diabetes is now considered reasonable, especially semaglutide, considering recent trials like SELECT that show event reduction in this group. For ACS survivors without

diabetes or obesity, routine use is not guideline-recommended. Still, it may be considered in select individuals at very high risk, based on individualized evaluation and shared decision-making [226].

The mechanisms of the previously described anti-inflammatory therapies are summarized in Table 1.

Table 1. Currently studied anti-inflammatory therapies in acute coronary syndromes.

Drug	Effects	Observations
Aspirin	Inhibits COX-1 and COX-2 enzymes Reduces inflammatory cytokines (TNF-α, IL-6, IL-1β) and MCP-1 Acetylates COX-2 to produce aspirin-triggered lipoxin A4 (potent anti-inflammatory mediator) Stimulates eNOS and reduces oxidative stress in vascular cells Inhibits platelet activation and reduces platelet-leukocyte aggregation Decreases endothelial activation and expression of adhesion molecules Protects LDL from oxidative modification Inhibits free radical formation and lipid peroxidation	Antiplatelet effects achieved at low doses (75–100 mg/day); anti-inflammatory effects at higher doses (300 mg/day)
Statins	Decrease inflammatory markers: IL-1β, CRP, IL-6, and TNF-α Inhibit leukocyte recruitment and adhesion to endothelium by reducing adhesion molecule expression (ICAM-1, VCAM-1, E-selectin, P-selectin) Decrease MPO activity and oxidative stress Reduce neutrophil activation and infiltration into atherosclerotic plaques Stabilize atherosclerotic plaques by reducing inflammation	Rosuvastatin (20 mg): 44% CRP reduction Atorvastatin (20 mg): 30% CRP reduction Benefits individuals without hyperlipidemia but with elevated inflammation (hsCRP $\geq$ 2 mg/L)
PCSK9 Inhibitors (evolocumab, alirocumab)	Reduce LDL cholesterol and inflammatory markers Decrease oxidative stress Stabilize atherosclerotic plaques Complement statin therapy for lipid and inflammation control	
Colchicine	Inhibits microtubule polymerization in neutrophils and monocytes Reduces neutrophil chemotaxis and adhesion to endothelium Decreases NLRP3 inflammasome activation Reduces IL-1β and IL-18 production Lowers inflammatory markers (hsCRP reduced from 4.27 mg/dL to 2.98 mg/dL) Reduces risk of major adverse cardiovascular events (MACE)	Reduces IL-1β and IL-18 production Lowers inflammatory markers (hsCRP reduced from 4.27 mg/dL to 2.98 mg/dL) Reduces risk of major adverse cardiovascular events (MACE)

Table 1. *Cont.*

Drug	Effects	Observations
Canakinumab (IL-1β inhibitor)	Monoclonal antibody targeting IL-1β Reduces first and total major cardiovascular events Significantly decreases hsCRP levels (median reduction from 4.2 mg/L) Reduces recurrent cardiovascular events in patients with residual inflammatory risk (hsCRP $\geq$ 2 mg/L) Inhibits IL-1β pathway, preventing downstream inflammatory cascade Reduces risk of recurrent MI, stroke, and cardiovascular death	Dose-dependent effect (50 mg, 150 mg, 300 mg subcutaneous every 3 months) 150 mg dose showed optimal risk–benefit profile Side effects: increased risk of fatal infections and sepsis
Anakinra (IL-1 receptor antagonist)	Recombinant IL-1 receptor antagonist blocking both IL-1α and IL-1β effects Reduces systemic inflammation in STEMI patients Decreases incidence of new-onset heart failure (9.4% vs. 25.7% placebo, $p = 0.03$) May reduce complications such as heart failure post-STEMI	No significant difference in infection rates compared to placebo (14% vs. 14%) No significant impact on end-systolic volume or ejection fraction in some studies Effectively reduces inflammation but cardiovascular benefit requires further validation
Low-dose IL-2	Expands regulatory T cells (Tregs) Restores Th17/Treg balance Has immune-suppressive and anti-inflammatory properties Promotes immune homeostasis and plaque stabilization	Under investigation for cardiovascular applications
Tocilizumab (IL-6 receptor inhibitor)	Monoclonal antibody against IL-6 receptor Significantly reduces inflammatory biomarkers (hsCRP, IL-6) Reduces troponin T area under the curve (AUC) in AMI patients Less microvascular obstruction observed Well tolerated in acute settings May reduce myocardial damage in STEMI patients undergoing PCI	Single dose (280 mg IV) before PCI reduces myocardial injury Not yet approved for ACS treatment; remains investigational
Ziltivekimab (IL-6 ligand inhibitor)	Novel monoclonal antibody targeting IL-6 ligand Strong anti-inflammatory effects in chronic kidney disease and atherosclerosis Reduces hsCRP levels by approximately 80–90% CRP reduction about twice that seen with canakinumab	Monthly subcutaneous injections May offer superior inflammation control compared to IL-1 inhibitors
Methotrexate (MTX)	Anti-inflammatory and immunosuppressive drug Reduces leukocyte adhesion Inhibits pro-inflammatory cytokine production Reduces CD4+, CD8+ T cell and NK cell activation Associated with reduced cardiovascular events in rheumatoid arthritis patients	Weekly dosing (15–20 mg) used in cardiovascular studies In STEMI patients: did not reduce IL-1β, IL-6, or hsCRP at 24 h or 30 days TETHYS trial showed no reduction in MACE in STEMI patients
NLRP3 Inflammasome Inhibitors (OLT1177, MCC950)	Prevent IL-1β and IL-18 release from foam cells and macrophages Reduce pyroptosis and inflammatory cell death Limit plaque inflammation and instability	Under investigation for cardiovascular applications
PAD4 Inhibitors	Target Protein Arginine Deiminase 4 (PAD4) Inhibit neutrophil extracellular trap (NET) formation Reduce thrombogenic NETs in ruptured plaques Decrease NET-mediated platelet activation and thrombosis	Experimental agents under development

Table 1. *Cont.*

Drug	Effects	Observations
Orticumab (OxLDL-targeting antibody)	Monoclonal antibody targeting oxidized LDL (oxLDL) epitopes Inhibits oxLDL-induced macrophage activation in atherosclerotic plaques Significantly reduces Fat Attenuation Index (FAI) score in right coronary artery (RCA) (p = 0.01 vs. baseline, p = 0.02 vs. placebo) Trend towards reduction in left circumflex (LCX) artery (p = 0.01 vs. baseline, p = 0.05 vs. placebo) Reduces coronary inflammation and residual inflammatory risk Targets oxidized LDL to reduce inflammatory oxLDL-mediated injury Addresses both skin and coronary disease inflammation	Effective in patients with elevated coronary inflammation at baseline (FAI score $\geq$ 50th centile) Tested in phase 2a trials in patients with psoriasis (associated with increased cardiovascular risk)
GLP-1 Receptor Agonists (liraglutide, semaglutide, dulaglutide)	Suppress pro-inflammatory cytokines (TNF-α, IL-1β, IL-6) Increase anti-inflammatory mediators (IL-10, adiponectin) Activate AMP-activated protein kinase (AMPK) pathway, inhibiting NF-κB Shift macrophages from pro-inflammatory M1 to anti-inflammatory M2 phenotype Reduce oxidative stress and endothelial dysfunction Reduce hsCRP by 15–40% and IL-6 by 10–25% (independent of weight loss) Cardiovascular benefits in high-risk patients with type 2 diabetes Reduce MACE, cardiovascular death, and heart failure hospitalization	ESC and ACC/AHA guidelines recommend for secondary prevention in ACS with diabetes Best results when started within first days to weeks after ACS Injectable and oral formulations available

5.17. C-Reactive Protein Apheresis in Acute Coronary Syndromes

C-reactive protein (CRP) plays a detrimental role in acute myocardial infarction (AMI) by mediating tissue damage and potentially worsening clinical outcomes. Acting as a primitive antibody, CRP binds to viable hypoxic myocardial cells, marking them for phagocytosis and exacerbating myocardial injury [227]. Plasma CRP levels rise within 48 h following myocardial infarction and inversely correlate with prognosis in acute coronary syndromes (ACS), suggesting that therapeutic CRP reduction may improve outcomes [227,228].

The CAMI-1 trial, a pilot study involving 83 STEMI patients, investigated the safety and efficacy of CRP apheresis performed at 24, 48, and 72 h post-AMI. The primary endpoint was reduction in myocardial infarction size as determined by cardiac magnetic resonance imaging (CMR). In the control group, CRP concentration directly correlated with larger infarct size (p = 0.002) and decreased myocardial function ($p \leq 0.001$). Notably, patients who underwent CRP apheresis showed no correlation between CRP levels and infarct size (p = 0.66) or left ventricular dysfunction (p = 0.79), suggesting that early CRP removal may attenuate myocardial damage and preserve cardiac function [229].

Emerging evidence supports the potential benefit of CRP apheresis in non-ST-elevation ACS (NSTE-ACS) as well. In a case series of 10 patients with NSTE-ACS complicated by cardiogenic shock, 2–4 sessions of CRP apheresis were performed following culprit vessel percutaneous coronary intervention (PCI) and standard medical therapy, resulting in no 30-day mortality and only 10% (1/10) mortality at one year. Another case series evaluated 7 NSTE-ACS patients with significantly elevated plasma CRP levels (>10 mg/L)

who underwent PCI followed by 2–4 cycles of CRP apheresis until CRP levels plateaued at 2–3 days post-PCI. The procedure was well tolerated with no relevant adverse effects, no in-hospital mortality, and no 30-day mortality. Notably, most patients (6/7) were male, and 4/7 had left circumflex artery stenosis or occlusion; one patient had concurrent SARS-CoV-2 infection, representing a potential confounder [229]. While these preliminary results are encouraging, long-term data on mortality and heart failure development remain unavailable. Ongoing clinical trials are currently evaluating CRP apheresis in patients undergoing coronary artery bypass grafting (CABG), which may further clarify its role in reducing inflammation-mediated myocardial injury and improving long-term cardiovascular outcomes (NCT04745468).

5.18. Main Gaps in Knowledge and Future Perspectives

There is no validated framework for identifying which ACS patients have "residual inflammatory risk" based on dynamic biomarkers, genetic signatures, or immune cell phenotypes. Extensive trials have not prospectively applied a multi-marker, multi-omics strategy for targeted therapy allocation. The ideal window for initiating anti-inflammatory agents—whether in the acute phase (hours to days) or chronic phase (weeks to months post-ACS)—remains unclear. Data suggest that efficacy and safety may differ based on timing, but definitive recommendations are lacking.

Significant trial limitations in the field of anti-inflammatory therapy for ACS include heterogeneity in patient selection and timing of intervention, unclear biomarkers to guide therapy, limited mechanistic endpoints, and safety concerns. These limitations impact the strength and applicability of clinical evidence for inflammation-targeted strategies.

Most trials focus on broad clinical endpoints (MACE, MI, death), with limited mechanistic endpoints such as plaque imaging, immune cell dynamics, or signaling pathway modulation. The specific molecular mechanisms underlying the benefits or harms of anti-inflammatory therapy remain underexplored.

Many trials enroll broad ACS populations without stratifying by residual inflammatory risk (e.g., baseline hsCRP, IL-6). This can dilute the apparent efficacy of treatments, as only some subgroups benefit (such as those with persistently elevated inflammation after ACS).

Randomization and treatment initiation times vary widely. Colchicine trials, for example, range from administration within hours post-infarction (CLEAR SYNERGY) to weeks later (COLCOT), resulting in inconsistent outcomes and challenging direct comparisons. Early therapy may interfere with beneficial inflammation needed for healing, while late therapy may miss the optimal window for efficacy.

Concomitant treatments (statins, antiplatelets, aggressive lipid-lowering) vary and may independently reduce inflammation, masking or amplifying the effects of the study drug. Differences in population characteristics and event rates may lead to variability across studies. Increased risk of infections (canakinumab) and unexplained non-cardiovascular mortality (colchicine, COPS trial) highlight the need for careful long-term safety assessment. Some adverse effects only become apparent with larger or longer studies.

Despite promising results, guideline recommendations for anti-inflammatory therapy remain cautious; robust, biomarker-driven criteria for patient selection are lacking, and current evidence does not support routine use in all ACS patients.

These challenges highlight why inflammation-targeted therapy is not yet standard for all ACS patients and indicate areas where future trial design can be improved.

Experimental and emerging molecular targets (NETosis, PAD4, pro-resolving mediators, epigenetic regulators, and immune cell engineering) have not yet been translated into adequately powered human trials. Their clinical potential and patient selection criteria require systematic evaluation. While genetic predisposition and polygenic risk scores

https://doi.org/10.3390/cells15010072

hold promise, their integration into routine ACS management and clinical trial design is preliminary, and there is no consensus on threshold or clinical utility.

Most large trials are limited in duration and do not provide full assessment of long-term safety, especially concerning immunosuppression, infection risk, and non-cardiovascular mortality.

Current guidelines do not universally endorse anti-inflammatory therapy in ACS outside secondary prevention with statins; recommendations await stronger evidence from well-designed, biomarker- and genetics-guided trials.

Addressing these gaps requires innovative integrative research—using multi-omics, immune profiling, adaptive trial designs, and mechanistic endpoints—to move from broad anti-inflammatory strategies to precision inflammation management in ACS patients.

A unique perspective in the field of ACS inflammation would emphasize the shift toward precision anti-inflammatory therapy, focusing on individualized risk stratification and targeting distinct inflammatory pathways based on patient-specific biomarkers and timing, rather than one-size-fits-all approaches. Original hypotheses could be centered on new molecular mechanisms, cellular interactions, or therapeutic windows that remain underexplored or controversial.

Recent advances in ACS research support the concept that anti-inflammatory therapies should not be applied indiscriminately, but instead rationed to patients with demonstrable residual inflammatory risk after event recovery. Multiplex panels measuring hsCRP, IL-6, the neutrophil-to-lymphocyte ratio, and novel genetic or epigenetic markers should guide the initiation and choice of immunomodulation. Furthermore, the therapeutic window for suppressing pathologic inflammation while preserving reparative processes is likely narrow and varies among individuals. Ongoing studies of NLRP3 inhibitors, NETosis blockers, adaptive immune modulators (e.g., low-dose IL-2, GLP-1RA), and advanced profiling will clarify how targeted therapy may optimize outcomes. Ultimately, integrated approaches combining anti-inflammatory, lipid-lowering, and metabolic interventions—each tailored to patient-specific molecular and immune profiles—may redefine secondary prevention in ACS.

Several promising but underexplored molecular targets for anti-inflammatory therapy in acute coronary syndromes (ACS) include NETosis and PAD4-mediated mechanisms, modulation of immune cell subsets, epigenetic regulators, and advanced chemokine signaling networks. These targets offer new strategies beyond traditional cytokine blockade and could help refine patient selection and optimize efficacy.

Neutrophil extracellular traps (NETs) directly contribute to plaque rupture, thrombosis, and microvascular injury during ACS. PAD4 (peptidyl-arginine-deiminase-4) is essential for NET formation, and its pharmacologic inhibition (e.g., GSK484, chloro-amidine) in preclinical models reduces infarct size, cardiac dysfunction, and prothrombotic risk. Targeting NETosis in ACS clinical trials is ongoing, but human data are limited.

Specialized pro-resolving mediators (SPMs)—such as lipoxins, resolvins, and protectins—actively terminate inflammation and promote tissue repair. Their therapeutic modulation represents a unique, underutilized approach to control inflammation and guide healing after myocardial infarction.

Fine-tuning specific immune cell subsets (e.g., promoting regulatory T cells with low-dose IL-2 or inhibiting CD8+ granzyme B activity) offers highly targeted options in ACS immune response. Agents such as CAR-Tregs targeting oxidized LDL show preclinical promise for local vascular tolerance induction.

Modulating microRNA profiles (e.g., miR-33, miR-146a), SUMOylation, phosphorylation, and ubiquitin-mediated signaling in inflammatory cells may regulate NLRP3 activation or downstream effects, potentially providing patient-specific intervention windows.

https://doi.org/10.3390/cells15010072

Drugs targeting less-studied chemokines (such as CCL2, CXCL1, CXCL5) and their receptors (ACKR1, CCR2, CXCR2) could selectively inhibit pathogenic leukocyte recruitment, extracellular matrix remodeling, and fibrosis post-ACS. There is preliminary evidence for protective and pathogenic roles depending on context and timing.

Monoclonal antibodies such as orticumab, or engineered regulatory immune cells (CAR-Tregs), targeting oxidized LDL and its epitopes could suppress local coronary artery inflammation and stabilize vulnerable plaques, but human application remains experimental.

Beyond established IL-1 antagonists, selective targeting of NLRP3 with agents like MCC950 and OLT1177 could offer more nuanced inflammatory control during ACS, especially in individuals with specific inflammasome activation profiles.

GLP-1RAs modulate immune responses and metabolic-inflammatory crosstalk and may provide protection, especially when timing is optimized during ACS hospitalization. Their effects on immune cell polarization (macrophage M2 vs. M1 shift) and vascular inflammation warrant further exploration.

These molecular pathways are beginning to draw research attention and represent highly innovative strategies for precision inflammation targeting in ACS. Including discussion or hypotheses around these targets can substantially increase the originality and impact of a review or research proposal in this field.

Emerging genetic profiling and polygenic risk models have a growing role in refining risk stratification and guiding therapeutic decisions for inflammation-targeted interventions in acute coronary syndromes (ACS). They allow for the identification of individual genetic variants and cumulative risk scores that influence disease susceptibility, residual inflammatory risk, and variable treatment response.

Advanced genetic profiling can identify patients with inherited susceptibility to ACS or more aggressive atheroinflammatory phenotypes, using genetic markers (e.g., variants in IL-6R, NLRP3, TLR4, CRP, and other inflammation-related genes). Polygenic risk scores (PRS), integrating hundreds or thousands of individual genetic variants, allow for robust prediction of overall ASCVD risk and can reveal those at increased residual inflammatory risk despite optimal conventional therapy.

Genetic variation affects both disease mechanisms and response to therapy. For example, patients carrying specific genetic variants or expression profiles in inflammasome or cytokine pathways may derive greater benefit from targeted anti-inflammatory drugs or may require dose adjustment or alternative strategies. This can help to optimize individualized care and avoid unnecessary treatment in those unlikely to benefit.

Genetic profiling supports the identification of novel mechanistic targets and enables more precise selection of trial populations. For example, enriched recruitment of patients with high polygenic inflammation risk or specific gene expression signatures (e.g., high NLRP3 activation) can improve trial yield and clarity of results. In addition, integrating genetic profiling with multiplex inflammatory biomarker panels supports a "multi-omics" approach for patient selection and risk prediction.

Differences among ethnic groups, family history, and unexplained outcomes may be clarified through genetic analysis, improving understanding of why some patient groups respond dramatically while others do not.

Routine genetic and polygenic profiling may soon complement standard clinicopathologic risk scores, further sharpening the selection of patients for anti-inflammatory therapies, whether colchicine, IL-1 antagonists, or newer agents.

Combining genetic predisposition (from PRS) with dynamic inflammatory markers (hsCRP, IL-6, NLRP3, etc.) can identify "super-responders" and help personalize both timing and intensity of inflammatory modulation post-ACS. This approach marks a key

transition in ACS management from one-size-fits-all secondary prevention to precision medicine, maximizing therapeutic benefit while minimizing risk and healthcare costs.

Inflammation is now recognized as a fundamental driver of acute coronary syndromes (ACS), influencing plaque instability, thrombosis, and post-infarction myocardial injury. Recent discoveries offer critical insights into pathophysiology, highlight the prognostic value of inflammatory biomarkers, and identify new therapeutic targets, moving the field beyond traditional risk factor management and antithrombotic therapies.

Inflammatory mechanisms in ACS involve complex interactions among innate and adaptive immune cells, including neutrophil extracellular trap formation, macrophage polarization, T helper subset imbalances, and overactivation of inflammatory cytokines and chemokines. Multiple biomarkers—such as C-reactive protein, interleukin-6, and the neutrophil-to-lymphocyte ratio—demonstrate value for prognostic risk stratification. Modern anti-inflammatory therapies, including colchicine and IL-1 inhibitors, have shown clinical efficacy in reducing recurrent events, though outcomes can depend on timing, dosing, and patient selection. Novel agents that target the NLRP3 inflammasome, NETosis, Th17/Treg imbalance, and IL-6 are under investigation, promising greater precision in managing residual inflammatory risk beyond lipid-lowering [230,231]. New anti-inflammatory medications such as colchicine, canakinumab, anakinra, and ziltivekimab show promise for reducing residual inflammation and cardiovascular events after ACS, with potential overlap in benefits for myocarditis due to shared inflammatory pathways. However, the 2025 guidelines (ESC for myocarditis/pericarditis and ACS) do not endorse their routine use for myocarditis post-ACS, limiting colchicine to Class IIb for selected ACS cases with uncontrolled risk and excluding others pending trial data from CLEAR [232], TACTIC [233], and ARTEMIS (NCT06118281). 2025 ESC myocarditis guidelines prioritize EMB/CMR for etiology before immunosuppression, omitting these agents except NSAIDs/colchicine for pericarditis features [234]. Theoretical benefit via IL-6 pathway inhibition exists for inflammatory myocarditis subtypes, but the absence of safety/efficacy data in EMB-proven cases contraindicates off-label use per the 2025 ESC guidelines. Risks include infections and HF exacerbation, so dedicated trials are desirable. No large-scale clinical trials specifically test IL-6 inhibitors such as tocilizumab, sarilumab, or ziltivekimab directly for the treatment of primary myocarditis. Evidence is limited to small studies, case reports, and trials in related conditions, such as COVID-19 myocarditis, immune checkpoint inhibitor (ICI)-associated myocarditis, or post-MI inflammation, which show potential benefits in reducing CRP and improving ejection fraction but lack robust outcome data.

An ideal anti-inflammatory medication post-ACS targets residual inflammation (e.g., hsCRP > 2 mg/L) via specific pathways, such as IL-6 or NLRP3, to reduce MACE by $\geq$25% while maintaining hemostatic neutrality for DAPT compatibility. It achieves rapid onset (<24 h CRP reduction), oral/short IV dosing, long half-life, and safety in CKD/HF subsets without elevating infection or GI risks.

The $\geq$25% MACE reduction threshold for ideal post-ACS anti-inflammatories sets a clinically meaningful benchmark, surpassing current agents like colchicine (7–23% relative risk reduction, often heterogeneous without mortality benefit). This aligns with landmark trials (e.g., CANTOS: canakinumab 20–25% in hsCRP-high; statins 25–30%) and regulatory standards for guideline endorsement (Class I/IIa), ensuring that the net benefit outweighs risks such as GI upset or infection.

Future anti-inflammatory treatment after ACS will shift toward personalized, pathway-specific therapies targeting IL-6, IL-1β, and the NLRP3 inflammasome, integrated with biomarkers such as hsCRP/IL-6 for patient selection. Expect multi-targeted regimens combining these with statins, SGLT2i, and antithrombotics, emphasizing rapid onset, myocardial salvage, and a $\geq$25% reduction in MACE in high-inflammation subsets. New

https://doi.org/10.3390/cells15010072

biomarkers and AI will play pivotal roles in future anti-inflammatory treatment after ACS by enabling precise patient selection, timing, and monitoring of therapies like IL-6 inhibitors. Emerging markers such as ARG1, HECW2, PFKFB3, and systemic indices (SIRI, NLR) outperform hsCRP alone in predicting MACE and immune infiltration, guiding personalized care beyond standard inflammation thresholds. AI models (e.g., machine learning via WGCNA/SVM-RFE [Weighted Gene Co-expression Network Analysis/Support Vector Machine—Recursive Feature Elimination], deep learning for miRNA-mRNA networks) identify biomarker panels from GEO data to predict inflammation trajectories and therapy response. AI models integrate multi-omic (genomics, proteomics, metabolomics) and clinical data to predict ACS risk through dimensionality reduction, feature fusion, and supervised learning frameworks such as MLPs, transformers, or ensemble methods. This enables precise stratification of inflammation-driven MACE risk, outperforming traditional scores. AI excels at identifying ACS patient subgroups benefiting most from anti-inflammatory therapy by clustering multi-omic, clinical, and imaging data into endotypes with differential treatment responses. Models like ANNs or transformers outperform GRACE/TIMI (C-index 0.73–0.85 vs. 0.67), reclassifying 6–18% more patients via NRI for high-inflammation phenotypes (e.g., hsCRP > 2 mg/L, elevated IL-6). Prospective trials will validate AI-stratified protocols, enabling guideline shifts and reducing overtreatment risks, such as infection.

5.19. Clinical Implications and Current Limitations

The implementation of anti-inflammatory strategies in ACS is rapidly evolving, with trials like COLCOT and CANTOS validating the reduction in cardiovascular events through selective targeting of inflammation. However, broad application in clinical practice remains limited by variable efficacy in different patient populations, uncertain optimal timing and duration, lack of validated biomarkers for patient selection, and concerns about long-term safety—especially infection risk. Recent neutral or safety-concerning findings in large trials (e.g., CLEAR SYNERGY for colchicine) underscore the need to tailor therapy to individual inflammatory profiles and to carefully monitor for adverse effects. While current ESC and ACC/AHA guidelines acknowledge the role of inflammation in ACS, they do not yet recommend routine use of anti-inflammatory agents outside of statin therapy, except in select high-risk cases.

Looking ahead, the future of ACS care rests on integrating precision anti-inflammatory interventions alongside optimized lipid management and secondary prevention. Multiplex biomarker panels, genetic risk scores, and advanced immune profiling are essential for identifying candidates with residual inflammatory risk who are most likely to benefit from targeted therapies. Ongoing large-scale trials and real-world cohort studies will clarify optimal timing, duration, and safety. Moving forward, research should focus on leveraging systems biology, multi-omics, and adaptive trial design to refine therapeutic selection, minimize harm, and further personalize cardiovascular care.

In conclusion, inflammation represents both a major residual risk and an exciting therapeutic frontier in ACS. The integration of individualized anti-inflammatory strategies with existing guideline therapies has the potential to profoundly improve outcomes for patients worldwide, provided future studies continue to address gaps in evidence, refine patient selection, and ensure long-term safety.

Author Contributions: Conceptualization, D.M.B., O.A., R.P. and A.D.B.; methodology, D.M.B. and A.T.; validation, D.M.B., C.M. and A.T.; formal analysis, A.D.B. and R.P.; investigation, D.M.B.; resources, C.M.; writing—original draft preparation, D.M.B. and A.D.B.; writing—review and editing, A.T. and O.A.; visualization, A.T.; supervision, C.M. and R.P.; project administration, C.M. and O.A.; funding acquisition, C.M. All authors have read and agreed to the published version of the manuscript.

Funding: We would like to acknowledge "Victor Babes" University of Medicine and Pharmacy Timisoara, for their support in covering the costs of publication for this research paper.

Institutional Review Board Statement: Not applicable.

Informed Consent Statement: Not applicable.

Data Availability Statement: No new data were created or analyzed in this study. Data sharing is not applicable to this article.

Conflicts of Interest: The authors declare no conflicts of interest.

Abbreviations

The following abbreviations are used in this manuscript:

ACS	Acute Coronary Syndrome
AKT	Protein Kinase B
AMI	Acute Myocardial Infarction
ASC	Apoptosis-associated Speck-like protein containing a CARD
ATP	Adenosine Triphosphate
CAD	Coronary Artery Disease
CANTOS	Canakinumab Anti-inflammatory Thrombosis Outcomes Study
CARD	Caspase Activation and Recruitment Domain
CCL4	C-C Motif Chemokine Ligand 4
CCR5	C-C Chemokine Receptor Type 5
CD40L	CD40 Ligand
CIRT	Cardiovascular Inflammation Reduction Trial
CKD	Chronic Kidney Disease
COLCOT	Colchicine Cardiovascular Outcomes Trial
CONSORT	Consolidated Standards of Reporting Trials
COVID	Coronavirus Disease
COX	Cyclooxygenase
CRP	C-Reactive Protein
CSF	Colony-Stimulating Factor
CT	Computed Tomography
CTLA	Cytotoxic T-Lymphocyte Associated Protein
DAMP	Damage-Associated Molecular Pattern
DNA	Deoxyribonucleic Acid
ECM	Extracellular Matrix
EMT	Epithelial–Mesenchymal Transition
ERK	Extracellular Signal-Regulated Kinase
ESC	European Society of Cardiology
FAI	Fat Attenuation Index
FDA	Food and Drug Administration
FDG	Fluorodeoxyglucose
HO	Heme Oxygenase
ICAM	Intercellular Adhesion Molecule
IFN	Interferon
IL	Interleukin
IVUS	Intravascular Ultrasound
LCK	Lymphocyte-Specific Protein Tyrosine Kinase
LCX	Left Circumflex Artery
LD	Linear Dichroism
LDL	Low-Density Lipoprotein
LOX	Lipoxygenase
LRR	Leucine-Rich Repeat

LVEF	Left Ventricular Ejection Fraction
MACCE	Major Adverse Cardiac and Cerebrovascular Events
MACE	Major Adverse Cardiovascular Events
MAPK	Mitogen-Activated Protein Kinase
MCP	Monocyte Chemoattractant Protein
MHC	Major Histocompatibility Complex
MI	Myocardial Infarction
MLR	Monocyte-to-Lymphocyte Ratio
MMP	Matrix Metalloproteinase
MPO	Myeloperoxidase
MTX	Methotrexate
NACHT	Neuronal Apoptosis Inhibitory Protein (NAIP), MHC Class II Transcription Activator (CIITA), Incompatibility Locus Protein from Podospora anserina (HET-E), and Telomerase-Associated Protein (TP1)
NADPH	Nicotinamide Adenine Dinucleotide Phosphate
NET	Neutrophil Extracellular Trap
NK	Natural Killer
NLR	Neutrophil-to-Lymphocyte Ratio
NLRP3	NOD-like Receptor Protein 3
NOD	Nucleotide-binding Oligomerization Domain
NOX2	NADPH Oxidase 2
NSTEMI	Non-ST-Elevation Myocardial Infarction
PAD4	Peptidylarginine Deiminase 4
PAMP	Pathogen-Associated Molecular Pattern
PCI	Percutaneous Coronary Intervention
PD	Programmed Cell Death
PET	Positron Emission Tomography
PI3K	Phosphoinositide 3-Kinase
PLR	Platelet-to-Lymphocyte Ratio
PMN	Polymorphonuclear Neutrophil
PPAR	Peroxisome Proliferator-Activated Receptor
RA	Rheumatoid Arthritis
RCA	Right Coronary Artery
RCT	Randomized Controlled Trial
RDW	Red Cell Distribution Width
RIR	Residual Inflammatory Risk
RNA	Ribonucleic Acid
ROS	Reactive Oxygen Species
RPR	Red Cell Distribution Width-to-Platelet Ratio
SII	Systemic Immune-Inflammation Index
SIRI	Systemic Inflammation Response Index
STEMI	ST-Elevation Myocardial Infarction
TCR	T-Cell Receptor
TGF	Transforming Growth Factor
TIMI	Thrombolysis in Myocardial Infarction
TLR	Toll-Like Receptor
TNF(R)	Tumor Necrosis Factor (Receptor)
Treg	Regulatory T Cell
UA	Unstable Angina
VCAM	Vascular Cell Adhesion Molecule
VEGF	Vascular Endothelial Growth Factor
WBC	White Blood Cell

https://doi.org/10.3390/cells15010072

References

1. Byrne, R.; Coughlan, J.J.; Rossello, X.; Ibanez, B.; Members of the Task Force for the 2023 ESCGuidelines for the Management of Acute Coronary Syndromes; Barbato, E.; Berry, C.; Chieffo, A.; Claeys, M.J.; Dan, G.-A.; et al. 2023 ESC Guidelines for the management of acute coronary syndromes. *Eur. Heart J.* **2023**, *44*, 3720–3826. [CrossRef] [PubMed]
2. Vrints, C.; Andreotti, F.; Koskinas, K.C.; Rossello, X.; Adamo, M.; Ainslie, J.; Banning, A.P.; Budaj, A.; Buechel, R.R.; Chiariello, G.A. 2024 ESC Guidelines for the management of chronic coronary syndromes. *Eur. Heart J.* **2024**, *45*, 3415–3537. [CrossRef] [PubMed]
3. Matter, M.A.; Paneni, F.; Libby, P.; Frantz, S.; Stähli, B.E.; Templin, C.; Mengozzi, A.; Wang, Y.-J.; Kündig, T.M.; Räber, L.; et al. Inflammation in acute myocardial infarction: The good, the bad and the ugly. *Eur. Heart J.* **2024**, *45*, 89–103. [CrossRef]
4. Spagnoli, L.G.; Bonanno, E.; Sangiorgi, G.; Mauriello, A. Role of Inflammation in Atherosclerosis. *J. Nucl. Med.* **2007**, *48*, 1800–1815. [CrossRef]
5. Kurihara, O.; Takano, M.; Miyauchi, Y.; Mizuno, K.; Shimizu, W. Vulnerable atherosclerotic plaque features: Findings from coronary imaging. *J. Geriatr. Cardiol.* **2021**, *18*, 577–584. [CrossRef]
6. Muller, J.E.; Abela, G.S.; Nesto, R.W.; Tofler, G.H. Triggers, acute risk factors and vulnerable plaques: The lexicon of a new frontier. *J. Am. Coll. Cardiol.* **1994**, *23*, 809–813. [CrossRef]
7. Virmani, R.; Kolodgie, F.D.; Burke, A.P.; Farb, A.; Schwartz, S.M. Lessons From Sudden Coronary Death: A Comprehensive Morphological Classification Scheme for Atherosclerotic Lesions. *Arterioscler. Thromb. Vasc. Biol.* **2000**, *20*, 1262–1275. [CrossRef]
8. Naghavi, M.; Libby, P.; Falk, E.; Casscells, S.W.; Litovsky, S.; Rumberger, J.; Badimon, J.J.; Stefanadis, C.; Moreno, P.; Pasterkamp, G.; et al. From Vulnerable Plaque to Vulnerable Patient. *Circulation* **2003**, *108*, 1664–1672. [CrossRef]
9. Stary, H.C.; Chandler, A.B.; Dinsmore, R.E.; Fuster, V.; Glagov, S.; Insull, W.; Rosenfeld, M.E.; Schwartz, C.J.; Wagner, W.D.; Wissler, R.W. A Definition of Advanced Types of Atherosclerotic Lesions and a Histological Classification of Atherosclerosis. *Circulation* **1995**, *92*, 1355–1374. [CrossRef]
10. Caldarelli, M.; Franza, L.; Cutrupi, S.; Menegolo, M.; Franceschi, F.; Gasbarrini, A.; Gambassi, G.; Cianci, R. Inflammasomes in Cardiovascular Diseases: Current Knowledge and Future Perspectives. *Int. J. Mol. Sci.* **2025**, *26*, 5439. [CrossRef]
11. Abderrazak, A.; Syrovets, T.; Couchie, D.; El Hadri, K.; Friguet, B.; Simmet, T.; Rouis, M. NLRP3 inflammasome: From a danger signal sensor to a regulatory node of oxidative stress and inflammatory diseases. *Redox Biol.* **2015**, *4*, 296–307. [CrossRef]
12. Mo, D.-G.; Liang, M.-T.; Xu, L.; Li, T.; Han, Q.-F.; Chen, C.; Yao, H.-C. The effect of NLRP3 inflammasome on cardiovascular prognosis in patients with acute coronary syndrome. *Sci. Rep.* **2025**, *15*, 1187. [CrossRef]
13. Liu, Y.; Li, C.; Yin, H.; Zhang, X.; Li, Y. NLRP3 Inflammasome: A Potential Alternative Therapy Target for Atherosclerosis. *Evid.-Based Complement. Altern. Med.* **2020**, *2020*, 1561342. [CrossRef]
14. Toldo, S.; Mezzaroma, E.; Buckley, L.F.; Potere, N.; Di Nisio, M.; Biondi-Zoccai, G.; Van Tassell, B.W.; Abbate, A. Targeting the NLRP3 inflammasome in car-diovascular diseases. *Pharmacol. Ther.* **2022**, *236*, 108053. [CrossRef] [PubMed]
15. Chai, R.; Xue, W.; Shi, S.; Zhou, Y.; Du, Y.; Li, Y.; Song, Q.; Wu, H.; Hu, Y. Cardiac Remodeling in Heart Failure: Role of Pyroptosis and Its Therapeutic Implications. *Front. Cardiovasc. Med.* **2022**, *9*, 870924. [CrossRef]
16. Seok, J.K.; Kang, H.C.; Cho, Y.-Y.; Lee, H.S.; Lee, J.Y. Regulation of the NLRP3 Inflammasome by Post-Translational Modifications and Small Molecules. *Front. Immunol.* **2021**, *11*, 618231. [CrossRef]
17. Mo, B.; Ding, Y.; Ji, Q. NLRP3 inflammasome in cardiovascular diseases: An update. *Front. Immunol.* **2025**, *16*, 1550226. [CrossRef] [PubMed]
18. Nordeng, J.; Schandiz, H.; Solheim, S.; Åkra, S.; Hoffman, P.; Roald, B.; Bendz, B.; Arnesen, H.; Helseth, R.; Seljeflot, I. The Inflammasome Signaling Pathway Is Actively Regulated and Related to Myocardial Damage in Coronary Thrombi from Patients with STEMI. *Mediat. Inflamm.* **2021**, *2021*, 5525917. [CrossRef] [PubMed]
19. Jiang, X.; Wang, F.; Wang, Y.; Gisterå, A.; Roy, J.; Paulsson-Berne, G.; Hedin, U.; Lerman, A.; Hansson, G.K.; Herrmann, J.; et al. Inflammasome-Driven Interleukin-1α and Interleukin-1β Production in Atherosclerotic Plaques Relates to Hyperlipidemia and Plaque Complexity. *JACC Basic Transl. Sci.* **2019**, *4*, 304–317. [CrossRef]
20. Wæhre, T.; Yndestad, A.; Smith, C.; Haug, T.; Tunheim, S.H.; Gullestad, L.; Frøland, S.S.; Semb, A.G.; Aukrust, P.; Damås, J.K. Increased Expression of Interleukin-1 in Coronary Artery Disease with Downregulatory Effects of HMG-CoA Reductase Inhibitors. *Circulation* **2004**, *109*, 1966–1972. [CrossRef]
21. Duncan, D.J.; Yang, Z.; Hopkins, P.M.; Steele, D.S.; Harrison, S.M. TNF-α and IL-1β increase Ca2+ leak from the sarcoplasmic reticulum and susceptibility to arrhythmia in rat ventricular myocytes. *Cell Calcium* **2010**, *47*, 378–386. [CrossRef]
22. Bujak, M.; Frangogiannis, N.G. The role of IL-1 in the pathogenesis of heart disease. *Arch. Immunol. Ther. Exp.* **2009**, *57*, 165–176. [CrossRef]
23. Ikeda, U.; Ito, T.; Shimada, K. Interleukin-6 and acute coronary syndrome. *Clin. Cardiol.* **2001**, *24*, 701–704. [CrossRef]
24. Tsioufis, P.; Theofilis, P.; Tsioufis, K.; Tousoulis, D. The Impact of Cytokines in Coronary Atherosclerotic Plaque: Current Therapeutic Approaches. *Int. J. Mol. Sci.* **2022**, *23*, 15937. [CrossRef] [PubMed]
25. López-Cuenca, Á.; Manzano-Fernández, S.; Lip, G.Y.; Casas, T.; Sánchez-Martínez, M.; Mateo-Martínez, A.; Pérez-Berbel, P.; Martínez, J.; Hernández-Romero, D.; Aniorte, A.I.R.; et al. Interleukin-6 and High-sensitivity C-reactive Protein for the Prediction of Outcomes in Non-ST-segment Elevation Acute Coronary Syndromes. *Rev. Esp. Cardiol.* **2013**, *66*, 185–192. [CrossRef]

26. Nakao, T.; Libby, P. IL-6 Helps Weave the Inflammatory Web during Acute Coronary Syndromes. *J. Clin. Investig.* **2023**, *133*, e167670. [CrossRef]
27. Yang, C.; Deng, Z.; Li, J.; Ren, Z.; Liu, F. Meta-analysis of the relationship between interleukin-6 levels and the prognosis and severity of acute coronary syndrome. *Clinics* **2021**, *76*, e2690. [CrossRef]
28. Mehta, N.N.; Degoma, E.; Shapiro, M.D. IL-6 and Cardiovascular Risk: A Narrative Review. *Curr. Atheroscler. Rep.* **2025**, *27*, 12. [CrossRef] [PubMed]
29. Fanola, C.L.; Morrow, D.A.; Cannon, C.P.; Jarolim, P.; Lukas, M.A.; Bode, C.; Hochman, J.S.; Goodrich, E.L.; Braunwald, E.; O'Donoghue, M.L. Interleukin-6 and the Risk of Adverse Outcomes in Patients After an Acute Coronary Syndrome: Observations From the SOLID-TIMI 52 (Stabilization of Plaque Using Darapladib—Thrombolysis in Myocardial Infarction 52) Trial. *J. Am. Heart Assoc.* **2017**, *6*, e005637. [CrossRef]
30. Akbari, T.; Fard, T.K.; Fadaei, R.; Rostami, R.; Moradi, N.; Movahedi, M.; Fallah, S. Evaluation of MMP-9, IL-6, TNF-α levels and peripheral blood mononuclear cells genes expression of MMP-9 and TIMP-1 in Iranian patients with coronary artery disease. *J. Cardiovasc. Thorac. Res.* **2023**, *15*, 223–230. [CrossRef]
31. Mourouzis, K.; Oikonomou, E.; Siasos, G.; Tsalamadris, S.; Vogiatzi, G.; Antonopoulos, A.; Fountoulakis, P.; Goliopoulou, A.; Papaioannou, S.; Tousoulis, D. Pro-inflammatory Cytokines in Acute Coronary Syndromes. *Curr. Pharm. Des.* **2020**, *26*, 4624–4647. [CrossRef]
32. Popova, V.; Geneva-Popova, M.; Kraev, K.; Batalov, A. Assessment of TNF-α expression in unstable atherosclerotic plaques, serum IL-6 and TNF-α levels in patients with acute coronary syndrome and rheumatoid arthritis. *Rheumatol. Int.* **2022**, *42*, 1589–1596. [CrossRef]
33. Tian, M.; Yuan, Y.; Li, J.; Gionfriddo, M.R.; Huang, R. Tumor necrosis factor-α and its role as a mediator in myocardial infarction: A brief review. *Chronic Dis. Transl. Med.* **2015**, *1*, 18–26. [CrossRef]
34. Haudek, S.B.; Taffet, G.E.; Schneider, M.D.; Mann, D.L. TNF provokes cardiomyocyte apoptosis and cardiac remodeling through activation of multiple cell death pathways. *J. Clin. Investig.* **2007**, *117*, 2692–2701. [CrossRef]
35. Konstantinidis, K.; Whelan, R.S.; Kitsis, R.N. Mechanisms of Cell Death in Heart Disease. *Arter. Thromb. Vasc. Biol.* **2012**, *32*, 1552–1562. [CrossRef]
36. Guo, R.; Wu, T.; Zheng, N.; Wan, Y.; Wang, J. Clinical Features of Acute Coronary Syndrome in Patients with Coronary Heart Disease and Its Correlation with Tumour Necrosis Factor in Cardiology. *Comput. Math. Methods Med.* **2022**, *2022*, 3439768. [CrossRef]
37. Gonzálvez, M.; Ruiz-Ros, J.A.; Pérez-Paredes, M.; Lozano, M.L.; García-Almagro, F.J.; Martínez-Corbalán, F.; Giménez, D.M.; Carrillo, A.; Carnero, A.; Cubero, T.; et al. Valor pronóstico del factor de necrosis tumoral alfa en pacientes con infarto agudo de miocardio con elevación del segmento ST. *Rev. Española Cardiol.* **2007**, *60*, 1233–1241. [CrossRef]
38. Shi, N.; Wei, L.; Wang, H.; Sun, S.; Yang, J.; Zhou, Y. Regulation of pyroptosis by natural products in atherosclerosis: Mechanisms and therapeutic potential. *Front. Pharmacol.* **2025**, *16*, 1626566. [CrossRef]
39. Xiong, C.; Yu, Q.; Gao, F.; Liu, S.; Zhang, J.; Ma, T.; Liu, S. Prognostic significance of IL-18 in acute coronary syndrome patients. *Clin. Cardiol.* **2024**, *47*, e24229. [CrossRef]
40. Kaplanski, G. Interleukin-18: Biological properties and role in disease pathogenesis. *Immunol. Rev.* **2018**, *281*, 138–153. [CrossRef]
41. Tenger, C.; Sundborger, A.; Jawien, J.; Zhou, X. IL-18 Accelerates Atherosclerosis Accompanied by Elevation of IFN-γ and CXCL16 Expression Independently of T Cells. *Arter. Thromb. Vasc. Biol.* **2005**, *25*, 791–796. [CrossRef]
42. Åkerblom, A.; James, S.K.; Lakic, T.G.; Becker, R.C.; Cannon, C.P.; Steg, P.G.; Himmelmann, A.; Katus, H.A.; Storey, R.F.; Wallentin, L.; et al. Interleukin-18 in patients with acute coronary syndromes. *Clin. Cardiol.* **2019**, *42*, 1202–1209. [CrossRef]
43. Hartford, M.; Wiklund, O.; Hultén, L.M.; Persson, A.; Karlsson, T.; Herlitz, J.; Hulthe, J.; Caidahl, K. Interleukin-18 as a Predictor of Future Events in Patients with Acute Coronary Syndromes. *Arter. Thromb. Vasc. Biol.* **2010**, *30*, 2039–2046. [CrossRef]
44. Aukrust, P.; Halvorsen, B.; Yndestad, A.; Ueland, T.; Øie, E.; Otterdal, K.; Gullestad, L.; Damås, J.K. Chemokines and Cardiovascular Risk. *Arterioscler. Thromb. Vasc. Biol.* **2008**, *28*, 1909–1919. [CrossRef]
45. Aukrust, P.; Berge, R.K.; Ueland, T.; Aaser, E.; Damås, J.K.; Wikeby, L.; Brunsvig, A.; Müller, F.; Forfang, K.; Frøland, S.S.; et al. Interaction between chemokines and oxidative stress: Possible pathogenic role in acute coronary syndromes. *J. Am. Coll. Cardiol.* **2001**, *37*, 485–491. [CrossRef]
46. Pandit, R.; Yurdagul, A. The Atherosclerotic Plaque Microenvironment as a Therapeutic Target. *Curr. Atheroscler. Rep.* **2025**, *27*, 47. [CrossRef]
47. Caidahl, K.; Hartford, M.; Ravn-Fischer, A.; Lorentzen, E.; Yndestad, A.; Karlsson, T.; Aukrust, P.; Ueland, T. Homeostatic Chemokines and Prognosis in Patients with Acute Coronary Syndromes. *J. Am. Coll. Cardiol.* **2019**, *74*, 774–782. [CrossRef]
48. Zhang, H.; Yang, K.; Chen, F.; Liu, Q.; Ni, J.; Cao, W.; Hua, Y.; He, F.; Liu, Z.; Li, L.; et al. Role of the CCL2-CCR2 axis in cardiovascular disease: Pathogenesis and clinical implications. *Front. Immunol.* **2022**, *13*, 975367. [CrossRef]
49. Hernández-Aguilera, A.; Fibla, M.; Cabré, N.; Luciano-Mateo, F.; Camps, J.; Fernández-Arroyo, S.; Martín-Paredero, V.; Menendez, J.A.; Sirvent, J.J.; Joven, J. Chemokine (C-C motif) ligand 2 and coronary artery disease: Tissue expression of functional and atypical receptors. *Cytokine* **2020**, *126*, 154923. [CrossRef]
50. Shao, Z.; Tan, Y.; Shen, Q.; Hou, L.; Yao, B.; Qin, J.; Xu, P.; Mao, C.; Chen, L.-N.; Zhang, H.; et al. Molecular insights into ligand recognition and activation of chemokine receptors CCR2 and CCR3. *Cell Discov.* **2022**, *8*, 44. [CrossRef]

51. Stangret, A.; Sadowski, K.A.; Jabłoński, K.; Kochman, J.; Opolski, G.; Grabowski, M.; Tomaniak, M. Chemokine Fractalkine and Non-Obstructive Coronary Artery Disease—Is There a Link? *Int. J. Mol. Sci.* **2024**, *25*, 3885. [CrossRef]
52. De Jager, S.C.A.; Bongaerts, B.W.C.; Weber, M.; Kraaijeveld, A.O.; Rousch, M.; Dimmeler, S.; Van Dieijen-Visser, M.P.; Cleutjens, K.B.J.M.; Nelemans, P.J.; Van Berkel, T.J.C.; et al. Chemokines CCL3/MIP1α, CCL5/RANTES and CCL18/PARC are Independent Risk Predictors of Short-Term Mortality in Patients with Acute Coronary Syndromes. *PLoS ONE* **2012**, *7*, e45804. [CrossRef]
53. de Jager, S.C.; Kraaijeveld, A.O.; Grauss, R.W.; de Jager, W.; Liem, S.-S.; van der Hoeven, B.L.; Prakken, B.J.; Putter, H.; van Berkel, T.J.; Atsma, D.E.; et al. CCL3 (MIP-1α) levels are elevated during acute coronary syndromes and show strong prognostic power for future ischemic events. *J. Mol. Cell. Cardiol.* **2008**, *45*, 446–452. [CrossRef]
54. de Jager, S.C.; Bot, I.; Kraaijeveld, A.O.; Korporaal, S.J.; Bot, M.; van Santbrink, P.J.; van Berkel, T.J.; Kuiper, J.; Biessen, E.A. Leukocyte-Specific CCL3 Deficiency Inhibits Atherosclerotic Lesion Development by Affecting Neutrophil Accumulation. *Arterioscler. Thromb. Vasc. Biol.* **2013**, *33*, e75–e83. [CrossRef]
55. Zhang, Y.-L.; Cao, H.-J.; Han, X.; Teng, F.; Chen, C.; Yang, J.; Yan, X.; Li, P.-B.; Liu, Y.; Xia, Y.-L.; et al. Chemokine Receptor CXCR-2 Initiates Atrial Fibrillation by Triggering Monocyte Mobilization in Mice. *Hypertension* **2020**, *76*, 381–392. [CrossRef]
56. Zhang, Y.; Zhang, X.; Zhang, X.; Cai, Y.; Cheng, M.; Yan, C.; Han, Y. Molecular Targets and Pathways Contributing to the Effects of Wenxin Keli on Atrial Fibrillation Based on a Network Pharmacology Approach. *Evid.-Based Complement. Altern. Med.* **2020**, *2020*, 8396484. [CrossRef]
57. Zhou, C.; Gao, Y.; Ding, P.; Wu, T.; Ji, G. The role of CXCL family members in different diseases. *Cell Death Discov.* **2023**, *9*, 212. [CrossRef]
58. Deng, J.; Jiang, R.; Meng, E.; Wu, H. CXCL5: A coachman to drive cancer progression. *Front. Oncol.* **2022**, *12*, 944494. [CrossRef]
59. Zeng, Z.; Lan, T.; Wei, Y.; Wei, X. CCL5/CCR5 axis in human diseases and related treatments. *Genes Dis.* **2022**, *9*, 12–27. [CrossRef]
60. Keeley, E.C.; Blotner, M.R.; Lipson, L.C.; Mehrad, B. CXCL5 gene polymorphisms and coronary collateralization. *Am. Heart J. Plus Cardiol. Res. Pract.* **2022**, *23*, 100220. [CrossRef]
61. Ravi, S.; Schuck, R.N.; Hilliard, E.; Lee, C.R.; Dai, X.; Lenhart, K.; Willis, M.S.; Jensen, B.C.; Stouffer, G.A.; Patterson, C.; et al. Clinical Evidence Supports a Protective Role for CXCL5 in Coronary Artery Disease. *Am. J. Pathol.* **2017**, *187*, 2895–2911. [CrossRef]
62. Murray, P.J.; Allen, J.E.; Biswas, S.K.; Fisher, E.A.; Gilroy, D.W.; Goerdt, S.; Gordon, S.; Hamilton, J.A.; Ivashkiv, L.B.; Lawrence, T.; et al. Macrophage Activation and Polarization: Nomenclature and Experimental Guidelines. *Immunity* **2014**, *41*, 14–20. [CrossRef]
63. Bajpai, G.; Bredemeyer, A.L.; Li, W.; Zaitsev, K.; Koenig, A.L.; Lokshina, I.V.; Mohan, J.; Ivey, B.; Hsiao, H.-M.; Weinheimer, C.J.; et al. Tissue Resident CCR2− and CCR2+ Cardiac Macrophages Differentially Orchestrate Monocyte Recruitment and Fate Specification Following Myocardial Injury. *Circ. Res.* **2019**, *124*, 263–278. [CrossRef]
64. Nahrendorf, M.; Swirski, F.K.; Aikawa, E.; Stangenberg, L.; Wurdinger, T.; Figueiredo, J.L.; Libby, P.; Weissleder, R.; Pittet, M.J. The healing myocardium sequentially mobilizes two monocyte subsets with divergent and complementary functions. *J. Exp. Med.* **2007**, *204*, 3037–3047. [CrossRef]
65. Shantsila, E.; Lip, G.Y.H. Monocytes in Acute Coronary Syndromes. *Arterioscler. Thromb. Vasc. Biol.* **2009**, *29*, 1433–1438. [CrossRef]
66. Ghattas, A.; Griffiths, H.R.; Devitt, A.; Lip, G.Y.; Shantsila, E. Monocytes in Coronary Artery Disease and Atherosclerosis. *J. Am. Coll. Cardiol.* **2013**, *62*, 1541–1551. [CrossRef]
67. Peet, C.; Ivetic, A.; Bromage, D.I.; Shah, A.M. Cardiac monocytes and macrophages after myocardial infarction. *Cardiovasc. Res.* **2020**, *116*, 1101–1112. [CrossRef] [PubMed] [PubMed Central]
68. Sager, H.B.; Kessler, T.; Schunkert, H. Monocytes and macrophages in cardiac injury and repair. *J. Thorac. Dis.* **2017**, *9*, S30–S35. [CrossRef]
69. Sager, H.B.; Hulsmans, M.; Lavine, K.J.; Moreira, M.B.; Heidt, T.; Courties, G.; Sun, Y.; Iwamoto, Y.; Tricot, B.; Khan, O.F.; et al. Proliferation and Recruitment Contribute to Myocardial Macrophage Expansion in Chronic Heart Failure. *Circ. Res.* **2016**, *119*, 853–864. [CrossRef]
70. Naruko, T.; Ueda, M.; Haze, K.; van der Wal, A.C.; van der Loos, C.M.; Itoh, A.; Komatsu, R.; Ikura, Y.; Ogami, M.; Shimada, Y.; et al. Neutrophil Infiltration of Culprit Lesions in Acute Coronary Syndromes. *Circulation* **2002**, *106*, 2894–2900. [CrossRef]
71. Papayannopoulos, V. Neutrophil extracellular traps in immunity and disease. *Nat. Rev. Immunol.* **2018**, *18*, 134–147. [CrossRef] [PubMed]
72. Mangold, A.; Alias, S.; Scherz, T.; Hofbauer, T.M.; Jakowitsch, J.; Panzenböck, A.; Simon, D.; Laimer, D.; Bangert, C.; Kammerlander, A.; et al. Coronary Neutrophil Extracellular Trap Burden and Deoxyribonuclease Activity in ST-Elevation Acute Coronary Syndrome Are Predictors of ST-Segment Resolution and Infarct Size. *Circ. Res.* **2015**, *116*, 1182–1192. [CrossRef] [PubMed]
73. Wu, Y.; Wei, S.; Wu, X.; Li, Y.; Han, X. Neutrophil Extracellular Traps in Acute Coronary Syndrome. 2023. *J. Inflamm.* **2023**, *20*, 17. [CrossRef]
74. Friedman, G.D.; Klatsky, A.L.; Siegelaub, A.B. The Leukocyte Count as a Predictor of Myocardial Infarction. *N. Engl. J. Med.* **1974**, *290*, 1275–1278. [CrossRef]
75. Borissoff, J.I.; Joosen, I.A.; Versteylen, M.O.; Brill, A.; Fuchs, T.A.; Savchenko, A.S.; Gallant, M.; Martinod, K.; ten Cate, H.; Hofstra, L.; et al. Elevated Levels of Circulating DNA and Chromatin Are Independently Associated with Severe Coronary Atherosclerosis and a Prothrombotic State. *Arter. Thromb. Vasc. Biol.* **2013**, *33*, 2032–2040. [CrossRef]
76. Zhang, Z.; Wang, Y.; Li, T.; Wang, H. NETosis in myocardial ischemia-reperfusion injury: From mechanisms to therapies (Review). *Biomed. Rep.* **2025**, *23*, 113. [CrossRef]

77. Szymańska, Z.; Staniewski, A.; Karpiński, M.; Zalewska, K.; Kalus, O.; Gramala, Z.; Maćkowiak, J.; Mertowski, S.; Filipiak, K.J.; Rahnama-Hezavah, M.; et al. The Role of Neutrophil Extracellular Networks in Cardiovascular Pathology. *Cells* **2025**, *14*, 1562. [CrossRef]
78. Megens, R.T.; Vijayan, S.; Lievens, D.; Döring, Y.; van Zandvoort, M.A.; Grommes, J.; Weber, C.; Soehnlein, O. Presence of luminal neutrophil extracellular traps in atherosclerosis. *Thromb. Haemost.* **2012**, *107*, 597–598. [CrossRef]
79. Mostafa, M.N.; Osama, M. The implications of neutrophil extracellular traps in the pathophysiology of atherosclerosis and atherothrombosis. *Exp. Biol. Med.* **2020**, *245*, 1376–1384. [CrossRef]
80. Awasthi, D.; Nagarkoti, S.; Sadaf, S.; Chandra, T.; Kumar, S.; Dikshit, M. Glycolysis dependent lactate formation in neutrophils: A metabolic link between NOX-dependent and independent NETosis. *Biochim. Biophys. Acta (BBA)-Mol. Basis Dis.* **2019**, *1865*, 165542. [CrossRef]
81. Yu, J.; Fu, Y.; Gao, J.; Zhang, Q.; Zhang, N.; Zhang, Z.; Jiang, X.; Chen, C.; Wen, Z. Cathepsin C from extracellular histone-induced M1 alveolar macrophages promotes NETosis during lung ischemia-reperfusion injury. *Redox Biol.* **2024**, *74*, 103231. [CrossRef]
82. Sun, L.; Wu, Q.; Nie, Y.; Cheng, N.; Wang, R.; Wang, G.; Zhang, D.; He, H.; Ye, R.D.; Qian, F. A Role for MK2 in Enhancing Neutrophil-Derived ROS Production and Aggravating Liver Ischemia/Reperfusion Injury. *Front. Immunol.* **2018**, *9*, 2610. [CrossRef]
83. AKurian, G.; Rajagopal, R.; Vedantham, S.; Rajesh, M. The Role of Oxidative Stress in Myocardial Ischemia and Reperfusion Injury and Remodeling: Revisited. *Oxid. Med. Cell. Longev.* **2016**, *2016*, 1656450. [CrossRef]
84. Guasti, L.; Dentali, F.; Castiglioni, L.; Maroni, L.; Marino, F.; Squizzato, A.; Ageno, W.; Gianni, M.; Gaudio, G.; Grandi, A.M.; et al. Neutrophils and clinical outcomes in patients with acute coronary syndromes and/or cardiac revascularisation. *Thromb. Haemost.* **2011**, *106*, 591–599. [CrossRef] [PubMed]
85. Takeda, S.; Emoto, T.; Yamashita, T.; Yamamoto, H.; Takaya, T.; Sawada, T.; Yoshida, T.; Inoue, M.; Suzuki, Y.; Hamana, T.; et al. Single-Cell RNA Sequencing Reveals an Immune Landscape of CD4+ T Cells in Coronary Culprit Plaques with Acute Coronary Syndrome in Humans—Brief Report. *Arter. Thromb. Vasc. Biol.* **2024**, *44*, 1135–1143. [CrossRef]
86. Flego, D.; Liuzzo, G.; Weyand, C.M.; Crea, F. Adaptive Immunity Dysregulation in Acute Coronary Syndromes. *J. Am. Coll. Cardiol.* **2016**, *68*, 2107–2117. [CrossRef] [PubMed]
87. Pryshchep, S.; Goronzy, J.J.; Parashar, S.; Weyand, C.M. Insufficient Deactivation of the Protein Tyrosine Kinase Lck Amplifies T-Cell Responsiveness in Acute Coronary Syndrome. *Circ. Res.* **2010**, *106*, 769–778. [CrossRef]
88. Chen, J.; Xiang, X.; Nie, L.; Guo, X.; Zhang, F.; Wen, C.; Xia, Y.; Mao, L. The emerging role of Th1 cells in atherosclerosis and its implications for therapy. *Front. Immunol.* **2023**, *13*, 1079668. [CrossRef] [PubMed]
89. Kehmeier, E.S.; Lepper, W.; Kropp, M.; Heiss, C.; Hendgen-Cotta, U.; Balzer, J.; Neizel, M.; Meyer, C.; Merx, M.W.; Verde, P.E.; et al. TNF-α, myocardial perfusion and function in patients with ST-segment elevation myocardial infarction and primary percutaneous coronary intervention. *Clin. Res. Cardiol.* **2012**, *101*, 815–827. [CrossRef]
90. Voloshyna, I.; Littlefield, M.J.; Reiss, A.B. Atherosclerosis and interferon-γ: New insights and therapeutic targets. *Trends Cardiovasc. Med.* **2014**, *24*, 45–51. [CrossRef]
91. Li, Q.; Wang, Y.; Wang, Y.; Chen, K.; Zhou, Q.; Wei, W.; Wang, Y. Treg/Th17 Ratio Acts as a Novel Indicator for Acute Coronary Syndrome. *Cell Biochem. Biophys.* **2014**, *70*, 1489–1498. [CrossRef]
92. Xia, Y.; Gao, D.; Wang, X.; Liu, B.; Shan, X.; Sun, Y.; Ma, D. Role of Treg cell subsets in cardiovascular disease pathogenesis and potential therapeutic targets. *Front. Immunol.* **2024**, *15*, 1331609. [CrossRef] [PubMed]
93. Santos-Zas, I.; Lemarié, J.; Zlatanova, I.; Cachanado, M.; Seghezzi, J.-C.; Benamer, H.; Goube, P.; Vandestienne, M.; Cohen, R.; Ezzo, M.; et al. Cytotoxic $CD8^+$ T cells promote granzyme B-dependent adverse post-ischemic cardiac remodeling. *Nat. Commun.* **2021**, *12*, 1483. [CrossRef] [PubMed]
94. Bocanegra-Zamora, F.; Espinosa-Bautista, F.; Jiménez-Rodríguez, G.M.; Masso, F.; Paez, A.; Gonzalez-Pacheco, H.; Patlán, M.; Eid-Lidt, G.; Amezcua-Guerra, L.M. Senescent CD4+ T-Cell Phenotypes and Inflammatory Milieu in the Coronary and Systemic Circulation in ST-Elevation Myocardial Infarction: An Exploratory Study. *J. Vasc. Res.* **2024**, *61*, 260–266. [CrossRef]
95. Schäfer, S.; Zernecke, A. CD8+ T Cells in Atherosclerosis. *Cells* **2020**, *10*, 37. [CrossRef]
96. Calabró, P.; Willerson, J.T.; Yeh, E.T. Inflammatory Cytokines Stimulated C-Reactive Protein Production by Human Coronary Artery Smooth Muscle Cells. *Circulation* **2003**, *108*, 1930–1932. [CrossRef] [PubMed]
97. Ahtesham, M.; Khan, S.W.; Khan, S.R.; Fayyaz, A.; Khan, Z.; Ullah, I.; Ahmad, Y.; Khan, S.W. C-reactive Protein (CRP) Levels as a Predictor of Adverse Cardiovascular Events in Acute Myocardial Infarction: A Prospective Study. *Cureus* **2025**, *17*, e93943. [CrossRef]
98. Bodí, V.; Sanchis, J. C-Reactive Protein in Acute Coronary Syndrome. Looking Back in Order to Move Forward. *Rev. Esp. Cardiol.* **2006**, *59*, 418–420. [CrossRef]
99. Armstrong, E.J.; Morrow, D.A.; Sabatine, M.S. Inflammatory Biomarkers in Acute Coronary Syndromes. *Circulation* **2006**, *113*, e72–e75.
100. Sheikh, A.; Yahya, S.; Sheikh, N.; Sheikh, A. C-reactive protein as a predictor of adverse outcome in patients with acute coronary syndrome. *Heart Views* **2012**, *13*, 7. [CrossRef]
101. Ray, K.K.; Cannon, C.P.; McCabe, C.H.; Cairns, R.; Tonkin, A.M.; Sacks, F.M.; Jackson, G.; Braunwald, E. Early and Late Benefits of High-Dose Atorvastatin in Patients with Acute Coronary Syndromes. *J. Am. Coll. Cardiol.* **2005**, *46*, 1405–1410. [CrossRef]

102. Gibson, C.M.; Pride, Y.B.; Hochberg, C.P.; Sloan, S.; Sabatine, M.S.; Cannon, C.P. Effect of Intensive Statin Therapy on Clinical Outcomes Among Patients Undergoing Percutaneous Coronary Intervention for Acute Coronary Syndrome. *J. Am. Coll. Cardiol.* **2009**, *54*, 2290–2295. [CrossRef] [PubMed]
103. Mitsis, A.; Sokratous, S.; Karmioti, G.; Kyriakou, M.; Drakomathioulakis, M.; Myrianthefs, M.M.; Eftychiou, C.; Kadoglou, N.P.E.; Tzikas, S.; Fragakis, N.; et al. The Role of C-Reactive Protein in Acute Myocardial Infarction: Unmasking Diagnostic, Prognostic, and Therapeutic Insights. *J. Clin. Med.* **2025**, *14*, 4795. [CrossRef] [PubMed]
104. EByrne, C.; Fitzgerald, A.; Cannon, C.P.; Fitzgerald, D.J.; Shields, D.C. Elevated white cell count in acute coronary syndromes: Relationship to variants in inflammatory and thrombotic genes. *BMC Med. Genet.* **2004**, *5*, 13. [CrossRef]
105. Núñez, J.; Nunez, E.; Bodí, V.; Sanchis, J.; Minana, G.; Mainar, L.; Santas, E.; Merlos, P.; Rumiz, E.; Darmofal, H.; et al. Usefulness of the Neutrophil to Lymphocyte Ratio in Predicting Long-Term Mortality in ST Segment Elevation Myocardial Infarction. *Am. J. Cardiol.* **2008**, *101*, 747–752. [CrossRef]
106. Sabatine, M.S.; AMorrow, D.; Cannon, C.P.; AMurphy, S.; ADemopoulos, L.; DiBattiste, P.M.; McCabe, C.H.; Braunwald, E.; Gibson, C. Relationship between baseline white blood cell count and degree of coronary artery disease and mortality in patients with acute coronary syndromes. *J. Am. Coll. Cardiol.* **2002**, *40*, 1761–1768. [CrossRef]
107. Alkhalfan, F.; Nafee, T.; Yee, M.K.; Chi, G.; Kalayci, A.; Plotnikov, A.; Braunwald, E.; Gibson, C.M. Relation of White Blood Cell Count to Bleeding and Ischemic Events in Patients with Acute Coronary Syndrome (from the ATLAS ACS 2-TIMI 51 Trial). *Am. J. Cardiol.* **2020**, *125*, 661–669. [CrossRef]
108. Chen, C.; Cong, B.L.; Wang, M.; Abdullah, M.; Wang, X.L.; Zhang, Y.H.; Xu, S.J.; Cui, L. Neutrophil to lymphocyte ratio as a predictor of myocardial damage and cardiac dysfunction in acute coronary syndrome patients. *Integr. Med. Res.* **2018**, *7*, 192–199. [CrossRef]
109. Lesmana, J.; Lefi, A. The relationship between neutrophil to lymphocyte ratio (NLR) with rehospitalisation and mortality in patients with acute coronary syndrome (ACS). *J. Pak. Med. Assoc.* **2024**, *74*, S9–S12. [CrossRef]
110. Soylu, K.; Gedikli, Ö.; Dagasan, G.; Aydin, E.; Aksan, G.; Nar, G.; Inci, S.; Yilmaz, Ö. Neutrophil-to-lymphocyte ratio predicts coronary artery lesion complexity and mortality after non-ST-segment elevation acute coronary syndrome. *Rev. Port. Cardiol.* **2015**, *34*, 465–471. [CrossRef]
111. Korkmaz, A.; Yildiz, A.; Gunes, H.; Duyuler, S.; Tuncez, A. Utility of Neutrophil–Lymphocyte Ratio in Predicting Troponin Elevation in the Emergency Department Setting. *Clin. Appl. Thromb.* **2015**, *21*, 667–671. [CrossRef] [PubMed]
112. Ridker, P.M.; Rane, M. Interleukin-6 Signaling and Anti-Interleukin-6 Therapeutics in Cardiovascular Disease. *Circ. Res.* **2021**, *128*, 1728–1746. [CrossRef] [PubMed]
113. Said, E.A.; Al-Reesi, I.; Al-Shizawi, N.; Jaju, S.; Al-Balushi, M.S.; Koh, C.Y.; Al-Jabri, A.A.; Jeyaseelan, L. Defining IL-6 levels in healthy individuals: A meta-analysis. *J. Med. Virol.* **2021**, *93*, 3915–3924. [CrossRef]
114. Tøllefsen, I.M.; Shetelig, C.; Seljeflot, I.; Eritsland, J.; Hoffmann, P.; Andersen, G.Ø. High levels of interleukin-6 are associated with final infarct size and adverse clinical events in patients with STEMI. *Open Heart* **2021**, *8*, e001869. [CrossRef]
115. Gabriel, A.S.; Martinsson, A.; Wretlind, B.; Ahnve, S. IL-6 levels in acute and post myocardial infarction: Their relation to CRP levels, infarction size, left ventricular systolic function, and heart failure. *Eur. J. Intern. Med.* **2004**, *15*, 523–528. [CrossRef] [PubMed]
116. Ridker, P.M.; Hennekens, C.H.; Buring, J.E.; Rifai, N. C-Reactive Protein and Other Markers of Inflammation in the Prediction of Cardiovascular Disease in Women. *N. Engl. J. Med.* **2000**, *342*, 836–843. [CrossRef]
117. Besse, S.; Nadaud, S.; Balse, E.; Pavoine, C. Early Protective Role of Inflammation in Cardiac Remodeling and Heart Failure: Focus on TNFα and Resident Macrophages. *Cells* **2022**, *11*, 1249. [CrossRef]
118. Kang, H.-J.; Kim, J.-W.; Lee, J.-Y.; Kim, S.-W.; Shin, I.-S.; Hong, Y.J.; Ahn, Y.; Jeong, M.-H.; Kim, J.-M. Time-Specific Associations of Tumor Necrosis Factor-α Levels and Polymorphisms (−850 C/T or −308 G/A) with Suicidal Ideation in Acute Coronary Syndrome Patients. *Front. Psychiatry* **2021**, *12*, 739823. [CrossRef]
119. Auda, H.J.; Barakat, A.M.; Sachet, H.S.; Aboqader, R.F.; Thamer, A.T. TNF-α and E-Selectin as Valuable Biomarkers in Patients with Acute Coronary Artery Syndrome. *Int. J. Mol. Cell Med.* **2025**, *14*, 694–704. [CrossRef]
120. Rafiqi, K.; Hoeks, C.B.; Løfgren, B.; Mortensen, M.B.; Bruun, J.M. Diagnostic Impact of Hs-CRP and IL-6 for Acute Coronary Syndrome in Patients Admitted to the ED with Chest Pain: Added Value to the HEART Score? *Open Access Emerg. Med.* **2023**, *15*, 333–342. [CrossRef]
121. Madjid, M.; Ali, M.; Willerson, J.T. Lipoprotein-associated phospholipase A2 as a novel risk marker for cardiovascular disease: A systematic review of the literature. *Tex. Heart Inst. J.* **2010**, *37*, 25–39. [PubMed]
122. Huang, Y.; Wu, Y.; Yang, Y.; Li, W.; Lu, J.; Hu, Y. Lipoprotein-associated phospholipase A2 and oxidized low-density lipoprotein in young patients with acute coronary syndrome in China. *Sci. Rep.* **2017**, *7*, 16092. [CrossRef] [PubMed]
123. Huang, T.; Zhu, B. The Value of Lp-PLA2 as a Biomarker for the Diagnosis of Plaque Stability in Atherosclerosis: A Meta-Analysis. *Clin. Appl. Thromb.* **2025**, *31*, 10760296251360015. [CrossRef]
124. Loria, V.; Dato, I.; Graziani, F.; Biasucci, L.M. Myeloperoxidase: A New Biomarker of Inflammation in Ischemic Heart Disease and Acute Coronary Syndromes. *Mediat. Inflamm.* **2008**, *2008*, 135625. [CrossRef] [PubMed]

125. Nofal, R.; Martini, N.; Hanna, M.; Almasri, I.-A.; Alsaadi, A.R.; Ali, T. Investigating soluble CD40 ligand as a prognostic factor among acute coronary syndromes patients: A multi-center prospective case-control study. *Medicine* **2024**, *103*, e39891. [CrossRef]
126. Adam, C.A.; Șalaru, D.L.; Prisacariu, C.; Marcu, D.T.M.; Sascău, R.A.; Stătescu, C. Novel Biomarkers of Atherosclerotic Vascular Disease—Latest Insights in the Research Field. *Int. J. Mol. Sci.* **2022**, *23*, 4998. [CrossRef]
127. Inoue, K.; Kodama, T.; Daida, H. Pentraxin 3: A Novel Biomarker for Inflammatory Cardiovascular Disease. *Int. J. Vasc. Med.* **2012**, *2012*, 657025. [CrossRef]
128. Ge, P.; Ni, T.; Liu, M.; Du, Q.; Xu, C.; Hu, T.; Gu, Y.; Liu, H.; Geng, J. TRAF3IP2 as a novel inflammatory biomarker for coronary artery disease: Development and validation of a multimodal prediction model. *Front. Endocrinol.* **2025**, *16*, 1644403. [CrossRef]
129. Kook, H.; Jang, D.H.; Kim, J.-H.; Cho, J.-Y.; Joo, H.J.; Cho, S.-A.; Park, J.H.; Hong, S.J.; Yu, C.W.; Lim, D.-S. Identification of plaque ruptures using a novel discriminative model comprising biomarkers in patients with acute coronary syndrome. *Sci. Rep.* **2020**, *10*, 20228. [CrossRef]
130. Jin, P.; Zhang, S.; Yang, L.; Zeng, Y.; Li, Y.; Tang, R. Analysis and validation of biomarkers and immune cell infiltration profiles in unstable coronary atherosclerotic plaques using bioinformatics and machine learning. *Front. Cardiovasc. Med.* **2025**, *12*, 1451255. [CrossRef]
131. Kumric, M.; Borovac, J.A.; Martinovic, D.; Kurir, T.T.; Bozic, J. Circulating Biomarkers Reflecting Destabilization Mechanisms of Coronary Artery Plaques: Are We Looking for the Impossible? *Biomolecules* **2021**, *11*, 881. [CrossRef] [PubMed]
132. Bom, M.J.; Levin, E.; Driessen, R.S.; Danad, I.; Van Kuijk, C.C.; van Rossum, A.C.; Narula, J.; Min, J.K.; Leipsic, J.A.; Pereira, J.P.B.; et al. Predictive value of targeted proteomics for coronary plaque morphology in patients with suspected coronary artery disease. *EBioMedicine* **2019**, *39*, 109–117. [CrossRef]
133. Schulte, C.; Zeller, T. microRNA-based diagnostics and therapy in cardiovascular disease-Summing up the facts. *Cardiovasc. Diagn. Ther.* **2015**, *5*, 17–36. [CrossRef]
134. Wexler, Y.; Nussinovitch, U. The Diagnostic Value of Mir-133a in ST Elevation and Non-ST Elevation Myocardial Infarction: A Meta-Analysis. *Cells* **2020**, *9*, 793. [CrossRef]
135. West, H.W.; Dangas, K.; Antoniades, C. Advances in Clinical Imaging of Vascular Inflammation. *JACC Basic Transl. Sci.* **2023**, *9*, 710–732. [CrossRef]
136. Klüner, L.V.; Oikonomou, E.K.; Antoniades, C. Assessing Cardiovascular Risk by Using the Fat Attenuation Index in Coronary CT Angiography. *Radiol. Cardiothorac. Imaging* **2021**, *3*, e200563. [CrossRef] [PubMed]
137. Kraaijenhof, J.M.; Nurmohamed, N.S.; Bom, M.J.; Gaillard, E.L.; Ibrahim, S.; Beverloo, C.Y.Y.; Planken, R.N.; Hovingh, G.K.; Danad, I.; Stroes, E.S.G.; et al. Plasma proteomics improves prediction of coronary plaque progression. *Eur. Heart J.-Cardiovasc. Imaging* **2025**, *26*, 489–499. [CrossRef] [PubMed]
138. Feng, X.; Zhang, Y.; Yi, S.; Lu, R. Effect of aspirin plus clopidogrel on inflammatory markers in patients with non-ST-segment elevation acute coronary syndrome. *Chin. Med. J.* **2006**, *119*, 32–36.
139. Layne, K.; Ferro, A. Antiplatelet Therapy in Acute Coronary Syndrome. *Eur. Cardiol. Rev.* **2017**, *12*, 33. [CrossRef]
140. Schrör, K.; Hohlfeld, T. Antiinflammatory effects of aspirin in ACS: Relevant to its cardio coronary actions? *Thromb. Haemost.* **2015**, *114*, 469–477. [CrossRef]
141. Dai, Y.; Ge, J. Clinical Use of Aspirin in Treatment and Prevention of Cardiovascular Disease. *Thrombosis* **2012**, *2012*, 245037. [CrossRef]
142. Ashidate, K.; Kawamura, M.; Mimura, D.; Tohda, H.; Miyazaki, S.; Teramoto, T.; Yamamoto, Y.; Hirata, Y. Gentisic acid, an aspirin metabolite, inhibits oxidation of low-density lipoprotein and the formation of cholesterol ester hydroperoxides in human plasma. *Eur. J. Pharmacol.* **2005**, *513*, 173–179. [CrossRef] [PubMed]
143. Steer, K.A.; Wallace, T.M.; Bolton, C.H.; Hartog, M. Aspirin protects low density lipoprotein from oxidative modification. *Heart* **1997**, *77*, 333–337. [CrossRef]
144. Awtry, E.H.; Loscalzo, J. Aspirin. *Circulation* **2000**, *101*, 1206–1218. [CrossRef]
145. Waterman, M.; Fuhrman, B.; Keidar, S.; Hayek, T. Aspirin Promotes Low Density Lipoprotein Susceptibility to Oxidative Modification in Healthy Volunteers. *Isr. Med. Assoc. J.* **2009**, *11*, 730–734. [PubMed]
146. Ridker, P.M.; Danielson, E.; Fonseca, F.A.; Genest, J.; Gotto, A.M.; Kastelein, J.J.; Koenig, W.; Libby, P.; Lorenzatti, A.J.; MacFadyen, J.G.; et al. Rosuvastatin to Prevent Vascular Events in Men and Women with Elevated C-Reactive Protein. *N. Engl. J. Med.* **2008**, *359*, 2195–2207. [CrossRef] [PubMed]
147. Diamantis, E.; Kyriakos, G.; Quiles-Sanchez, L.V.; Farmaki, P.; Troupis, T. The Anti-Inflammatory Effects of Statins on Coronary Artery Disease: An Updated Review of the Literature. *Curr. Cardiol. Rev.* **2017**, *13*, 209–216. [CrossRef] [PubMed]
148. Chamani, S.; Kooshkaki, O.; Moossavi, M.; Rastegar, M.; Soflaei, S.S.; McCloskey, A.P.; Banach, M.; Sahebkar, A. The effects of statins on the function and differentiation of blood cells. *Arch. Med. Sci.* **2022**, *19*, 1314–1326. [CrossRef]
149. Zhou, T.; Zhou, S.H.; Qi, S.S.; Shen, X.Q.; Zeng, G.F.; Zhou, H.N. The effect of atorvastatin on serum myeloperoxidase and CRP levels in patients with acute coronary syndrome. *Clin. Chim. Acta* **2006**, *368*, 168–172. [CrossRef]
150. Oesterle, A.; Laufs, U.; Liao, J.K. Pleiotropic Effects of Statins on the Cardiovascular System. *Circ. Res.* **2017**, *120*, 229–243. [CrossRef]
151. Zivkovic, S.; Maric, G.; Cvetinovic, N.; Lepojevic-Stefanovic, D.; Cvijan, B.B. Anti-Inflammatory Effects of Lipid-Lowering Drugs and Supplements—A Narrative Review. *Nutrients* **2023**, *15*, 1517. [CrossRef] [PubMed]

152. Karmaus, P.W.F.; Shi, M.; Perl, S.; Biancotto, A.; Candia, J.; Cheung, F.; Kotliarov, Y.; Young, N.; Fessler, M.B.; CHI Consortium. Effects of rosuvastatin on the immune system in healthy volunteers with normal serum cholesterol. *JCI Insight* **2019**, *4*, e131530. [CrossRef]
153. Khurana, S.; Gupta, S.; Bhalla, H.L.; Nandwani, S.; Gupta, V. Comparison of anti-inflammatory effect of atorvastatin with rosuvastatin in patients of acute coronary syndrome. *J. Pharmacol. Pharmacother.* **2015**, *6*, 130–135. [CrossRef]
154. Schwartz, G.G.; Olsson, A.G.; Ezekowitz, M.D.; Ganz, P.; Oliver, M.F.; Waters, D.; Zeiher, A.; Chaitman, B.R.; Leslie, S.; Stern, T. Effects of atorvastatin on early recurrent ischemic events in acute coronary syndromes: The MIRACL study: A randomized controlled trial. *JAMA* **2001**, *285*, 1711–1718. [CrossRef]
155. Murphy, S.A.; Cannon, C.P.; Wiviott, S.D.; McCabe, C.H.; Braunwald, E. Reduction in recurrent cardiovascular events with intensive lipid-lowering statin therapy compared with moderate lipid-lowering statin therapy after acute coronary syndromes from the PROVE IT-TIMI 22 (Pravastatin or Atorvastatin Evaluation and Infection Therapy-Thrombolysis In Myocardial Infarction 22) trial. *J. Am. Coll. Cardiol.* **2009**, *54*, 2358–2362.
156. Song, X.; Zhou, X.; Li, Z.; Sun, H.; Liu, H.; AG; Hao, Y.; Liu, J.; Liu, J.; Zhao, D.; et al. Early Statin Therapy and In-Hospital Outcomes in Acute Coronary Syndrome Patients Presenting with Advanced Killip Class at Admission: Findings from the CCC-ACS Project. *Am. J. Cardiovasc. Drugs* **2022**, *22*, 685–694. [CrossRef]
157. Momtazi, A.A.; Sabouri-Rad, S.; Gotto, A.M.; Pirro, M.; Banach, M.; Awan, Z.; Barreto, G.E.; Sahebkar, A. PCSK9 and inflammation: A review of experimental and clinical evidence. *Eur. Heart J.-Cardiovasc. Pharmacother.* **2019**, *5*, 237–245. [CrossRef]
158. Nordmann, A.; Schwartz, G.; Vale, N.; Bucher, H.C.; Briel, M. Cochrane corner: Early statin therapy in acute coronary syndromes—What is the clinical benefit? *Heart* **2016**, *102*, 653–654. [CrossRef] [PubMed]
159. Punch, E.; Klein, J.; Diaba-Nuhoho, P.; Morawietz, H.; Garelnabi, M. Effects of PCSK9 Targeting: Alleviating Oxidation, Inflammation, and Atherosclerosis. *J. Am. Heart Assoc.* **2022**, *11*, e023328. [CrossRef] [PubMed]
160. Katsuki, S.; Jha, P.K.; Aikawa, E.; Aikawa, M. The role of proprotein convertase subtilisin/kexin 9 (PCSK9) in macrophage activation: A focus on its LDL receptor-independent mechanisms. *Front. Cardiovasc. Med.* **2024**, *11*, 1431398. [CrossRef]
161. Wu, N.-Q.; Shi, H.-W.; Li, J.-J. Proprotein Convertase Subtilisin/Kexin Type 9 and Inflammation: An Updated Review. *Front. Cardiovasc. Med.* **2022**, *9*, 763516. [CrossRef]
162. Luo, J.; Liao, W.; Wang, X.; Xu, R.; Li, W.; Li, W.; Liu, K.; Huang, K.; Ma, Y.; Wang, T.; et al. PCSK9 inhibitors for anti-inflammation in atherosclerosis: Protocol for a systematic review and meta-analysis of randomised controlled trials. *BMJ Open* **2022**, *12*, e062046. [CrossRef]
163. Ruscica, M.; Tokgözoğlu, L.; Corsini, A.; Sirtori, C.R. PCSK9 inhibition and inflammation: A narrative review. *Atherosclerosis* **2019**, *288*, 146–155. [CrossRef] [PubMed]
164. Cao, Y.-X.; Li, S.; Liu, H.-H.; Li, J.-J. Impact of PCSK9 monoclonal antibodies on circulating hs-CRP levels: A systematic review and meta-analysis of randomised controlled trials. *BMJ Open* **2018**, *8*, e022348. [CrossRef]
165. Baruch, A.; Mosesova, S.; Davis, J.D.; Budha, N.; Vilimovskij, A.; Kahn, R.; Peng, K.; Cowan, K.J.; Harris, L.P.; Gelzleichter, T.; et al. Effects of RG7652, a Monoclonal Antibody Against PCSK9, on LDL-C, LDL-C Subfractions, and Inflammatory Biomarkers in Patients at High Risk of or with Established Coronary Heart Disease (from the Phase 2 EQUATOR Study). *Am. J. Cardiol.* **2017**, *119*, 1576–1583. [CrossRef]
166. Ridker, P.M.; Revkin, J.; Amarenco, P.; Brunell, R.; Curto, M.; Civeira, F.; Flather, M.; Glynn, R.J.; Gregoire, J.; Jukema, J.W.; et al. Cardiovascular Efficacy and Safety of Bococizumab in High-Risk Patients. *N. Engl. J. Med.* **2017**, *376*, 1527–1539. [CrossRef] [PubMed]
167. Marfella, R.; Prattichizzo, F.; Sardu, C.; Paolisso, P.; D'ONofrio, N.; Scisciola, L.; La Grotta, R.; Frigé, C.; Ferraraccio, F.; Panarese, I.; et al. Evidence of an anti-inflammatory effect of PCSK9 inhibitors within the human atherosclerotic plaque. *Atherosclerosis* **2023**, *378*, 117180. [CrossRef] [PubMed]
168. Sun, C.; Zheng, W.; Liang, L.; Liu, Z.; Sun, W.; Tang, R. Ezetimibe Improves Rosuvastatin Effects on Inflammation and Vascular Endothelial Function in Acute Coronary Syndrome Patients Undergoing PCI. *J. Interv. Cardiol.* **2021**, *2021*, 2995602. [CrossRef]
169. Yoshikawa, M.; Honda, A.; Arashi, H.; Shibahashi, E.; Otsuki, H.; Kawada-Watanabe, E.; Ogawa, H.; Yamaguchi, J.; Hagiwara, N. Addition of Ezetimibe to Intensive Lipid-Lowering Therapy Is Associated with a Lower Incidence of Heart Failure in Patients with Acute Coronary Syndrome. *Circ. J.* **2024**, *88*, 1819–1824. [CrossRef]
170. Correia, L.C.L. Ezetimibe: Clinical and Scientific Meaning of the IMPROVE-IT Study. *Arq. Bras. Cardiol.* **2016**, *106*, 247–249. [CrossRef]
171. Kastelein, J.J.; Akdim, F.; Stroes, E.S.; Zwinderman, A.H.; Bots, M.L.; Stalenhoef, A.F.; Visseren, F.L.; Sijbrands, E.J.; Trip, M.D.; Stein, E.A.; et al. Simvastatin with or without Ezetimibe in Familial Hypercholesterolemia. *N. Engl. J. Med.* **2008**, *358*, 1431–1443. [CrossRef]
172. Takahashi, M. Role of NLRP3 Inflammasome in Cardiac Inflammation and Remodeling after Myocardial Infarction. *Biol. Pharm. Bull.* **2019**, *42*, 518–523. [CrossRef] [PubMed]
173. Mo, D.-G.; Wang, L.; Han, Q.-F.; Yu, K.; Liu, J.-H.; Yao, H.-C. NLRP3 Inflammasome May Be a Biomarker for Risk Stratification in Patients with Acute Coronary Syndrome. *J. Inflamm. Res.* **2022**, *15*, 6595–6605. [CrossRef] [PubMed]
174. Tong, Y.; Wang, Z.; Cai, L.; Lin, L.; Liu, J.; Cheng, J. NLRP3 Inflammasome and Its Central Role in the Cardiovascular Diseases. *Oxid. Med. Cell. Longev.* **2020**, *2020*, 4293206. [CrossRef]

175. Gao, R.; Shi, H.; Chang, S.; Gao, Y.; Li, X.; Lv, C.; Yang, H.; Xiang, H.; Yang, J.; Xu, L.; et al. The selective NLRP3-inflammasome inhibitor MCC950 reduces myocardial fibrosis and improves cardiac remodeling in a mouse model of myocardial infarction. *Int. Immunopharmacol.* **2019**, *74*, 105575. [CrossRef]
176. Ismael, S.; Zhao, L.; Nasoohi, S.; Ishrat, T. Inhibition of the NLRP3-inflammasome as a potential approach for neuroprotection after stroke. *Sci. Rep.* **2018**, *8*, 5971. [CrossRef] [PubMed]
177. Marchetti, C.; Swartzwelter, B.; Gamboni, F.; Neff, C.P.; Richter, K.; Azam, T.; Carta, S.; Tengesdal, I.; Nemkov, T.; D'Alessandro, A.; et al. OLT1177, a β-sulfonyl nitrile compound, safe in humans, inhibits the NLRP3 inflammasome and reverses the metabolic cost of inflammation. *Proc. Natl. Acad. Sci. USA* **2018**, *115*, E1530–E1539. [CrossRef]
178. Toldo, S.; Mauro, A.G.; Cutter, Z.; Van Tassell, B.W.; Mezzaroma, E.; Del Buono, M.G.; Prestamburgo, A.; Potere, N.; Abbate, A. The NLRP3 Inflammasome Inhibitor, OLT1177 (Dapansutrile), Reduces Infarct Size and Preserves Contractile Function After Ischemia Reperfusion Injury in the Mouse. *J. Cardiovasc. Pharmacol.* **2019**, *73*, 215–222. [CrossRef]
179. Sánchez-Fernández, A.; Skouras, D.B.; Dinarello, C.A.; López-Vales, R. OLT1177 (Dapansutrile), a Selective NLRP3 Inflammasome Inhibitor, Ameliorates Experimental Autoimmune Encephalomyelitis Pathogenesis. *Front. Immunol.* **2019**, *10*, 2578. [CrossRef]
180. Buckley, L.F.; Libby, P. Colchicine's Role in Cardiovascular Disease Management. *Arter. Thromb. Vasc. Biol.* **2024**, *44*, 1031–1041. [CrossRef]
181. Tong, D.C.; Quinn, S.; Nasis, A.; Hiew, C.; Roberts-Thomson, P.; Adams, H.; Sriamareswaran, R.; Htun, N.M.; Wilson, W.; Stub, D.; et al. Colchicine in Patients with Acute Coronary Syn-drome. *Circulation* **2020**, *142*, 1890–1900. [CrossRef]
182. Tardif, J.-C.; Kouz, S.; Waters, D.D.; Bertrand, O.F.; Diaz, R.; Maggioni, A.P.; Pinto, F.J.; Ibrahim, R.; Gamra, H.; Kiwan, G.S.; et al. Efficacy and Safety of Low-Dose Colchicine after Myocardial Infarction. *N. Engl. J. Med.* **2019**, *381*, 2497–2505. [CrossRef]
183. Banach, M.; Penson, P.E. Colchicine and Cardiovascular Outcomes: A Critical Appraisal of Recent Studies. *Curr. Atheroscler. Rep.* **2021**, *23*, 32. [CrossRef]
184. Ma, Z.; Chen, J.; Jin, K.; Chen, X. Colchicine and coronary heart disease risks: A meta-analysis of randomized controlled clinical trials. *Front. Cardiovasc. Med.* **2022**, *9*, 947959. [CrossRef]
185. Tong, D.C.; Bloom, J.E.; Quinn, S.; Nasis, A.; Hiew, C.; Roberts-Thomson, P.; Adams, H.; Sriamareswaran, R.; Htun, N.M.; Wilson, W.; et al. Colchicine in Patients with Acute Coronary Syndrome: Two-Year Follow-Up of the Australian COPS Randomized Clinical Trial. *Circulation* **2021**, *144*, 1584–1586. [CrossRef]
186. Bouabdallaoui, N.; Tardif, J.-C.; Waters, D.D.; Pinto, F.J.; Maggioni, A.P.; Diaz, R.; Berry, C.; Koenig, W.; Lopez-Sendon, J.; Gamra, H.; et al. Time-to-treatment initiation of colchicine and cardiovascular outcomes after myocardial infarction in the Colchicine Cardiovascular Outcomes Trial (COLCOT). *Eur. Heart J.* **2020**, *41*, 4092–4099. [CrossRef]
187. Jolly, S.S.; d'Entremont, M.A.; Lee, S.F.; Mian, R.; Tyrwhitt, J.; Kedev, S.; Montalescot, G.; Cornel, J.H.; Stanković, G.; Moreno, R.; et al. Colchicine in Acute Myocardial Infarction. *N. Engl. J. Med.* **2025**, *392*, 633–642. [CrossRef] [PubMed]
188. Tardif, J.-C.; Kouz, S. Efficacy and safety of colchicine and spironolactone after myocardial infarction: The CLEAR-SYNERGY trial in perspective. *Eur. Heart J. Acute Cardiovasc. Care* **2024**, *13*, 843–844. [CrossRef]
189. Laudani, C.; Abbate, A.; Angiolillo, D.J.; Galli, M. CLEAR results, cloudy impact: Colchicine's neutral role in ST-segment elevation myocardial infarction. *Eur. Heart J.-Cardiovasc. Pharmacother.* **2025**, *11*, 215–217. [CrossRef] [PubMed]
190. Thompson, P.L.; Nidorf, S.M. Anti-inflammatory therapy with canakinumab for atherosclerotic disease: Lessons from the CANTOS trial. *J. Thorac. Dis.* **2018**, *10*, 695–698. [CrossRef] [PubMed]
191. Baylis, R.A.; Gomez, D.; Mallat, Z.; Pasterkamp, G.; Owens, G.K. The CANTOS Trial. *Arter. Thromb. Vasc. Biol.* **2017**, *37*, e174–e177. [CrossRef] [PubMed]
192. Hassan, M. CANTOS: A breakthrough that proves the inflammatory hypothesis of atherosclerosis. *Glob. Cardiol. Sci. Pract.* **2018**, *2018*, 2. [CrossRef]
193. Abbate, A.; Van Tassell, B.W.; Biondi-Zoccai, G.; Kontos, M.C.; Grizzard, J.D.; Spillman, D.W.; Oddi, C.; Roberts, C.S.; Melchior, R.D.; Mueller, G.H.; et al. Effects of Interleukin-1 Blockade with Anakinra on Adverse Cardiac Remodeling and Heart Failure After Acute Myocardial Infarction [from the Virginia Commonwealth University-Anakinra Remodeling Trial (2) (VCU-ART2) Pilot Study]. *Am. J. Cardiol.* **2013**, *111*, 1394–1400. [CrossRef]
194. Sriranjan, R.; Zhao, T.X.; Tarkin, J.; Hubsch, A.; Helmy, J.; Vamvaka, E.; Jalaludeen, N.; Bond, S.; Hoole, S.P.; Knott, P.; et al. Low-dose interleukin 2 for the reduction of vascular inflammation in acute coronary syndromes (IVORY): Protocol and study rationale for a randomised, double-blind, placebo-controlled, phase II clinical trial. *BMJ Open* **2022**, *12*, e062602. [CrossRef]
195. Ashour, D.; Ramos, G. Insights from the LILACS trial on translational T cell regulation in cardiology. *Nat. Cardiovasc. Res.* **2025**, *4*, 652–654. [CrossRef]
196. Su, J.-H.; Luo, M.-Y.; Liang, N.; Gong, S.-X.; Chen, W.; Huang, W.-Q.; Tian, Y.; Wang, A.-P. Interleukin-6: A Novel Target for Cardio-Cerebrovascular Diseases. *Front. Pharmacol.* **2021**, *12*, 745061. [CrossRef]
197. Dimitroglou, Y.; Aggeli, C.; Theofilis, P.; Tsioufis, P.; Oikonomou, E.; Chasikidis, C.; Tsioufis, K.; Tousoulis, D. Novel Anti-Inflammatory Therapies in Coronary Artery Disease and Acute Coronary Syndromes. *Life* **2023**, *13*, 1669. [CrossRef]
198. Parums, D.V. Editorial: Tocilizumab, a Humanized Therapeutic IL-6 Receptor (IL-6R) Monoclonal Antibody, and Future Combination Therapies for Severe COVID-19. *Med. Sci. Monit.* **2021**, *27*, e933973-1–e933973-3. [CrossRef] [PubMed]

199. Broch, K.; Anstensrud, A.K.; Woxholt, S.; Sharma, K.; Tøllefsen, I.M.; Bendz, B.; Aakhus, S.; Ueland, T.; Amundsen, B.H.; Damås, J.K.; et al. Randomized Trial of Interleukin-6 Receptor Inhibition in Patients with Acute ST-Segment Elevation Myocardial Infarction. *J. Am. Coll. Cardiol.* **2021**, *77*, 1845–1855. [CrossRef] [PubMed]
200. Elrosasy, A.; Sabbagh, D.; Assaf, M.; Tarakhan, H.; Afyouni, A.; Elgendy, M.O.; Abdelaty, L.N.; Omar, R.H.; Zabady, A.H. Efficacy and safety of ziltivekimab in patients with chronic kidney disease susceptible to inflammatory diseases: A systematic review and meta-analysis of randomized controlled trials. *Future J. Pharm. Sci.* **2024**, *10*, 168. [CrossRef]
201. Ridker, P.M.; Devalaraja, M.; Baeres, F.M.M.; Engelmann, M.D.M.; Hovingh, G.K.; Ivkovic, M.; Lo, L.; Kling, D.; Pergola, P.; Raj, D.; et al. IL-6 inhibition with ziltivekimab in patients at high atherosclerotic risk (RESCUE): A double-blind, randomised, placebo-controlled, phase 2 trial. *Lancet* **2021**, *397*, 2060–2069. [CrossRef] [PubMed]
202. Ridker, P.M. From RESCUE to ZEUS: Will interleukin-6 inhibition with ziltivekimab prove effective for cardiovascular event reduction? *Cardiovasc. Res.* **2021**, *117*, e138–e140. [CrossRef]
203. Perkovic, V.; Tuttle, K.; Sattar, N.; Lincoff, A.M.; Navar, A.M.; Marx, N.; Hvelplund, A.; Baeres, F.M.; Engelmann, M.D.; Hovingh, G.K.; et al. WCN25-888 Design of the Zeus Trial: Interleukin 6 Inhibition with Ziltivekimab for Cardiovascular Protection in Chronic Kidney Disease. *Kidney Int. Rep.* **2025**, *10*, S767–S768. [CrossRef]
204. Petrie, M.; Borlaug, B.; Buchholtz, K.; Ducharme, A.; Hvelplund, A.; Ping, C.L.S.; Mendieta, G.; Hardt-Lindberg, S.Ø.; Voors, A.A.; Ridker, P.M. HERMES: Effects Of Ziltivekimab Versus Placebo On Morbidity And Mortality In Patients with Heart Failure with Mildly Reduced Or Preserved Ejection Fraction And Systemic Inflammation. *J. Card. Fail.* **2024**, *30*, 126. [CrossRef]
205. Zhang, J.; Xu, D.-L.; Liu, X.-B.; Bi, S.-J.; Zhao, T.; Sui, S.-J.; Ji, X.-P.; Lu, Q.-H. Darapladib, a Lipoprotein-Associated Phospholipase A2 Inhibitor, Reduces Rho Kinase Activity in Atherosclerosis. *Yonsei Med. J.* **2016**, *57*, 321–327. [CrossRef] [PubMed]
206. O'Donoghue, M.L.; Braunwald, E.; White, H.D.; Steen, D.P.; Lukas, M.A.; Tarka, E.; Steg, P.G.; Hochman, J.S.; Bode, C.; Maggioni, A.P.; et al. Effect of Darapladib on Major Coronary Events After an Acute Coronary Syndrome. *JAMA* **2014**, *312*, 1006–1015. [CrossRef]
207. Mangoni, A.A.; Sotgia, S.; Zinellu, A.; Carru, C.; Pintus, G.; Damiani, G.; Erre, G.L.; Tommasi, S. Methotrexate and cardiovascular prevention: An appraisal of the current evidence. *Ther. Adv. Cardiovasc. Dis.* **2023**, *17*, 17539447231215213. [CrossRef]
208. Marks, J.L.; Edwards, C.J. Protective effect of methotrexate in patients with rheumatoid arthritis and cardiovascular comorbidity. *Ther. Adv. Musculoskelet. Dis.* **2012**, *4*, 149–157. [CrossRef]
209. Ridker, P.M.; Everett, B.M.; Pradhan, A.; MacFadyen, J.G.; Solomon, D.H.; Zaharris, E.; Mam, V.; Hasan, A.; Rosenberg, Y.; Iturriaga, E.; et al. Low-Dose Methotrexate for the Prevention of Atherosclerotic Events. *N. Engl. J. Med.* **2019**, *380*, 752–762. [CrossRef]
210. Moreira, D.M.; Lueneberg, M.E.; da Silva, R.L.; Fattah, T.; Gottschall, C.A.M. MethotrexaTE THerapy in ST-Segment Elevation MYocardial InfarctionS. *J. Cardiovasc. Pharmacol. Ther.* **2017**, *22*, 538–545. [CrossRef]
211. Farina, C.J.; Davidson, M.H.; Shah, P.K.; Stark, C.; Lu, W.; Shirodaria, C.; Wright, T.; A Antoniades, C.; Nilsson, J.; Mehta, N.N. Inhibition of oxidized low-density lipoprotein with orticumab inhibits coronary inflammation and reduces residual inflammatory risk in psoriasis: A pilot randomized, double-blind placebo-controlled trial. *Cardiovasc. Res.* **2024**, *120*, 678–680. [CrossRef]
212. Posey, A.; June, C.; Schwab, R. Chimeric Antigen Receptor T Regulatory Cells for the Treatment of Atherosclerosis. U.S. patent 12,473,342, 18 November 2025.
213. Schwab, R.D.; Degaramo, D.; Hong, S.J.; Bi, X.; Faruqi, A.; Aguilar, W.; Brookens, S.K.; Keane, J.T.; Liu, F.; Musunuru, K.; et al. OxLDL-targeted Chimeric Antigen Receptor T Regulatory Cells Reduce Atherosclerotic Plaque Development. *Circulation* **2025**, *153*. [CrossRef] [PubMed]
214. Du, M.; Yang, W.; Schmull, S.; Gu, J.; Xue, S. Inhibition of peptidyl arginine deiminase-4 protects against myocardial infarction induced cardiac dysfunction. *Int. Immunopharmacol.* **2020**, *78*, 106055. [CrossRef]
215. Luo, Y.; Arita, K.; Bhatia, M.; Knuckley, B.; Lee, Y.-H.; Stallcup, M.R.; Sato, M.; Thompson, P.R. Inhibitors and Inactivators of Protein Arginine Deiminase 4: Functional and Structural Characterization. *Biochemistry* **2006**, *45*, 11727–11736. [CrossRef]
216. Zheng, Z.; Zong, Y.; Ma, Y.; Tian, Y.; Pang, Y.; Zhang, C.; Gao, J. Glucagon-like peptide-1 receptor: Mechanisms and advances in therapy. *Signal Transduct. Target. Ther.* **2024**, *9*, 234. [CrossRef] [PubMed]
217. Skrobucha, A.; Pindlowski, P.; Krajewska, N.; Grabowski, M.; Jonik, S. Anti-inflammatory effects of glucagon-like peptide-1 (GLP-1) in coronary artery disease: A comprehensive review. *Front. Cardiovasc. Med.* **2024**, *11*, 1446468. [CrossRef]
218. Alharbi, S.H. Anti-inflammatory role of glucagon-like peptide 1 receptor agonists and its clinical implications. *Ther. Adv. Endocrinol. Metab.* **2024**, *15*, 20420188231222367. [CrossRef] [PubMed]
219. Yaribeygi, H.; Maleki, M.; Jamialahmadi, T.; Sahebkar, A. Anti-inflammatory benefits of semaglutide: State of the art. *J. Clin. Transl. Endocrinol.* **2024**, *36*, 100340. [CrossRef]
220. Lincoff, A.M.; Brown-Frandsen, K.; Colhoun, H.M.; Deanfield, J.; Emerson, S.S.; Esbjerg, S.; Hardt-Lindberg, S.; Hovingh, G.K.; Kahn, S.E.; Kushner, R.F.; et al. Semaglutide and Cardiovascular Outcomes in Obesity without Diabetes. *N. Engl. J. Med.* **2023**, *389*, 2221–2232. [CrossRef]

221. Kolkailah, A.A.; Lingvay, I.; Dobrecky-Mery, I.; Aharonovich, A.; David, J.P.; Holse, C.; Rasmussen, S.; McGuire, D.K. Effects of once-weekly subcutaneous semaglutide on coronary artery disease outcomes in patients with type 2 diabetes with or at high risk for cardiovascular disease: Insights from the SUSTAIN-6 trial. *Diabetes Obes. Metab.* **2023**, *25*, 1117–1120. [CrossRef]
222. Zeng, H.; Hu, J.; Zhuo, Y.; Wang, M.; Gao, L.; Tang, Z.; Zhang, J.; Yin, P.; Gu, J.; Wang, C. Effect of GLP-1RA on coronary progression and cardiovascular outcomes in type 2 diabetic patients after PCI: A prospective cohort study. *Sci. Rep.* **2025**, *15*, 31824. [CrossRef]
223. Karakasis, P.; Patoulias, D.; Kassimis, G.; Koufakis, T.; Klisic, A.; Doumas, M.; Fragakis, N.; Rizzo, M. Therapeutic Potential of Sodium-glucose Co-transporter-2 Inhibitors and Glucagon-like Peptide-1 Receptor Agonists for Patients with Acute Coronary Syndrome: A Review of Clinical Evidence. *Curr. Pharm. Des.* **2024**, *30*, 2109–2119. [CrossRef] [PubMed]
224. Sabouret, P.; Ecarnot, F.; De Rosa, S.; Ray, K.K. What about glucagon-like peptide-1 receptor agonist for all? Recent data and perspectives. *Eur. Heart J.* **2023**, *44*, 4499–4502. [CrossRef] [PubMed]
225. Rao, S.V.; O'Donoghue, M.L.; Ruel, M.; Rab, T.; Tamis-Holland, J.E.; Alexander, J.H.; Baber, U.; Baker, H.; Cohen, M.G.; Cruz-Ruiz, M.; et al. 2025 ACC/AHA/ACEP/NAEMSP/SCAI Guideline for the Management of Patients with Acute Coronary Syndromes: A Report of the American College of Cardiology/American Heart Association Joint Committee on Clinical Practice Guidelines. *Circulation* **2025**, *85*, 2135–2237.
226. Gupta, N.; Zayyad, Z.; Bhattaram, R.; Tiu, D.; Dau, J.; Guburxani, V.; Kalzuna, S.D.; Shroff, A.R. Beyond Blood Sugar: A Scoping Review of GLP-1 Receptor Agonists in Cardiovascular Care. *Cardiol. Ther.* **2025**, *14*, 351–366. [CrossRef]
227. Torzewski, J.; Brunner, P.; Ries, W.; Garlichs, C.D.; Kayser, S.; Heigl, F.; Sheriff, A. Targeting C-Reactive Protein by Selective Apheresis in Humans: Pros and Cons. *J. Clin. Med.* **2022**, *11*, 1771. [CrossRef]
228. Torzewski, J.; Mattecka, S.; Ries, W.; Garlichs, C.D.; Heigl, F.; Fiedler, J.; Sheriff, A. Case report: C-reactive protein apheresis in cardiogenic shock: Case series from the C-reactive protein apheresis in acute myocardial infarction-registry. *Front. Drug Discov.* **2023**, *3*, 1286710. [CrossRef]
229. Ries, W.; Torzewski, J.; Heigl, F.; Pfluecke, C.; Kelle, S.; Darius, H.; Ince, H.; Mitzner, S.; Nordbeck, P.; Butter, C.; et al. C-Reactive Protein Apheresis as Anti-inflammatory Therapy in Acute Myocardial Infarction: Results of the CAMI-1 Study. *Front. Cardiovasc. Med.* **2021**, *8*, 591714. [CrossRef]
230. Przytuła, N.; Podolec, J.; Przewłocki, T.; Podolec, P.; Kabłak-Ziembicka, A. Inflammasomes as Potential Therapeutic Targets to Prevent Chronic Active Viral Myocarditis—Translating Basic Science into Clinical Practice. *Int. J. Mol. Sci.* **2025**, *26*, 11003. [CrossRef]
231. Cabral, J.E.; Wu, A.; Zhou, H.; Pham, M.A.; Lin, S.; McNulty, R. Targeting the NLRP3 inflammasome for inflammatory disease therapy. *Trends Pharmacol. Sci.* **2025**, *46*, 503–519. [CrossRef]
232. Ray, K.K.; Nicholls, S.J.; Li, N.; Louie, M.J.; Brennan, D.; Lincoff, A.M.; ENissen, S. Efficacy and safety of bempedoic acid among patients with and without diabetes: Prespecified analysis of the CLEAR Outcomes randomised trial. *Lancet Diabetes Endocrinol.* **2024**, *12*, 19–28. [CrossRef] [PubMed]
233. Bawamia, B.; Spray, L.; Wangsaputra, V.K.; Bennaceur, K.; Vahabi, S.; Stellos, K.; Kharatikoopaei, E.; Ogundimu, E.; Gale, C.P.; Keavney, B.; et al. Activation of telomerase by TA-65 enhances immunity and reduces inflammation post myocardial infarction. *Geroscience* **2023**, *45*, 2689–2705. [CrossRef] [PubMed]
234. Schulz-Menger, J.; Collini, V.; Gröschel, J.; Adler, Y.; Brucato, A.; Christian, V.; Ferreira, V.M.; Gandjbakhch, E.; Heidecker, B.; Kerneis, M.; et al. 2025 ESC Guidelines for the management of myocarditis and pericarditis. *Eur. Heart J.* **2025**, *46*, 3952–4041. [CrossRef] [PubMed]

Disclaimer/Publisher's Note: The statements, opinions and data contained in all publications are solely those of the individual author(s) and contributor(s) and not of MDPI and/or the editor(s). MDPI and/or the editor(s) disclaim responsibility for any injury to people or property resulting from any ideas, methods, instructions or products referred to in the content.

cells

MDPI

Review

Molecular Mechanisms of Atrial Fibrillation Recurrence After Successful Catheter Ablation

Muhammad Sanusi [1], Roopeessh Vempati [1], Dinakaran Umashankar [1], Suha Tarannum [2], Yash Varma [3], Fawaz Mohammed [3], Maneeth Mylavarapu [4], Faiza Zakaria [1], Rajiv Nair [3], Yeruva Madhu Reddy [5] and Christian Toquica Gahona [3,*]

[1] Department of Internal Medicine, Trinity Health Oakland/Wayne State University, Pontiac, MI 48341, USA; muhammad.sanusi@trinity-health.org (M.S.); roopeessh.vempati@gmail.com (R.V.)
[2] Department of Family Medicine, Western Michigan Homer Stryker M.D. School of Medicine, Kalamazoo, MI 49008, USA
[3] Department of Cardiology, Trinity Health Oakland/Wayne State University, Pontiac, MI 48341, USA
[4] Department of Cardiology, Endeavor Health Cardiovascular Institute, Glenview, IL 60026, USA; dr.maneeth.mylavarapu@gmail.com
[5] Electrophysiology Division, Department of Cardiology, Kansas University Medical Center, Kansas City, KS 66160, USA
* Correspondence: christian.toquicagahona@trinity-health.org or christian.toquica@trinity-health.org

Abstract

Atrial fibrillation (AF) is the most common sustained cardiac arrhythmia globally, linked to significant cardiovascular morbidity and mortality. Catheter ablation has emerged as a primary therapeutic approach, yet substantial recurrence rates limit its long-term efficacy. This review critically examines the molecular mechanisms underlying AF recurrence post-ablation, synthesizing recent findings from current literature. Key molecular pathways identified include structural remodeling mediated by fibrosis involving transforming growth factor-beta 1 (TGF-β1) and matrix metalloproteinases (MMPs), ion-channel dysregulation, inflammatory pathways, autonomic nervous system imbalance, and genetic and epigenetic alterations. Despite considerable advances, critical gaps persist due to small, heterogeneous studies and insufficient long-term follow-up. Comprehensive mechanistic research integrating genomics, proteomics, and advanced imaging is urgently needed to better characterize these pathways. Future studies must validate biomarkers such as TGF-β1, MMPs, connexins, and novel markers like GDF-15 and relaxin. Clinical translation of these molecular insights through precision diagnostics and personalized interventions holds great promise to enhance patient selection, optimize ablation strategies, reduce recurrence, and ultimately improve clinical outcomes in AF management.

Keywords: atrial fibrillation recurrence; catheter ablation; left atrial remodeling; fibrosis; connexins and gap junctions; ion-channel remodeling; inflammation and oxidative stress; autonomic nervous system remodeling; genetic susceptibility; MicroRNAs

1. Introduction

Atrial fibrillation (AF) is the most prevalent sustained cardiac arrhythmia, impacting more than 33 million people globally [1]. Its occurrence rises significantly with age, and as population demographics shift, the prevalence of AF is projected to more than double within the next 40 years [2]. AF not only doubles the risk of premature death but is also linked to serious cardiovascular complications, including heart failure, stroke, and myocardial infarction [3–6].

Catheter ablation is a tailored intervention that disrupts the underlying mechanisms driving AF initiation and persistence by eliminating triggers, altering the electroanatomical substrate, and modulating the autonomic nervous system [7]. In the past two decades, catheter ablation for atrial fibrillation (AF) has evolved from a last-resort treatment for patients with severe, drug-resistant symptoms to a widely accepted first-line therapy for individuals with varying types and severities of AF [8–10]. Numerous studies have established that catheter ablation is more effective than antiarrhythmic medications for restoring and maintaining normal sinus rhythm [11,12]. Reflecting this evidence, the latest guidelines from the European Society of Cardiology and the American Heart Association/American College of Cardiology/Heart Rhythm Society advocate for catheter ablation in patients with symptomatic atrial fibrillation (AF) [11,12].

While catheter ablation has emerged as a highly effective treatment for atrial fibrillation (AF), its long-term effectiveness is often hindered by considerable recurrence rates [13,14]. This review aims to shed light on the molecular mechanisms underlying AF recurrence after initially successful catheter ablation (Figure 1).

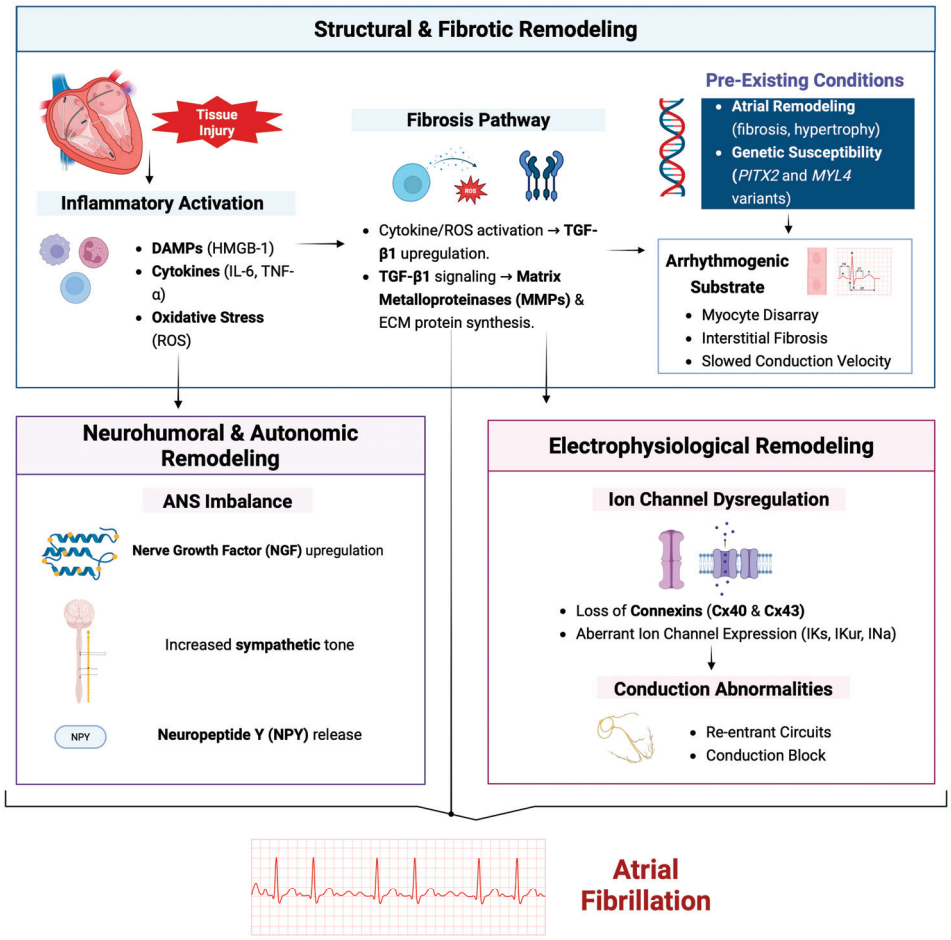


Figure 1. Mechanisms of atrial fibrillation: structural, neurohumoral, and electrophysiological remodeling. Created in BioRender. Mylavarapu, M. (2025) https://BioRender.com/5nc7afi (accessed on 20 December 2025).

2. Structural Remodeling

2.1. Fibrosis and Extracellular Matrix (ECM) Alterations

Atrial fibrosis is associated with both the electrophysiological and structural remodeling of atrial tissue and plays a significant role in the development of atrial fibrillation (AF) [15]. While electrical remodeling can be fully restored several weeks after recovery

to sinus rhythm, structural remodeling rarely returns to normal, making it more likely for AF to recur. These findings suggest that atrial structural remodeling may play a more critical role in the recurrence and persistence of AF compared to electrical remodeling. Transforming growth factor-β1 (TGF-β1) is a key cytokine that initiates and promotes the synthesis and metabolism of interstitial collagen in the atria. During fibrosis, TGF-β1 can induce the overexpression of extracellular matrix (ECM) proteins, leading to significant changes in cardiac structure and tissue [16,17].

Atrial remodeling is a key characteristic of atrial fibrillation (AF) that creates an irregular environment for electrical conduction, leading to ectopic or re-entrant activity. Transforming growth factor-beta 1 (TGF-β1) plays a crucial role in the atrial remodeling process, including tissue repair and the formation of fibrosis, and is considered a significant factor in causing atrial fibrosis. Studies of atrial specimens from patients undergoing cardiac surgery have shown that TGF-β1 is selectively involved in the development of atrial fibrosis. This occurs through its receptors: TGF-β1 receptor 1 and receptor 2 along with the classical SMAD signalling pathway [18]. Furthermore, the differences observed between atrial and ventricular fibrosis may be attributed to variations in the binding ability of TGF-β1 to its receptors or differences in the phosphorylation levels. Overall, these findings highlight that atrial fibrosis is an important contributor to the onset and maintenance of AF [19].

2.2. Role of Transforming Growth Factor-Beta (TGF-β) and Matrix Metalloproteinases (MMPs)

TGF-β1 has been postulated to be a cause of AF by inducing and maintaining AF through the initiation of atrial fibrosis [20]. Collagen, TGF-β1 mRNA, and plasma TGF-β1 concentrations gradually increase in subjects' sinus rhythm, for both paroxysmal AF and persistent AF, suggesting that plasma TGF-β1 concentrations positively correlate with the degree of atrial fibrosis [21]. Studies in patients with nonvalvular AF have shown that high plasma TGF-β1 concentrations are indicative of low left atrial (LA) endocardial voltage [22]. For example, a study measuring the degree of fibrosis in the LA tissue of patients with persistent AF who underwent open heart surgery for valvular heart disease found that plasma TGF-β1 concentrations correlated with the degree of fibrosis [23]. Moreover, preoperative plasma TGF-β1 concentrations were found to predict the persistence of AF 1 year after surgical maze procedures. Taken together, these findings suggest that TGF-β1 is involved in the mechanisms of atrial fibrosis and AF pathogenesis and that plasma TGF-β1 concentrations may be a surrogate marker of atrial fibrosis. However, plasma TGF-β1 concentrations are also affected by noncardiogenic factors such as the kidneys, lungs, and liver. We therefore measured serum TGF-β1 concentration as an indicator of the level of atrial fibrosis in patients with AF. We found that serum TGF-β1 concentration was significantly lower in patients with AF without recurrence than in those with recurrence, suggesting that serum TGF-β1 concentration correlates with AF recurrence [19].

A group of enzymes capable of degrading almost all ECM proteins, matrix metalloproteinases (MMPs), contribute to both normal and pathological tissue remodeling [24–29]. The balance between activated MMPs and tissue inhibitors of metalloproteinases (TIMPs) controls the extent of myocardial ECM remodeling [30,31], including the atrial tissue. However, recent studies have demonstrated the existence of alternative MMP inhibitors [32–35], namely reversion-inducing cysteine-rich protein with Kazal motifs (RECK), which is thought to be an important regulator of ECM remodeling [32,36,37].

In several cohorts, higher pre-ablation TGF-β1 or MMP-9 levels predicted AF recurrence even after adjustment for left atrial diameter, AF type, and standard clinical risk factors, suggesting incremental prognostic value beyond chamber size alone [19,38,39]. However, most studies did not fully adjust for advanced imaging markers of fibrosis (e.g., LGE-MRI late enhancement or low-voltage area burden), so a substantial part of the

association is likely mediated by the degree of underlying atrial myopathy rather than being completely independent. Conceptually, the TGF-β1/MMP axis promotes extracellular matrix accumulation, collagen cross-linking, and myocyte–fibroblast uncoupling. These changes create low-voltage areas and regions of slow, heterogeneous conduction that facilitate re-entry. In this framework, elevated TGF-β1 and MMP-9 levels probably identify more diffuse atrial disease in which both pulmonary-vein reconnection and extra-PV substrate-related circuits are more likely to occur, rather than pointing to a single dominant mechanism of recurrence. It is therefore more accurate to view these biomarkers as integrators of global atrial injury and fibrosis, which interact with procedural factors (durability of PVI, extent of substrate modification) to determine long-term outcome.

Progression of atrial structural remodeling results in the need for more invasive ablation strategies, i.e., complex fractionated electrogram (CFAE) ablation or intra-atrial linear ablation. Despite such aggressive treatment, the post-ablation recurrence rate is higher in these cases than in cases with a less remodeled atrium treated with PVI alone [40,41].

In a study by Okumura et al., Baseline serum MMP-2, carboxylterminal telopeptide of collagen type I (ICTP), and Brain natriuretic peptide (BNP) levels were significantly higher in patients who experienced AF recurrence than in those who did not (860.3 ± 120.8 ng/mL vs. 687.0 ± 122.5 ng/mL; 3.2 ± 1.1 ng/mL vs. 2.7 ± 0.6 ng/mL; 105.0 [38.5–133.0] pg/mL vs. 38.9 [20.8–72.9] pg/mL, $p < 0.05$ for all) [40]. Myocardial collagen turnover biomarker levels are associated with post-ablation AF recurrence. A 2-month post-ablation elevation in MMP-2 levels suggests that wound healing persists for that long after ablation. The levels of systemic and intracardiac biomarkers of both inflammation and collagen turnover were similar, which implies that these serum biomarkers may originate in the systemic circulation rather than in the heart [42].

2.3. Cellular Hypertrophy and Myocyte Disarray

Myocyte hypertrophy and cellular disarray, as seen in patients with hypertrophic cardiomyopathy (HCM), can also increase the risk of recurrence of atrial fibrillation. Atrial myocyte hypertrophy increases LA wall thickness, thus reducing the likelihood of creating durable transmural lesions. HCM is commonly associated with LA dilatation, remodeling, and diffuse interstitial fibrosis, thus increasing the risk of elicitation of triggering from extra-pulmonary vein foci [43]. Additionally, a multicenter study found that most patients require re-do procedures, that efficacy was obtained with the concomitant administration of anti-arrhythmic drugs (AADs) in most patients, and that efficacy was time-dependent [44]. The probability of post-ablation recurrence of atrial arrhythmias was found to be two-fold higher in patients with HCM compared with that in controls, after either single or multiple procedures. AADs were found to be paramount in maintaining sinus rhythm, as shown by a five-fold higher probability of AAD use after ablation in patients with HCM. Nonetheless, the combination of catheter ablation with AADs was associated with a success rate as high as 75% after a single procedure [43,45–47]. Treatment with AADs in HCM patients is less effective than in patients without HCM. Appropriate selection of specific AADs can overcome this limitation. Amiodarone and sotalol are the most frequently used AADs in this clinical setting, the former being the most effective and the latter being better tolerated. Dofetilide is also well tolerated, and recent data suggest a high efficacy during long-term follow-up [43].

2.4. Impact on Conduction Velocity and Arrhythmogenic Substrate Formation

AF substrate is, at least in part, dynamic, with rate-dependent effective refractory periods and conduction velocities. These electrophysiological factors can lead to the so-

https://doi.org/10.3390/cells15010036

called functional phenomena. The atrium, under higher rates and conduction velocities, is more prone to functional phenomena than the ventricle, leading to complex electric wavefront dynamics during AF [48]. Frontera, A et al. summarized that dual high-density mapping during sinus rhythm and after an atrial extra stimulus reveals differences in areas with conduction abnormalities, particularly represented by pivot sites and zones of slow conduction. The change in direction and velocity of the traveling wavefront, when an extra stimulus is delivered with a short coupling interval, uncovers "functional" rhythm-dependent conduction abnormalities that can predict atrial fibrillation (AF) recurrences during follow-up. Functional conduction abnormalities are found at sites with preserved voltage and are often associated with anatomical structures such as the esophagus and the sinus of Valsalva in the ascending aorta. Pulmonary vein isolation (PVI) remains the primary treatment for AF; however, this procedure does not address the entire complexity of AF pathogenesis. Success rates for PVI typically range from 50% to 70% in patients with persistent AF (PsAF), and a considerable number of patients experience recurrent AF episodes. As a result, current treatment options for these patients are still limited. This study highlighted a new methodology for characterizing the atrial substrate in patients with AF. The mapping protocol performed during sinus rhythm, combined with the application of an extra stimulus delivered from the coronary sinus, is both easily reproducible and reliable in any electrophysiology laboratory. Identifying slow conduction sites and pivot points during either sinus rhythm or paced rhythm can provide a better characterization of the substrate that sustains localized reentrant circuits [49].

While catheter ablation for paroxysmal AF yields satisfying outcomes in terms of AF recurrence, persistent AF remains associated with high recurrence rates. Therefore, patients with persistent AF may require different ablation strategies [50]. Lukito et al., in their meta-analysis, investigated and performed a diagnostic test meta-analysis on whether slow left atrial conduction velocity (LACV) in the anterior wall calculated by electroanatomic mapping predicts atrial fibrillation (AF) recurrence after catheter ablation. Seven studies involved a sample size of 1428 patients, with a mean follow-up duration of 13 months. Patients with AF recurrence have slower LACV in the anterior wall (mean difference − 0.16 m/s [−0.18, −0.15], $p < 0.001$). Slow LACV in the anterior wall, defined as LACV below 0.70–0.88 m/s, was associated with increased AF (adjusted OR 3.41 [1.55, 7.50], $p = 0.002$). Slow LACV in the anterior wall has an AUROC of 0.80 [0.76–0.83], sensitivity of 70% [52, 84], specificity of 76% [67, 83], positive likelihood ratio of 2.9 [2.3, 3.6], negative likelihood ratio of 0.39 [0.25, 0.63] for predicting AF recurrence post ablation [50]. Tissue fibrosis occurs due to various insults, leading to intercellular gap junction remodeling and abnormal distribution, which results in altered conduction and atrial strain [51,52]. Myocardial fibrosis promotes remodeling, which increases the resting membrane potential of myocytes, causing decreased conduction velocity and resulting in shortened action potential duration and refractory period. These conduction disturbances may contribute to the development of re-entrant circuits in AF. Hence, slow LACV may serve as an indicator of left atrial remodeling or fibrosis and is closely related to the development and recurrence of AF [53]. Low voltage areas and slow conduction velocities more accurately depict atrial fibrosis and interatrial conduction block, which are closely associated with conduction issues and an increased risk of AF recurrence [54]. Determining the association between slow LACV and AF recurrence may pave the way for utilizing high-density mapping systems and noninvasive cardiac studies to detect slow conduction by identifying prolonged P-wave duration or regions of potential re-entry, such as left atrial heterogeneity through late gadolinium enhancement (LGE). This may improve the prognostication of AF recurrence post-PVI [55]. High-density mapping studies show that zones of slow conduction and pivot points tend to co-localize with areas of LGE-MRI fibrosis and low-

voltage substrate in the left atrium [56,57]. A greater burden in these regions has been associated with higher recurrence rates and with inducible organized atrial tachycardias after ablation, particularly in patients with persistent AF. These observations have been reproduced across different mapping platforms and multipolar catheters, although the absolute thresholds used to define "low voltage" and "slow conduction" vary with catheter geometry, filtering, and pacing protocol. At present, left atrial conduction velocity, pivot zones, and slow-conducting areas are best considered qualitative markers of underlying atrial myopathy that can complement imaging and voltage mapping, rather than fully standardized metrics that can be applied interchangeably across all systems.

2.5. Ion-Channel Dysregulation

The mechanisms underlying AF induction and maintenance are incompletely understood, but it is generally accepted that re-entry is the major mechanism of AF maintenance. Re-entry induction requires an appropriate vulnerable substrate, as well as a trigger that initiates re-entry within the substrate. Long-term AF causes profound alterations in atrial structure (cardiomyocyte hypertrophy, glycogen accumulation, and interstitial fibrosis). These lead to inhomogeneous conduction slowing that promotes the development of anatomically fixed re-entry circuits. Atrial remodeling is clinically important as it indicates the large resistance of persistent AF to treatment [58].

2.6. Electrophysiological and Structural Determinants

Atrial fibrillation (AF) recurrence following catheter ablation (CA) is influenced by multiple electrophysiological and structural factors, including left atrial (LA) asynchrony, abnormal atrial voltage, and altered conduction patterns. Emerging evidence suggests that heterogeneity in atrial conduction and remodeling of the LA substrate contribute significantly to post-ablation arrhythmia recurrence [59].

Recent studies utilizing pulsed-wave tissue Doppler imaging (PW-TDI) have demonstrated that LA asynchrony is a key determinant of AF recurrence [60]. Two novel indices, the difference between the longest and shortest P-A0 intervals (DLS) and the standard deviation of activation times across four LA sites (SD4), have been proposed to quantify asynchrony. Notably, patients experiencing AF recurrence exhibited significantly higher DLS (43 ± 16 ms vs. 35 ± 16 ms; $p = 0.01$) and SD4 (20 ± 8 ms vs. 16 ± 7 ms; $p = 0.004$) than those without recurrence. Additionally, LA scarring, as indicated by low-voltage areas (<0.5 mV) on electroanatomical mapping, was associated with prolonged DLS (46 ± 19 ms vs. 36 ± 16 ms; $p = 0.04$) and SD4 (23 ± 9 ms vs. 16 ± 7 ms; $p = 0.009$). These findings underscore the role of conduction heterogeneity and delayed atrial activation in sustaining AF and increasing the likelihood of post-ablation recurrence. Structural remodeling of the LA further contributes to AF persistence and recurrence. Among patients undergoing electroanatomical mapping, all individuals with low-voltage areas exhibited a distinct "U-pattern" of atrial activation, characterized by conduction propagating from the inferior to anterosuperior regions. In contrast, patients with normal LA voltage demonstrated a D-pattern of activation, consistent with conduction through Bachmann's bundle. The strong association between the U-pattern, LA scarring, and AF recurrence suggests that interatrial conduction block and altered atrial excitation patterns play a pivotal role in post-ablation outcomes [60].

Multivariate analysis further supported these findings, identifying DLS (HR: 1.02, $p = 0.008$) and SD4 (HR: 1.35, $p = 0.031$) as independent predictors of AF recurrence and the presence of atrial scarring [61]. Interestingly, LA size ($p = 0.08$) and age ($p = 0.35$) were not significant predictors, highlighting the importance of functional conduction abnormalities over structural enlargement in determining ablation success [61]. These observations align

https://doi.org/10.3390/cells15010036

with prior research demonstrating that total atrial conduction time, as assessed by tissue Doppler imaging, is a reliable predictor of AF recurrence following CA.

From a clinical perspective, these findings suggest that pre-procedural assessment of LA asynchrony and conduction abnormalities could enhance risk stratification and guide ablation strategies. The presence of delayed anterior LA activation and conduction block across Bachmann's bundle may serve as markers of advanced atrial remodeling, warranting a tailored approach to ablation in these patients [60]. Although the study had limitations, including a relatively small cohort of persistent AF cases and individuals with extensive LA scarring, it provides a novel electrophysiological framework for predicting post-ablation outcomes and optimizing patient selection.

2.7. Role of Connexins and Gap Junctions

AF recurrence following CA is influenced by electrophysiological and structural remodeling of the atria [62]. One critical component of this process is the gap junctional network, which facilitates impulse propagation between cardiomyocytes. Gap junctions, composed of connexins (Cxs), play a crucial role in maintaining synchronized atrial activation. Disruptions in connexin expression, localization, and function have been linked to increased AF susceptibility, conduction heterogeneity, and reentrant activity, which may contribute to post-ablation recurrence [62]. Gap junctions in the atria primarily comprise Cx40, Cx43, and Cx45, with Cx40 being the predominant connexin in atrial tissue [63]. Remodeling of these connexins has been widely observed in AF, with Cx40 and Cx43 displaying altered expression patterns, lateralization from intercalated disks, and abnormal hemichannel activity [64,65]. Cx40 downregulation or redistribution has been strongly associated with conduction heterogeneity and AF recurrence, supporting its role in sustaining arrhythmic substrates [66]. Multifaceted mechanisms contribute to connexin remodeling and AF recurrence, including gene mutations, transcriptional dysregulation, and post-translational modifications. Several mutations in the GJA5 gene encoding Cx40 have been identified in idiopathic and familial AF cases, leading to impaired gap junction function and reduced electrical coupling [67]. Similarly, Cx43 mutations (GJA1) have been linked to conduction slowing and reentrant arrhythmias, suggesting that dysfunctional connexin interactions may create a substrate for AF persistence [68]. Beyond genetic alterations, connexin phosphorylation and trafficking defects contribute to AF-associated gap junction remodeling. Increased lateralization of Cx40 and Cx43 from intercalated disks has been documented in chronic AF, resulting in abnormal conduction and increased reentry [65,69]. These findings indicate that gap junction remodeling, rather than total connexin depletion, plays a predominant role in AF recurrence. The implications of connexin dysfunction extend to therapeutic strategies aimed at reducing AF recurrence post-ablation. Beta-blockers such as metoprolol have been shown to mitigate gap junction remodeling, restoring normal Cx43 distribution and reducing conduction heterogeneity [69]. Moreover, connexin gene therapy and pharmacological modulation of hemichannel function have been explored as potential AF interventions [70].

In summary, connexin dysregulation and gap junction remodeling play a pivotal role in AF recurrence after catheter ablation. The loss of coordinated atrial conduction due to altered Cx40 and Cx43 expression, mislocalization, and impaired electrical coupling provides an arrhythmogenic substrate that sustains AF. Targeting gap junction integrity and connexin function represents a promising approach to improving long-term outcomes in post-ablation AF patients.

https://doi.org/10.3390/cells15010036

3. Inflammatory Pathways

Inflammation plays a key role in recurrent atrial fibrillation (AF) following ablation. Mechanical and surgical injury triggers the release of inflammatory mediators, including cytokines and chemokines, leading to atrial remodeling and sustaining AF [71]. Rosenberg et al. highlight that ablation therapy increases damage-associated molecular patterns (DAMPs), inflammatory cytokines, immune cell activity, and collagen remodeling, contributing to AF recurrence. DAMPs, such as HMGB-1, mtDNA, heat shock proteins (HSPs) 27, 70, and 60, along with the NLRP3 inflammasome, activate toll-like receptors (TLRs), contributing to atrial remodeling via initiation of sterile immune responses [72].

Several studies have examined individual inflammatory mediators in AF recurrence. Cao et al. identified the TGF-β1 C-509T polymorphism as an independent predictor of AF recurrence, with elevated TGF-β1 promoting atrial fibrosis [73]. Tian et al. also linked higher serum TGF-β1 to extensive fibrosis and increased AF recurrence risk [19]. Wei et al.'s study of 150 AF patients undergoing radiofrequency catheter ablation found that elevated growth differentiation factor-15 (GDF-15) levels were associated with left atrial remodeling and higher recurrence rates [74]. Zakynthinos et al. highlighted the role of endothelial dysfunction in AF persistence, noting that higher asymmetric dimethylarginine (ADMA) levels—an inhibitor of nitric oxide synthase (NOS)—are linked to increased AF recurrence [75].

Inflammatory cytokines such as CRP, TNF-α, IL-2, and IL-6 contribute to recurrent AF by recruiting PMNs, macrophages, and fibroblasts, driving ECM remodeling. Angiotensin-II-stimulated TGF-β1 further promotes collagen deposition, leading to atrial fibrosis. Systemic inflammation thus plays a critical role in structural remodeling, fibrosis, and conduction abnormalities, sustaining AF persistence [72]. Endothelial dysfunction contributes to fibrosis and electrical remodeling, further promoting atrial substrate modifications that favor AF initiation and maintenance [75]. Most studies that evaluated inflammatory biomarkers in the ablation setting followed a common sampling pattern: blood was drawn at baseline, repeated at 24–72 h after the procedure, and in some cases at 1 week and 3 months. High baseline hs-CRP and IL-6 and larger early post-procedural rises have been associated with a greater risk of AF recurrence, particularly within the first 3–6 months after ablation [76–79]. CRP levels often peak around days 2–3 after RF ablation and then decline, whereas patients who maintain sinus rhythm tend to show a more pronounced long-term decrease in inflammatory markers. By contrast, GDF-15 and relaxin have been studied mainly as baseline risk markers. Elevated pre-ablation GDF-15 seems to reflect a higher overall cardiovascular risk burden and has shown inconsistent associations with AF incidence and recurrence [80]. Baseline serum relaxin has been more consistently linked to AF recurrence after RF ablation, although data are still limited to small cohorts [81,82]. Systematic data on serial GDF-15 and relaxin measurements over time, and how their trajectories relate to late (>12 months) recurrence, are still lacking. Differences between energy sources may influence biomarker profiles. RF ablation typically causes larger and more prolonged CRP and IL-6 elevations than cryoballoon ablation in some series, whereas robust comparative data for PFA are only now emerging from ongoing trials [83–85]. Taken together, these observations suggest that baseline inflammatory status and early post-procedural inflammatory response provide complementary information about short- and intermediate-term recurrence risk, but we still lack a validated, energy-specific biomarker algorithm to guide clinical decisions.

Multiple studies [71,72,75,86] highlight oxidative stress as a key driver of atrial remodeling and recurrent AF. Reactive oxygen species (ROS) induce cellular damage, alter ion channels, and disrupt atrial electrical properties. Major ROS sources in atrial tissue include mitochondrial dysfunction, NADPH oxidases, and uncoupled nitric oxide syn-

https://doi.org/10.3390/cells15010036

thases. Polymorphonuclear cells (PMNs) also release myeloperoxidase (MPO) and activate NADPH oxidase, generating free radicals through nitric oxide (NO) uncoupling. This cascade promotes atrial fibrosis, structural remodeling, and AF progression.

4. Autonomic Nervous System (ANS) Imbalance

Imbalances in the autonomic nervous system (ANS), including heightened sympathetic and parasympathetic activity, disrupt atrial electrophysiology and contribute to AF [72,86]. Choi et al. highlight the intrinsic cardiac autonomic system, particularly the ganglionated plexi, in modulating atrial electrophysiology, where imbalances trigger atrial tachyarrhythmia and elevate AF risk [87].

Molecular mediators like nerve growth factor (NGF) and catecholamines play key roles in autonomic nervous system (ANS) remodeling, contributing to AF pathogenesis. NGF overexpression enhances sympathetic innervation, altering atrial electrophysiology and creating a substrate for AF. Excessive catecholamine release, particularly norepinephrine, increases adrenergic signaling, promoting triggered activity, shortening refractory periods, and increasing repolarization dispersion. These changes drive atrial remodeling, increasing AF susceptibility and persistence [71].

5. Genetic and Epigenetic Factors

The cardiac action potential, a marvel of biological engineering, forms the basis of the cardiac conduction system and is primarily influenced by the intricate shift of sodium, calcium, and potassium ions. This complex exchange of biological molecules, orchestrated by intercalated disks between myocytes, plays a crucial role in propagating the action potential [88].

Several potassium channels, including the delayed-rectifier potassium current, IKs, are expressed in cardiac cells. These channels are responsible for maintaining the resting membrane potential, a crucial factor in the heart's electrical activity. They play a vital role in the different repolarization phases. The KCNQ1 gene encodes the cardiac IKs channel, and it was the first disease gene linked to adult-onset familial atrial fibrillation (AF). The KCNA5 gene encodes Kv1.5, a component of the voltage-gated IKur potassium channel. KCNA5 is a promising candidate gene for familial AF due to its atrium-specific functional expression [89]. Other gain-of-function mutations have also been identified in the KCNE1, KCNE2, KCNE, KCNE5, KCNQ1, and KCNJ2 genes as causes of AF. Furthermore, mutations in the SCN5A gene, which encodes a cardiac sodium channel, have also been linked to this condition [90].

The *MYL4* gene is responsible for the atrium's electrical, contractile, and structural integrity. It plays a crucial role in the normal functioning of the atrium, ensuring its proper electrical activity, contractility, and structural stability. A loss-of-function variant in the MYL4 gene was identified as causing early atrial fibrosis, which in turn leads to atrial cardiomyopathy and atrial arrhythmia. This gene is a key player in maintaining the atrium's health, and any variations in its function can lead to atrial fibrillation [91]. Titin (*TTN*) is considered a critical AF gene, as previously mentioned. The gene encodes a giant sarcomere protein, titin, expressed in all chambers of the human heart. Titin-truncating variants (TTNtv) have been shown to predispose individuals to AF directly [92].

Catheter ablation is a commonly used technique to manage rhythm in atrial fibrillation (AF). However, for many patients, it may not be beneficial due to the recurrence of AF. Since it is an intervention with several health risks, predicting which patients are more likely to benefit from the procedure would be advantageous. Although still in its early stages, the potential of genetic risk scores, along with other relevant factors, to aid physicians in determining whether to perform catheter ablation on patients is a promising development.

https://doi.org/10.3390/cells15010036

Polymorphisms in the chromosome locus 4q25, which contains two single-nucleotide polymorphisms (SNPs) (rs2200733, shown to be most strongly associated with atrial fibrillation (AF), and rs10033464, near pituitary homeobox 2 (PITX2)), have been shown to influence the risk of AF recurrence after catheter ablation [93]. Genome-wide association studies (GWASs) have been conducted to identify these variations, and PITX2 is a transcription factor that plays a crucial role in the embryologic development of the heart, the suppression of sinus node formation in the left atrium [94], and the formation of the pulmonary vein myocardial sleeves [95]. It has been found to impact AF recurrence significantly [96].

Several circulating microRNAs (miRNAs) have been explored as predictive biomarkers of AF recurrence after ablation. Small studies suggest that miR-21, miR-29, and newer candidates such as miR-451a and miR-15a-5p may differentiate patients who relapse from those who remain in sinus rhythm, but findings are heterogeneous, and sample sizes are modest [97]. MiR-1, a muscle-specific microRNA (miRNA) and the most abundantly expressed miRNA in both ventricles and atria, has been shown to exert a proarrhythmic effect by modulating the inwardly rectifying potassium channel subfamily J member 2 (KCNJ2) through enhanced expression [98]. This upregulation is significantly observed in cardiomyocytes from patients with atrial fibrillation (AF) [99]. Importantly, multiple studies have also demonstrated that miRNAs are involved in various cardiovascular processes, including cardiac remodeling, fibrosis, inflammation, and arrhythmogenesis [100,101]. They have proven to be attractive candidates as biomarkers due to their stability in circulation and tissue-specific expression patterns [102,103]. Zhou Q. et al. revealed that plasma miR-21 levels are strongly correlated with left atrial low-voltage areas (LVAs), which are directly indicative of atrial fibrosis. Patients with lower miR-21 levels showed better outcomes after ablation, suggesting that it may serve as a potential predictor and marker of ongoing atrial remodeling [104]. The proarrhythmic effect of MiR-1 emphasizes its potential as a promising target for further research into the role of miR-1 in AF. Beyond miR-1 and other ion-channel-modulating miRNAs, AF-related atrial fibrosis appears to reflect an imbalance between pro-fibrotic and anti-fibrotic microRNAs. Pro-fibrotic miRNAs, such as miR-21, miR-132, miR-199, miR-208, and miR-34a, promote fibroblast activation, collagen synthesis, and TGF-β/Smad signaling, whereas anti-fibrotic miRNAs, such as the miR-29 family, miR-30, miR-133, and miR-101, restrain extracellular matrix deposition and fibrotic gene expression [105].

However, in the context of AF, global DNA methylation levels are significantly increased in AF patients, positively correlating with age and suggesting a role in cardiac inflammation and fibroblast activation [106,107]. Histone deacetylation, catalyzed by distinct classes of histone deacetylases (HDACs), is linked to gene silencing [108]. Emerging evidence suggests a crucial role for HDACs in regulating the post-transcriptional expression of various proteins in cardiomyocytes within the context of atrial fibrillation (AF), particularly those related to cytoskeletal and conductive proteins [109]. Conversely, their role in contractile and ion channels remains unclear. However, the potential of HDAC inhibition to significantly block or halt the progression of AF is a promising development, further underscoring the importance of HDAC as a potential therapeutic target in AF [109]. Nonetheless, the molecular mechanisms require further exploration. Further methylation analysis of left atrial tissue from patients with permanent atrial fibrillation (AF) revealed 417 differentially methylated cytosine–phosphate–guanine (CpG) sites involved in inflammation activation, sodium and potassium ion transport, fibrosis, and the reduction in lipid metabolism [110]. Hypermethylation of DNA suppresses the expression of antiproliferative and anti-myofibroblast differentiation genes in the human heart, accelerating cardiac fibrosis and AF recurrence [111,112].

https://doi.org/10.3390/cells15010036

6. Neurohumoral Factors and Circulating Biomarkers

The sympathetic co-transmitter neuropeptide Y (NPY) is a promising biomarker for sympathetic hyperactivity following myocardial infarction [113] and heart failure [114]. Increasing evidence indicates that the autonomic nervous system plays a role in inducing AF. NPY has been recognized as a biomarker of neuromodulation in AF through its receptors in the left atrium [115]. A study comparing persistent or long-standing atrial fibrillation (AF) with paroxysmal AF suggested a link between AF progression and left atrial NPY receptor expression [116]. This indicates that neuromodulation is present. Song et al. concluded that NPY could inhibit fibrosis by reducing apoptosis in atrial myocytes and suppressing the activation of Akt (protein kinase) in cardiac fibroblasts, consequently increasing the incidence of AF post-ablation [117]. Circulating NPY concentrations are higher in patients with AF than in those in sinus rhythm, and levels tend to increase with AF persistence and symptom burden [118]. Elevated pre-operative NPY has also been associated with an increased risk of post-operative AF after cardiac surgery [119]. Experimental work in canines suggests that long-term changes in NPY signaling after circumferential PV ablation may influence AF inducibility and atrial remodeling, but these findings have not yet translated into routine peri-ablation monitoring of NPY in humans [119].

Substance P (SP) is an 11-amino acid peptide that belongs to the tachykinin family of neuropeptides [120]. SP is primarily found in C-fiber sensory nerves that innervate the coronary arterial system, the intrinsic cardiac neural plexus, intrinsic nerve bundles, and interganglionic nerves in the atria, as well as occasionally in cardiomyocytes [120]. Yu et al. paced dog hearts at 600 beats per minute to induce atrial fibrillation and discovered that, while there was an increase in sympathetic nerve fibers in the atria, there was a significant loss of substance P (SP)-containing nerve fibers [120]. Given that most cardiac sympathetic (SP) activity is in the atria and that SP can influence heart rate, leading to bradycardia, it is reasonable to conclude that a loss of SP could contribute to atrial fibrillation. Neuromodulatory strategies that target cardiac ganglionated plexi or enhance vagal tone (e.g., GP ablation, low-level vagus nerve stimulation, ethanol infusion into the vein of Marshall) have shown that acute changes in autonomic tone can impact AF initiation and maintenance [121–123]. Small mechanistic studies have reported that biomarkers such as NPY, S100B and other nerve-related proteins can reflect acute autonomic injury during AF ablation and might predict maintenance of sinus rhythm [116,124,125]. However, dynamic measurements of NPY or substance P before and after neuromodulatory procedures remain sparse, and their direct value for predicting long-term AF recurrence after catheter ablation is unproven. Autonomic neuropeptides should therefore be viewed as promising mechanistic markers rather than established clinical tools at this time.

Two biomarkers reflect and modulate AF: N-terminal pro-B-type natriuretic peptide (NT-proBNP) [126] and high-sensitivity C-reactive protein (hs-CRP) [127]. Both biomarkers have been shown to predict AF recurrence, irrespective of radiofrequency catheter ablation of AF (RFCA). A multicenter study by Carballo et al. found that NT-proBNP levels at 6 months post-RFCA were significantly higher in patients with AF recurrence compared to those without ($p = 0.001$, Wilcoxon rank sum test) [78]. Additionally, a meta-analysis indicated that elevated high-sensitivity C-reactive protein and Interleukin-6 are also strong markers of AF recurrence [76].

The left atrial appendage (LAA) is a remnant of the embryonic left atrium, while the smooth-walled left atrium arises from the primordial pulmonary veins and their branches. The LAA is an actively contracting structure, and studies have shown that it is more distensible than the left atrium [128]. As a result, the LAA may help maintain left atrial pressure by activating stretch-sensitive receptors and influencing the actions of the atrial natriuretic factor (ANF), which increases heart rate, diuresis, and natriuresis [129]. Atrial arrhythmias,

https://doi.org/10.3390/cells15010036

such as atrial fibrillation (AF), are known predisposing factors for thrombus formation, with the left atrial appendage (LAA) serving as a primary site. The function and morphology of the LAA are believed to contribute to the origin of thrombus. Echocardiographic measurements of LAA function are directly correlated with the risk of thromboembolism. Lower LAA velocities have been associated with ischemic stroke and the formation of thrombi. Three known morphologic features of the LAA linked to ischemic stroke are its shape, orifice size, and fibrosis [130].

Growth differentiation factor-15 (GDF-15) is a member of the transforming growth factor β (TGF-β) cytokine family, which is widely distributed in mammalian tissues, including the prostate, intestinal mucosa, and kidney. It has been shown to play multiple roles in various pathologies, such as cardiovascular disease [131]. A study by Kempf et al. found that GDF-15 contributes to cardiomyocyte repair in response to tissue inflammation, oxidative stress, and injury, exhibiting both anti-apoptotic and anti-hypertrophic properties [132]. Suppression of Tumorigenicity-2 (ST-2) belongs to the interleukin-1 (IL-1) receptor family and can be used in conjunction with GDF-15 as a marker of cardiac stress. It has two forms, soluble ST2 (sST-2) and transmembrane ST-2 (ST-2L), both of which are upregulated in response to myocyte stretch, similar to brain natriuretic peptide (BNP) [133]. Wei et al. found that the expression of GDF-15 in serum was elevated in the persistent AF group compared to the paroxysmal AF group and also increased in the recurrence group compared to the non-recurrence group; however, it decreased after RFCA [74]. This suggests the potential of using GDF-15 to predict AF recurrence after ablation. In a study by Gizatulina et al., sST2 was identified as the only independent predictor of AF recurrence. A 10-unit increase in sST2 was associated with a 2.10-fold increase in the risk of AF recurrence. Serum sST2 levels at a cut-off value of 36 ng/mL or greater can serve as a predictor [134].

Relaxin, a peptide hormone of the insulin superfamily, promotes the remodeling of the extracellular matrix [135]. It has emerged as a natural suppressor of age-related fibrosis in various tissues, including the skin, lungs, kidneys, and heart. Several downstream pathological processes are involved, including reduced expression of transforming growth factor-β (TGF-β) and tumor necrosis factor-α (TNF-α), as well as increased activity of matrix metalloproteinases (MMPs), which leads to decreased fibrosis [135]. Hao Zhou et al. demonstrated that relaxin is associated with fibrosis-related biomarkers and is significantly elevated in atrial fibrillation (AF) [136]. A study by Qu et al. demonstrated that elevated pre-RFCA relaxin levels are associated with post-RFCA AF recurrence [82]. The exact mechanism by which relaxin contributes to atrial fibrillation (AF) recurrence is not fully understood, but it may be related to its effects on atrial remodeling and fibrosis.

7. Emerging Exposures

Emerging research links microplastics and nanoplastics (MNPs) to systemic inflammation, oxidative stress, and endothelial dysfunction, key contributors to cardiovascular diseases like AF [137]. MNPs trigger inflammation, activating immune cells and causing genomic instability, which leads to vascular endothelial dysfunction [138]. A landmark *New England Journal of Medicine* study reported that patients with MNPs in carotid plaque had roughly a 4–5-fold higher risk of myocardial infarction, stroke, or death compared with those without detectable plastics, supporting a link between plastic contamination of the vasculature and adverse cardiovascular events [139]. However, specific studies linking microplastics to AF recurrence post-ablation are currently lacking. Given the established role of inflammation and oxidative stress in AF pathogenesis, further research is warranted to explore potential connections between microplastic exposure and AF outcomes.

https://doi.org/10.3390/cells15010036

8. Ablation Energy Sources and Their Biological Footprint

Radiofrequency and cryoballoon ablation create lesions by heating or freezing tissue, whereas pulsed field ablation (PFA) uses short, high-voltage electrical pulses to cause non-thermal electroporation of cell membranes. Preclinical and early clinical data show that PFA is relatively selective for cardiomyocytes, while largely sparing nearby structures such as the esophagus, pulmonary veins, and phrenic nerve, although rare phrenic nerve injury has been reported [85,140,141]. Randomized trials and meta-analyses demonstrate that PFA is non-inferior to conventional thermal ablation for 1-year freedom from atrial arrhythmias, with similar acute pulmonary vein isolation rates and shorter procedure times [142,143]. Repeat-procedure data suggest that lesion durability and pulmonary vein reconnection rates are comparable between PFA and high-power radiofrequency ablation, with some series showing numerically lower reconnection after PFA, although differences are modest and still under investigation [144–146]. In terms of systemic response, RF and cryoablation trigger marked rises in inflammatory and myocardial injury markers (hs-CRP, IL-6, fibrinogen, and troponin), which relate to early recurrence [79,147]. Early work suggests that PFA may produce a different inflammatory and biomarker profile, potentially reflecting its non-thermal mechanism, but head-to-head data are still limited, and ongoing studies are specifically addressing this question [84].

9. Therapeutic Implications

9.1. Colchicine

Colchicine was introduced to cardiology nearly four decades ago for treating recurrent pericarditis [148]. In recent years, its role has expanded to other cardiovascular conditions. Atrial fibrillation (AF) is the most common complication following cardiac surgery. Given colchicine's efficacy in preventing pericardiotomy syndrome, several trials have evaluated its role in preventing postoperative atrial fibrillation (POAF). A systematic review and meta-analysis demonstrated a significant reduction in POAF (RR: 0.70, 95% CI: 0.58–0.84, $p = 0.0001$) [149]. However, only two of the six included trials showed a positive effect, while four showed neutral results. Data on hospital length of stay were inconsistent [150,151], and no study has demonstrated a reduction in all-cause mortality.

Ablation procedures for AF trigger a proinflammatory response, contributing to early AF recurrence [152]. Colchicine has shown benefit in reducing AF recurrence at 3- and 12-month post-ablation (RR: 0.57, 95% CI: 0.39–0.83, $p = 0.0032$; RR: 0.58, 95% CI: 0.42–0.80, $p = 0.0008$) [149,153]. Larger trials are needed to confirm colchicine's effectiveness in secondary AF prevention.

9.2. Corticosteroids

Corticosteroids, which modulate multiple inflammatory pathways, have been studied in both POAF and AF recurrence after catheter ablation (CA). Koyama et al. reported a reduction in immediate AF recurrence ($\leq$3 days post-PVI) with low-dose corticosteroids for three days; however, recurrence between 4 and 30 days was unchanged. At 14 months, AF-free survival was higher in the corticosteroid group (85% vs. 71%, $p = 0.032$) [154]. In contrast, a study by Won et al. found no significant reduction in recurrence with pre-procedure IV corticosteroids [155].

IV corticosteroids have been shown to alter levels of IL-6, IL-8, IL-10, CRP, nitric oxide, endothelin-1, and complement C4 [156]. One study found that IV hydrocortisone before PVI increased the need for radiofrequency ablation and dormant PV conduction [157]. Despite some positive signals, the role of corticosteroids in secondary AF prevention remains uncertain due to their potential adverse effects, such as GI bleeding and infections.

https://doi.org/10.3390/cells15010036

9.3. Methotrexate

Methotrexate is associated with a lower incidence of new-onset AF in patients with seropositive rheumatoid arthritis [158]. Though the exact mechanism is unclear, its anti-inflammatory properties may contribute to risk reduction.

9.4. Cardiac Drugs with Pleiotropic Effects

Renin–angiotensin system (RAS) inhibitors have shown benefits in both primary and secondary AF prevention. Meta-analyses indicate reduced recurrence after electrical cardioversion and in patients with paroxysmal AF [159].

Baia-Bezerra et al. demonstrated that sacubitril–valsartan (SV) significantly reduced AF recurrence post-CA compared to ACEi/ARB (RR: 0.54; 95% CI: 0.41–0.70; $p = 0.000004$; $I^2 = 80\%$) [160]. Similarly, Sun et al. found that RAS inhibitors lowered AF recurrence post-ablation (RR: 0.85; 95% CI: 0.72–0.99; $p = 0.03$), with SV showing even greater benefit (RR: 0.50; 95% CI: 0.37–0.68; $p < 0.00001$) [161].

Although a specific mechanism is not well defined, losartan has been shown to reduce stress-induced electrical remodeling in atrial cardiomyocytes [162], and Goette et al. reported increased Erk1/Erk2 and ACE expression in AF patients [163], suggesting a role in atrial fibrosis.

9.5. Statins and PCSK9 Inhibitors

Statins have been shown to reduce AF recurrence after CA, independent of LDL-lowering effects [164]. Mechanistically, they reduce lysyl oxidase, collagen deposition, and cross-linking—key processes in atrial remodeling [164].

While PCSK9 inhibitors have not been studied in randomized AF trials, preclinical data suggest that evolocumab may reduce AF susceptibility in animal models [165]. However, a clinical trial found that alirocumab did not significantly affect AF incidence post-acute coronary syndrome (HR: 0.91; 95% CI: 0.77–1.09) [166].

9.6. Metformin

Metformin activates AMPK and inhibits fibroblast differentiation and atrial fibrosis, key substrates for AF [167]. An observational study showed it reduced AF and ventricular arrhythmias compared to sulfonylureas [168]. The ongoing phase 4 trial (NCT04625946) is evaluating metformin's role in preventing AF recurrence post-CA [169].

9.7. Sodium–Glucose Cotransporter 2 Inhibitors

Sodium–glucose cotransporter 2 inhibitors (SGLT2i) reduce AF recurrence after CA, as shown in a recent meta-analysis [170]. They are also associated with reduced hospitalizations and ischemic stroke risk. A population study confirmed lower AF recurrence post-ablation in type 2 diabetes patients on SGLT2i [171].

Mechanistically, SGLT2i affects atrial electrophysiology by modulating sodium (INa), potassium (Ito, IKs), and calcium (ICa-L) currents, leading to reduced arrhythmogenicity [172].

9.8. Glucagon-like-Peptide-1 Receptor Agonists

Emerging data support the use of glucagon-like-peptide-1 receptor agonists (GLP-1 RAs) in reducing AF recurrence post-CA, particularly in patients with type 2 diabetes and obesity [173]. A recent meta-analysis confirmed this association [174]. Animal models show that GLP-1 RAs prevent atrial fibrosis, electrical remodeling, and conduction abnormalities [175].

https://doi.org/10.3390/cells15010036

9.9. n-3 Polyunsaturated Fatty Acids (PUFAs)

PUFAs have shown potential in reducing POAF, with greater benefit seen when the EPA/DHA ratio is <1 [176]. However, other studies have reported increased AF recurrence risk, especially at higher doses [177].

PUFAs offer multiple protective effects, including anti-inflammatory, anti-thrombotic, and antihypertensive properties, as well as favorable myocardial remodeling and electrophysiology [178]. In canine models, omega-3 PUFAs reduced atrial fibrosis, apoptosis, and stress-related proteins in the left atrium [179]. Further research is needed to clarify their role in AF prevention post-CA.

10. Future Therapeutic Targets

Targeting the complex mechanisms underlying AF—including inflammation, oxidative stress, and RAAS activation—may lead to novel therapies. Potential approaches include modulating inflammatory mediators such as HSP27, HSP60, IL-10, and the NLRP3 inflammasome, or using antibodies against DAMPs [180]. However, translating these targets into effective therapies remains a challenge.

Genetic polymorphisms affecting inflammatory responses suggest that personalized therapies based on individual inflammatory profiles may be necessary. Atrial-specific potassium channels like IKur and IK, ACh have been studied in phase II/III trials but have not demonstrated sufficient efficacy [168].

The TASK1 potassium channel is a promising target. TASK1 inhibition via small molecules or gene therapy has shown antiarrhythmic effects in preclinical studies [181]. Canakinumab, an anti-IL-1β monoclonal antibody, did not significantly reduce AF recurrence after ECV but did reduce AF burden [182].

Several additional agents show promise in preclinical models, though discussion of these is beyond the scope of this review and is detailed elsewhere [183].

11. Limitations of Current Research and Future Directions

Despite considerable advances, existing studies exhibit notable limitations, including small sample sizes, heterogeneity in patient populations, and insufficient long-term follow-up data. The molecular pathways leading to structural and electrical remodeling remain incompletely understood, particularly the precise roles and interactions of TGF-β1, matrix metalloproteinases (MMPs), and connexins in atrial fibrosis and conduction abnormalities. Moreover, inflammatory mediators, oxidative stress, and autonomic dysregulation in AF recurrence have yet to be fully characterized in clinical populations.

Future research must prioritize comprehensive mechanistic studies integrating genomics, proteomics, and advanced imaging to clarify these molecular pathways. Larger, multicenter trials with diverse patient cohorts and standardized outcome measures are essential to validate biomarkers such as serum TGF-β1, MMPs, connexins, and novel circulating markers like GDF-15 and relaxin. Additionally, exploring emerging risk factors like microplastic-induced inflammation could unveil new intervention targets. Ultimately, advancing the molecular understanding of AF recurrence will enhance patient selection, improve ablation strategies, and foster the development of personalized therapeutic approaches.

12. Conclusions

In summary, significant molecular mechanisms contributing to AF recurrence following catheter ablation include structural remodeling and fibrosis mediated by TGF-β1 and MMPs, ion-channel dysregulation, inflammatory responses, autonomic nervous system imbalance, and genetic and epigenetic alterations. Each of these mechanisms holds considerable clinical relevance, as they not only influence the likelihood of AF recurrence

https://doi.org/10.3390/cells15010036

but also provide actionable targets for enhancing therapeutic efficacy. As clinical practice evolves, integrating molecular insights through precision diagnostics and tailored therapeutic interventions holds immense promise. Future clinical approaches should incorporate comprehensive biomarker profiling and personalized treatment strategies to refine patient selection, optimize ablation procedures, and improve long-term outcomes, ultimately reducing AF recurrence and associated cardiovascular complications (Table 1).

Table 1. Mechanism key findings.

Mechanism	Key Findings
Fibrosis and ECM Alterations	• Atrial fibrosis significantly contributes to AF recurrence, involving irreversible structural remodeling compared to reversible electrical remodeling. • TGF-β1 promotes atrial fibrosis by inducing collagen synthesis and ECM alterations through classical SMAD signaling pathways. • Variations in TGF-β1 receptor interactions differentiate atrial from ventricular fibrosis.
Role of TGF-β and MMPs	• Elevated plasma and serum TGF-β1 concentrations positively correlate with atrial fibrosis severity and AF recurrence. • Matrix metalloproteinases (MMPs) and their inhibitors regulate ECM remodeling; elevated MMP-2 levels persist post-ablation and predict recurrence. • Aggressive ablation strategies targeting structurally remodeled atria (e.g., CFAE ablation) have higher recurrence rates.
Cellular Hypertrophy & Myocyte Disarray	• Cellular hypertrophy and disarray, especially in hypertrophic cardiomyopathy (HCM), increase recurrence risk by causing thicker atrial walls, diffuse fibrosis, and triggering ectopic activity beyond pulmonary veins. • Combining catheter ablation with anti-arrhythmic drugs improves outcomes in HCM patients, despite high recurrence risk.
Conduction Velocity & Arrhythmogenic Substrate Formation	• Functional conduction abnormalities (e.g., slow conduction velocity in left atrium) are predictive of AF recurrence post-ablation. • Slow conduction velocities indicate structural remodeling, fibrosis, and atrial strain, predisposing to re-entry circuits and persistent AF.
Ion-Channel Dysregulation	• Ion-channel dysfunction contributes to conduction slowing and re-entry circuit formation, pivotal to maintaining persistent AF.
Connexins and Gap Junctions	• Connexin (Cx40, Cx43) remodeling disrupts electrical coupling, facilitating arrhythmogenic substrates and increased recurrence. • Therapeutic modulation (e.g., beta-blockers) targeting gap junction integrity reduces recurrence risk.
Inflammatory Pathways	• Post-ablation inflammation involving cytokines (CRP, TNF-α, IL-6) and DAMPs promotes fibrosis, structural remodeling, and AF recurrence.
Autonomic Nervous System Imbalance	• ANS imbalances enhance susceptibility to AF recurrence through autonomic remodeling, affecting atrial electrophysiology.
Genetic & Epigenetic Factors	• Specific genetic variants and epigenetic changes (DNA methylation, histone modifications) influence AF susceptibility and recurrence risk post-ablation.
Neurohumoral Factors & Biomarkers	• Elevated circulating biomarkers (GDF-15, relaxin, NT-proBNP, and hs-CRP) correlate strongly with structural remodeling and AF recurrence.
Nanoplastics & Microplastics (MNPs)	• MNPs induce systemic inflammation, oxidative stress, and endothelial dysfunction, all critical mechanisms in cardiovascular disease progression. • Although direct evidence linking MNP exposure and AF recurrence post-ablation is lacking, the established role of inflammation and oxidative stress in AF supports further research into potential connections.

Author Contributions: Conceptualization, M.S., C.T.G. and Y.M.R.; methodology, M.S., R.V., D.U., S.T., Y.V., F.M., M.M. and F.Z.; investigation, M.S., R.V., D.U., S.T., C.T.G., Y.V., F.M., M.M., F.Z. and Y.M.R.; resources, C.T.G. and Y.M.R.; data curation, M.S., R.V., D.U., S.T. and F.Z.; writing—original draft preparation, M.S., R.V., D.U., S.T. and F.Z.; writing—review and editing, M.S., R.V., D.U., S.T., C.T.G., Y.V., F.M., M.M., F.Z., R.N. and Y.M.R.; visualization, M.S., R.V., Y.V., F.M., R.N. and M.M.; supervision, C.T.G. and Y.M.R.; project administration, M.S., R.V. and C.T.G. All authors have read and agreed to the published version of the manuscript.

Funding: This research received no external funding.

Institutional Review Board Statement: Not applicable.

Informed Consent Statement: Not applicable.

Data Availability Statement: Not applicable.

Conflicts of Interest: The authors declare no conflicts of interest.

Abbreviations

The following abbreviations are used in this manuscript:

AF	Atrial fibrillation
AAD	Anti-arrhythmic drug
ACEi	Angiotensin-converting enzyme inhibitor
ADMA	Asymmetric dimethylarginine
AMPK	AMP-activated protein kinase
ANS	Autonomic nervous system
ANF	Atrial natriuretic factor
AUROC	Area under the receiver operating characteristic
BNP	Brain natriuretic peptide
CA	Catheter ablation
CFAE	Complex fractionated atrial electrogram
CpG	Cytosine–phosphate–guanine
CRP	C-reactive protein
Cx	Connexin
DAMPs	Damage-associated molecular patterns
DLS	Difference between the longest and shortest P-A0 interval
ECM	Extracellular matrix
ECV	Electrical cardioversion
GWAS	Genome-wide association study
GDF-15	Growth differentiation factor-15
GI	Gastrointestinal
HDAC	Histone deacetylase
HCM	Hypertrophic cardiomyopathy
HMGB-1	High-mobility group box-1
HR	Hazard ratio
hs-CRP	High-sensitivity C-reactive protein
ICa-L	L-type calcium current
ICTP	Carboxylterminal telopeptide of collagen type I
IL	Interleukin
INa	Sodium current
IKur	Ultrarapid delayed rectifier potassium current
IKs	Slow delayed rectifier potassium current
IV	Intravenous
LA	Left atrium / Left atrial
LAA	Left atrial appendage
LACV	Left atrial conduction velocity
LGE	Late gadolinium enhancement
LVAs	Low-voltage areas
MAPK	Mitogen-activated protein kinase
miRNA	MicroRNA
MMP	Matrix metalloproteinase
MNPs	Microplastics/nanoplastics
MPO	Myeloperoxidase
mtDNA	Mitochondrial DNA
NF-κB	Nuclear factor kappa-B
NGF	Nerve growth factor
NO	Nitric oxide
NOS	Nitric oxide synthase
NPY	Neuropeptide Y

https://doi.org/10.3390/cells15010036

NT-proBNP	N-terminal pro–B-type natriuretic peptide
OR	Odds ratio
PCSK9	Proprotein convertase subtilisin/kexin type 9
PITX2	Paired-like homeodomain transcription factor 2
PMNs	Polymorphonuclear neutrophils
POAF	Postoperative atrial fibrillation
PsAF	Persistent atrial fibrillation
PUFAs	Polyunsaturated fatty acids
PVI	Pulmonary vein isolation
PW-TDI	Pulsed-wave tissue Doppler imaging
RAAS	Renin–angiotensin–aldosterone system
RECK	Reversion-inducing cysteine-rich protein with Kazal motifs
RFCA	Radiofrequency catheter ablation
ROS	Reactive oxygen species
RR	Relative risk
sST2	Soluble suppression of tumorigenicity-2
SNP	Single-nucleotide polymorphism
SP	Substance P
SV	Sacubitril–valsartan
TASK1	Twik-related acid-sensitive potassium channel 1
TGF-β1	Transforming growth factor-beta 1
TIMP	Tissue inhibitor of metalloproteinase
TLR	Toll-like receptor
TNF-α	Tumor necrosis factor-alpha
TTN	Titin
TTNtv	Titin-truncating variant

References

1. Chugh, S.S.; Havmoeller, R.; Narayanan, K.; Singh, D.; Rienstra, M.; Benjamin, E.J.; Gillum, R.F.; Kim, Y.-H.; McAnulty, J.H.; Zheng, Z.-J.; et al. Worldwide Epidemiology of Atrial Fibrillation: A Global Burden of Disease 2010 Study. *Circulation* **2014**, *129*, 837–847. [CrossRef]
2. Krijthe, B.P.; Kunst, A.; Benjamin, E.J.; Lip, G.Y.H.; Franco, O.H.; Hofman, A.; Witteman, J.C.M.; Stricker, B.H.; Heeringa, J. Projections on the Number of Individuals with Atrial Fibrillation in the European Union, from 2000 to 2060. *Eur. Heart J.* **2013**, *34*, 2746–2751. [CrossRef]
3. Benjamin, E.J.; Wolf, P.A.; D'Agostino, R.B.; Silbershatz, H.; Kannel, W.B.; Levy, D. Impact of Atrial Fibrillation on the Risk of Death: The Framingham Heart Study. *Circulation* **1998**, *98*, 946–952. [CrossRef] [PubMed]
4. Vermond, R.A.; Geelhoed, B.; Verweij, N.; Tieleman, R.G.; Van der Harst, P.; Hillege, H.L.; Van Gilst, W.H.; Van Gelder, I.C.; Rienstra, M. Incidence of Atrial Fibrillation and Relationship With Cardiovascular Events, Heart Failure, and Mortality: A Community-Based Study From the Netherlands. *J. Am. Coll. Cardiol.* **2015**, *66*, 1000–1007. [CrossRef]
5. Lin, H.J.; Wolf, P.A.; Kelly-Hayes, M.; Beiser, A.S.; Kase, C.S.; Benjamin, E.J.; D'Agostino, R.B. Stroke Severity in Atrial Fibrillation. The Framingham Study. *Stroke* **1996**, *27*, 1760–1764. [CrossRef]
6. Soliman, E.Z.; Safford, M.M.; Muntner, P.; Khodneva, Y.; Dawood, F.Z.; Zakai, N.A.; Thacker, E.L.; Judd, S.; Howard, V.J.; Howard, G.; et al. Atrial Fibrillation and the Risk of Myocardial Infarction. *JAMA Intern. Med.* **2014**, *174*, 107–114. [CrossRef] [PubMed]
7. Walters, T.E.; Nisbet, A.; Morris, G.M.; Tan, G.; Mearns, M.; Teo, E.; Lewis, N.; Ng, A.; Gould, P.; Lee, G.; et al. Progression of Atrial Remodeling in Patients with High-Burden Atrial Fibrillation: Implications for Early Ablative Intervention. *Heart Rhythm* **2016**, *13*, 331–339. [CrossRef]
8. Jaïs, P.; Haïssaguerre, M.; Shah, D.C.; Chouairi, S.; Gencel, L.; Hocini, M.; Clémenty, J. A Focal Source of Atrial Fibrillation Treated by Discrete Radiofrequency Ablation. *Circulation* **1997**, *95*, 572–576. [CrossRef] [PubMed]
9. Calkins, H.; Kuck, K.H.; Cappato, R.; Brugada, J.; Camm, A.J.; Chen, S.-A.; Crijns, H.J.G.; Damiano, R.J.; Davies, D.W.; DiMarco, J.; et al. 2012 HRS/EHRA/ECAS Expert Consensus Statement on Catheter and Surgical Ablation of Atrial Fibrillation: Recommendations for Patient Selection, Procedural Techniques, Patient Management and Follow-up, Definitions, Endpoints, and Research Trial Design. *Eur. Eur. Pacing Arrhythm. Card. Electrophysiol. J. Work. Groups Card. Pacing Arrhythm. Card. Cell. Electrophysiol. Eur. Soc. Cardiol.* **2012**, *14*, 528–606. [CrossRef]

10. Calkins, H.; Hindricks, G.; Cappato, R.; Kim, Y.-H.; Saad, E.B.; Aguinaga, L.; Akar, J.G.; Badhwar, V.; Brugada, J.; Camm, J.; et al. 2017 HRS/EHRA/ECAS/APHRS/SOLAECE Expert Consensus Statement on Catheter and Surgical Ablation of Atrial Fibrillation. *Heart Rhythm* **2017**, *14*, e275–e444. [CrossRef]
11. January, C.T.; Wann, L.S.; Alpert, J.S.; Calkins, H.; Cigarroa, J.E.; Cleveland, J.C.; Conti, J.B.; Ellinor, P.T.; Ezekowitz, M.D.; Field, M.E.; et al. 2014 AHA/ACC/HRS Guideline for the Management of Patients with Atrial Fibrillation: Executive Summary: A Report of the American College of Cardiology/American Heart Association Task Force on Practice Guidelines and the Heart Rhythm Society. *Circulation* **2014**, *130*, 2071–2104. [CrossRef]
12. Kirchhof, P.; Benussi, S.; Kotecha, D.; Ahlsson, A.; Atar, D.; Casadei, B.; Castella, M.; Diener, H.-C.; Heidbuchel, H.; Hendriks, J.; et al. 2016 ESC Guidelines for the Management of Atrial Fibrillation Developed in Collaboration with EACTS. *Eur. Heart J.* **2016**, *37*, 1609–1678. [CrossRef]
13. Packer, D.L.; Mark, D.B.; Robb, R.A.; Monahan, K.H.; Bahnson, T.D.; Poole, J.E.; Noseworthy, P.A.; Rosenberg, Y.D.; Jeffries, N.; Mitchell, L.B.; et al. Effect of Catheter Ablation vs Antiarrhythmic Drug Therapy on Mortality, Stroke, Bleeding, and Cardiac Arrest Among Patients With Atrial Fibrillation: The CABANA Randomized Clinical Trial. *JAMA* **2019**, *321*, 1261–1274. [CrossRef] [PubMed]
14. Kuck, K.-H.; Brugada, J.; Fürnkranz, A.; Metzner, A.; Ouyang, F.; Chun, K.R.J.; Elvan, A.; Arentz, T.; Bestehorn, K.; Pocock, S.J.; et al. Cryoballoon or Radiofrequency Ablation for Paroxysmal Atrial Fibrillation. *N. Engl. J. Med.* **2016**, *374*, 2235–2245. [CrossRef] [PubMed]
15. Jaïs, P.; Cauchemez, B.; Macle, L.; Daoud, E.; Khairy, P.; Subbiah, R.; Hocini, M.; Extramiana, F.; Sacher, F.; Bordachar, P.; et al. Catheter Ablation versus Antiarrhythmic Drugs for Atrial Fibrillation: The A4 Study. *Circulation* **2008**, *118*, 2498–2505. [CrossRef]
16. Khan, R.; Sheppard, R. Fibrosis in Heart Disease: Understanding the Role of Transforming Growth Factor-Beta in Cardiomyopathy, Valvular Disease and Arrhythmia. *Immunology* **2006**, *118*, 10–24. [CrossRef] [PubMed]
17. Verheule, S.; Sato, T.; Everett, T.; Engle, S.K.; Otten, D.; Rubart-von der Lohe, M.; Nakajima, H.O.; Nakajima, H.; Field, L.J.; Olgin, J.E. Increased Vulnerability to Atrial Fibrillation in Transgenic Mice with Selective Atrial Fibrosis Caused by Overexpression of TGF-Beta1. *Circ. Res.* **2004**, *94*, 1458–1465. [CrossRef]
18. Rahmutula, D.; Marcus, G.M.; Wilson, E.E.; Ding, C.-H.; Xiao, Y.; Paquet, A.C.; Barbeau, R.; Barczak, A.J.; Erle, D.J.; Olgin, J.E. Molecular Basis of Selective Atrial Fibrosis Due to Overexpression of Transforming Growth Factor-B1. *Cardiovasc. Res.* **2013**, *99*, 769–779. [CrossRef]
19. Tian, Y.; Wang, Y.; Chen, W.; Yin, Y.; Qin, M. Role of Serum TGF-B1 Level in Atrial Fibrosis and Outcome after Catheter Ablation for Paroxysmal Atrial Fibrillation. *Medicine* **2017**, *96*, e9210. [CrossRef]
20. Li, Y.; Jian, Z.; Yang, Z.Y.; Chen, L.; Wang, X.F.; Ma, R.Y.; Xiao, Y.B. Increased Expression of Connective Tissue Growth Factor and Transforming Growth Factor-Beta-1 in Atrial Myocardium of Patients with Chronic Atrial Fibrillation. *Cardiology* **2013**, *124*, 233–240. [CrossRef]
21. Xiao, H.; Lei, H.; Qin, S.; Ma, K.; Wang, X. TGF-Beta1 Expression and Atrial Myocardium Fibrosis Increase in Atrial Fibrillation Secondary to Rheumatic Heart Disease. *Clin. Cardiol.* **2010**, *33*, 149–156. [CrossRef]
22. Kim, S.K.; Park, J.H.; Kim, J.Y.; Choi, J.I.; Joung, B.; Lee, M.-H.; Kim, S.S.; Kim, Y.-H.; Pak, H.-N. High Plasma Concentrations of Transforming Growth Factor-β and Tissue Inhibitor of Metalloproteinase-1: Potential Non-Invasive Predictors for Electroanatomical Remodeling of Atrium in Patients with Non-Valvular Atrial Fibrillation. *Circ. J. Off. J. Jpn. Circ. Soc.* **2011**, *75*, 557–564. [CrossRef]
23. On, Y.K.; Jeon, E.-S.; Lee, S.Y.; Shin, D.-H.; Choi, J.-O.; Sung, J.; Kim, J.S.; Sung, K.; Park, P. Plasma Transforming Growth Factor Beta1 as a Biochemical Marker to Predict the Persistence of Atrial Fibrillation after the Surgical Maze Procedure. *J. Thorac. Cardiovasc. Surg.* **2009**, *137*, 1515–1520. [CrossRef]
24. Rundhaug, J.E. Matrix Metalloproteinases and Angiogenesis. *J. Cell. Mol. Med.* **2005**, *9*, 267–285. [CrossRef]
25. Pistol, G.; Matache, C.; Calugaru, A.; Stavaru, C.; Tanaseanu, S.; Ionescu, R.; Dumitrache, S.; Stefanescu, M. Roles of CD147 on T Lymphocytes Activation and MMP-9 Secretion in Systemic Lupus Erythematosus. *J. Cell. Mol. Med.* **2007**, *11*, 339–348. [CrossRef] [PubMed]
26. Moshal, K.S.; Tyagi, N.; Moss, V.; Henderson, B.; Steed, M.; Ovechkin, A.; Aru, G.M.; Tyagi, S.C. Early Induction of Matrix Metalloproteinase-9 Transduces Signaling in Human Heart End Stage Failure. *J. Cell. Mol. Med.* **2005**, *9*, 704–713. [CrossRef]
27. Li, H.; Sun, B. Toll-like Receptor 4 in Atherosclerosis. *J. Cell. Mol. Med.* **2007**, *11*, 88–95. [CrossRef]
28. Jinga, D.C.; Blidaru, A.; Condrea, I.; Ardeleanu, C.; Dragomir, C.; Szegli, G.; Stefanescu, M.; Matache, C. MMP-9 and MMP-2 Gelatinases and TIMP-1 and TIMP-2 Inhibitors in Breast Cancer: Correlations with Prognostic Factors. *J. Cell. Mol. Med.* **2006**, *10*, 499–510. [CrossRef]
29. Anghelina, M.; Moldovan, L.; Zabuawala, T.; Ostrowski, M.C.; Moldovan, N.I. A Subpopulation of Peritoneal Macrophages Form Capillarylike Lumens and Branching Patterns in Vitro. *J. Cell. Mol. Med.* **2006**, *10*, 708–715. [CrossRef] [PubMed]
30. Spinale, F.G. Matrix Metalloproteinases: Regulation and Dysregulation in the Failing Heart. *Circ. Res.* **2002**, *90*, 520–530. [CrossRef] [PubMed]

31. Spinale, F.G.; Coker, M.L.; Bond, B.R.; Zellner, J.L. Myocardial Matrix Degradation and Metalloproteinase Activation in the Failing Heart: A Potential Therapeutic Target. *Cardiovasc. Res.* **2000**, *46*, 225–238. [CrossRef]
32. Oh, J.; Takahashi, R.; Kondo, S.; Mizoguchi, A.; Adachi, E.; Sasahara, R.M.; Nishimura, S.; Imamura, Y.; Kitayama, H.; Alexander, D.B.; et al. The Membrane-Anchored MMP Inhibitor RECK Is a Key Regulator of Extracellular Matrix Integrity and Angiogenesis. *Cell* **2001**, *107*, 789–800. [CrossRef]
33. Herman, M.P.; Sukhova, G.K.; Kisiel, W.; Foster, D.; Kehry, M.R.; Libby, P.; Schönbeck, U. Tissue Factor Pathway Inhibitor-2 Is a Novel Inhibitor of Matrix Metalloproteinases with Implications for Atherosclerosis. *J. Clin. Investig.* **2001**, *107*, 1117–1126. [CrossRef]
34. Mott, J.D.; Thomas, C.L.; Rosenbach, M.T.; Takahara, K.; Greenspan, D.S.; Banda, M.J. Post-Translational Proteolytic Processing of Procollagen C-Terminal Proteinase Enhancer Releases a Metalloproteinase Inhibitor. *J. Biol. Chem.* **2000**, *275*, 1384–1390. [CrossRef]
35. Welm, B.; Mott, J.; Werb, Z. Developmental Biology: Vasculogenesis Is a Wreck without RECK. *Curr. Biol. CB* **2002**, *12*, R209–R211. [CrossRef]
36. Noda, M.; Oh, J.; Takahashi, R.; Kondo, S.; Kitayama, H.; Takahashi, C. RECK: A Novel Suppressor of Malignancy Linking Oncogenic Signaling to Extracellular Matrix Remodeling. *Cancer Metastasis Rev.* **2003**, *22*, 167–175. [CrossRef] [PubMed]
37. Echizenya, M.; Kondo, S.; Takahashi, R.; Oh, J.; Kawashima, S.; Kitayama, H.; Takahashi, C.; Noda, M. The Membrane-Anchored MMP-Regulator RECK Is a Target of Myogenic Regulatory Factors. *Oncogene* **2005**, *24*, 5850–5857. [CrossRef] [PubMed]
38. Wu, C.-H.; Hu, Y.-F.; Chou, C.-Y.; Lin, Y.-J.; Chang, S.-L.; Lo, L.-W.; Tuan, T.-C.; Li, C.-H.; Chao, T.-F.; Chung, F.-P.; et al. Transforming Growth Factor-B1 Level and Outcome after Catheter Ablation for Nonparoxysmal Atrial Fibrillation. *Heart Rhythm* **2013**, *10*, 10–15. [CrossRef]
39. Wu, G.; Wang, S.; Cheng, M.; Peng, B.; Liang, J.; Huang, H.; Jiang, X.; Zhang, L.; Yang, B.; Cha, Y.; et al. The Serum Matrix Metalloproteinase-9 Level Is an Independent Predictor of Recurrence after Ablation of Persistent Atrial Fibrillation. *Clinics* **2016**, *71*, 251–256. [CrossRef]
40. Ouyang, F.; Bänsch, D.; Ernst, S.; Schaumann, A.; Hachiya, H.; Chen, M.; Chun, J.; Falk, P.; Khanedani, A.; Antz, M.; et al. Complete Isolation of Left Atrium Surrounding the Pulmonary Veins: New Insights from the Double-Lasso Technique in Paroxysmal Atrial Fibrillation. *Circulation* **2004**, *110*, 2090–2096. [CrossRef] [PubMed]
41. Lin, Y.-J.; Tai, C.-T.; Kao, T.; Chang, S.-L.; Lo, L.-W.; Tuan, T.-C.; Udyavar, A.R.; Wongcharoen, W.; Hu, Y.-F.; Tso, H.-W.; et al. Spatiotemporal Organization of the Left Atrial Substrate After Circumferential Pulmonary Vein Isolation of Atrial Fibrillation. *Circ. Arrhythm. Electrophysiol.* **2009**, *2*, 233–241. [CrossRef] [PubMed]
42. Okumura, Y.; Watanabe, I.; Nakai, T.; Ohkubo, K.; Kofune, T.; Kofune, M.; Nagashima, K.; Mano, H.; Sonoda, K.; Kasamaki, Y.; et al. Impact of Biomarkers of Inflammation and Extracellular Matrix Turnover on the Outcome of Atrial Fibrillation Ablation: Importance of Matrix Metalloproteinase-2 as a Predictor of Atrial Fibrillation Recurrence. *J. Cardiovasc. Electrophysiol.* **2011**, *22*, 987–993. [CrossRef] [PubMed]
43. Penela, D.; Sorgente, A.; Cappato, R. State-of-the-Art Treatments for Atrial Fibrillation in Patients with Hypertrophic Cardiomyopathy. *J. Clin. Med.* **2021**, *10*, 3025. [CrossRef]
44. Castagno, D.; Di Donna, P.; Olivotto, I.; Frontera, A.; Calò, L.; Scaglione, M.; Arretini, A.; Anselmino, M.; Giustetto, C.; De Ferrari, G.M.; et al. Transcatheter Ablation for Atrial Fibrillation in Patients with Hypertrophic Cardiomyopathy: Long-term Results and Clinical Outcomes. *J. Cardiovasc. Electrophysiol.* **2021**, *32*, 657–666. [CrossRef]
45. Ha, H.S.K.; Wang, N.; Wong, S.; Phan, S.; Liao, J.; Kumar, N.; Qian, P.; Yan, T.D.; Phan, K. Catheter Ablation for Atrial Fibrillation in Hypertrophic Cardiomyopathy Patients: A Systematic Review. *J. Interv. Card. Electrophysiol.* **2015**, *44*, 161–170. [CrossRef]
46. Zhao, D.-S.; Shen, Y.; Zhang, Q.; Lin, G.; Lu, Y.-H.; Chen, B.-T.; Shi, L.-S.; Huang, J.-F.; Lu, H.-H. Outcomes of Catheter Ablation of Atrial Fibrillation in Patients with Hypertrophic Cardiomyopathy: A Systematic Review and Meta-Analysis. *Europace* **2016**, *18*, 508–520. [CrossRef]
47. Providencia, R.; Elliott, P.; Patel, K.; McCready, J.; Babu, G.; Srinivasan, N.; Bronis, K.; Papageorgiou, N.; Chow, A.; Rowland, E.; et al. Catheter Ablation for Atrial Fibrillation in Hypertrophic Cardiomyopathy: A Systematic Review and Meta-Analysis. *Heart* **2016**, *102*, 1533–1543. [CrossRef]
48. Antzelevitch, C.; Burashnikov, A. Overview of Basic Mechanisms of Cardiac Arrhythmia. *Card. Electrophysiol. Clin.* **2011**, *3*, 23–45. [CrossRef]
49. Frontera, A.; Villella, F.; Cristiano, E.; Comi, F.; Latini, A.; Ceriotti, C.; Galimberti, P.; Zachariah, D.; Pinna, G.; Taormina, A.; et al. The Functional Substrate in Patients with Atrial Fibrillation Is Predictive of Recurrences after Catheter Ablation. *Heart Rhythm* **2024**, *22*, 1401–1410. [CrossRef] [PubMed]
50. Lukito, A.A.; Raffaello, W.M.; Pranata, R. Slow Left Atrial Conduction Velocity in the Anterior Wall Calculated by Electroanatomic Mapping Predicts Atrial Fibrillation Recurrence after Catheter Ablation-Systematic Review and Meta-Analysis. *J. Arrhythmia* **2024**, *40*, 1077–1084. [CrossRef]

51. McDowell, K.S.; Vadakkumpadan, F.; Blake, R.; Blauer, J.; Plank, G.; MacLeod, R.S.; Trayanova, N.A. Mechanistic Inquiry into the Role of Tissue Remodeling in Fibrotic Lesions in Human Atrial Fibrillation. *Biophys. J.* **2013**, *104*, 2764–2773. [CrossRef]
52. Mahnkopf, C.; Badger, T.J.; Burgon, N.S.; Daccarett, M.; Haslam, T.S.; Badger, C.T.; McGann, C.J.; Akoum, N.; Kholmovski, E.; Macleod, R.S.; et al. Evaluation of the Left Atrial Substrate in Patients with Lone Atrial Fibrillation Using Delayed-Enhanced MRI: Implications for Disease Progression and Response to Catheter Ablation. *Heart Rhythm* **2010**, *7*, 1475–1481. [CrossRef]
53. Okubo, Y.; Oguri, N.; Sakai, T.; Uotani, Y.; Furutani, M.; Miyamoto, S.; Miyauchi, S.; Okamura, S.; Tokuyama, T.; Nakano, Y. Conduction Velocity Mapping in Atrial Fibrillation Using Omnipolar Technology. *Pacing Clin. Electrophysiol.* **2024**, *47*, 19–27. [CrossRef]
54. Qi, D.; Guan, X.; Liu, X.; Liu, L.; Liu, Z.; Zhang, J. Slow Conduction Velocity Predicts Atrial Fibrillation Recurrence after Radiofrequency Ablation. *J. Cardiovasc. Electrophysiol.* **2024**, *35*, 461–468. [CrossRef] [PubMed]
55. Fukumoto, K.; Habibi, M.; Ipek, E.G.; Zahid, S.; Khurram, I.M.; Zimmerman, S.L.; Zipunnikov, V.; Spragg, D.; Ashikaga, H.; Trayanova, N.; et al. Association of Left Atrial Local Conduction Velocity With Late Gadolinium Enhancement on Cardiac Magnetic Resonance in Patients With Atrial Fibrillation. *Circ. Arrhythm. Electrophysiol.* **2016**, *9*, e002897. [CrossRef] [PubMed]
56. McGann, C.; Akoum, N.; Patel, A.; Kholmovski, E.; Revelo, P.; Damal, K.; Wilson, B.; Cates, J.; Harrison, A.; Ranjan, R.; et al. Atrial Fibrillation Ablation Outcome Is Predicted by Left Atrial Remodeling on MRI. *Circ. Arrhythm. Electrophysiol.* **2014**, *7*, 23–30. [CrossRef] [PubMed]
57. Gu, Y.; Shao, Y.; Li, S.; Liu, T. Research Progress of Low-Voltage Areas Associated with Atrial Fibrillation. *Rev. Cardiovasc. Med.* **2023**, *24*, 320. [CrossRef] [PubMed]
58. Voigt, N.; Dobrev, D. Ion Channel Remodelling in Atrial Fibrillation. *Eur. Cardiol. Rev.* **2011**, *7*, 97. [CrossRef]
59. Dinov, B.; Knopp, H.; Löbe, S.; Nedios, S.; Bode, K.; Schönbauer, R.; Sommer, P.; Bollmann, A.; Arya, A.; Hindricks, G. Patterns of Left Atrial Activation and Evaluation of Atrial Dyssynchrony in Patients with Atrial Fibrillation and Normal Controls: Factors beyond the Left Atrial Dimensions. *Heart Rhythm* **2016**, *13*, 1829–1836. [CrossRef]
60. Löbe, S.; Knopp, H.; Le, T.-V.; Nedios, S.; Seewöster, T.; Bode, K.; Sommer, P.; Bollmann, A.; Hindricks, G.; Dinov, B. Left Atrial Asynchrony Measured by Pulsed-Wave Tissue Doppler Is Associated With Abnormal Atrial Voltage and Recurrences of Atrial Fibrillation After Catheter Ablation. *JACC Clin. Electrophysiol.* **2018**, *4*, 1640–1641. [CrossRef] [PubMed]
61. den Uijl, D.W.; Gawrysiak, M.; Tops, L.F.; Trines, S.A.; Zeppenfeld, K.; Schalij, M.J.; Bax, J.J.; Delgado, V. Prognostic Value of Total Atrial Conduction Time Estimated with Tissue Doppler Imaging to Predict the Recurrence of Atrial Fibrillation after Radiofrequency Catheter Ablation. *EP Europace* **2011**, *13*, 1533–1540. [CrossRef] [PubMed]
62. Guo, Y.-H.; Yang, Y.-Q. Atrial Fibrillation: Focus on Myocardial Connexins and Gap Junctions. *Biology* **2022**, *11*, 489. [CrossRef] [PubMed]
63. Chaldoupi, S.-M.; Loh, P.; Hauer, R.N.W.; de Bakker, J.M.T.; van Rijen, H.V.M. The Role of Connexin40 in Atrial Fibrillation. *Cardiovasc. Res.* **2009**, *84*, 15–23. [CrossRef] [PubMed]
64. Polontchouk, L.; Haefliger, J.A.; Ebelt, B.; Schaefer, T.; Stuhlmann, D.; Mehlhorn, U.; Kuhn-Regnier, F.; De Vivie, E.R.; Dhein, S. Effects of Chronic Atrial Fibrillation on Gap Junction Distribution in Human and Rat Atria. *J. Am. Coll. Cardiol.* **2001**, *38*, 883–891. [CrossRef]
65. Kostin, S.; Klein, G.; Szalay, Z.; Hein, S.; Bauer, E.P.; Schaper, J. Structural Correlate of Atrial Fibrillation in Human Patients. *Cardiovasc. Res.* **2002**, *54*, 361–379. [CrossRef]
66. Wetzel, U.; Boldt, A.; Lauschke, J.; Weigl, J.; Schirdewahn, P.; Dorszewski, A.; Doll, N.; Hindricks, G.; Dhein, S.; Kottkamp, H. Expression of Connexins 40 and 43 in Human Left Atrium in Atrial Fibrillation of Different Aetiologies. *Heart Br. Card. Soc.* **2005**, *91*, 166–170. [CrossRef]
67. Gollob, M.H.; Jones, D.L.; Krahn, A.D.; Danis, L.; Gong, X.-Q.; Shao, Q.; Liu, X.; Veinot, J.P.; Tang, A.S.L.; Stewart, A.F.R.; et al. Somatic Mutations in the Connexin 40 Gene (GJA5) in Atrial Fibrillation. *N. Engl. J. Med.* **2006**, *354*, 2677–2688. [CrossRef]
68. Thibodeau, I.L.; Xu, J.; Li, Q.; Liu, G.; Lam, K.; Veinot, J.P.; Birnie, D.H.; Jones, D.L.; Krahn, A.D.; Lemery, R.; et al. Paradigm of Genetic Mosaicism and Lone Atrial Fibrillation: Physiological Characterization of a Connexin 43-Deletion Mutant Identified from Atrial Tissue. *Circulation* **2010**, *122*, 236–244. [CrossRef]
69. Dhein, S.; Rothe, S.; Busch, A.; Rojas Gomez, D.M.; Boldt, A.; Reutemann, A.; Seidel, T.; Salameh, A.; Pfannmüller, B.; Rastan, A.; et al. Effects of Metoprolol Therapy on Cardiac Gap Junction Remodelling and Conduction in Human Chronic Atrial Fibrillation. *Br. J. Pharmacol.* **2011**, *164*, 607–616. [CrossRef]
70. Igarashi, T.; Finet, J.E.; Takeuchi, A.; Fujino, Y.; Strom, M.; Greener, I.D.; Rosenbaum, D.S.; Donahue, J.K. Connexin Gene Transfer Preserves Conduction Velocity and Prevents Atrial Fibrillation. *Circulation* **2012**, *125*, 216–225. [CrossRef]
71. Nattel, S.; Heijman, J.; Zhou, L.; Dobrev, D. Molecular Basis of Atrial Fibrillation Pathophysiology and Therapy: A Translational Perspective. *Circ. Res.* **2020**, *127*, 51–72. [CrossRef]
72. Rosenberg, J.H.; Werner, J.H.; Plitt, G.D.; Noble, V.V.; Spring, J.T.; Stephens, B.A.; Siddique, A.; Merritt-Genore, H.L.; Moulton, M.J.; Agrawal, D.K. Immunopathogenesis and Biomarkers of Recurrent Atrial Fibrillation Following Ablation Therapy in Patients with Preexisting Atrial Fibrillation. *Expert Rev. Cardiovasc. Ther.* **2019**, *17*, 193–207. [CrossRef] [PubMed]

73. Cao, H.; Zhou, Q.; Lan, R.; Røe, O.D.; Chen, X.; Chen, Y.; Wang, D. A Functional Polymorphism C-509T in TGFβ-1 Promoter Contributes to Susceptibility and Prognosis of Lone Atrial Fibrillation in Chinese Population. *PLoS ONE* **2014**, *9*, e112912. [CrossRef]
74. Wei, Y.; Liu, S.; Yu, H.; Zhang, Y.; Gao, W.; Cui, M.; Li, L. The Predictive Value of Growth Differentiation Factor-15 in Recurrence of Atrial Fibrillation after Catheter Ablation. *Mediators Inflamm.* **2020**, *2020*, 8360936. [CrossRef]
75. Zakynthinos, G.E.; Tsolaki, V.; Oikonomou, E.; Pantelidis, P.; Gialamas, I.; Kalogeras, K.; Zakynthinos, E.; Vavuranakis, M.; Siasos, G. Unveiling the Role of Endothelial Dysfunction: A Possible Key to Enhancing Catheter Ablation Success in Atrial Fibrillation. *Int. J. Mol. Sci.* **2024**, *25*, 2317. [CrossRef]
76. Boyalla, V.; Harling, L.; Snell, A.; Kralj-Hans, I.; Barradas-Pires, A.; Haldar, S.; Khan, H.R.; Cleland, J.G.F.; Athanasiou, T.; Harding, S.E.; et al. Biomarkers as Predictors of Recurrence of Atrial Fibrillation Post Ablation: An Updated and Expanded Systematic Review and Meta-Analysis. *Clin. Res. Cardiol.* **2022**, *111*, 680–691. [CrossRef]
77. Henningsen, K.M.A.; Nilsson, B.; Bruunsgaard, H.; Chen, X.; Pedersen, B.K.; Svendsen, J.H. Prognostic Impact of Hs-CRP and IL-6 in Patients Undergoing Radiofrequency Catheter Ablation for Atrial Fibrillation. *Scand. Cardiovasc. J. SCJ* **2009**, *43*, 285–291. [CrossRef] [PubMed]
78. Carballo, D.; Noble, S.; Carballo, S.; Stirnemann, J.; Muller, H.; Burri, H.; Vuilleumier, N.; Talajic, M.; Tardif, J.-C.; Keller, P.-F.; et al. Biomarkers and Arrhythmia Recurrence Following Radiofrequency Ablation of Atrial Fibrillation. *J. Int. Med. Res.* **2018**, *46*, 5183–5194. [CrossRef] [PubMed]
79. Lim, H.S.; Schultz, C.; Dang, J.; Alasady, M.; Lau, D.H.; Brooks, A.G.; Wong, C.X.; Roberts-Thomson, K.C.; Young, G.D.; Worthley, M.I.; et al. Time Course of Inflammation, Myocardial Injury, and Prothrombotic Response After Radiofrequency Catheter Ablation for Atrial Fibrillation. *Circ. Arrhythm. Electrophysiol.* **2014**, *7*, 83–89. [CrossRef]
80. Tan, Z.; Song, T.; Huang, S.; Liu, M.; Ma, J.; Zhang, J.; Yu, P.; Liu, X. Relationship between Serum Growth Differentiation Factor 15, Fibroblast Growth Factor-23 and Risk of Atrial Fibrillation: A Systematic Review and Meta-Analysis. *Front. Cardiovasc. Med.* **2022**, *9*, 899667. [CrossRef]
81. Aragón-Herrera, A.; Couselo-Seijas, M.; Feijóo-Bandín, S.; Anido-Varela, L.; Moraña-Fernández, S.; Tarazón, E.; Roselló-Lletí, E.; Portolés, M.; Martínez-Sande, J.L.; García-Seara, J.; et al. Relaxin-2 Plasma Levels in Atrial Fibrillation Are Linked to Inflammation and Oxidative Stress Markers. *Sci. Rep.* **2022**, *12*, 22287. [CrossRef]
82. Qu, X.; Chen, L.; Sun, L.; Chen, C.; Gao, Z.; Huang, W.; Zhou, H. Serum Relaxin Level Predicts Recurrence of Atrial Fibrillation after Radiofrequency Catheter Ablation. *Heart Vessels* **2019**, *34*, 1543–1551. [CrossRef]
83. Kalenderoglu, K.; Hayiroglu, M.I.; Cinar, T.; Oz, M.; Bayraktar, G.A.; Cam, R.; Gurkan, K. Comparison of Inflammatory Markers for the Prediction of Atrial Fibrillation Recurrence Following Cryoablation. *Biomark. Med.* **2024**, *18*, 717–725. [CrossRef]
84. University Hospital. Bordeaux Inflammatory Response Following "Pulsed Field Ablation" vs. Radiofrequency Ablation of Paroxysmal Atrial Fibrillation-2. 2025. Available online: https://www.clinicaltrials.gov (accessed on 18 March 2025).
85. Meng, F.; Jin, S.; Liu, N. Cardiac Selectivity in Pulsed Field Ablation. *Curr. Opin. Cardiol.* **2025**, *40*, 37–41. [CrossRef]
86. Wong, G.R.; Nalliah, C.J.; Lee, G.; Voskoboinik, A.; Prabhu, S.; Parameswaran, R.; Sugumar, H.; Anderson, R.D.; Ling, L.-H.; McLellan, A.; et al. Genetic Susceptibility to Atrial Fibrillation Is Associated With Atrial Electrical Remodeling and Adverse Post-Ablation Outcome. *JACC Clin. Electrophysiol.* **2020**, *6*, 1509–1521. [CrossRef] [PubMed]
87. Choi, E.; Zhao, Y.; Everett, T.H.; Chen, P. Ganglionated Plexi as Neuromodulation Targets for Atrial Fibrillation. *J. Cardiovasc. Electrophysiol.* **2017**, *28*, 1485–1491. [CrossRef] [PubMed]
88. Saffitz, J.E. Gap Junctions: Functional Effects of Molecular Structure and Tissue Distribution. *Adv. Exp. Med. Biol.* **1997**, *430*, 291–301. [CrossRef]
89. Fatkin, D.; Otway, R.; Vandenberg, J.I. Genes and Atrial Fibrillation: A New Look at an Old Problem. *Circulation* **2007**, *116*, 782–792. [CrossRef] [PubMed]
90. Feghaly, J.; Zakka, P.; London, B.; MacRae, C.A.; Refaat, M.M. Genetics of Atrial Fibrillation. *J. Am. Heart Assoc.* **2018**, *7*, e009884. [CrossRef]
91. Peng, W.; Li, M.; Li, H.; Tang, K.; Zhuang, J.; Zhang, J.; Xiao, J.; Jiang, H.; Li, D.; Yu, Y.; et al. Dysfunction of Myosin Light-Chain 4 (MYL4) Leads to Heritable Atrial Cardiomyopathy With Electrical, Contractile, and Structural Components: Evidence From Genetically-Engineered Rats. *J. Am. Heart Assoc.* **2017**, *6*, e007030. [CrossRef]
92. Ahlberg, G.; Refsgaard, L.; Lundegaard, P.R.; Andreasen, L.; Ranthe, M.F.; Linscheid, N.; Nielsen, J.B.; Melbye, M.; Haunsø, S.; Sajadieh, A.; et al. Rare Truncating Variants in the Sarcomeric Protein Titin Associate with Familial and Early-Onset Atrial Fibrillation. *Nat. Commun.* **2018**, *9*, 4316. [CrossRef]
93. Roberts, J.D.; Marcus, G.M. The Burgeoning Field of Ablatogenomics. *Circ. Arrhythm. Electrophysiol.* **2015**, *8*, 258–260. [CrossRef]
94. Gudbjartsson, D.F.; Arnar, D.O.; Helgadottir, A.; Gretarsdottir, S.; Holm, H.; Sigurdsson, A.; Jonasdottir, A.; Baker, A.; Thorleifsson, G.; Kristjansson, K.; et al. Variants Conferring Risk of Atrial Fibrillation on Chromosome 4q25. *Nature* **2007**, *448*, 353–357. [CrossRef]

95. Mommersteeg, M.T.M.; Brown, N.A.; Prall, O.W.J.; de Gier-de Vries, C.; Harvey, R.P.; Moorman, A.F.M.; Christoffels, V.M. Pitx2c and Nkx2-5 Are Required for the Formation and Identity of the Pulmonary Myocardium. *Circ. Res.* **2007**, *101*, 902–909. [CrossRef]
96. Cai, L.; Yin, Y.; Ling, Z.; Su, L.; Liu, Z.; Wu, J.; Du, H.; Lan, X.; Fan, J.; Chen, W.; et al. Predictors of Late Recurrence of Atrial Fibrillation after Catheter Ablation. *Int. J. Cardiol.* **2013**, *164*, 82–87. [CrossRef]
97. Lage, R.; Cebro-Márquez, M.; Vilar-Sánchez, M.E.; González-Melchor, L.; García-Seara, J.; Martínez-Sande, J.L.; Fernández-López, X.A.; Aragón-Herrera, A.; Martínez-Monzonís, M.A.; González-Juanatey, J.R.; et al. Circulating miR-451a Expression May Predict Recurrence in Atrial Fibrillation Patients after Catheter Pulmonary Vein Ablation. *Cells* **2023**, *12*, 638. [CrossRef]
98. Kakimoto, Y.; Tanaka, M.; Kamiguchi, H.; Hayashi, H.; Ochiai, E.; Osawa, M. MicroRNA Deep Sequencing Reveals Chamber-Specific miR-208 Family Expression Patterns in the Human Heart. *Int. J. Cardiol.* **2016**, *211*, 43–48. [CrossRef] [PubMed]
99. Girmatsion, Z.; Biliczki, P.; Bonauer, A.; Wimmer-Greinecker, G.; Scherer, M.; Moritz, A.; Bukowska, A.; Goette, A.; Nattel, S.; Hohnloser, S.H.; et al. Changes in microRNA-1 Expression and IK1 up-Regulation in Human Atrial Fibrillation. *Heart Rhythm* **2009**, *6*, 1802–1809. [CrossRef] [PubMed]
100. Van Den Berg, N.W.E.; Kawasaki, M.; Berger, W.R.; Neefs, J.; Meulendijks, E.; Tijsen, A.J.; De Groot, J.R. MicroRNAs in Atrial Fibrillation: From Expression Signatures to Functional Implications. *Cardiovasc. Drugs Ther.* **2017**, *31*, 345–365. [CrossRef] [PubMed]
101. Silva, A.M.G.D.; Araújo, J.N.G.D.; Freitas, R.C.C.D.; Silbiger, V.N. Circulating MicroRNAs as Potential Biomarkers of Atrial Fibrillation. *BioMed Res. Int.* **2017**, *2017*, 7804763. [CrossRef]
102. Boxhammer, E.; Dienhart, C.; Rezar, R.; Hoppe, U.C.; Lichtenauer, M. Deciphering the Role of microRNAs: Unveiling Clinical Biomarkers and Therapeutic Avenues in Atrial Fibrillation and Associated Stroke—A Systematic Review. *Int. J. Mol. Sci.* **2024**, *25*, 5568. [CrossRef]
103. Komal, S.; Yin, J.-J.; Wang, S.-H.; Huang, C.-Z.; Tao, H.-L.; Dong, J.-Z.; Han, S.-N.; Zhang, L.-R. MicroRNAs: Emerging Biomarkers for Atrial Fibrillation. *J. Cardiol.* **2019**, *74*, 475–482. [CrossRef]
104. Zhou, Q.; Maleck, C.; Von Ungern-Sternberg, S.N.I.; Neupane, B.; Heinzmann, D.; Marquardt, J.; Duckheim, M.; Scheckenbach, C.; Stimpfle, F.; Gawaz, M.; et al. Circulating MicroRNA-21 Correlates With Left Atrial Low-Voltage Areas and Is Associated With Procedure Outcome in Patients Undergoing Atrial Fibrillation Ablation. *Circ. Arrhythm. Electrophysiol.* **2018**, *11*, e006242. [CrossRef]
105. Sygitowicz, G.; Maciejak-Jastrzębska, A.; Sitkiewicz, D. A Review of the Molecular Mechanisms Underlying Cardiac Fibrosis and Atrial Fibrillation. *J. Clin. Med.* **2021**, *10*, 4430. [CrossRef]
106. Shen, K.; Tu, T.; Yuan, Z.; Yi, J.; Zhou, Y.; Liao, X.; Liu, Q.; Zhou, X. DNA Methylation Dysregulations in Valvular Atrial Fibrillation. *Clin. Cardiol.* **2017**, *40*, 686–691. [CrossRef] [PubMed]
107. Felisbino, M.B.; McKinsey, T.A. Epigenetics in Cardiac Fibrosis: Emphasis on Inflammation and Fibroblast Activation. *JACC Basic Transl. Sci.* **2018**, *3*, 704–715. [CrossRef] [PubMed]
108. Tao, H.; Shi, K.-H.; Yang, J.-J.; Li, J. Epigenetic Mechanisms in Atrial Fibrillation: New Insights and Future Directions. *Trends Cardiovasc. Med.* **2016**, *26*, 306–318. [CrossRef]
109. Scholz, B.; Schulte, J.S.; Hamer, S.; Himmler, K.; Pluteanu, F.; Seidl, M.D.; Stein, J.; Wardelmann, E.; Hammer, E.; Völker, U.; et al. HDAC (Histone Deacetylase) Inhibitor Valproic Acid Attenuates Atrial Remodeling and Delays the Onset of Atrial Fibrillation in Mice. *Circ. Arrhythm. Electrophysiol.* **2019**, *12*, e007071. [CrossRef]
110. Zhao, G.; Zhou, J.; Gao, J.; Liu, Y.; Gu, S.; Zhang, X.; Su, P. Genome-Wide DNA Methylation Analysis in Permanent Atrial Fibrillation. *Mol. Med. Rep.* **2017**, *16*, 5505–5514. [CrossRef] [PubMed]
111. Tao, H.; Yang, J.-J.; Chen, Z.-W.; Xu, S.-S.; Zhou, X.; Zhan, H.-Y.; Shi, K.-H. DNMT3A Silencing RASSF1A Promotes Cardiac Fibrosis through Upregulation of ERK1/2. *Toxicology* **2014**, *323*, 42–50. [CrossRef]
112. Lv, M.; Ge, W.; Li, Z.; Wang, C.; Zhang, Y. DNA Methylation in Atrial Fibrillation and Its Potential Role in Precision Medicine. *Methods Mol. Biol.* **2020**, *2204*, 123–131. [CrossRef] [PubMed]
113. Kalla, M.; Hao, G.; Tapoulal, N.; Tomek, J.; Liu, K.; Woodward, L.; Oxford Acute Myocardial Infarction (OxAMI) Study; Dall'Armellina, E.; Banning, A.P.; Choudhury, R.P.; et al. The Cardiac Sympathetic Co-Transmitter Neuropeptide Y Is pro-Arrhythmic Following ST-Elevation Myocardial Infarction despite Beta-Blockade. *Eur. Heart J.* **2020**, *41*, 2168–2179. [CrossRef]
114. Ajijola, O.A.; Chatterjee, N.A.; Gonzales, M.J.; Gornbein, J.; Liu, K.; Li, D.; Paterson, D.J.; Shivkumar, K.; Singh, J.P.; Herring, N. Coronary Sinus Neuropeptide Y Levels and Adverse Outcomes in Patients With Stable Chronic Heart Failure. *JAMA Cardiol.* **2020**, *5*, 318–325. [CrossRef]
115. Jelavic, M.M.; Țica, O.; Pintaric, H.; Țica, O. Circulating Neuropeptide Y May Be a Biomarker for Diagnosing Atrial Fibrillation. *Cardiology* **2023**, *148*, 593–595. [CrossRef] [PubMed]
116. Stavrakis, S.; Morris, L.; Takashima, A.D.; Elkholey, K.; Van Wagoner, D.R.; Ajijola, O.A. Circulating Neuropeptide Y as a Biomarker for Neuromodulation in Atrial Fibrillation. *JACC Clin. Electrophysiol.* **2020**, *6*, 1575–1576. [CrossRef]

117. Song, Q.; Zhang, N.; Zhang, Y.; Zhang, A.; Li, H.; Bai, S.; Shang, L.; Du, J.; Hou, Y. Multiomics Analysis of Canine Myocardium after Circumferential Pulmonary Vein Ablation: Effect of Neuropeptide Y on Long-Term Reinduction of Atrial Fibrillation. *J. Cell. Mol. Med.* **2024**, *28*, e18582. [CrossRef]
118. Wang, P.; Guo, J.; Li, Y.; Liu, H.; Kang, X.; Liu, S.; Zhang, Y. Circulating Neuropeptide Y May Be a Biomarker for Diagnosing Atrial Fibrillation. *Cardiology* **2023**, *148*, 517–527. [CrossRef]
119. Zhang, J.; He, Y.; Yin, Z.; Li, R.; Zhang, X.; Wang, Y.; Wang, H. Circulating Neuropeptide Y as a Biomarker in Postoperative Atrial Fibrillation Cases Administered Off-Pump Coronary Bypass Graft Surgery. *Heliyon* **2024**, *10*, e31251. [CrossRef]
120. Yu, Y.; Liu, L.; Jiang, J.Y.; Qu, X.F.; Yu, G. Parasympathetic and Substance P-Immunoreactive Nerve Denervation in Atrial Fibrillation Models. *Cardiovasc. Pathol.* **2012**, *21*, 39–45. [CrossRef]
121. Stavrakis, S.; Po, S. Ganglionated Plexi Ablation: Physiology and Clinical Applications. *Arrhythmia Electrophysiol. Rev.* **2017**, *6*, 186–190. [CrossRef] [PubMed]
122. Avazzadeh, S.; McBride, S.; O'Brien, B.; Coffey, K.; Elahi, A.; O'Halloran, M.; Soo, A.; Quinlan, L.R. Ganglionated Plexi Ablation for the Treatment of Atrial Fibrillation. *J. Clin. Med.* **2020**, *9*, 3081. [CrossRef]
123. Aksu, T.; Skeete, J.R.; Huang, H.H. Ganglionic Plexus Ablation: A Step-by-Step Guide for Electrophysiologists and Review of Modalities for Neuromodulation for the Management of Atrial Fibrillation. *Arrhythm Electrophysiol. Rev.* **2022**, *12*, e02. [CrossRef]
124. Scherschel, K.; Hedenus, K.; Jungen, C.; Lemoine, M.D.; Rübsamen, N.; Veldkamp, M.W.; Klatt, N.; Lindner, D.; Westermann, D.; Casini, S.; et al. Cardiac Glial Cells Release Neurotrophic S100B upon Catheter-Based Treatment of Atrial Fibrillation. *Sci. Transl. Med.* **2019**, *11*, eaav7770. [CrossRef]
125. Zafeiropoulos, S.; Stavrakis, S. Impact of Pulsed Field Ablation on Autonomic Nervous System. *JACC Clin. Electrophysiol.* **2023**, *9*, 494–496. [CrossRef] [PubMed]
126. Mark Richards, A.; Lainchbury, J.G.; Troughton, R.W.; Nicholls, G.; Frampton, C.M.; Yandle, T.G. Plasma Amino-Terminal pro-B-Type Natriuretic Peptide Predicts Postcardioversion Reversion to Atrial Fibrillation. *J. Am. Coll. Cardiol.* **2003**, *41*, 99. [CrossRef]
127. Dernellis, J.; Panaretou, M. C-Reactive Protein and Paroxysmal Atrial Fibrillation: Evidence of the Implication of an Inflammatory Process in Paroxysmal Atrial Fibrillation. *Acta Cardiol.* **2001**, *56*, 375–380. [CrossRef]
128. Davis, C.A.; Rembert, J.C.; Greenfield, J.C. Compliance of Left Atrium with and without Left Atrium Appendage. *Am. J. Physiol.-Heart Circ. Physiol.* **1990**, *259*, H1006–H1008. [CrossRef]
129. Al-Saady, N.M.; Obel, O.A.; Camm, A.J. Left Atrial Appendage: Structure, Function, and Role in Thromboembolism. *Heart* **1999**, *82*, 547–554. [CrossRef]
130. Yaghi, S.; Song, C.; Gray, W.A.; Furie, K.L.; Elkind, M.S.V.; Kamel, H. Left Atrial Appendage Function and Stroke Risk. *Stroke* **2015**, *46*, 3554–3559. [CrossRef]
131. Unsicker, K.; Spittau, B.; Krieglstein, K. The Multiple Facets of the TGF-β Family Cytokine Growth/Differentiation Factor-15/Macrophage Inhibitory Cytokine-1. *Cytokine Growth Factor Rev.* **2013**, *24*, 373–384. [CrossRef] [PubMed]
132. Kempf, T.; Eden, M.; Strelau, J.; Naguib, M.; Willenbockel, C.; Tongers, J.; Heineke, J.; Kotlarz, D.; Xu, J.; Molkentin, J.D.; et al. The Transforming Growth Factor-β Superfamily Member Growth-Differentiation Factor-15 Protects the Heart From Ischemia/Reperfusion Injury. *Circ. Res.* **2006**, *98*, 351–360. [CrossRef]
133. Wang, T.J.; Wollert, K.C.; Larson, M.G.; Coglianese, E.; McCabe, E.L.; Cheng, S.; Ho, J.E.; Fradley, M.G.; Ghorbani, A.; Xanthakis, V.; et al. Prognostic Utility of Novel Biomarkers of Cardiovascular Stress: The Framingham Heart Study. *Circulation* **2012**, *126*, 1596–1604. [CrossRef]
134. Gizatulina, T.P.; Mamarina, A.V.; Martyanova, L.U.; Belonogov, D.V.; Kolunin, G.V.; Petelina, T.I.; Shirokov, N.E.; Gorbatenko, E.A. The Soluble ST2 Level Predicts Risk of Atrial Fibrillation Recurrences in Long-Term Period after Radiofrequency Ablation. *BMC Cardiovasc. Disord.* **2024**, *24*, 460. [CrossRef]
135. Teichman, S.L.; Unemori, E.; Teerlink, J.R.; Cotter, G.; Metra, M. Relaxin: Review of Biology and Potential Role in Treating Heart Failure. *Curr. Heart Fail. Rep.* **2010**, *7*, 75–82. [CrossRef]
136. Zhou, H.; Qu, X.; Gao, Z.; Zheng, G.; Lin, J.; Su, L.; Huang, Z.; Li, H.; Huang, W. Relaxin Level in Patients With Atrial Fibrillation and Association with Heart Failure Occurrence: A STROBE Compliant Article. *Medicine* **2016**, *95*, e3664. [CrossRef]
137. Mahmud, F.; Sarker, D.B.; Jocelyn, J.A.; Sang, Q.-X.A. Molecular and Cellular Effects of Microplastics and Nanoplastics: Focus on Inflammation and Senescence. *Cells* **2024**, *13*, 1788. [CrossRef] [PubMed]
138. Zheng, H.; Vidili, G.; Casu, G.; Navarese, E.P.; Sechi, L.A.; Chen, Y. Microplastics and Nanoplastics in Cardiovascular Disease—A Narrative Review with Worrying Links. *Front. Toxicol.* **2024**, *6*, 1479292. [CrossRef] [PubMed]
139. Marfella, R.; Prattichizzo, F.; Sardu, C.; Fulgenzi, G.; Graciotti, L.; Spadoni, T.; D'Onofrio, N.; Scisciola, L.; Grotta, R.L.; Frigé, C.; et al. Microplastics and Nanoplastics in Atheromas and Cardiovascular Events. *N. Engl. J. Med.* **2024**, *390*, 900–910. [CrossRef] [PubMed]
140. Di Monaco, A.; Vitulano, N.; Troisi, F.; Quadrini, F.; Romanazzi, I.; Calvi, V.; Grimaldi, M. Pulsed Field Ablation to Treat Atrial Fibrillation: A Review of the Literature. *J. Cardiovasc. Dev. Dis.* **2022**, *9*, 94. [CrossRef]

141. Oda, Y.; Nogami, A.; Igarashi, D.; Usui, R.; Uno, K. A Case Report of Persistent Phrenic Nerve Injury by Pulsed Field Ablation: Lessons from Anatomical Reconstruction and Electrode Positioning. *Hear. Case Rep.* **2025**, *11*, 763–766. [CrossRef]
142. Reddy, V.Y.; Gerstenfeld, E.P.; Natale, A.; Whang, W.; Cuoco, F.A.; Patel, C.; Mountantonakis, S.E.; Gibson, D.N.; Harding, J.D.; Ellis, C.R.; et al. Pulsed Field or Conventional Thermal Ablation for Paroxysmal Atrial Fibrillation. *N. Engl. J. Med.* **2023**, *389*, 1660–1671. [CrossRef]
143. Maurhofer, J.; Kueffer, T.; Madaffari, A.; Stettler, R.; Stefanova, A.; Seiler, J.; Thalmann, G.; Kozhuharov, N.; Galuszka, O.; Servatius, H.; et al. Pulsed-Field vs. Cryoballoon vs. Radiofrequency Ablation: A Propensity Score Matched Comparison of One-Year Outcomes after Pulmonary Vein Isolation in Patients with Paroxysmal Atrial Fibrillation. *J. Interv. Card. Electrophysiol.* **2024**, *67*, 389–397. [CrossRef]
144. Reinsch, N.; Füting, A.; Hartl, S.; Höwel, D.; Rausch, E.; Lin, Y.; Kasparian, K.; Neven, K. Pulmonary Vein Isolation Using Pulsed Field Ablation vs. High-Power Short-Duration Radiofrequency Ablation in Paroxysmal Atrial Fibrillation: Efficacy, Safety, and Long-Term Follow-up (PRIORI Study). *Europace* **2024**, *26*, euae194. [CrossRef]
145. Chen, J.-C.; Mao, Y.-J.; Huang, Q.-Y.; Cheng, Z.-D.; He, S.-B.; Xu, Q.-X.; Zhang, Y. Meta-Analysis of Thermal Versus Pulse Field Ablation for Pulmonary Vein Isolation Durability in Atrial Fibrillation: Insights From Repeat Ablation. *Clin. Cardiol.* **2025**, *48*, e70151. [CrossRef]
146. Reddy, V.Y.; Neuzil, P.; Koruth, J.S.; Petru, J.; Funosako, M.; Cochet, H.; Sediva, L.; Chovanec, M.; Dukkipati, S.R.; Jais, P. Pulsed Field Ablation for Pulmonary Vein Isolation in Atrial Fibrillation. *JACC* **2019**, *74*, 315–326. [CrossRef]
147. Yin, G.; Yao, L.; You, L. Inflammation Response Post-Radiofrequency Ablation for Atrial Fibrillation: Implications for Early Atrial Fibrillation Recurrence. *Pol. Heart J. Kardiologia Pol.* **2025**, *83*, 570–576. [CrossRef]
148. Ozen, S.; Demirkaya, E.; Erer, B.; Livneh, A.; Ben-Chetrit, E.; Giancane, G.; Ozdogan, H.; Abu, I.; Gattorno, M.; Hawkins, P.N.; et al. EULAR Recommendations for the Management of Familial Mediterranean Fever. *Ann. Rheum. Dis.* **2016**, *75*, 644–651. [CrossRef]
149. Kommu, S.; Arepally, S. The Effect of Colchicine on Atrial Fibrillation: A Systematic Review and Meta-Analysis. *Cureus* **2023**, *15*, e35120. [CrossRef] [PubMed]
150. Zarpelon, C.S.; Netto, M.C.; Jorge, J.C.M.; Fabris, C.C.; Desengrini, D.; Jardim, M.d.S.; Silva, D.G. da Colchicine to Reduce Atrial Fibrillation in the Postoperative Period of Myocardial Revascularization. *Arq. Bras. Cardiol.* **2016**, *107*, 4–9. [CrossRef] [PubMed]
151. Imazio, M.; Brucato, A.; Ferrazzi, P.; Rovere, M.E.; Gandino, A.; Cemin, R.; Ferrua, S.; Belli, R.; Maestroni, S.; Simon, C.; et al. Colchicine Reduces Postoperative Atrial Fibrillation: Results of the Colchicine for the Prevention of the Postpericardiotomy Syndrome (COPPS) Atrial Fibrillation Substudy. *Circulation* **2011**, *124*, 2290–2295. [CrossRef] [PubMed]
152. Koyama, T.; Sekiguchi, Y.; Tada, H.; Arimoto, T.; Yamasaki, H.; Kuroki, K.; Machino, T.; Tajiri, K.; Zhu, X.D.; Kanemoto, M.; et al. Comparison of Characteristics and Significance of Immediate versus Early versus No Recurrence of Atrial Fibrillation after Catheter Ablation. *Am. J. Cardiol.* **2009**, *103*, 1249–1254. [CrossRef]
153. Deftereos, S.; Giannopoulos, G.; Kossyvakis, C.; Efremidis, M.; Panagopoulou, V.; Kaoukis, A.; Raisakis, K.; Bouras, G.; Angelidis, C.; Theodorakis, A.; et al. Colchicine for Prevention of Early Atrial Fibrillation Recurrence after Pulmonary Vein Isolation: A Randomized Controlled Study. *J. Am. Coll. Cardiol.* **2012**, *60*, 1790–1796. [CrossRef] [PubMed]
154. Koyama, T.; Tada, H.; Sekiguchi, Y.; Arimoto, T.; Yamasaki, H.; Kuroki, K.; Machino, T.; Tajiri, K.; Zhu, X.D.; Kanemoto-Igarashi, M.; et al. Prevention of Atrial Fibrillation Recurrence with Corticosteroids after Radiofrequency Catheter Ablation: A Randomized Controlled Trial. *J. Am. Coll. Cardiol.* **2010**, *56*, 1463–1472. [CrossRef] [PubMed]
155. Won, H.; Kim, J.-Y.; Shim, J.; Uhm, J.-S.; Pak, H.-N.; Lee, M.-H.; Joung, B. Effect of a Single Bolus Injection of Low-Dose Hydrocortisone for Prevention of Atrial Fibrillation Recurrence after Radiofrequency Catheter Ablation. *Circ. J. Off. J. Jpn. Circ. Soc.* **2013**, *77*, 53–59. [CrossRef] [PubMed]
156. Yared, J.-P.; Bakri, M.H.; Erzurum, S.C.; Moravec, C.S.; Laskowski, D.M.; Van Wagoner, D.R.; Mascha, E.; Thornton, J. Effect of Dexamethasone on Atrial Fibrillation after Cardiac Surgery: Prospective, Randomized, Double-Blind, Placebo-Controlled Trial. *J. Cardiothorac. Vasc. Anesth.* **2007**, *21*, 68–75. [CrossRef]
157. Andrade, J.G.; Khairy, P.; Nattel, S.; Vanella, A.; Rivard, L.; Guerra, P.G.; Dubuc, M.; Dyrda, K.; Thibault, B.; Talajic, M.; et al. Corticosteroid Use during Pulmonary Vein Isolation Is Associated with a Higher Prevalence of Dormant Pulmonary Vein Conduction. *Heart Rhythm* **2013**, *10*, 1569–1575. [CrossRef]
158. Kim, H.W.; Han, M.; Jung, I.; Ahn, S.S. New-Onset Atrial Fibrillation in Seropositive Rheumatoid Arthritis: Association with Disease-Modifying Anti-Rheumatic Drugs Treatment. *Rheumatology* **2024**, *63*, 630–638. [CrossRef]
159. Schneider, M.P.; Hua, T.A.; Böhm, M.; Wachtell, K.; Kjeldsen, S.E.; Schmieder, R.E. Prevention of Atrial Fibrillation by Renin-Angiotensin System Inhibition a Meta-Analysis. *J. Am. Coll. Cardiol.* **2010**, *55*, 2299–2307. [CrossRef]
160. Baía Bezerra, F.; Rodrigues Sobreira, L.E.; Tsuchiya Sano, V.K.; de Oliveira Macena Lôbo, A.; Cavalcanti Orestes Cardoso, J.H.; Alves Kelly, F.; Aquino de Moraes, F.C.; Consolim-Colombo, F.M. Efficacy of Sacubitril-Valsartan vs. Angiotensin-Converting Enzyme Inhibitors or Angiotensin Receptor Blockers in Preventing Atrial Fibrillation Recurrence after Catheter Ablation: A Systematic Review and Meta-Analysis. *Herz* **2025**, *50*, 135–141. [CrossRef]

161. Sun, Q.; Cui, W.; Zhang, X.; Tian, Y.; Huang, G.; He, W.; Zhao, Y.; Zhao, X.; Li, D.; Liu, X. A Systematic Review and Meta-Analysis of Renin-Angiotensin System Inhibitors and Angiotensin Receptor Neprilysin Inhibitors in Preventing Recurrence After Atrial Fibrillation Ablation. *J. Cardiovasc. Pharmacol.* **2024**, *83*, 220–227. [CrossRef]
162. Saygili, E.; Rana, O.R.; Saygili, E.; Reuter, H.; Frank, K.; Schwinger, R.H.G.; Müller-Ehmsen, J.; Zobel, C. Losartan Prevents Stretch-Induced Electrical Remodeling in Cultured Atrial Neonatal Myocytes. *Am. J. Physiol. Heart Circ. Physiol.* **2007**, *292*, H2898–H2905. [CrossRef]
163. Goette, A.; Arndt, M.; Röcken, C.; Spiess, A.; Staack, T.; Geller, J.C.; Huth, C.; Ansorge, S.; Klein, H.U.; Lendeckel, U. Regulation of Angiotensin II Receptor Subtypes during Atrial Fibrillation in Humans. *Circulation* **2000**, *101*, 2678–2681. [CrossRef] [PubMed]
164. Peng, H.; Yang, Y.; Zhao, Y.; Xiao, H. The Effect of Statins on the Recurrence Rate of Atrial Fibrillation after Catheter Ablation: A Meta-Analysis. *Pacing Clin. Electrophysiol. PACE* **2018**, *41*, 1420–1427. [CrossRef] [PubMed]
165. Han, X.; Gao, Y.; He, M.; Luo, Y.; Wei, Y.; Duan, Y.; Zhang, S.; Yu, H.; Kan, J.; Hou, T.; et al. Evolocumab Prevents Atrial Fibrillation in Rheumatoid Arthritis Rats through Restraint of PCSK9 Induced Atrial Remodeling. *J. Adv. Res.* **2024**, *61*, 211–221. [CrossRef] [PubMed]
166. Lopes, R.D.; Guimarães, P.O.; Schwartz, G.G.; Bhatt, D.L.; Bittner, V.A.; Budaj, A.; Dalby, A.J.; Diaz, R.; Goodman, S.G.; Harrington, R.A.; et al. Effect of Alirocumab on Incidence of Atrial Fibrillation After Acute Coronary Syndromes: Insights from the ODYSSEY OUTCOMES Trial. *Am. J. Med.* **2022**, *135*, 915–918. [CrossRef]
167. Saljic, A.; Heijman, J.; Dobrev, D. Emerging Antiarrhythmic Drugs for Atrial Fibrillation. *Int. J. Mol. Sci.* **2022**, *23*, 4096. [CrossRef]
168. Ostropolets, A.; Elias, P.A.; Reyes, M.V.; Wan, E.Y.; Pajvani, U.B.; Hripcsak, G.; Morrow, J.P. Metformin Is Associated With a Lower Risk of Atrial Fibrillation and Ventricular Arrhythmias Compared With Sulfonylureas: An Observational Study. *Circ. Arrhythm. Electrophysiol.* **2021**, *14*, e009115. [CrossRef]
169. Metformin as an Adjunctive Therapy to Catheter Ablation in Atrial Fibrillation | Clinical Research Trial Listing (Atrial Fibrillation) (NCT04625946). Available online: https://www.trialx.com/clinical-trials/listings/225558/metformin-as-an-adjunctive-therapy-to-catheter-ablation-in-atrial-fibrillation/ (accessed on 19 June 2025).
170. Abdelhadi, N.A.; Ragab, K.M.; Elkholy, M.; Koneru, J.; Ellenbogen, K.A.; Pillai, A. Impact of Sodium-Glucose Co-Transporter 2 Inhibitors on Atrial Fibrillation Recurrence Post-Catheter Ablation Among Patients With Type 2 Diabetes Mellitus: A Systematic Review and Meta-Analysis. *J. Cardiovasc. Electrophysiol.* **2025**, *36*, 673–682. [CrossRef]
171. Abu-Qaoud, M.R.; Kumar, A.; Tarun, T.; Abraham, S.; Ahmad, J.; Khadke, S.; Husami, R.; Kulbak, G.; Sahoo, S.; Januzzi, J.L.; et al. Impact of SGLT2 Inhibitors on AF Recurrence After Catheter Ablation in Patients With Type 2 Diabetes. *JACC Clin. Electrophysiol.* **2023**, *9*, 2109–2118. [CrossRef]
172. Paasche, A.; Wiedmann, F.; Kraft, M.; Seibertz, F.; Herlt, V.; Blochberger, P.L.; Jávorszky, N.; Beck, M.; Weirauch, L.; Seeger, T.; et al. Acute Antiarrhythmic Effects of SGLT2 Inhibitors-Dapagliflozin Lowers the Excitability of Atrial Cardiomyocytes. *Basic Res. Cardiol.* **2024**, *119*, 93–112. [CrossRef]
173. Patel, H.; Sheth, A.; Nair, A.; Patel, B.; Thakkar, S.; Narasimhan, B.; Mehta, N.; Azad, Z.; Kowlgi, G.N.; Desimone, C.V.; et al. Long-Term Impact of GLP-1 Receptor Agonists on AF Recurrence After Ablation in Obese Patients. *J. Cardiovasc. Electrophysiol.* **2025**, *36*, 1808–1816. [CrossRef]
174. Karakasis, P.; Fragakis, N.; Patoulias, D.; Theofilis, P.; Kassimis, G.; Karamitsos, T.; El-Tanani, M.; Rizzo, M. Effects of Glucagon-Like Peptide 1 Receptor Agonists on Atrial Fibrillation Recurrence After Catheter Ablation: A Systematic Review and Meta-Analysis. *Adv. Ther.* **2024**, *41*, 3749–3756. [CrossRef] [PubMed]
175. Bohne, L.J.; Jansen, H.J.; Dorey, T.W.; Daniel, I.M.; Jamieson, K.L.; Belke, D.D.; McRae, M.D.; Rose, R.A. Glucagon-Like Peptide-1 Protects Against Atrial Fibrillation and Atrial Remodeling in Type 2 Diabetic Mice. *JACC Basic Transl. Sci.* **2023**, *8*, 922–936. [CrossRef] [PubMed]
176. Wang, H.; Chen, J.; Zhao, L. N-3 Polyunsaturated Fatty Acids for Prevention of Postoperative Atrial Fibrillation: Updated Meta-Analysis and Systematic Review. *J. Interv. Card. Electrophysiol. Int. J. Arrhythm. Pacing* **2018**, *51*, 105–115. [CrossRef] [PubMed]
177. Jia, X.; Gao, F.; Pickett, J.K.; Al Rifai, M.; Birnbaum, Y.; Nambi, V.; Virani, S.S.; Ballantyne, C.M. Association Between Omega-3 Fatty Acid Treatment and Atrial Fibrillation in Cardiovascular Outcome Trials: A Systematic Review and Meta-Analysis. *Cardiovasc. Drugs Ther.* **2021**, *35*, 793–800. [CrossRef]
178. Marcus, M.D.; Link, M.S. Omega-3 Fatty Acids and Arrhythmias. *Circulation* **2024**, *150*, 488–503. [CrossRef]
179. Tu, T.; Li, B.; Li, X.; Zhang, B.; Xiao, Y.; Li, J.; Qin, F.; Liu, N.; Sun, C.; Liu, Q.; et al. Dietary ω-3 Fatty Acids Reduced Atrial Fibrillation Vulnerability via Attenuating Myocardial Endoplasmic Reticulum Stress and Inflammation in a Canine Model of Atrial Fibrillation. *J. Cardiol.* **2022**, *79*, 194–201. [CrossRef]
180. Hu, Y.-F.; Chen, Y.-J.; Lin, Y.-J.; Chen, S.-A. Inflammation and the Pathogenesis of Atrial Fibrillation. *Nat. Rev. Cardiol.* **2015**, *12*, 230–243. [CrossRef]

181. Wiedmann, F.; Beyersdorf, C.; Zhou, X.B.; Kraft, M.; Paasche, A.; Jávorszky, N.; Rinné, S.; Sutanto, H.; Büscher, A.; Foerster, K.I.; et al. Treatment of Atrial Fibrillation with Doxapram: TASK-1 Potassium Channel Inhibition as a Novel Pharmacological Strategy. *Cardiovasc. Res.* **2022**, *118*, 1728–1741. [CrossRef]
182. Krisai, P.; Blum, S.; Schnabel, R.B.; Sticherling, C.; Kühne, M.; von Felten, S.; Ammann, P.; Pruvot, E.; Albert, C.M.; Conen, D. Canakinumab After Electrical Cardioversion in Patients With Persistent Atrial Fibrillation: A Pilot Randomized Trial. *Circ. Arrhythm. Electrophysiol.* **2020**, *13*, e008197. [CrossRef]
183. Wiedmann, F.; Schmidt, C. Novel Drug Therapies for Atrial Fibrillation. *Nat. Rev. Cardiol.* **2024**, *21*, 275–276. [CrossRef] [PubMed]

Disclaimer/Publisher's Note: The statements, opinions and data contained in all publications are solely those of the individual author(s) and contributor(s) and not of MDPI and/or the editor(s). MDPI and/or the editor(s) disclaim responsibility for any injury to people or property resulting from any ideas, methods, instructions or products referred to in the content.

MDPI AG
Grosspeteranlage 5
4052 Basel
Switzerland
Tel.: +41 61 683 77 34

Cells Editorial Office
E-mail: cells@mdpi.com
www.mdpi.com/journal/cells



Disclaimer/Publisher's Note: The title and front matter of this reprint are at the discretion of the Guest Editors. The publisher is not responsible for their content or any associated concerns. The statements, opinions and data contained in all individual articles are solely those of the individual Editors and contributors and not of MDPI. MDPI disclaims responsibility for any injury to people or property resulting from any ideas, methods, instructions or products referred to in the content.





Academic Open
Access Publishing

mdpi.com

ISBN 978-3-7258-9174-0